Thesis submitted for the degree of Doctor of Philosophy

The sedimentology and chemostratigraphy of the Nafun Group, Huqf Supergroup, Oman.

by

M.E. Gretta McCarron



Department of Earth Sciences
&
St. Cross College
Trinity Term 1999

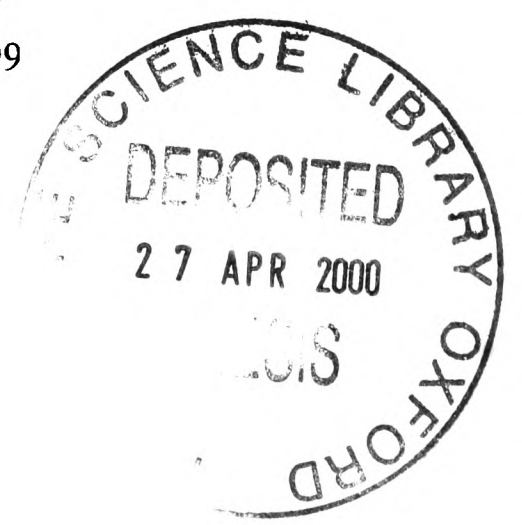


TABLE OF CONTENTS

	Page
Short abstract	i
Long abstract	ii
Acknowledgements	vi
Chapter One Introduction	
1.1 INTRODUCTION	**I**
1.2 REGIONAL SETTING	**1**
1.3 TECTONO-STRATIGRAPHIC HISTORY	**3**
1.3.1 Huqf Supergroup	6
1.4 HUQF SUPERGROUP NOMENCLATURE	**10**
1.5 HUQF STRATIGRAPHY AND FACIES ASSOCIATIONS	**12**
1.6 PROJECT DEVELOPMENT	**13**
Chapter Two Chronostratigraphy	
2.1 INTRODUCTION	**15**
2.2 BIOSTRATIGRAPHY	**16**
2.2.1 Previous work	16
2.2.2 Present study	16
2.3 RADIOMETRIC DATES	**17**
2.3.1 Previous work	17
2.4 NEW GHADIR MANQIL DATES	**19**
2.5 NEW FARA FORMATION DATES	**22**
2.6 SIGNIFICANCE OF THE NEW DATES	**24**
2.6.1 Ghadir Manqil	24
2.6.2 Fara Formation	25
Chapter Three Khufai Formation	
3.1 INTRODUCTION	**27**
3.2 METHODS	**27**
3.3 PREVIOUS WORK	**31**
3.4 SUBDIVISION OF THE KHUFAI FORMATION	**32**
3.5 FACIES ASSOCIATION A: FETID DOLOSTONES/LIME-MUDSTONE	**33**
3.5.1 Facies A1: Fetid laminated dolo/limestone	33
3.5.2 Facies A2: Fetid lime-mudstone	35
3.5.3 Facies Association A synthesis	35
3.6 FACIES ASSOCIATION B: GRAINSTONES	**36**
3.6.1 Facies B1: Oncolitic-ooidal grainstone/packstone/boundstone	37

3.6.2 Facies B2: Fetid intraclast/peloidal wackestone 38
3.6.3 Facies B3: Fetid intraclast grainstone 41
3.6.4 Facies Association B synthesis 41
3.7 FACIES ASSOCIATION C: GRAINSTONE-STROMATOLITE CYCLES 42
3.7.1 Facies C1: Ooidal-intraclast grainstone/packstone 44
3.7.2 Facies C2: Cherty microbial laminites/stromatolites 46
3.7.3 Facies C3: Intraclast lag breccia 48
3.7.4 Facies C4: Dolosiltite 49
3.7.5 Facies Association C synthesis 49
3.8 FACIES ASSOCIATION D: LITHARENITES 50
3.8.1 Facies D1: Calcareous quartz-arenites 51
3.8.2 Facies Association D synthesis 52
3.9 FACIES ASSOCIATION E: OOIDAL-INTRACLAST GRAINSTONES 52
3.9.1 Facies E1: Ooidal-intraclast grainstone 52
3.9.2 Facies E2: Ooidal grainstone 54
3.9.3 Facies Association E synthesis 54
3.10 ASSOCIATION A SYNTHESIS 55

Chapter Four Shuram Formation

4.1 INTRODUCTION 57
4.2 METHODS 58
4.3 PREVIOUS WORK 58
4.4 SUBDIVISIONS OF THE SHURAM FORMATION 60
4.5 LOWER MEMBER OF THE SHURAM FORMATION 62
4.5.1 Huqf area 62
4.5.2 Facies S1: Red and green siltstones 62
4.5.3 Oman Mountains 64
4.5.4 Facies S5: Conglomeratic litharenites from the Oman Mountains 64
4.5.5 Facies S6: Black heterolithic limestones 65
4.5.6 Lower member of the Shuram Formation synthesis 66
4.6 MIDDLE MEMBER OF THE SHURAM FORMATION 66
4.6.1 Huqf area 66
4.6.2 Facies S2: Flat-pebble conglomerates 69
4.6.3 Oman Mountains 70
4.6.4 Facies S8: green and purple siltstones 71
4.6.5 Middle member of the Shuram Formation synthesis 71
4.7 UPPER MEMBER OF THE SHURAM FORMATION 71
4.7.1 Huqf area 71
4.7.2 Facies S3: Silty pelsparite 72

4.7.3 Facies S4: Oosparite 73
4.7.4 Oman Mountains 74
4.7.5 Facies S9: Recrystallized limestones 74
4.7.6 Upper member of the Shuram Formation synthesis 75
4.8 SHURAM FORMATION SYNTHESIS 75

Chapter Five Buah Formation

5.1 INTRODUCTION 77
5.2 METHODS 78
5.3 PREVIOUS WORK 78
5.4 SUBDIVISION S OF THE BUAH FORMATION 80
5.5 FACIES ASSOCIATION A: LIMESTONES 80
5.5.1 Facies A1: Crinkly laminites 82
5.5.2 Facies A2: Silty limestone 86
5.5.3 Facies Association A synthesis 87
5.6 FACIES ASSOCIATION B: SHOAL STROMATOLITES AND GRAINSTONES 88
5.6.1 Facies B1: Compound stromatolites 88
5.6.2 Facies B2: Silty/peloidal wackestone 89
5.6.3 Facies B3: Recrystallized grainstone 91
5.6.4 Facies B4: Ooidal grainstone 93
5.6.5 Facies Association B synthesis 94
5.7 FACIES ASSOCIATION C: PERITIDAL STROMATOLITES AND EVAPORITES 94
5.7.1 Facies C1: Vuggy muddy carbonates 95
5.7.2 Facies C2: Stromatolites 95
5.7.3 Facies Association C synthesis 97
5.8 FACIES ASSOCIATION D: SABKHA 97
5.8.1 Facies D1: Red silty dolostone 98
5.8.2 Facies D2: Quartz-arenite 98
5.8.3 Facies D3: Red/brown anhydritic dolostones 99
5.8.4 Facies Association D synthesis 99
5.9 FACIES ASSOCIATION E: THE DISTAL DEPOSITS OF WADI BANI AWF 99
5.9.1 Facies E1: Black crinkly laminites 100
5.9.2 Facies E2: Recrystallized evaporitic-laminites 101
5.9.3 Facies E3: Rhythmites 101
5.9.4 Facies E4: Carbonate and shale laminites 102
5.9.5 Facies E5: Laminites with slumps and auto-brecciation 102
5.9.6 Facies E6: Breccia 103

5.9.7 Facies E7: Cherty ooid grainstones 104
5.9.8 Facies E8: Facies Association E synthesis 104
5.10 BUAH FORMATION SYNTHESIS 104

Chapter Six Chemostratigraphy
6.1 INTRODUCTION 106
6.2 PRINCIPLES OF CARBON- AND OXYGEN-ISOTOPE CHEM-STRATIGRAPHY 107
6.2.1 The Global Carbon Cycle 107
6.2.2 Carbon isotope fractionation 108
6.2.3 Vertical and lateral changes in the isotope composition of sea water 108
6.2.4 Post-depositional isotope fractionation in sedimentary and organic carbonates 109
6.2.5 Oxygen-isotope fractionation 109
6.2.6 Post-depositional isotope fractionation in sedimentary and microbial carbonates 110
6.3 ELEMENTAL CHEMISTRY OF THE HUQF CARBONATES 110
6.3.1 Mg/Ca ratios 111
6.3.2 Strontium (Sr) and Sr/Ca ratios 112
6.3.3 Iron (Fe) 114
6.3.4 Mn/Sr (as a proxy for diagenetic exchange) 115
6.3.5 Mn and Fe (as a proxy for diagenetic exchange) 118
6.4 DATA CORRECTION 120
6.4.1 Component analyses and corrections 120
6.4.2 Carbon/Oxygen-isotope covariation 127
6.4.3 Oxygen-isotope values 128
6.4.4 Summary 129
6.5 DISCUSSION OF THE KHUFAI FORMATION DATA 130
6.5.1 Regional variation 134
6.5.2 Interpreting the Khufai Formation signature 135
6.6 DISCUSSION OF THE SHURAM FORMATION DATA 135
6.6.1 Regional variation 138
6.6.2 Interpreting the Shuram Formation signature 138
6.7 DISCUSSION OF THE BUAH FORMATION DATA 139
6.7.1 Regional variation 144
6.7.2 Interpreting the Buah Formation signature 144
6.8 CARBON ISOTOPIC SIGNATURE SYNTHESIS 145

Chapter Seven Discussion

7.1 INTRODUCTION **148**

7.2 CHRONOSTRATIGRAPHIC POSITION **148**

7.3 BASIN SEQUENCE STRATIGRAPHY **149**

7.3.1 Recommended revision of Huqf Supergroup nomenclature 154

7.4 CHEMOSTRATIGRAPHY - BASINAL AND GLOBAL **155**

7.4.1 Khufai, Shuram and Buah Formation mineralogy 155

7.4.2 Chemostratigraphic signature 157

7.4.3 Global correlation 160

7.5 BASINAL REVIEW **163**

REFERENCES **165**

LIST OF FIGURES

1.1 Simplified tectonic map of Oman with Huqf Supergroup outcrops 1
1.2 Simplified geological map of the North Oman Mountains 2
1.3 The Arabian peninsula, with Precambrian terranes 3
1.4 Schematic reconstruction of accretionary evolution of the Arabian Shield 4
1.5 The Rodinia Supercontinent 4
1.6 Late Neoproterozoic continental reconfiguration 5
1.7 Arabian plate tectonic reconstruction 6
1.8 Ghadir Manqil Formation from south to north Oman 7
1.9 Al Halfayn Formation log 8
1.10 Ghadir Manqil Formation log 9
1.11 Huqf Supergroup nomenclature 11

2.1 Chronostratigraphy of the terminal Neoproterozoic 15
2.2 Map of eastern Oman with basement and Precambrian exposures 18
2.3 Schematic log of the Ghadir Manqil Formation, showing ash beds 21
2.4 Ghadir Manqil Formation discordia 22
2.5 Summary log of the basal Fara Formation showing ash beds 23
2.6 Fara Formation discordia 24

3.1 Sketch map of the Huqf Supergroup in east-central Oman 28
3.2 Sketch map of the Huqf Supergroup in the Oman Mountains 29
3.3 Khufai Formation summary logs 30
3.4 Subdivisions of the Khufai Formation 31
3.5 Logs of grainstone-stromatolite cycles 43

4.1 Summary logs of the Shuram Formation 59
4.2 Subdivisions of the Shuram Formation 60
4.3 Palaeocurrent measurements of the middle and upper Shuram Formation 68

5.1 Summary logs of the Buah Formation 79
5.2 Subdivisions of the Buah Formation 80

6.1 Plots of 1000Sr/Ca against Mg/Ca 112
6.2 Mn (ppm) against 1000Sr/Ca 114
6.3 Mn/Sr for the Nafun Group 115
6.4 Covariance plots of Mn (ppm) against Sr (ppm) 116
6.5 Mn/Sr against $\delta^{13}C$ for the Nafun Group 117
6.6a Crossplots of Mn/Sr and $\delta^{13}C$ for the Huqf area 118
6.6b Crossplots of Mn/Sr and $\delta^{13}C$ for the Oman Mountains 118
6.7a Crossplots of Mn (ppm) and Fe (ppm) against $\delta^{13}C$ 119

6.7b Crossplots of Mn (ppm) and Fe (ppm) against $\delta^{18}O$ 119
6.8a Khufai Formation component plot 122
6.8b Shuram Formation component plot 123
6.8c Buah Formation component plot 124
6.9 Nafun Group original $\delta^{13}C$ and $\delta^{18}O$ data 125
6.10 Nafun Group corrected $\delta^{13}C$ and $\delta^{18}O$ data 126
6.11a Nafun Group $\delta^{13}C$ and $\delta^{18}O$ covariation 127
6.11b Shuram and Buah formations $\delta^{13}C$ and $\delta^{18}O$ covariation 128
6.12 $\delta^{13}C$ and $\delta^{18}O$ data of the Khufai Formation in the Huqf area 131
6.13 $\delta^{13}C$ and $\delta^{18}O$ data of the Khufai Formation in the Oman Mountains 132
6.14 $\delta^{13}C$ and $\delta^{18}O$ data of the Shuram Formation 137
6.15 $\delta^{13}C$ and $\delta^{18}O$ data of the Buah Formation in the Huqf area 141
6.16 $\delta^{13}C$ and $\delta^{18}O$ data of the Buah Formation in the Oman Mountains 142

7.1 Huqf Supergroup within a global chronostratigraphic framework 149
7.2 Gamma ray log with $\delta^{13}C$ and $\delta^{18}O$ data of the Nafun Group 150
7.3 Sequence-stratigraphic interpretations for the Khufai, Shuram and Buah formations 151
7.4 Sequence-stratigraphic interpretations for the Hadash, Masirah Bay and Khufai formations 152
7.5 Summary log of the Huqf Supergroup with climatic and environmental interpretations and recommended nomenclature revision 157
7.6 Correlation of the Huqf carbon-isotope excursions with global reference sections 161

LIST OF TABLES

1.1 Facies Associations of the Khufai, Shuram and Buah formations 12

2.1 Radiometric dates from Oman 18
2.2 U-Pb Isotope Dilution Analyses, Oman 26

3.1 Khufai Formation Facies Associations A-E with subfacies 32

4.1 Shuram Formation Facies S1-S9 61

5.1 Buah Formation Facies Associations A-D 81

6.1 Trace-element data 147

LIST OF PLATES

1.1 Basement, Hadash Formation and Masirah Bay Formation
2.1 Biostratigraphy and ash beds
3.1 Khufai Formation overview
3.2 Huqf Supergroup in the Oman Mountains
3.3 Facies Association A in the Huqf area
3.4 Khufai Formation in the Oman Mountains
3.5 Facies Association B
3.6 Facies Association C
3.7 Facies Association C
3.8 Facies Association D and E
4.1 Lower and middle members of the Shuram Formation
4.2 Middle member of the Shuram Formation
4.3Upper member of the Shuram Formation
4.4 Shuram Formation in the Oman Mountains
5.1 Overview of the Buah Formation in Wadi Shuram
5.2 Facies Association A
5.3 Facies Association B
5.4 Facies Association B
5.5 Facies Association C in the Mukhaibah dome
5.6 Facies Association C in the Khufai dome
5.7 Facies Association D
5.8 Facies Associations A and B in Wadi Bani Kharus
5.9 Facies Association E in Wadi Bani Awf
5.10 Facies Association E in Wadi Bani Awf
6.1 Khufai Formation cathodoluminescence photomicrographs
6.2 Shuram Formation cathodoluminescence photomicrographs
6.3 Buah Formation cathodoluminescence photomicrographs

The sedimentology and chemostratigraphy of the Nafun Group,

Huqf Supergroup,

Oman.

Thesis submitted to Oxford University for the Degree of Doctor of Philosophy, Trinity Term 1999, by M.E. Gretta McCarron, St. Cross College and Department of Earth Sciences.

Short Abstract

Two glacial units have been identified within the Abu Mahara Group, with the upper being overlain by a 'cap carbonate' (the Hadash Formation). Ash beds from the lower glacial unit are dated herein by U-Pb zircon methods at 723+10/-16 Ma. The Hadash Formation is succeeded by the Nafun Group which is overlain by the volcaniclastic Fara Formation. An ignimbrite unit within the Fara Formation is dated herein by U-Pb zircon methods at 544±3.3 Ma.

The lithologies of the Nafun Group are found to indicate shallow marine deposits in the Huqf area of east-central, Oman and more distal deposits in the Oman Mountains of north Oman. The east-central Khufai Formation carbonates shoal-upward from mid-ramp settings to intertidal carbonates with outer-ramp carbonates in the Oman Mountains. There was arguably a slight draw-down in the uppermost Khufai Formation before the drowning of the carbonate ramp by the Shuram Formation siliciclastics. These red and green siliciclastics are typically swaley cross-stratified upward, indicative of storm deposition. An increase in carbonates in the upper Shuram Formation leads gradationally into the lower Buah Formation. The Buah Formation carbonates preserve another upward-shoaling trend from subwave base to sabkha deposits in east-central Oman. In Wadi Bani Awf, the coeval sediments are shown to contain slump structures and brecciated beds of the ramp slope, with thick breccia units representing slope failure deposits. The Oman Mountains therefore preserves the margin of a carbonate platform.

The dramatic positive and negative to positive excursions recorded in the stable isotope stratigraphy through the Nafun Group are argued to largely reflect sea water $\delta^{13}C$ signatures and may perhaps be explained in terms of climatic changes identified lithologically. The top of both carbonate formations are sequence boundaries with the maximum flooding surfaces identified within the siliciclastic formations.

The sedimentology and chemostratigraphy of the Nafun Group,
Huqf Supergroup,
Oman.

M.E. Gretta McCarron
St. Cross College

Long Abstract

The aim of this work has been to characterise surface exposures of sediments of the Nafun Group in the Huqf Supergroup (a major hydrocarbon source and reservoir) and to define a time-frame for the deposition of these commercially important sediments using bio-, chrono- and chemostratigraphic techniques. The Huqf Supergroup comprises the Abu Mahara, the Nafun and the Ara groups. A review of the sometimes confusing Huqf Supergroup nomenclature has been undertaken and a revision is recommended for further use based on the tectono-stratigraphic evolution of the formations and new data acquired during the course of the present study. The Nafun Group (unrevised), which provides the main focus of this thesis, is exposed in east-central Oman and in the Oman Mountains of north Oman, where detailed stratigraphical logging was undertaken. This was followed by petrographic work and geochemical studies to help elucidate the depositional environments.

Despite considerable effort, biostratigraphic controls on the time frame have not been enhanced by this study, except for rare samples of questionable *Nimbia occlusa* discovered at the base of the Shuram Formation in the Mukhaibah dome area and in the Middle Shuram Formation in Wadi Aswad area. There was considerable success, however, in the discovery of ash beds suitable for dating by U-Pb zircon methods. Reconnaissance logging was undertaken and ash bands were identified within a diamictite unit in the lower Ghadir Manqil Formation and the volcaniclastic Fara Formation of the Oman Mountains. These have yielded an age of 723+10/-16 Ma for the lower Ghadir Manqil Formation and an age of 544±3.3 Ma for the middle of the Fara Formation. These dates place the Huqf Supergroup firmly within the Neoproterozoic to Precambrian-Cambrian boundary interval. These new dates suggest that two glacial units within the Ghadir Manqil Formation in the Oman Mountains could be equivalent to the Sturtian and Marinoan glaciations. The upper, possibly Marinoan glacial

deposits are overlain by a dolostone unit *c.* 5m thick that is considered similar to the 'cap carbonates' described from above other Marinoan glaciations world-wide. This carbonate unit, which can be traced laterally across Oman, is herein identified as the 'Hadash Formation' as it is very well exposed near the village of Hadash in the Oman Mountains.

The Hadash Formation is overlain by red and green siltstones of the Masirah Bay Formation which contain trough cross-stratified sandstones in the Huqf area and are interpreted as shallow-marine deposits. The Masirah Bay Formation has been previously included in the Abu Mahara Group (Bell 1993; Rabu *et al.* 1986) but, in the revision of the present study, is transferred to the Nafun Group.

A detailed study was carried out on the lithofacies of the Khufai, Shuram and Buah formations in the Huqf area and the Oman Mountains. Microfacies analysis was also carried out to elucidate the depositional and diagenetic environments. In Chapter 3, the Khufai Formation facies have been grouped into facies associations A, B, C, D and E. The Huqf area facies indicate upward shoaling from outer ramp deposits in Association A, through grainstones (B), to intertidal cycles in Association C, whereas Association E represents intertidal and shoal deposition. In the Oman Mountains, the formation is very much thinner and formed of fetid, muddy limestones suggestive of deeper-water, more distal facies. Different stromatolite morphologies are described and identified where possible. It is concluded that the Khufai Formation formed on a carbonate ramp, with more proximal deposition in the Huqf area and deeper waters in the north and west, so that outer-ramp deposition is found in the Oman Mountains.

In Chapter 4, the Shuram formation is divided into lower, middle and upper members on the basis of sedimentary structures and carbonate facies upwards. The base of the Shuram Formation comprises deep-water sandstone with rafted limestone clasts and limestones in several areas in the Oman Mountains whereas, in the Huqf area, the basal sediments comprise shallow-water flat-pebble conglomerates and siltstones. The lower Shuram Formation sediments tend to be very homogenous throughout Oman, comprising planar-bedded red and green siltstones and mudstones which are heavily cleaved in the Oman Mountains. Relatively quiet deposition at the base of the Shuram Formation gives way to storm deposits within the middle member which is marked by an increase in evidence for current activity, with ubiquitous swaley-cross-stratification and dewatering structures. Within the middle member, there is an increase in the number and thickness of carbonate interbeds. These storm deposits continue into the upper member with the progradation of ooid and peloidal shoals forming

siliciclastic-carbonate cycles, each *c.* 3 to 12m thick. These comprise red and green siltstone overlain by silty pelsparite with variable occurrences of oosparite, followed by flat-pebble conglomerate at the top. The upper Shuram Formation grades-upward into the succeeding Buah Formation. Humid tropical weathering is suggested to have provided the source for extensive red siltstone and mudstones.

In Chapter 5, the Buah Formation is divided into a lower member and an upper member, with facies grouped into five associations: A, B, C, D and E. Associations A to D represent proximal shelf/platform deposition while E is composed of facies that formed in an outer platform-edge to slope setting. Association A grades up from the underlying Shuram Formation and is formed of crinkly laminites, with edgewise flake-breccias forming a lithostratigraphic marker traceable from the Huqf area to the Oman Mountains. These are overlain by compound stromatolites of Association B which, in turn, are succeeded by stromatolites interbedded with cross-stratified grainstones. The upper Buah Formation consists of peritidal facies of Association C that are interbedded with, and grade-upward into, sabhka facies (D). The complete upper member of the Buah Formation was only observed in the Mukhaibah dome area. Thus the Buah Formation in the Huqf area and in Wadi Bani Kharus of the Oman Mountains appears to represent a general upward shoaling from subtidal crinkly laminites through shoal deposits to peritidal and sabhka deposits. Facies of Association E occur further west in Wadi Bani Awf , where they indicate slope deposition with slump structures, auto-brecciation and resedimented slope breccias. Thus, the Buah Formation was deposited on a shallow platform that extended across the Huqf area and into Wadi Bani Kharus of the Oman Mountains. The platform edge to slope lies between Wadi Bani Kharus and Wadi Bani Awf. The Buah Formation is erosively overlain by the Thumaylah Formation of the Cambrian Haima Group in the Huqf area. In Wadi Bani Kharus it is unconformably overlain by the Permian Khuff Formation whereas in Wadi Bani Awf it is conformably overlain by the Fara Formation of Precambrian-Cambrian boundary age.

In Chapter 6, the chemostratigraphy of the Nafun Group is analysed. After detailed petrographic and cathodoluminescence analyses, 316 samples showing good textural preservation and lack of alteration were selected for stable isotope stratigraphy. 48 of these samples, representing different facies, were chosen for trace-elemental analysis of the carbonate fraction. These data have been used to elucidate the role of diagenetic overprinting. Elemental cross-plots, component analyses and $\delta^{13}C$ v $\delta^{18}O$ covariance plots are used to define diagenetic trends and, as far as possible, to backtrack to the primary $\delta^{13}C$ signal. The $\delta^{13}C$ values for the Khufai Formation are very heavy, reaching up to 6‰ in the

Huqf area and up to 8‰ in the Oman Mountains. The Shuram Formation records a fall to very light $\delta^{13}C$ signatures, with values still reaching -5‰ after correction for diagenesis. These remarkably negative values rise gradually into the lower Buah Formation. The middle Buah Formation sees the return to lighter $\delta^{13}C$ values of around 1‰ in both the Huqf area and the Oman Mountains. These data are discussed in terms of lithofacies, water depth and regional variations. This dynamic $\delta^{13}C$ signature through the Nafun Group is typical of the Late Neoproterozoic, and possible forcing mechanisms include both climate change and palaeogeography.

In Chapter 7, a synthesis of the research includes a suggested revised chronostratigraphy for the Nafun Group based on the U-Pb zircon dates. The new lithostratigraphic information and the carbon isotope-stratigraphy are integrated with subsurface gamma-ray data to allow a broad sequence-stratigraphic interpretation of the succession. Here, it is suggested that the Hadash Formation represents the transgressive with the *mfs* within the lower Masirah Bay Formation while the Khufai Formation represents the highstand deposition. A second cycle begins near the top of the Khufai Formation with a *mfs* in the lower member of the Shuram Formation. The middle and upper Shuram Formation represents the early highstand whereas the Buah Formation represents latest highstand to lowstand deposition. It is clear from this that there was a close linkage between mechanisms controlling the $\delta^{13}C$ curve and sequence stratigraphic processes.

The palaeo-environmental significance of the lithologies and the carbon-isotope signature is then considered. The evidence clearly suggests a change from arid climatic conditions within the Khufai Formation to humid and stormy conditions during the Shuram Formation, leading back to arid conditions again within the Buah Formation and the Ara Group. These were, perhaps, minor fluctuations compared with those of to the preceding glacial events of the Abu Mahara Group and the very extensive evaporite deposits of the succeeding Ara Group. Taken together, these dramatic climatic changes may, in part, be explained by feedbacks in the carbon cycle, perhaps combined with continental drift across equatorial latitudes at this time. Further work is required to establish the mechanism that was driving these major changes in climate and the carbon cycle in the lead-up to the 'Cambrian explosion'.

Acknowledgements

I would like to thank my supervisors, Philip Allen and Martin Brasier, for their advice, support and their entertaining discussions by the campfire (often inspired by my bean chilli). PDO are thanked for their generous funding of this project. Salim Al Maskery from PDO showed us how to live safely in the desert while providing feasts for us every evening. Charlotte Schreiber, John Grotzinger and Albert Matter are thanked for their very useful discussions on the outcrops. I also enjoyed many lively discussions on Precambrian geology and geochemistry with John Lindsay, Chris Nicholas, Graham Shields, Dave Wright and Maria Mange. I would like to thank my undergraduate supervisors Ken Jones and Alastair Ruffel for their support and encouragement throughout my career so far.

Many technical staff in the department have helped me and thanks are due to: Owen Green, Phil and Jeremy, Steve Baker, Richard McAvoy, Steve Wyatt and Steve Usher. Diana Relton, John O'Sullivan, Carol Coggins and Barbara did an excellent job of helping me sort out my very complicated field trips. I would like to thank Julie Cartlidge, Richard Corfield, Roy Goodwin and Steve Wyatt for smoothing my way through the age lab.

Fiona and Margaret, my first office mates, are thanked for their patience with my impatience of computers. My palaeolab mates are thanked for sharing the dungeon with me and making it a very bright place to spend many hours, Helen, Liz and Louise and of late Chris, Sam and David.

My train of field assistants deserve my gratitude for sharing many intrepid experiences with me in the desert. Thanks to Judith, Jason, Dave, Nathan and Liz for sharing my bean chilli without complaint.

My pals in Oxford are thanked for many cheerful evenings. Debbie for her culinary delights, Jacky, Fiona and Joël for many trips to the theatre, movies and of course St. Cross bar. Special thanks to Jake for proof-reading my thesis and numerous discussions over the merits of travel and good wine. This thesis is dedicated to my Mum and my very large and wonderful family.

Chapter One - Introduction

1.1 INTRODUCTION

1.2 REGIONAL SETTING

1.3 TECTONO-STRATIGRAPHIC HISTORY

1.4 HUQF SUPERGROUP NOMENCLATURE

1.5 HUQF STRATIGRAPHY AND FACIES ASSOCIATIONS

1.5 PROJECT DEVELOPMENT

1.1 INTRODUCTION

The impetus for this project results from the knowledge that the Huqf Supergroup sediments are components in a proven hydrocarbon play (Lake 1996; Nederlof & al Ruwehy 1996). Huqf source sediments are deeply buried beneath the Oman salt basins and thus lie beyond the resolution of seismic and core analysis. Petroleum Development Oman, which has the Omani Government as a majority shareholder together with its shareholder the Shell Oil Company, have funded this project with a view to gaining a better understanding of the surface exposures of the Huqf Supergroup. The chief focus of the project was to characterise the exposed sediments of the Huqf Supergroup and to define a time frame for their deposition using bio-, chemo- and chronostratigraphic methods. A further goal has been the integration of these new data within a regional context, to help define basin and biosphere development at this time in Earth history.

1.2 REGIONAL SETTING

Rocks of the Huqf Supergroup crop out in two main areas: in the core of the Jebel Akhdar in the Oman Mountains and in an area of east-central Oman known as the Huqf-Haushi Uplift (Figure 1.1). Exposure also occurs in the Saih Hatat region of the Eastern Oman Mountains.

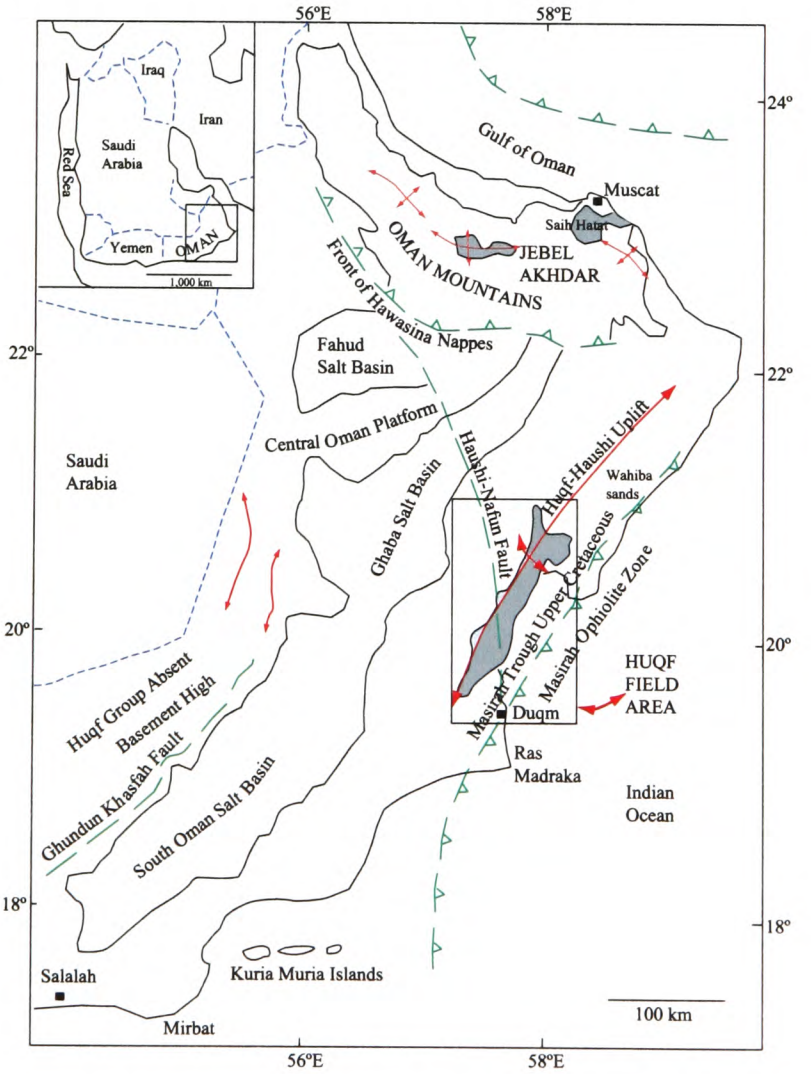


Figure 1.1 Simplified tectonic map of Oman showing distribution of the Huqf Supergroup outcrop in blue.

However, as these have undergone complex deformation (Glennie *et al.* 1977; Mann & Hanna 1990; Rabu 1993) they were not included in the present study.

The Huqf-Haushi Uplift (Figure 1.1), is an inlier of Neoproterozoic strata which extends for *c.* 180km north-northeastwards of Duqm before disappearing under the Wahiba Sands in the northeast. Its maximum outcrop width is 40km. The inlier is surrounded by onlapping Cambrian to Cretaceous sequences that rest unconformably on the eroded Neoproterozoic-Cambrian strata. To the west is the subsurface Ghaba Salt Basin, whose subsidence was coeval with the intermittent uplift of the Neoproterozoic-Cambrian strata in the Huqf-Haushi Uplift (Ries & Shackleton 1990). These surface and subsurface sediments are relatively undeformed.

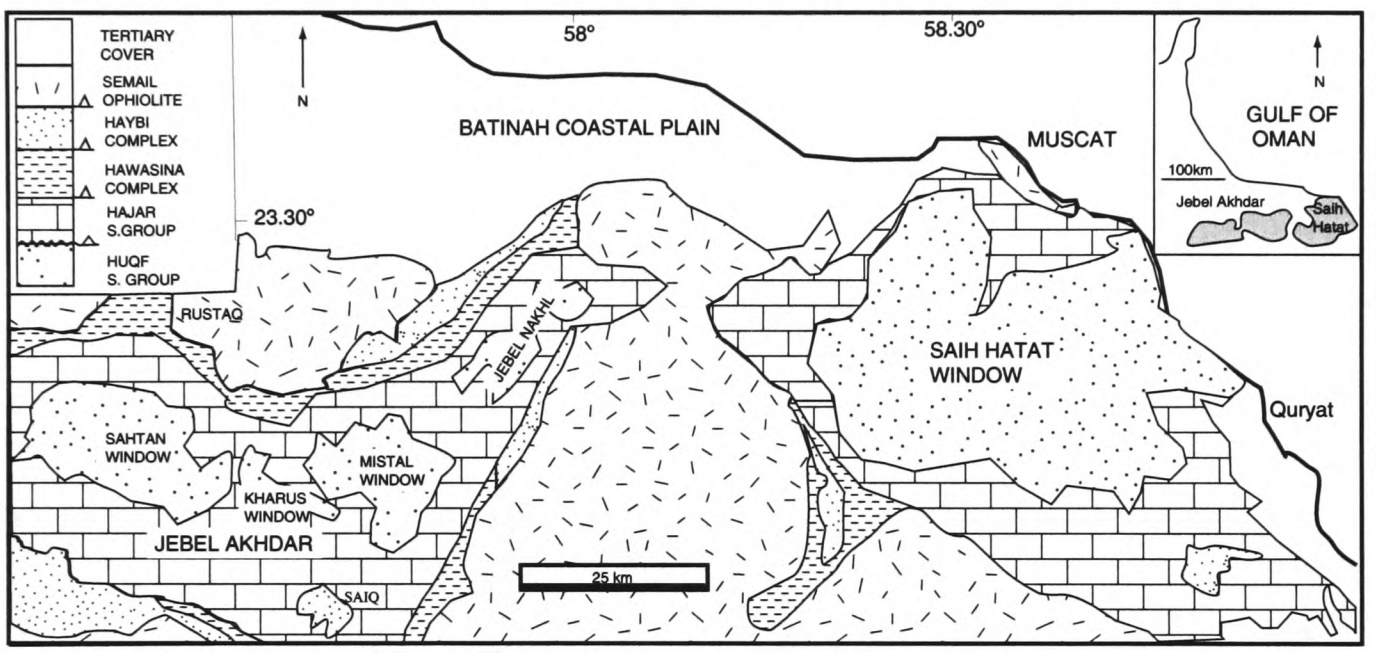


Figure 1.2 Simplified geological map of the central Oman Mountains showing the distribution of the Huqf Supergroup rocks (after Glennie *et al.* 1974).

The Oman Mountains form an arcuate belt parallel to the Gulf of Oman that is some 30-130km wide and extends 700km in a NW-SE direction. The Neoproterozoic-Cambrian strata are exposed in a series of erosional windows beneath middle-Permian platform carbonates of the Hajar Supergroup (Figure 1.2). From west to east these are: 1) the Sahtan, Kharus, Mistal, and Saiq Windows at the core of the Jebel Akhdar; 2) Jebel Nakhl; and 3) Saih Hatat in the east. The pre-Permian rocks of the central Oman Mountains have been affected by at least two major tectonic events: a late Palaeozoic deformation, and a late Cretaceous thrusting which emplaced both the Semail ophiolite and the Tethyan thrust sheets onto the Arabian continental margin (Mann & Hanna 1990). The deformation and metamorphism both increase in intensity towards the east and northeast of the Oman Mountains. Only the less deformed rocks of the Sahtan, Kharus and Mistal Windows have been included in the present study.

1.3 TECTONO-STRATIGRAPHIC HISTORY

The Sultanate of Oman is situated on the south-eastern margin of the Arabian Plate (Figure 1.3). It is bounded to the south by the Gulf of Aden Spreading Zone, to the east by the Masirah Transform Fault and the Owen Fracture Zone and to the north by the Zagros-Makram convergent plate margin which has resulted in the formation of the Oman Mountains.

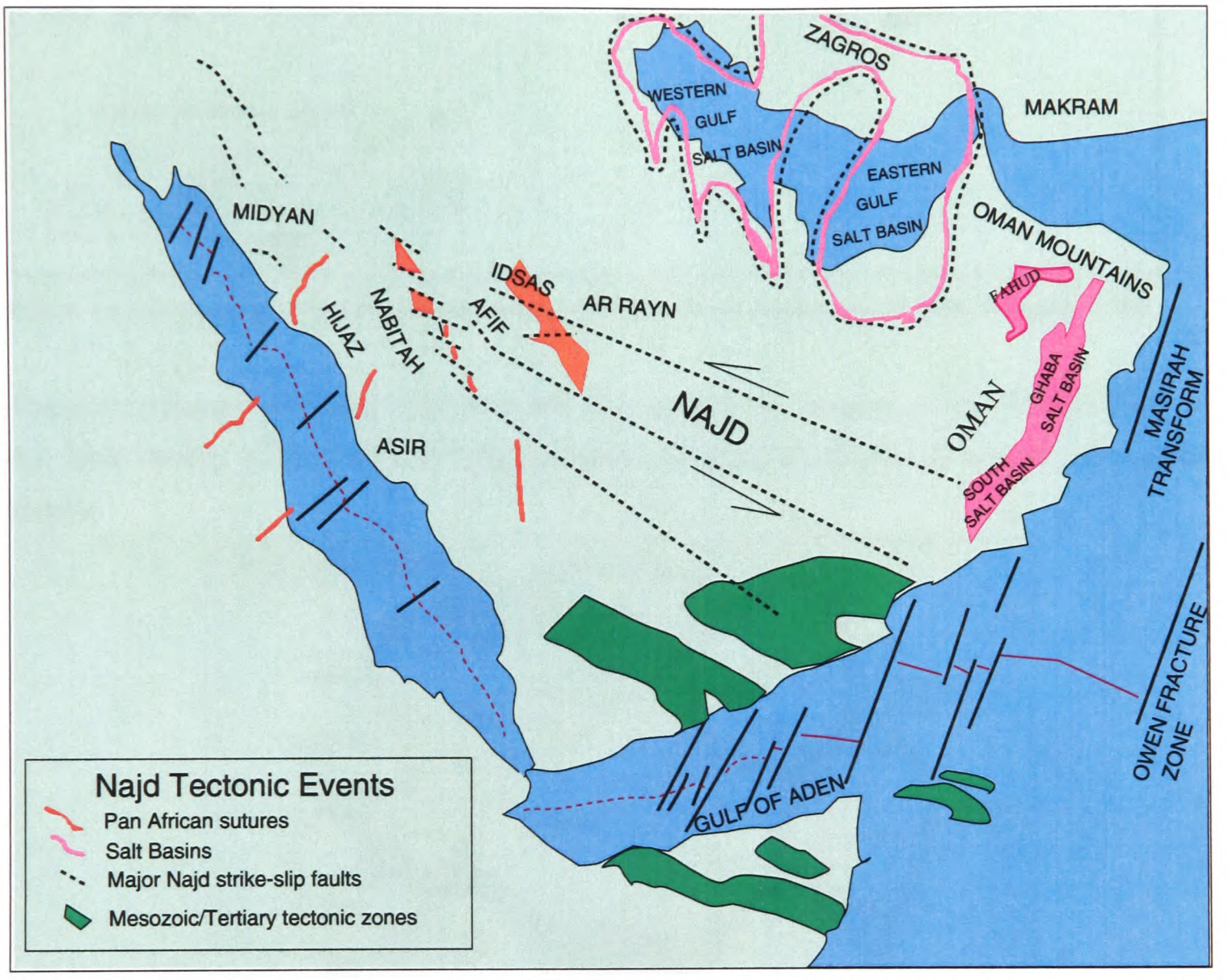


Figure 1.3 The Arabian Peninsula, with Precambrian terranes (Midyan, Hijaz, Asir, Nabitah, Afif and Ar Rayn) in the Arabian Shield area with the Neoproterozoic-Cambrian Najd sinistral strike-slip fault system. Microplate boundaries are based on Stoeser & Camp (1985); other data after Looseveld *et al.* (1996).

Stoeser & Camp (1985), Husseini (1989), Husseini & Husseini (1990) and Looseveld *et al.* (1996) have all provided similar tectonic models for the evolution of the Arabian and adjoining plates in the Neoproterozoic. This process began when the Nubian-Arabian shield was fused together with a complex of accretionary collisional tectonics which terminated with the formation of the Nabitah and Idsas thrust belts. This involved the initial formation of the western part of the Arabian shield by the fusion of three island-arc terranes: the Asir, Hijaz and Midyan (Figure 1.3). The Afif terrane was added along the Nabitah suture between

c. 680 and 640 Ma (Figures 1.3; 1.4). Finally, during the Idsas orogeny, the Ar Rayn terrane was sutured onto the Arabian shield around 640-620 Ma.

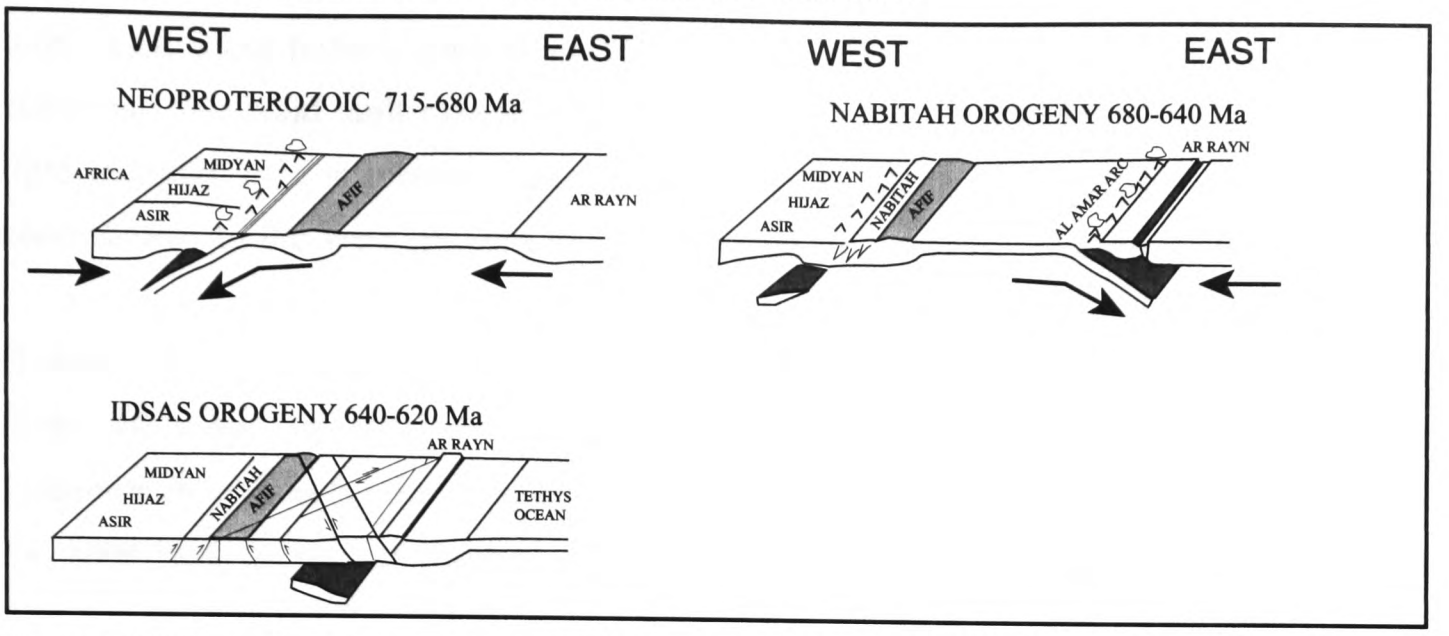


Figure 1.4 Schematic reconstruction of accretionary evolution of the Arabian Shield (after Husseini 1989).

These accretionary processes closed oceans and merged the terranes of the Middle East with the north-eastern African edge of Gondwanaland, forming an extensive area of mountainous stature.

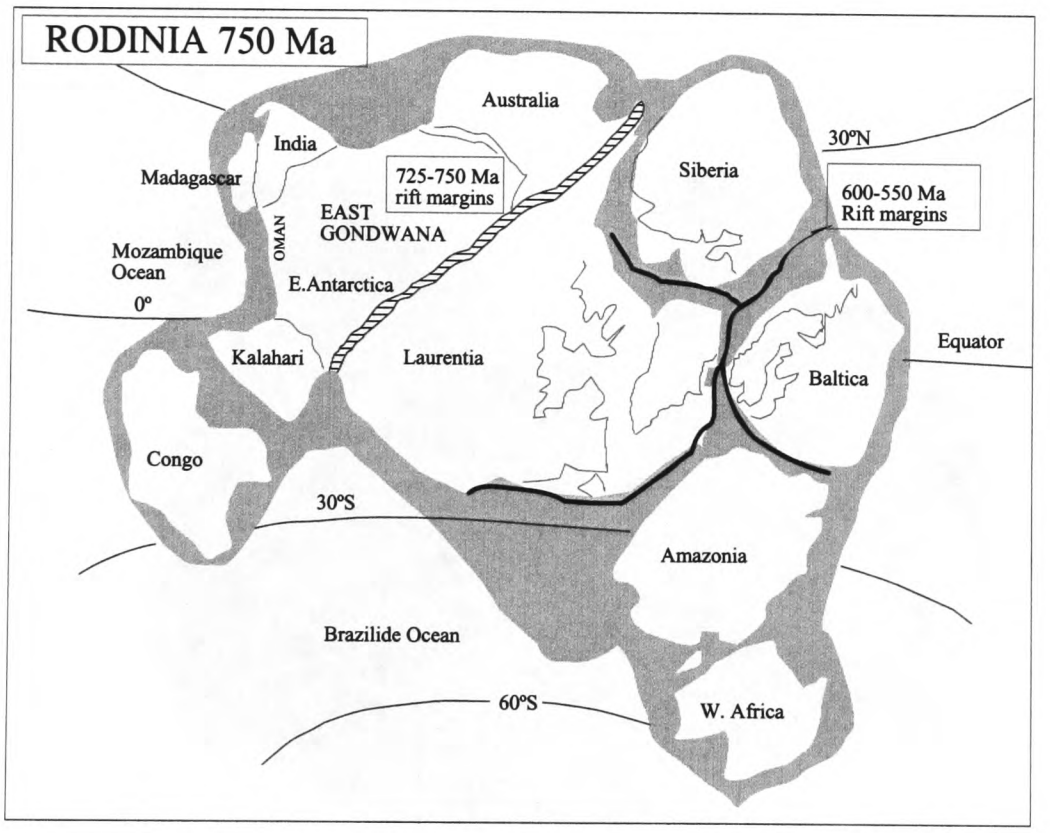


Figure 1.5 The Rodinia supercontinent at ~ 780 Ma after Torsvik *et al.* (1995) and Handke *et al.* (1999). Cross-hatched area between East Antarctica, Australia and Laurentia shows location of the proposed 750-725 Ma rift margins; heavy lines between Laurentia, Siberia, Baltica and Amazonia show location of proposed 600-550 Ma rift margins.

From 630 Ma to 550 Ma, further tectonic events included emplacement of peraluminous and peralkaline granites, folding and faulting accompanied by greenschist metamorphism and the

development of the Najd fault zone, a major sinistral strike-slip fault system with up to 300km displacement (Stoeser & Camp 1985; Husseini 1989). Stoeser & Camp (1985) interpreted these latter events to mark the final phase of continuous compression related to collision. The Najd fault system resulted from collision in which the Ar Rayn block was a rigid indenter of continental crust which impinged on the arc terranes to the west. This confinement to the west resulted in displacement to the north and northwest.

Husseini (1989) interpreted the Najd fault system as having formed during the transformation from collisional to extensional tectonics, accompanied also by alkali-rich granites and volcanics as well as by the development of salt-filled extensional basins. The final phase of the Najd fault motion is sinistral and the system consists of a series of braided *en-echelon* fractures with sinuous and branching geometry and a slight convergence to the north-west (Beydoun 1991). With completion of cratonisation by about 550Ma associated with the end of activity in the Najd sinistral system, epicontinental subsidence developed differentially and resulted in the formation of broad basins. This faulting led to the creation of a number of rift-related basins and crustal sags on conjugate and other trends. Greenwood *et al.* (1980) suggested the 'Infracambrian salt basins' of Oman were possible examples of these structures.

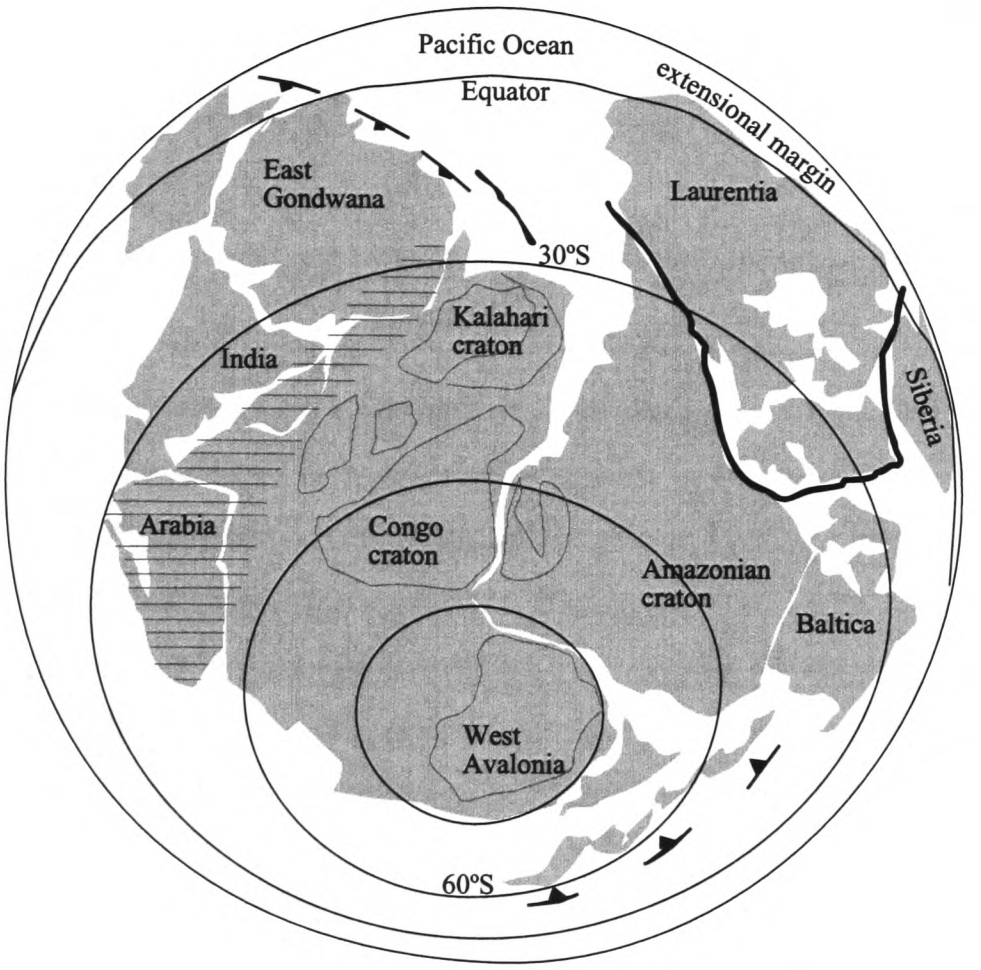


Figure 1.6 Late Neoproterozoic (545Ma) continental configuration of 'Pannotia' after Dalziel (1997).

Dalziel (1997) has recently attempted to reconstruct the final supercontinent of the Neoproterozoic, which he has called 'Pannotia', meaning 'all southern' (Figure 1.6). In his view, this involved the opening of the Pacific Ocean basin along with uplift and erosion of orogens within the newly assembled Gondwana portion of Pannotia. A collisional mountain range (striped ornament) extended for up to 7,500km from Arabia to the Pacific margin of Antarctica.

In the late Neoproterozoic, Arabia with Turkey, central and northwest Iran, Afghan, India and other plates appear collectively to have formed part of a long and wide 'northern' passive margin of Gondwana, bordering a Palaeo-Tethys ocean (Beydoun 1991; Figure 1.7; McKerrow *et al.* 1992.).

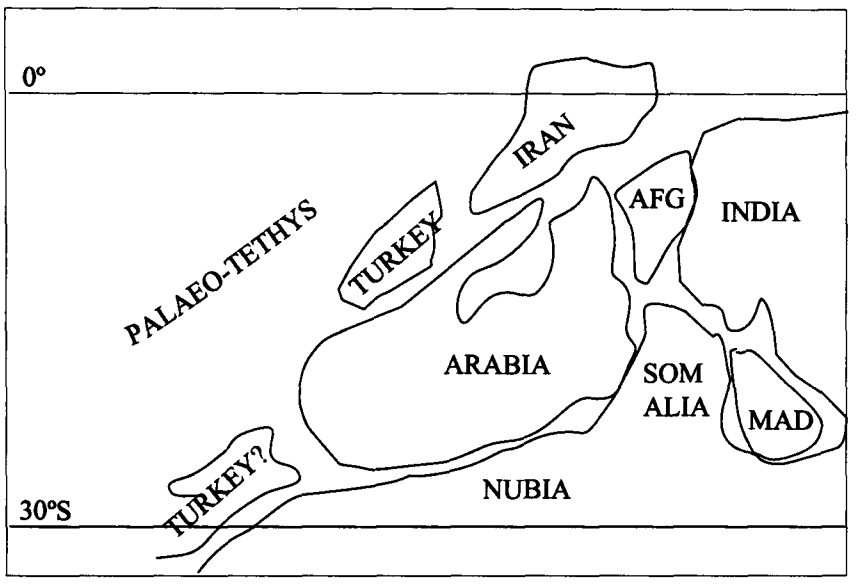


Figure 1.7 Neoproterozoic plate tectonic reconstruction of Arabia and adjoining terranes according to Beydoun (1991).

Much of this region was covered intermittently by shallow epeiric seas that bordered lowlands made up of portions of the shields, with the aerial extent of these seas changing in response to transgressions and regressions. According to Beydoun (1991), the orientation of the passive margin rotated between north-westerly facing in the latest Neoproterozoic with oscillations to a westerly setting in the Cambrian. The width of the epeiric shelf seas along this margin was at least 2,000km and may have reached 3,000km from the evidence of palaeogeography and stratigraphic correlation and facies patterns (Beydoun 1986, 1988).

1.3.1 Huqf Supergroup

In Oman, the crystalline basement rocks crop out in the south, along the coast at Mirbat (Figure 1.1) where they also form the Kuria Muria Islands. These rocks comprise

metamorphic and igneous basement intruded by dolerites, granodiorites and granites and are unconformably overlain by the diamictites thought to be of Huqf Supergroup age.

The lowest deposits of the Huqf Supergroup in the type area of the Huqf-Haushi Uplift were first described by Kassler (1965) who defined the lowest, Abu Mahara Formation on clastics in the Khufai dome area. Bell (1993) redefined the Abu Mahara Group on the basis of well logs and surface exposures and regional seismic lines. He separated the Group into two formations: the lower Ghadir Manqil Formation, succeeded by the Masirah Bay Formation.

Masirah Bay Formation:	Transition Member
	Clastic Member
	Basal Carbonate Member
Ghadir Manqil Formation:	Clastic Member
	Diamictite Member
	Volcanic Member

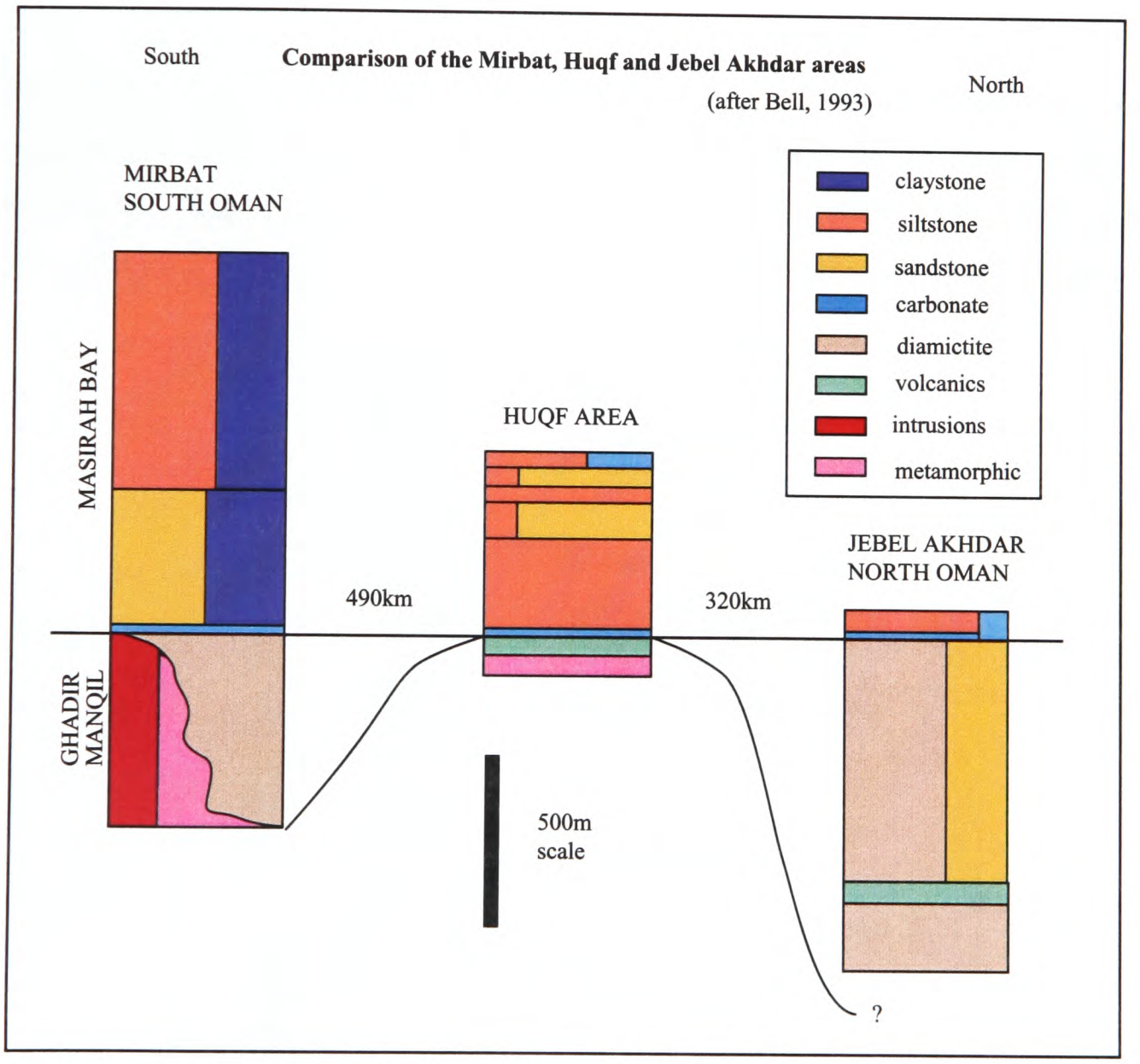


Figure 1.8 Comparison of Ghadir Manqil Formation lithologies from south to north Oman, based on Bell (1993).

The interpreted regional seismic line 920721C (Figure 2; Bell 1993) suggests that the great thickness variation of Abu Mahara sediments may have been deposited in a rifting basin. In

the Mirbat area, diamictites believed to belong to the Ghadir Manqil Formation range in thickness from 600m to zero metres over a distance of 8km. This drastic lateral variation could represent either infill of a syn-sedimentary basin or half-graben or it could represent infill of an existing topography. The abundance of volcaniclastic sediments within the Ghadir Manqil Formation in north Oman would support the former interpretation. The interbedding of diamictites and volcanics in Wadi Mistal in the Oman Mountains shows that active volcanism and glacial conditions were partly contemporaneous.

Termination of the Ghadir Manqil glacial episode resulted in a sea-level rise, which covered areas like the Huqf area where no glacial sediments had been deposited (Kapellos *et al.* 1992). Although the Basal Carbonate Member is only 20m it is of great regional extent (Figure 1.8) and since it is commonly overlain by black shales (Plate 1.1f), it has been considered as part of the major flooding event that resulted from deglaciation (Bell 1993).

In central Oman, the basement crops out in the northern part of the Huqf area. Here, foliated biotite granodiorite is exposed *c.*15km north-west of the village of Al Jobah (Plate 1.1a). This is overlain by green rhyolites and a volcaniclastic breccia (Plate 1.1b) which is capped by a thin silcrete horizon and overlain by finely laminated pale grey dolostones (Figure 1.9).

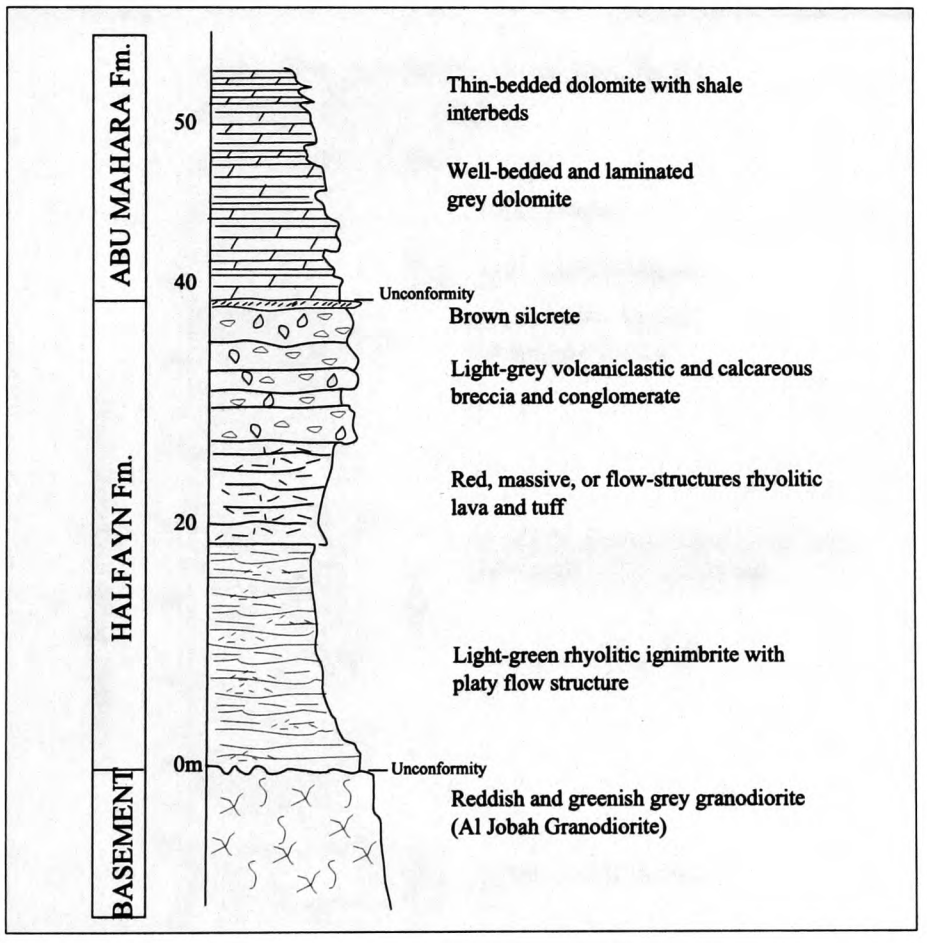


Figure 1.9 Al Jobah Granodiorite (basement) overlain by the Halfayn Formation and Abu Mahara Formation according to Dubreuilh *et al.* (1992).

The volcaniclastic sediments have been termed the Halfayn Formation (Dubreuilh *et al.* 1992) who also interpreted the overlying dolostones as a unit at the base of the Abu Mahara Formation, implying a lateral equivalent of the basal carbonate member of Bell (1993). Gorin *et al.* (1982) in their study of the Huqf Supergroup, examined the Abu Mahara Formation from borehole data (Core 17, Khufai dome) which bottomed in a volcanic rock of trachytic texture. Unfortunately, there is not enough information to correlate the Core 17 volcanics with the Halfayn Formation.

The crystalline basement is not exposed in the Oman Mountains. The Ghadir Manqil equivalents here has been called the Mistal Formation (Figure 1.10), described by Kapp and Llewellyn (1965), Glennie *et al.* (1974), Beurrier *et al.* (1986) and Rabu *et al.* (1986). The Mistal Formation, which represents the oldest exposed sedimentary unit in the Oman Mountains, has been divided into four members by Rabu *et al.* (1986; Figure 1.10). The lowermost Ghubrah Member is a diamictite; the Saqla Member mainly comprises pillow basalts and the thick Fiq Member is composed of extensive lithic wackes and pyritic shales with dropstones and conglomerates. The uppermost Amq Member comprises a basal carbonate and overlying siltstones that are clearly the equivalent of the Masirah Bay Formation of Bell (1993).

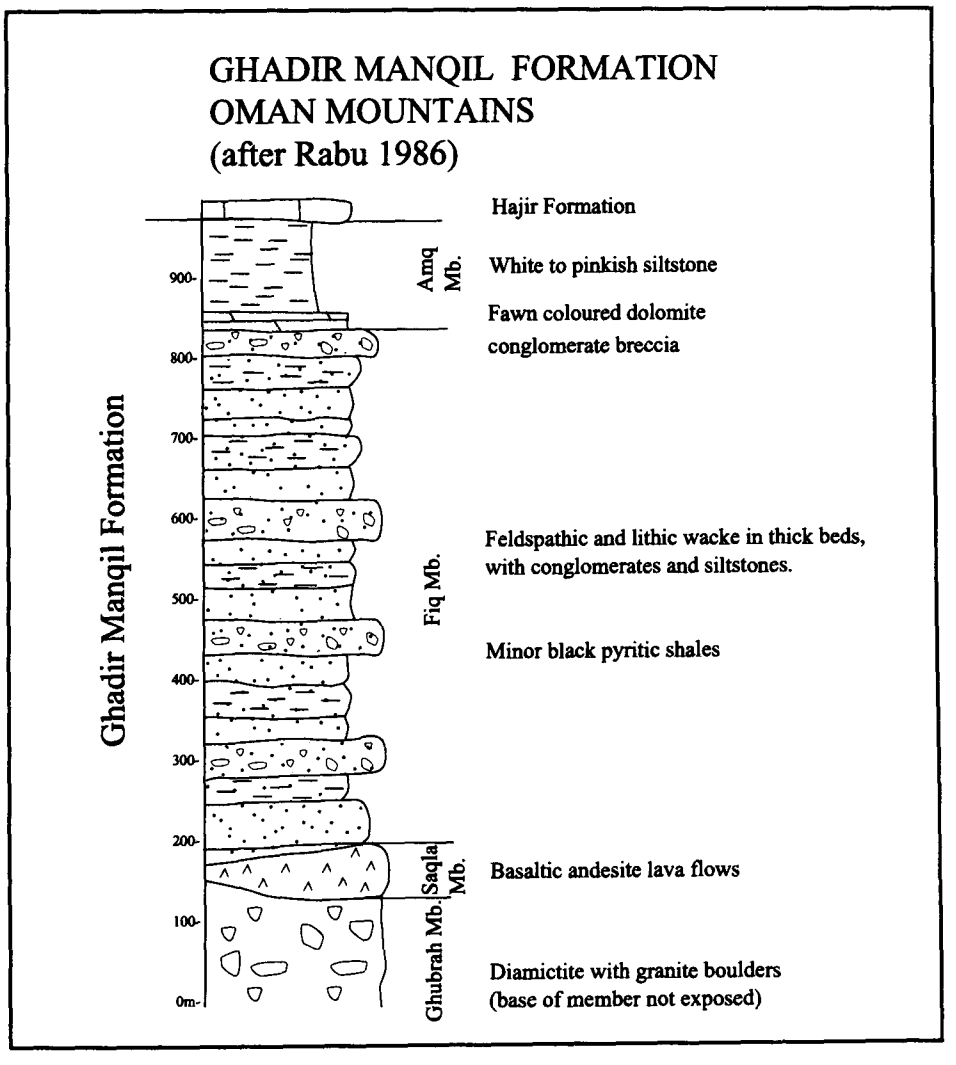


Figure 1.10 Stratigraphic log of the Ghadir Manqil (Mistal) Formation, after Rabu (1986).

After deposition of the regionally extensive Basal Carbonate Member there is an absence of rapid changes in facies or thickness, suggesting tectonic quiescence. This implies that subsidence continued by thermal sag of the basin as opposed to active extension along basin bounding faults (Bell 1993). During this thermal sag period, the sediments of the Nafun Group were deposited.

1.4 HUQF SUPERGROUP NOMENCLATURE

Carter (1852) and Lees (1928) published early reports on the 'argillaceous beds of Dhofar' and 'Mirbat sandstone' that overlie the crystalline basement in southern Oman. The outcrops of the Huqf Supergroup were first studied by Iraq Petroleum Co. geologists (Gorin *et al.* 1982) while Morton (1959) first mentioned a fourfold subdivision. Beydoun (1960) used the terminology of First and Second Clastic Groups (Abu Mahara and Shuram Formations) and First and Second Dolomite Groups (Khufai and Buah Formations). The PDO geologist, P Kassler defined the Abu Mahara, Khufai, Shuram and Buah formations of the Huqf area while Tschopp (1967) first correlated these formations with similar sequences in Jebel Akhdar, defining the Mistal, Hajir, Mi'aidin, and Kharus Formations. Looseveld *et al.* (1996) were the first to present a new stratigraphy which refers to the Huqf unit as a supergroup.

These previous researchers have, along with PDO geologists, used different nomenclatures and definitions for the formations of the Huqf Supergroup (Figure 1.11). To avoid confusion, a uniformity of terms will be used in the present study by applying widely used names to all coeval formations.

The Ghadir Manqil Formation (Mistal Formation of some previous authors) overlies basement, infills basin topography and is capped by a thin carbonate unit which can be traced throughout Oman on seismic lines (Bell 1993). This 'cap carbonate' is best observed near Hadash village in Wadi Mistal 577259(E) UTM 2257962(N) and is, therefore, referred to herein as the Hadash Formation (Plates 1.1c&d) being a mapable unit of regional extent. Therefore, the Ghadir Manqil Formation, the Hadash Formation and the Masirah Bay Formation make up the Abu Mahara Group (Rabu 1988, 1993; Bell 1993) (Figure 1.11). While the Hadash Formation was only observed in the Oman Mountains, the Masirah Bay Formation and the overlying Nafun Group are laterally extensive in east-central Oman (Huqf area) and the Oman Mountains.

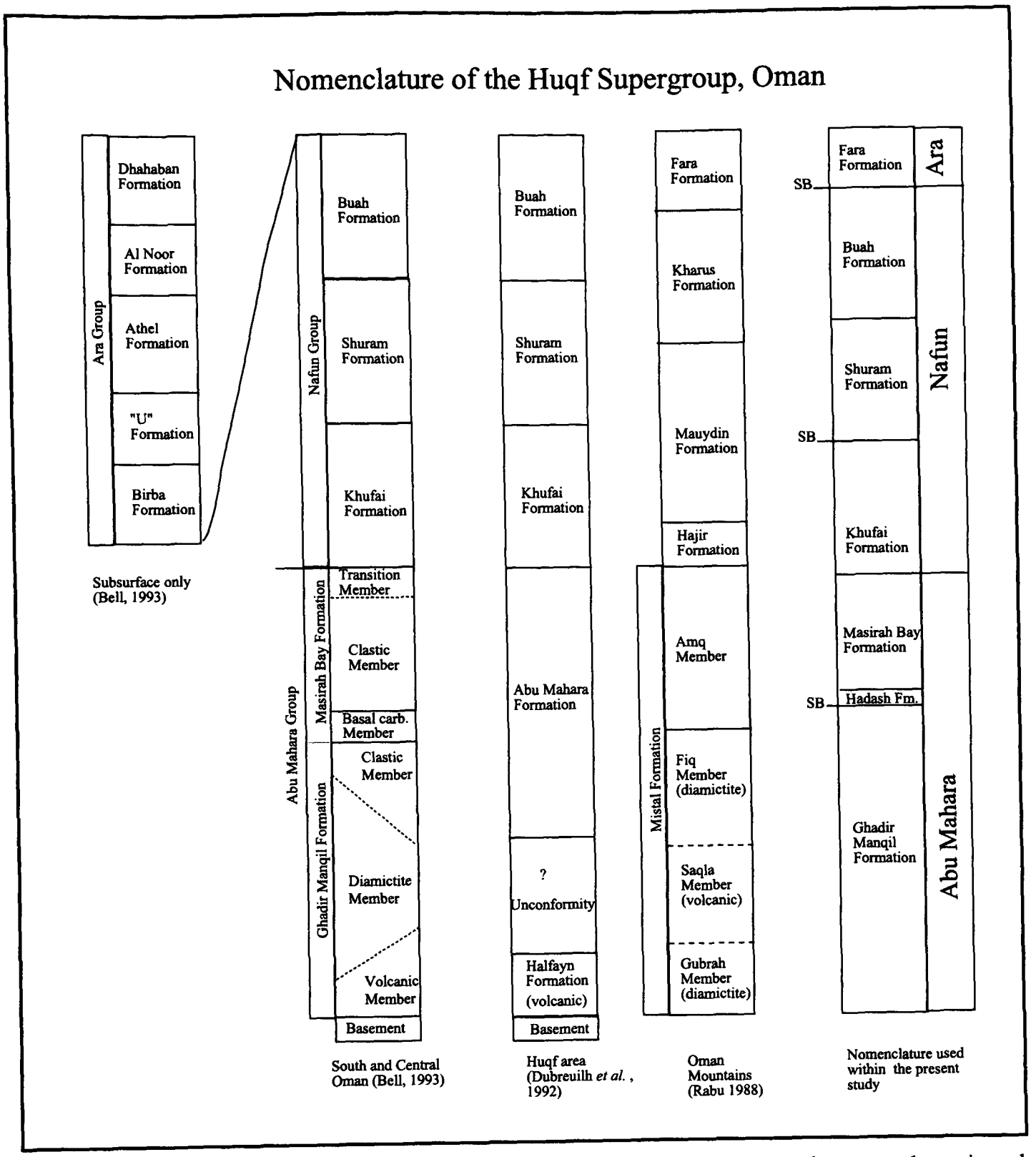


Figure 1.11 Huqf Supergroup nomenclature used to-date and within the present study, logs are schematic and not to scale.

The Nafun Group is formed of the dolomitic Khufai Formation, and the siliciclastic/carbonate cycle that comprises the Shuram and Buah formations. These three formations were deposited in a layercake depositional pattern (Bell 1993) and are the chief subject of this thesis (Figure 1.11). A reconnaissance study of the overlying Fara Formation was undertaken with a view to the identification of ash beds and the procurement of samples suitable for absolute age dating. As the uppermost formation of the Huqf Supergroup in outcrop, it is considered coeval with part of the Ara Group of the subsurface. The base of the Fara

Formation comprises organic-rich carbonates and cherts but becomes volcaniclastic upwards. The Ara Group of the subsurface is formed of carbonates, shales and evaporites.

1.5 HUQF STRATIGRAPHY AND FACIES ASSOCIATIONS

The majority of published research on the geology of the Huqf Supergroup has been concerned with outcrops, structural geology and tectonics of the Oman Mountains (e.g. Kapp & Llewellyn 1965; Glennie *et al.* 1974; Rabu *et al.* 1986; Beurrier *et al.* 1986). The sedimentology and structure of the Huqf Supergroup in east-central Oman (Huqf area) has also been studied (e.g. Kassler 1965; Gorin *et al.* 1982; Gass *et al.* 1990; Ries & Shackelton 1990; Wright *et al.* 1990). Many recent in-house PDO reports have been written on the stratigraphy and tectonics of the Huqf Supergroup (e.g. Kapellos *et al.* 1992; Bell 1993; Looseveld *et al.* 1995; Pilcher & Buckley 1995; Mc Carron 1996).

This present study is concerned with regional correlation of the Huqf formations from the Huqf area to the Oman Mountains. To this end, the formations have been subdivided into facies and facies associations based on similar lithological characteristics and environmental interpretation.

	Huqf (Proximal)	**Wadi Bani Awf, Oman Mountains (Distal)**
Upper Buah Formation		Association E Slope and distal deposits
Association D	Sabhka	E7 Platform/slope grainstones
Association C	Peritidal stromatolites and mudstones	E6 and E5 Slope deposits
Lower Buah Formation		E4 and E3 Distal deposits
Association B	Platform stromatolites and grainstones	E2 and E1 Subtidal laminites
Association A	Subtidal crinkly laminites	
Upper Shuram Member		
Facies S4 and S3	Prograding platformal deposits	Prograding recrystallized limestones (S9)
Middle Shuram Member		
Facies S1 and S2	Stormy shoreface deposits	Crenulated siltstones with minor carbonates
Lower Shuram Member		
Facies S1 and S2	Distal fine-grained deposits	Conglomeratic sandstones and shales (S5,S6)
Khufai Formation		
Association E	Shoal grainstones	
Association D	Inner-ramp arenites	
Association C	Inner-ramp stromatolites	
Association B	Mid-ramp shoal grainstones	Outer-ramp fetid grainstones
Association A	Fetid laminites	Outer-ramp fetid laminites

Table 1.1 Khufai, Shuram and Buah Formation Facies Associations as defined in the present study.

Detailed descriptions of facies and associations are given in Chapters 3 (Khufai Formation), 4 (Shuram Formation) and 5 (Buah Formation).

1.6 PROJECT DEVELOPMENT

The initial remit of this project, the study all of the formations of the Huqf Supergroup, was attempted during the first field season (4.1.96-10.3.96) but was deemed too ambitious during the second season because of the vast scale and thickness of the exposures and the inhospitable terrain. The first field season in Oman involved a reconnaissance study of most of the exposure in the Huqf area and the Oman Mountains, and summary logs were made of the Nafun Group sediments. Samples were also collected for microfacies analysis. Prior to the second field season, a report for PDO was written on the lithofacies and microfacies of the Nafun Group.

The first part of the second field season (28.11.96-23.2.97) involved logging and sampling the Fara Formation for ash bands with a view to dating the section. A reconnaissance study of the Ghadir Manqil Formation was carried out in the Oman Mountains involving summary logs of specific sections along with a search for ash bands. During the second field season it was agreed to make only a reconnaissance study of the lowermost Ghadir Manqil and Masirah Bay formations and the uppermost Fara Formation in the Oman Mountains. The focus, therefore, switched to a more detailed field study and stable-isotope stratigraphy of the Nafun Group, (Khufai, Shuram and Buah formations) in both the Huqf area and the Oman Mountains.

The aim of the reconnaissance studies of the lowermost and uppermost formations was to identify ash beds which, hopefully, would yield absolute ages bracketing the time of Huqf Supergroup deposition. Fortunately, a zircon-bearing tuffaceous ash was discovered in the Ghadir Manqil Formation of Wadi Mistal, and a 20m-thick zircon-bearing ignimbritic unit was identified in the Fara Formation of Wadi Bani Awf, both in the Oman Mountains. These sections were subsequently logged and sampled for geochronology (see Chapter 2).

A more detailed study of the Nafun Group was undertaken with the aim of characterising the sediments by means of carefully located and logged sections from selected traverses, analysing their environments of deposition and their lateral variation, leading to the development of depositional models. These sediments were also sampled for chemostratigraphy, and these new data can be integrated with global reference sections to help further definition of the age of the sediments. A concerted effort was also made to improve the impoverished biostratigraphic control.

During the third field season (2.1.98-18.2.98) a two-week workshop was held on the Huqf Supergroup in Muscat followed by field excursions to the Oman Mountains and the Huqf area

involving Shell personnel, geologists and academics. This provided an excellent forum for discussion of lithofacies, environments and basin dynamics. Field-work focused on lateral facies variations where facies were walked out laterally and special attention was given to formation boundaries in the search for evidence of significant breaks. More attention was given to stromatolite morphologies and their variation temporally and spatially. Specific horizons were sampled or re-sampled for geochemistry and for palynology. Jonathan Leather began his PhD research on the Ghadir Manqil, Hadash and Masirah Bay formations during this field season

A fourth trip to Oman (14.2.99-24.2.99) involved the introduction of two post-doctoral workers, Chris Nicholas and Andrea Cozzi, to the Huqf Supergroup sediments and their exposures across Oman. Specific problems, such as the lateral variation of the Upper Buah Formation, became the focus for further research at this time.



Plate 1.1a Exposure of granodioritic basement near Al Jobah in the north of the Huqf area. Hammer for scale



Plate 1.1b Exposure of granodioritic basement on the horizon with rhyolitic volcanics (green) and volcaniclastic breccias (foreground) of the Halfayn Fm.



Plate 1.1c Diamictites of the Ghadir Manqil Fm. overlain by a brown weathering 'cap dolostone', recessive Masirah Bay Fm is unconformably overlain by the Permian. Wadi Mistal in the Oman Mountains.

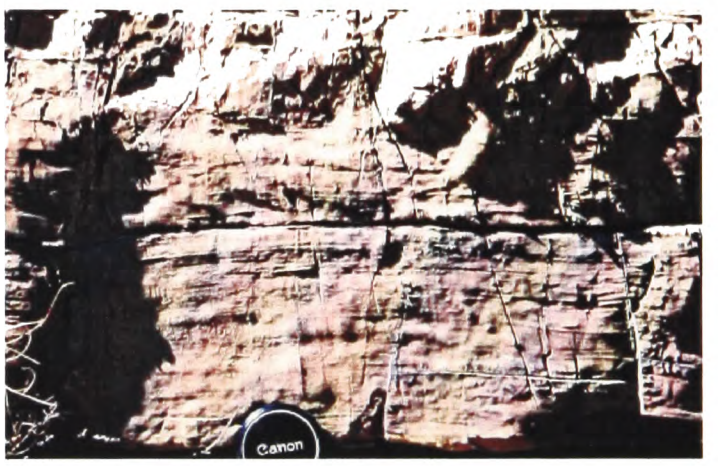


Plate 1.1d Planar laminations with minor scours within the 'cap dolostone', Hadash Fromation, of the Abu Mahara Group. Hadash village in Wadi Mistal. Lens cap 50mm.



Plate 1.1e Masirah Bay Formation in the Khufai dome, Huqf area. Trough cross-bedded sandstones overlain by green and red siltstones; Khufai carbonates at the top of the ridge.

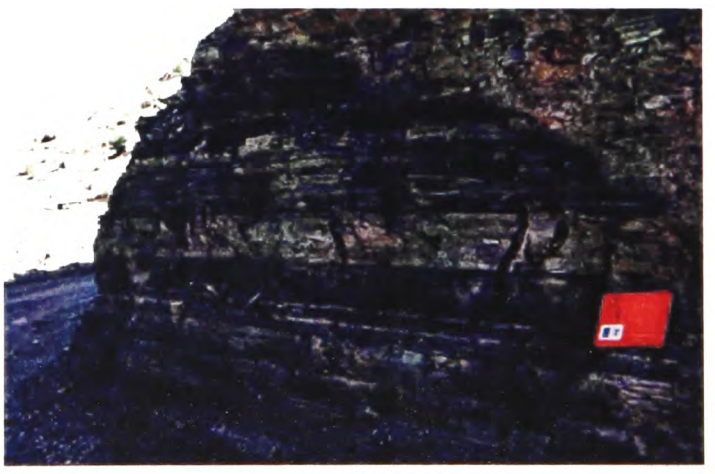


Plate 1.1f Masirah Bay Formation near Hadash in Wadi Mistal, dark organic-rich shale interbeds within siltstones. Notebook 225x176mm

Chapter Two - Chronostratigraphy

2.1 INTRODUCTION

2.2 BIOSTRATIGRAPHY

2.3 RADIOMETRIC DATES

2.4 NEW GHADIR MANQIL DATES

2.5 NEW FARA FORMATION DATES

2.6 SIGNIFICANCE OF NEW DATES

2.1 INTRODUCTION

An important aim of this project has been to determine the age of the Huqf Supergroup sediments. Bio-, chemo-, sequence and chronostratigraphic methods have been applied with a view to defining a reliable age. This chapter reviews previous biostratigraphic and chronostratigraphic work and outlines research undertaken in the present study, including new and significant U-Pb dates. Analyses and methods are given in the appendix.

The Neoproterozoic Era spans the interval between 1000 Ma and the base of the Cambrian System, which has been recently dated at *c.* 543 Ma (Bowring *et al.* 1993; Conway Morris 1993; Grotzinger *et al.* 1995). Figure 2.1 outlines the major events of the late Neoproterozoic that are pertinent to the present study.

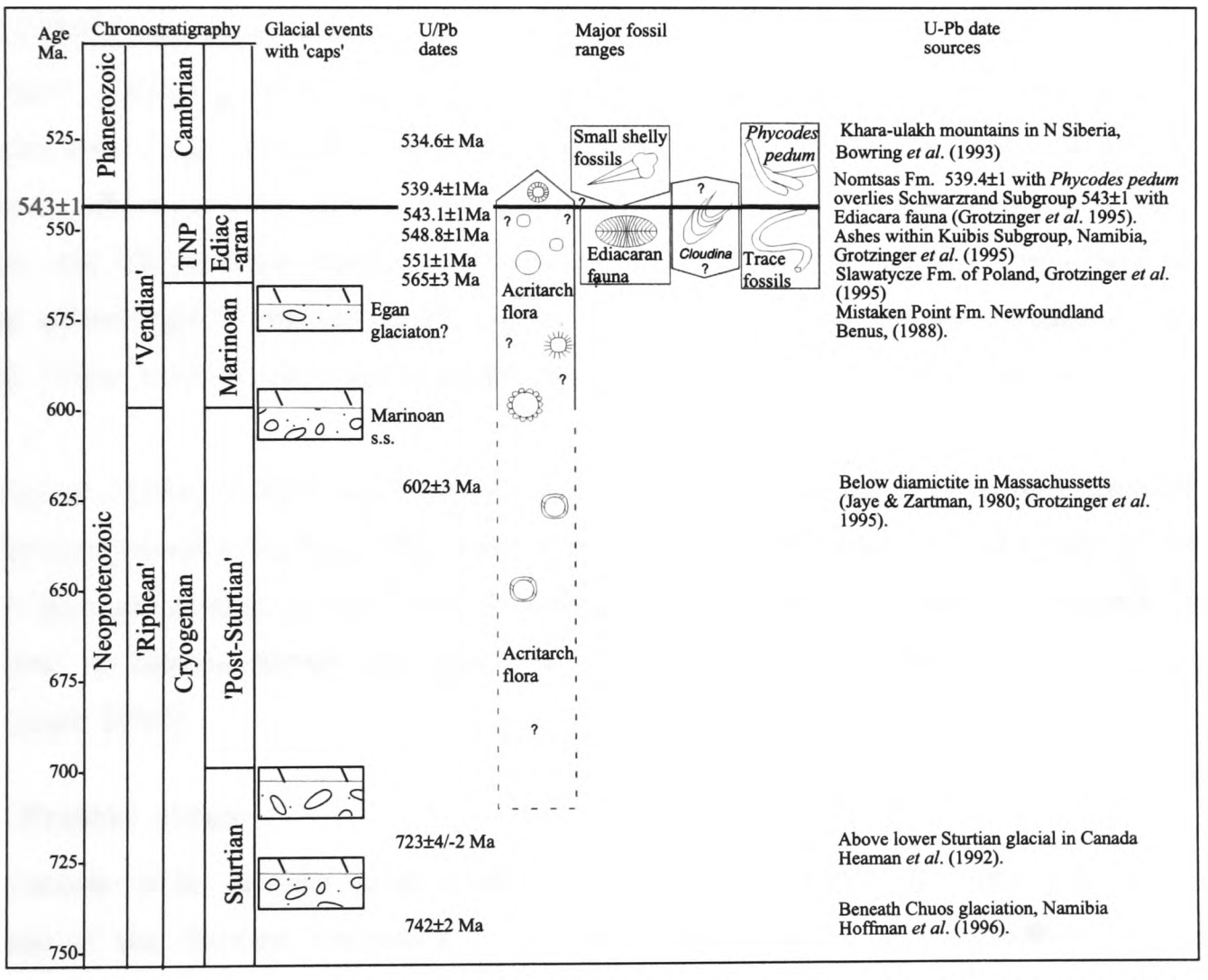


Figure 2.1 Chronostratigraphy of the terminal Neoproterozoic with major glacial events, present U/Pb dates and fossil ranges.

2.2 BIOSTRATIGRAPHY

The biostratigraphic control on the Huqf Supergroup is poor. One of the aims of this study was to try to improve this by examination of surface exposures for body or trace fossils.

2.2.1 Previous work

Mattes & Conway Morris (1990) have reported the presence of *Cloudina* cf. *hartmannae* (Plate 2.1b) from thrombolitic carbonates of Stringer 2 of the Ara Formation in borehole Birba North-1 where it is associated with the calcimicrobe *Angulocellularia,* known from the lower Cambrian of Siberia and Mongolia (Riding & Voronova 1982, 1984). Based on this association, Conway Morris *et al.* (1990) suggested that the Ara Group may be of Cambrian age. The credibility of this calcimicrobe for biostratigraphy was questioned by Grant (1990) who infers a late Neoproterozoic age for the Ara Group.

Knoll (1990) and Mattes & Conway Morris (1990) examined cores from the Suwaihat area that have yielded a very similar assemblages of acritarchs. Knoll (1990) reported an acritarch assemblage from the Ghadir Manqil Formation between the diamicite and the cap carbonate which they interpret as similar to late Riphean to Vendian forms from northern Europe and the Siberian platform. Mattes & Conway Morris (1990) discovered a very similar assemblage to that of Knoll (1990) yet they attribute the assemblage to the Ara Group. These workers have not reported any microflora from the Nafun Group.

Gorin *et al.* (1982) in their study of the Buah Formation identified columnar stromatolites and the calcimicrobe *Nubecularites antis* from the Khufai Formation. This latter species was said to be characteristic of the latest Neoproterozoic to earliest Cambrian Nemakit-Daldyn "horizon" in Siberia, though the utility of such forms for biostratigraphy is questionable (e.g. Grant 1990).

2.2.2 Present study

In the course of the present study, a discoidal marking was found approximately 5m above the base of the Shuram Formation in the Mukhaibah dome. This comprises an annular, discoidal ridge preserved in positive hyporelief. The structure is 24mm wide and the marginal ridge is up to 2mm high and up to 7mm wide. Similar samples have been found about 50m from the top of the Shuram Formation in Wadi Aswad. These are about 8mm to 20mm in diameter with 4mm thick marginal ridges that have 2mm relief (Plate 2.1a). These traces may be compared with those described as *Nimbia occlusa* from the late Precambrian rocks of the White Sea (Fedonkin 1980; D. McIlroy pers.comm. 1998). The

latter markings have only been found in float and are devoid of the characteristic central tubercle, which means that the *Nimbia* interpretation is very tentative.

Samples were collected by the writer from Masirah Bay Formation shales, lower Shuram Formation shales and the shaley carbonates of the Buah Formation in Wadi Bani Awf and were submitted to PDO for palynofacies analysis. None of the samples have yielded any positive results.

Despite extensive examination of outcrops and thin sections, no other macrofossils have been identified in the present study, although stromatolites abound and microfossil filaments have been found in bituminous cherts of the Khufai Formation.

Interpretation

The biostratigraphic control on the Huqf Supergroup is very poor. This may, in part, be a reflection of basin restriction. Although *Nimbia occlusa* is considered an Ediacaran fossil, the samples described from the Shuram Formation are not convincingly biogenic. *Cloudina* from the lower part of the Ara Group is indicative of a latest Neoproterozoic age (Grant 1990, Knoll & Walter 1992; Brasier *et al.* 1997) which would suggest that the Ara Group is either wholly latest Neoproterozoic or possibly passes up into the Cambrian.

2.3 RADIOMETRIC DATES

The most accurate method of dating any sequence is by absolute age dating of volcanic events, preferably by U-Pb methods. No such dates have been established from the Huqf Supergroup to date, so it was an aim of this study to identify ash beds suitable for dating by the isotope dilution methods (Tucker *et al.* 1990; Tucker & McKerrow 1995) in Prof. R.W. Tucker's Laboratory at the University of Washington in St. Louis, Missouri.

2.3.1 Previous work

Although some radiometric dates for the Oman basement have been published in the literature, most remain unpublished although they may be referred to in the explanatory notes accompanying BRGM geological maps of Oman and in internal PDO reports (Spriggs 1994; Spriggs & Russell 1997). Some important isochrons are reported below in Table 2.1 with the location of the dated rocks shown in Figure 2.2.

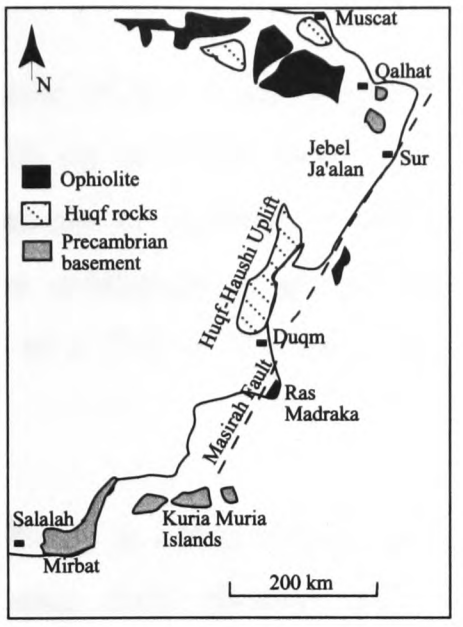


Figure 2.2 Map of eastern Oman showing location of dated basement outcrops and Precambrian exposures, after Gass *et al.* (1990).

Jebel Ja'alan

The Jebel Ja'alan intrusive complex lies *c.* 50km SSW of Sur in east-central Oman and comprises a suite of granitic-dioritic plutonic rocks intruded into a metamorphic basement which have yielded dates of *c.*815-834 Ma by a variety of techniques (Table 2.1).

Jebel Ja'alan	**Method**	**Date**
Pallister *et al.* 1988	$^{207}Pb/^{206}Pb$ zircon tonalite	834±6 Ma (intrusion age)
Roger *et al.* 1991	U-Pb zircon granodiorite	824±8 Ma (intrusion age)
Wursten *et al.* 1991	K-Ar several rock types	815-828 Ma (pluton cooling age)
Al Hallaniyah Island		
FM consultants	K-Ar granitic gneiss and granite	799±9 and 812±10 Ma
Gass *et al.* 1990	Rb/Sr 7granitic complex samples	772±8 (MSWD 1.6) (intrusion age)
Platel *et al.* 1992b	U-Pb zircons biotite-amphibolite	780±10 Ma
Mirbat area		
Kramers & Frei 1992	U-Pb zircon granodiorite gneiss	799±10 Ma (metamorphic event)
Kramers & Frei 1992	Rb/Sr muscovite from granite	745±7 Ma
Gass *et al.*1990	Rb/Sr whole rock granodiorite	706±40 Ma (late-tectonic intrusion)
Core 17 trachyte		
Gorin *et al.* 1982	K-Ar	654±16 Ma
Halfayn rhyolites and granites		
Kramers & Frei 1992	Rb/Sr isochron	556±11 Ma
Birba carbonates, Ara Group		
Russell & Amthor 1996	Pb/Pb	529±16 Ma

Table 2.1 Radiometric dates from the crystalline basement of Oman, Halfayn Formation volcaniclastics and carbonates of the Ara Group.

Al Hallaniyah Island

Al Hallaniyah Island is the largest of the Kuria Muria Islands that lie off the coast of Southeast Oman. These islands lie on an 80km long E-W trending line (17°30'N:55°36'-56°20'E). They are composed mainly of crystalline orthogneissic basement comparable to the Arabian-Nubian Shield. These orthogneisses of the basement are intruded by a granitic complex, which has yielded ages of *c.* 772 to 799 Ma, using various techniques (Table 2.1).

Mirbat

The Mirbat area of southeast Oman is about 50km northeast of Salalah. It contains a metamorphic terrain (Juffa gneiss, Sadh gneiss) with syn-deformational granodioritic intrusions. These have yielded ages of *c.* 745 to 799 Ma using various techniques (Table 2.1) Post-metamorphic basic and acidic dyke swarms cut the terrain.

Jan Kramers (1999 pers.comm., at a group meeting in the University of Bern), has also produced Rb-Sr dates from medium- to coarsely-crystalline red granites from Mirbat, along with others from granitic pebbles from the overlying diamictite and from the Halfayn Formation rhyolitic volcanics from the Al Jobah area. All of these samples yielded a combined Rb/Sr isochron age of 556±11 (Framers & Frei 1992) now refined to 547±5 Ma. These have an initial isotope ratio of 0.7114±0.0004 with 95% confidence. Russell & Amthor (1996) have produced a Pb/Pb radiometric date on carbonates from the Birba Formation (Stringer 1) of the Ara Group of 529±16 Ma.

The crystalline basement of the east and southern margins of Oman suffered a regional metamorphic event that involved crustal melting and magmatic intrusion. The protoliths of the metamorphic basement included calc-alkaline igneous rocks indicative of subduction-related magnatism. This metamorphic event is dated at around 840-820 Ma at Jebel Ja'alan and 820-800 Ma in Mirbat (Table 2.1). Syn-tectonic igneous activity occurred producing a suite of granitic dioritic plutonic intrusions dated at 830-815 Ma in the north and 800-780 Ma in the south. Subsequent post-metamorphic granitic intrusive activity continued up until about 750 Ma. These data would be consistent with the accretion of an island arc terrain onto the edge of the Arabian Shield, an interpretation generally invoked to explain the Pan-African orogeny regionally (Gass *et al.* 1990).

2.4 NEW GHADIR MANQIL DATES

During the first and second field seasons reconnaissance studies were undertaken on all the formations of the Huqf Supergroup, with the aim of finding datable ash beds. An ash bed was

discovered in the Ghubrah Member of the Ghadir Manqil Formation in Wadi Mistal (Figure 2.3). The Ghubrah Member comprises red/brown diamictites with numerous granitic, limestone, rhyolitic and vesicular pillow-basalts clasts, some of which have glacially striated surfaces. The clasts are generally poorly sorted and angular, set within a medium- to fine-grained red-sandy matrix. In Wadi Hajir, there are pyritic shales with dropstones, thick conglomeratic beds with scoured bases and turbiditic sandstones. Here, diamictites with metre-scale granitic boulders are overlain by a 5m-thick iron-rich 'cap dolostone', which is superseded by the Masirah Bay Formation.

The diamictite-dolostone contact is also very well exposed near Hadash village in Wadi Mistal, hence this dolostone has been termed the Hadash Formation and is considered to be the uppermost formation of the Abu Mahara Group. Overlying the Hadash Formation near Hadash village are rhythmic beds of fine-sandstones and siltstones of the Masirah Bay Formation; these are locally very organic-rich, especially along the road going up to the village (Plate 1.1f).

The sampled ash bed occurs along the roadside on the wadi floor below the village of Wakan 577518(E) UTM 2563048(N) (Plates 2.1c/d). In contrast to the host diamictites, the ash is a pale-grey colour, up to 2m thick and extends laterally for over 100m but it could not be traced on the opposite side of the wadi. This unit is composed of 9 fining-up beds, each *c.* 10-30cm thick accompanied by minor beds of poorly sorted agglomerates. The bases of the agglomerates comprise volcaniclastic breccia with angular, fine-grained rhyolitic clasts up to 2-3cm in size, which fine-upward to medium-grained tuff. The upper part of some tuffaceous beds are fine-grained and planar laminated which could represent fallout from suspension or an upper-stage plane bed developed during waning flow of a thin undercurrent.

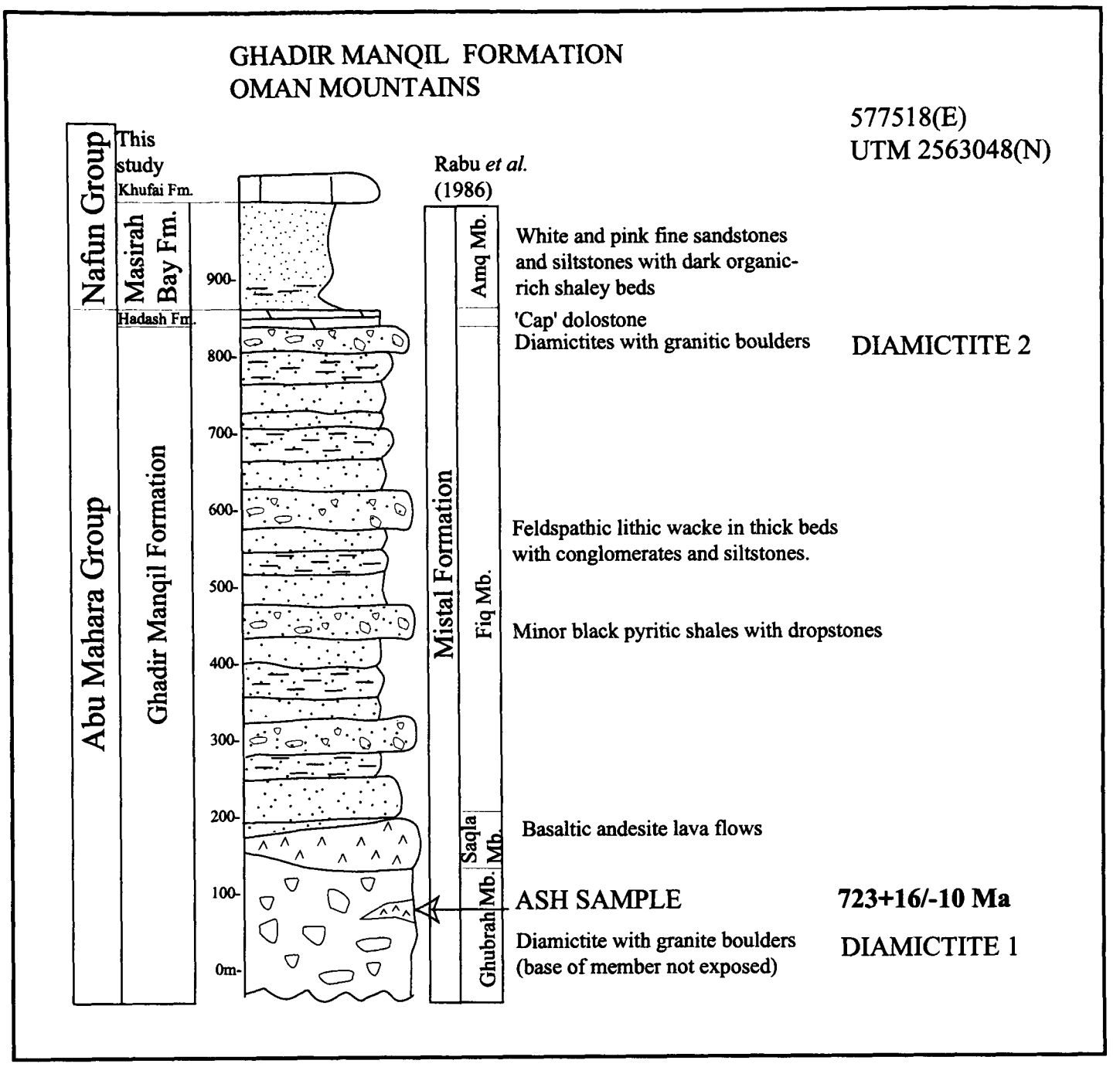


Figure 2.3 Schematic log of the Ghadir Manqil Formation from the Oman Mountains with data from Rabu *et al.* (1986) and the present study, showing the location of the ash bed, and new age date.

The sampled band is approximately 20cm thick, with arenaceous clasts within a fine-grained matrix, and lies about 1.5m above the base of the unit. In thin section, the rock is highly sericitized with a strong tectonic fabric that makes a primary volcanic origin somewhat ambiguous. The separated zircon grains, however, are very small (<250μm long), well faceted, euhedral prisms which are totally consistent with an eruptive igneous origin (R.W. Tucker, pers.comm., 1998).

Ten single grains or small fractions (2-4 grains) of zircon were analysed from sample GM6 and produced the discordia shown in Figure 2.4. Seven of these (1-7, Table 2.2) are discordant but co-linear with a high probability (66%) of defining an upper-intercept age of 723+16/-10 Ma (95% confidence level). This upper intercept age is interpreted to represent

the time of zircon crystallization and hence the age of the ash. The lower-intercept age is defined as 248+107/-115 Ma, which indicates a period of Pb-loss which may or may not have geological significance, especially given the large error of the age. Three samples do not plot on this regression line; they are interpreted to contain a trace component of inherited zircon, either as an old component in any grain or a xenocrystic grain in a multigrain fraction (R.W. Tucker pers.comm., 1998).

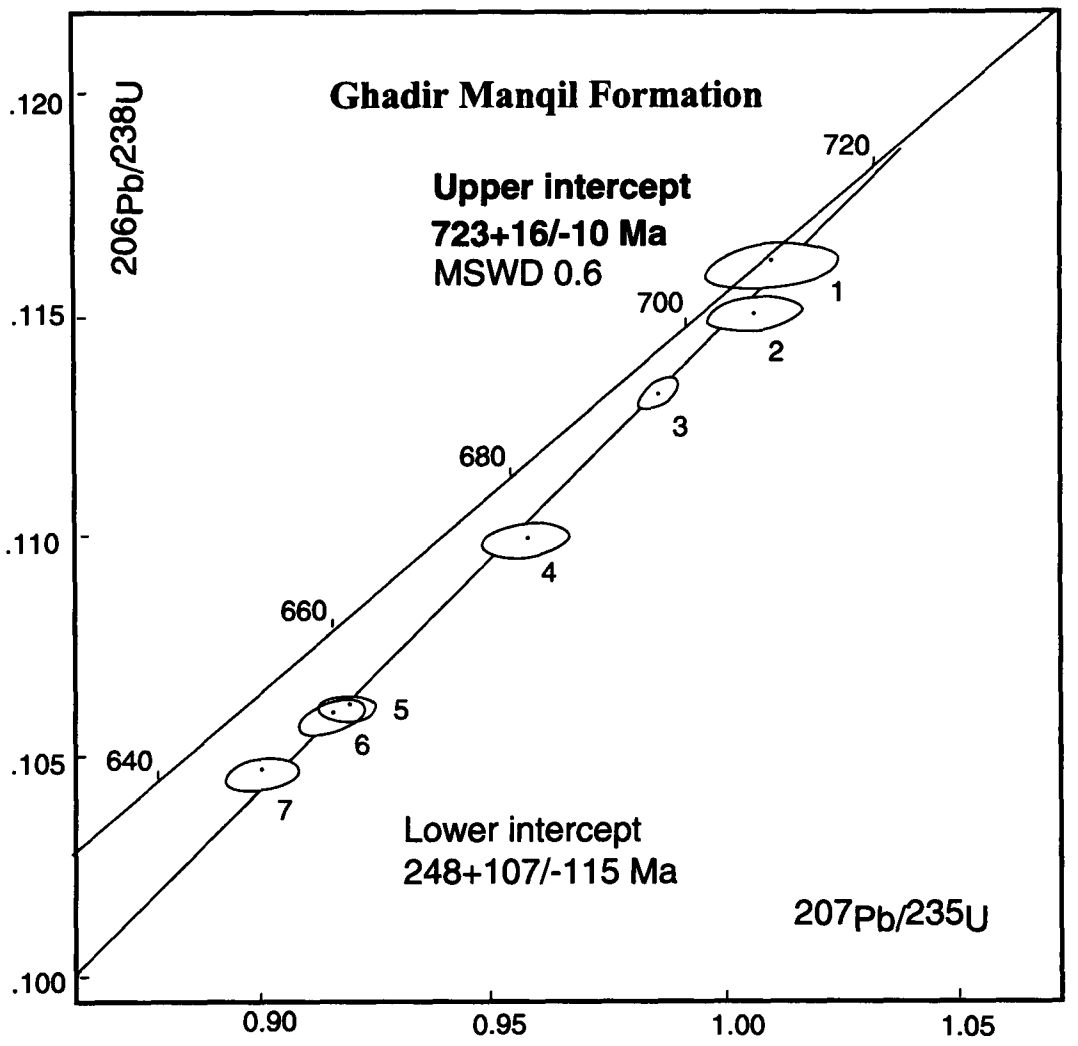


Figure 2.4 Ghadir Manqil Formation discordia, from data of Prof. R.W. Tucker.

2.5 NEW FARA FORMATION DATES

A reconnaissance survey of the Fara Formation in Wadi Bani Awf was carried out with a view to sampling the volcanic beds. A summary log of the basal part of this formation is presented in Figure 2.5 along with the stratigraphic location of the ash sample.

The Fara Formation has a gradational lower contact with the Buah Formation, and is organic-rich and cherty at the base, becoming more carbonate rich upwards. After 140m of section there is a sharp influx of volcaniclastic sediments in the form of tuffaceous litharenites, which are overlain by a unit of pale-grey ignimbrites. The latter are very fine-grained, with black fiammé and welded-tuff textures.

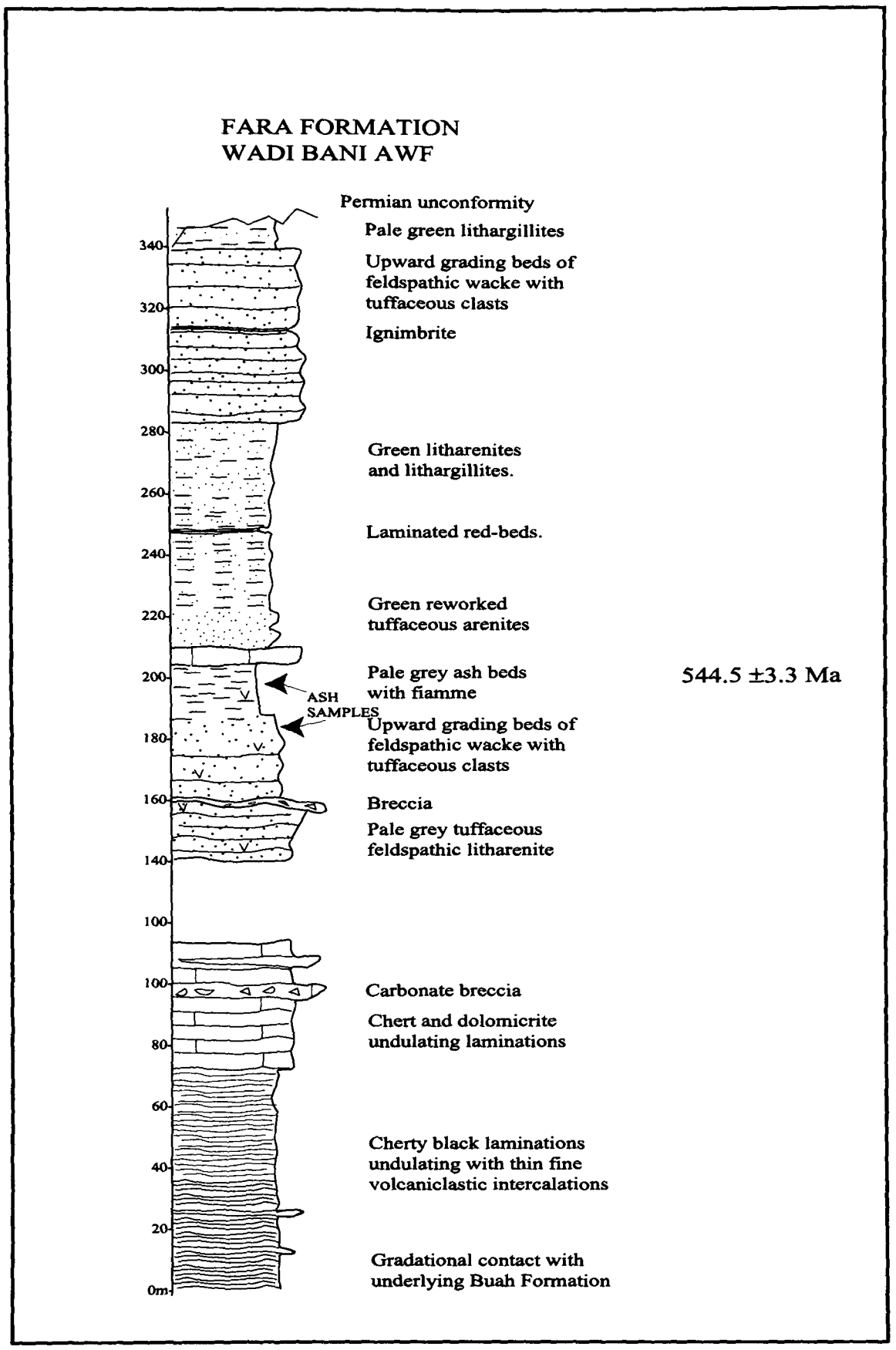


Figure 2.5 Summary log of the basal Fara Formation from which the ash samples were taken for U/Pb age dating.

The samples selected for analyses are from the top of the unit of tuffaceous litharenites located on the western side of the wadi behind the mosque, whilst the fine-grained ignimbrite with conspicuous fiamme textures crops out directly across the wadi from the mosque, on the eastern side 547432(E) UTM 2574724(N). In thin section, these contain an aphanitic matrix with volcaniclastic cuspate phenocrysts. The welded texture is occluded by microquartz. The extracted zircon crystals are predominantly pink, euhedral, well faceted

without overgrowths, are up to 300μm in size and considered to be typically volcanic in origin (R.W. Tucker pers.comm., 1998).

Six single grains and small fractions were analysed (Figure 2.6). Two of these are concordant at 545 and 533 Ma, but the younger analysis is less precise owing to its low content of radiogenic-Pb and poor measurement precision. Nonetheless, four analyses regress to common discordia with an upper-intercept age of 544.5±3.3 Ma (weighted mean $^{207}Pb/^{206}Pb$ ages) (Figure 2.6). The date of 545 Ma is assumed to be the crystallization age of the zircons and therefore the eruption age of the ash. Two other analyses (5+6, Table 2.2) yield older $^{207}Pb/^{206}Pb$ ages indicative of the trace presence of inherited zircons.

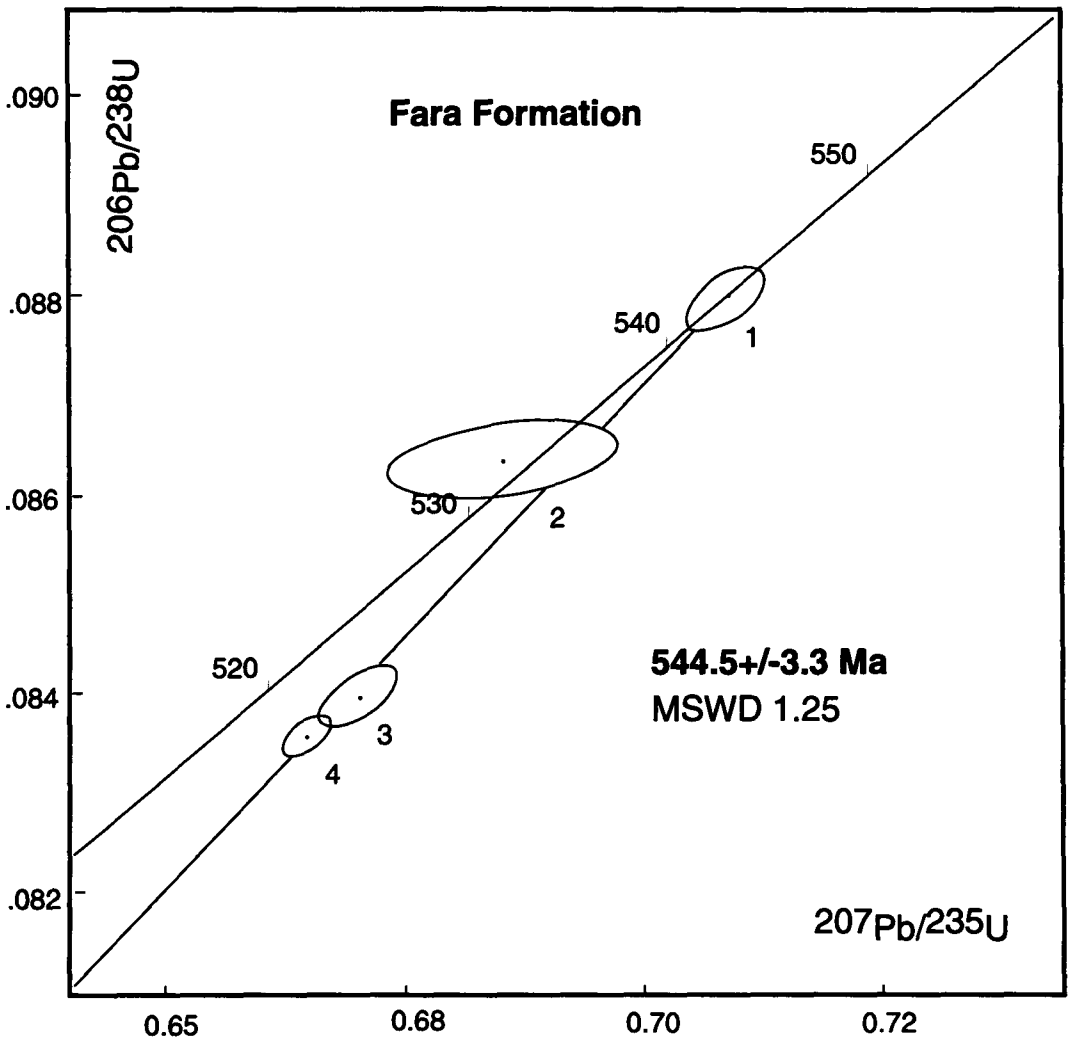


Figure 2.6 Fara Formation discordia, from data of Prof. R.W. Tucker.

2.6 SIGNIFICANCE OF THE NEW DATES

2.6.1 Ghadir Manqil

The U-Pb zircon age of 723+10/-16 Ma for the diamictites of the Ghadir Manqil Formation suggests that this glacial event is of Sturtian rather than Marinoan age. This is the first U-Pb date acquired from any Neoproterozoic glaciation (Figure 2.1). As this date comes from close to the base of the formation and is overlain by upwards of 900m of section before

encountering more diamictites with an extensive 'cap dolostone', the younger glacial could well be of Marinoan age, implying that two distinct Neoproterozoic glacial events are preserved in Oman. This hypothesis is supported by the observations that the Hadash Formation is similar to supposedly Marinoan cap carbonates described by Kennedy *et al.* (1998) and Prave (1999). The stable isotopes of the Hadash Formation have been measured and their isotopic signature would also concur with this interpretation (Figures 6.9 and 6.10 and Jon Leather pers. comm., 1999).

It could, however, be argued that these zircons have been reworked from earlier volcanic deposits or from the basement. That could mean that the various glaciations could all relate to a single, possibly Marinoan glaciation. Kaufman *et al.* (1997) have inferred early and late Marinoan glacial events from Spitzbergen, from carbon-isotope peaks. So the diamictites of the Ghadir Manqil Formation may represent two events within the Marinoan cryogen. However, the dates that would support this second hypothesis are considered rather dubious as one is a K-Ar date (trachytes from Core 17) which is easily reset. The Halfayn date is a combined Rb/Sr date and if the Halfayn rhyolite analysis is considered independently it gives a date with a very large error (546±42 Ma) and is considered unreliable.

As the majority of the basement dates are between 840-800 Ma (Table 2.1) the zircons are not considered to represent reworked basement zircons. Therefore, they most likely record a volcanic event that occurred during the glaciation, implying the presence of Sturtian glacial sediments in Oman.

2.6.2 Fara Formation

The Fara Formation date of 544±3.3 Ma is within the error of the published date for the Precambrian/Cambrian boundary (Bowring *et al.* 1993; Grotzinger *et al.* 1995). This has major implications for the age of the Huqf Supergroup and implies that we could yet find trace fossils and small shelly fauna in the upper part of the Fara Formation. This date also implies that the Nafun Group straddles the Ediacaran time interval even though no Ediacara soft-bodied fauna has been found in these sediments. Maybe the preservation potential did not exist in Oman or possibly the environments were too marginal and inhospitable to the Ediacara fauna.

Table 1. U-Pb Isotope Dilution Analyses, Oman.

FRACTIONS		CONCENTRATIONS					ATOMIC RATIOS								AGE [Ma]	
No.	Properties	Wt [µg]	Pb rad [ppm]	U [ppm]	Pb com [pg]	Th/U	$^{206}Pb/^{204}Pb$		$^{207}Pb/^{206}Pb$	±	$^{207}Pb/^{235}U$	±	$^{206}Pb/^{238}U$	±	$^{207}Pb/^{206}Pb$	±
	(1)	(2)	(2)	(2)	(3)	(4)	(5)		(6)		(6)		(6)		(6)	
HUQF ASH																
1	1gr,cl,pp,p	1	30.1	247	2.0	0.494	1,294		0.06306	34	1.0100	57	0.11617	20	710.2	11.3
2	1gr,cl,pp,p	3	21.0	162	2.1	0.766	1,757		0.06343	24	1.0063	41	0.11505	16	722.8	8.0
3	2gr,cl,pp,p	6	39.4	326	11.0	0.563	1,293		0.06312	9	0.9857	18	0.11326	14	712.4	2.9
4	1gr,cl,pp,p	2	41.3	341	2.8	0.678	1,468		0.06315	22	0.9573	36	0.10995	16	713.3	7.2
5	2gr,cl,pp,p	2	49.8	394	1.9	1.00	2,736		0.06284	16	0.9198	26	0.10617	11	702.8	5.4
6	4gr,cl,pp,p	13	39.3	345	66.4	0.575	466.8		0.06270	16	0.9164	28	0.10600	18	698.2	5.3
7	1gr,cl,pp,p	2	42.9	351	9.4	0.916	529.0		0.06243	22	0.9008	34	0.10466	15	688.8	7.4
†8	1gr,cl,pp,p	2	40.0	324	1.7	0.526	1,280		0.07021	35	1.1125	59	0.11492	20	934.5	10.1
†9	1gr,cl,pp,p	3	40.3	321	2.6	0.842	2,831		0.06396	13	0.9416	22	0.10678	16	740.2	4.3
†10	2gr,cl,pp,p	5	31.9	284	4.8	0.492	2,049		0.06345	11	0.9371	19	0.10712	13	723.3	3.7
FARA FORMATION																
1	1gr,cl,pp,p	6	9.45	107	1.9	0.930	1,865		0.05838	9	0.7078	14	0.08793	13	544.2	3.4
2	1gr,cl,pp,p	2	13.5	129	2.8	1.11	540.9		0.05791	30	0.6890	39	0.08630	16	526.3	11.4
3	1gr,cl,pp,p	5	10.6	108	1.9	0.925	1,477		0.05848	9	0.6766	14	0.08392	13	547.9	3.3
4	4gr,cl,pp,m-p	10	9.95	97.3	2.3	1.13	2,299		0.05837	6	0.6722	9	0.08352	8	543.7	2.4
†5	3gr,cl,pp,p	9	14.6	130	19.6	0.784	382.8		0.06120	30	0.8382	43	0.09933	18	646.2	10.4
†6	5gr,cl,pp,m-p	7	8.5	80.4	3.2	0.770	1,017		0.06002	27	0.7763	37	0.09381	10	604.4	9.8

Notes:

(1) Cardinal number indicates the number of zircon grains analyzed (*e.g.* 3 grains); all grains were selected from non-paramagnetic separates at 0° tilt at full magnetic field in Frantz Magnetic Separator; cl= clear; pp = pale pink; p = prismatic in form; m-p = middle parts from prisms. All zircon grains were abraded following Krogh (1982).

(2) Concentrations are known to ± 30% for sample weights of about 20 µg and ± 50% for samples ≤ 5 µg.

(3) Corrected for 0.0215 mole fraction common-Pb in the ^{205}Pb-^{235}U spike.

(4) Calculated Th/U ratio assuming that all ^{208}Pb in excess of blank, common-Pb, and spike is radiogenic ($\lambda\ ^{232}Th = 4.9475 \times 10^{-11}\ y^{-1}$).

(5) Measured, uncorrected ratio.

(6) Ratio corrected for fractionation, spike, blank, and initial common-Pb (at the determined age from Stacey and Kramers (1975)). Pb fractionation correction = 0.094%/amu (±0.025% 1σ); U fractionation correction = 0.111%/amu (± 0.02% 1σ). U blank = 0.2 pg; Pb blank ≤ 10 pg. Absolute uncertainties (1σ) in the Pb/U and $^{207}Pb/^{206}Pb$ ratios calculated following Ludwig (1980). This column lists the $^{206}Pb/^{238}U$ age (± 1σ absolute). U and Pb half-lives and isotopic abundance ratios from Jaffey *et al.* (1971).



Plate 2.1a Nimbia occlusa like markings from the Middle Shuram Fm. (178m) in Wadi Aswad, Huqf area.

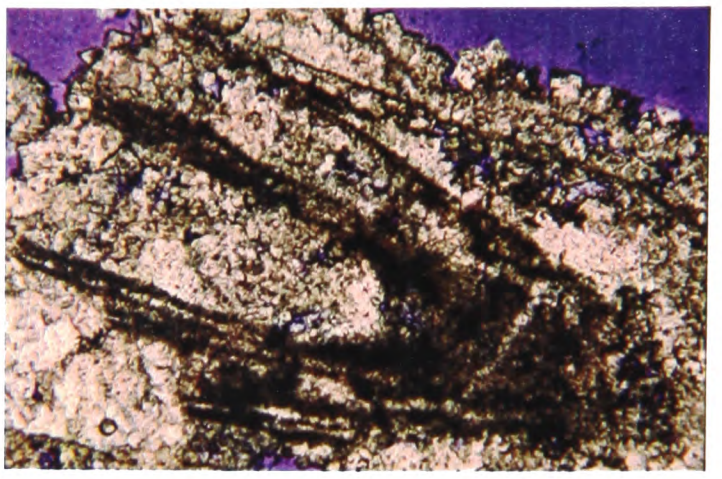


Plate 2.1b Longitudinal section of Cloudina from the Ara Fm. (A.Matter, Bern University) Horizontal fov. 3mm

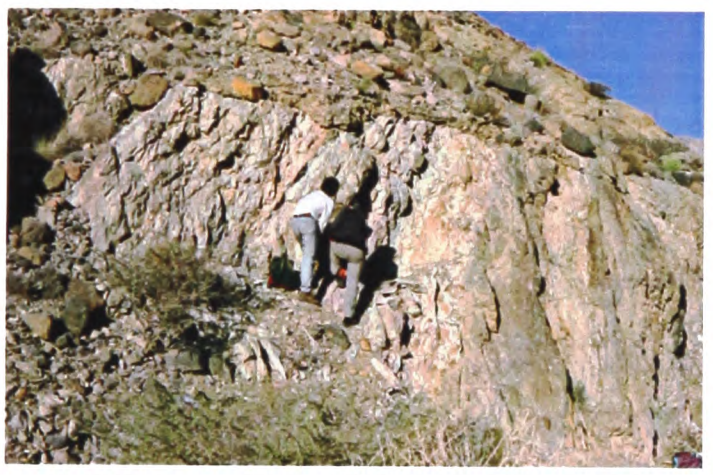


Plate 2.1c Ash band (pale) within the diamictites of the Ghubrah Member of the Ghadir Manqil Fm. in Wadi Mistal near Wakan village. Facing north.



Plate 2.1d Sampled ash bed, decimetre-scale fining-up beds. Notebook 225x176mm.



Plate 2.1d Ash bed from the Fara Formation in Wadi Bani Awf. Darker laminae contain fiamme and pumice.



Plate 2.1e Ash bed from the Fara Formation in Wadi Bani Awf. Fiamme and pumice-rich beds.

Chapter Three - Khufai Formation

3.1 INTRODUCTION

3.2 METHODS

3.3 PREVIOUS WORK

3.4 SUBDIVISIONS OF THE KHUFAI FORMATION

3.5 FACIES ASSOCIATION A:

3.6 FACIES ASSOCIATION B:

3.7 FACIES ASSOCIATION C:

3.8 FACIES ASSOCIATION D:

3.9 FACIES ASSOCIATION E:

3.10 KHUFAI FORMATION SYNTHESIS

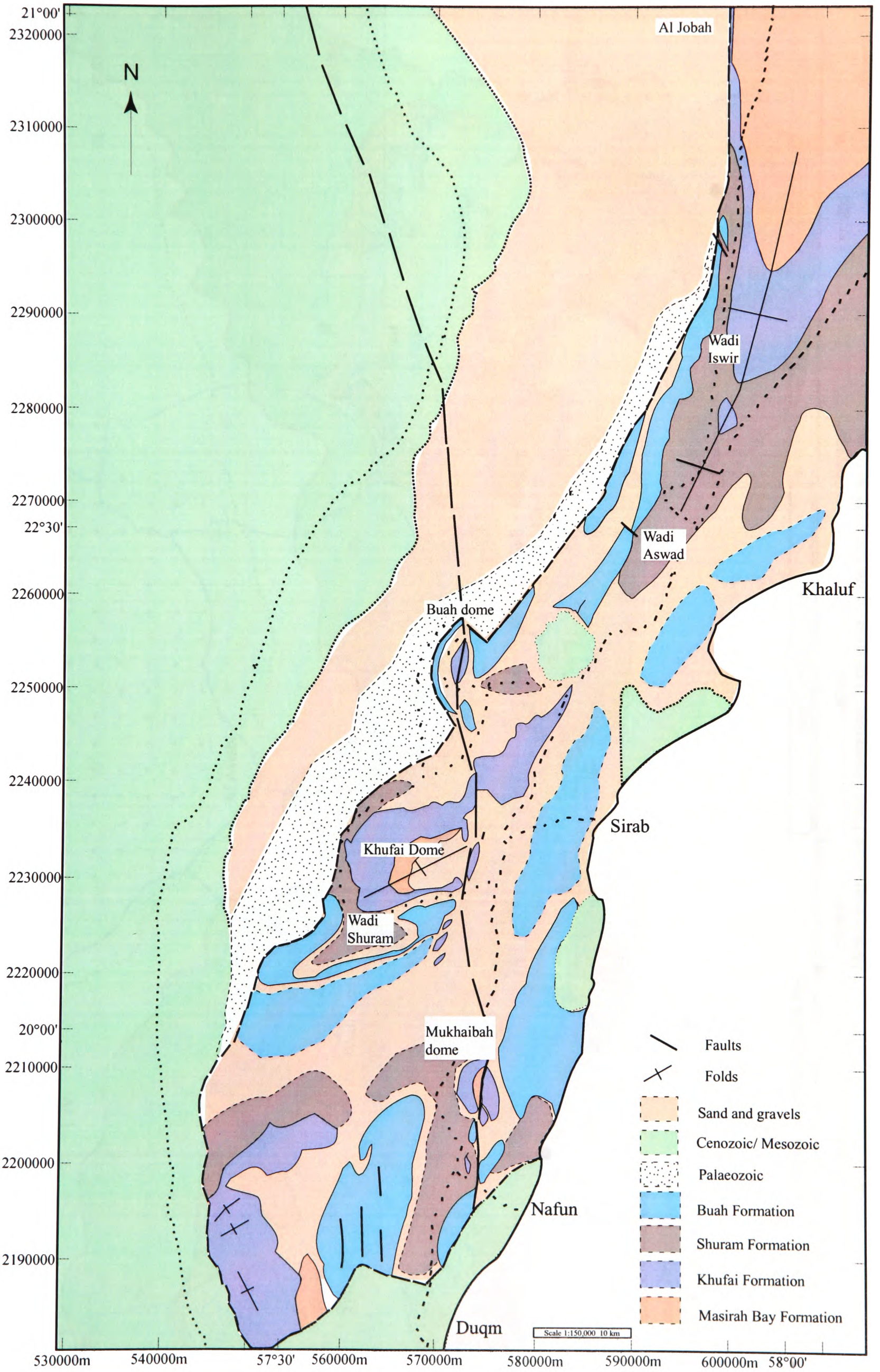
3.1 INTRODUCTION

The Khufai Formation is a mappable unit of carbonates that are widely distributed in the Huqf area (Figure 3.1) and the Oman Mountains (Figure 3.2). In the Oman Mountains, coeval carbonates have been termed the Hajir Formation by Kapp & Llewellyn (1965) after the type section in Wadi Hajir but for simplicity, in this study, the latter will also be referred to as the Khufai Formation. In the Huqf region, the Khufai Formation conformably overlies the silty carbonates of the Masirah Bay Formation whilst in the Oman Mountains it conformably supersedes siliciclastics coeval with the Masirah Bay Formation.

Previous workers have correlated the Khufai Formation in the Oman Mountains with the Khufai Formation in the Huqf area yet a detailed study of both areas by a single author had not been carried out. The aim of this chapter is to characterise the sediments of the Khufai Formation in both the Huqf area and the Oman Mountains (Plates 3.1 and 3.2), establish regional facies variation and develop a carbonate model. Summary logs from sections through the Khufai Formation in the south-east of Oman (Mukhaibah dome) to the northwest of Oman (Oman Mountains) are shown in Figure 3.3. These allow an overview of the Khufai Formation lithologies and show the five main facies associations defined in the present study. The inset shows the interpreted ramp model for these units and a lithological key. Detailed lithological logs are in Appendix 3 and the plates are presented at the end of the chapter.

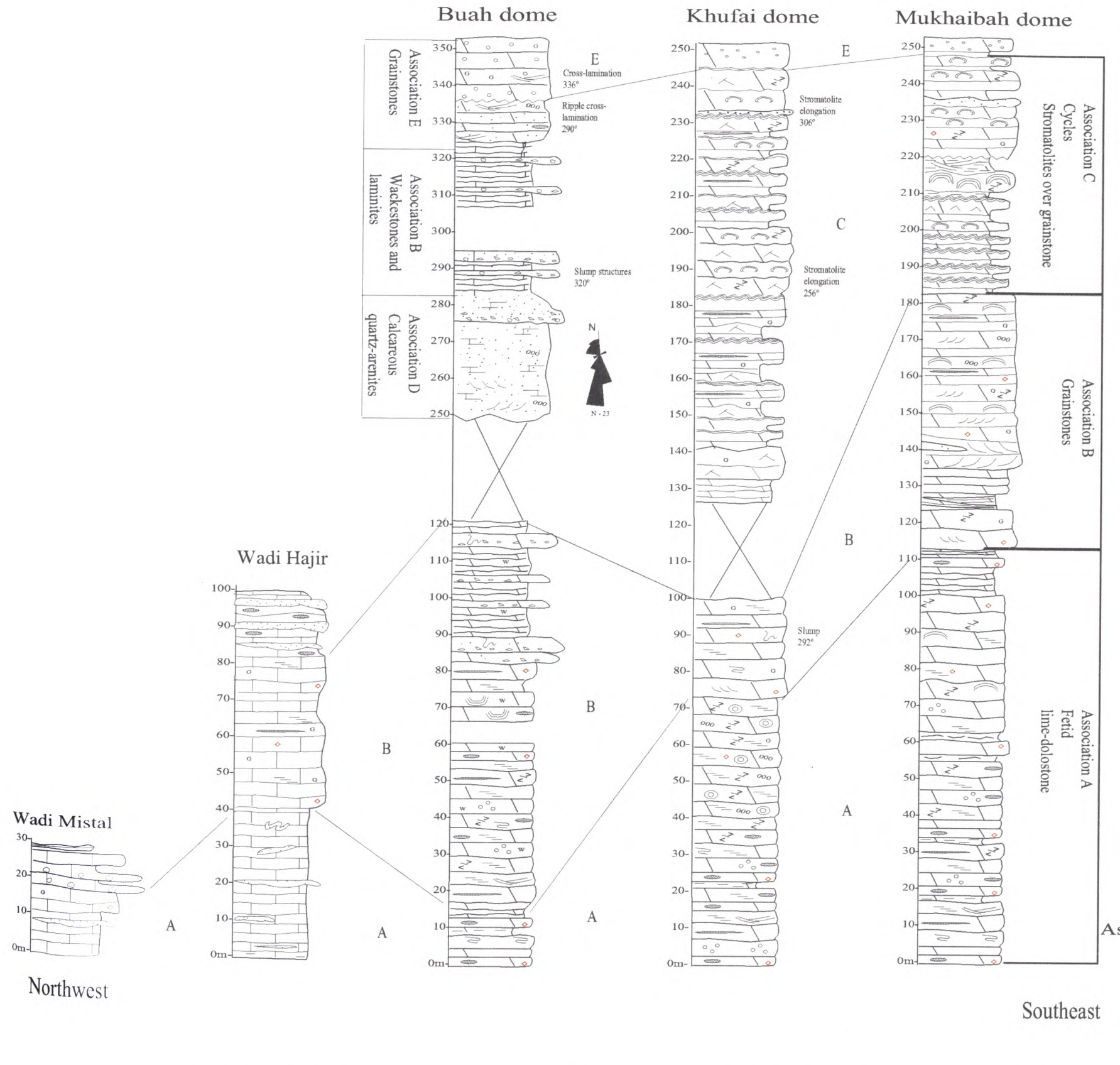
3.2 METHODS

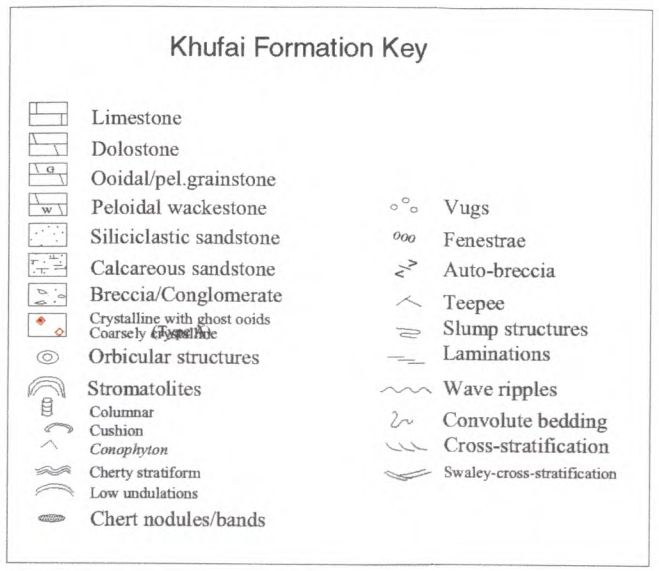
Relatively complete and well-exposed sections of the Khufai Formation crop out in the core of three anticlines, called the Buah dome, the Khufai dome, and the Mukhaibah dome in the Huqf region (Figure 3.1). In the Oman Mountains, complete sections occur in Wadi Hajir and in Wadi Mistal (Figure 3.2). Sections at these localities were logged in detail with the aim of characterising lithologies, facies variation and establishing palaeoenvironments. These were then used to define genetic depositional units. Supplementary sections were studied at other locations to test the validity of the genetic subdivision of the succession across the region. Representative facies samples were collected for petrographic and microfacies studies. This combined information has enabled the identification of facies, sub-facies, and depositional settings, and leads to a ramp-depositional model for this formation (Inset, Figure 3.3).

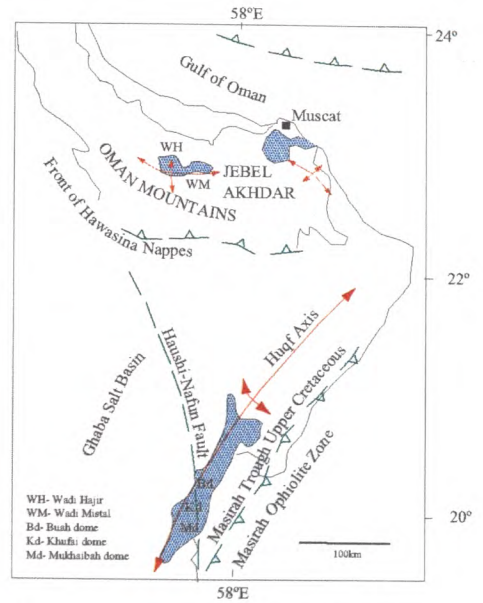


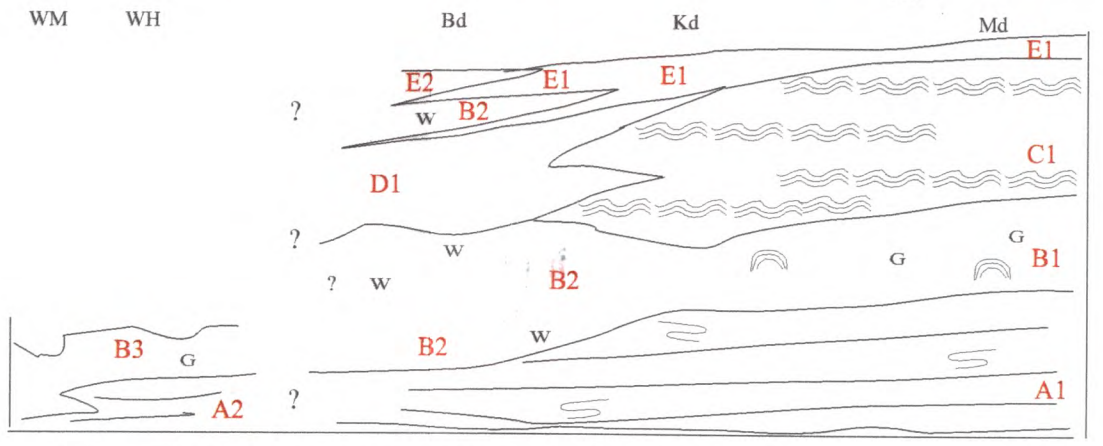
Sketch map of the Huqf Supergroup Formations in East-Central Oman

Figure 3.1

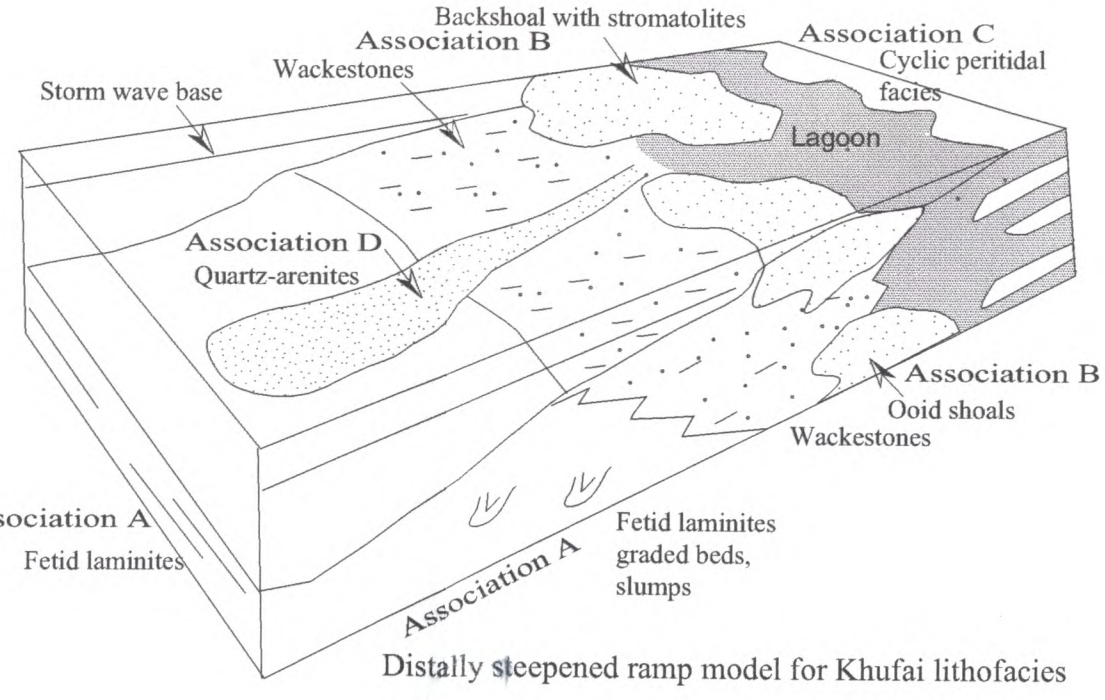








NW Khufai Formation lateral facies variation across Oman SE



Distally steepened ramp model for Khufai lithofacies

Figure 3.3 Khufai Formation summary logs showing lateral variation of lithofacies units referred to in text and Table 3.1. Inserts show location map, lateral facies variation, depositional model and key to lithostratigraphic symbols used.

3.3 PREVIOUS WORK

The Khufai Formation was first described by Beydoun (1960,1964) in his review of the Huqf Supergroup where he described the Khufai Formation as the First Dolomite. Kapp & Llewellyn (1965) during their survey of the geology of the Oman Mountains described the Khufai Formation and defined the type section in Wadi Hajir. Kassler (1965) while working in the Haushi, Central Huqf and Masirah Island areas, defined the type section in the Khufai dome, concluding that the formation was deposited in a complex of intertidal to supratidal environments. The dolomitized lime mudstones were taken to represent tidal-flat deposits, the lime sands representing deposits of tidal channels while the stromatolites were thought to indicate supratidal and marsh sediments. Later work carried out by Glennie *et al.* (1974), Rabu *et al.* (1986) and Hughes Clarke (1988) concurs with these interpretations.

More recent detailed work adds to these earlier studies. Figure 3.4 shows subdivisions that these previous workers have applied to the Khufai Formation as well as those used in the present study. Gorin *et al.* (1982) interprets the basal unit of the Khufai Formation as representing an upper intertidal to supratidal regime whilst Wright *et al.* (1990) interpret it as representing a low-oxygen, sub-wave base, probably sub-storm wave base ramp setting. Both groups interpret the middle and upper Khufai Formation as representing shoal to intertidal/peritidal environments of deposition which is in agreement with the interpretation reached by Dubreuilh *et al.* (1992).

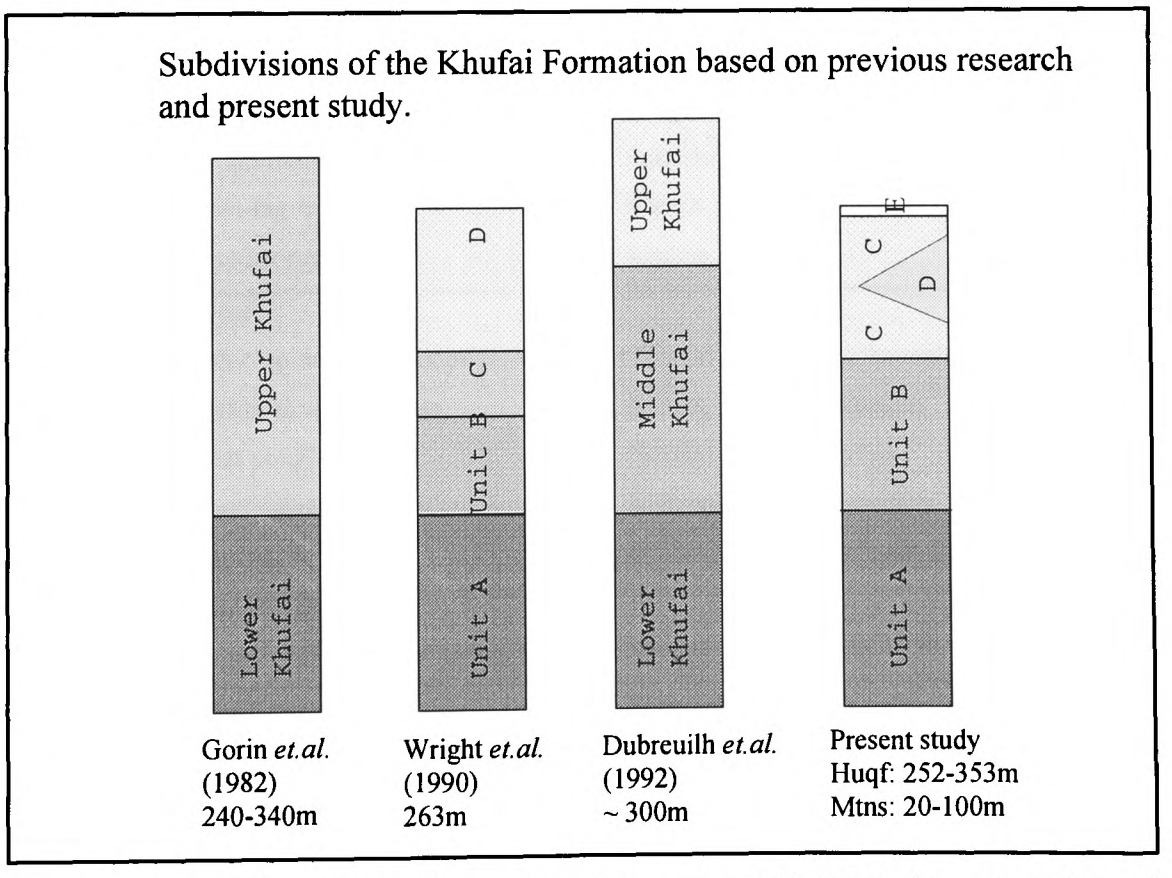


Figure 3.4 Lithological units defined by earlier workers shown alongside the facies association units defined and described within the present study.

3.4 SUBDIVISION OF THE KHUFAI FORMATION

In the Khufai and Mukhaibah domes of the Huqf area, the lithostratigraphic units of the Khufai Formation are thick and easily recognised by their topographic expression (Plate 3.1). Here, the Khufai Formation is approximately 250m thick and can be divided into five lithostratigraphic associations, termed A-E (Table 3.1). In the Buah dome, the Khufai Formation is only intermittently exposed and is made lithologically distinct by an extensive influx of siliciclastic sandstones toward the top of the formation. In the Oman Mountains, the Khufai Formation comprises well-indurated, black limestones that form ridges that are cut by narrow gorges and gullies (Plate 3.2). Here, the lithological character is relatively homogenous, consisting dominantly of recrystallized lime mudstones and grainstones. In the Oman Mountains, thickness varies considerably from as much as 100m in Wadi Hajir, to 20m in Wadi Mistal, to absence in Wadi Mu'aydin.

Summary of sedimentary facies in the Khufai Formation			
Facies	**Lithology**	**Sedimentary structures**	**Interpretation**
Association E	**Intraclast grainstones**		
E1	Ooidal-intraclast grainstones	Cross-beds, ripples	Shoal environment
E1a	Peloidal-intraclast grainstones	Fenestrae, auto-breccia	Intertidal
E2	Ooidal grainstones	Cross-beds, ripples	Shoal environment
Association D	**Litharenites**		
D1	Calcareous feldspathic-arenite	Cross-beds, ripples	Channel on mid-ramp
Association C	**Grainstone - Stromatolite cycles**		
C1	Ooidal-intraclast grainstones/packstones	Teepee, fenestrae	Backshoal
C1a	Cherty peloidal grainstone w/teepees	Teepee, fenestrae	Lagoonal - Inner ramp
C2	Cherty laminites/stromatolites	Auto-breccia, fenestrae	Intertidal to supratidal
C3	Intraclast-lag breccia	Scours	Peritidal
C4	Lime-mudstones	Swales, fenestrae	Intertidal - lagoonal
Association B	**Grainstones**		
B1	Oncolithic/ooidal grainstones/packstones	Tabular cross-beds,channels	Shoal to backshoal
B2	Fetid peloidal wackestones	Scours, swaley lamination	Shallow mid-ramp
B2a	Intraclast conglomerates	Normal grading, scours	Shallow mid-ramp
B2b	Black and white laminites	Soft-sediment deformation	Lagoonal
B3	Fetid grainstones	Grading, scours, soft-sed-def.	Outer-ramp
Association A	**Fetid dolo/limestones**		
A1	Laminated, cherty, vuggy dolostone	Slumps, auto-breccia	Slope, partly anoxic
A2	Lime mudstones	Planar beds	

Table 3.1 Khufai Formation Facies Associations A-E showing lithologies with sub-facies. These are described in approximate stratigraphic order from the base of the formation (Association A) upwards.

3.5 FACIES ASSOCIATION A: FETID DOLOSTONES/LIME-MUDSTONES

In the Huqf area, Association A (Plate 3.1) appears visually striking in outcrop as it is forms prominent ridges of thickly bedded dark-grey, fine- to medium-grained neomorphosed dolomites. In the Oman Mountains, it forms thick exposures of black limestones that produce deep-gullies and escarpments. Association A is regionally very homogenous, consisting of dark fetid dolostones (A1, Huqf area) and limestones (A2, Oman Mountains) that smell of hydrogen sulphide when cracked with a hammer.

The thickness of Association A varies across the area, reaching a maximum of 115m in the Mukhaibah dome in the south, then thinning northward to 75m in the Khufai dome and 16m in the Buah dome. In the Oman Mountains, the black lime mudstones are less than 50m thick and are bedded on a 10-50cm scale.

3.5.1 Facies A1: Fetid laminated dolo/limestones

These grey/brown dolomites are characterised by faint laminations that are dark grey and sub-millimetre to a centimetre thick. These laminae are planar to undulating, with lateral development of truncation structures and rare swaley cross-lamination. There is rare evidence for normal graded bedding on a centimetre scale. Slump structures range from a few centimetres to several metres in scale, occurring as flat-lying isoclinal-fold structures (Plate 3.3e) or as upright to inclined antiformal structures which convey vergence to the northwest.

At the base of the unit, laterally extensive beds contain subspherical vugs that range from a few microns to 5mm in diameter. The vugs are fringed by calcite halos and are more abundant toward the top of the beds. A bedding sub-parallel, laminoid, fenestral fabric becomes more prevalent upward, formed by laminoid fenestrae with irregular walls up to 5mm long and 2mm wide that are generally oriented subparallel to the bedding surface (Plate 3.3a). These laminoid-fenestral textures are associated with subspherical orbicular structures (similar to the 'jelly-roll' of Demicco & Hardie (1994) a term proposed for structures known as "enrolling of mats" in Davies 1970) that are especially well-developed in the Khufai dome area (Plate 3.3b).

Brecciated beds where the laminations are disassociated and fragmented *in situ*, produce a chaotic jumble of fragments bounded above and below by planar laminated beds (Plate 3.3c). In the Mukhaibah dome, the extensive brecciated beds are chertified, which imparts a reticulate fabric to the rock. Chert occurs as nodules, or as elliptical, lensoidal and/or tabular

lenses up to 10cm thick. These cherts are laterally extensive and commonly contain dolomite inclusions in the form of clasts. The cherts sometimes retain the dark laminations of the original dolomite precursor.

In thin section, facies A1 consist for the most part, of neomorphosed dolospar which is rich in rod-shaped micro-inclusions. Rarely, however, thin micritic laminae are preserved, sandwiched between laminae of coarse-grained carbonate that is rich in rod-shaped inclusions. Dolomite grains have vermicular textures in some samples (Plate 3.3f). The micritic laminations contain minor detrital silt-grade quartz and feldspar grains. Many laminated dolomites enclose voids which are laminoid to subspherical in nature. Some fenestrae result from intergranular porosity where, despite neomorphism, relict peloids are discernible. Many of these fenestrae are empty but some are partly or wholly occluded by calcite spar. Microquartz and chalcedony occlude some fenestrae. In thin section, auto-brecciated dolomites (Plate 3.3d) are observed to contain chalcedonic microquartz or sparry calcite.

Interpretation

The laminated dolostones are of fine-grained micritic carbonate thought to be derived from an inner-ramp shoal. Graded-bedding and swaley cross-lamination suggest an episodic influx of sediment, perhaps from waning currents during off-ramp transport of sediment during storms. The truncation surfaces and slump-folding indicate slope failure and initial down-slope transport of autochthonous sediments.

Subspherical fenestrae are suggested to have been produced by air or gas bubbles trapped during deposition of the host sediment or by post-depositional decay of organic matter (Cloud 1960; Demicco & Hardie 1994). Laminoid fenestrae have polygenetic origins; for example, *a)* desiccation, *b)* moulds caused by the degradation of fleshy cyanobacterial mats, *c)* gases generated by organic decay which lift subaqueous mats or buried mats to produce laminoid fenestrae or *d)* compaction of subspherical gas bubbles (Hardie & Ginsburg 1977; Grover & Read 1978). These structures are herein interpreted as the result of organic matter decay rather than as desiccation structures because of the lack of other evidence for shallow-water/exposure such as desiccation polygons. The fetid nature of the rock implies that it was organic-rich.

In-situ auto-brecciation can occur as result of slope failure which, disrupts the bed to cause brecciation or slump fold structures. Gorin *et al.* (1982) interpreted brecciation as the result of evaporite dissolution. Evidence for relict evaporites, however, has not been found in this

facies and the presence of slump structures is more consistent with a slope origin for the brecciated beds.

The prevalent chertification may have resulted from active photosynthesis by indigenous cyanobacteria, which are believed to create alkaline environments with pH values >10. Such environments would corrode detrital quartz, saturating the pore waters with silica in solution. A subsequent decrease in algal activity, thereby lowering the pH, combined with a decrease in water volume such as that caused by evaporation, could then cause the dissolved silica to precipitate (Blatt, Middleton & Murray 1980; Knoll 1985; Hesse 1989). Within this facies, there is no micro- or macro-scale evidence of former autotrophic microbial communities, except for the fetid nature of the rocks. This suggests that organic matter was partially preserved indicating sub-oxic conditions beneath the sediment/water interface.

3.5.2 Facies A2: Fetid lime-mudstone

The lower Khufai Formation in the Oman Mountains consists of black, fetid, pyritic limestones which are bedded on a 12-20cm scale (Plates 3.4a/b). The limestones are argillaceous and contain pyrite cubes that are exposed on the weathered surfaces. The beds are planar and devoid of evidence of current activity. Reworked intraclasts form minor lenses with scoured bases that pinch and swell laterally. Interbedded mudstones have often suffered soft-sediment deformation. In thin section, the mudstones are formed of recrystallized calcite spar with a marble texture, interlaminated with micrite. Some have evidence for detrital micritic intraclasts (Plate 3.4e). Numerous late hairline calcite-spar veins occur.

Interpretation

The presence of pyrite and the fetid nature of the limestones suggest that an organic-rich precursor sediment accumulated in a sub-oxic depositional environment (Berner 1981; Berner 1984; Sheilds *et al.* 1997) . The lack of sedimentary structures is taken to indicate that a quiet, possibly outer-ramp environment in which periodic influxes of reworked intraclasts represent storm events. The contortion of the grainstone lenses possibly results from gravitational loading on a sloping seabed.

3.5.3 Facies Association A synthesis

Although the laminated, fenestral, cherty dolomites of the Huqf area were interpreted by Gorin *et al.* (1982) to be microbial (stratiform stromatolite) sediments deposited in an upper intertidal to supratidal setting, there is clearly no physical evidence for this interpretation on

either a micro- or macro-scale. Accepting that micro-scale structures could be obscured by recrystallization, macro-scale evidence for intertidal/lagoonal stromatolites is well-preserved elsewhere in the formation. The absence of these fabrics in Facies Association A is taken to indicate deposition in a deeper, sub-photic zone environment.

The extensive recrystallization is unique to this facies of the Khufai Formation and probably indicates that this was originally a fine-grained or micritic carbonate deposit. The fine-grained material, the horizontal continuity of beds with planar boundaries and lack of shallow-water sedimentary structures are all indicative of a relatively deep marine environment, as suggested by Wright *et al.* (1990). The fetid nature of these dolo/limestones suggests that the organic-rich precursor was deposited in sub-oxic conditions. Sub-oxic conditions would enable at least partial decay of organic matter and the formation of the fenestral fabrics observed. The fetid nature of the rocks contradicts the argument of Gorin *et al.* (1982) for a shallow intertidal-supratidal regime because such an environment is likely to have been well oxygenated and hence unlikely to preserve abundant organic matter.

As no microbial textures are seen one can best infer a detrital origin for these sediments, probably sourced from the shallow inner ramp. This conclusion is supported by the combined occurrence of rare normal-graded bedding, truncation surfaces, cross-lamination, *in-situ* brecciation and slump structures. Slump structures, gravitational loading and *in-situ* breccias also testify to the presence of a slope. The lack of megabreccias or re-sedimentation of shallow sediments would indicate a shallow slope with a dip only large enough to allow for local failure in the form of auto-brecciation. Hence the Huqf area sediments are considered to have been deposited on an outer-ramp shallow slope setting whilst the Oman Mountains lime-mudstones are considered to represent more distal outer-ramp facies.

3.6 FACIES ASSOCIATION B: GRAINSTONES

In the outcrops of the Khufai Formation in the Mukhaibah dome and Khufai dome the contact between Facies Associations A and B is immediately apparent because of a colour change from the dark, fetid, laminated dolostones of facies A1 to the pale non-fetid grainstones of facies B1 (Plate 3.1). In the Mukhaibah dome, the flaggy beds of muddy carbonates (A1) are interbedded with the more resistant cross-stratified ooidal/oncolitic grainstones (B1) thus imparting a rhythmic appearance (Log in Appendix 3). This contrast is not so dramatic in the Buah dome where facies B2 is dominated by fetid intraclast wackestones, fetid mudstones and minor conglomerates. In the Oman Mountains, facies B3

has the same outcrop character as facies A2 but is marked by an increase in beds with reworked intraclasts.

Association B is 68m thick in the Mukhaibah dome but only *c.* 27m is seen in the Khufai dome, where it is overlain by a gap in exposure caused by a peneplanation surface at the top of the dome structure. Bed thickness varies between decimetre- to metre-scale in both areas. In the Buah dome, Association B comprises 106m of facies B3. Here, the bed thickness is on a centimetre- to decimetre-scale. Facies Association B in the Oman Mountains comprises the upper-half of the formation, being approximately 50m thick in Wadi Hajir and is distinguished by an increase in the proportion of reworked grainstone beds relative to mudstone beds. In Wadi Hajir, there is a gradual increase in bed thickness upward from decimetre- to metre-scale.

Facies B2 in the Buah dome, comprises intraclast-wackestones and fissile mudstones which become conglomeratic upwards (Log Appendix 3). Intraclast beds containing low-angle swales, soft-sediment deformation structures and graded-bedding are interbedded with or grade-up into fine-grained mudstones (Plate 3.5e). In the upper part of this facies the fetid wackestones are interbedded with fine-grained planar bedded dark and light laminites. This sub-facies is laterally extensive across all of the Buah dome (Plate 3.5a).

Facies B3 in the Oman Mountains, generally has an erosional contact with the underlying mudstones, is normally graded on a few centimetre scale and consists of peloidal intraclasts with detrital and authigenic quartz and feldspar grains.

3.6.1 Facies B1: Oncolitic-ooidal grainstone/packstone/boundstone

Facies B1 is formed of medium-scale, tabular-cross bedded grainstones/packstones that are non-fetid, pale cream/grey coloured with a well-indurated blocky appearance. Locally, these contain spaced, laterally-linked-hemispheroid stromatolite domes (LLH-S of Logan *et al.* 1964) with 10-20cm synoptic relief visible on bedding surfaces. Chert laminations and nodules are also present. Faint millimetre- and centimetre-scale lamination and scour-structures can be seen within the decimetre- to metre-scale beds. Siliciclastic sandstones occur locally in channels a few metres wide and up to 20cm deep in the lower part of the unit. In the Khufai dome, facies B1, exposed for *c.* 27m of section, forms a pale-grey cliff of decimetre-scale beds of grainstones with low-angle cross-bedding, local ripples and minor chert nodules.

Thin sections reveal that this facies consists of oncoliths and aggregate-coated-grains up to 1.5mm in diameter with subrounded ooids, up to 500μm in diameter, imparting a bimodal coarse and fine fabric within a packstone texture. The ooids in this facies are pseudo-ooids with only the micritic rim preserved, their internal structure being neomorphosed to microspar. Laterally, this facies contains millimetre-scale micritic laminations that form a boundstone with local micro-relief. In the Khufai dome, facies B1 is composed of pseudo-ooids, aggregate-grains and oncolitic grains that are up to 1mm in diameter with a micritic cortex. The cores have been leached and are replaced by an inclusion-free microspar which also forms the cement. Some of the samples retain a thin fibrous isopachous fringe cement around the intraclasts. This facies varies from grainstone to packstone with minor boundstone laminations, while some samples contain centimetre-scale interbeds of oncolitic-ooidal grainstone and oncolitic-ooidal packstone. Thin, micritised surfaces with differential packing and cementation above and below, are common throughout this facies (Plate 3.5b).

Interpretation

The ooid-oncolitic grainstones described above are similar to modern ooid and intraclastic sand ribbons and shoals (0-3m water depths) on high-energy sublittoral platforms described by Hagan & Logan (1974) in that the sediments have well-defined layering, micritised surfaces interpreted as hardgrounds, with reworked intraclasts and calcareous algae attached to clasts. Alternating coarse and fine layers and basal erosional surfaces suggest that the sediments were intermittently reworked during storms. Fibrous cements in lime sands indicate submarine lithification of sand bodies that were immobile for long periods (Hagan & Logan 1974). These periods of lower-energy and perhaps non-deposition, possibly provided the necessary conditions to enable the development of the boundstones and laterally-linked low-domal stromatolites. The ooid grainstones are interpreted as prograding lime sand sheets that form on the shallow ramp between tidal-flat, cyclic carbonates/lagoonal mudstones (Association C) and outer-ramp fine-grained laminated dolostones of Facies Association A.

3.6.2 Facies B2: Fetid intraclast/peloidal wackestone

Facies B2 is intermittently exposed and laterally extensive in the Buah dome area, where it consists of dark-grey centimetre-scale beds at the base, rising to 40cm-thick beds upwards. This facies is characterised by fetid, brown/grey siliceous intraclast wackestones with undulating fine- and coarse-grained laminations that alternate with centimetre-bedded, fissile, muddy-dolostones. Coarser beds have erosional contacts with the underlying units and contain swaley low-angle cross-lamination. Upwards in the section, there is an increase in

conglomeratic beds (up to 40cms thick) formed of matrix-supported, rounded to subrounded, pebble-to-cobble sized, clasts of pink/grey micritic dolomite. Conglomeratic beds are dominantly normally-graded on a 20-40cm-scale and fine-up into mudstones (Plate 3.5e). Spherical chalcedonic chert nodules a few millimetres in diameter are ubiquitous throughout this facies.

In thin section, facies B2 is represented by a range of textures from neomorphosed microspar with micritic intraclasts to ooid/intraclast packstone to conglomeratic wackestone (Plates 3.5c/d). The intraclasts usually consist of dark micrite and may be organic-rich and are angular-to-rounded. Typically they average 1.5mm in diameter but can be up to 1cm. Ooids are approximately 500μm in diameter and are neomorphosed to spar. Catagraphs with micritic outlines are typically rounded to subrounded and approximately 250μm diameter. Conglomeratic wackestones consist of micritic, peloidal, ooidal and stromatolite intraclasts up to a few centimetres in size with detrital quartz and feldspars up to 500μm in diameter. These clasts are sometimes broken and brecciated and are generally enclosed in a neomorphosed microspar matrix. Minor detrital quartz and feldspar influxes occur in fining-up laminations that are approximately 500μm thick. Cherts formed of spherulitic quartz nodules tend to occur parallel to the lamination.

Interpretation

Markello & Read (1981) interpreted similar wackestones from the Upper Cambrian Nolichucky Formation as representing low-energy, sub-wave base deposits in which some of the fine carbonate may have been carried from adjacent shallow-water areas to accumulate together with intraclast grains. The cross-stratified wackestones are higher energy winnowed ramp sediments that may have been formed above fair-weather wave-base or in sub-wave base settings that were subject to periodic reworking of bottom sediments. The majority of clasts are sourced from the interbedded micritic muddy dolomites, which probably reflects early cementation of this facies. Basal erosion/scour surfaces, swaley-lamination and mud caps indicate fining-upward layers generated by erosion and redeposition of sediments during and following storms. Basal erosion surfaces may have formed from the action of high-energy storm waves that scour and suspend bottom sediments and redeposit winnowed material as storm lags. Only during these storm events, when conglomerates are deposited, is there evidence for stromatolite intraclasts and detrital siliciclastics. This facies is, therefore, interpreted as representing storm-reworked mid-ramp carbonates that formed below normal wave-base but above storm wave-base, following the carbonate ramp model described by Burchette & Wright (1992).

3.6.2a Sub-facies B2a: Intraclast conglomerates

Interbedded with facies B2 and with hybrid calcarenites are intraclast conglomerate beds which invariably have erosional bases. Some beds contains soft-sediment deformation structures. These comprise beds up to 40cm thick and contain fine-grained dolomitic intraclasts that can be up to 50cm in diameter. Commonly, however, the intraclasts are of cobble size. The intraclasts are usually normally graded and overlain by dolomudstone (Plate 3.5e).

In thin section, this facies consists of variably sized angular micritic intraclasts within a microspar matrix. In some samples, subrounded detrital quartz and feldspar grains up to 1mm in diameter are present, along with detrital angular intraclasts up to 5mm in diameter, formed of ooidal grapestones, silty micrite, ooids and organic-rich micrite. These grains are matrix supported within a microspar cement which is partially replaced by spar. Other samples consist of paler inclusion-poor microspar intraclasts within an inclusion-rich microspar cement and are variably recrystallized.

Interpretation

The erosional nature of the bed contacts and the soft-sediment deformation structures both suggest that this facies is rapidly deposited on the shelf as storm related event beds.

3.6.2b Sub-facies B2b: Light and dark laminites

This facies is interbedded with calcarenite facies (D1) and peloidal wackestone facies (B2). It comprises persistent, millimetre- to centimetre-scale, laminites formed of dark-grey and pale-grey, fetid, planar-bedded limestone (Plate 3.5a) together with very minor quartz sand intercalations within micro-channels. The persistent nature of this lithofacies is very striking in the Buah dome area where it outcrops for *c.* 5km along strike.

In thin section, this facies is formed of layers of anastomosing dolomicrite with detrital fine-grained siliciclastics alternating with blocky calcispar. The spar crystals tend to be elongate, perpendicular to laminations and are radial-fibrous (pseudo-spheroids). Spherulitic nodules of fibrous quartz with length-slow microscopic textures commonly occur preferentially within the spar laminae.

Interpretation

The regular, planar laminations suggest a quiet environment of deposition such as a lagoon but could also represent outer-ramp below wave-base environments. Length-slow chalcedony

has been taken to indicate precursor evaporites (Folk & Pittman 1971; Milliken 1979). This facies, therefore, is taken to represent organic-rich lagoonal facies which were deposited in a partly anoxic environment.

3.6.3 Facies B3: Fetid intraclast grainstone

This facies occurs in the Oman Mountains, where it forms decimetre-scale interbeds within the black fetid lime-mudstones of facies A2 (Plate 3.4a). Typically the beds pinch and swell laterally and rest on very irregular scoured lower surfaces (Plate 3.4b). Although normally graded bedding occurs, there is very little evidence of other sedimentary structures.

In thin section, the rocks of B3 are formed of angular micrite intraclasts, grapestones and ooids that are up to 400μm in diameter and are commonly neomorphosed such that only the micritic cortex remains. Quartz and feldspar grains that are up to 500μm in diameter have irregular corroded margins. These siliciclastic grains contain carbonate inclusions and are observed to embay ooid grains and intraclasts. The matrix is formed of neomorphosed spar. Framboid and euhedral pyrite is ubiquitous.

Interpretation

The lack of sedimentary structures, such as cross-stratification, and the presence of graded beds with irregular scour bases suggest a quiet-water environment with infrequent storms. The fetid micritic intraclasts were rafted basinward by strong currents during storm events and deposited as graded tempestites, interbedded with lime-mudstone that are typical of the outer-ramp facies (Read 1985; Pratt & James 1986; Burchette & Wright 1992). The fetid nature of these sediments, along with the existence of euhedral pyrite, would indicate that the environment of deposition was at least partly anoxic with preservation of organic carbon. Abundant cubic and framboidal pyrite indicates reducing conditions below the sediment-water interface. The carbonate inclusions within the silicate grains suggest these are authigenic in origin despite the lack of euhedral terminations characteristic of authigenic minerals (Scholle 1978). Silica replacement is commonly associated with micro-environments of high organic content (Scholle 1978).

3.6.4 Facies Association B synthesis

In the Mukhaibah dome area, the lateral development of stromatolites in facies B1 indicates a well-oxygenated moderate energy environment possibly of a shoal to back shoal inner-ramp setting. Facies B1 of the Khufai dome area, represents an aerated, moderate to high-energy

environment with minor slump-structures and ripple-lamination perhaps of a more distal inner-ramp (Reineck & Singh 1973). Thus the mid-Khufai interval reveals an upward-shoaling depositional sequence formed by aggradation and progradation of the ramp from the Mukhaibah dome area in the south-east to the Khufai Formation area in the northwest. Shoaling of the deeper-ramp beds is indicated by the appearance of grainstone/packstone accompanied by channel fills, local stromatolites and cross-stratification. In the Buah dome area, the intraclast/peloidal wackestones of facies B2 indicates deposition beneath fair-weather-wave base, probably in a storm dominated shallow mid-ramp environment. In the Oman Mountains, the lack of sedimentary structures within facies B3 suggests possible deeper-water conditions.

This lateral variation in lithologies represents facies change across the basin. These spatial variations are accentuated within Association B relative to Association A and may reflect differential subsidence within the basin indicated by deepening to the north and west.

3.7 FACIES ASSOCIATION C: GRAINSTONE-STROMATOLITE CYCLES

Facies Association C is dominated by shallowing-upward cycles that are discernible on the satellite image (Appendix 1) and consist of recessive bases and resistant desert-varnished cherty caps. These cycles therefore form resistant ridges in outcrop, particularly in the Khufai dome, where they are overlain by recessive beds from the base of the superjacent cycle (Plates 3.6a/b). Facies Association C is 104m thick in the Khufai dome whilst only 58m thick in the Mukhaibah dome. It is absent in the Buah dome where there is an influx of calcareous quartz-arenites (Facies Association D) at the same stratigraphic level. In the Oman Mountains, the Khufai Formation comprises Facies Associations A and B only (Figure 3.3).

Towards the top of Facies Association C in the Khufai dome area there is an influx of detrital siliciclastics up to 3m thick which is trough-cross bedded and may represent the lateral extension of Facies Association D from the Buah dome.

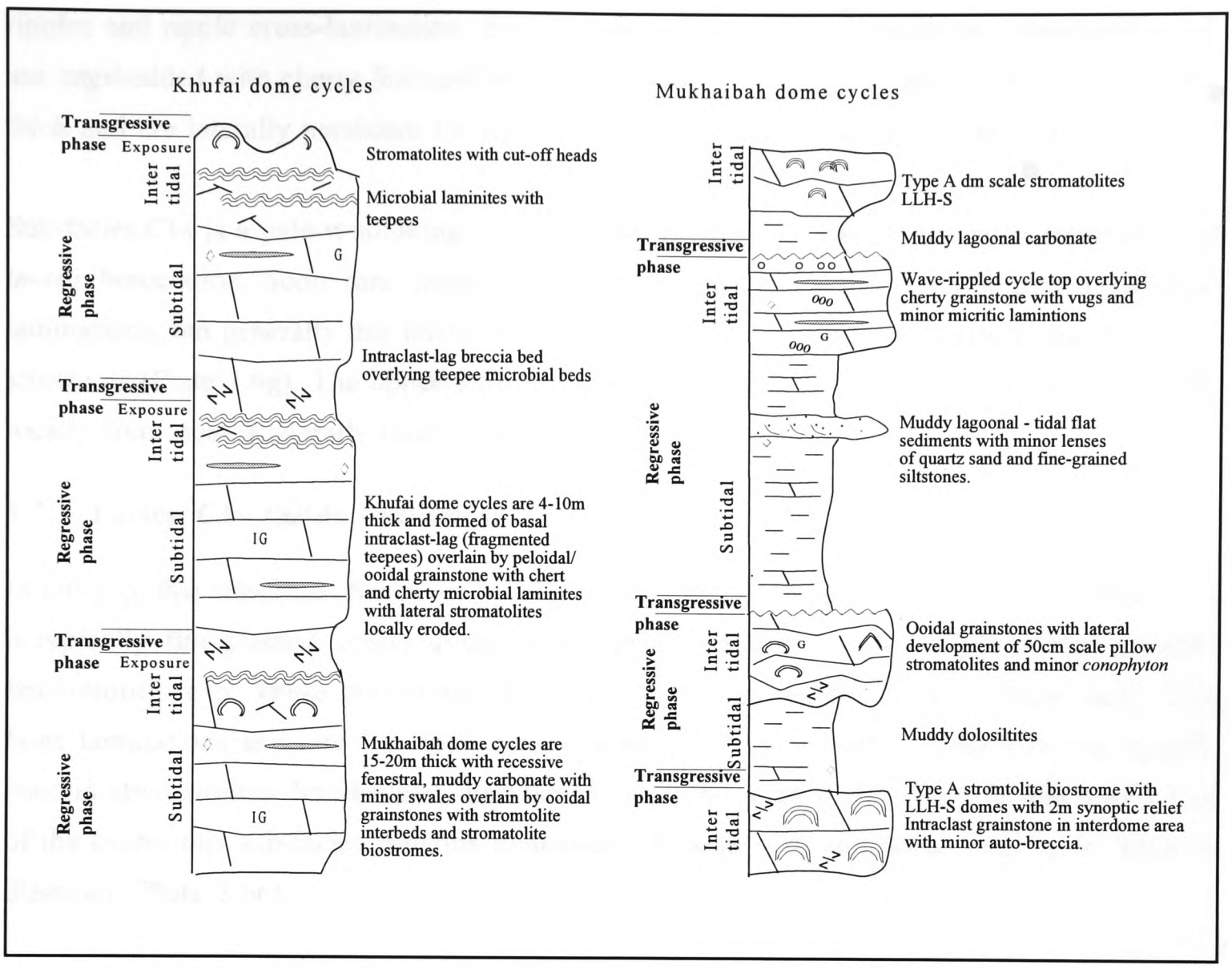


Figure 3.4 Facies Association C Grainstone-Stromatolite cycles in the Khufai dome and the Mukhaibah dome.

In the Khufai dome, Facies Association C is formed of shallowing-upward cycles on a 2-10m scale (Figure 3.4). The cycles comprise cherty dolomitized grainstones (C1) with rare low-angle swales passing up into cherty microbial laminites with stromatolites (C2) and teepee structures. The microbial laminations can be preferentially replaced by chert. These cherts have often been desert-varnished to a deep brown colour. Some tops of the cycles contain truncated stromatolite heads and *in-situ* brecciation of the lamination (Plate 3.7h). Locally, the cycle tops are marked by teepee structures and intraclast beds (facies C3). These cycles are laterally persistent throughout the Khufai dome outcrop area (Plate 3.6a).

The basal 20m of this Association in the Mukhaibah dome has cycles similar to those described from the Khufai dome, here, being some 2-4m thick. The middle and upper part of this unit is intermittently exposed and formed of cycles of recessive lime-mudstone with minor detrital siltstones overlain by ooidal grainstones and/or stromatolite biostromes (Log in Appendix 3). The stromatolite types at the Mukhaibah dome area are quite variable, and form large biostromes of up to 200m across. The ooidal grainstones, here, contain wave-

ripples and ripple cross-lamination that were later colonised by stratiform stomatolites and are interbedded with cherty fenestral limestones (Plate 3.7g). These higher cycles are 15-20m thick and are laterally persistent for up to 200m in the Mukhaibah dome outcrop area.

Sub-facies C1a is a pale-weathering, cherty, fine-grained dolomite with teepee structures and *in-situ* brecciation. Some rare cross-stratification is preserved in C1a with occasional faint laminations, but generally this facies is devoid of structure except for laterally spaced teepee structures (Plate 3.6g). The upper part of the cycle consists of stratiform stromatolites that locally form domes laterally (facies C2).

3.7.1 Facies C1: Ooidal-intraclast grainstones/packstones

In outcrop, this sub-facies forms the bulk of the shallowing-upward cycles of Association C. It is typically fine-grained, cream in colour and grades-upward into the brown desert-varnished stromatolitic cap. These grainstone/packstones are planar bedded on a 10-50cm scale with faint laminations and rare low-angle swales. They infill stromatolitic relief and can, locally, contain stromatolites. Interbedded chert bands are up to 10cm in thickness. In the upper part of the cycles this sub-facies contains numerous fenestrae with rectilinear vugs up to 3mm in diameter (Plate 3.6c).

Thin-section analysis indicates that many ooids have undergone aggrading neomorphism such that only a micritic cortex is preserved around a microspar carbonate core. These ooids have diameters between 500μm and 750μm and retain hints of a fringe cement within a clear spar matrix. Some ooid cores are replaced by secondary microquartz chert though the micritic cortex of the ooid is preserved. This sub-facies is interbedded with microbial laminites, where it overlies cherty stromatolite laminations. These are interlaminated with micritic/stromatolitic laminations which are eroded and brecciated laterally. Rare oomouldic porosity occurs whilst intergranular porosity is occluded by calcite spar.

Interpretation

The lower lithologies of the cycles consist of variably neomorphosed ooid-intraclast grainstones/packstones. The thin fringe cement and the lack of deformation of the ooids and intraclasts suggests early cementation at the sediment-water interface. The pervasive recrystallization of the ooid grains suggests an aragonite precursor (Tucker 1984). These sediments have only local development of swaley or low-angle cross-beds, indicating periodic higher-energy turbulent-water conditions. These could have formed by shedding from the

shoal area, for example, during relative sea-level rise. The increase in cherty microbial laminites, stromatolites and reworked intraclasts in the upper part of the cycle, would suggest shallowing. Eroded and brecciated laminations yield evidence for exposure which resulted in the *in-situ* formation of intraclasts. The abundant fenestrae and pseudo-evaporite structures are taken to indicate an arid environment with enhanced evaporation and salinity.

3.7.1a Sub-facies C1a: Cherty peloidal grainstone with teepee structures

This facies occurs above Facies Association B grainstones in the Khufai dome and is typically found in the lower parts of shallowing-upward cycles. It forms recessive, pale white/grey, flaggy, faintly laminated dolostone beds which are generally 10-30cm thick. Plates 3.6g/h show peloidal grainstone with spherical vugs (precursor evaporites) up to 1mm in diameter which occur along laminations. These are interbedded with chert bands up to 20cm thick. Teepee structures with up to 20cm anticlinal relief occur on a metre-scale spacing along the bed (Plate 3.6g).

Thin sections of chert bands (Plate 3.6h) reveal that microquartz replaces the matrix within the peloidal grainstone. Peloids are subrounded, some 20-50μm in diameter and occasionally occur in event beds. They are interbedded with 2-3mm thick undulating, micritic laminations. Non-chertified grainstones are dominant. These reveal micritic peloids up to 140μm in diameter within 2-3mm thick event beds which have typically undergone differential cementation and recrystallization.

Interpretation

Folk (1962) defined peloids as structureless micritic grains less than 0.2mm. Although peloids are often assumed to be faecal in origin this is not considered the case here due to the lack of evidence for organisms that might produce faecal pellets. There are no tracks or trails or signs of bioturbation in these sediments. This suggests that the peloids formed by flocculation of muddy carbonate grains within the water column. Differential cementation and recrystallization is possibly a reflection of early cementation on the seafloor. Pervasive expansive cementation of submarine hardgrounds initiates lateral compressive deformation which effects upward wedging and push-apart deformation forming teepee ridges (Demicco & Hardie 1994; p184). This facies probably formed in a lagoonal setting.

3.7.2 Facies C2: Cherty microbial laminites/stromatolites

3.7.2a Sub-facies C2a: Cherty microbial laminites

In outcrop, this sub-facies forms the brown-weathering and resistant caps to Association C cycles (Plate 3.2e). It consists of flat and undulating laminites which display the cryptalgal textures such as described those by Aitken (1967). This sub-facies consists of a microscale alternation of clastic laminae (peloids, ooids and flakes) with interbedded dolomicrite laminae. The microbial laminites occur as units a few centimetres to 2m thick that are locally chertified. Some laminations are crenulate in appearance and contain laminar fenestrae now occluded by dolospar (Plate 3.6d). Laminites may show desiccation structures such as disruption, flaking, curling-up of lamination and teepee structures.

3.7.2b Sub-facies C2b: Laterally-spaced-hemispheroids, 50cm scale

Laterally, the cherty microbial laminations of sub-facies C2b form flat-topped-domes (Plate 3.6e) of close-linked-hemispheroid (LLH-C) to spaced-linked-hemispheroid (LLH-S) stromatolites which can have up to 2-3m lateral spacing with synoptic relief of 40-50cm. Domes generally have a diameter of 20-40cm and several have asymmetric heads, with thicker laminae developed on one side, suggesting a preferred direction of growth. In one of the cycles these stromatolites have cut-off heads (Plate 3.7h). Stromatolite relief is infilled with fine-grained grainstones or intraclast grainstones.

3.7.2c Sub-facies C2c: 'Type A' stromatolite, smooth mm laminated domes

'Type A' stromatolites of sub-facies C2c are characterised by 1-2mm pale micrite and darker more recessive microspar laminations that are not crenulate but smooth, thickening in the domal area and thinning toward the edges. In thin section (Plate 3.7d), this consistent alteration is seen with microspar and micrite interfingering at the lamination edges. These laminae form domes with up to 1m synoptic relief and 2m in diameter. The domes are close-linked-hemispheroids to spaced-linked-hemispheroids and form a biostrome some 200m in lateral extent in the Mukhaibah dome. In the uppermost part of Facies Association C in the Mukhaibah dome area the synoptic relief of 'Type A' stromatolites decreases to *c.* 10cms (Plate 3.7b). Microbial laminites also nucleate on, and help to preserve, climbing-wave-ripples (Plate 3.7f).

3.7.2d Sub-facies C2d: Conophyton

Conophyton stromatolites are recorded in the Mukhaibah dome section and are formed of smooth 'Type A' stromatolite laminations sub-mm to 2mm thick with up to 25cm synoptic relief (Plate 3.7e). These retain a conical outline with a base diameter of approximately 40cm. Associated 'egg-carton' stromatolites with diameters of 15cm, synoptic relief of 6cm and dome spacing of 14-15cm, appear to nucleate on wave rippled grainstones.

3.7.2e Sub-facies C2e: Pillow-shaped stromatolites

Pillow stromatolites are also formed of 'Type A' stromatolite laminations that are 1-3mm thick in domes and thin at edges. Pillow-shaped stromatolites have a narrow base and grow laterally and upward to form a pillow shape with a diameter of approximately 18cm and 10cm synoptic relief (Plate 3.7c).

Interpretation

In the Khufai dome area, the stromatolites are dominantly stratiform laminites, although flat-topped close-linked-hemispheroid (LLH-C) to spaced-linked-hemispheroid (LLH-S) types do occur locally. The alternation of micrite and intraclast laminations indicate a trapping and binding mechanism in which the mats bound calcareous muds and detrital grains that were ultimately covered to form laminated sediments beneath the algal sheaths. Continuous mats and algal bound sediments are characteristically developed in marine, intertidal, mud-flat environments (Logan *et al.* 1964) between low-water and high-water. Hoffman (1967) demonstrated that thicker laminae are formed on the up-current side of algal heads. If so, this would indicate a dominantly north-westerly current direction in the Khufai dome area. The abundance of ooid and intraclast grainstones, and current-elongate stromatolites, indicates that much of the deposition was in the surf zone; that is, from where the waves first agitate the sea bottom to where the wave energy is finally dissipated (Hoffman 1975). The stromatolite domes may well have formed in the lower intertidal zone where current energy is strongest, while the microbial laminites with teepees could indicate a relative shallowing (cf. Gebelin 1969).

In the Mukhaibah dome area, the stromatolite character is quite different, with the morphology of 'Type A' (smooth lamination) tending to dominate. *Conophyton* and pillow-shaped stromatolites occur together and tend to nucleate on, and be interbedded with, ooidal grainstones. Conical laminated stromatolites are also developed in subtidal lagoonal sediments of the early Proterozoic Rocknest Formation in Northwest Territories, Canada (Grotzinger

1986b). In the present study, the ooid grainstones of facies C1 are taken to represent shoreward migration of the shoal facies or barrier into the lagoon during times of relative sea-level rise. These grainstones are overlain and interbedded with microbial laminites of Facies C2 (Log in Appendix 3). Metre-scale 'Type A' LLH-C stromatolites form an extensive biostrome of compound forms that probably represents a period of deeper water conditions within the lagoon. Stromatolite nucleation may have been relatively rapid as suggested by their growth on, and preservation of, climbing wave-ripples. The commonly uniform, homogenous lamination of 'Type A' might be taken to indicate that they were not trapping and binding forms but the result of *in-situ* precipitation (Pope *et. al.* 1999). The neomorphic fabric of these types (Plate 3.7d) suggests that bladed cement crusts were precipitated onto microbial laminae while the stromatolites were still growing. A process in which photosynthetic uptake of CO_2 from the seawater raised the pH and induced calcite precipitation, probably enabled early cementation of the biostromes (John Grotzinger, pers comm.).

3.7.3 Facies C3: Intraclast lag breccia

Intraclast lags form thin beds that occur at the base of some cycles. These beds comprise pebble- to boulder-sized clasts and, for the most part, are related to large scale teepees at the tops of underlying cycles. In the Khufai dome, these teepees are interbedded with cut-off stromatolite heads in which the uppermost laminations are erosively removed (Plate 3.7h). In the Mukhaibah dome, desiccation polygons were observed on loose boulders but could not be found *in-situ*. Here, intraclast lags were not observed although *in-situ* brecciation is common.

Interpretation

Teepee structures had the effect of curling-up the mat, which was then susceptible to brecciation. Stromatolite laminations suffered erosional truncation probably as a consequence of sub-aerial exposure. The fragments were reworked in the swash zone to form smaller lithoclasts. These are inferred to have formed at the start of transgressive phases, leading to breccia sheets that cover the tidal-flat lithologies of facies C2, or more rarely, were mobilised into erosional channels. *In-situ* brecciation within the Mukhaibah dome cycles is considered to result from evaporite dissolution.

3.7.4 Facies C4: Dolosiltite

Facies C4 is found only in the Mukhaibah dome where it forms the base of Facies Association C cycles. The pale pink/grey muddy carbonates of C4 are poorly exposed, forming recessive units. This facies is bedded on a decimetre-scale, with minor interbeds of chert. Minor influxes of medium grain-size quartz-arenites have basal scours. In some of the cycles, this facies contains swaley-cross stratification.

Thin sections reveal that this facies is formed of dolosiltite with minor grains of detrital quartz and feldspar silt up to 20μm in size. Minor clay-rich laminations also occur, alternating with vuggy laminated dolostone having rectilinear vugs up to 300μm in diameter.

Interpretation

The fine grained sediments of this facies typically occur on the inner-ramp, where tidal-flats were submerged following transgression, leading to carbonate silts and muds being deposited along with siliciclastics. Swaley-cross-stratification reflects reworking of sediment above storm-wave base by oscillatory currents (Hamblin & Walker 1979) and indicate that water depths at maximum transgression were close to storm-wave base in the Mukhaibah dome area.

3.7.5 Facies Association C synthesis

Khufai dome cycles commence with transgressive lag deposits (C3), grainstones (C1) are overlain by microbial laminites and stromatolites with teepee structures (C2), followed occasionally by exposure surfaces. Initially, shallow flooding of the shoal complex (B1) occurs with the deposition of lagoonal peloidal grainstones with teepee structures (C1). During subsequent fall in relative sea-level, the shoal complex became established again with the deposition of shoal grainstones. Oscillations become more enhanced up-section with the cycles consisting of ooidal-intraclast grainstones, overlain by microbial laminites that laterally contain current-elongate stromatolites. When relative sea-level fell, these earlier formed sediments were exposed in the vadose zone, leading to the formation of teepees, fenestrae and intraclast-lag breccias. Such cyclical sequences in the shoal complex reflect minor oscillations in sea level (Fairchild & Herrington 1989; Grotzinger 1989). These Khufai dome cycles are, therefore, taken to represent submergence to intertidal or subtidal depths during each cyclic transgression, followed by aggradation to sea level and final sub-aerial exposure during relative sea-level fall.

The basal cycles of Mukhaibah dome are very similar to those of the Khufai dome. Up-section, the cycles become thicker (averaging 15-20m) and consist of dolomudstones or dolosiltstone overlain by wave-rippled ooidal-grainstones with stromatolites or stromatolite biostromes. Although evidence exists for evaporite pseudomorphs, conclusive exposure surfaces were not found in the Mukhaibah dome cycles. Cycles here were initiated by rapid transgression and flooding of the carbonate tidal-flats and lagoons developed behind the grainstone shoals of facies B1 on the inner-ramp. The upward increase in clastic carbonate beds within shale-based cycles (Log in Appendix 3) indicates progressive migration of the carbonate tidal-flats over deeper-lagoonal sediments cf. Grotzinger (1986). Stromatolite build-ups are thin (1-2m) because deposition occurred under stable or shallowing conditions with limited space for upward growth of mounds. Absence of large build-ups in the upper part of the section may be related to shallowing and increased restriction cf. Read (1980). Shoaling then developed a sand-flat setting, which was subjected to frequent wave reworking of ooidal grainstones that overlie the lime-mudstones of low-energy tidal-flat to lagoonal setting. Microbial-rich ooidal sheets and lenses are taken to be channel fill and storm layers. Mats are thought to have developed periodically on wave-rippled, ooidal sediments of the shallow, subtidal-lower intertidal sand flats. Shallowing of the channelled sand flats was accompanied by deposition of massive fenestral beds of the low-energy tidal-flats.

Absence of distinct marker beds makes it difficult to correlate cycles across the Huqf area but, in general, the Khufai dome appears to preserve inner-ramp shoal facies, whereas the Mukhaibah dome preserves proximal lagoonal to intertidal facies. The lack of cyclicity in the Buah dome area is presumably a reflection of a deeper mid-ramp setting. Marked conglomeratic intervals there may indicate the onset of transgressive intervals. In the Oman Mountains, outer-ramp facies B2 continue through the middle and upper part of the Khufai Formation.

3.8 FACIES ASSOCIATION D: LITHARENITES

Facies Association D is marked by an influx of siliciclastics and is 33m thick in the Buah dome but only 3m thick in the Khufai dome (Figure 3.3). The possible lateral equivalent of Facies Association D is only 1m thick in the Mukhaibah dome.

The basal 26m of this Facies Association in the Buah dome is placed in facies D1 which consists of feldspathic-litharenites that are poorly indurated and only intermittently exposed (Log and ternary diagram in Appendix 3). Further north, in the Buah dome outcrop area, these feldspathic-litharenites are interbedded with muddy carbonates resulting in fining-up

cycles on a scale of 1-2m. Toward the top of Facies Association D, facies D1 becomes more calcareous intraclasts forming a calci-litharenite and is interbedded with conglomerates of sub-facies B2a and intraclast-wackestones of facies B2.

Facies D1 has an erosional lower contact and consists of pale-creamy calcareous coarse feldspathic-litharenite in beds up to 2m thick. Beds fine-up, on 30-50cm, scale from coarse- to medium-sands.

3.8.1 Facies D1: Calcareous feldspathic-arenite

This facies is dominated by well-sorted calcareous feldspathic arenites that occur in 2m-scale beds that roughly fine-up. These have a blocky appearance and minor silt partings a few centimetres thick. These coarse- to medium-calcarenites contain low-angle swaley cross-lamination at the base but become planar-laminated upwards, cross-set thickness 10cm. Bi-directional palaeoflow appears to be to the west and south. Upwards, an increase in carbonate intraclasts is marked by a colour change to grey-weathering, along with a more flaggy appearance and thinner beds, about 20-50cm thick. Beds become more planar upward with asymmetrical ripple-cross-lamination locally developed. Ripple wavelength 10cm with waveheight 1cm. Some beds fine-up to siltstones which suffers loading from the overlying sandstone bed. Toward the top of this facies, the calcarenites are medium-grained, bedded on a finer scale of 10-30cm and contain dewatering structures. Interbedded with these are 10-40cm scale, fining-up beds of conglomerates with rare dolomitic clasts up to 50cm (B2a).

In thin section, this facies is composed of subrounded-subangular quartz and feldspar grains between 500μm and 900μm in diameter (Plate 3.8h). These grains have variable amounts of syntaxial overgrowth cements. Many of the quartz grains are cracked, strained and contain lath-shaped inclusions of sillimanite and opaque oxides. The feldspars are variably altered while all the grains are corroded and, in places, partially replaced by calcite. Intraclasts are composed of subrounded micritic clasts with minor ooids and oncoliths usually between 500μm and 900μm in diameter. These contain minor glauconites and heavy minerals usually deposited along cross or planar lamination. Some samples, especially toward the top of the unit, have a patchy poikolithic spar cement which replaces earlier micritic cement. In some samples, this facies has a sharp planar upper-contact with a fine-grained muddy carbonate.

Interpretation

These are interpreted as tidal channels that cut across the shallow mid-ramp area. They appear to have been deposited during storm events, as is indicated by the erosional nature of lower contacts and by the swaley cross-lamination probably formed during storms below the fair-weather wave base. The fact that the beds grade-up from swaley cross-laminated to planar-laminated also suggests a setting below fair-weather wave base and above storm-wave base. Normal-grading of the calcarenite beds and conglomerate interbeds would further suggest a storm/event origin for these sediments. The lateral variation would confirm this hypothesis. Initially comprising predominantly feldspathic arenites (Appendix 3), these become more calcareous upwards with clasts 50/50 carbonate/siliciclastic might reflect changes in relative sea-level. Palaeocurrent structures indicate a source area to the east. Silliminite inclusions in quartz grains would indicate metamorphic origin (Scholle 1979).

3.8.2 Facies Association D synthesis

The facies of Facies Association D reveal a general upward-shallowing. This basinward migration of facies suggests that this lithofacies formed part of a lowstand prograding wedge. Finer grained calcarenites in the north of the outcrop area may be a reflection of their greater distance from the source area, which is considered to be in the east from palaeocurrent data. The 3m thick, cross-bedded lithic-arkosic sandstones in the Khufai dome area may be a southern prolongation of facies D1. Association D is interbedded with intraclast conglomerates in the Buah dome which suggests that storm events occurred on a shallow-ramp setting. The dominance of fine-grained micritic clasts suggests deposition by off-shore currents that reworked clasts from early lithified, possibly more proximal lagoonal settings. Association D is succeeded by finely laminated lagoonal limestones.

3.9 FACIES ASSOCIATION E: OOIDAL-INTRACLAST GRAINSTONES

Facies Association E is the uppermost unit of the Khufai Formation in the Huqf area and is 21m thick in the Buah dome, 10m thick in the Khufai dome and only 3-4m thick in the Mukhaibah dome. Dominantly comprising cross-bedded oncolithic-ooidal grainstones, this unit has thin interbeds of stromatolitic limestones and fenestral, auto-brecciated, ooidal-intraclast grainstones. This unit forms a pale-grey resistant ridge in outcrop.

3.9.1 Facies E1: Ooidal-intraclast grainstone

This facies is dominated by cream-grey metre-thick beds of oncolithic grainstones that are locally desert-varnished. Ooids and grapestones weather out from the matrix. In the Buah

dome, this facies preserves low-angle cross-stratification that overlies planar beds (Plate 3.8c). Bi-directional cross-sets reveal a dominant palaeoflow to the south and northwest. Flat topped wave ripples also occur, with a 10cm wavelength and a height of 1cm.

In thin section, the grainstones are formed of well-preserved ooids and grapestones up to 1.5mm across. These have micrite cortices. Intraclasts of micrite, microspar and grapestones up to 3mm across also occur (Plate 3.8d). Some ooids are neomorphosed to microspar but the concentric fabric is still visible. All have an isopachous fringe cement which was originally aragonite but has since been replaced by blocky calcite spar (Plates 3.8d/f). Intergranular porosity is occluded by microquartz and calcite spar. In the Mukhaibah dome, the isopachous fringe is also replaced by spar, with intergranular porosity occluded by chalcedony and megaquartz. Sparry calcite occurs in vugs with rare anhydrite and gypsum.

Interpretation

Oolitic and grapestone facies cover large areas of modern carbonate platforms from water depths of around 9m to the intertidal zone (Tucker & Wright 1990). The isopachous acicular cements could indicate a shallow-marine origin for these ooidal-intraclast beds (Tucker 1981; Flügel 1982; Harwood 1988) The cross-stratification in these grainstones suggest deposition in a high-energy shoal environment.

3.9.1a Sub-facies E1a: Peloidal-intraclast grainstone

This sub-facies is interbedded with facies E1 in the Buah dome and the Khufai dome. It comprises decimetre-scale beds of pale-grey peloidal-intraclast grainstones with minor stromatolites and cross-lamination. The stromatolites have mm-scale, smooth, laminations with up to 20cm of synoptic relief. This facies is auto-brecciated and contains numerous fenestrae with evaporite pseudomorphs (Plate 3.8e).

In thin section, this subfacies comprises ooids of up to 300μm in diameter, which are partly neomorphosed to spar within a sparry calcite cement. Laterally, this facies is more peloidal-rich with micritic intraclasts up to 100μm in size within a microspar cement, alternating with undulating micritic laminations. Minor detrital quartz occurs in some samples in the Buah dome.

Interpretation

This facies represents deposition in an environment with variable energies. The ooidal grainstones represent higher-energy events possibly depositing shoal ooids as spillover fans into the lagoon. The deposition of peloids and microbial laminites and stromatolite growth may indicate the less energetic background conditions of the lagoon. The fenestral and auto-brecciated structures and evaporite pseudomorphs suggests restricted, arid conditions prevailed, leading to evaporite deposition and subsequent dissolution with auto-brecciation. This facies is therefore most likely to represent an intertidal to supratidal environment of deposition.

3.9.2 Facies E2: Ooidal grainstone

The pale cream-grey, ooidal grainstones of facies E2 lie directly beneath the flat-pebble-conglomerate carbonates of the Shuram Formation at Nafun in the Mukhaibah dome area (Plate 3.8a). This facies is approximately 50cm thick and is exposed over some kilometers in the Mukhaibah dome area. This is the only place where the contact between the Khufai Formation and the Shuram Formation is visible in the Huqf area.

In thin section, this facies (Plates 3.8b) consists of ooids with a bimodal size distribution. The larger ooids have a maximum diameter of approximately 1.25mm and are perfectly preserved as low-Mg calcite with a concentric structure and a fibrous outer rim which is commonly 200-250μm thick. The core is usually of fibrous calcite nucleated on lath-shaped grains now dissolved or, more rarely, occluded by calcite spar. The smaller ooids are 500-570μm in diameter, and are darker and presumably organic-rich with a clotted microspar texture. Compaction has resulted in chemical dissolution along grain contacts, leading to localised concavo-convex contacts. The cement is an inclusion-free calcite spar with a crystal size of up to 150μm. There are also minor patches of haematite.

Interpretation

The excellent preservation of textures in this facies suggests that the precursor carbonate was a low-Mg calcite. This excellent preservation and cement fabric is very similar to that of the carbonates in the overlying Shuram Formation. It could be therefore that this facies actually marks the base of the Shuram Formation.

3.9.3 Facies Association E synthesis

Facies Association E represents an overall deepening in the Huqf region. In the Buah dome area, the lagoonal laminites are overlain be fenestral peloidal-intraclast grainstones that in turn are overlain by cross-bedded ooidal grainstones of the shoal/barrier. In the Khufai dome, ooidal grainstones overlie intermittently exposed intertidal stromatolitic cycles, while in the Mukhaibah dome they overlie intertidal/lagoonal cycles. This indicates overall shallowing followed by a shoreward progradation of facies which is suggestive of a relative increase in water depth.

3.10 KHUFAI FORMATION SYNTHESIS

The sediments of the Khufai Formation display a pattern of deposition consistent with a carbonate ramp setting. Proximal sedimentation took place in the Huqf area to the south and distal sedimentation in the Oman Mountains to the north (Figure 3.3). The basal beds of the Khufai Formation conformably overlie the siliciclastic dominated Masirah Bay Formation in both areas. Initiation of carbonate production may have been related to a reduced siliciclastic influx, possibly caused by either long term sea-level rise or by decreased rates of uplift and/or erosion in the hinterland source area. Basal deposits of the Khufai Formation ramp sequence (Association A) consist of outer-ramp dolostones in the Huqf area and lime-mudstones of the outer-ramp in the Oman Mountains.

In the Huqf area, the overlying Association B suggests a build-up of grainstone shoals in the south with mid-ramp wackestones in the more northern Buah dome area. In the Oman Mountains, Facies Association B represents influxes of intraclast grainstones as storm or higher-energy deposits that disrupted the background lime-mud sedimentation.

Association C is marked by asymmetric cyclicity in the Mukhaibah dome and Khufai dome which suggests relative sea-level rise, leading to aggradation followed by a relatively slow regression. Peritidal cycles are controlled by a number of factors, chiefly, sediment supply combined with subsidence/eustasy and/or relative sea-level change. Although Milankovich-related orbital forcing periodicities have been postulated by many workers as a factor in the formation of peritidal cycles the lack of biostratigraphic or chronostratigraphic control makes it difficult to confirm such controls in the Khufai Formation.

Facies Association D is characterised by the influx of siliciclastic sedimentation in the form of channels that cut across the tidal-flats onto the carbonate ramp. This may be evidence of a

lowered-base level caused by a relative sea-level fall which brought coarse siliciclastics onto the mid-ramp, or the siliciclastics may have been due to deflation and offshore winds. In the Buah dome, these sands are associated with planar, thin laminites of dark and light carbonates of possible lagoonal origin.

Facies Association E consists of ooidal-intraclast grainstones that mark a return to higher energy shoal conditions across the Huqf area.

Thus, the present study has shown that the Khufai Formation does record shallow peritidal deposits across Oman as has been previously reported by earlier workers (Kapp & Llewellyn (1965); Glennie *et al.* (1974) and Rabu *et al.* (1986). In deference to these authors the Khufai Formation of the Oman Mountains is considered here to represents deposition in a deeper, outer-ramp setting (Figure 3.3). Association A in the Huqf area, has been interpreted as intertidal to supratidal deposits by Gorin *et al.* (1982) and as sub-storm wave base ramp deposits by Wright *et al.* (1990); the latter interpretation is more in agreement with observations made during the course of this study.

The Khufai Formation represents a general shallowing-upward carbonate cycle from slope outer-ramp facies of Facies Association A to the cross-stratified grainstones and back-shoal mid-ramp deposits of Association B. Further shallowing occurs in the inner-ramp peritidal carbonate cycles with evaporites and exposure surfaces of Association C in the Khufai dome and Mukhaibah dome that are probably the stratigraphic equivalent of channel sandstones of Association D in the Buah dome. Facies Association E at the top represents a deepening across the whole Huqf area.



Khufai Formation in Mukhaibah dome

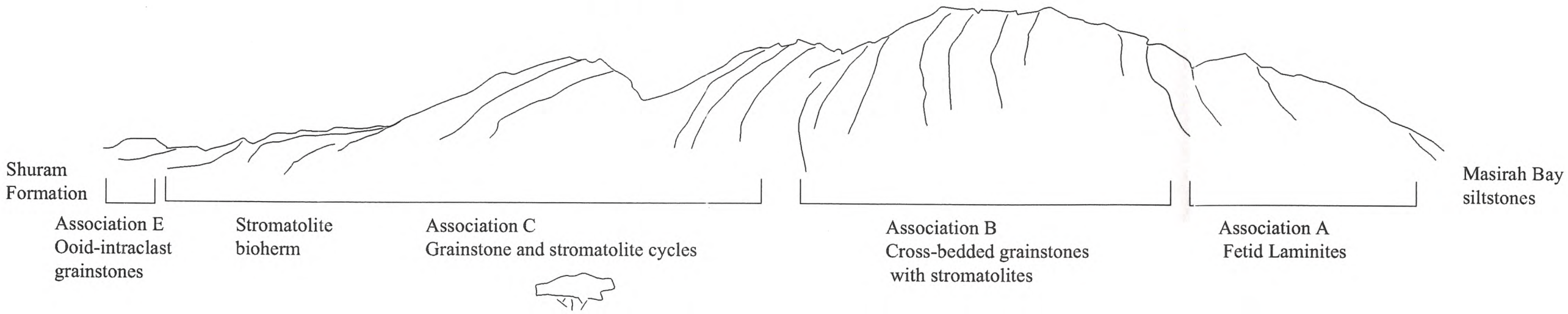


Plate 3.1

Huqf Supergroup exposures in Wadi Hajir,
Oman Mountains



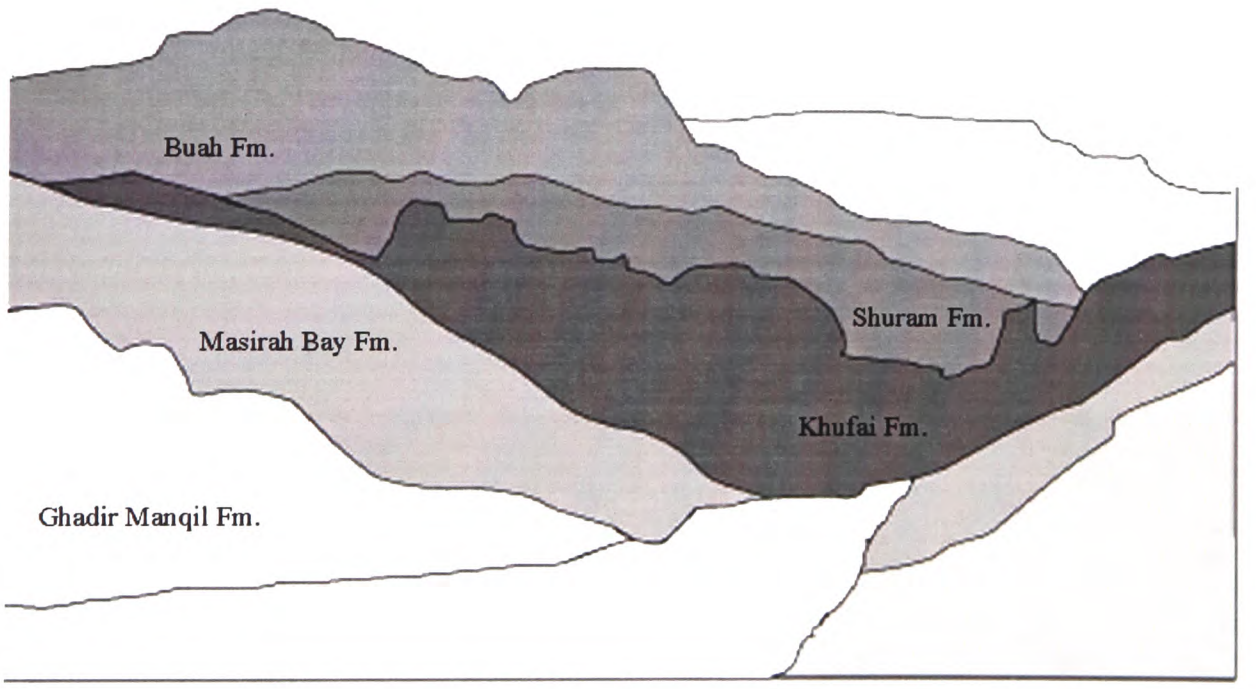


Plate 3.2

Facies Association A in the Huqf area

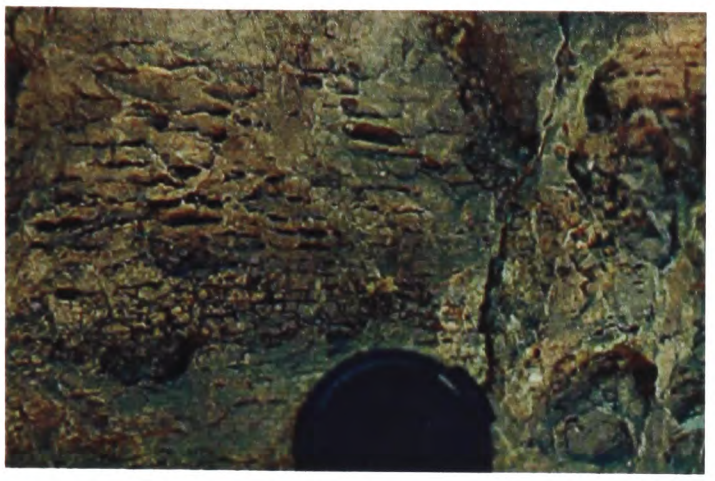


Plate 3.3a Facies A1 fetid dolostones with laminoid fenestrae, subparallel to the lamination
Lens cap 50mm 33m Kd

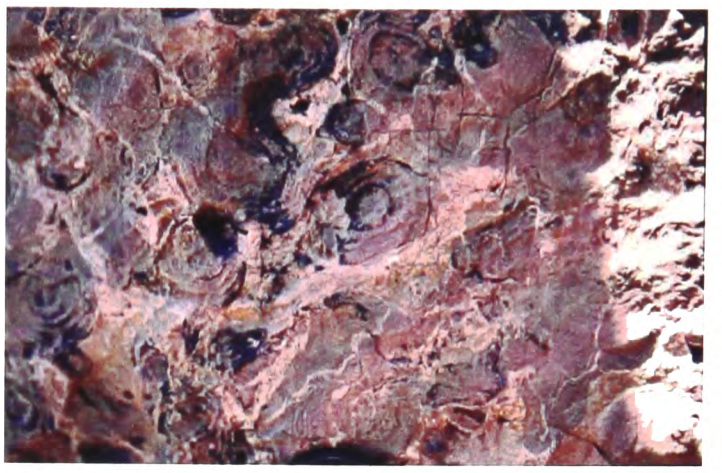


Plate 3.3b Facies A1 fetid dolostones with orbicular structures. Lens cap 50mm 73m Kd.



Plate 3.3c Facies A1 fetid dolostones with in-situ auto-brecciated lamination in the Khufai dome.
Pencil for scale.

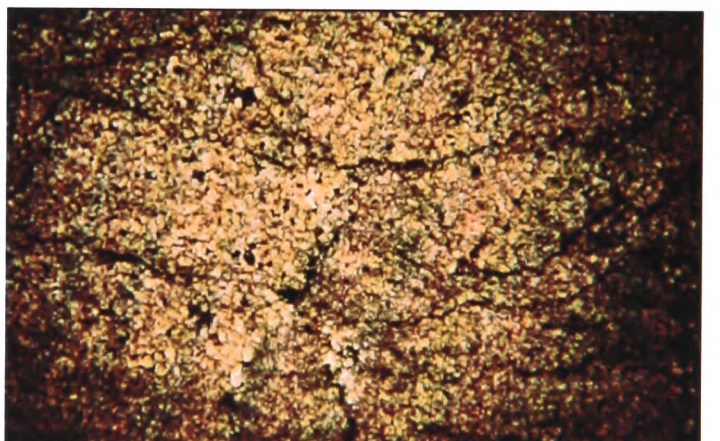


Plate 3.3d Photomicrograph of fetid dolostones (A1) with auto-brecciated lamination of dolomicrospar with minor chert. Horizontal fov. 2.45mm ppl. 98m Md



Plate 3.3e Facies A1 fetid dolostones with isoclinal slump fold at 13m in the Khufai dome
Lens cap 50mm

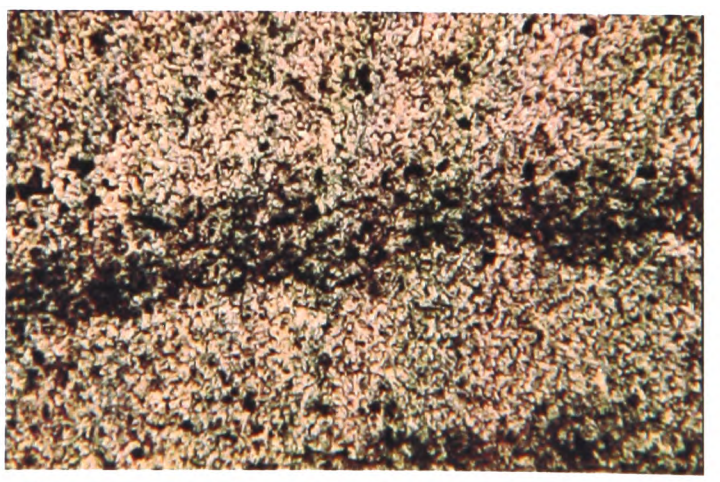


Plate 3.3f Photomicrograph of fetid dolostones (A1) laminites with vermicular dolomicrospar and organic-rich micritic laminations. Horizontal fov. 2.45mm ppl. 71m Kd

Plate 3.3

Khufai Formation in the Oman Mountains

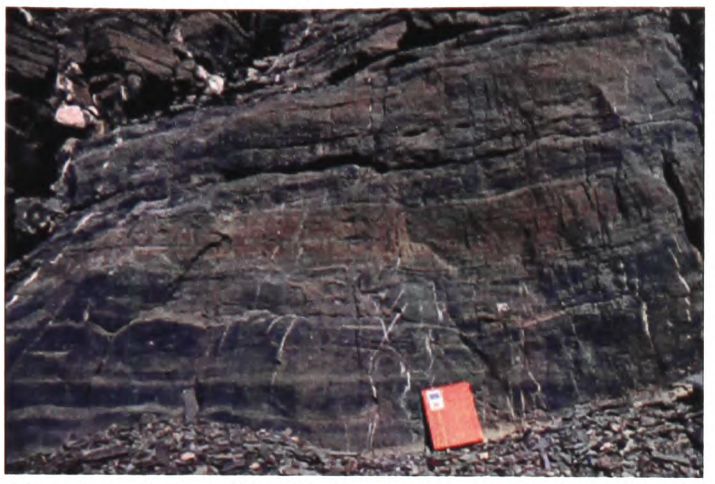


Plate 3.4a Typical Khufai Formation in the Oman Mountains Fetid lime-mudstones (A2) with thin dolostones and grainstone interbeds (brown). Notebook 225x176mm. Wadi Mistal



Plate 3.4b Fetid lime-mudstones (A2) are dark grey with fetid grainstones (B3). Decimetre-scale beds. Wadi Hajir.

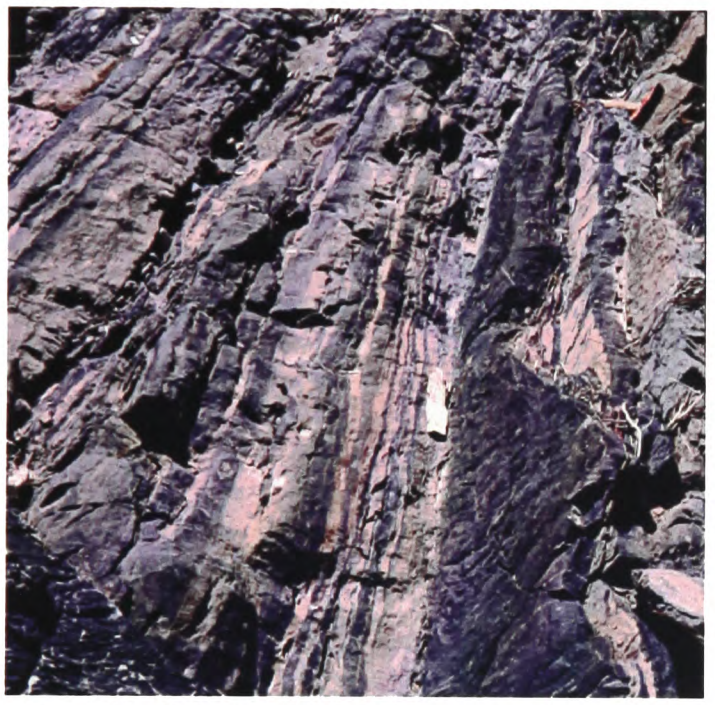


Plate 3.4c Khufai/Shuram contact in Wadi Bani Awf, muddy grey limestones with thin red mudstones and coarse siliciclastic conglomerates (under hammer). Hammer for scale.



Plate 3.4d Khufai/Shuram contact in Wadi Hajir, muddy grey limestones with thin (<30cm) beds of quartz litharenites. Tape measure for scale.

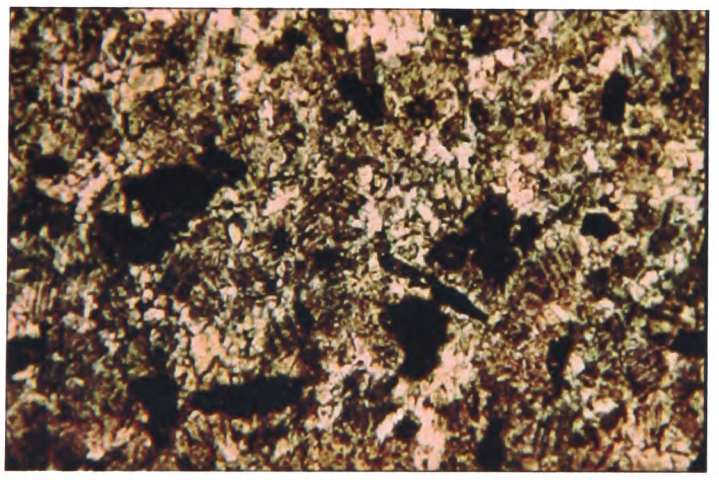


Plate 3.4e Photomicrograph of recrystallized lime-mudstone with micritic intraclasts (B3). Horizontal fov. 2.45mm ppl. 10m Wadi Hajir

Khufai Formation Facies Association B



Plate 3.5a Facies B2b Black and white laminites
Lens cap 50mm 305m Bd

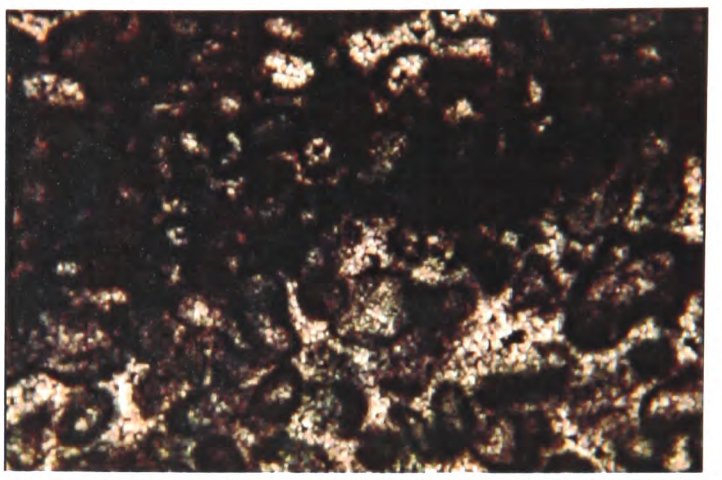


Plate 3.5b Photomicrograph of Facies B1 ooidal grainstone/packstone with hardground surfaces.
Horizontal fov. 2.45mm ppl. 99m Kd



Plate 3.5c Facies B2 fetid peloidal wackestone with swaley cross-lamination. Hammer for scale. 27m Bd

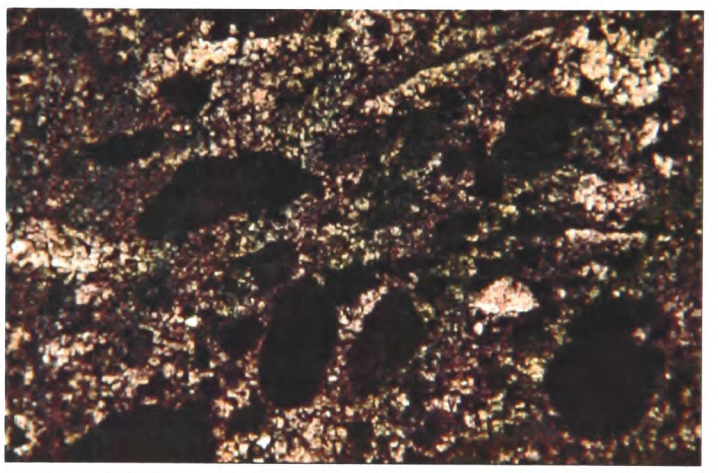


Plate 3.5d Photomicrograph of Facies B2 peloidal wackestone with organic-rich micritic intraclasts and chert nodules.
Horizontal fov. 2.45mm ppl. 59m Bd



Plate 3.5e Facies B2a intraclast conglomerate with muddy dolomitic clasts. Notebook and pencil for scale 293m Bd

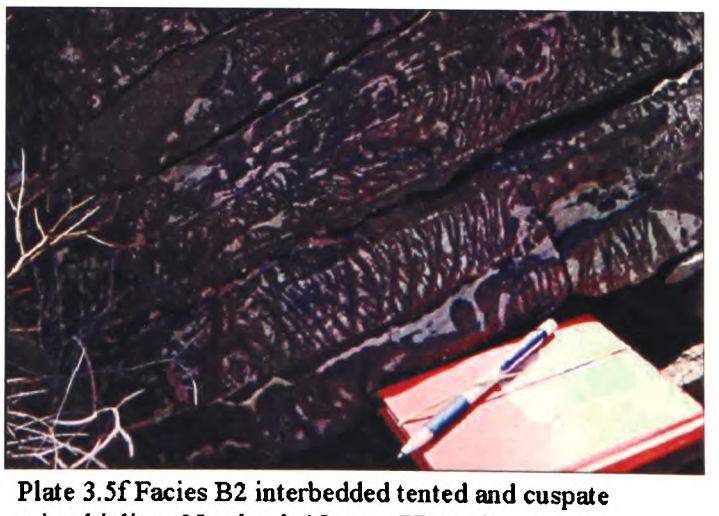


Plate 3.5f Facies B2 interbedded tented and cuspate microbialites. Notebook 15mm. 77m Bd

Facies C Grainstone-stromatolite cycles



Plate 3.6a Facies C in the Khufai dome, where individual cycles estend laterally for up to 5km.
Liz Ross for scale.



Plate 3.6b Facies C cycles are formed of fine-grained grainstones overlain by cherty microbial laminites and stromatolites with teepee structures. Hammer for scale.

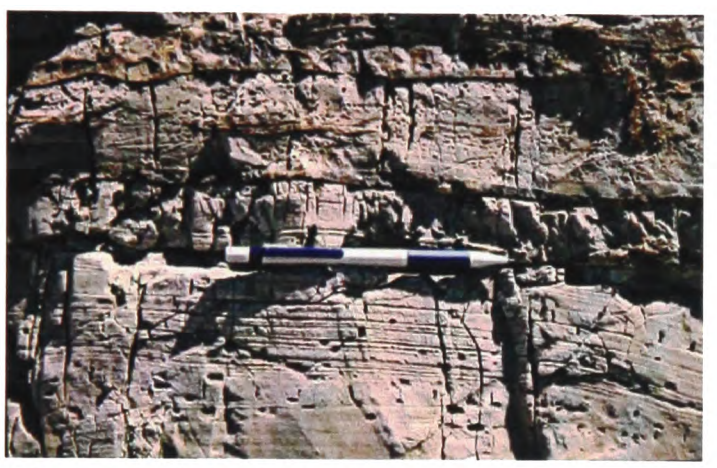


Plate 3.6c Subfacies C1a ooidal-intraclast grainstone, laminated with vugs from mid-to-upper cycle.

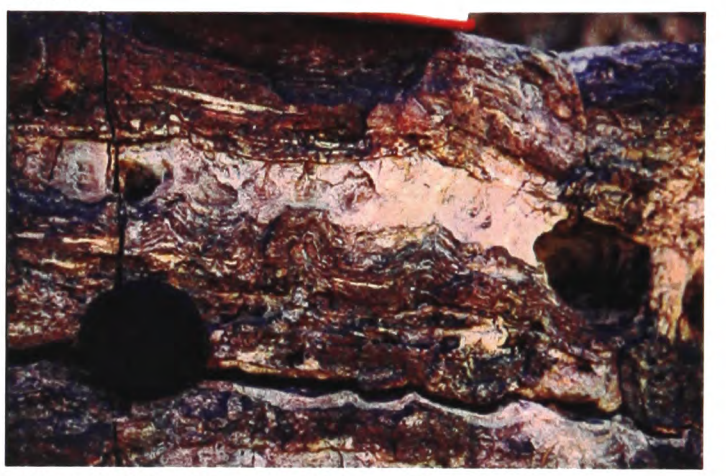


Plate 3.6d Crinkly microbial laminites from the cycle top (Facies C2). Lens cap 50mm 154m Kd
210m Kd



Plate 3.6e Subfacies C2b laterally-linked hemispheroids with flat domes. Lens cap 50mm 196m Kd

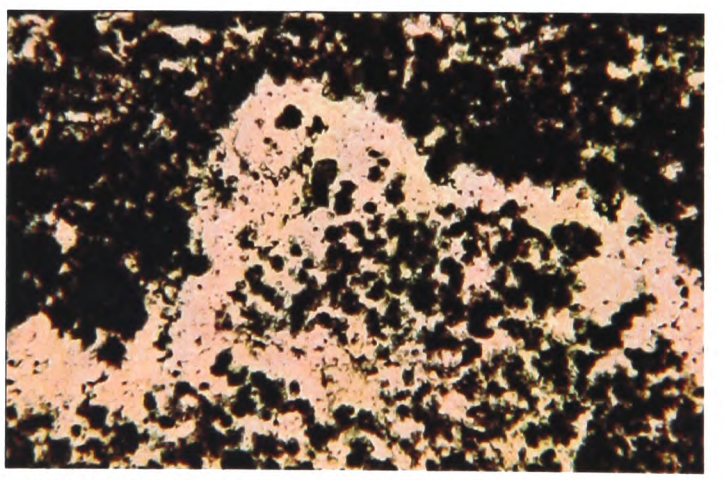


Plate 3.6f Photomicrograph of cherty microbial laminites (C2a) from the cycle top. Horizontal fov. 2.45mm ppl.
171m Kd



Plate 3.6g Subfacies C1b cherty peloidal grainstone with teepee structure. Lens cap 50mm 196m Kd

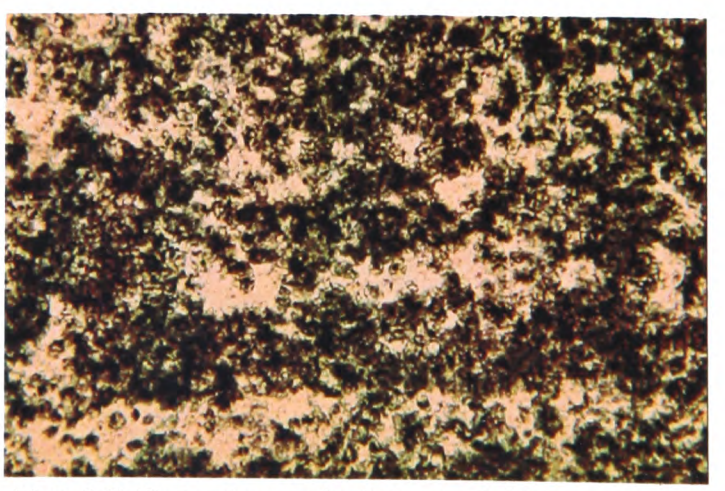


Plate 3.6h Photomicrograph of cherty peloidal grainstone (C1b). Horizontal fov. 2.45mm ppl.
158m Kd

Facies C Grainstone-stromatolite cycles



Plate 3.7a Fenestral laminated grainstone (C1) from the upper part of the peritidal cycles in the Mukhaibah dome. Pencil for scale.



Plate 3.7b Type A stromatolites with smooth, mm laminations forming laterally-spaced-domes (C2c). Lens cap 50mm. 255m Md



Plate 3.7c Type A stromatolites with smooth, mm laminations forming pillow-shaped domes (C2e). Lens cap 50mm. 251m Md

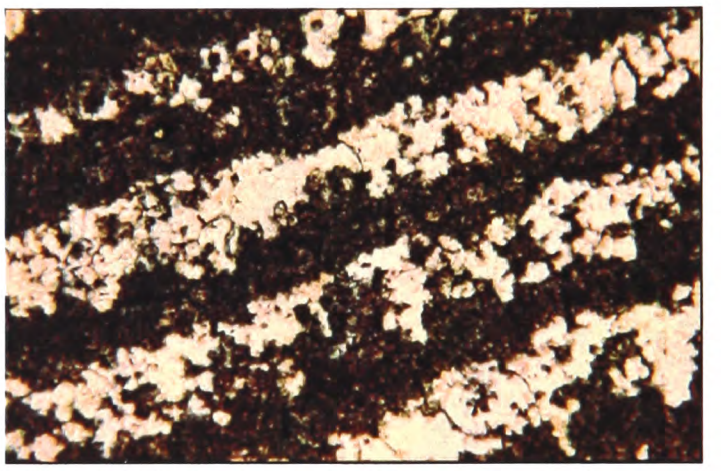


Plate 3.7d Photomicrograph of Type A stromatolite with alternating micrite and clear spar laminae. Horizontal fov. 2.45mm ppl. 235m Md



Plate 3.7e Conophyton stromatolites have a conical shape with an egg-carton appearance on the bedding surface (C2d). Pencil for scale. 192m Md



Plate 3.7f Microbial mats colonize and stabilize wave-ripple lamination overlain by pillow-shaped domes. Pencil for scale. 250m Md

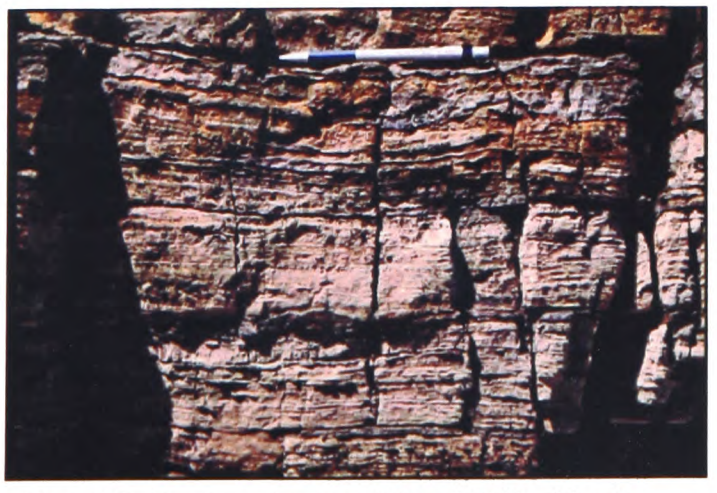


Plate 3.7g Cherty grainstones (C1 and C1b) with minor-scours and swales. Pencil for scale. 261m Md

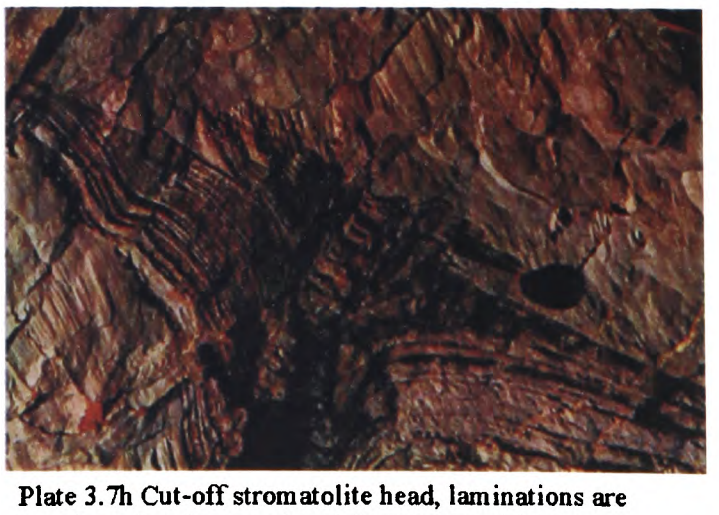


Plate 3.7h Cut-off stromatolite head, laminations are terminated owing to subaerial exposure which lead to desiccation and fragmentation. Lens cap 50mm. 225m Kd

Facies D and E
Uppermost Khufai Formation

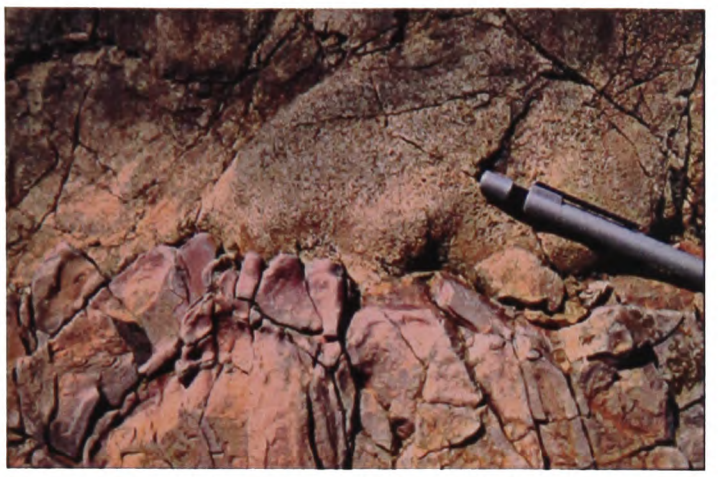


Plate 3.8a Ooidal grainstone (E2) overlain by silty flat-pebble-conglomerate of the Shuram Formation. Khufai/Shuram contact near Nafun in the Md.

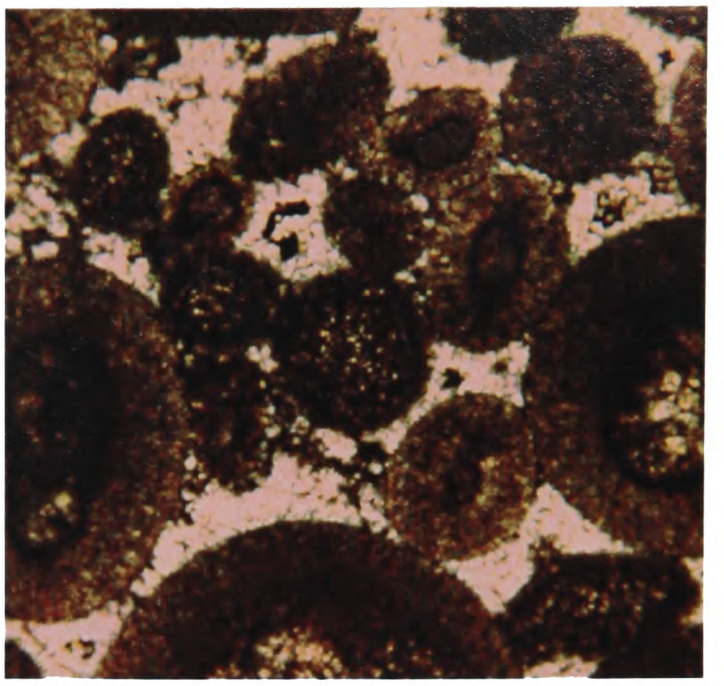


Plate 3.8b Photomicrograph of ooidal grainstones (E2) that are very similar to those of the Shuram Formation. Horizontal fov. 2.45mm ppl. 262m Md



Plate 3.8c Ooidal-intraclast grainstone (E1) with cross-stratification. Notebook 225x176mm 349m Bd

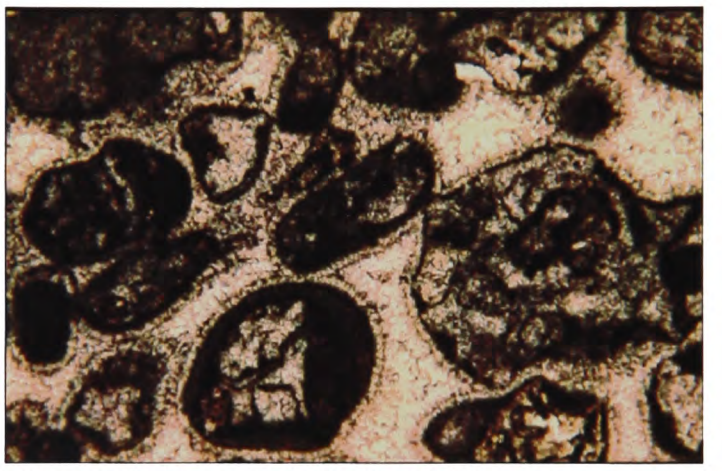


Plate 3.8d Photomicrograph of ooidal-intraclast grainstones (E1) with fringe cement and late calcite spar. Horizontal fov. 2.45mm ppl. 350m Bd



Plate 3.8e Peloidal-intraclast grainstone (E1b) with auto-brecciated laminations and fenestrae. Lens cap 50mm. 346m Bd

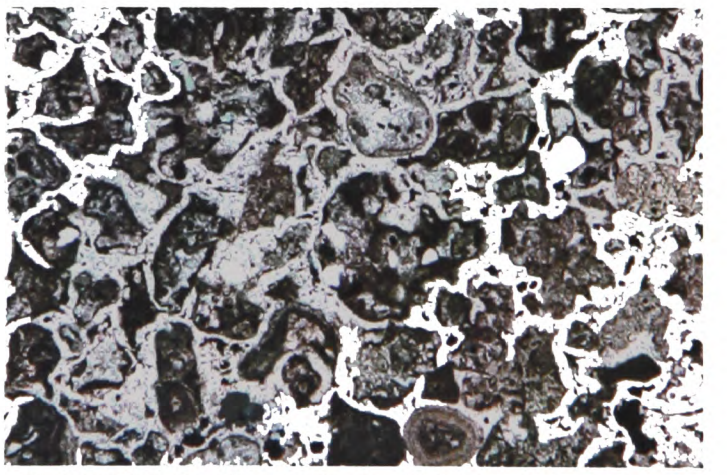


Plate 3.8f Photomicrograph of ooidal-intraclast grainstones/packstone (E1) with fringe cement. Horizontal fov. 2.45mm ppl. 351m Bd



Plate 3.8g Peloidal-intraclast grainstone (E1b) with climbing wave-ripples. Lens cap 50mm. 339m Bd

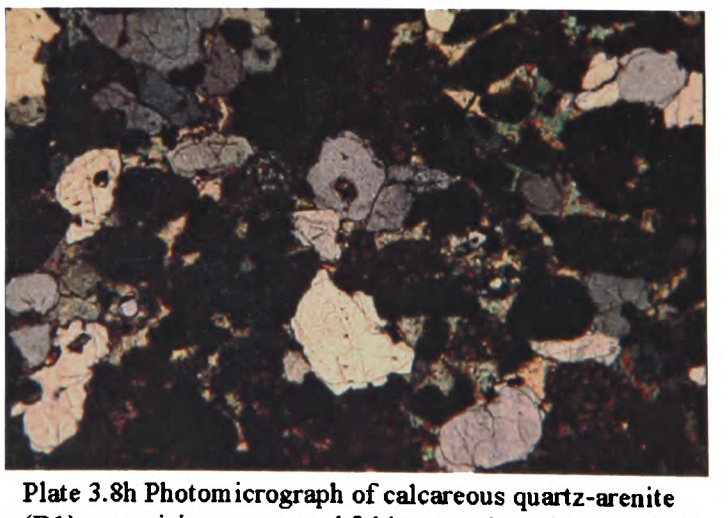


Plate 3.8h Photomicrograph of calcareous quartz-arenite (D1) comprising quartz and feldspar grains with syntaxial overgrowths and detrital peloids within a carbonate cement. Horizontal fov. 2.45mm xpl. 272m Bd

Chapter Four - Shuram Formation

4.1 INTRODUCTION

4.2 METHODS

4.3 PREVIOUS WORK

4.4 SUBDIVISION OF THE SHURAM FORMATION

4.5 LOWER MEMBER OF THE SHURAM FORMATION

4.6 MIDDLE MEMBER OF THE SHURAM FORMATION

4.7 UPPER MEMBER OF THE SHURAM FORMATION

4.8 SHURAM FORMATION SYNTHESIS

4.1 INTRODUCTION

In the Huqf area, the siliciclastics of the Shuram Formation are discontinuously exposed and form low-lying topography (Plate 4.1a) whilst in the Oman Mountains, the sediments have undergone tectonic deformation resulting in pencil-cleaved siltstones forming extensive topography (Plate 4.4a). Two separate type sections have been defined for the Shuram Formation, one in Wadi Shuram in the Huqf area (Kassler 1965) and another in Wadi Mi'aidin in the Oman Mountains (Kapp & Lewellyn 1965). The Shuram Formation in the Oman Mountains has been termed the Mi'aidin Formation after the type section locality at Wadi Mi'aidin. The name Mu'aydin Formation was introduced by Rabu *et. al.* (1986) as this spelling is derived from the officially accepted transliteration of the Arabic. In the present study, priority is given to the term 'Shuram Formation' which will be used for both the Huqf area and the Oman Mountains. The lower and middle members of the Shuram Formation have been defined, during this study, from sections in the Huqf area near Nafun in the Mukhaibah dome area and Wadi Shuram, whereas the upper member of the Shuram Formation has been defined in Wadi Aswad.

In the Huqf area, the basal red and green siliciclastics of the Shuram Formation contrast greatly with the underlying ooidal grainstones of the Khufai Formation. This contact is only exposed in the Nafun area of the Mukhaibah dome (Plate 4.1a). In the Oman Mountains, the Khufai/Shuram contact is best seen in Wadi Bani Awf and in Wadi Bani Kharus where the fetid limestones of the Khufai Formation are overlain by coarse conglomeratic sandstone beds that are interbedded with fetid muddy limestones that grade-up, locally, to organic-rich shales (Log in Appendix 4).

Kassler (1965) separated the Shuram Formation into two well-defined parts, the lower part being made up of fissile red-brown argillaceous siltstones to silty shales while the upper part is characterised by the intercalation of thin limestones. These were described therein as recrystallized peloidal-ooidal grainstones and fissile silty and micaceous lime-mudstones with flat-pebble conglomerates. Kassler considered the boundary between the Shuram Formation and the Buah Formation to occur at the base of continuous beds of dolomite. Wright *et. al.* (1990) and Gorin *et. al.* (1982) considered the upper boundary of the Shuram Formation to be marked by the disappearance of siltstone intercalations, which is the criterion followed in the present study.

The aim of this chapter is to characterise the sediments of the Shuram Formation in both the Huqf area and the Oman Mountains, to establish regional facies variation, and to develop a comprehensive model accounting for depositional dynamics. Figure 4.1 is a summary log giving an overview of the lower, middle and upper members of the Shuram

Formation as defined in the present study. Detailed lithological logs are in Appendix 4 while the plates are at the back of the chapter.

4.2 METHODS

The lower and middle members of the Shuram Formation were logged in the Mukhaibah dome area where there is complete exposure. Further observations were made at other localities to establish regional variation and palaeocurrent trends (Figure 4.3). The upper member of the Shuram Formation was logged in detail in Wadi Aswad and further studies were made in the Mukhaibah dome and Wadi Shuram for lateral thickness variations within the siltstone/carbonate cycles. In the Oman Mountains, observations were made through the sections with lithological logs recorded from the lower and upper members in Wadi Bani Awf. Representative facies samples were collected for petrographic and microfacies examination.

4.3 PREVIOUS WORK

Most previous workers (Kassler 1965; Hughes Clark 1988; and Gorin *et. al.* 1982) have recognised two units in the Shuram Formation of the Huqf area (Figure 4.2). These workers interpret their lower Shuram Formation siliciclastics to represent low-energy marine deposits whilst the overlying grainstones of their upper Shuram Formation represents the progressive development of higher-energy shoal environments.

Dubreuilh *et. al.* (1992) recognised three units within the Shuram Formation of the Huqf area, with the lowermost siltstones representing proximal marine deposition and the middle member of convoluted siltstones with interbedded oolites representing transgressive deposits. Their uppermost member comprised purple-to-green claystones-siltstones and pale-grey oolitic limestones which were taken to mark a return to proximal and occasionally emergent conditions.

Kapp & Llewellyn (1965) and Rabu *et. al.* (1986) measured between 500m and 800m of Shuram Formation in the Oman Mountains where the stratigraphy is highly deformed. Rabu *et. al.* (1986) defined three units: their lowermost unit is about 50m thick and comprises mauve siltstones with rust coloured sandstone interbeds; the middle unit is approximately 700m thick and is formed of homogenous millimetre-laminated mauve to green siltstones; and the uppermost unit is 50m thick and marked by an influx of centimetre-thick beds of intercalated carbonates. These carbonates thicken-upward and grade into the overlying Buah Formation. These earlier workers concluded that the Shuram Formation of the Oman Mountains represents a typical tidal-flat/littoral sequence.

Shuram Formation

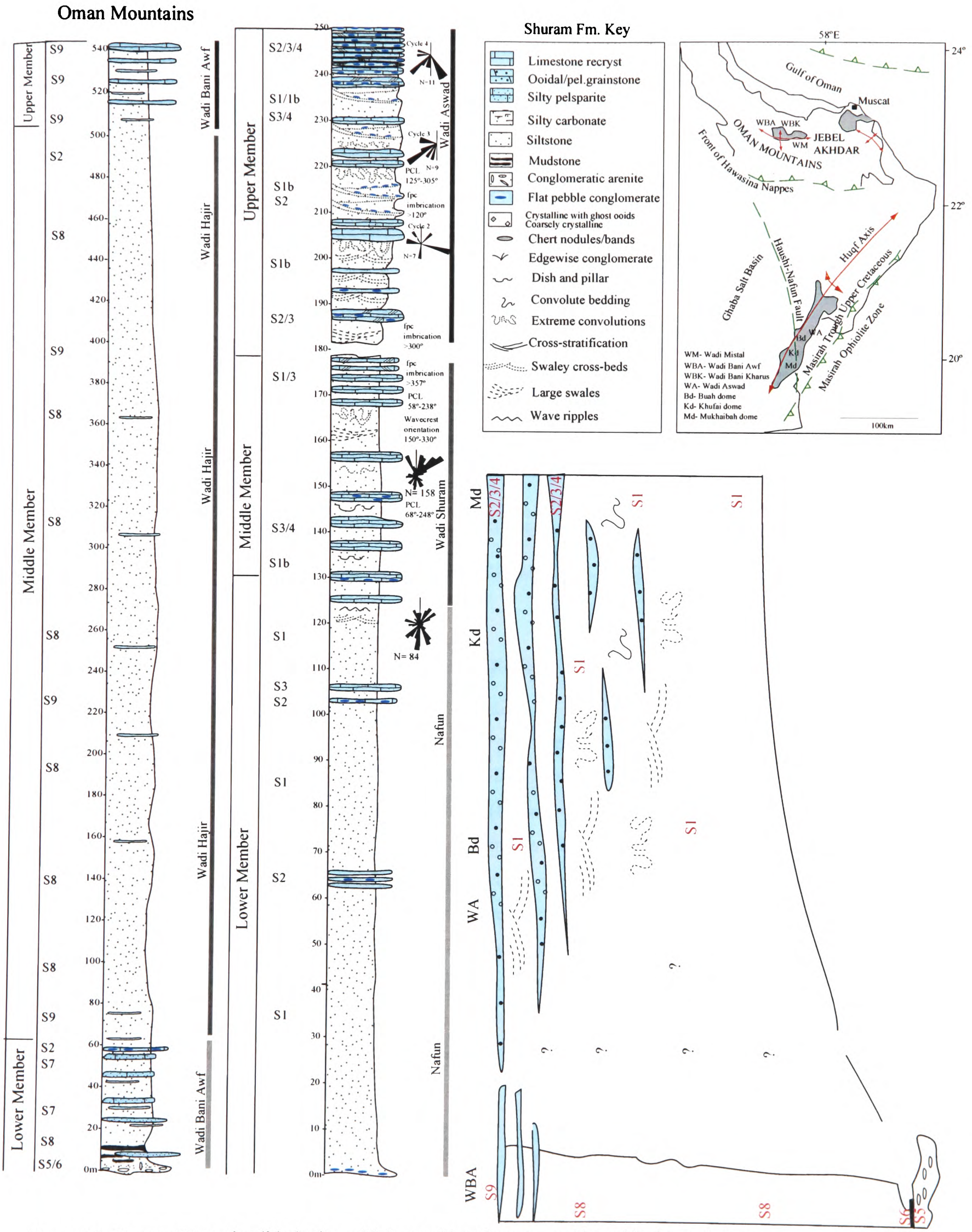


Figure 4.1 Shuram Formation lithologies, with key and location map and lateral facies variation.

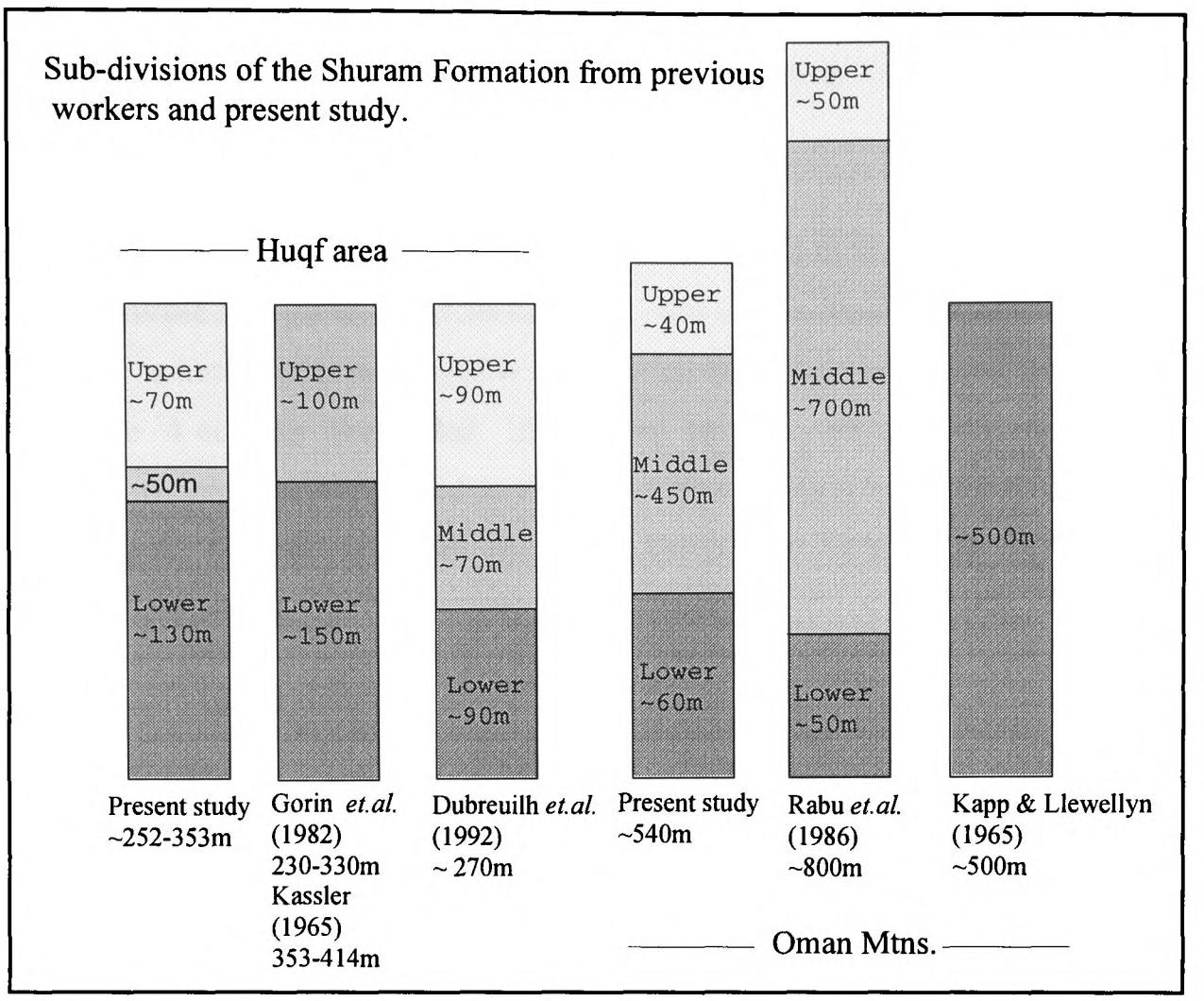


Figure 4.2 shows the subdivisions of the Shuram Formation from the present study as well as those defined by previous workers.

4.4 SUBDIVISION OF THE SHURAM FORMATION

In the present study, the Shuram Formation is divided into lower, middle and upper members based on lithological character and facies associations that are considered to have environmental significance. In the Huqf area, the lower member is best exposed in the Nafun area of the Mukhaibah dome (Figure 4.1) where it is seen to comprise red-brown and green siltstones and buff sandstones. The middle member occurs after about 130m of section and is chiefly characterised by an increase in current activity in the form of swaley cross-lamination, wave and current ripples and dewatering structures. There is also an increase in the number of thin limestone interbeds in the upper part of the middle member (Figure 4.1). The upper member is marked by thicker carbonate beds containing cross-stratified grainstones that are interbedded with siliciclastics and silty carbonates to form asymmetric siliciclastic-carbonate cycles. The siliciclastic content progressively diminishes toward the base of the overlying Buah Formation.

In the Oman Mountains, the basal Shuram Formation is locally conglomeratic with 2-3m thick beds of coarse calcarenites and quartz sandstones containing rafted limestone blocks of the underlying Khufai Formation. In Wadi Bani Awf, these are overlain by

approximately 10m of organic-rich shales (Log in Appendix 4). Elsewhere in the Oman Mountains the lower member, which is approximately 60m thick, comprises siltstones with thin centimetre-scale carbonate interbeds and thin sandy limestone beds up to 50cm thick.

In Wadi Hajir the middle member is up to 500m thick, and is formed of very planar, very homogenous purple and green siliciclastics with rare carbonate interbeds (Plate 4.4b). The upper member is about 40m thick and is marked by thin carbonate interbeds that thicken upwards (Plate 4.4c). In the Wadi Bani Awf section, seven asymmetric cycles of siliciclastics-carbonates are recorded at the top of the Shuram Formation (Plate 4.4d). As in the Huqf area, the contact with the Buah Formation is marked by a reduction in conspicuous siliciclastics.

The Shuram Formation lithologies are very homogenous and laterally persistent. Changes in sedimentary regime are marked by sedimentary structures and the relative proportions of the different lithologies present. Table 4.1 shows the facies of the Shuram Formation with facies S1 to S4 being described from the Huqf area and facies S5 to S9 described from the Oman Mountains. In the Huqf area, the lower member of the Shuram Formation comprises, for the most part, red and green siltstones (S1), with minor influxes of flat-pebble conglomerates (S2), and silty pelsparites (S3). The middle member comprises the same facies but there is greater evidence for current activity and disruption of bedding. The upper member of the Shuram Formation is composed of the same three facies with cross-stratified oosparites (S4) becoming the more dominant lithology.

Shuram Formation Facies			
Facies	**Lithology**	**Structures**	**Interpretation**
Oman Mountains			
S9	Recrystallized limestones		
S8	Siltstones	Starved ripples	Below wave base
S7	Sandy limestone	Cross-lamination	
S6	Organic-rich lime-mudstones		Below wave base
S5	Conglomeratic quartz-litharenites	Scours, graded-beds	
Huqf area			
S4	Oosparites	Cross-bedding, stylolite	Shoal
S3	Pelsparites	Cross-lamination	Shoal
S2	Flat-pebble conglomerates	Scour bases	
S1	Red and green siltstones	Dewatering structures	Below wave base
S1b	Carbonate cemented siltstones	Swaley cross-beds	

Table 4.1 Shuram Formation facies and sub-facies for the Huqf area and the Oman Mountains. These facies are described from the base of the section upwards in more or less stratigraphic order.

In the Oman Mountains, conglomeratic quartz-litharenites (S5) and organic-rich lime-mudstones (S6) occur at the base of the Shuram Formation in Wadi Bani Awf and in Wadi Bani Kharus. They have a combined thickness of about 10m. The lower member in the Oman Mountains contains thin beds of sandy limestones (S7) and flat-pebble conglomerates. The middle member is composed of planar bedded siltstones (S8) with very minor recrystallized limestones. The upper member shows a gradual increase in limestone intercalations that grade upward into the overlying Buah Formation.

4.5 LOWER MEMBER OF THE SHURAM FORMATION

4.5.1 Huqf area

The most continuous exposure of the lower member of the Shuram Formation occurs in the Mukhaibah dome near Nafun where its contact with the underlying Khufai Formation can be observed. Overlying the ooidal grainstones of the Khufai Formation is a few centimetre thick unit of grey silty carbonate and flat-pebble conglomerates which are overlain by the characteristic red-brown siliciclastics of the lower member. There is no evidence for a significant erosional break at this transition from ooidal grainstones to silty carbonates and siliciclastics. The influx of fine-grained siliciclastics which flooded the Khufai carbonate platform (Plate 4.1a) may be a response to a rapid rise in sea level.

The lower member of the Shuram Formation is approximately 130m thick and comprises Facies S1, red and green very fissile and finely laminated siltstones, that are with no evidence for current activity (Log in Appendix 4). After deposition of approximately 100m of very homogenous fine-grained siliciclastics, very minor influxes of silty peloidal carbonates and flat-pebble conglomerates occur.

4.5.2 Facies S1: Red and green siltstones

Facies S1 is very striking in the field as it forms low-lying outcrops with a strong red-brown colouration and predominates in the lower member of the Shuram Formation (Plate 4.1c). In the lower-part of the member this facies is laminated on a mm-scale and weathers into fissile plates with a crumbly texture.

In thin-section (Plate 4.1f), this facies comprises quartz and feldspar grains that are sub-angular and up to 100μm in size with abundant grains of muscovite and biotite and some chlorite. Well-rounded zircon and rutile grains occur along with glauconite within an iron clay-rich matrix (Adams *et al.* 1984).

4.5.2a Sub-facies S1b: Carbonate-cemented siltstones

These comprise more resistant, less fissile siltstones which are green-grey to red in colour and occur in the uppermost part of the lower member of the Shuram Formation. They are millimetre-laminated with local swaley cross-lamination.

In thin-section (Plates 4.1e/4.3e), the carbonate-cemented siltstones are normally graded with sub-angular quartz and feldspar grains, up to 100μm in size, and numerous mica grains. The laminae are between 300μm and 1mm thick. There are rounded detrital zircon, rutile grains and opaques. Some samples contain phosphatic fragments and others, in the upper part of section, contain glaucony. Iron-rich micritic peloids occur and are sometimes concentrated along the lamination. The cement is formed of recrystallized inclusion-rich sparry iron-poor calcite

Interpretation

The lateral continuity and homogenous nature of the finely laminated siltstones of the basal 130m of the lower member of the Shuram Formation (Figure 4.1) suggests deposition in a low-energy marine environment.

The red colouration reflects the liberation of oxidised Fe^{3+} from ferrous silicates such as biotite, amphibole and pyroxene which leads to the formation of authigenic haematite resulting in red beds (Turner 1978). The precipitation of authigenic haematite can only occur in oxidizing conditions (Garrels & Christ 1965) which is dependent upon the rate of organic productivity, the rate of surface oxidation of organic matter and the overall sedimentation rate. The green interbeds (Plate 4.1c) may reflect periodic water stagnation with no currents or turbulence to aerate the environment so that iron may have remained reduced. This could have increased alkalinity and enhanced $CaCO_3$ precipitation, so that the green bands could then become more carbonate-rich.

Authigenic glaucony is quite abundant in the silty carbonates of Facies S1b. Glaucony tends to form at the sediment water interface and is associated with organic matter and generally positive but fluctuating Eh conditions. Glauconitization occurs in a semi-confined micro-environment, sufficiently confined to allow concentration of ions and crystal growth not possible in open seawater (Odin & Letolle 1980).

Phosphatic grains occur within Facies S1 and S1b and are thought to result from vertical mixing of deeper water with the waters of the shallow shelf which leads to an increase in temperature of the deeper water and, in consequence, waters of deep-sea origin became phosphate supersaturated. Phosphate precipitation occurs in shallow-marine

environments where iron, organic compounds and relatively oxidizing conditions are necessary for its genesis (Odin & Letolle 1980).

The association of phosphatization and glauconitization may indicate a warm climate which would facilitate the temperature changes required for the former and the liberation of large amounts of iron from the continents that are required for the latter. Their combined occurrence might also indicate a relatively condensed sequence (Sheldon 1980; Jenkyns 1997).

4.5.3 Oman Mountains

The basal Shuram Formation in the Oman Mountains is characterised by an influx of coarse quartz-arenites, with locally graded conglomeratic interbeds (Log in Appendix 4). In Wadi Hajir, these coarse quartz-arenites form beds up to 40cm thick within dark organic-rich limestones. In Wadi Bani Awf and Wadi Bani Kharus, these coarse quartz-arenites form beds up to 3m thick and contain rafted clasts of dark limestone up to a few metres in diameter. These coarse conglomeratic beds are both normally graded and reverse-graded. In Wadi Bani Awf and at Hadash village, the coarse quartz-arenites are overlain by black organic-rich shales, whilst elsewhere the overlying sediments comprise green and purple siltstones. These siltstones are millimetre-centimetre bedded, finely laminated to micro-lenticular, slightly micaceous quartz-siltstones with minor shales. They contain subordinate sandy recrystallized limestones in beds up to 2cm thick, many of which pinch out laterally. Within these sandier beds some evidence for low-angle cross-lamination was observed. Starved ripples were observed in the sandier beds and minor flat-pebble conglomerates occur within the carbonate beds.

4.5.4 Facies S5: Conglomeratic litharenites from the Oman Mountains

In Wadi Bani Kharus and Wadi Bani Awf and to a lesser extent in Wadi Hajir and at Hadash village, the well indurated black limestones of the top Khufai Formation are immediately overlain by decimetre-scale recrystallized limestones with thin red-clay interbeds and conglomeratic quartz-litharenites. In Wadi Bani Awf (Log in Appendix 4), the conglomeratic litharenites form four beds between 1 and 3m thick with rafted Khufai limestone clasts up to a few meters in diameter. Conglomeratic litharenite beds have scour bases and pinch-and-swell laterally. The lower-part of some beds fine-up whilst the upper-part coarsens-up. Laterally, in Wadi Hajir and at Hadash Village, this facies is much thinner and finer-grained, forming brown-weathering beds on a decimetre scale.

In thin-section, this facies comprises black organic-rich limestone intraclasts with cream and brown micritic and stromatolitic intraclasts with detrital quartz grains within a microspar matrix. The sub-rounded quartz grains contain numerous micro-inclusions and

are up to 1mm in diameter. Often, these grains have corroded outlines and are partially replaced by calcite spar. Detrital organic-rich, micritic, stromatolitic and ooidal intraclasts also occur and these are up to 3mm in size. There are many pyrite grains which are up to 300μm in diameter. These detrital grains are matrix-supported within a partially recrystallized microspar.

4.5.5 Facies S6: Black heterolithic limestones

Dark organic-rich limestone with thin red-clay interbeds alternate with the coarse conglomeratic litharenites and comprise beds on a few centimetres scale that have sharp planar contacts. These recrystallized limestones become more sandy upward resulting in more heterolithic facies. Locally, they contain isoclinal fold and slump structures with traces of low-angle cross-lamination and have irregular scour and undulating contacts.

Thin-sections of these black limestones reveal varying amounts of organic matter, pyrite and detrital silts within a micritic or microspar matrix. Many samples comprise laminations of sub-centimetre scale that are typically planar but can have micro-scour bases. Some of these laminae are formed of iron-rich peloids that fine upward. Some have sub-millimetre thick detrital laminae with quartz grains up to 100μm in size. Most are formed of micrite with minor detrital silt-grade quartz, feldspars and micas. Numerous pyrite cubes and framboids occur with some authigenic quartz. Some micro-stylolites occur whilst iron-rich surfaces with different lithologies above and below are more akin to erosional hardgrounds. Vugs and veins are occluded by calcite spar or quartz. Upward this facies becomes much more organic-rich with a greater clay component.

Sub-facies S6b: Organic-rich shale

Above the uppermost conglomeratic litharenite bed the limestones become very organic-rich and shaley attaining a thickness of approximately 15m before the return of 'normal' sedimentation in the form of purple and green siltstones. The organic-rich shales are very black, recessive and fragmented by calcite veins.

In thin-section, these are formed of very dark, organic-rich, micritic limestones with minor detrital feldspar and quartz grains up to 500μm in size along with abundant euhedral pyrite. Some samples have thin sheared quartz veins.

Interpretation

Black, fetid, organic-rich limestone was the background sedimentation within the Oman Mountains in late Khufai times. The limestones are pyritic with variable amounts of peloids, micrite and microspar recrystallization. The influx of conglomeratic litharenites

represents the first influx of Shuram Formation siliciclastics onto the Khufai Formation outer-ramp. These thick beds with scour bases and large clasts of the Khufai-type limestones therefore represent erosion of the Khufai ramp. Stromatolitic and ooidal grainstone intraclasts, as well as rafted clasts of facies S6, suggest erosional reworking of adjacent lithologies. The lateral change in thickness of these conglomeratic beds may indicate that these are localised flows that thin laterally.

The interbedded limestones represent the background sedimentation. The upward increase in black organic-rich shales suggests a relatively deeper water with increasing anoxia along with the presence of abundant organic matter leading to the formation of pyrite.

4.5.6 Lower member of the Shuram Formation synthesis

The red and green siliciclastics of the Shuram Formation represent a sharp change in depositional regime from the carbonates of the Khufai Formation. They are interpreted as low-energy shallow marine deposits based on the homogenous nature of the sediments and the lack of sedimentary structures except for planar bedding. The thin flat-pebble conglomerate interbeds represent periods of higher energy, possibly storm events. The red and green colouration of these sediments suggests fluctuating Eh and pH conditions in the depositional and diagenetic environments.

In the Oman Mountains, the influx of conglomeratic litharenites containing reworked clasts of Khufai limestone represents redeposition of submarine eroded sediments. Owing to the discontinuous exposure it is difficult to discern whether the variable thickness within the Khufai Formation here results from depositional lateral variation or from erosional downcutting. This conglomeratic transgressive lag deposit is overlain by black shaly carbonates possibly representing a condensed horizon. The rest of the lower Shuram Formation in the Oman Mountains comprises purple and green siltstones formed in a low-energy shallow marine environment.

4.6 MIDDLE MEMBER OF THE SHURAM FORMATION

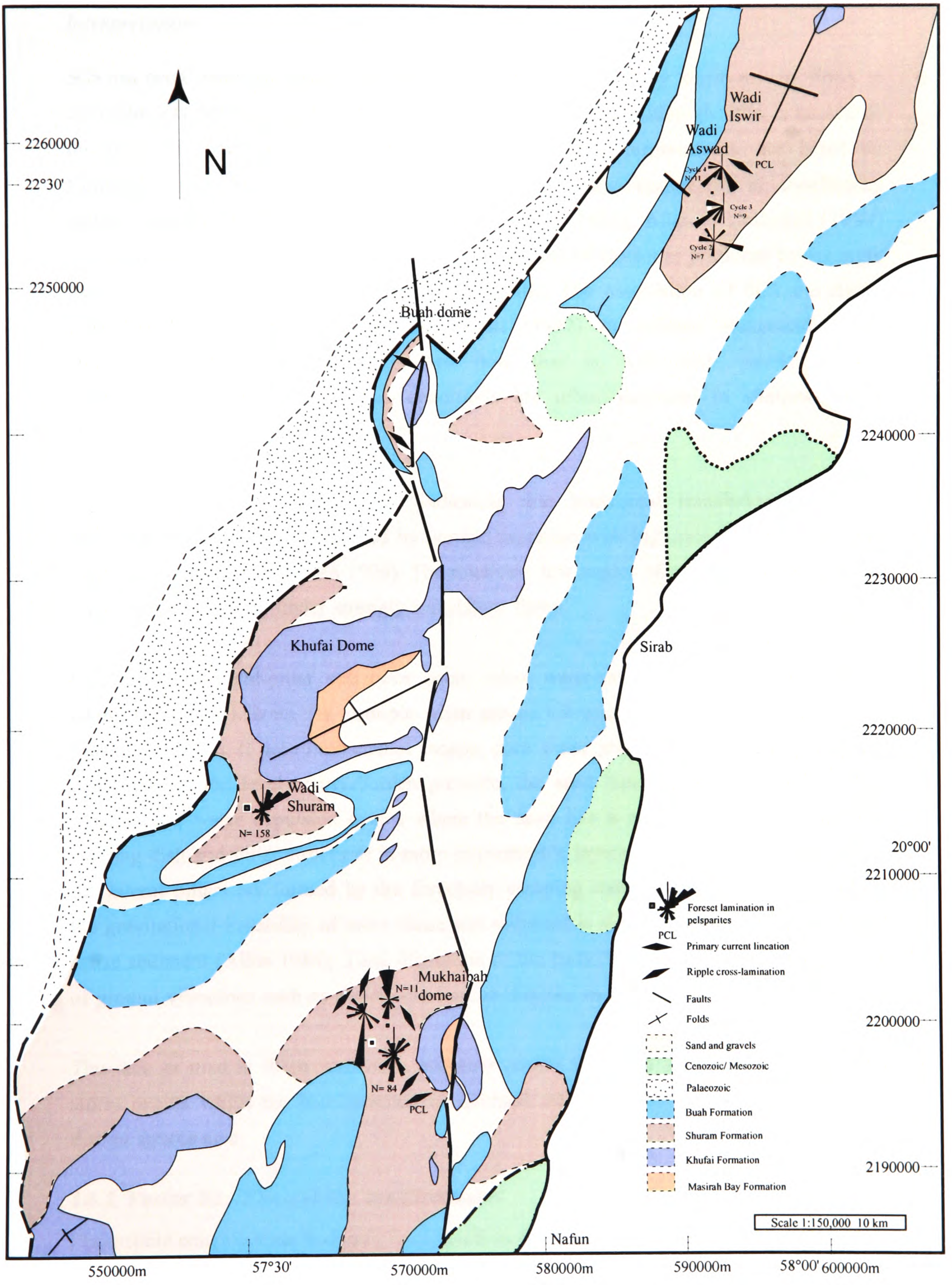
4.6.1 Huqf area

The middle member of the Shuram Formation is approximately 20-50m thick and is marked by a dramatic increase in sedimentary structures within the red and green siltstones of Facies S1. Thin (<50cms) carbonate interbeds occur comprising cross-stratified oosparite and pelsparite with minor flat-pebble conglomerates (Plates 4.2a/f). In the Mukhaibah dome area, Facies S1 is observed to contain swaley cross-stratified (SCS)(Cheel & Leckie 1993) beds overlain by climbing wave-ripples (Plates 4.2c/e)(Allen

1968). The sandstones are characterised by broad concave-up depressions or swales with wavelengths of up to 5m. The bounding surfaces of the swaley cross-set margins are erosional yet very low angle, <10°. The basal swale laminae are generally concordant with the lower bounding surface (Plates 4.1c/d) and are typically less than 50cm deep. No discernible grain size change has been detected across the set boundaries and the only evidence for a coarse lag is in the form of thin flat-pebbles that, locally, line the lower bounding surfaces. Hummocks were rarely observed. Palaeocurrent analysis of these structures was thwarted by the fact that they were never observable in three dimensions. However, flat-pebble imbrication indicates rather variable transport directions chiefly to the north, northeast and northwest.

Climbing wave-ripples and sinusoidal/trochoidal wave-ripples are interbedded with planar laminations and overlie SCS beds. Ripple sets attain a thickness of a few centimetres and wavelengths of a few decimetres. Most have suffered stoss-side erosion whilst rare sigmoidal laminae occur (Plate 4.2d). Some ripple sets are intercalated with plane beds whilst others are intercalated with undulating accretionary laminations (Plate 4.2c). Angles of climb, where measurable, were roughly between 13° and 18°. Ripple foreset laminae, measured from Nafun, give a palaeoflow direction to the southwest. Near Sedrah, ripples have a RI of 9-10 and a palaeoflow direction measured from foreset laminae of 081°-261°. A ripple index of 10 which can be either wave or current derived (Allen 1968) were observed at a number of locations. Trochoidal and sinuous to straight-crested wave-ripples preserved on the bedding surfaces of fine-grained sandstone have dominant wave-crest orientations between 120° and 160°, indicating a wave propagation direction of approximately SW-NE. This is supported by primary current lineations, which although rarely observed, indicate a NE/SW palaeoflow direction (Figure 4.3).

Soft-sediment deformation structures and dewatering dish-and-pillar structures are ubiquitous. Convoluted laminations are typically between a decimetre and 2m thick, with the former being the most common. Dish-and-pillar structures from a few centimetres up to 1m in diameter (Plate 4.1b/c/h) are the most dominant deformation structure. The dishes are flat, sub-horizontal and concave-upwards and appear to be formed of more carbonate-rich sediments (S1b) whilst the pillars are thin, sub-vertical and typically comprises Facies S1. Plate 4.1b shows how dewatering along the pillar has buckled the overlying laminae to create an antiformal structure. Load casts a few-cm deep were observed at the boundary of green siltstones overlying red siltstones. Some of the structures are observed to result from loading of coarser sands into the horizontally laminated siltstones. The tops of some of these dish and pillar structures are locally eroded by the swaley cross-laminations above. Massively contorted beds occur locally demonstrating wholesale deformation of the bedded sediments (Plate 4.1g).



Schematic map with palaeocurrent measurements from the middle and upper members of the Shuram Formation

Figure 4.3

Interpretation

SCS has been described and interpreted as a structure formed by storm-driven flows in environments between the lower shoreface and the foreshore. Although little is known of the physical conditions that produce SCS, most early interpretations are based on similarities with hummocky cross-stratification and their association in shoaling-up marine successions (Walker 1982, McCrory & Walker 1986). Allen & Underhill (1989) interpreted SCS from the Bencliff Grit, (Upper Jurassic) of Dorset as produced by strongly translatory flows that are not environment specific. The association of SCS and ripple cross-stratification was interpreted by Arnott (1992) to indicate compound cross-stratification generated under combined flow, that is, with both oscillatory and unidirectional components. These conditions are often produced in shallow-marine environments during storm events.

Climbing wave-ripples (Plate 4.2c) indicating that horizontal translation was more important initially but was replaced by vertical accretion with high rates of net deposition during waning currents (Allen 1970). The relatively low angles of climb recorded suggests rapid ripple migration under strongly translatory flows.

Dewatering dish-and-pillar structures occur when water-saturated sand is subjected to lateral pressure gradients, for example when ground vibrations are caused by water waves passing overhead. If pore fluid cannot escape, pore water pressure will increase and when it approaches the level of overburden pressure, the sand liquefies (Leeder 1982). After liquefaction, water expulsion occurs where the sand has a connection to the surface, creating dish-and-pillar structures in more impermeable layers that form the dishes whilst the lateral pillars are formed by the forcefully escaping water. Load casts are caused by the gravitational instability of more dense wet sediment is superimposed on a layer of less dense sediment (Allen 1984). Total disruption of the beds (Plate 4.1g) is probably a result of ground vibrations such as the effect of an earthquake shock.

The lack of mud in these sediments probably results from the recurrent winnowing by storm events whilst the homogenous fine-grained nature of the sands suggests a rather distant source area.

4.6.2 Facies S2: Flat-pebble conglomerates

Flat-pebble conglomerate beds and lenses such as those shown in Plate 4.3b are ubiquitous throughout the Shuram Formation. They can occur intercalated with, but predominately overlie, ooidal and peloidal grainstones to form beds up to 30cm thick, but more often they form thin lenses that pinch-out laterally. Flat pebbles are deposited along erosional

scours and along swales within the siltstones of Facies S1 (Plate 4.2a). The pebbles are flat, rounded to elliptical in shape, typically between 0.5mm and 10cm in size and 0.5-1cm thick. These pebble-beds are grey to red-purple in colour and the pebbles, despite their plate-like shape, are rarely broken or bent. They are generally poorly sorted and randomly orientated or with a preferred orientation of long axes on the bedding plane, and vertically-stacked to flat-lying in cross-section (Plate 4.2b). On some bedding surfaces the pebbles are within a very glaucony-rich carbonate.

Thin-section analyses show the flat pebbles are formed of laminated silty peloidal grainstones identical in fabric and composition to Facies S4. The outer margin of the pebbles is often iron-stained and rich in opaques. The pebbles also contain numerous opaques and glaucony pellets. The matrix is generally a peloidal or ooidal grainstone/wackestone where the ooids have a thin isopachous fringe cement.

Interpretation

The pebbles from the flat-pebble conglomerate are clearly derived from Facies S3 and therefore represent reworking of early lithified thin limestone beds. Early lithification of these sediments was probably enhanced by: *(a),* slow rates of sedimentation and general lack of movement of bottom sediments; *(b),* presence of a sufficient reservoir of seawater supersaturated with respect to $CaCO_3$ (which may have been enhanced by bacterial production of bicarbonate below the oxidising zone in the sediments) and *(c),* presence of a suitable substrate, specifically porous and permeable carbonate grainstones. Sepkoski (1982) suggests these deposits would also need to be protected from immediate current reworking. The presence of authigenic glaucony, believed to form during periods of slow sedimentation, would support this view.

Early lithified thin beds may have been ripped up during storm events and subsequently redeposited. Storm reworking is also indicated by the fact that flat-pebble conglomerates line erosional channels within the siliciclastics of Facies S1.

4.6.3 Oman Mountains

About 60m above the Khufai/Shuram Formation contact the lithologies become a monotonous green and purple siltstone which is heavily cleaved with local intense shearing. Beds are folded, some are overturned, and a crenulation cleavage is ubiquitous. Minor coarsely crystalline quartz veins occur. The homogenous nature of this lithology makes it difficult to decipher the extent of folding and possible repetition of section but the thickness is estimated to be approximately 450m based on the section in Wadi Hajir.

Numerous hours were spent in search of trace fossils within these lithologies but they have yielded nothing.

4.6.4 Facies S8: Green and purple siltstones

The green and red/purple siltstones from the Oman Mountains are very homogenous and are heavily cleaved. In outcrop, they have very planar, centimetre-scale bedding forming alternating green and purple bands that weather-out into thin pencils (Plates 4.4a/b). Sub-millimetre scale fine and coarse banding is evident in thin-sections. The purple siltstones do not contain porphroblasts but are generally fine-grained with hints of normal grading (Plates 4.4e/f). The green siltstones are rich in chlorite porphyroblasts within a fine-grained quartz, feldspar and micaceous matrix (Plates 4.4g/h).

4.6.5 Middle member of the Shuram Formation synthesis

SCS indicates deposition from a high suspended load which, along with the large size of the swales in the middle member, probably reflects storm-driven transport on the shoreface. Flat-pebble imbrication along swales suggest the dominant palaeoflow was to the northwest. Wave-ripples were most likely generated on the sea bed as the translatory storm-driven currents waned, or in fairweather periods.

The common occurrence of soft-sediment deformation and dewatering-structures might suggest rapid sedimentation. This interpretation is, however, contradicted by the omnipresence of glaucony within the carbonate interbeds. The soft-sediment deformation structures, therefore, probably result from pulsating pore pressures caused by the frequent storm events and/or seismic shaking. The intermittent carbonate sedimentation possibly occurred during lulls in the terrigenous input which enabled the establishment of a carbonate factory. The low-angle cross-stratification within the pelsparites suggests a relatively high-energy environment of deposition.

The middle member of the Shuram Formation, therefore, represents an increase in turbulence and current velocities on the shallow shelf, especially in the form of storm events. The relatively thin carbonate interbeds represent sediment reworking, possibly from a nearby shoal.

4.7 UPPER MEMBER OF THE SHURAM FORMATION

4.7.1 Huqf Area

The upper member of the Shuram Formation is intermittently exposed across the Huqf area where it is dominated by siliciclastic-carbonate cyclicity (Log in Appendix 4). The thickest exposure of the upper Shuram Formation, approximately 70m, is at Wadi Aswad

(Plate 4.3a) where cycles can be traced laterally for some kilometres. Thinner cycles occur in Wadi Shuram, in the Mukhaibah dome area and at the Buah dome.

Within the upper member these siliciclastic-carbonate cycles thicken upwards (Log in Appendix 4) and a progressive increase in the thickness of the interbedded carbonates also occurs. The contact with the overlying Buah Formation is characterised by a decrease in siliciclastic input relative to carbonate, as well as a change in the carbonate character.

The siliciclastic part of the cycles is composed of red and green siltstones (S1 and S1b) that are swaley-cross laminated with local climbing wave-ripples and minor soft-sediment deformation structures. The carbonates comprise peloidal grainstones and ooidal grainstones with varying amounts of silts. These are cross-stratified with decimetre-scale bimodal cross-sets and are intensely stylolitised and glauconitic (Plate 4.3c). Flat-pebble conglomerates form thin interbeds and are observed to cap most of the cycles (Plate 4.3b). Flat-pebble conglomerates also occur within channel structures that scour into the underlying siliciclastics and line the bases of swales (Plate 4.2a).

4.7.2 Facies S3: Silty pelsparite

Pelsparites occur as tabular units overlying the recessive siltstones of Facies S1 and are intercalated with oosparite facies and flat-pebble conglomerates. They are generally purple-grey coloured and often contain medium-scale cross-stratification. In hand specimen, they have a mottled texture and when they are intercalated with flat-pebble conglomerate they often impart a green colouration.

In thin-sections (Plate 4.3e), the peloids are micritic and between 50 to 200μm in diameter often with irregular outlines and packed with skeletal inclusions. Some of the peloids have discoidal to prolate ellipsoid shapes. Some samples contain small radial ooids and grain aggregates. Many contain variable amounts of siliciclastics with detrital-rich laminae composed of silt-grade quartz, feldspars and micas with minor rutile, tourmaline and zircons grains. Sometimes the siliciclastics occur as discrete laminae but are also dispersed throughout the sample. Opaques are abundant, as is authigenic glaucony. Micro-stylolites commonly cause sutured grain contacts. The cement is an inclusion-free, equant, xenotopic mosaic of sparry carbonate. Some peloids have undergone dissolution and reprecipitation which has resulted in only relict fabric preservation (Plates 6.2g/h).

Interpretation

The irregular shapes and diverse sizes of the peloids and the occurrence of ooids and grain aggregates suggest that these represent 'pseudopellets' formed of carbonate mud that has been reworked by water currents. This interpretation is supported by the presence of flat-

pebble conglomerates of the same facies which suggests early lithification at the sediment-water interface followed by subsequent reworking. These particles therefore represent 'small intraclasts', an interpretation supported by the presence of cross-stratification and interlaminated siliciclastics. Glaucony is considered to form during periods of relatively slow sedimentation which is in accordance with shallow-water environments and restricted sedimentation associated with the pseudopeloids described by Carss and Carozzi (1965).

4.7.3 Facies S4: Oosparite

Ooidal grainstones are a minor component of the carbonate units above the recessive siltstones. Oosparites are generally green-grey coloured and interbedded with peloidal grainstones and flat-pebble conglomerates.

In thin-sections, the ooids are dark-brown micrite with diameters between 0.3-1mm. Ooids are both radial and concentric but dominantly radial. Cores are often recrystallized with numerous micro-inclusions. Many of the ooids have a central core of columnar calcite crystals with a 'radial-with-dark-rays' fabric and an outer cortex of 'radial-concentric' fabric. Some of these cortical radial fibrous crystal fans have a radial undulose extinction whilst others have an extinction cross (Plate 4.3d). In some samples, this cortex is not developed on the ooid cores giving a pseudo bimodal texture (Plates 4.3d/f). Some ooids are perfectly spherical but many of the ooids are squashed and have sutured contacts with micro-stylolites common. A fitted fabric where the ooids have a rhombic shape is locally observed. Oosparites contain variable amounts of detrital quartz, feldspars and mica grains that are sub-angular, silt-grade and occur both in thin laminae and randomly in the interstices between ooid grains. The cement changes from sparry calcite with crystals up to 50μm in size to micrite. In some samples, ooids have an acicular fringe cement often associated with hardground surfaces.

Interpretation

The outward radiating aggregates of fibrous crystals are similar to ooids from the Great Salt Lake (Sandberg 1975) and other primary radial ooids. Similar Holocene oolitic sediments are forming today in protected Persian Gulf lagoons where ooids are moved only during storms, and sustained low-energy periods allow the precipitation of thick radial oolitic cortexes (Loreau & Purser 1973). The excellent state of textural preservation of the Shuram Formation ooids suggests that they were formed of low-Mg calcite rather than aragonite (Tucker 1985). Flat-pebble conglomerates also provide evidence for early cementation beneath the sediment-water interface, a process which, in addition to mechanical compaction, may have resulted in the fitted fabric preserved in some of the ooids. The pseudo-bimodal texture (the presence of populations of small and

large ooids) in some samples is considered a reflection of growth state rather than different areas of origin. The preservation of a thin fringe cement would suggest shallow-marine cementation whilst the inclusion-free equant sparry cements are possibly early diagenetic with meteoric influence. The occurrence of detrital silts within the cements suggest mechanical infiltration prior to or coeval with the early cementation.

Most Phanerozoic ooids form on platform-margin shoals. Facies S4 occurs, however, in thin layers quite dissimilar to large oolitic shoals, suggesting that these are allochthonous and possibly brought onto the siliciclastic shelf during storms. Alternatively, they may represent thin prograding wedges of a local carbonate shoal, with the ooids having precipitated from local basin waters *in situ*.

4.7.4 Oman Mountains

In the Oman Mountains, the upper member of the Shuram Formation is best seen in Wadi Bani Awf where the transition with the Buah Formation is exposed along the wadi floor. The upper member of the Shuram Formation here is approximately 50m thick, and is composed of siliciclastics with centimetre-scale interbeds of recrystallized limestones. At the transition into the Buah Formation thicker siliciclastic-carbonate cycles occur. These comprise nine asymmetric cycles (Plate 4.4d) (from 2m to 8m in thickness) with siliciclastic bases overlain by recrystallized limestones with minor edgewise flake-breccias. Rare occurrences of symmetrical wave-ripples were observed within some of the fine-sandstone beds. The base of the Buah Formation is marked at the base of the first thick carbonate unit.

4.7.5 Facies S9: Recrystallized limestones

Recrystallized limestones occur as thin beds (cm-scale) within the purple and green siltstones of the upper member of the Shuram Formation of the Oman Mountains (Plate 4.4c). These grade upward into the black limestones of the Buah Formation. Thin-sections reveal that they are composed of recrystallized calcite spar.

Interpretation

The pervasive recrystallization of these limestones makes an environmental interpretation very difficult. The lack of structures formed by current activity would indicates a relatively quiet environment. These recrystallized limestones grade-up into the black limestones of the Buah Formation which might suggest that these are more distal deposits similar to the black laminites of Facies E1 (Chapter 5).

4.7.6 Upper member of the Shuram Formation synthesis

Wave-ripple cross-lamination and primary current lineations from Facies S1 record palaeoflows in a NE-SW and a NW-SE directions (Figure 4.3). This upper member is marked by an increase in carbonate interbed thickness. These are dominated by silty pelsparites with ubiquitous low-angle cross-lamination giving highly variable current directions (Figure 4.3). This variation may result from shoreline irregularity or deposition during storm events.

The cycles of the upper member of the Shuram Formation are characterised by relatively thick basal siliciclastics with swales and convoluted bedding overlain by silty pelsparites and oosparites which have erosional bases and are capped by flat-pebble conglomerates. This coarsening-up sequence is very similar to those described by Markello & Read (1981) from the Appalachians which contain interlayered silty muds, storm-reworked parallel and hummocky laminated silts with thick beds of shoreface cross-bedded sands that occur as progradational sheets and lobes that fine seaward. These prograde during storms when sediments are transported and deposited in deeper-water environments. In a similar manner, the Shuram Formation carbonates may have formed by progradation of sandy sheets and lobes over the shoreface siltstones. Some conglomerate caps might have formed during subsequent storms by erosion of the previous storm-deposited silty carbonates that had become cemented at or near to the sediment-water interface. The scattered nature of the Shuram Formation exposure and the lack of marker horizons makes it difficult to map the lateral continuity of the carbonate interbeds throughout the area. However, the general thickening upward of the carbonates would reflect a progressive shoaling-up into the basal Buah Formation.

4.8 SHURAM FORMATION SYNTHESIS

The fine clastics of the lower member of the Shuram Formation in the Huqf area represent a sharp change from the underlying shoal carbonates. In the Oman Mountains, the fetid limestones are interbedded with conglomeratic sandstones overlain by shaley carbonates that are considered to represent transgressive deposits overlain by *mfs* shales. The open shelf fine sandstones of the lower Shuram Formation therefore were deposited within early HST.

The storm-dominated deposits of the middle member of the Shuram Formation could well reflect a different climatic regime in which the shelf was being traversed by tropical storms and hurricanes (Spjeldnaes 1981; Walker 1990). The increase in carbonate preservation in cycles in the upper member of the Shuram Formation into the Buah Formation suggests a progressive shoaling upward. The increasing thickness of cycles

upwards through the upper member indicates that accommodation space continued to be generated and was filled by plentiful sediment supplies from the Shuram landmass.

Lower and Middle Members of the Shuram Formation



Plate 4.1a Khufai Fm. carbonates in the foreground are overlain by Shuram Fm. siliciclastic representing a parallel unconformity at Nafun, south of the Md.

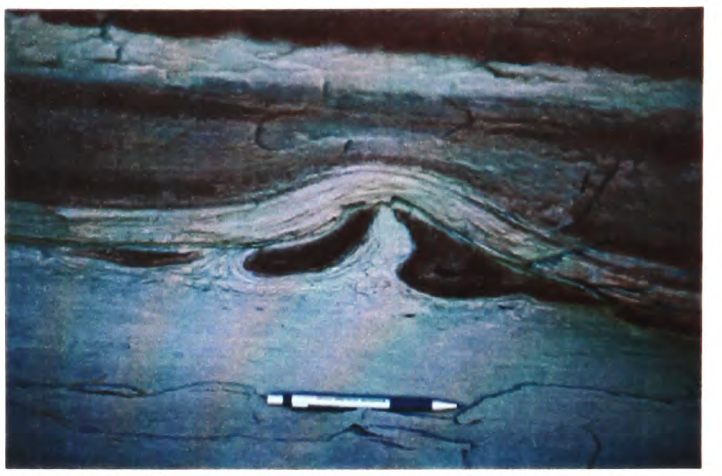


Plate 4.1b Lithofacies S1 red and green siltstones with dish-and-pillar structures. Pencil for scale. Md

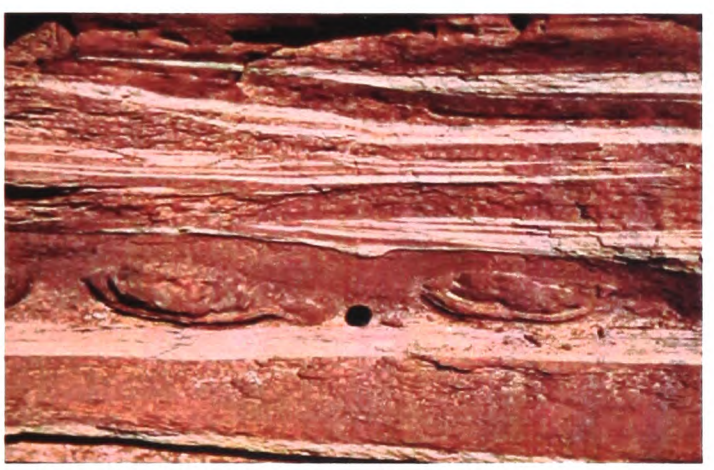


Plate 4.1c Lithofacies S1 and S1b red and green siltstones with dish-and-pillar structures overlain by swales. Lens cap 50mm. Wadi Shuram

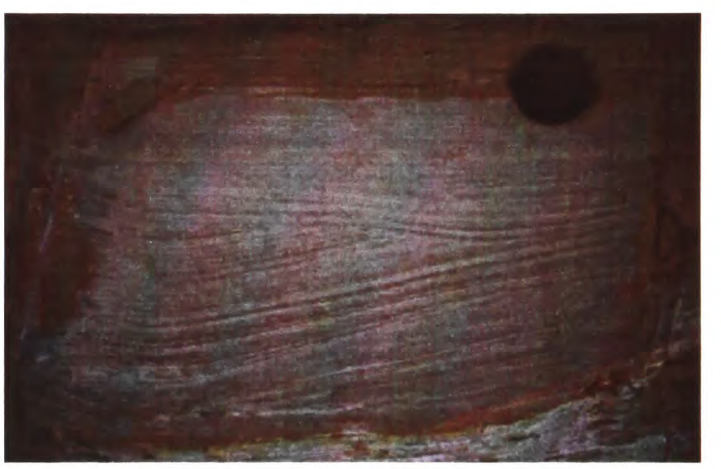


Plate 4.1d Lithofacies S1 red and green siltstones swaley cross-stratification. Lens cap 50mm. Khaluf

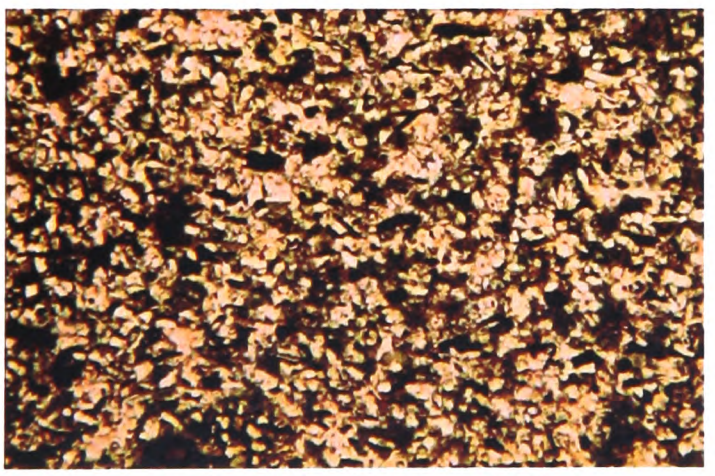


Plate 4.1e Carbonate cemented siltstone (S1b) with quartz, feldspar, mica grains and glauconite and pyrite. Horizontal fov. 2.45mm. ppl. 198m WA

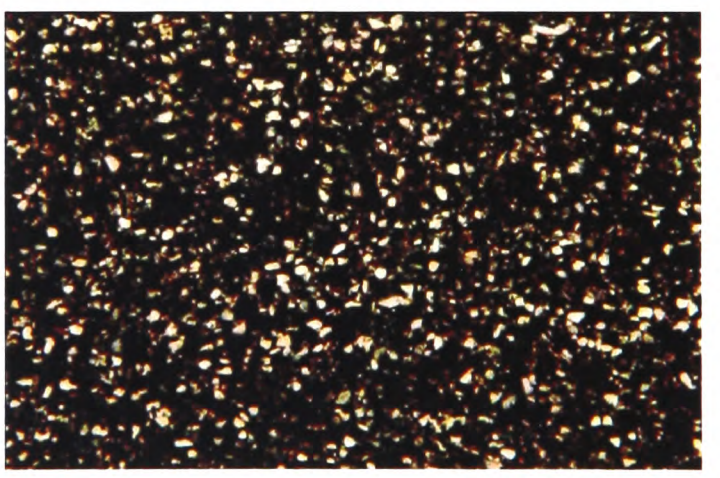


Plate 4.1f Red and green siltstone (S1) with quartz, feldspar, mica grains within an iron-clay rich matrix. Horizontal fov. 2.45mm. xpl. 238m Bd

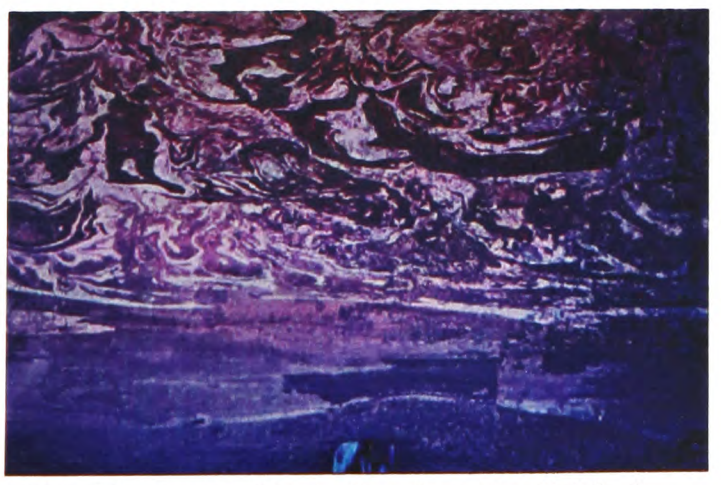


Plate 4.1g Contorted laminations formed by fluidized flow within Facies S1. Backpack for scale. 203m Wadi Aswad

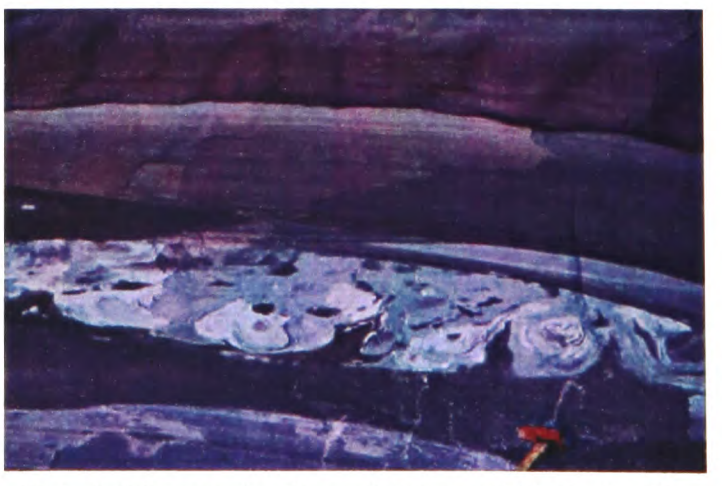


Plate 4.1h Dewatering flame structures within Facies S1. Hammer for scale. Md

Plate 4.1

Middle Members of the Shuram Formation



Plate 4.2a Flat-pebble conglomerate (S2) form channel fill. Hammer for scale. West of Nafun.



Plate 4.2b Profile view of Flat-pebble conglomerate (S2) bed in the Buah dome. Lens cap 50mm.

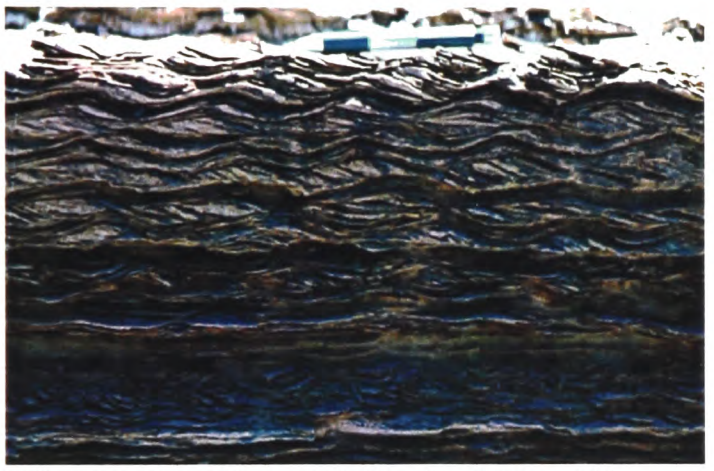


Plate 4.2c Accretionary and migration ripples within Facies S1, red and green siltstone near Nafun. Pencil for scale.

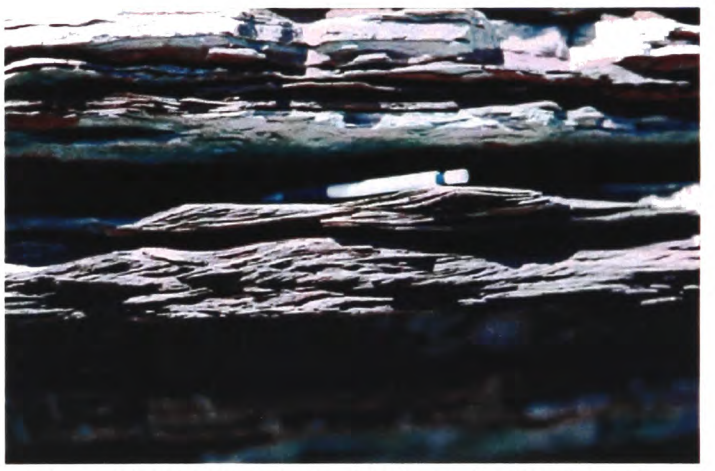


Plate 4.2d Climbing ripples within Facies S1, red and green siltstone near Nafun. Pencil for scale.

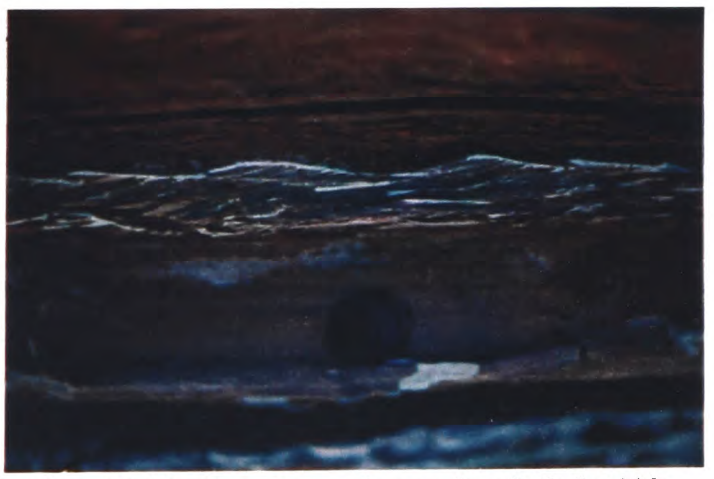


Plate 4.2e Ripples with very low angles of climb within Facies S1, red and green siltstone near Nafun. Lens cap 50mm.

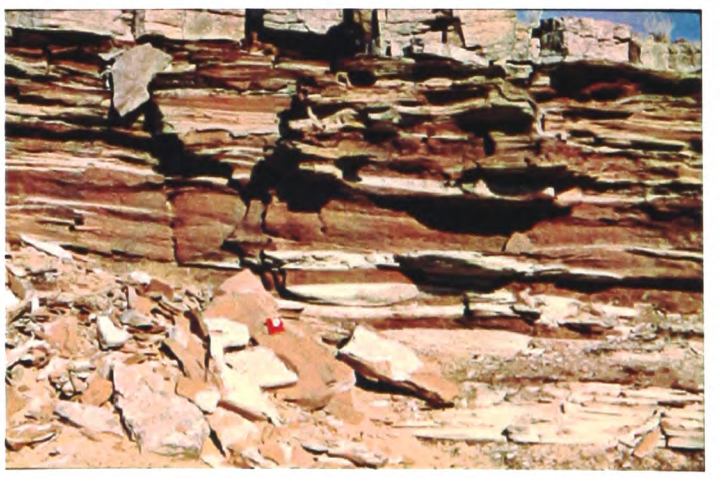


Plate 4.2f Characteristic red and green colour of S1 siliciclastics with silty peloidal interbeds. Notebook 225x176mm. Wadi Shuram

Plate 4.2

Upper Shuram Formation



Plate 4.3a Siliciclastic-carbonate cycles of the upper member of the Shuram Formation in Wadi Aswad. Judith Hodgson for scale.



Plate 4.3b Plan view of flat-pebble conglomerate (S2) bed from cycle top in Wadi Aswad. Hammer for scale.



Plate 4.3c Low-angle cross-stratification within pelsparite (S3) in Wadi Aswad. Lens cap 50mm.

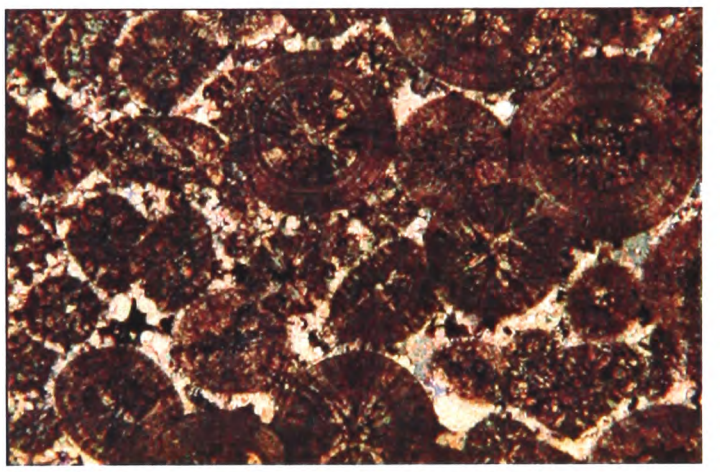


Plate 4.3d Photomicrograph of facies S4, oosparite with cross-extinction and fitted texture within calcite-spar matrix. Horizontal fov. 2.45mm. xpl. 241m WA

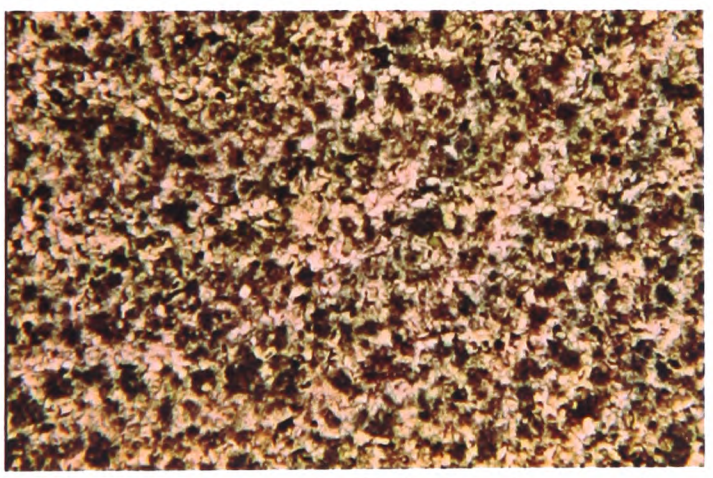


Plate 4.3e Photomicrograph of facies S3, pelsparite with micritic peloidal clasts and minor glauconite within a calcite-spar matrix. Horizontal fov. 2.45mm. ppl. 240m WA



Plate 4.3f Photomicrograph of facies S4, oosparite with columnar calcite cores to radial and concentric ooids with a calcite-spar matrix. Horizontal fov. 2.45mm. ppl. 241m WA

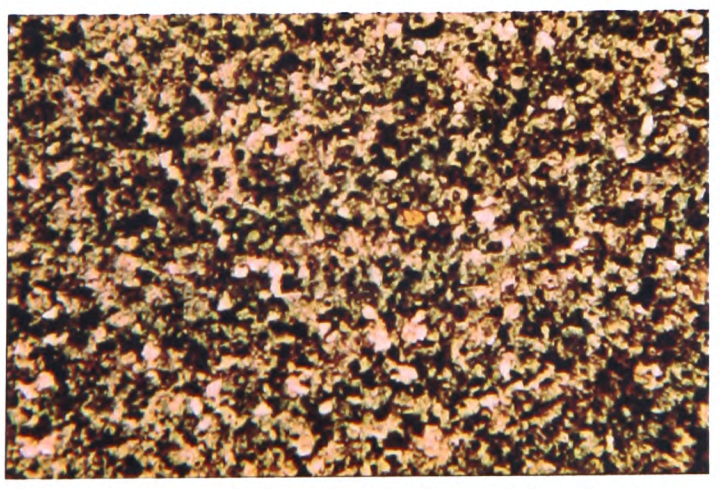


Plate 4.3g Photomicrograph of subfacies S1b, carbonate cemented siltstone with phosphate. Horizontal fov. 2.45mm. ppl. 178m Wadi Shuram

Shuram Formation in the Oman Mountains



Plate 4.4a Overview of the middle member of the Shuram Formation in Wadi Bani Awf. Car for scale.

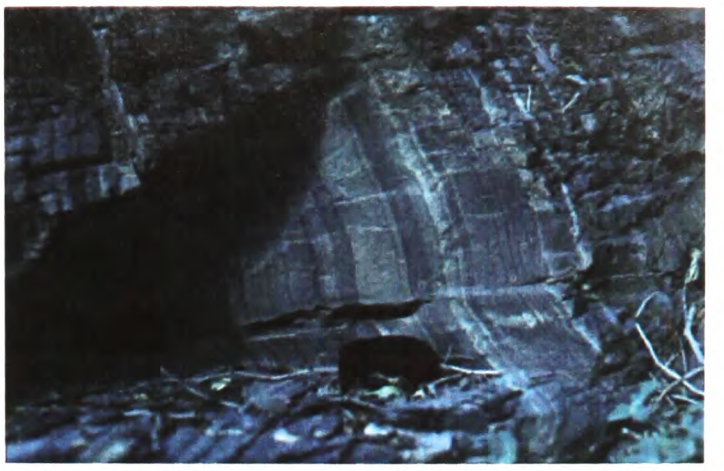


Plate 4.4b Purple and green banding within Lithofacies S1 in Wadi Hajir. Lens cap 50mm.



Plate 4.4c Siliciclastic-carbonate interbeds from the upper member of the Shuram Formation in Wadi Bani Awf. Notebook 225x176mm.



Plate 4.4d Siliciclastic (brown) and carbonate (grey) cycles (2-8m thick) of the uppermost Shuram Formation in Wadi Bani Awf. Jon and Tim for scale.

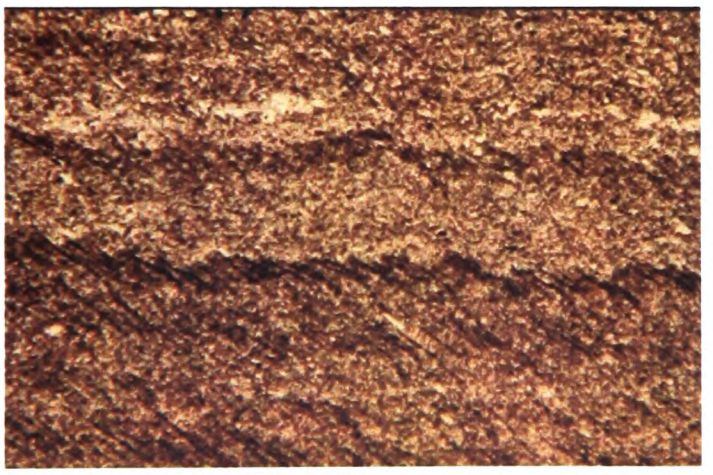


Plate 4.4e Purple siltstones (S1) from the Oman Mountains with strong crenulation cleavage. Horizontal fov. 2.45mm. ppl.

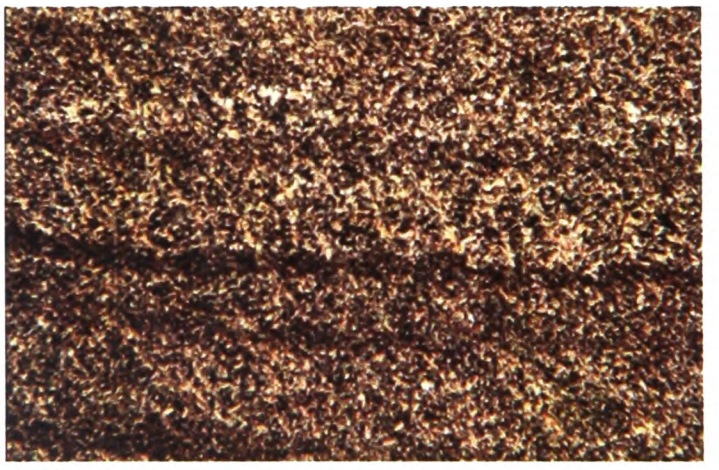


Plate 4.4f Purple siltstones (S1) from the Oman Mountains with strong crenulation cleavage. Horizontal fov. 2.45mm. xpl.

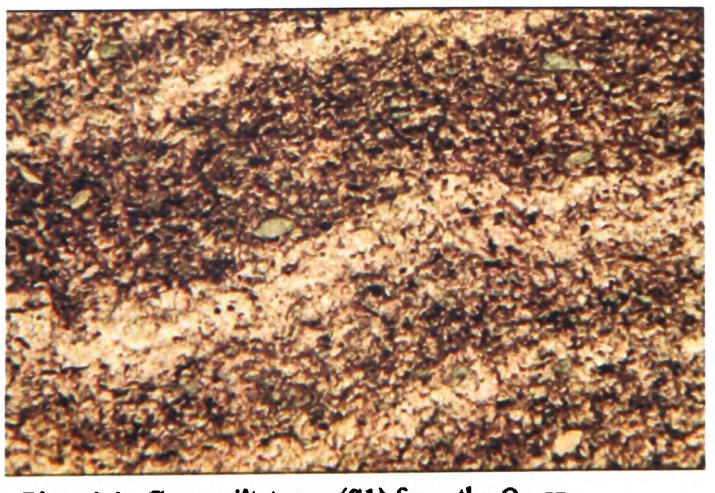


Plate 4.4g Green siltstones (S1) from the Oman Mountains, laminated and crenulated with chlorite porphyroblasts. Horizontal fov. 2.45mm. ppl.

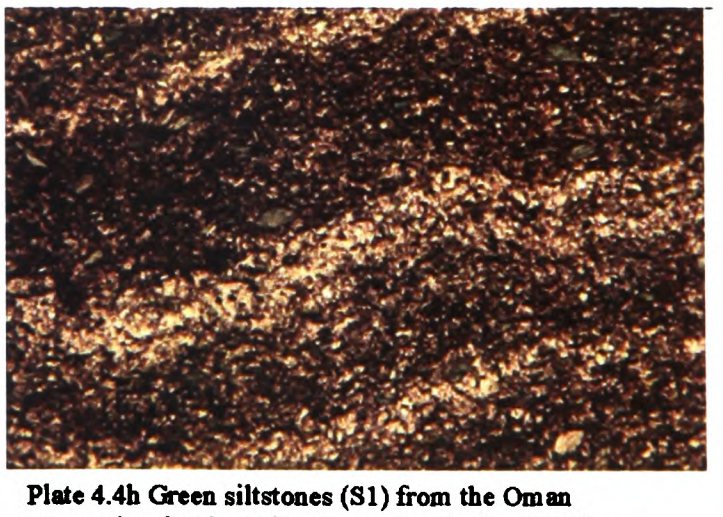


Plate 4.4h Green siltstones (S1) from the Oman Mountains, laminated and crenulated with chlorite porphyroblasts. Horizontal fov. 2.45mm. xpl.

Chapter Five - Buah Formation

5.1 INTRODUCTION

5.2 METHODS

5.3 PREVIOUS WORK

5.4 SUBDIVISIONS OF THE BUAH FORMATION

5.5 FACIES ASSOCIATION A:

5.6 FACIES ASSOCIATION B:

5.7 FACIES ASSOCIATION C:

5.8 FACIES ASSOCIATION D:

5.9 FACIES ASSOCIATION E:

5.10 BUAH FORMATION SYNTHESIS

5.1 INTRODUCTION

The Buah Formation is a mappable unit of carbonates that is widely distributed in the Huqf area (Figure 2.1) and in the Oman Mountains (Figure 2.2). The original type section for the Buah Formation has been defined by Kassler (1965) in the Buah dome of the Huqf area. Further work completed by Gorin *et. al.* (1982) redefined a new, more complete, type section in the Mukhaibah dome. In the Oman Mountains, the type section of the coeval Kharus Formation carbonates has been defined by Kapp and Llewellyn (1965) in Wadi Bani Awf. The similarity and correlation between the Buah Formation and the Kharus Formation (Burns & Matter 1993; Burns *et al.* 1994) indicate that these terms are synonyms. Since the term 'Buah Formation' is more widely used in the literature, and is the term used for this formation throughout Oman, this name will be used here.

In all outcrops studied, the Buah Formation grades-up from the siliciclastics and carbonates of the underlying Shuram Formation. This gradational contact has resulted in various workers picking different horizons as the base of the Buah Formation. Kassler (1965) placed the base of the Buah Formation at the first appearance of dolomites, that is, above Facies Association A of the present study. Gorin *et. al.* (1982) defined the base of the Buah Formation as the top of a ridge-forming bed, equivalent to the top of the basal rhythm in Facies Association A. Wright *et. al.* (1990) described the base as being marked by the sharp disappearance of red siltstones and cross-bedded grainstones, with a thin flat-pebble conglomerate of reworked Shuram lithologies marking the contact.

The olive-grey crinkly laminites with edgewise flake-breccias of Facies Association A are very distinctive in the field. In the present study, therefore, the first 1m thick occurrence of this facies without interbedded siltstones is taken to mark the base of the Buah Formation.

As no previous workers have studied the lithology of the Buah Formation in both the Huqf area and the Oman Mountains, the aim of this chapter is to characterise the sediments in both regions, with a view to establishing facies and their regional variation. This allows the development of a comprehensive model to account for depositional dynamics. Figure 5.1 shows summary logs of the Buah Formation from sections in the south-east of Oman (Mukhaibah dome) to the northwest of Oman (Wadi Bani Kharus). These allow an overview of the lower and upper Buah Formation lithologies with the four platformal Facies Associations (A-D) and the more distal slope Facies Association (E) defined during the present study. Insets show the interpreted platform model for these facies and a lithological key. Detailed lithological logs are in Appendix 5, whereas plates are placed at the end of the chapter.

5.2 METHODS

In the Huqf area a complete, well-exposed section of the Buah Formation can be seen in the Mukhaibah dome area whilst incomplete sections crop-out in the Khufai dome (not fully exposed) and the Buah dome areas (due to erosion) (Figures 2.1 & 2.2). In the Oman Mountains, complete sections occur in Wadi Bani Awf and Wadi Hajir whilst the top of the section is cut-out by the overlying Permian unconformity in Wadi Bani Kharus. Sections at the above localities were logged in detail with the aim of characterising facies, and establishing palaeoenvironments. These were then used to define genetic depositional units. Observations were made and sections were studied at other locations to test the validity of the genetic subdivision of the formation across the region. Representative facies samples were collected for petrographic and microfacies examination. This combined information has enabled the identification of facies, sub-facies and depositional settings and leads to a distally steepened platform model for this formation. In this model, platform sedimentation occurred in the Huqf area, Wadi Bani Kharus and Wadi Hajir (A-D) whilst sedimentation in Wadi Bani Awf represents slope/distal deposits (E) (Figure 5.2).

5.3 PREVIOUS WORK

Kapp & Llewellyn (1965), Glennie *et. al.* (1974) and Beurrier *et. al.* (1986) described the Buah Formation in Wadi Bani Awf during their surveys of the geology of the Oman Mountains and concluded that the formation was deposited in a tidal-flat environment. Kapp & Llewellyn (1965) also recognised indications of some shallow carbonate-bank influence in the upper part of the formation. Kassler (1965) and later, Hughes Clarke (1988), interpreted the Buah Formation in the Huqf area as tidal-flat limestones overlain by supratidal dolomites with evaporites and stromatolites.

More recent detailed studies add to these earlier works. Figure 5.2 shows the subdivisions applied to the Buah Formation by these workers as well as those interpreted in the present study. Gorin *et. al.* (1982) recognised two units in the Buah Formation of the Huqf area. The lower, flagstone facies with clusters of intraclasts, which they interpreted as subtidal to supratidal, is overlain by dolomitized intervals of stratiform and linked domal stromatolites. They identified cherty dolomites with stromatolites and evaporites overlain by red-green anhydrite-rich claystones which they interpreted to represent a period of emergence. These authors concluded that the Buah Formation represents an overall shoaling sequence from shallow subtidal to intertidal and supratidal conditions.

BUAH FORMATION

Wadi Bani Awf

Wadi Bani Kharus

Buah dome

Khufai dome

Mukhaibah dome

Upper Buah Formation

Lower Buah Formation

Stromatolite elongation = 188°

Stromatolite elongation = 188°

Wavecrest orientation = 154°

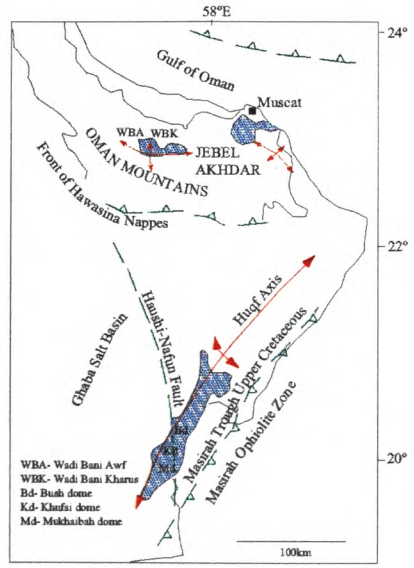
N=16

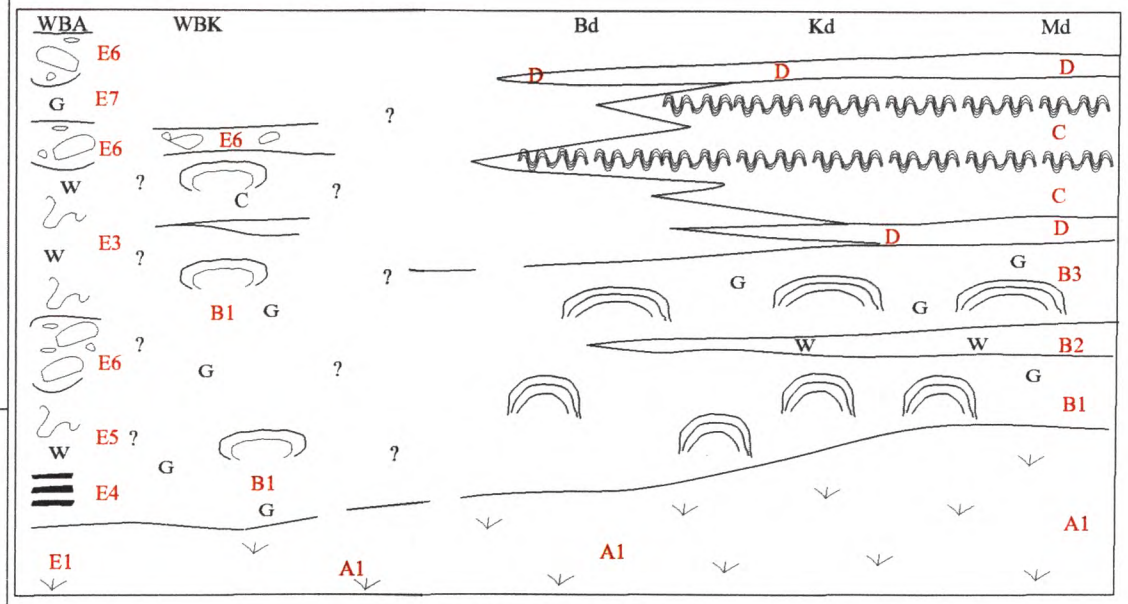
NORTHWEST

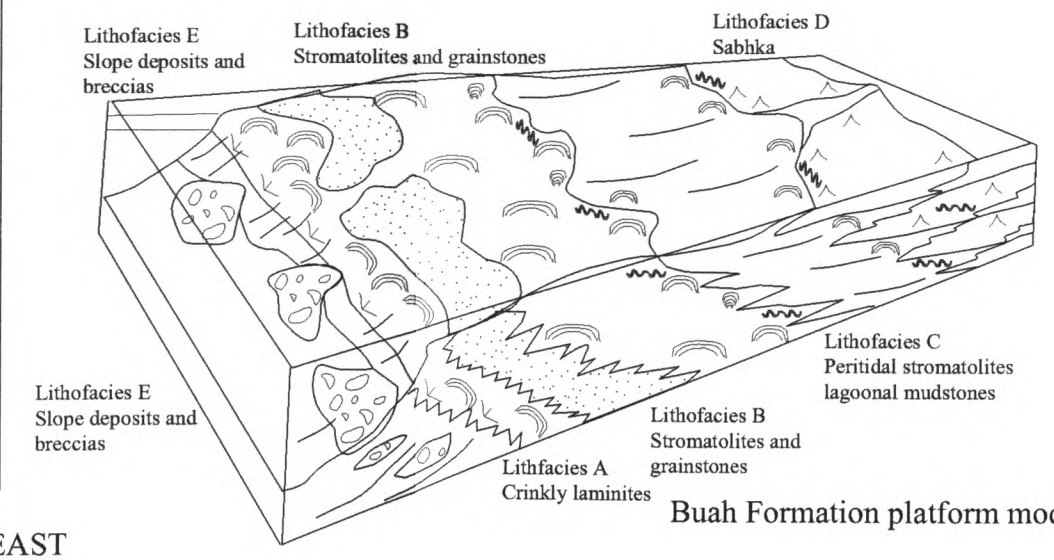
SOUTHEAST

Buah Formation Key

- Limestone
- Dolomite
- Ooidal/pel.grainstone
- Peloidal wackestone
- Sandstone
- Calcareous sandstone
- Carbonates and shales
- Silty carbonate
- Nodular wackestones
- Breccia
- Crystalline with ghost ooids / Coarsely crystalline
- Flat pebbles
- Stromatolites
- Flat topped LLH-S
- Pseudo-columnar
- Columnar
- Cherty stratiform
- Cushion shaped
- Chert nodules/bands
- Edgewise flake-breccia
- Fenestrae
- Auto-breccia
- Teepee
- Anhydrite rosettes
- Wave ripples
- Convolute bedding
- Cross-stratification
- Swaley-cross-stratification







Buah Formation platform model

Figure 5.1 Buah Formation summary logs showing lateral variation of Lithofacies Associations referred to in the text. Insert shows location map, lateral facies variation, platform depositional model and lithological key.

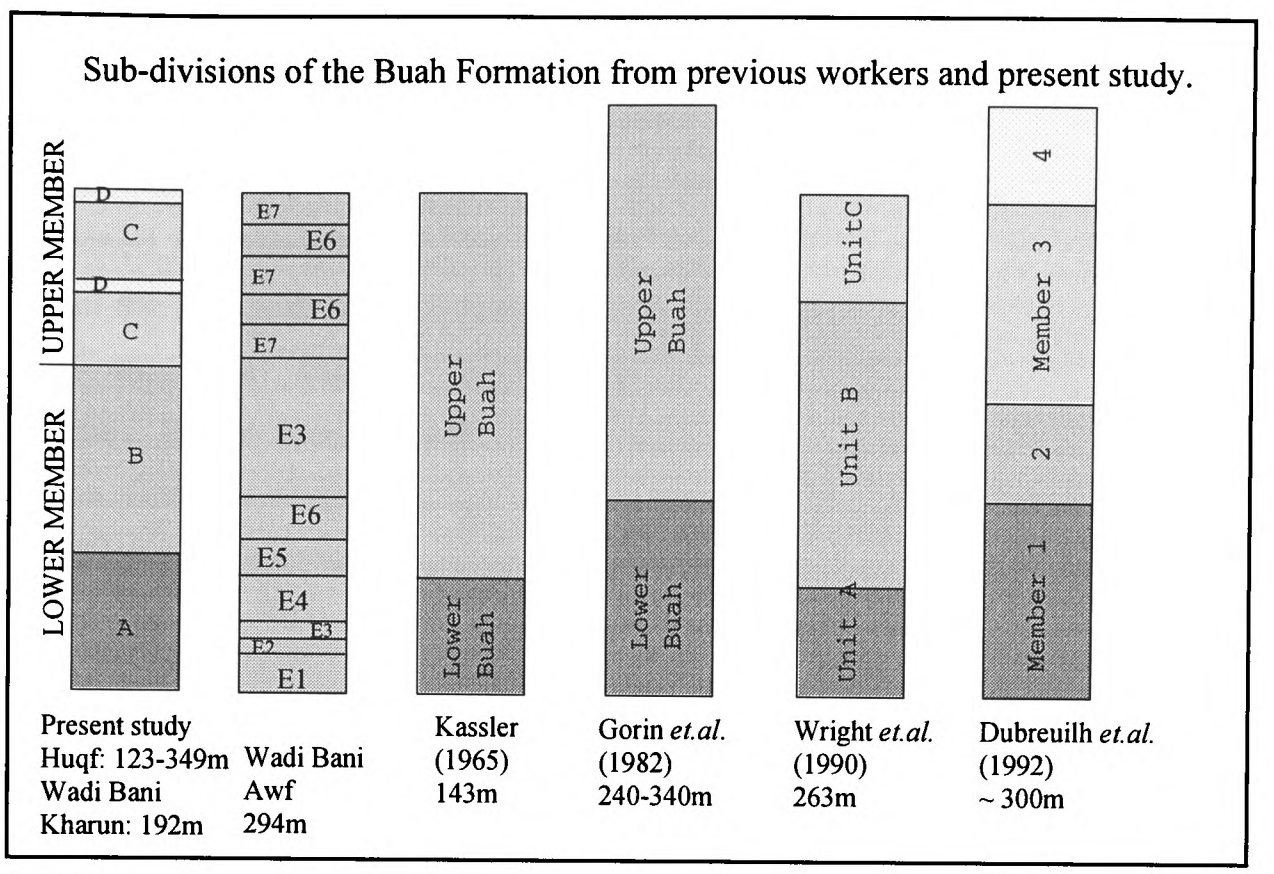


Figure 5.2 Subdivisions of the Buah Formation based on exposed sections in the Huqf area of Oman

Wright, *et al.* (1990) subdivided the Buah Formation into 3 units, and contradicted Gorin *et al.* (1982) by interpreting the lower flagstone facies as low-energy subwave base deposits. Their interpretation of the Upper Buah Formation as low-energy peritidal lagoons behind a prograding shoal reef complex, however, broadly concurs with Gorin *et al.* (1982).

Dubreuilh *et al.* (1992) deduced a similar depositional environment for the four members of the Buah Formation defined by them in the Huqf area. Their Member 1 comprises flagstone carbonates whilst Member 2 is characterised by detrital input forming red-brown sandstones with stromatolite structures. Member 3 is mostly dolomitic limestones with domal, biostrome-forming stromatolites with cherty pseudo-columnar structure. Member 4 is characterised by red, friable, argillaceous sandstone with algal-mat carbonates and evaporites.

5.4 SUBDIVISION OF THE BUAH FORMATION

In the present study, the Buah Formation is divided into two members, which in the Mukhaibah dome and the Khufai dome, can be identified by their topographic expression forming two prominent ridges above generally low-lying topography (Plate 5.1). The lower member of the Buah Formation consists of Facies Association A: Limestones, and Facies Association B: Stromatolites and grainstones (Figure 5.2). This relatively homogenous lower member is between 60 to 150m thick throughout the Huqf area and in Wadi Bani Kharus in the Oman Mountains. The most complete exposure of the upper

member occurs in the Mukhaibah dome and comprises two peritidal/sabhka cycles (Figure 5.1), with Facies Association C: Peritidal, and Facies Association D: Sabkha (Log in Appendix 5). Intermittent exposure of Facies Association C occurs in the Khufai dome area (Log in Appendix 5) whilst close by at Sirab, Facies Association C and D both occur. In the Buah dome area, (Log in Appendix 5) Facies Association C and D occur but are greatly thinned (approximately 15m) or possibly eroded. These four facies associations identified in the Mukhaibah dome section are broadly based on interbedded facies that are considered to have similar environmental significance as well as weathering characteristics. Facies Association E: Deep-water carbonates are specific to the Wadi Bani Awf section (Log in Appendix 5). The units described by previous workers that are defined in Figure 5.2 are based on field studies in the Huqf area only.

Summary of proximal sedimentary facies in the Buah Formation				
Facies	**Sub-facies**	**Lithology**	**Structures**	**Interpretation**
Facies Association D		**Sabkha**		
D1		Red silty dolomites		Sabkha
D2		Quartz arenites	Cross-stratification	Channel deposit
D3		Red/brown anhydritic dolomites		Sabkha
Facies Association C		**Peritidal stromatolites and mudstones**		
C1		Vuggy muddy carbonates	Planar, vuggy	Lagoonal
C2		Domal Stromatolites LLH		Peritidal
	C2a	Cherty pseudo-columnar		Peritidal
	C2b	Cottage-loaf stromatolites		Lagoonal
Facies Association B		**Shoal stromatolites and grainstones**		
B1		Compound stromatolites		
B2		Silty/peloidal wackestone	Swales, truncation	Subwave base
	B2a	Ooidal wackestone		Shoal
B3		Recrystallized grainstone	Cross-stratification	Shoal
	B3a	Recrystallized tabular stromatolites		
	B3b	Cushion stromatolites		
	B3c	Turbinate stromatolites		
	B3d	Columnar stromatolites		
B4		Ooidal grainstone	Cross-stratification	Shoal
Facies Association A		**Limestones**		
A1		Crinkly laminites	Nodular, undulations	Subwave base
	A1a	Edgewise flake-breccia	Cluster, imbricate	Subwave base
	A1b	Flat-pebble conglomerate		
A2		Silty limestone	Swales	

Table 5.1 Buah Formation Facies Associations with facies and sub-facies; A and B form the Lower Buah Member whilst C and D constitute the Upper Buah Member. The facies and sub-facies are described from the base of the formation upwards in more or less stratigraphic order.

5.5 FACIES ASSOCIATION A: LIMESTONES

The base of Facies Association A is the contact between the Buah and the Shuram Formations which, in this study, is considered to occur at the base of the first metre-thick

occurrence of crinkly laminites (facies A1), without conspicuous detrital siltstones. In the field, this facies is distinctive because of its olive-grey colour and topographic expression as it forms ridges overlying the wadi floor comprising the hollowed-out Shuram Formation (Plate 5.1). As shown on Plates 5.2a/b from Wadi Shuram, Facies Association A comprises asymmetric rhythms of a few metres thickness that are particularly characteristic of this association across the region. Facies Association A is between 30-70m thick (Figure 5.1).

Facies Association A is composed of two main facies: crinkly laminites (A1) formed of lime mudstones with a crinkly/nodular texture, and silty limestone (A2); with sub-facies: edgewise flake-breccias (A1a), and flat-pebble conglomerates (A1b). These facies occur in asymmetric rhythms of silty limestone and crinkly laminites with interbedded edgewise flake-breccias that are sometimes capped by a thin beds of flat-pebble conglomerate (Figure 5.1 and Logs).

The micro-nodular texture of the limestones with edgewise flake-breccia interbeds is very distinctive (Plates 5.2c/d) and these are laterally persistent even into the Oman Mountains where they form dark-grey beds (Plate 5.8e) that mark the base of the Buah Formation there. The crinkly laminites are bedded on a decimetre-scale with interbeds or thin lenses of edgewise flake-breccias (Plates 5.2c/e). Silty limestones are planar, millimetre-laminated with minor truncation-surfaces and swales locally developed, and are of variable thickness (Plate 5.2b).

In the Huqf area, the asymmetric rhythms are often capped by thin beds of silty flat-pebble conglomerates that are brown weathering. Similar facies and lithological characteristics occur in the Oman Mountains, where the lithologies tend to be black, massive and crystalline (Plate 5.8e).

5.5.1 Facies A1: Crinkly laminites

Facies A1 is olive-grey-weathering with planar (Plate 5.2c) sub-millimetre to 5mm-scale laminations that form beds up to 10cm thick. Thicker laminae are formed of crystalline carbonate while thin laminae are micrite/clay-rich. Crinkly laminae have a loose nodular-texture with low-amplitude undulations that pinch and swell on a scale of a few millimetres, and/or pinch-out laterally. In the Khufai dome area, these locally thicken to centimetre-scale beds and can thus form laterally extensive nodular beds. Here the nodular beds are separated by yellow silt-rich clays.

Thin-section studies reveal that the coarser laminations comprise a hypidiotopic mosaic of inclusion-rich crystals up to 15μm in size that typically occur in nodular bands up to

5mm thick. The calcimicrite and clay-rich laminations are 250-750μm thick, and contain detrital quartz, feldspar and mica grains up to 50μm in size (Plate 5.2d). Authigenic quartz grains occur in some samples as do coarse crystals of rectangular- to rhomb-shaped calcispar. Minor bitumen occurs within some clay-rich laminae.

Interpretation

Although algal filaments are not preserved, crinkly laminites contain many of the criteria suggested by Logan *et al.* (1964), Aitken (1967) and Burne & Moore (1987) for the recognition of organo-sedimentary deposits that have accreted as a result of a benthic microbial community trapping and binding and/or forming the locus for mineral precipitation. These include: *a),* lamination cannot be explained by settling of sediment in still water, by deposition from variable current velocity, or by periodic chemical precipitation; *b),* laminae do not pinch and swell to compensate for relief but bear an encrusting relationship; *c),* common small-scale disconformities; and *d),* thin edgewise flake-breccias of carbonate rock that are identical with the crinkly laminated carbonates and of similar lamina thickness are commonly associated. Domal stromatolite structures were not observed in the crinkly laminites of Facies A1. Up-section, however, crinkly laminites form LLH-S. These stratiform stromatolites are considered to be of trapping and binding type because the darker organic-rich layer contains detrital silt-grade quartz and feldspar grains. Gorin *et al.* (1982) observed domal stromatolites with synoptic relief of a few centimetres in this facies.

Modern microbial communities tend to form a cohesive mat covering shallow subtidal, intertidal to supratidal surfaces. In late Proterozoic times, however, before the advent of bottom-disturbing metazoans and metaphytes, microbial communities probably had a greater distribution over a wider variety of environments than in more recent times (Garret 1970; Hofmann 1973).

Similar nodular textures have been described from the Lower Magnesian Limestone of Yorkshire (Upper Permian, Zechstein Basin) and are interpreted as having been formed after deposition of the sediments by mineral segregation within lime-rich layers (Fuzesy 1980). This concretionary activity took place in micro-environments where ammonia was generated locally from decomposing organic matter. Ammonia decreased the hydrogen-ion concentration so the micro-environments created were favourable for the precipitation of calcium carbonate. Concentration of calcium carbonate was highest in the inner part of the concretion creating paler outer margins. These outer margins are subsequently preferentially dolomitized owing in part to higher porosities. Concretions

are compacted and flattened by the weight of overlying sediments, creating the observed crinkly appearance.

5.5.1a Sub-facies A1a: Edgewise flake-breccia

Edgewise flake-breccias are formed of crystalline carbonate intraclasts a few centimetres long and a few millimetres thick (Plate 5.2e) that occur as clusters or beds within facies A1. Lenses or clusters of vertically-stacked imbricate clasts are up to 20cm in lateral extent and a few centimetres high. These are often located in depressions on the underlying lamina and are spaced at intervals (of up to 1m) along the lamination. Some laminae are observed to curl-up and are continuous with the outer margin of the edgewise cluster (Plate 5.2e). Where these vertically stacked clusters could be observed on bedding surfaces they appear to have a rough polygonal outline. As well as occurring as imbricate clusters, intraclasts can also be randomly oriented and imbricated in beds up to 10cm thick that are interbedded with crinkly laminites of facies A1. Edgewise flake-breccia beds are observed to become more abundant in the upper-part of the rhythms, which are capped by silty flat-pebble conglomerates (Plate 5.2f).

Petrographically, the edgewise flakes are formed of microspar just like their host crinkly laminites (Plate 5.2h). Occasionally they can be vertically imbricated and some clasts can be cracked yet rarely broken whilst others are bent. Locally the intraclasts are only vaguely discernible from the host sediment except for a faint iron-rich coating around intraclast rims.

Interpretation

Subwave base hypothesis

Hoffman (1974) described similar lithologies from Lower Proterozoic rocks exposed near the Great Slave Lake, Canada and interpreted these as representing surf-zone deposits. Grotzinger (1986) interpreted similar edgewise conglomerates from the early Proterozoic Rocknest Formation of Canada as deposited by oscillatory shear currents during storms between fair-weather and storm wavebase. Gorin *et al.* (1982) interpreted these structures as shallow subtidal low-energy storm deposits which passed upward into supratidal environments characterised by desiccation and sub-aerial exposure. Wright *et al.* (1990) did not find associated stromatolites or desiccation structures or even evidence for transport, so interpreted the edgewise flake-breccias as soft-sediment deformation features that were possibly related to dewatering.

The intimate association of this facies with the calcisiltites of facies A2 suggests that both are subaqueous deposits. This interpretation is supported by the lack of evidence for

sub-aerial exposure in the form of mud-cracks, fenestral fabrics or desiccation polygons. The edgewise flake-breccia clusters are, therefore, interpreted as non-actualistic sedimentary structures where lithified microbial mat has been fragmented during storm events and subsequently redeposited (Pflüger & Gresse 1996). The lack of evidence for transport and the observed imbrication of clasts (forming clusters) may be the result of an inherent cohesive nature of the fragments.

Peritidal hypothesis

The upturned lamination observed at the edge of some clusters is reminiscent of submarine pseudo-anticlines formed as a result of early lithification of the mat (Asserto & Kendall 1977). Dewatering of carbonate supersaturated pore-waters may have enhanced the teepee structures and provided the necessary medium from which $CaCO_3$ could have been precipitated to form *in situ* clusters.

The polygonal outline to edgewise-breccias and the curling-up of the lamination into pseudo-teepee structures are phenomena that recall structures described from ephemeral lakes in the Coorong Lagoon of South Australia (Dave Wright, pers. comm.). In this modern setting, their formation is due to interference between resurgent seasonal groundwater below lake margins and lithified crusts that seal the lake sediments. In the Coorong analogue, prograding microbial mats occur on marginal flats which are alternatively flooded and dried. Within the Coorong carbonates, sedimentary structures indicative of subaerial exposure and desiccating conditions abound. However, such structures were not observed in facies A1 and A1a of the present study and therefore a subaqueous mode of formation is most likely.

An alternative hypothesis to explain the genesis of edgewise clusters is that they are bladed crystals that grew within these teepee structure. These radiating clusters are similar in form and size to radiating acicular gypsum crystals described from the Coxco Dolomite Member, of the Palaeoproterozoic Teena Dolomite in the Mc Arthur Basin of Australia, (Jackson *et al.*, 1987). There, radiating bundles of six-sided gypsum crystals were replaced by aragonite in a two-stage process: initially a thin film of calcium carbonate was deposited around the gypsum crystals forming a thin skin of carbonate, groundwater subsequently dissolve out the remaining gypsum, without dissolving the carbonate to leave a hollow mould of the crystal which was later infilled with carbonate. Deflation and the formation of rip-up clasts and their remobilisation during flood events could explain the interbedded random-textured breccia observed at the tops of rhythms. Further work, such as a more concentrated field study and geochemical analysis would have to be carried out to determine the mode of origin of these structures.

5.5.1b Sub-facies A1b: Flat-pebble conglomerate

Flat-pebble conglomerate beds are only a few-centimetres thick and form resistant caps to the rhythmites within Facies Association A (Plate 5.2a). They are pale-brown weathering and contain discoidal flat-pebbles (Plate 5.2f) and are overlain by recessive calcisiltite. Relatively small flat-pebbles ranging up to a few centimetres in horizontal diameter and up to 5mm in thickness are rafted and randomly orientated on the bedding plane.

Thin-sections reveal iron-rich peloids up to 100μm enveloped in dolomite rhombs and ooids 100-250μm with solid cores and radial cortices (Plate 5.2g). Minor phosphatic grains occur, commonly in the ooid core. The matrix is formed of carbonate microspar with minor detrital quartz, feldspar and mica grains up to 100μm in size. The long flat-pebbles are formed of peloidal wackestone, silty-peloidal wackestone and micrite.

Interpretation

The fact that flat-pebble intraclasts are formed of micrite and silty peloidal-wackestone and have lost their angularity indicates that they are locally sourced yet they have undergone some transportation. The iron-rich phosphatic nature of these deposits suggest a period of non- or slow-deposition. As rhythm caps, these probably represent reworking on the sea floor as part of condensed sequences and/or are associated with transgressive events. Similar mud chip intraclasts form on the present-day tidal-flats of north-western Andros Island by the erosion of cyanobacterial-bound sediment (Hardie 1977). The lack of fenestral fabrics or desiccation polygons in facies A1b suggest that these are subtidal deposits rather than subaerial.

5.5.2 Facies A2: Silty limestone

The silty limestones of Facies A2 are pale grey and recessive in outcrop. The more silty end-member (that forms the lower-part of the rhythms) weathers as thin millimetre-thick plates reminiscent of the underlying Shuram Formation. The calcisiltite part of the rhythm varies in thickness, being thickest in the Mukhaibah dome area and thinner in the Khufai dome, whilst in the Buah dome calcisiltite is rare (Figure 5.1). The more carbonate-rich end-member tend to have thicker lamination with low-angle swales and rare ripples developed locally; these are interbedded with facies A1 on a decimetre scale (Plate 5.2c below pencil).

Thin-section analysis reveals that the terrigenous detrital component of this facies varies from 0-30% of the rock with quartz, feldspar and mica grains up to 100μm in size. The sub-angular quartz and feldspars are corroded and partially replaced by microspar. Iron-rich peloids up to 100μm in diameter form 25% of the rock and these are often partly

replaced by euhedral dolomite rhombs. These detrital grains are matrix-supported by subhedral inclusion-rich microspar with crystals up to 100μm in diameter or passing laterally into micrite. Pyrite grains are numerous.

Interpretation

This facies overlies the flat-pebble conglomerates and represents an influx of terrigenous material onto the carbonate-rich platform. The scouring low-angle swales are taken to indicate storm events and increased wave energy possibly resulting from minor transgressions across the platform. The fine-grained nature of the sediments and the swaley-cross stratification suggests that these accumulated close to the fair-weather wavebase.

5.5.3 Facies Association A synthesis

From the evidence acquired in this study, the sediments of Facies Association A have most probably been deposited in a subwave base environment. This interpretation is supported by the presence of swaley cross-lamination and the lack of features indicative of peritidal environments such as: fenestrae, teepee structures and desiccation polygons that are ubiquitous within peritidal facies in Associations C and D.

The lithologies of Facies Association A have biogenic and detrital origins and are considered to have accumulated between fair-weather and storm-wave base. This interpretation concurs with Wright *et al.* (1990) but contradicts all the other earlier workers. Facies Association A is distinctive because it is formed dominantly of limestone, like the underlying Shuram Formation, whereas the rest of the Buah Formation is composed mostly of dolostone. In the Oman Mountains, the very dark colour, muddy fetid lithologies with pyrite crystals and lack of siliciclastics indicate an organic-rich precursor and possibly a subtidal environment of deposition. In the Huqf area, the rhythms probably represent transgressions of sea level with an increase in siliciclastic deposition followed by a slow carbonate catch-up phase involving colonisation by microbial mats and storm deposition of detrital carbonates. Early lithification of these sediments enabled their reworking into flake breccias which were deposited upon the stratiform mat during storm events. Flat pebbles deposited upon initiation of each new transgressive cycle were probably sourced from early lithified thin silty limestone beds. The presence of iron and phosphate in the reworked flat-pebble conglomerate beds would be consistent with recycling of nutrients, from deeper water into shallower depths, that possibly encouraged the establishment of microbial communities.

5.6 FACIES ASSOCIATION B: SHOAL STROMATOLITES AND GRAINSTONES

In the field, Facies Association B has a sharp lower contact with the rhythms of Facies Association A. It is pale pink/grey in colour and forms more massive dolomitic beds (Plate 5.3a). This Facies Association is between 60-100m thick and is formed of two grainstone-stromatolite facies (B1 and B3) separated by a thin silty lime-wackestones facies (B2). The basal part of the facies association in the Buah dome, the Khufai dome and Wadi Bani Kharus comprises Facies B1, which forms an extensive biostrome of large LLH-S stromatolites with diameters of up to 10m (Plate 5.3b). In the Mukhaibah dome, the lower part of the facies association is composed of cross-stratified grainstones with relict evaporites (Plate 5.3e)(Log, Appendix 5).

Recessive silty/peloidal wackestones (B2) and ooidal-wackestones of sub-facies B2a, are brown weathering and nodular bedded (Plate 5.4e) units that directly overlie Facies B1 in the field. This influx of peloids, ooids and siliciclastics is thickest in the Mukhaibah dome (6-8m) but pinches out toward the Buah dome in the north.

The wackestones are overlain by a major ridge of stromatolites and grainstones of facies B3. These recrystallized peloidal/ooidal grainstones, with locally developed cross-stratification interfinger with large, flat-topped stromatolites of sub-facies B3a. Evaporite pseudomorphs occur throughout this facies association, being particularly extensive in the upper-part of the Association. Locally, in the Buah dome area, columnar stromatolites (B3d) occur whereas in the Oman Mountains, the dominant stromatolite type are cushion forms (B3b). A thin unit of cross-stratified ooidal grainstones (B4) overlie the stromatolites in the Buah dome (Log, Appendix 5). Here, and in the Khufai dome, Facies Association B is overlain by an interval with no exposure. In the Mukhaibah dome, it is directly overlain by muddy carbonates and cherty stromatolites of Facies Association C of the upper member of the Buah Formation.

5.6.1 Facies B1: Compound stromatolites

This facies comprises crinkly, coarsely laminated carbonate which forms laterally extensive stratiform (tabular) and domal stromatolite biostromes. This facies differs from Facies Association A in that the crinkly-laminations are coarser and laterally form very large stromatolite domes (Plate 5.3b). Laminae are of wrinkled- to wavy-type (Plate 5.3c) whilst domes are sub-spherical to tabular. The ubiquitous edgewise flake-breccia of sub-facies A1a is rarely seen in Facies Association B except locally between stromatolite domes.

These stromatolites comprise low sub-spherical domes of LLH-C type having up to 25-30cm synoptic relief. They coalesce to form metre-scale domes that, in turn, are overlain

by tabular stratiform mats with sub-vertical edges and synoptic relief of up to 3m (Plate 5.3c). These large composite stromatolites can be up to 10m in diameter (Plate 5.3b). Interdome areas are infilled with either peloidal grainstone or edgewise flake-breccias. In outcrop, these stromatolites are grey-yellow in colour and record elongation in a NE/SW direction. Local breccia horizons occur in the Khufai dome area which appear to be concentrated between stromatolite domes. This biostrome horizon is everywhere formed of micrite and calcispar laminations (Plate 5.3d).

Interpretation

Many workers have used stromatolite morphology along with modern analogues to aid environmental interpretation (Logan *et al.* 1964, Gebelein 1969, Grotzinger 1986a). The compound domal stromatolites of facies B1 are similar to those described by Grotzinger (1986a) and Bertrand-Sarfati & Moussine-Pouchkine (1983) from high-energy shoal-water reef complexes. The elongation of these domes indicates that they were affected by current activity and thus represent development above fairweather wave base. The breccia horizons probably formed in channels cut between the elongate stromatolites.

Because these overlie the crinkly laminites formed below fairweather-wave base, they may be taken to indicate a general shoaling with the development of a stromatolite reef system from the Huqf area to the Oman Mountains. In the Mukhaibah dome, the cross-stratified grainstones with evaporite moulds form the lateral equivalents of these stromatolite biostromes (B1). These may have formed in an area of higher energy such as tidal channels that became partially restricted, resulting in the formation of evaporites.

5.6.2 Facies B2: Silty/peloidal wackestone

This facies which is recessive in the field, overlies the large stromatolite biostrome of B1 in the Khufai dome and the grainstones with evaporite moulds in the Mukhaibah dome. Silty/peloidal wackestones consist of nodular, heterolithic beds 2-3cm thick (Plates 5.4e/f) comprising coarse silt-grade carbonate and fissile muddy carbonate. This facies is laterally extensive, being thickest in the Mukhaibah dome and in the Khufai dome areas (*c.* 7m) but appears to pinch-out toward the Buah dome in the north. Sedimentary structures comprise local swales, truncation surfaces and wave ripples with wave-crest orientation towards 154° (Log, Appendix 5).

Thin-section analysis reveals iron-rich micritic peloids up to 100μm in diameter along with ooids having diameters of up to 200μm that preserve both radial and concentric textures. Detrital feldspar, quartz and mica grains of up to 100μm in size occur, as do phosphatic grains (Plate 5.4d). Some samples contain micritic and silty/peloidal intraclasts up to a centimetre long but only a millimetre thick. These are matrix

supported in a fine-grained carbonate which is iron-rich in patches. Oomouldic porosity is partly replaced by authigenic quartz.

5.6.2a Sub-facies B2a: Ooidal grainstones

This sub-facies crops-out everywhere in the Huqf area at the same stratigraphic level and forms thin intercalations of up to a metre-thick within the silty/peloidal wackestone facies (B2). In outcrop, subfacies B2a is conspicuous because the ooids and grapestones have a distinctive dark organic clay-rich coating (Plate 5.4g). These form a grainstone within a patchy muddy-carbonate cement with late sparry calcite veins.

Thin-section studies reveal that the ooids are formed of perfect spheres up to 800μm in diameter with pseudo-axial cross-extinction. Ooidal-grapestones, with diameters up to 2.4mm, comprise ooids and silty-intraclasts and are surrounded by a dark organic clay-rich concentric laminae approximately 10μm thick. Generally ooids and grapestones are replaced by coarse inclusion-rich dolospar with syntaxial overgrowths in which only the micrite cortex is preserved. Many of these ooids are fragmented and float in a fine- to medium-grained crystalline carbonate matrix that is rich in detrital silt-grade quartz, feldspar and mica grains.

Interpretation

Cook & Taylor (1977) interpreted similar facies from the Ordovician of Nevada as having been deposited in shallow subtidal shelf waters below active wave base. Similar nodular limestones formed of wackestones and mudstones from the Mid-Triassic in southern Hungary have been interpreted by Török (1998) as outer-ramp deposits.

These silty/peloidal wackestones of B2 overlie the large compound stromatolites (B1) and thus mark a great change in sedimentation with the influx of siliciclastics, iron-rich peloids and phosphatic grains. The low-angle swaley cross-stratification and truncation surfaces suggest sub-wave base deposits, which in turn would suggest a relative deepening from the underlying stromatolites that could have formed above fairweather-wave base. The fragmented ooids of sub-facies B2a suggests reworking of ooids from a nearby shoal whereas the micritic intraclasts are possibly reworked outer-ramp rip-up clasts. Facies B2, being laterally extensive across the Huqf area, is herein interpreted as representing a basin-wide relative deepening, transgressive event where siliciclastics and intraclasts were transported by wind-forced geostrophic currents and by storm-surge ebb currents. This interpretation is supported by the occurrence of phosphatic grains which are often associated with up-welling currents (Cook and Shergold 1979).

5.6.3 Facies B3: Recrystallized grainstone

In all sections studied in the Huqf area (Figure 5.1), recrystallized grainstones form the major part of Facies Association B. They form a major resistant ridge (Plate 5.1) and are grey/brown weathering with a sucrosic sparry dolomite appearance whilst the fresh surface imparts a pink pigmentation. They are formed, for the most part, of crinkly laminations with a wavy to nodular appearance accentuated by dark-grey clay-rich partings. In outcrop, this facies weathers-in to form large cavernous structures of up to 3m wide and about 1m high (Plate 5.4a). Locally, this facies contains low-angle planar cross-stratification. In the upper part of the lower Buah Formation, this facies contains lath-shaped vugs a few millimetres long and rosettes (Plate 5.4h).

In thin-section, recrystallized grainstones are formed of idiotopic, non-equant, dolomite crystals with ghost ooids or peloids that are rich in micro-inclusions. Coarse anhedral crystals are up to 500μm in size while smaller subhedral crystals are 100μm. These occur in undulating coarse bands up to 5mm thick while finer bands are 500μm with dark micro-stylolites containing fine-grained pyrite grains and clays. Minor detrital quartz and feldspar grains of up to 50μm in size occur. Locally, lath shaped vugs are ubiquitous in some sections; whereas most are empty, some are filled by calcite spar with rare relict anhydrite remaining in a few.

Interpretation

This facies is interpreted as an ooidal/peloidal shoal environment with relatively high energy indicated by the locally developed cross-stratification. Fine-grained siliciclastics were probably blown in by the wind. The occurrence of pyrite suggests the presence of precursor organic matter. The pervasive recrystallization of this facies may be a reflection of an original high porosity that enabled the through-flow of supersaturated fluids resulting in dissolution and reprecipitation. Alternatively, the original mineralogy may have been aragonite or high Mg-calcite and therefore more prone to recrystallization. Compaction with pressure-solution resulted in the formation of stylolites. The lath and rosette shaped vugs indicate precursor evaporites, suggesting that arid, hypersaline environments prevailed, especially toward the top of the section.

5.6.3a Sub-facies B3a: Tabular stromatolites

Tabular stromatolites are flat-topped and form extensive biostromes throughout the Buah Formation in the upper-part of Facies Association B. These biostromes are traceable for up to 70m laterally and appear to build upon the grainstone facies. Individual stromatolite structures comprise laminae which are flat, in most of the dome, but plunge steeply at the edges; with up to 1m synoptic relief, individual domes can be up to 20m in diameter.

These grow vertically and laterally, with grainstones and intraclast breccias filling the 'interdome' space. In the Khufai dome area, stromatolites are observed in channels within the grainstones.

In thin-section, this sub-facies is formed of coarse, euhedral dolospar with faint relict peloids or ooids (Plate 5.4c). The laminae are approximately 250-500μm thick with inter-crystalline porosity occluded by quartz. Skeletal organic and iron-rich inclusions are abundant.

5.6.3b Sub-facies B3b: Cushion stromatolites

Cushion stromatolites are dominant at a similar stratigraphic level in the Wadi Bani Kharus section (Log, Appendix 5). Here, the stromatolites are formed of wavy crinkly laminations that thicken and thin laterally; the 'domes' extending laterally for 1m with 50cm of synoptic relief. Upward in the section, the stromatolite relief diminishes to approximately 20-30cm and these, in turn, are overlain by small LLH-C stromatolites with only 1-2cm of synoptic relief. Thin-section analysis shows that these are formed of alternating microspar and micrite laminations that are locally contain possible evaporite pseudomorphs (Plate 5.8g).

5.6.3c Sub-facies B3c: Turbinate shaped stromatolites

In Wadi Bani Kharus, columnar stromatolites form laterally extensive biostromes up to 2m thick. These biostromes comprise cushion-domes, pseudo-columnar and turbinate-columnar stromatolites formed of irregular millimetre-thick crinkly laminae having up to 20cm synoptic relief. Turbinate forms (Plates 5.8a/b) have bases approximately 2cm in diameter but expand upward to 20cm in diameter. Synoptic relief varies from 2-20cm. In thin-section, these are formed of irregular undulating laminations of calcimicrite and calcispar.

5.6.3d Sub-facies B3d: Columnar stromatolites

In the Buah dome area, columnar stromatolites form a unit approximately 30cm thick that occurs above the large-scale compound stromatolites (B1). These consist of erect, uniform, sub-cylindrical columns with gentle convex-upward laminae and diameters of up to 2cm. They have a sub-centimetre spacing and synoptic relief of up to 5cm. They are similar to the SH-C type of Logan *et al.* (1964) and Bertrand-Sarfati (1992). Gorin *et al.* (1982) recognised a resemblance of this stromatolite to *Gymnosolen* Steinmann.

Interpretation

The variation in form of these stromatolite types is largely limited to synoptic relief. This is considered a function of palaeo-water depth, with shallow-water forms having lower synoptic relief. Tabular stromatolites are observed to build upon the grainstones and interfinger with them, and therefore could have formed in quieter areas of the shoal environment and/or when the energy levels were dissipated. The relatively low synoptic relief of these forms also suggests relatively shallow water. The upward decrease in synoptic relief recorded in sub-facies B3b at Wadi Bani Kharus indicates that shallowing also occurred in this locality. The gradation from LLH-S→SH-C stromatolite observed in the Buah Formation is similar to that recorded from recent stromatolites in the intertidal zone in Shark Bay, Western Australia (Logan *et al.* 1964). A peritidal environment of deposition is, therefore, inferred for sub-facies B3d in the Buah dome.

5.6.4 Facies B4: Ooidal grainstone

Facies B4 infills stromatolite relief, and is approximately 6m thick in the Buah dome area. These cross-stratified ooidal grainstones are bedded on a metre-scale and are grey/brown weathering. Cross-sets are up to 50cm thick and planar, with bi-directional flow toward the northwest and south-west. In Wadi Bani Kharus, Facies B4 is commonly chertified and interbedded with turbinate stromatolites.

Thin-sections reveal that, in the Buah dome area, this facies is formed of micritic ooidal/peloidal grainstones/packstone with a sparry cement. The grains are in places coated by bitumen. Minor grapestone grains also occur. In Wadi Bani Kharus, this facies is formed of a recrystallized grainstone/packstone lithology with only the micritic cortex of ooidal grains remaining. Some micritic intraclasts also occur. Ooids and intergranular porosity are occluded by chalcedonic quartz and megaquartz (Plate 5.8d).

Interpretation

The cross-stratification in Facies B4 in the Buah dome is indicative of deposition in a high-energy environment. This suggests a relative deepening as these directly overlie the peritidal columnar stromatolites (B3e) (Bertrand-Sarfati 1976). Sedimentary structures indicative of current energy were not observed in Facies B4 in Wadi Bani Kharus, although, grainstone/packstone facies are taken to indicate at least moderate energy conditions. The fact that ooidal grainstones are interbedded with turbinate stromatolites suggests that energy levels varied repeatedly.

5.6.5 Facies Association B synthesis

The large composite stromatolites of facies B1 represent the development of a stromatolite reef complex stretching from the Huqf area to the Oman Mountains. In the Mukhaibah dome area to the south, the stratigraphically equivalent cross-stratified grainstones with evaporites possibly represent a back-reef environment. The influx of iron- and phosphate-rich silty/peloidal wackestones with low-angle swales and truncation surfaces marks a period of increased water depth which caused the reworking of early lithified seafloor into clasts. The upper part of Facies Association B is characterised by a general shoaling-upward to high-energy grainstones interfingering with tabular stromatolites. The lateral extent of this facies across the Huqf area and into the Oman Mountains suggests that shallow platform carbonates had become established across nearly the whole region at this time.

Facies Association B records fluctuating relative sea-levels across the Huqf area and into the Oman Mountains. The crinkly laminite facies (A1) followed by the stromatolite reef build-up lithofacies (B1) is suggested to reflect an overall transgression whilst the influx of phosphatic-rich peloidal wackestones of Facies B2, occurred during a flooding event. The catch-up phase of carbonate deposition occurs with an aggradational unit of grainstones and stromatolites (B3). By the end of Facies Association B times, partly restricted evaporitic conditions were becoming established.

5.7 FACIES ASSOCIATION C: PERITIDAL STROMATOLITES AND EVAPORITES

Facies Association C is well-developed in the Mukhaibah dome and the Khufai dome areas but it is remarkably thinned in the Buah dome area (Figure 5.1). Although almost complete exposure occurs in the Mukhaibah dome area, interpretation is hindered by poor preservation owing to extensive weathering. Facies Association C is formed of shallowing-upward peritidal cycles on a 3-10m scale. The lower part of the cycles comprises carbonate mudstones (C1) whereas the upper part consists of domal stromatolites overlain by cherty columnar stromatolites (C2) and minor ooidal grainstones.

In the Mukhaibah dome, three recessive cycles comprise approximately 20m of section and overlie Facies Association B. These cycles form a dip in topography between the two massive ridges produced by the Facies Association B grainstones and the peritidal cycles of the upper-part of Facies Association C. These cycles are rich in evaporite pseudomorphs, are auto-brecciated and are locally capped by intraclast or ooidal grainstones with columnar stromatolites. Above these recessive cycles is 35m of muddy

carbonates (C1) with a 2m-thick interbed of cross-bedded coarsely crystalline calcite and a 1m thick cap of red anhydrite-rich cherty carbonate (D3) (Log, Appendix 5).

The upper part of Facies Association C is exposed in the Mukhaibah dome and the Khufai dome and is characterised by 1-10m scale cycles. These cycles are formed of recessive fine-grained carbonate (C1) overlain by fenestral, auto-brecciated, cherty stromatolites that contain considerable evidence for precursor evaporites and are capped by cherty columnar stromatolites (C2). Although cherty stromatolites and grainstones occur in Wadi Bani Kharus, peritidal cycles similar to those of Facies Association C have not been observed there.

5.7.1 Facies C1: Vuggy muddy carbonates

Facies C1 is pale-green/grey with a chalky texture, very fine-grained, recessive and is generally covered by scree in outcrop. In the Mukhaibah dome, this facies forms a 35m thick unit near the base of Facies Association C. This unit is not observed in the Khufai dome or the Buah dome areas; however, a lack of exposure is recorded at this stratigraphic level in both of these localities. These muddy carbonates consist of tabular beds, approximately 10cm thick, that form the lowermost part of the peritidal cycles. No sedimentary structures were observed in this facies. Irregular millimetre-scale vugs which are partially stained pink are observed higher in the section.

Thin-sections reveal a structureless, fine-grained, micrite-microspar (Plate 5.6h). Irregular millimetre-scale vugs are often occluded by clear microspar. Some vugs have rectilinear outlines. Patchy relict anhydrite occurs in some thin-sections.

Interpretation

This facies is taken to represent lagoonal deposition because of the fine-grained, homogenous microfacies. The lack of sedimentary structures suggests a very quiet environment of deposition. Vugs with rectilinear outlines have been interpreted by Tucker (1982) as an indication of precursor evaporites. Rare relict anhydrite indicates the environment was arid and hypersaline.

5.7.2 Facies C2: Stromatolites

The stromatolites of facies C2 form biostromes and bioherms of LLH-S domes that build upon the recessive muddy carbonates of facies C1 (Plate 5.5d). Biostromes vary in thickness from 1-10m and are generally capped by pseudo-columnar stromatolites. These contain ubiquitous fenestrae and auto-brecciation in the Mukhaibah dome area where they are poorly preserved. Similar facies have slightly better preservation in the Khufai dome area.

5.7.2a Sub-facies C2a: Domal stromatolites

Pale-grey to yellow weathering, these LLH-S stromatolites form biostromes some tens of metres in lateral extent, with up to 2m of synoptic relief (Plate 5.5d). Stromatolites have diameters of up to 4m and are typically formed of smooth, fine-grained, millimetre-thick laminae that are locally fenestral and auto-brecciated. Fenestrae are sub-circular with diameters up to 1cm (Plate 5.5e). Some laminae are replaced by chert. These large domes form the main body of the peritidal cycles of Facies Association C. Higher in Facies Association C of the Khufai dome, the synoptic relief diminishes to decimetre-scale. In the Mukhaibah dome, the uppermost cycle is extensively contorted and brecciated (Plate 5.5b). In thin-section, these stromatolites are formed of dolomicrite laminations alternating with cherty or dolospar laminations. Within these laminations are numerous laths and rosette-shaped vugs that are occluded by spar or chalcedonic quartz.

5.7.2b Sub-facies C2b: Cherty pseudo-columnar stromatolites

Pseudo-columnar stromatolites (Plate 5.6a) occur dominantly in the upper-part of Facies Association C, typically at the tops of the peritidal cycles where they form ridges in outcrop. Columnar-stromatolites weather dark to pale-grey and are built from smooth sub-millimetre laminations to form stromatolites with up to 10cm of synoptic relief and diameters up to 3cm. Laminae thicken in the axial area and thin at the steeply dipping margins and the 'domes' are convex upwards with concave 'interdomal' laminae. Laminae are smooth with high inheritance and are formed of alternating microspar and micrite. Many of these are replaced by chert which has been desert varnished subsequently (Plate 5.6a). Some laminae contain calcite spar pseudomorphs after anhydrite nodules and laths (Plate 5.6d). In plan view, these form close-spaced sub-circular structures with diameters up to 4cm.

Thin-sections of chertified forms reveal that the laminations (Plate 5.6b) are between 300μm and 1mm thick and formed of chert and micrite alternations whereas others are formed of micrite and spar alternations. Some samples contain alternations of peloidal grains and micritic laminations.

5.7.2c Sub-facies C2c: Cottage-loaf stromatolites

This sub-facies was only observed in the Buah dome area, where it is pale-grey to pink weathering and contains minor pseudo-columnar and dominantly cottage-loaf stromatolites with diameters up to 30cm and with a few centimetres of synoptic relief.

Interpretation

The large LLH-S domal stromatolites at the base of the biostromes are very regularly laminated, auto-brecciated and fenestral. Fenestral or birdseye fabrics suggest intertidal environments (Shinn 1968). However, the rectilinear outline of some of the fenestrae probably reflects precursor evaporites whilst the auto-brecciation of the beds is probably caused by evaporite dissolution. The local erosion and brecciation of stromatolite domes in the Mukhaibah dome area (Log, Appendix 5) indicates these were subjected to periods of sub-aerial exposure. These domal stromatolites are interpreted to have formed in a peritidal marine environment.

The upward-grading from large compound stromatolites to pseudo-columnar forms indicates an upward shallowing. This interpretation is supported by the presence of numerous evaporite moulds and by auto-brecciation of the lamination. The inter-lamination of peloidal grains with microbial laminae suggests that the stromatolites were trapping and binding forms. Chert probably preferentially replaced the organic-rich laminae. Stromatolite forms without evidence for peloids could have formed by *in-situ* precipitation; this is supported by the uniform smooth lamination with high inheritance morphology. Pope *et. al.* (1999) describe similar features associated with changes in water chemistry between carbonate and evaporite transitions, which allow chemical processes to dominate over biological processes.

5.7.3 Facies Association C synthesis

Facies Association C represents deposition in lagoonal to supratidal environments probably behind the shoal reef complex of Facies Association B. The ubiquitous precursor evaporites indicate that hypersalinity and arid environments prevailed. Lagoonal and supratidal sedimentation probably occurred in the lee of Facies B2, which may have formed an effective barrier at this time. Alternatively, there may have been a relative sea-level fall which resulted in the progradation of supratidal facies belts.

5.8 FACIES ASSOCIATION D: SABKHA

Facies Association D is formed of three facies: recessive, silty dolostones (D1); cross-stratified, quartz-arenites (D2) and silty carbonates with gypsum crystals and enterolithic quartz after anhydrite (D3; Plate 5.7a). In the Mukhaibah dome area, sabkha facies occur above the peritidal facies of Association C (Figure 5.1; Plate 5.7a) to form two peritidal/sabhka cycles. Facies Association D is best observed in the Buah dome area where, despite intermittent exposure, facies D3 contains interbedded ferruginous silcrete horizons (Plate 5.7b). This horizon is unconformably overlain by aeolian sandstones of the Thumaylah Formation of the Cambrian Haima Group. Facies Association D is not

exposed in the section studied in the Khufai dome but its lateral equivalent is exposed along the road to Sirab. Unfortunately, the time limitations of the present study made it impossible to study that section in detail.

5.8.1 Facies D1: Red silty dolostones

This facies is very fine-grained, and forms recessive units 1-2m thick in outcrop in the Mukhaibah dome. It has a pink-red colouration and a chalky texture as is found at the base of peritidal cycles in the upper part of Facies Association C. These red silty dolostones contain low-angle swaley cross-laminations but are typically planar laminated.

In thin-section, this facies comprises a micritic matrix with thin, sub-millimetre, laminations of detrital quartz, feldspars and mica grains less than 50μm in size. Numerous phyllosilicates occur along with minor phosphatic grains.

Interpretation

This facies includes the first influx of terrigenous siltstones into a carbonate-dominated lagoonal environment. The swaley cross-lamination suggests that these influxes represent storm events or at least deposition during periods of higher energy in the lagoon. This may also indicate a periodic increase in water depth.

5.8.2 Facies D2: Quartz-arenites

This facies has an erosional contact with the underlying pink beds of facies D1 in the Mukhaibah dome (Plate 5.7b). Only locally exposed, this facies is 3.2m thick, a white/brown colour and is composed of low-angle cross-bedded quartz-arenite with well-rounded grains.

Thin-sections reveal a bimodal distribution with rounded to sub-rounded quartz grains, some 500-900μm in diameter, with diagenetic overgrowths (Plate 5.7c). Sub-rounded quartz grains of 100-200μm in size have boundaries that are partly obscured by overgrowth cement. Minor feldspars, mica, glauconite and chert grains occur. Overgrowth cementation occludes almost all of the pore space, resulting in irregular compromise boundaries between adjacent overgrowths.

Interpretation

This mature quartz-arenite is interpreted as having been deposited within the tidal-flat environment. The quartz sand was probably sourced by deflation of the continental sabkha hinterland.

5.8.3 Facies D3: Red/brown anhydritic dolostones

This facies is approximately 3m thick and is exposed in the Mukhaibah dome where it crops out close to the base of the Upper Buah Formation. It overlies the pale-grey muddy carbonates of Facies C1 and is formed of red enterolithic beds of anhydrite-rich carbonate with quartz-rich and micritic lamina that undulate and are slightly brecciated. The upper bedding surface contains discoidal casts of gypsum crystals. This facies is best observed in the Buah dome area where it is 1-3m thick and formed of red and grey muddy carbonates disrupted and brecciated in places, with chert stringers a few millimetres thick showing micro-teepee structures. Locally, this facies contains centimetre-scale stringers of detrital angular quartz and carbonate clasts. In the Buah dome, this facies is capped by an undulating ferruginous crust up to 10cm thick. Three such crusts recur at intervals of 20-30cm.

Thin-section analysis reveals medium-grained crystalline carbonate with iron-rich clay laminae and anhydrite-rich patches. Spherulitic quartz nodules occur with numerous anhydrite relicts whilst micro-quartz laminae pseudomorph a nodular anhydrite texture (Plates 5.7d/e). Subhedral dolomite rhombs are zoned, non-equant and contain relict evaporites. Minor detrital quartz grains occur.

Interpretation

This facies is typical of sabkha deposition on supratidal-flats. The enterolithic fabric and abundance of anhydrite or of chalcedonic quartz after anhydrite suggests the presence of palaeo-exposure surfaces. Aeolian quartz grains can accumulate by adhesion to the moist sabkha surface and are typical of supratidal-zone sabkha deposits (Schreiber 1986). The ferruginous crusts observed in the Buah dome area are interpreted as possible silcrete horizons. These beds are overlain by aeolian sandstones of the Cambrian Thumaylah Formation.

5.8.4 Facies Association D synthesis

Facies Association D in the Mukhaibah dome records tidal-flat deposits overlain by a supratidal sabkha followed by a relative deepening with the deposition of peritidal stromatolites of facies C2. In the Buah dome, the sabkha red-beds contain silcrete horizons and are erosionally overlain by the aeolian sandstones of the Cambrian Thumaylah Formation. Facies Association D of the Mukhaibah dome is the lateral equivalent of this silcrete horizon of the Buah dome and is therefore taken to represent the top of the Buah Formation here.

5.9 FACIES ASSOCIATION E: THE DISTAL DEPOSITS OF WADI BANI AWF

The Buah Formation sediments of Wadi Bani Awf are well exposed along the wadi floor in Wadi Bani Awf and are dominated by distal slope facies (Figure 5.1). These have been divided into facies representing characteristic lithological types. The basal Facies E1 grades-upward from the underlying siliciclastic/carbonate cycles of the Shuram Formation.

Summary of distal sedimentary facies in the Buah Formation			
Association E	**Lithology**	**Structures**	**Interpretation**
E7	Cherty ooidal grainstones		Platform-slope
E6	Massive breccia		Slope
E5	Slumped laminites	Slumps, breccia	Slope
E4	Carbonate and shale laminites	Planar	Deep water
E3	Rhythmites	Slumps, s.s.def.	Slope
E2	Recrystallized evaporitic-laminites		
E1	Black crinkly laminites	Nodular	Wave base

Table 5.2 Buah Formation distal Facies Association E with facies E1 to E7, all of which crop out in Wadi Bani Awf in the Oman Mountains. The facies are described from the base of the formation upwards in approximate stratigraphic order.

5.9.1 Facies E1: Black crinkly laminites

This facies forms the basal 55m of the Buah Formation in Wadi Bani Awf and comprises dark grey, nodular limestones with edgewise breccia interbeds (Log, Appendix 5). The dark-grey colour makes Facies E1 a marker bed throughout the Oman Mountains. The basal part of this facies contains silty carbonates with thin carbonate stringers. After 34m of section, the siliciclastics die out and the millimetre-laminated black limestones are bedded on a 10-50cm scale. These form massive, well-indurated, resistant beds that are packed with hairline calcite veins. Upward, Facies E1 becomes more thinly bedded with millimetre-scale silt intercalations and weathered-out pyrite cubes.

This facies is totally recrystallized, being formed of calcimicrospar and calcispar. Being very similar to the crinkly laminites of the Huqf area these also form mm-cm scale nodular beds with rare edgewise flake-breccia interbeds. Some sections contain millet-seed quartz and feldspar grains especially concentrated along stylolites. This facies is extensively stylolitised with iron-rich clay solution seams. Pyrite cubes are ubiquitous and authigenic quartz is prevalent upwards.

Interpretation

These black crinkly laminites are quite similar to facies B1 in the Huqf area and are also interpreted as having been deposited in a sub-wave base environment as the beds are planar laminated, and devoid of sedimentary structures that indicate current activity. The

dark colouration and abundance of pyrite indicates the presence of precursor organic matter.

5.9.2 Facies E2: Recrystallized evaporitic-laminites

This facies comprises 9m of section and is characteristically sub-millimetre, planar to nodular laminae that are formed of recrystallized microspar with numerous evaporite relicts and pyrite grains. Higher in the facies, authigenic quartz forms regular six-sided porphyroblasts possibly pseudomorph gypsum (Plate 5.9g). The top 6m of this unit comprises a 'cottage-cheese fabric' formed of microspar intercalated with micrite (Plate 5.9f).

Interpretation

The cottage-cheese fabric of the dolospar is similar to nodular anhydrite fabrics from sabhka-type environments described in the literature (Schreiber 1986, Kendall & Harwood 1996). However, in this instance there is no evidence for fenestral fabrics nor desiccation structures to suggest a similar sabhka environment for these deposits. The pervasive recrystallization of this facies and the lack of sedimentary structures make it very difficult to define the environment of deposition. The occurrence of pyrite suggests reducing conditions below the sediment-water interface whilst the dark colour might reflect a high organic content. The adjacent sub-wave base Facies of E1 and slope Facies E3 suggest that Facies E2 also represents deeper-marine deposition.

5.9.3 Facies E3: Rhythmites

This facies occurs twice in the section: the lower exposure is 15m thick whilst the upper one is 86m thick and crops out between the lower and upper breccia units in the upper part of the Buah Formation. In the field, it has a banded appearance, composed of light-grey dololutite alternating with dark-grey bands of dolosiltite which are locally cherty, especially close to the contact with the massive breccia. Laminations are sub-millimetre- to centimetre-scale with dolosiltite composing the thickest laminae. These are commonly planar bedded but scours, soft-sediment deformation structures and auto-brecciation are locally developed. Slump folds on the scale of a few-centimetres occur (Plate 5.10d). Some of the detrital beds are normally graded.

In thin-section, the base of this unit is formed of alternating planar beds of micrite and microspar with minor cherts and stylolites (Plate 5.10g). Laminations consist of microspar alternating with detrital laminations formed of quartz, feldspar, and muscovite grains up to 100μm in size, pyrite and micritic peloids (Plate 5.10e). The detrital laminations often have erosional bases. Toward the top of this facies, the intraclasts include broken and fragmented ooids.

Interpretation

This facies is inferred to represent periplatformal, fine-grained carbonate derived from the shelf margin. Grading suggests episodic influx of sediment, perhaps as thin and dilute, distal turbidites produced during off-shelf transport of sediment during storms. Slump folding and truncation surfaces within the rhythmites indicate upper-slope failure and initial down-slope transport of autochthonous rhythmite masses.

5.9.4 Facies E4: Carbonate and shale laminites

This facies is 44m thick and comprises millimetre- to centimetre-scale interbeds of fine-grained organic-rich carbonate and dark organic-rich siltstone (Plate 5.9d). Bed thickness is on a centimetre-scale with very planar contacts and are without any sedimentary structures indicative of current activity.

Thin-section analysis reveals that these comprise minor detrital quartz, feldspars and mica grains up to 50μm in size that are matrix-supported within clay and organic-rich micrite. These alternate with paler, inclusion-rich microspar beds having minor detrital quartz, feldspars and mica but with large (up to 100μm) pyrite cubes. Thin lenses of peloids, quartz, feldspar and mica grains occur within a sparry matrix; these lenses can be up 100μm thick and pinch out laterally (Plate 5.9e).

Interpretation

These organic-rich shales and carbonates are interpreted to have formed in a deep water setting. This environment is suggested by the dark colour, planar and parallel bedding, thin laminae and lack of wave produced sedimentary structures. The pyrite and organic-rich nature of this facies indicates that at least partly anoxic conditions prevailed at the sediment/water interface. The influx of terrigenous siliciclastics possibly reflects a relative increase in water depth or may indicate a change in the climatic or tectonic regime.

5.9.5 Facies E5: Laminites with slumps and auto-brecciation

This facies comprises 28m of section and is formed of undulating, contorted and planar beds of dark-grey and creamy-white dolomicrite and dolospar. Laterally these are folded into slump structures and numerous auto-breccia patches (Plates 5.9c and 5.10f). Thin-section analysis reveals that the laminites are formed of microspar and spar alternations. Stylolites are common.

Interpretation

The fine-grained nature of this facies along with the lack of wave produced sedimentary structures indicate a deep-water environment of deposition. The ubiquitous auto-

brecciation and slump structures suggest the presence of a slope where minor failure caused the *in-situ* disassociation and brecciation of the beds. The pervasive recrystallization of this facies possibly reflects the original fine-grained aragonitic or high Mg-calcite mudstones. Similar dark and light laminations have been interpreted as structures formed by evaporite dissolution (Schreiber 1986; Tucker 1991).

5.9.6 Facies E6: Breccia

The lower breccia unit is 30m thick, and erosively overlies the laminites of facies E5 and appears to thin toward the east. This is a massively bedded unit that lacks textural changes from the base to the top. It is pale-grey weathering with pale dolomitic clasts up to 2m in diameter. The clasts are angular, often fragmented, poorly-sorted, randomly oriented and matrix supported (Plate 5.9a). They are composed of micrite, grainstones and rarely microbial laminites. Thin-sections reveal that this facies is formed of angular dolomicrospar clasts within a microspar matrix (Plate 5.9b). Sometimes it is very difficult to recognise the clasts within the matrix.

Two more breccia units occur in the upper part of the Buah Formation in Wadi Bani Awf. Of these, the lower is 6m thick whilst the upper is almost 12m thick (Plate 5.10b). In Wadi Bani Kharus, similar breccia units are 5m and 10m thick, with the upper unit being unconformably overlain by the Permian Khuff Formation. These breccias also have erosive contacts and are massively bedded with poorly sorted angular clasts. Clast sizes vary from a few millimetres to 2m. The clasts exhibit random orientation, are devoid of any obvious normal or reverse grading and are supported by a grainstone matrix. Thin-section analysis reveals that the background sedimentation was an ooidal-grapestone wackestone with fragmented angular breccia clasts composed of micrite, stromatolites and ooidal wackestone (Plate 5.10b).

Interpretation

As the lowermost massive breccia unit is interbedded with the slope Facies E5, it is interpreted to represent catastrophic failure of the slope which resulted in downslope transportation in the form of a debris flow. The large size, very angular nature, poor sorting and homogeneity of the clasts indicate limited transportation. The breccia was probably deposited as periplatformal detritus at the foot of an escarpment. The unit appears to thicken away from the platform margin near Wadi Bani Kharus.

The upper breccia unit is interpreted as being a slump or slide deposit that formed as a gravity flow which entrained platformal sediments. Although this facies occurs in Wadi Bani Awf and Wadi Bani Kharus, its lateral geometry has not been determined.

5.9.7 Facies E7: Cherty ooid grainstones

Two units of facies E7 occur near the top of the succession at Wadi Bani Awf. The lower exposure is 6m thick while the upper one is approximately 13m thick. Facies E7 comprises metre-scale beds of massive pale-grey ooidal grainstones with thin planar beds 2-3cm thick. The matrix of the upper breccia unit of facies E6 is formed of ooidal grainstones similar to facies E7.

Thin-sections reveal this facies to be formed of ooidal grainstones/packstones. The ooids and oncoliths, up to 2mm in diameter, are concentric with a 'brick calcite' fabric (Plate 5.10a). Some ooids are replaced by megaquartz or calcite spar. The matrix is an inclusion-rich calcite spar.

Interpretation

This facies represents deposition in an agitated environments, although no sedimentary structures were observed in outcrop, these probably represent reworked platformal grainstones. The brick fabric retained in the ooids indicates an aragonite precursor (Tucker 1984).

5.9.8 Facies Association E synthesis

The basal Facies E1 is similar to the facies A observed in the Huqf area and is, therefore, taken to represent deposition below fair-weather wave base. These may have been partially restricted leading to the occurrence of putative evaporites. The massive unit of organic-rich carbonates (E2 and E3) and shales (E4) indicates a period of anoxic deep marine deposition. The overlying slope facies (E5) possibly represents redeposited grainstones with the intercalated breccia (E6) horizons representing *in-situ* slope failure. There is a general shoaling toward the top of the Buah Formation in Wadi Bani Awf to reworked shallow marine deposits (E7). These reworked shoal sediments are interbedded with two massive units of breccia (E6) which may result from contemporaneous tectonic activity, as similar breccia units also overlies the columnar stromatolites of Wadi Bani Kharus. In Wadi Bani Kharus, the breccia unit is unconformably overlain by the Permian Khuff Formation. The base of the overlying Fara Formation in Wadi Bani Awf is taken at the first influx of volcaniclastic silts.

5.10 BUAH FORMATION SYNTHESIS

Figure 5.1 illustrates the interpreted platform model of deposition for the Buah Formation. The lower member of the Buah Formation grades-upward from the silty carbonates and siltstones of the Shuram Formation and represent deposition below fair-weather wave base (Facies Association A) shoaling-up to reef forming, large-scale

compound stromatolites (Facies Association B). A possible flooding event is marked by the overlying silty peloidal wackestones. A general upward shoaling occurs within the upper part of the Lower Buah Formation, with the deposition of a thick unit of tabular stromatolites and cross-bedded grainstones over the whole region. This period represents platform deposition across nearly all of Oman (except Wadi Bani Awf) that became progressively more evaporitic upwards, reflecting an arid climate and at least limited basin restriction.

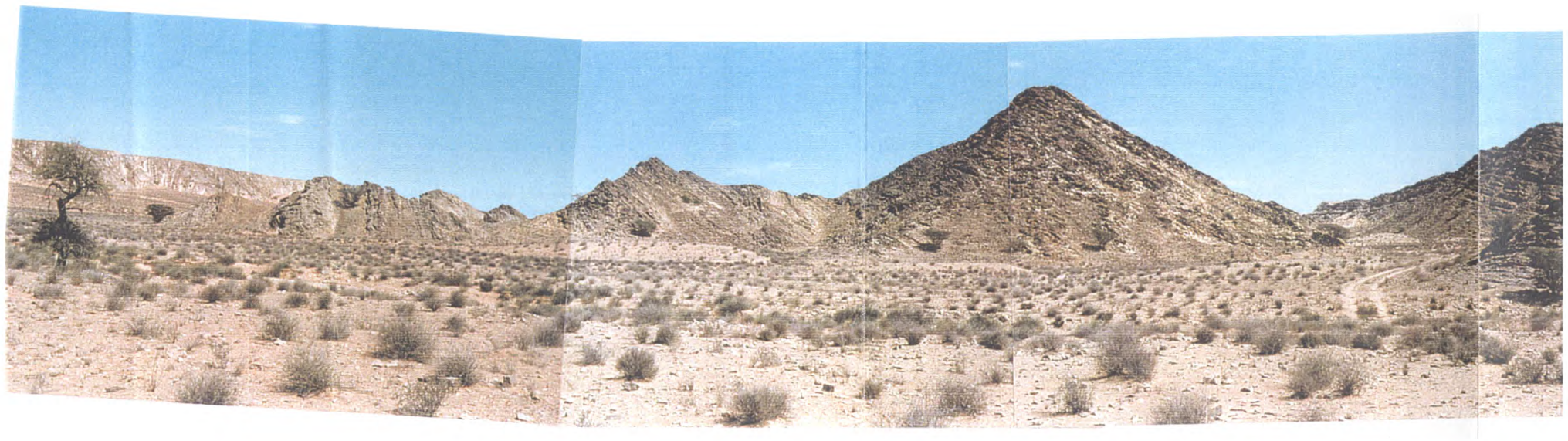
A marked change occurs in the intermittently exposed upper member of the Buah Formation where the stromatolites of Association C are very fine-grained and smooth laminated as opposed to the coarsely recrystallized laminations that characterise the lower member of the Buah Formation. The upper member is characterised by peritidal cyclicity with recessive lagoonal mudstones being overlain by stromatolites showing abundant evaporite pseudomorphs, fenestrae and auto-brecciation indicative of peritidal deposition. The extensive chertification of these facies probably reflects supratidal meteoric mixing, resulting in pH changes that enhance silica precipitation (Maliva *et al.* 1989).

Facies Association D is taken to represents a lagoonal to sabkha environment. Sabkha deposits represent progradation of supratidal-flats along protected coastlines. Facies Association D in the Buah dome is erosionally overlain by the Thumaylah Formation aeolian sandstones of Cambrian age (Dubreuilh *et al.* 1992).

Facies Association E of Wadi Bani Awf is characterised by deeper-water deposits that are organic-rich. These give way to slope deposition with extensive breccia units caused by gravitational and slope failure. Cherty ooidal grainstones in the upper part of Facies Association E suggests reworking of shoal sediments.

Thus the Buah Formation in the Huqf area and in Wadi Bani Kharus represents a gradual shoaling from below fair-weather wavebase deposition to supratidal and sub-aerial deposition. In Wadi Bani Awf, the Buah Formation represents deeper marine deposition of distal mudstones, turbidites and slope deposits with slope-failure breccias.

Overall the Buah Formation is taken to represent deposition on a carbonate platform, with the shallow water deposits of the Huqf area and Wadi Bani Kharus forming on the platform whereas the organic-rich muddy carbonates of Wadi Bani Awf represent slope and distal sedimentation (Figure 5.1).



Buah Formation in Wadi Shuram

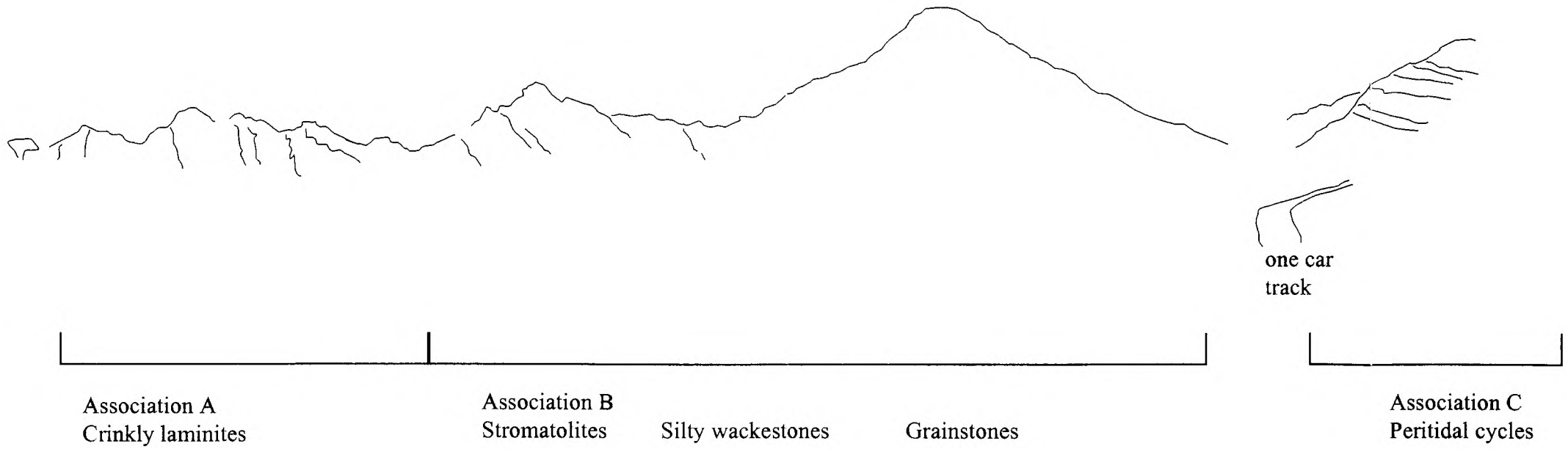


Plate 5.1

Lithofacies Association A Crinkly laminites

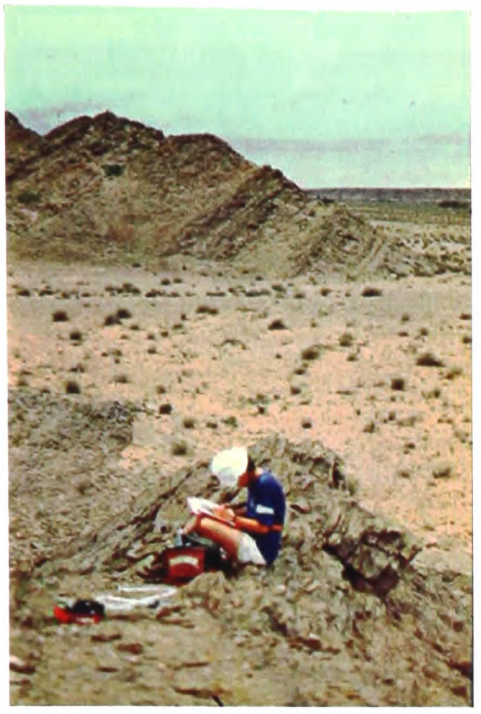


Plate 5.2a Crinkly laminites (A1) and silty limestones (A2) forming rhythms on the southern limb of the Kd anticline in Wadi Shuram. author for scale.

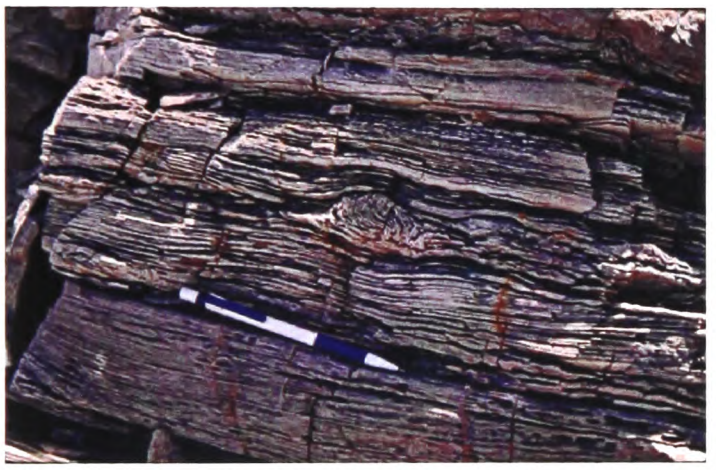


Plate 5.2c Facies A1, crinkly laminites (A1) formed of planar crinkly laminations with minor swales (below pen) in the Mukhaibah dome. Pencil for scale

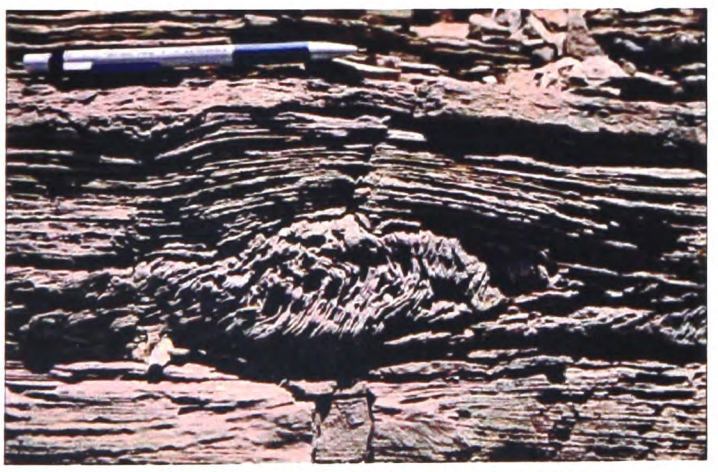


Plate 5.2e Subfacies A1a, edgewise flake-breccia cluster within crinkly laminations in the Mukhaibah dome. Pencil for scale

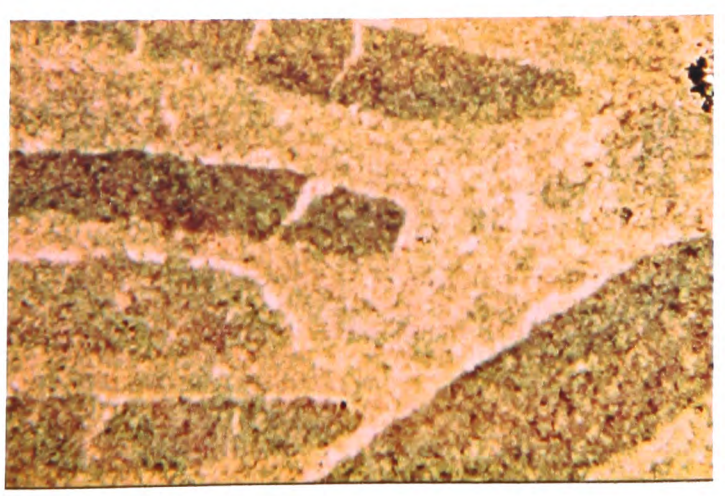


Plate 5.2g Photomicrograph of edgewise flake-breccia (A1a) Horizontal fov 2.45mm ppl.

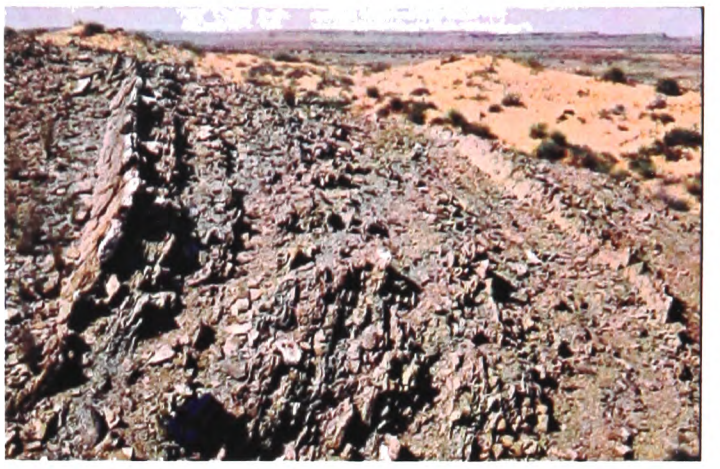


Plate 5.2b Crinkly laminite (A1) and silty limestone (A2) rhythms in the Mukhaibah dome. Backpack for scale.

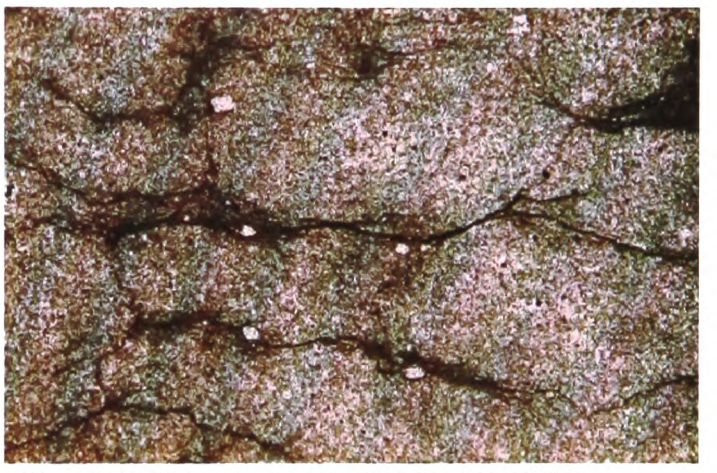


Plate 5.2d Photomicrograph of Facies A1, crinkly laminites containing microspar with clay-rich inter-laminations. Horizontal fov. 2.45mm ppl. 74m Md

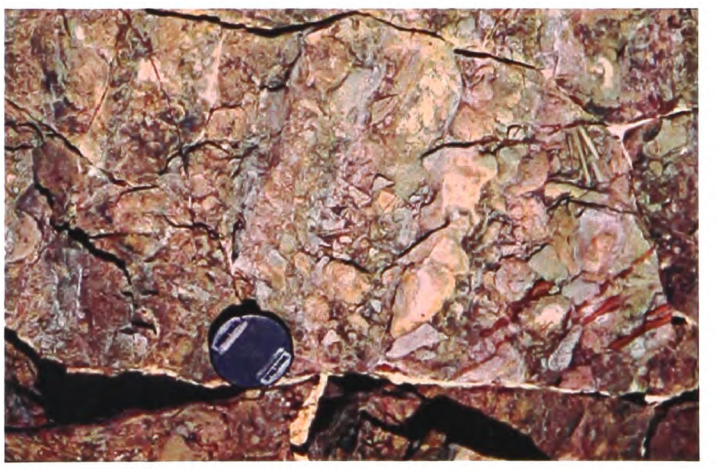


Plate 5.2f Subfacies A1b, flat-pebble conglomerate horizons form thin caps to the rhythms.
Lens cap 50mm

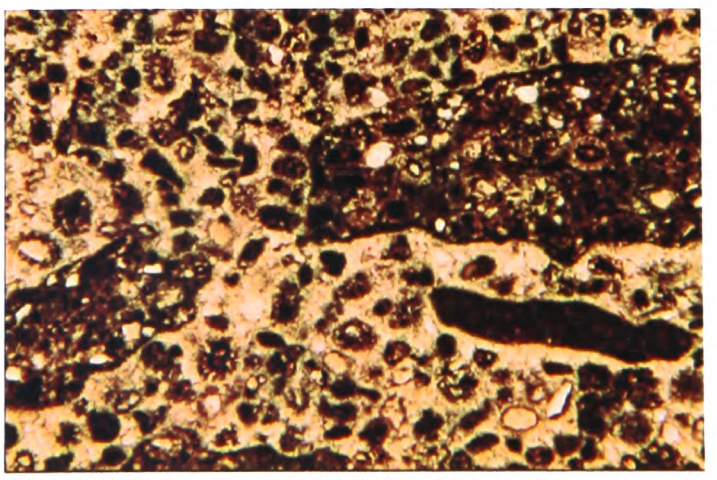


Plate 5.2h Photomicrograph of flat-pebble conglomerate (A1b) Horizontal fov 2.45mm ppl. 45m Md

Facies Association B: Stromatolites and grainstones



Plate 5.3a Overview of Facies B3, stromatolites and grainstones, facing east in Wadi Shuram.



Plate 5.3b Large compound stromatolite of Facies B1, at the western end of Wadi Shuram. Dave Wright for scale.

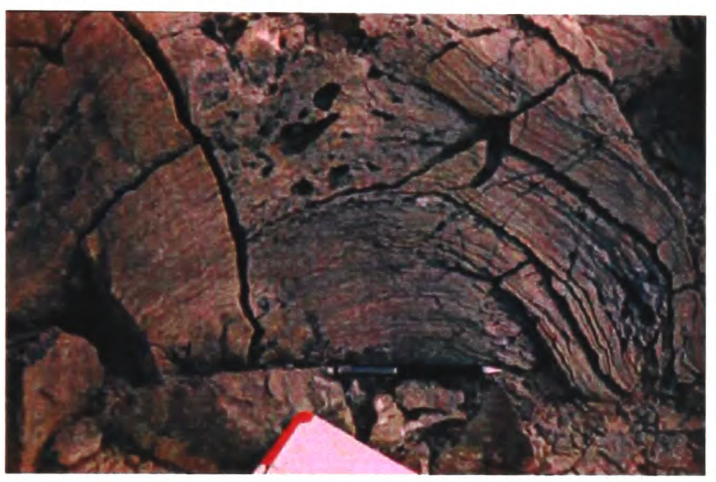


Plate 5.3c Compound stromatolite of Facies B1, showing internal lamination and steeply-dipping margins. Pencil for scale.



Plate 5.3d Photomicrograph of compound stromatolite of Facies B1, with ill-defined micritic and microspar laminations. Horizontal fov. 2.45mm. ppl.



Plate 5.3e Cross-stratification within recrystallised grainstones of Facies B1 in the Mukhaibah dome. Pencil for scale. 77m

Lithofacies Association B Lower Buah Formation



Plate 5.4a Cavernous weathering of stromatolites and grainstones (B3) at 121m in the Mukhaibah dome. Hammer for scale



Plate 5.4b Tabular stromatolite laminae (B3a) retain a crinkly-nodular texture. 112m in the Mukhaibah dome. Lens cap 50mm.

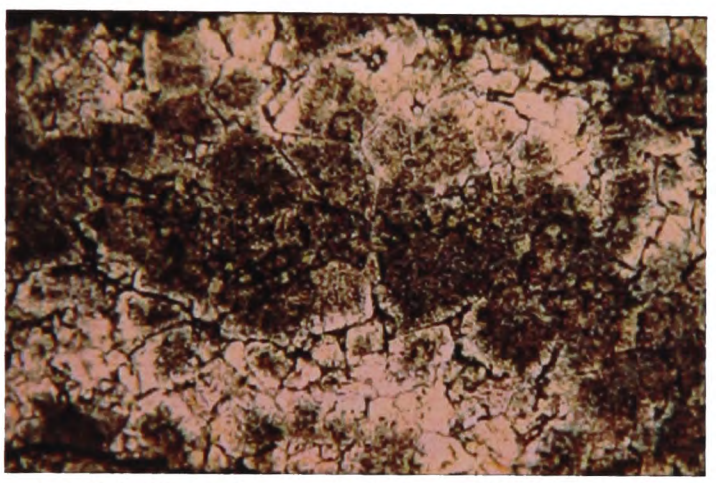


Plate 5.4c Photomicrograph of recrystallised tabular stromatolite, coarse dolospar with inclusion-rich laminae. Horizontal fov. 0.9mm ppl. 44m Bd

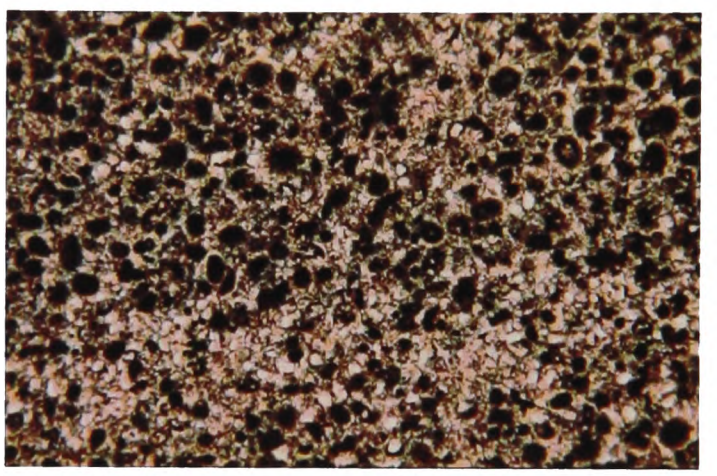


Plate 5.4d Photomicrograph of silty peloidal wackestone (B2). Horizontal fov. 2.45mm ppl. 55m Kd



Plate 5.4e Recessive, brown silty peloidal wackestone (B2). Beds are a few-cm. thick, have a nodular appearance with rare ripplesa and truncation surfaces. backpack for scale.



Plate 5.4f Heterolithic beds within silty peloidal wackestone (B2). Beds are a few-cm. thick. 85m Md

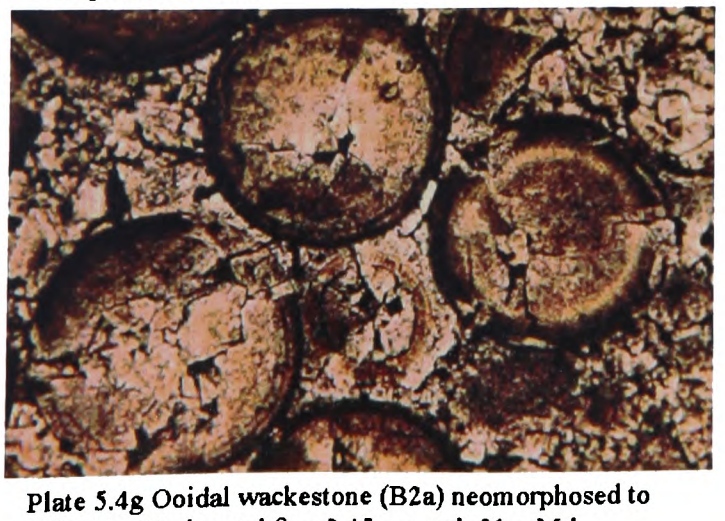


Plate 5.4g Ooidal wackestone (B2a) neomorphosed to dolospar. Horizontal fov. 2.45mm ppl. 81m Md



Plate 5.4h Recrystallised grainstone (B3) with anhydrite rosettes. 157m Kd
Lens cap 50mm

Lithofacies Association C in the Mukhaibah dome

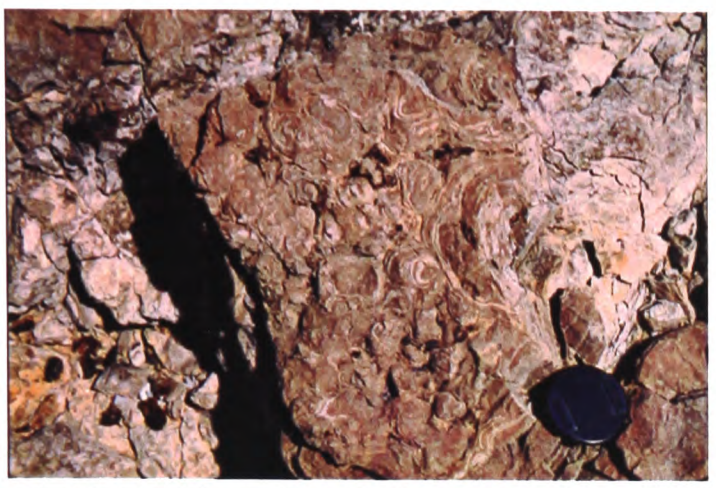


Plate 5.5a Bedding surface of columnar stromatolites (B3d) at top of peritidal cycle at 137m Md.
Lens cap 50mm



Plate 5.5b Uppermost peritidal cycle with stromatolite laminations contorted and brecciated. 249m Md
Lens cap 50mm

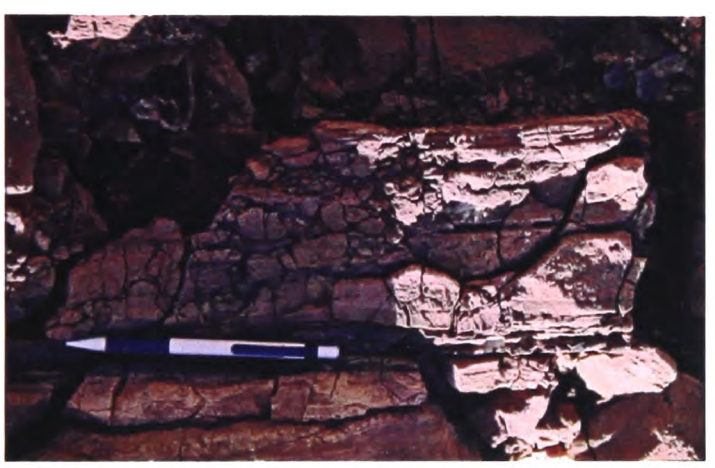


Plate 5.5c Auto-brecciated laminations within peritidal cycle (Facies C). 190m Md
Pencil for scale



Plate 5.5d LLH-C stromatolite domes (C2) from peritidal cycles at 194m Md
Backpack for scale

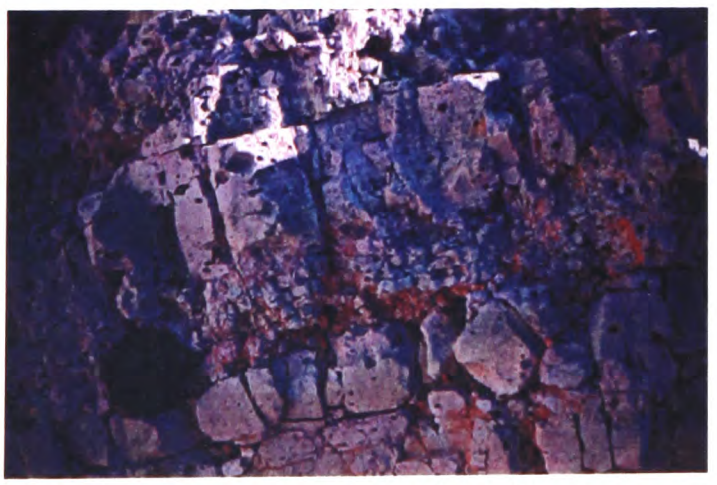


Plate 5.5e Vuggy, fenestral laminations with auto-brecciation from peritidal facies C2 at 202m Md
Lens cap 50mm

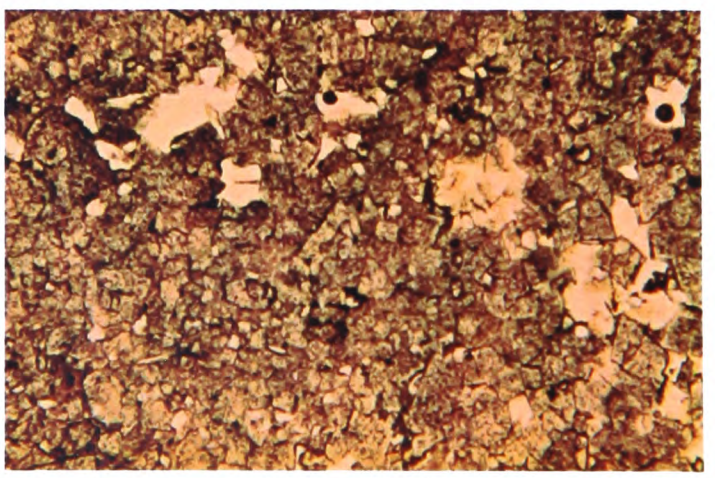


Plate 5.5f Recrystallised vuggy dolospar from peritidal facies C2. Horizontal fov. 2.45mm ppl.

Plate 5.5

Lithofacies Association C in the Khufai dome



Plate 5.6a Cherty columnar stromatolites (C2a) from peritidal facies at 347m Kd
Notebook and pencil for scale

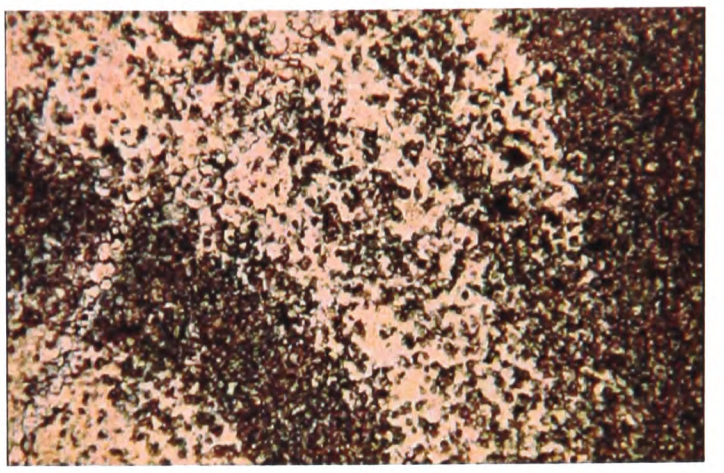


Plate 5.6b Photomicrograph of cherty columnar stromatolites (C2a), microspar and spar laminations.
Horizontal fov. 2.45mm ppl. 337m Kd



Plate 5.6c Nodular-ball textured dolostones interbedded with stromatolites from peritidal facies (C2). 321m Kd
Lens cap 50mm

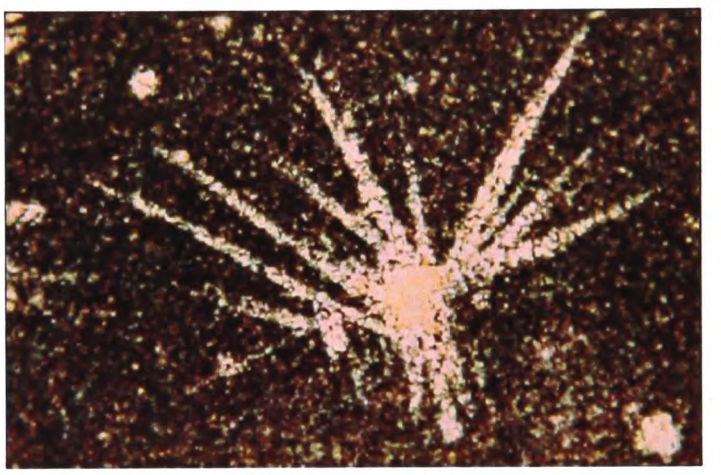


Plate 5.6d Photomicrograph of 5.6c, micritic dolostone with anhydrite rosette. 321m Kd
Horizontal fov. 2.45mm ppl.



Plate 5.6e Cherty stromatolites (C2) within pale-yellow dolomicrites from peritidal facies. 310m Kd
Notebook and pencil for scale.

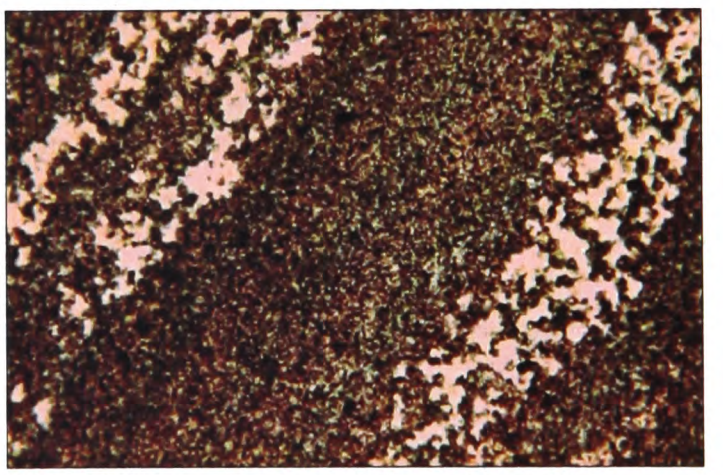


Plate 5.6f Photomicrograph of cherty stromatolites (C2) at 310m Kd
Horizontal fov. 2.45mm ppl.



Plate 5.6g Peritidal cycle base with recessive muddy carbonate (C1) overlain by stromatolitic dolostone (C2). 296m Kd



Plate 5.6h Photomicrograph of recessive muddy carbonates (5.6g) facies C1 from the lower part of the peritidal cycles. Horizontal fov. 2.45mm ppl. 170m Kd

Lithofacies Association D Sabhka



Plate 5.7a Overview of Facies Association D from the Mukhaibah dome. Ridge to left of picture is top of Association C. Backpack for scale.

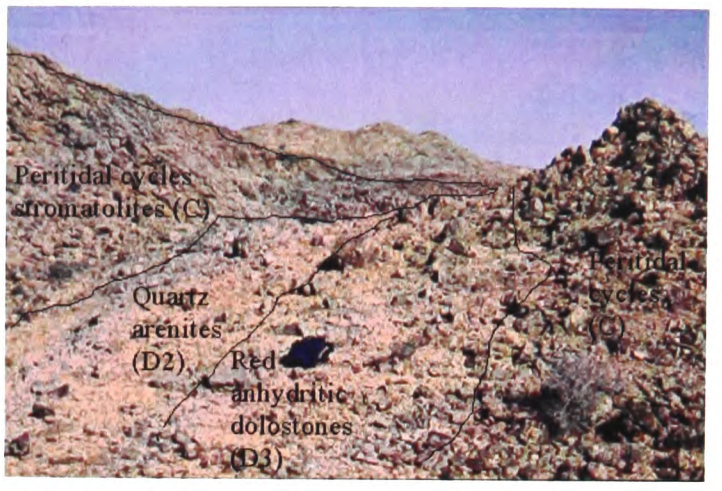


Plate 5.7b Sabhka Association D, with facies outlined. Backpack for scale

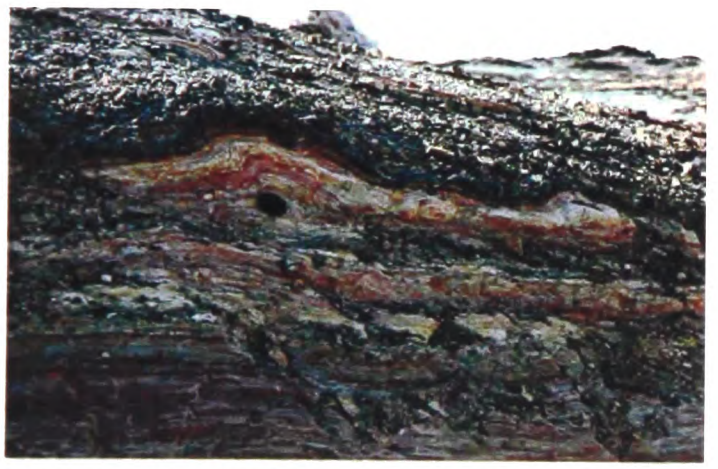


Plate 5.7c Sabhka siltstones (D3) with enterolithic folds and ferruginous crusts. Bd
Lens cap 50mm

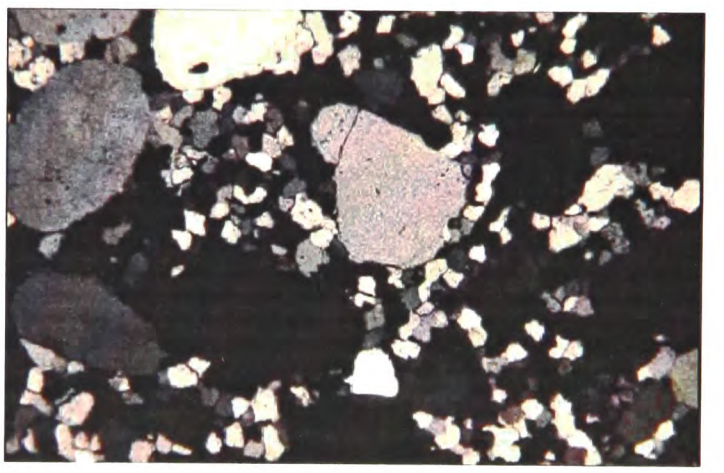


Plate 5.7d Photomicrograph of bimodal quartz arenites (D2) note overgrowths on grains.
Horizontal fov. 2.45mm xpl. 254m Md

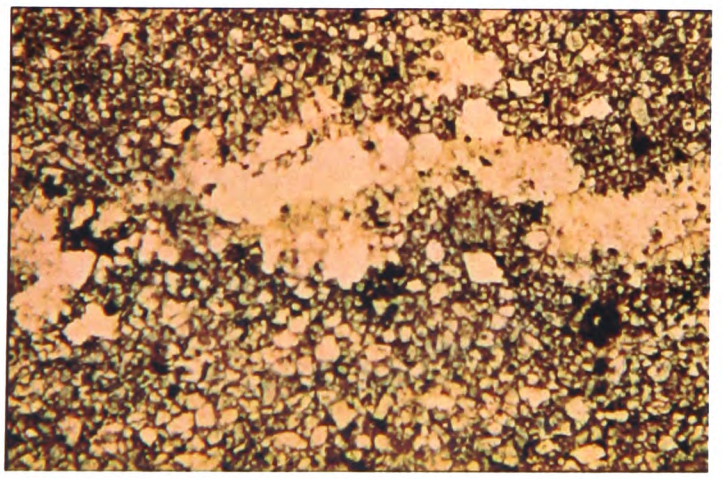


Plate 5.7e Photomicrograph anhydritic dolostones (D3) with enterolithic folds of chert containing anhydrite relicts.
Horizontal fov. 2.45mm ppl. 186m Md

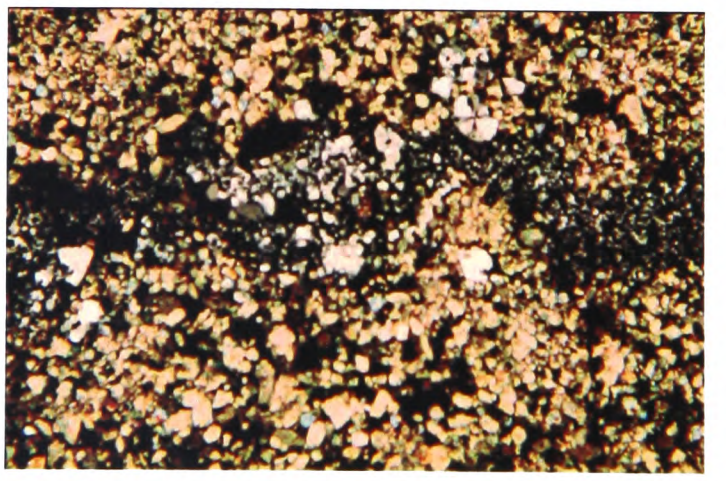


Plate 5.7f Photomicrograph anhydritic dolostones (D3) with enterolithic folds of chert containing anhydrite relicts.
Horizontal fov. 2.45mm xpl. 186m Md

Lithofacies Association A and B in Wadi Bani Kharus



Plate 5.8a Turbinate stromatolites (C3c) from Wadi Bani Kharus at 144m
Notebook 225x176mm

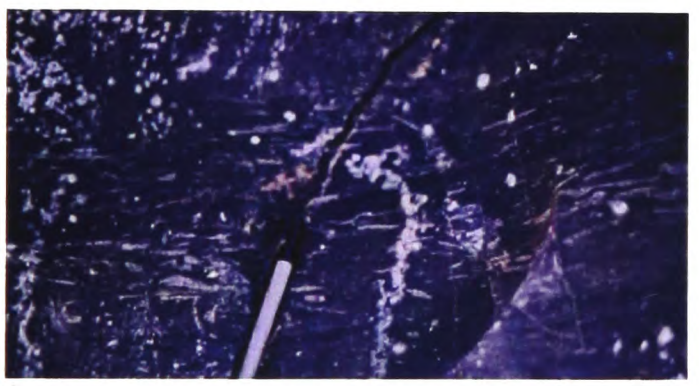


Plate 5.8c Recrystallised intraclast wackestone (B2) at 86m in Wadi Bani Kharus.
Pencil for scale

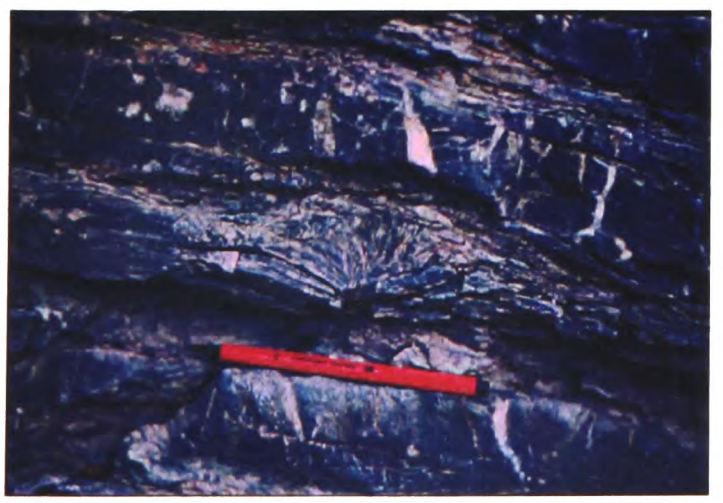


Plate 5.8e Edgewise flake-breccia (A1a) forming imbricated cluster within crinkly laminites (A1).
Pencil for scale

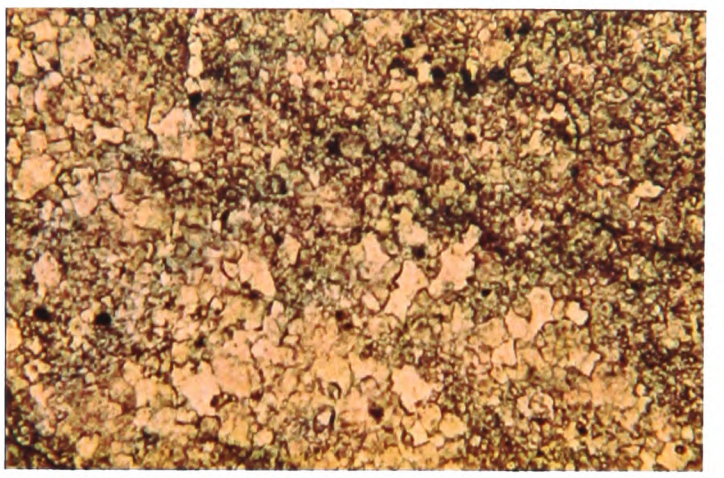


Plate 5.8b Photomicrograph of (B3c)turbinate stromatolites, undulating microspar and spar laminations. 108m
Horizontal fov. 2.45mm ppl.

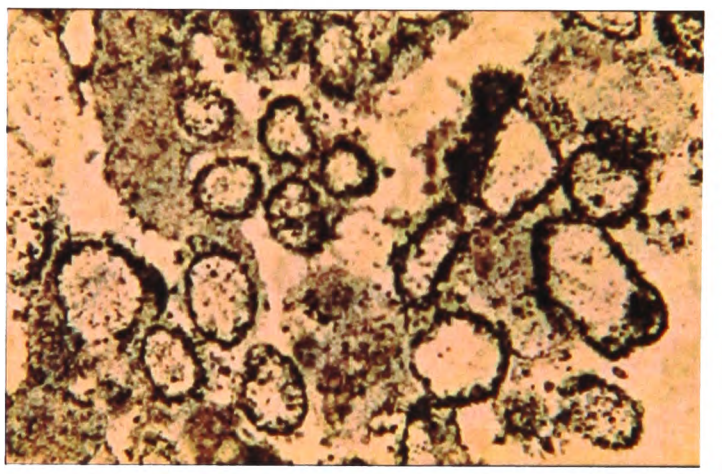


Plate 5.8d Photomicrograph of (B4) cherty ooidal grainstone. 163m
Horizontal fov. 2.45mm ppl.

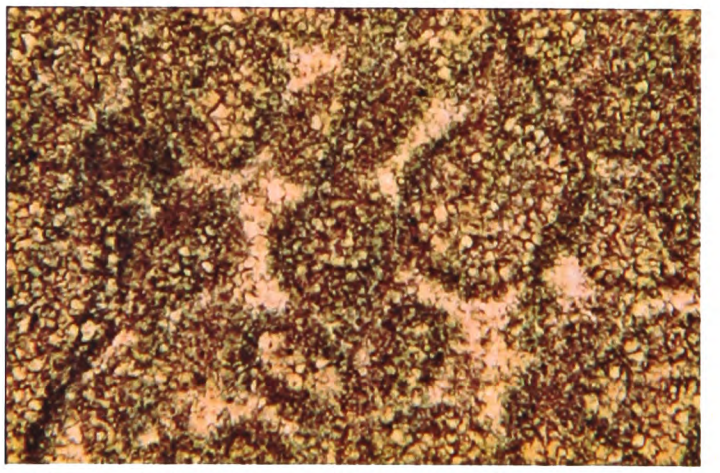


Plate 5.8f Photomicrograph of recrystallised grainstone (B3). 95m
Horizontal fov. 2.45mm ppl.

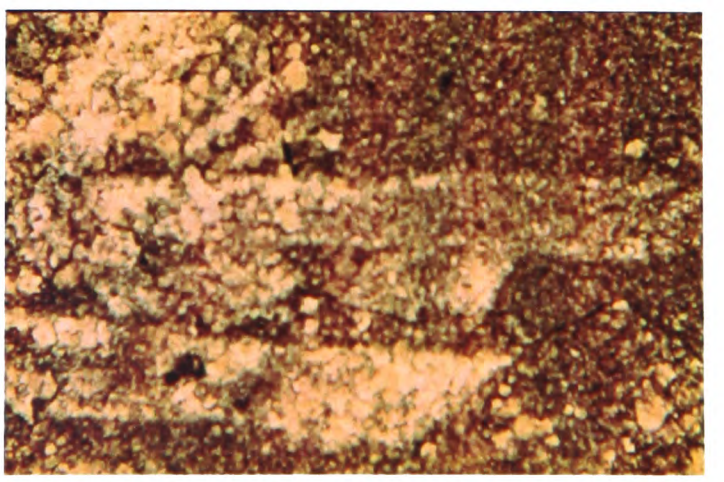


Plate 5.8g Photomicrograph of cushion stromatolites (B3b) with spar pseudomorphs after gypsum. 148m
Horizontal fov. 2.45mm ppl.

Plate 5.8

Lithofacies Association E in Wadi Bani Awf



Plate 5.9a Facies E6 Breccia with randomly orientated, poorly sorted clasts that are matrix supported. 161m WBA

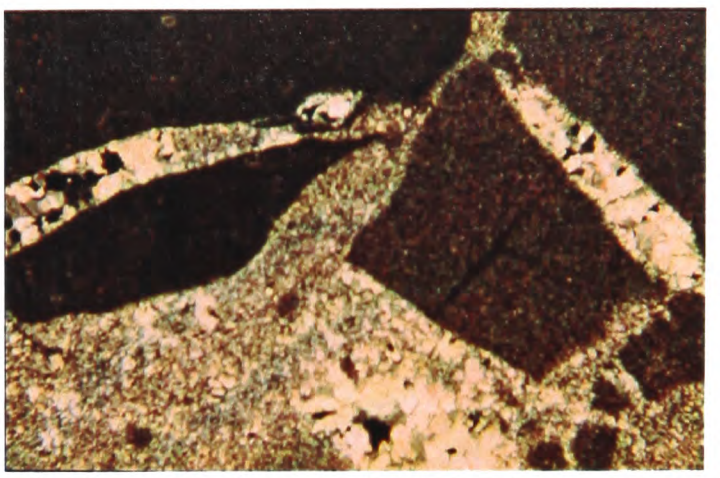


Plate 5.9b Photomicrograph of Facies E6 Breccia with fragmented, angular micritic clasts within a sparry matrix. Horizontal fov. 2.45mm ppl. 154m WBA



Plate 5.9c Dark grey and white laminations with extensive auto-brecciation and slump folds up to 1m. (E5) Hammer for scale. 125-152m WBA

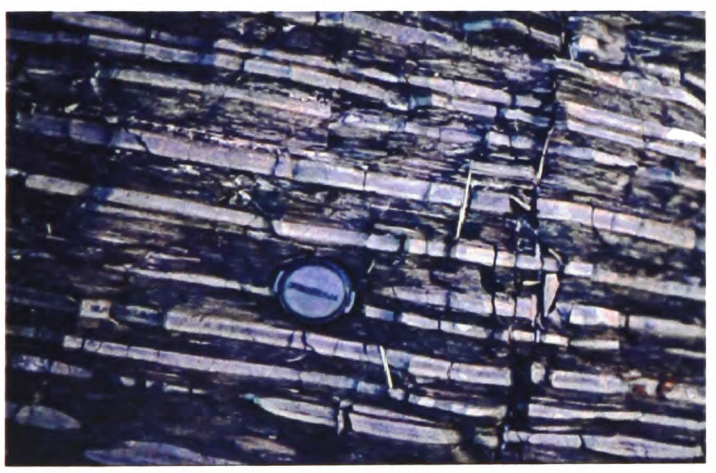


Plate 5.9d Carbonate and shale interbeds (E4), planar, cm-scale bands that are dark-grey and organic-rich. Lens cap 50mm 80-124m WBA

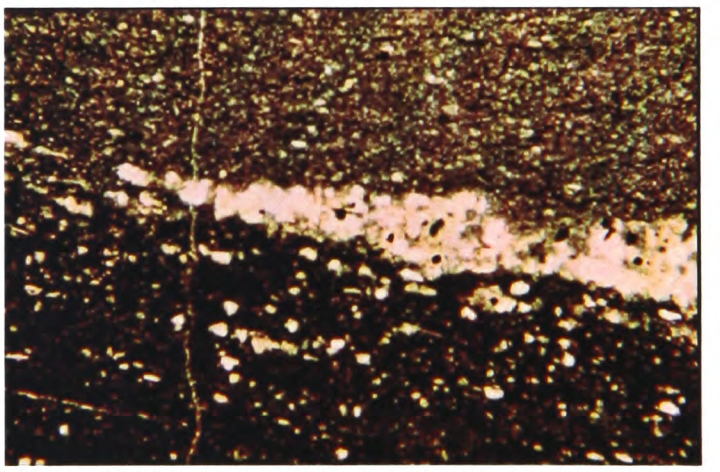


Plate 5.9e Photomicrograph of carbonate and shale interbeds (E4), dark organic-rich laminae alternates with silty microspar with minor spar. Horizontal fov. 2.45mm ppl. 108m WBA

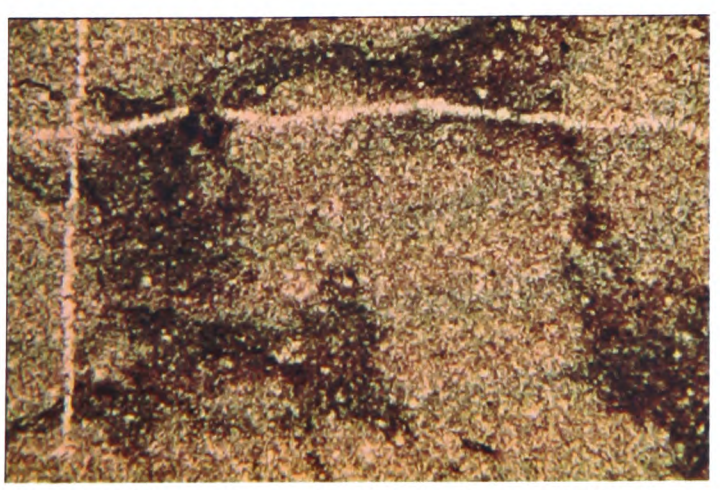


Plate 5.9f Photomicrograph of facies E2 recrystallised nodular laminations with 'chicken-wire' fabric possibly after precursor evaporites. Horizontal fov. 2.45mm ppl. 63m WBA

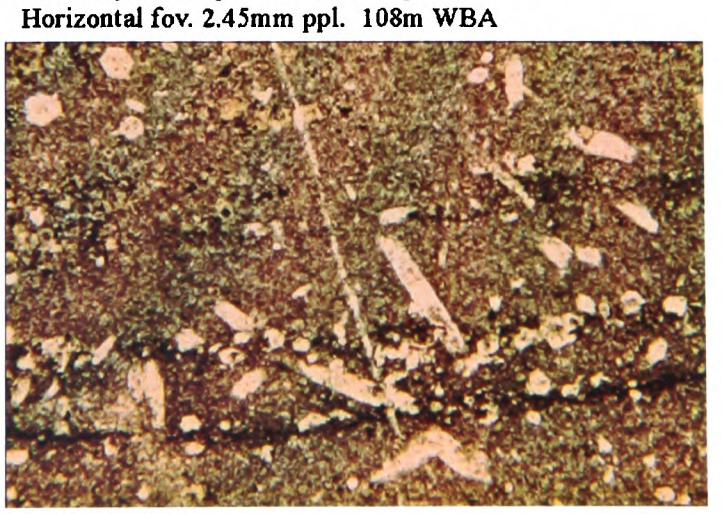


Plate 5.9g Photomicrograph of facies E2 recrystallised nodular laminations with authigenic quartz possible pseudomorphs after gypsum. Horizontal fov. 2.45mm ppl. 57m WBA

Plate 5.9

Lithofacies Association E in Wadi Bani Awf

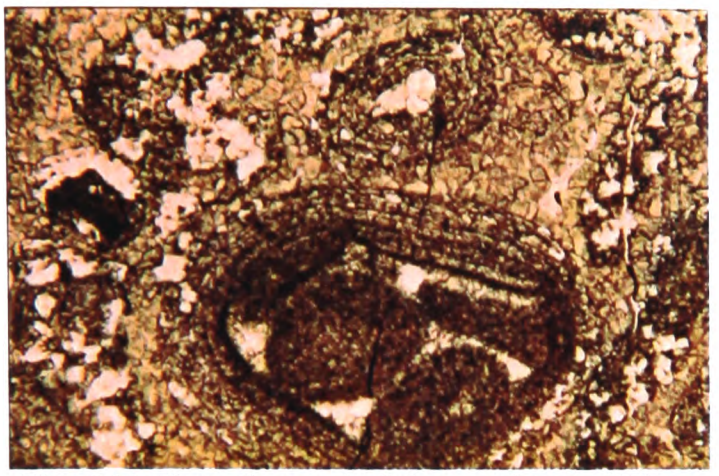


Plate 5.10a Photomicrograph of cherty grainstone (E7), ooids (laminae have brick texture) and grapestones within a cherty matrix. Horizontal fov. 2.45mm. ppl. 275m WBA

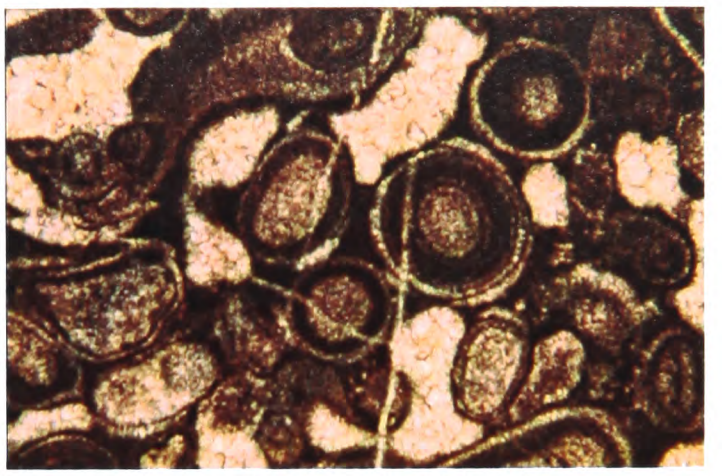


Plate 5.10b Photomicrograph of ooidal wackestone/ packstone matrix in the upper part of the lower breccia. Horizontal fov. 2.45mm. ppl. 182m WBA

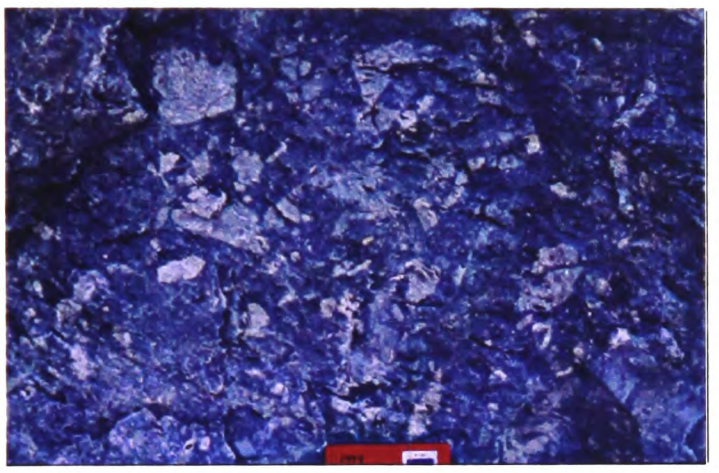


Plate 5.10c Uppermost breccia (E6) clasts matrix supported within an ooid-grainstone matrix. Notebook for scale 225x176mm. 280m WBA

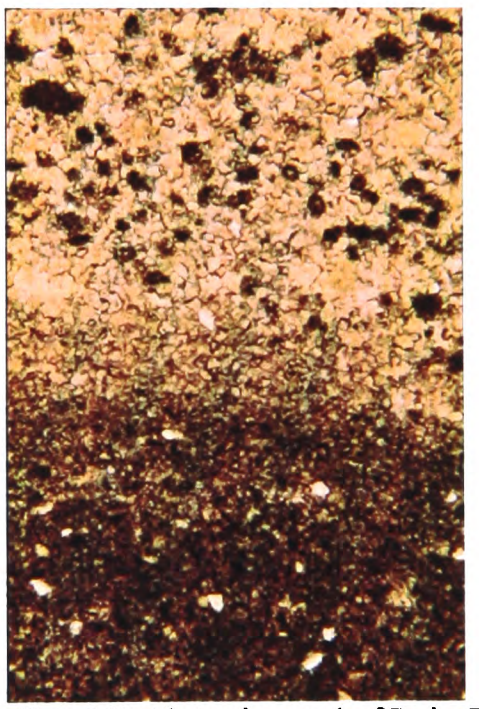


Plate 5.10e Photomicrograph of Facies E3, rhythmites dark micritic lamination alternating with sparite laminations with minor intraclasts. Horizontal fov. 2.45mm ppl. 232m WBA

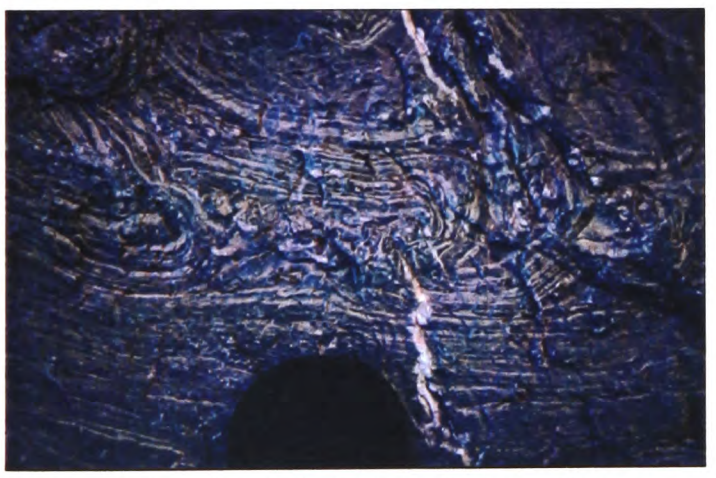


Plate 5.10d Facies E3 rhythmites with slump-folding and soft sediment deformation. Lens cap 50mm. 198m WBA



Plate 5.10f Facies E3 rhythmites with slump-folding and auto-brecciation. Hammer for scale 231m WBA

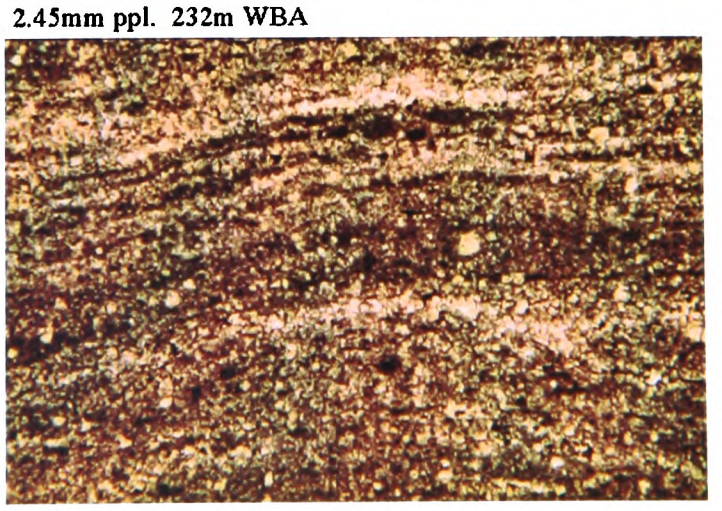


Plate 5.10g Photomicrograph of Facies E3, rhythmites undulating microspar and spar laminations. Horizontal fov. 2.45mm ppl. 218m WBA

Chapter Six - Chemostratigraphy

6.1 INTRODUCTION

6.2 BACKGROUND THEORY

6.3 TRACE ELEMENTS

6.4 DATA CORRECTION

6.5 DISCUSSION OF KHUFAI FORMATION

6.6 DISCUSSION OF SHURAM FORMATION

6.7 DISCUSSION OF BUAH FORMATION

6.8 CARBON ISOTOPE SIGNATURE SYNTHESIS

6.1 INTRODUCTION

The sediments of the Khufai, Shuram and Buah formations have good potential for the acquisition of chemostratigraphic data as they are well preserved dolostones and limestones that have been relatively free from tectonic alteration. The excellent preservation of fine-scale fabrics suggest that dolomitization was a syngenetic reaction that took place in the presence of fluids isotopically similar to seawater (Tucker 1983). If this is so, then, early cementation would have occluded pore-spaces isolating the dolomite crystals from alteration by later diagenetic fluids. Dolomite in isotopic equilibrium with calcite ought, in theory, to be enriched in ^{13}C by about 2‰ (Sheppard & Schwarcz 1970) though, in practice, the difference appears to be minimal (Kaufman & Knoll 1995). Most studies of Proterozoic limestones and dolostones have demonstrated empirically that they normally retain a C-isotopic composition that must be close to that of their precursor $CaCO_3$ (Tucker 1983; Knoll *et al.* 1986; Derry *et al.* 1992; Narbonne *et al.* 1994).

Whole-rock carbon isotopic studies have recently revealed stratigraphic patterns of $\delta^{13}C$ fluctuations of relative large magnitude through the late Neoproterozoic (Derry *et al.* 1994; Kaufman & Knoll 1995; Pelechaty 1998) and these may be used to improve the relatively coarse stratigraphic resolution provided by sparse Neoproterozoic fossils. Burns and Matter (1993) have produced a carbon-isotope curve for the Huqf Supergroup from 409 samples obtained from two outcrop sections (one in Central Oman and one in the Oman Mountains) and two wells (well MQ on the flank of the Ghaba Salt Basin and well T on the flank of the South Oman Salt Basin; Figure 1.1). Their data revealed positive $\delta^{13}C$ values of around +4‰PDB for the Khufai Formation with a sharp decrease to -4‰PDB in the Shuram Formation, followed by a slow increase to +2‰PDB in the upper Buah Formation.

The carbon-isotope curve of the present study is based on 316 samples from 11 different sections across Oman. These samples were selected as 'least altered' based on good fabric preservation, detailed petrography and cathodoluminescence techniques. Forty-eight samples representing different lithofacies were analysed for minor and major elements and this data is used as a further screen for diagenesis. Cross-plots of elemental and isotopic data as well as component analysis techniques are used to backtrack to the least-altered isotope signature. Analytical methods are described in Appendix 6 along with carbon and oxygen data for all the samples analysed.

The aim of this work is primarily to ascertain the stable isotopic character of the Huqf carbonate sediments in the Huqf area and Oman Mountains regions; and to examine the influence of water depth and facies on this signature and establish regional variations.

6.2 PRINCIPLES OF CARBON AND OXYGEN ISOTOPE CHEMOSTRATIGRAPHY

Isotopes are atoms of the same element whose nuclei contain the same number of protons but a different number of neutrons. The isotopic compositions of elements of low atomic number are variable because their isotopes are fractionated by natural chemical and physical processes. This fractionation is due to slight variations in the physical and chemical properties of isotopes proportional to differences in their masses. Differences due to fractionation are the basis of stable isotopic investigations in palaeoceanography (Anderson & Arthur 1983).

In stable-isotope geochemistry, the ratio between two different isotopes of the same element is measured. For stable-isotope geochemistry of carbon, the ratio of ^{13}C to ^{12}C (expressed as $\delta^{13}C$ and quoted in ‰) is measured and for stable-isotope geochemistry of oxygen the ^{18}O to ^{16}O ratio (expressed as $\delta^{18}O$ and quoted in ‰) is measured in a sample of calcium carbonate. These ratios are calibrated against the universal PDB standard, enabling the comparison of ratios from different samples and different laboratories (Anderson & Arthur 1983).

6.2.1 The Global Carbon Cycle

Conditions were such on the primitive earth that water vapour discharged from the mantle condensed to form oceans in which sizeable quantities of CO_2 entered into solution. Bicarbonate and carbonate ions were then precipitated to form sedimentary carbonate, according to the equilibrium system:

$$CO_{2\ (gas)} \leftrightarrow CO_{2(aq)} \leftrightarrow HCO_3^- \leftrightarrow CO^{2-}{}_3$$

This provided a mechanism for transferring volatile and dissolved carbon dioxide from the atmosphere and ocean to the solid crust. A second sink for atmospheric carbon dioxide was established after the initiation of prokaryotic microbial ecosystems in the Archaean. Biological or autotrophic carbon fixation (involving enzymatic reduction of CO_2) has effectively competed with the inorganic carbonate-forming process for the removal of carbon dioxide from the surficial exchange reservoir. This biological flux results in the deposition of kerogen and related substances that constitute the bulk of fossil organic matter. This large scale partitioning between the oxidised (carbonate) and reduced (kerogen) reservoir forms the basis of the biogeochemical carbon cycle.

6.2.2 Carbon-isotope fractionation

Carbon consists principally of two stable-isotopes, the light isotope ^{12}C with 98.89% abundance and the heavy isotope ^{13}C with 1.1% abundance (Anderson & Arthur 1983). The shortlived radioactive isotope ^{14}C occurs only in trace amounts. Autotrophic (e.g. photosynthetic) carbon fixation primarily involves the assimilation of carbon dioxide and dissolved bicarbonate ions by micro-organisms and plants. The bulk of primary biological production in the present carbon cycle is due either to chemically or solar-powered reduction of CO_2 to organic matter. Work performed by Park & Epstein (1960) confirmed that all photosynthesis discriminates against ^{13}C with the preferential uptake of ^{12}C, owing to a kinetic isotope effect inherent in the first irreversible enzymatic CO_2-fixing reaction (Schidlowski & Aharon 1988). This means that the conversion of inorganic carbon to living matter leads to a marked enrichment of the light carbon-isotope in the newly generated organic substances, while the heavy isotope is preferentially retained in the residual substrate. Thus the basic configuration of the global carbon cycle reflects the activity of the Earth's biosphere.

6.2.3 Vertical and lateral changes in the isotopic composition of sea water

Depth, ecology, water energy, proximity to land, the nature of circulation into and out of the region and many other factors contribute to fluctuations in the ambient seawater $\delta^{13}C$ and $\delta^{18}O$. Today, the world average surface water has a $\delta^{13}C$ of +2.0‰ PDB but the deeper waters have lower values: $\delta^{13}C$ of +1.0‰ to 0.5‰ PDB for North Atlantic Deep Water, +0.5‰ to -0.5‰ PDB for the deep Pacific and 0.5‰ to 0.0‰ PDB for the deep Indian Ocean (Prothero 1994).

Photosynthesis takes place in the photic zone of the oceans with maximum photosynthesis occurring in the upper 20m. As photosynthesis preferentially absorbs the lighter isotope ^{12}C, this results in an enrichment of ^{13}C in surface waters. The organic matter incorporated into the photosynthetic biomass sinks into deeper water where it becomes oxidised by bacterial respiration. This has the effect of releasing ^{12}C back into deeper waters so that a $\delta^{13}C$ gradient becomes established between shallow and deep waters. Absolute values of $\delta^{13}C$ in the photic zone also vary with productivity and surface water mixing, meaning that $\delta^{13}C$ can be used as an indication of palaeo-productivity in the oceans (Brasier 1995a).

6.2.4 Post-depositional isotope fractionation in sedimentary and organic carbonates

During diagenesis and metamorphism the primary isotopic signatures of both carbon species are apt to suffer secondary overprints as part of the overall changes experienced by their host rocks during their long geological history. Carbonate sediments deposited in shallow marine environments can become exposed to meteoric waters which are charged with CO_2 and thus highly corrosive. The unstable primary mineralogical assemblage of high-Mg calcite and aragonite transforms to the more stable low-Mg calcite by sequential dissolution-reprecipitation under such conditions (Land 1967; Bathurst 1975; Tucker & Wright 1990). This is a rock-dominated system in which the precursor mineral phases play a dominant role in controlling the chemistry and isotopic composition of waters in the microenvironment. Diagenetically stabilised sedimentary carbonates can therefore preserve the isotopic composition of original carbonate muds within *c.* ±1‰ of primary values (Schidlowski & Aharon 1988). Hence carbonates can closely reflect the $^{13}C/^{12}C$ ratio of the parent bicarbonate pool, which makes the marine C_{carb} record a fairly reliable sensor for the isotopic evolution of oceanic HCO_3^{2-}.

The carbon-isotope value of marine organic matter is about 25% more negative than inorganic bicarbonate (Marshall 1992), thus the degradation of organic matter has the potential to significantly alter the carbon-isotope composition of marine carbonate sediment. Reactions of organic-matter degradation include microbially mediated reduction of iron, manganese, sulphate and nitrate under sub-oxic conditions, and methanogenesis under anoxic conditions (Coleman & Raiswell 1981; Glumac & Walker 1998). Most of these reactions release organogenic carbon, which decreases the $\delta^{13}C$ value of dissolved bicarbonate and any precipitated carbonate phases (Irwin *et al.* 1977).

During metamorphism, carbonates with siliceous impurities can undergo decarbonation reactions in which the primary carbonate phases (limestone and dolomite) react with Ca-Mg silicates, with a concomitant release of CO_2. Decarbonation processes of this type start at 300°-400°C and increase with metamorphic grade. Thus the $\delta^{13}C$ of metamorphosed impure carbonates can be shifted by 2-5‰ in a negative direction (Kaufman & Knoll 1995)

6.2.5 Oxygen-isotope fractionation

Oxygen has three stable-isotopes with approximate abundances of ^{16}O = 99.63%, ^{17}O = 0.0375% and ^{18}O = 0.1995% (Anderson & Arthur 1983). In contrast to carbon, oxygen-isotope fractionation is strongly temperature-dependent; the $\delta^{18}O$ becomes depleted by

about 1‰ for every 4°C increase at near-surficial temperatures (Marshall 1992). The oxygen isotopic composition of modern surface waters is affected by evaporation, condensation and the mixing of water bodies. During glaciation, the trapping of large volumes of isotopically negative water in continental ice caps changes the composition of contemporaneous ocean water. Total melting of the present ice cap would result in a decrease in ocean composition of approximately 0.5 to 0.9‰ with the total difference between glacial and interglacial being about 1.2‰ (Marshall 1992).

Biogenic fractionation or 'vital effects' can also result in the non-equilibrium fractionation of oxygen isotopes in biominerals but this is not likely to be of significance in Precambrian sequences.

6.2.6 Post-depositional isotope fractionation in sedimentary and microbial carbonates

While C in the waters of the diagenetic microenvironment originates mostly from the precursor carbonate phases, the proportion of oxygen from this source (as opposed to that from pore waters) is negligible. Hence the oxygen isotopes of diagenetically modified carbonates are not likely to reflect the primary isotopic composition. Where a sediment has been buried deeper than about 400m, elevated temperatures result in cementation and recrystallization processes that act to decrease $\delta^{18}O$ values (Marshall 1992). Sub-aerial exposure also results in meteoric diagenetic alteration of $\delta^{18}O$ values by the precipitation of carbonate depleted in ^{18}O (Kaufman & Knoll 1995). On the other hand, evaporation can preferentially remove the lighter ^{16}O from the upper parts of the water mass, resulting in carbonates depleted in ^{16}O (Pierre 1988).

6.3 ELEMENTAL CHEMISTRY OF THE HUQF CARBONATES

Concentrations of Mn, Sr, Mg and Ca are important for understanding the degree of alteration associated with meteoric and burial diagenesis and dolomitization (Hudson 1977; Brand & Veizer 1981; Land 1980; Marshall 1992). In the diagenetic environment, stabilisation of an original metastable carbonate assemblage is achieved through complementary textural, mineralogical and chemical changes which involve the dissolution-reprecipitation reaction:

$$CaCO_3 + H_2O + CO_2 \leftrightarrow Ca(HCO_3)_2$$

Trace elements such as Sr^{2+}, Mn^{2+}, Fe^{2+}, Pb^{2+}, Zn^{2+} and Na^{+} will substitute to varying degrees for Ca^{2+} in the $CaCO_3$ lattice owing to different partition coefficients and large compositional differences in marine and meteoric water (Brand & Veizer 1980). Open or

partly closed diagenetic systems and/or single or multiple dissolution-reprecipitation events will lead, in general, to a decrease in concentrations of these elements in which $K_{calcite\text{-}water} < 1$ (Sr^{2+}, Na^{+}, Mg^{2+}) and to an increase for those with $K > 1$ (Mn^{2+}, Fe^{2+}, Zn^{2+}).

Elemental and stable-isotope data for the selected subset of 48 samples are presented in Table 6.1. All samples analysed in this way were free of secondary veins and vugs and are considered to be representative of the lithofacies described in preceding chapters. The complete stable-isotope dataset is presented in Appendix 6.

6.3.1 Mg/Ca ratios

The Mg/Ca ratio of seawater is primarily related to ocean floor spreading rates. When rates are high, increased pumping of seawater through mid-ocean ridge basalts extracts Mg^{2+} during low-grade metamorphism and releases Ca^{2+}, so that the Mg/Ca ratio decreases. It is believed that high Mg/Ca ratios favour the precipitation of aragonite, high Mg-calcite and dolomite whereas low Mg/Ca ratios will preferentially precipitate low Mg-calcite (Tucker 1992). Dolomite is considered to form in evaporitic environments or in meteoric-marine mixing zones or on burial (Fairchild 1980; Dunham & Olsen 1980; Tucker & Wright 1990). In shallow-water environments, anaerobic microbial activity may also promote dolomite precipitation and early dolomitization in recent sediments (Vasconcelos & McKenzie 1997, D. Wright pers. comm., 1997)

The Mg/Ca ratios show quite a considerable scatter through the formations (Table 6.1). The Khufai Formation dolostones show an average Mg/Ca ratio of 0.585 with a standard deviation of 0.168 whilst the limestones have a mean of 0.176 and standard deviation of 0.213 (Table 6.1). The Shuram Formation limestones have very low ratios of 0.028 with standard deviation of 0.013. While in the Oman Mountains, mean values in the Shuram/Buah Formation cycles are around 0.022 and standard deviation of 0.010. Values similar to the Shuram Formation are recorded in the basal limestones of the Buah Formation (mean 0.019). The dolostones of the Buah Formation record an increase in values up-section from 0.66 to 0.97 with a mean of 0.76 with similar mean values recorded in the Buah Formation of the Oman Mountains. These high values are assumed to reflect the more evaporitic nature of the sediments in the Upper Buah Formation.

Mg/Ca ratio may be used to characterise the carbonate mineralogy of a sample. The lithological description of samples as limestones and dolostones is too simplistic as most samples comprise calcite and dolomite phases. 'Ideal calcite' will have Mg/Ca ratios tending

towards zero, whilst 'ideal dolomite' will have Mg and Ca in a ratio of 1:1 within the crystal lattice (Veizer 1978; Veizer 1983; Nicholas 1996). Mg/Ca ratios are plotted against 1000Sr/Ca in Figure 6.1, to show that most samples of the Khufai Formation fit well into the 'ideal dolomite' (circles) field, with the Oman Mountains samples being formed of 'ideal calcite' (diamonds). The Shuram Formation limestones appear formed of 'ideal calcite' while most Buah Formation samples cluster within the 'ideal dolomite' field, with the supratidal samples showing Mg-enrichment.

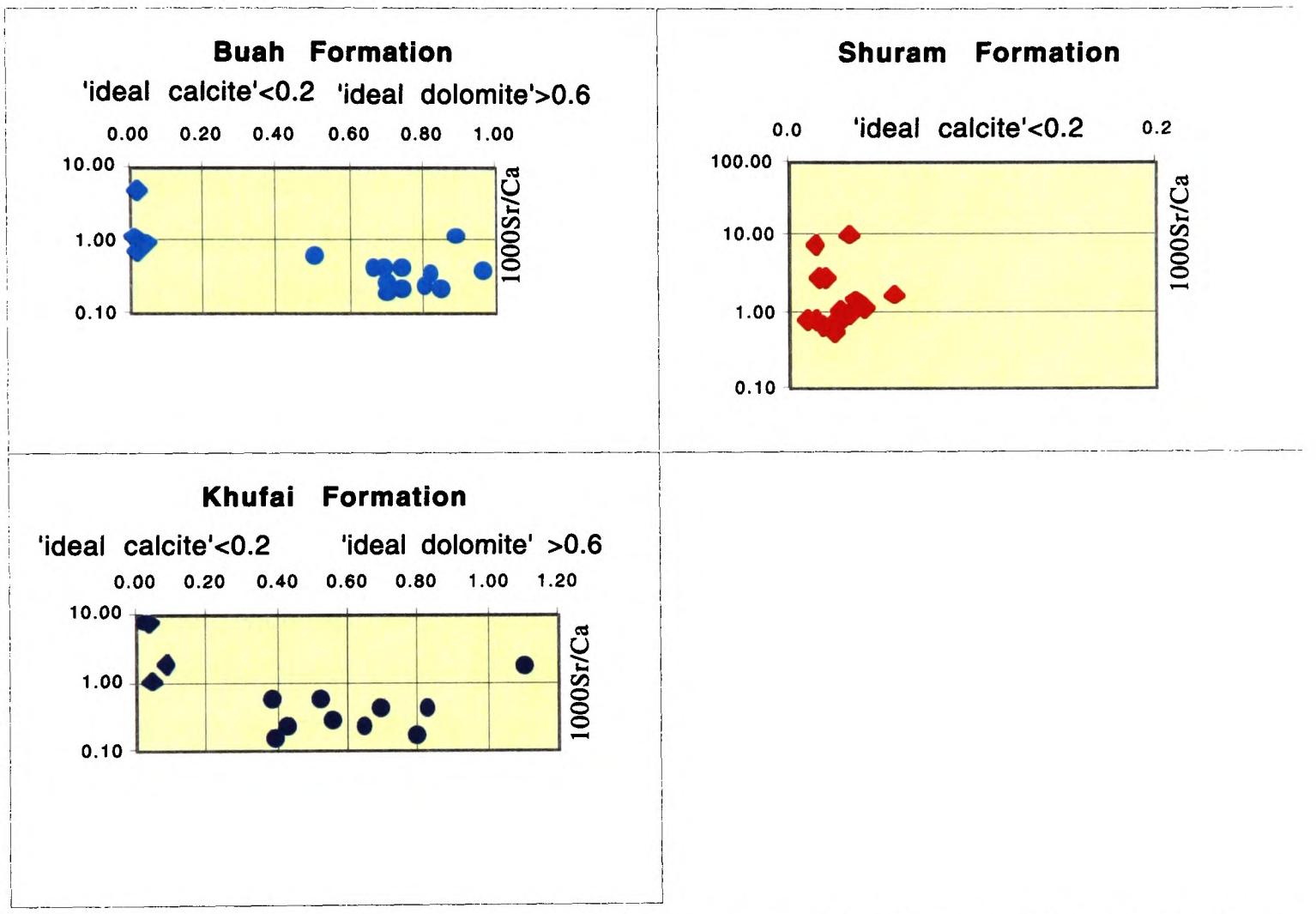


Figure 6.1 Plots of 1000xSr/Ca against Mg/Ca show 'ideal calcite' v 'ideal dolomite' (Veizer 1983; Nicholas 1996). Circles represent dolostone samples while diamonds represent limestone samples. Diagenetic pathways are a function of decreasing 1000xSr/Ca and increasing Mn ppm concentrations

6.3.2 Strontium (Sr) and Sr/Ca ratios

The two primary sources of Sr in the ocean are the continental crust (by subaerial weathering and river transport) and the oceanic crust (by hydrothermal activity at the mid-ocean ridges and submarine alteration of basalts). Strontium concentrations reach 10,000 ppm in modern marine aragonitic ooids and cements whilst values in high Mg-calcite vary between about 1,000 and 2,000 ppm (Tucker & Wright 1990). In modern hypersaline and evaporative dolomites, Sr values range from 600-900 ppm, while in mixing zones values are found between 100-250 ppm (Land 1973). Values for the Buah Formation and Khufai Formation are between 25 and 369 ppm with the majority being below 100 ppm (Table

6.1). Similar very low values have been recorded in Precambrian dolomites from the Beck Spring Formation of Eastern California which were interpreted as mixing-zone replacement dolomites (Tucker 1983; Zempolich *et al.* 1988). Tucker (1983) also suggested that Sr may have been depleted from the initial marine precipitate of calcian-dolomite during stabilisation to well-ordered stoichiometric dolomite.

The Shuram Formation limestones have moderate Sr ppm, with values between 190 and 552, the majority of which are between 200 and 300. Lorens (1981) determined that limestones in equilibrium with precipitating fluids have a Sr/Ca ratio close to modern seawater and would have Sr contents of 400-500 ppm. The Shuram Formation carbonates could, therefore, actually record slight strontium depletion and indicate some measure of diagenetic alteration. An interesting aspect of the Shuram/Buah Formation contact is that Facies A1 (Crinkly laminites) is very enriched in Sr relative to the rest (Table 6.1). In the Oman Mountains the cycles across the Shuram/Buah Formation boundary record high Sr contents of between 1010 and 3390 ppm suggesting an aragonite or high-Mg calcite precursor carbonate.

Diagenetic pathways are a function of decreasing Sr/Ca and increasing Mn ppm concentrations (Nicholas 1996; Veizer 1983). 1000Sr/Ca against Mn ppm is plotted for the formations of the Nafun Group in Figure 6.2. Dolostones with less than 400 ppm Mn and limestones with less than 200 ppm Mn are considered 'least altered' (Nicholas 1996).

Burns & Matter (1993) published the $^{87}Sr/^{86}Sr$ ratios for outcrop samples from the Huqf area. These show a gradual increase from about 0.7080 at the bottom of the Khufai Formation to approximately 0.7086 at the top of the Buah Formation. As these values are all within the range of Phanerozoic carbonates they were considered by the authors to indicate a rock-buffered diagenetic system. In such a system, the carbon-isotope ratios are more likely to record the signatures of the primary carbonate.

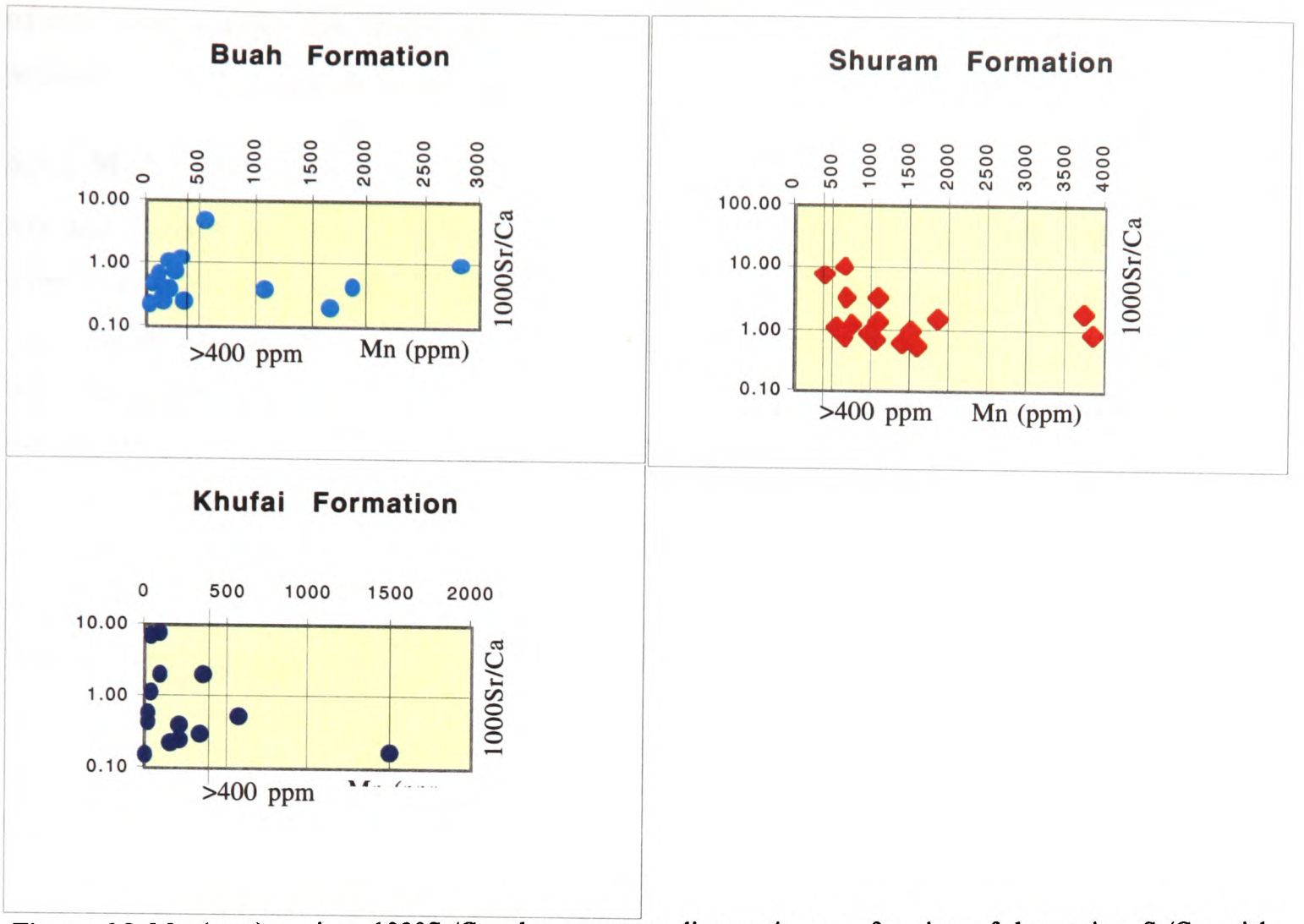


Figure 6.2 Mn (ppm) against 1000Sr/Ca plots measure diagenesis as a function of decreasing Sr/Ca with increasing Mn ppm concentrations. Samples with Mn concentrations greater than 400 ppm are considered 'altered' (Nicholas 1994). Circles represent dolomite samples whilst diamonds represent limestone samples.

6.3.3 Iron (Fe)

Modern carbonates have very little Fe and Mn (tens of ppm) as these elements have very low concentrations in seawater. Diagenetic porewaters however, have high concentrations of these elements, especially if they have negative Eh, which is commonly the case in burial environments (Tucker 1986a). Fe is also relatively enriched in carbonates of the Shuram Formation (Table 6.1) which might be argued to reflect a higher concentration of these elements in the diagenetic fluids. Alternatively, as the Shuram Formation consists predominately of red siliciclastic siltstones and mudrocks, elevated Fe concentrations may have been more related to seawater chemistry. For example, Beukes & Klein (1993) have invoked a density-stratified ocean to explain the precipitation of banded iron formations in the Proterozoic. This model requires surface waters which are oxic and deeper waters enriched in dissolved ferrous iron. The precipitation of iron-bearing minerals then takes place along an oxycline determined by the downward flux of organic matter from the photic zone and by the upward transport of ferrous iron from deeper water. Where the organic flux is low, ferrous iron is oxidised upon contact with oxic surface waters, causing precipitation

of iron oxides along the chemocline but where the organic flux is high then black shales accumulate (Grotzinger & Knoll 1995).

6.3.4 Mn/Sr (as a proxy for diagenetic exchange)

Mn and Sr have markedly different distribution coefficients in calcite, Mn being preferred over Sr to replace Ca in the calcite lattice during dissolution-recrystallisation events. During meteoric diagenesis, Sr is expelled from marine carbonates whilst Mn is incorporated, so that Mn/Sr ratios can be a useful tool for screening samples (Veizer 1983). Correlation with isotopic ratios has been taken to suggest that diagenetic recrystallization of carbonate incurs predictable trace element exchange in an open system (Marshall 1992). However, absolute concentrations of Mn, Fe, and Sr may result either from an open system or reflect absolute availability of reduced Mn and Fe in the original seawater or in diagenetic fluids (Graham Shields, pers. comm.).

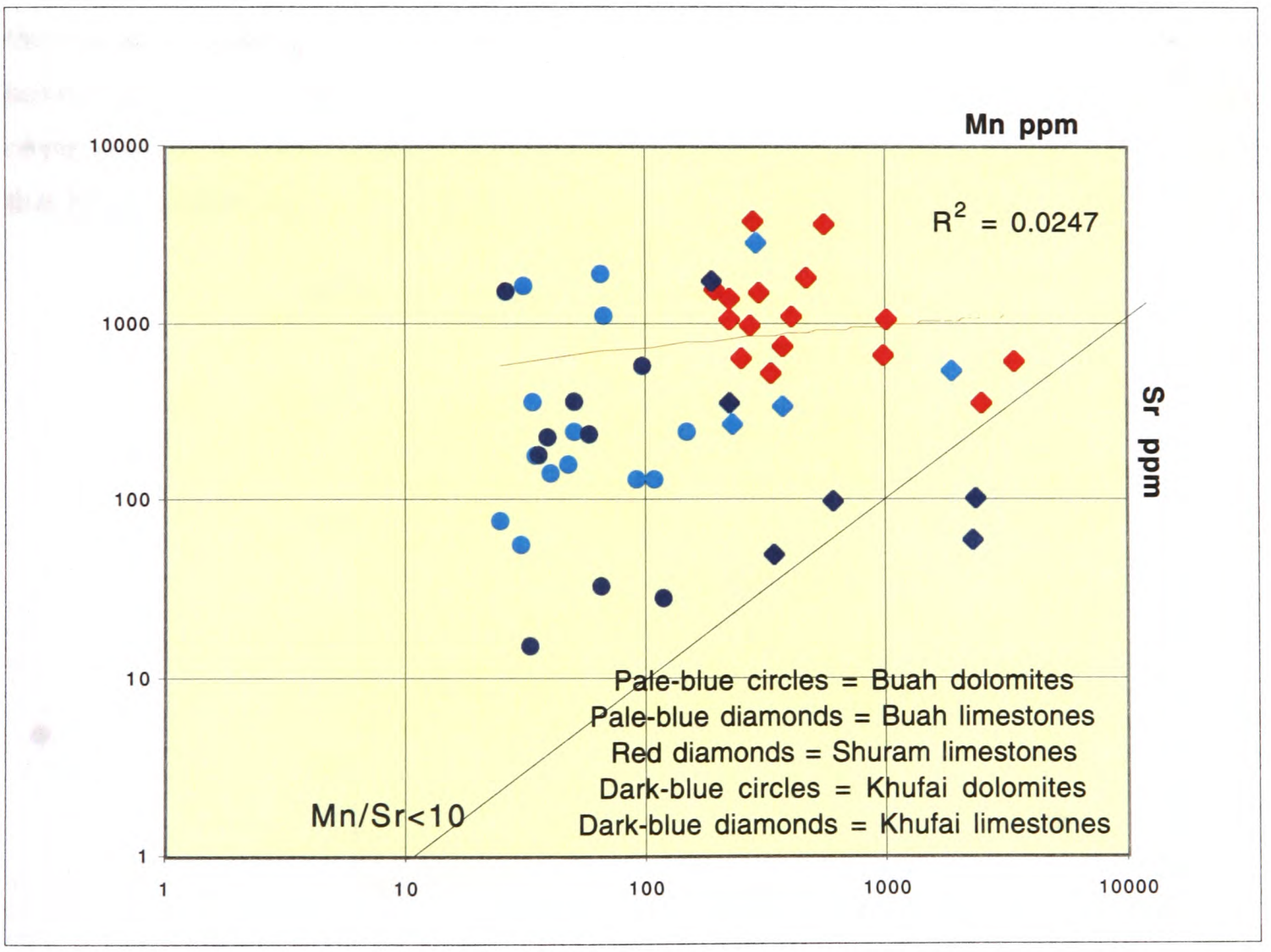


Figure 6.3 Mn/Sr plot for the Nafun Group carbonates, which shows values very similar to previously published Precambrian data. Diamonds are limestones whilst circles are dolostones. The pale red line is the log regression line showing a covariance coefficient of R^2=0.0247.

The Mn/Sr plot for the carbonates of the Nafun Group (Figure 6.3) shows that the data scatter is quite similar to that of other published Precambrian data (e.g. Veizer *et al.* 1992, Fig. 3). With progressive diagenesis one would expect an increase in Mn to the detriment of Sr. However, no such trend is obvious within the Nafun Group carbonates (Figure 6.3). The Shuram Formation limestones have higher Mn and Sr contents than most of the dolomites of the Buah and Khufai Formations. The most Sr-enriched Khufai samples are slightly depleted in Mn while the samples with higher Mn values have lower Sr concentrations, suggesting that these latter samples have undergone some diagenesis. This plot also shows how most samples contain less than 400 ppm Mn, indicating they are most likely not to have undergone open system diagenesis (Nicholas 1994).

There is a possible Mn/Sr covariation from the Shuram Formation through to the Buah Formation as seen on Figure 6.3. These two datasets have therefore been plotted alone to see if they have a statistically significant covariance (Figure 6.4). As this plot indicates there is no evidence for a statistical covariance. When the formation data sets are plotted individually there is again no significant evidence for covariation. There may be a slight covariation of the Mn/Sr ratios of some of the samples of the Buah Formation suggesting that these samples may have undergone some measure of meteoric diagenesis (Figure 6.4).

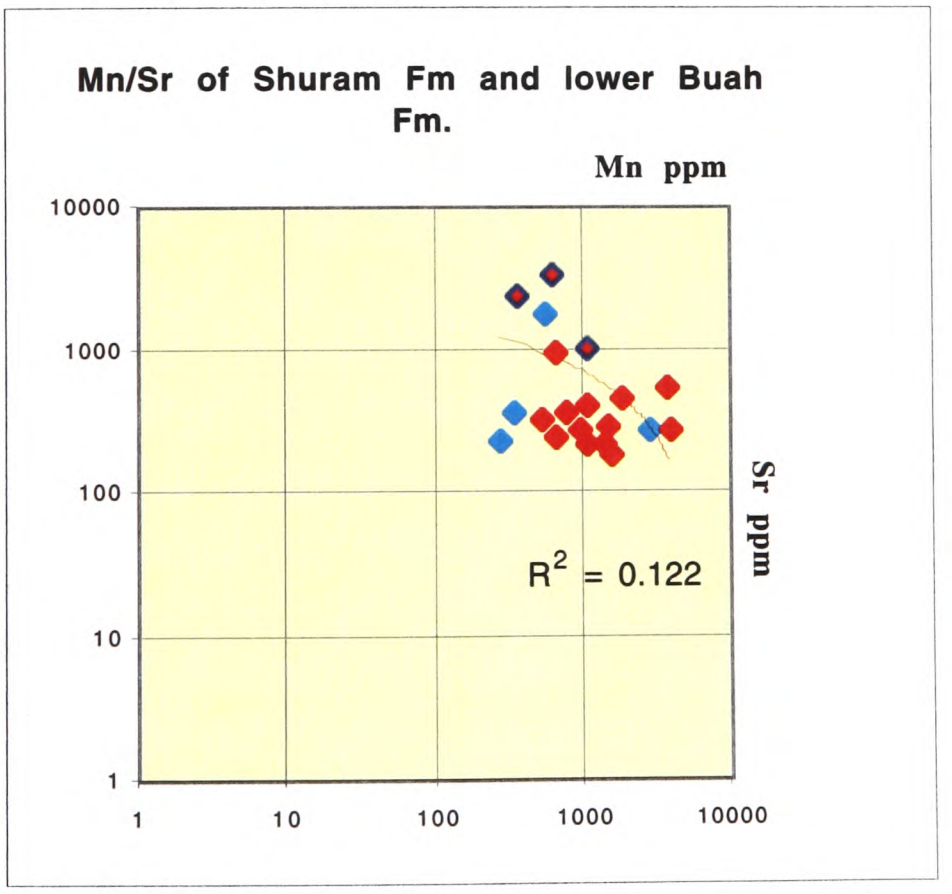


Figure 6.4 Covariance plots Mn (ppm) against Sr (ppm) for the limestones of the Shuram and lower Buah formations. Diamonds are limestones, darkened rims represent samples from the Oman Mountains. The red line is the log regression line showing a coefficient of covariance of R^2=0.122. The Buah Formation dolostones were previously included but the limestone data shows a better covariance coefficient.

According to Kaufman & Knoll (1995) and Kaufman *et al.* (1993), limestones and dolostones with Mn/Sr <10 commonly retain near primary $\delta^{13}C$ abundances but they had highest confidence with Mn/Sr values of <3. As can be seen from Figure 6.5 and Table 6.1 the vast majority of samples retain Mn/Sr ratios of <10 with somewhat less at values of <3.

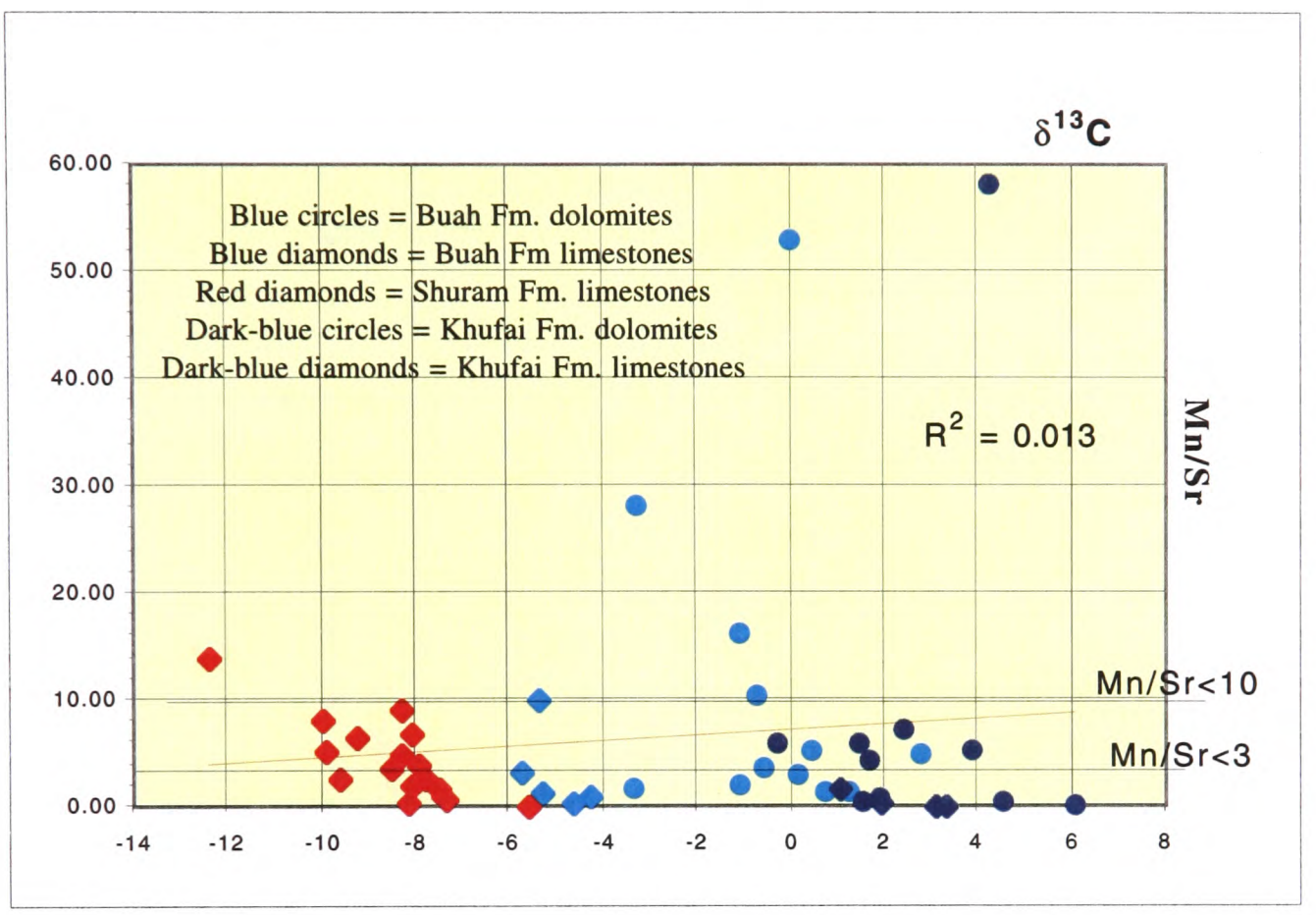


Figure 6.5 Mn/Sr ratios plotted against $\delta^{13}C$ for the formations of the Nafun Group. The limestones of the Shuram Formation and the lower Buah Formation have the most negative carbon isotopic signature. The majority of the samples have Mn/Sr ratios below 10.

Mn/Sr ratios have been plotted against $\delta^{13}C$ for covariant analysis of the different formations in the Huqf area and the Oman Mountains. The general lack of significant clear covariance with an R^2 value of only 0.013 (Figures 6.5, 6.6a, 6.6b) for the Khufai and Buah Formations suggest that these samples have not been systematically recrystallized in an open diagenetic system. The Shuram Formation does, however, show some indication of covariance, having an R^2 value of 0.7161, and has possibly suffered diagenesis in an open system.

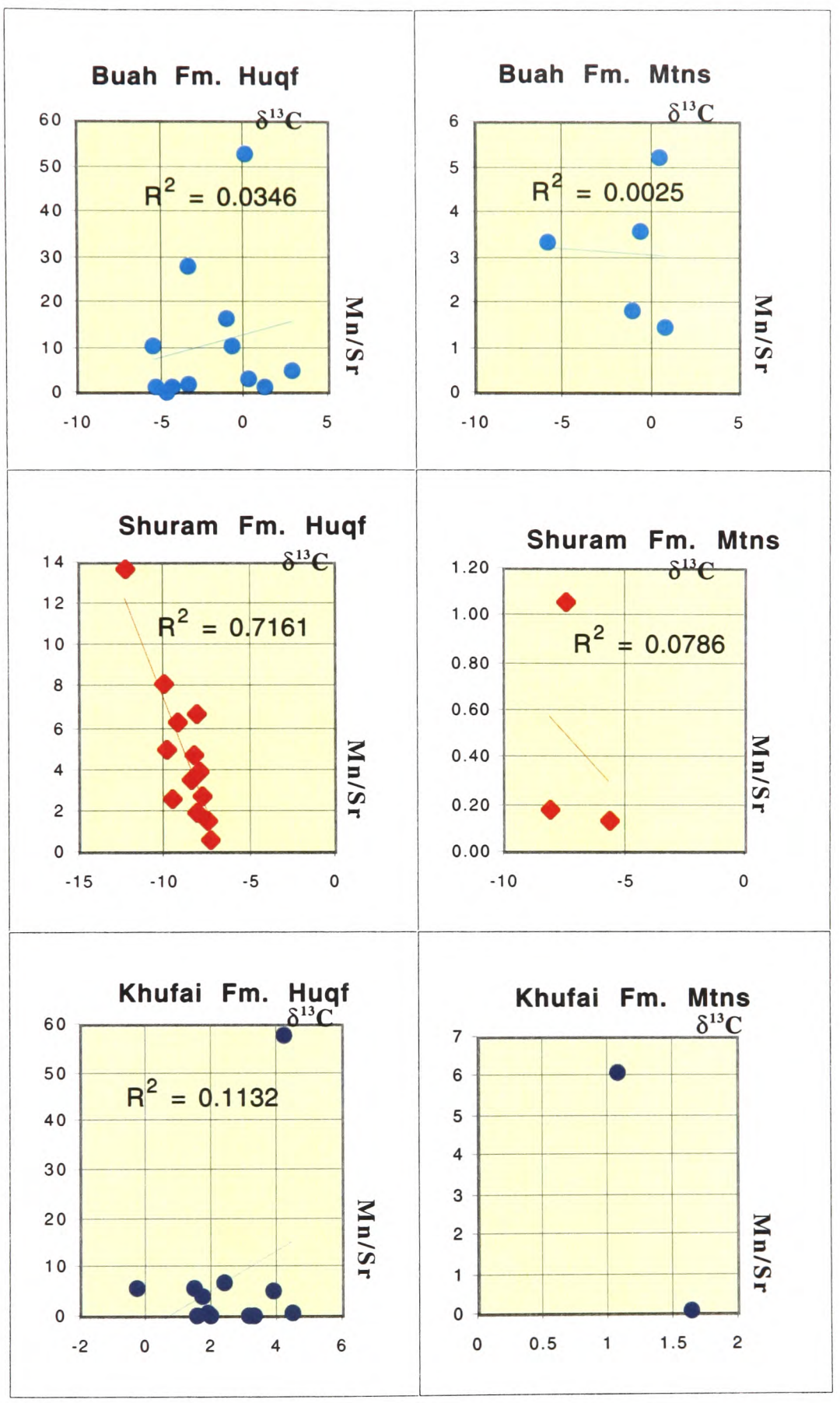


Figure 6.6a and 6.6b Crossplots of Mn/Sr for each formation in the Huqf area (a) and the Oman Mountains (b). No clear covariance is obvious within the Buah or Khufai formations but there is a relatively good covariance in the Shuram Formation of the Huqf area.

6.3.5 Mn and Fe (as a proxy for diagenetic exchange)

Mn and Fe are incorporated into the calcite lattice under reducing conditions; such conditions occur rarely in the Phanerozoic depositional environments but are common in

the diagenetic environment (Brasier *et al.* 1992). Hence cross-plots of these elements against stable isotopic values can be used to extrapolate back towards primary marine values (Marshall 1992). Crossplots of Fe and Mn against isotopic data are shown in Figure 6.7.

6.7a **6.7b**

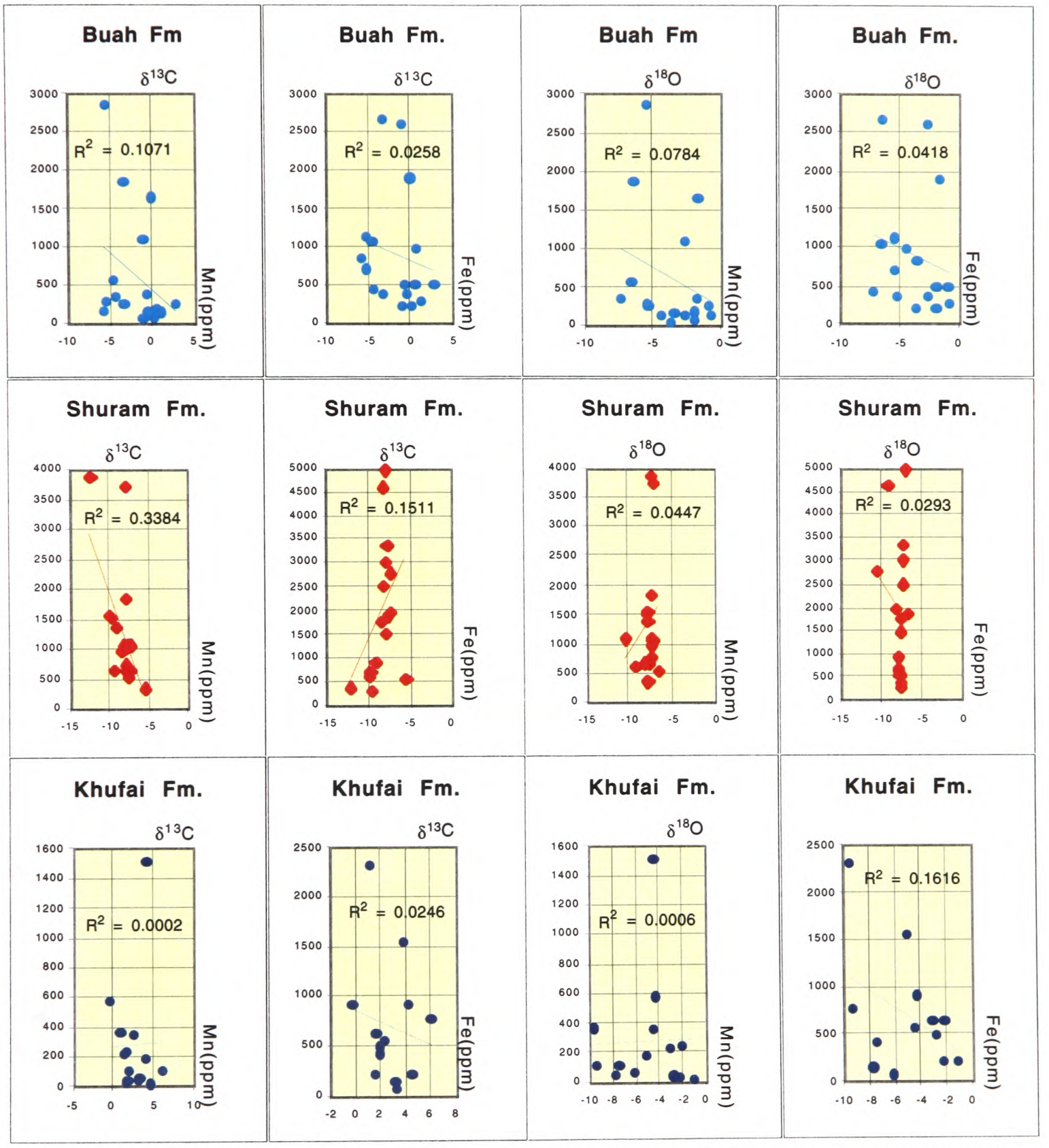


Figure 6.7a and 6.7b Cross-plots of Mn and Fe concentrations against carbon isotopic data (a) and against oxygen isotopic data (b) for all the formations.

From this it is apparent that no systematic covariance occurs between Mn or Fe and $\delta^{13}C$ or $\delta^{18}O$ values for any of the formations, which means it is not possible to use the Mn and Fe backstripping method (Marshall 1992) on these data.

In well-oxygenated groundwaters, ferric ions are common and thus iron is not usually incorporated into the cements. Manganese is precipitated preferentially with respect to iron in near-surface oxygenated waters since Mn^{2+} is slightly more soluble in a wider range of Eh conditions than is Fe^{2+}. Thus Mn^{2+} can occur in more oxidizing waters than Fe^{2+}, leading to cements rich in Mn^{2+} and poor in Fe^{2+} (Harris *et al.* 1985). There is a relative enrichment in Fe ppm within the upper Shuram Formation and Associations A and B of the lower Buah Formation whilst Mn ppm shows no consistent trends (Table 6.1). Elsewhere, Fe ppm remains relatively low, suggesting that diagenetic environments were generally well-oxygenated or that Fe^{2+} was not brought into the depositional environment. However, Fe/Mn ratios (Table 6.1) do not appear to show a corresponding trend which suggests that as Fe ppm increased so did Mn ppm. Correlation of isotope ratios and Mn and Fe concentrations would suggest diagenetic concentrations within an open system. As figures 6.7a and 6.7b show, however, no such correlations exist in this instance. This suggests that the concentration of these elements in the crystal lattice was determined more by redox conditions or their availability within the depositional system. The higher contents of Fe and Mn in the upper Shuram Formation and lower Buah Formation could be explained, for example, by deposition in a more humid climate while the Khufai or upper Buah Formations retain many features characteristic of arid climatic conditions. During humid climatic periods, there is higher continental discharge, hydration, content of organic matter, and lower Eh and pH which leads to higher content of dissolved, colloidal and suspended Fe in surface waters and its precipitation, coagulation and settling upon entering marginal marine basins (Tucker 1992; Krauskopf & Bird 1995).

6.4 DATA CORRECTION

A literature search was undertaken to evaluate processes recommended for the estimation and correction of diagenetic overprints. These corrections can be used as a control to show whether major stable isotopic trends are robust to the effects of diagenesis. In the subsequent discussion (Sections 6.5; 6.6 and 6.7), both primary and corrected data will be considered.

6.4.1 Component analyses and corrections

The component-analysis method is used to differentiate the amount of alteration between least altered (e.g. ooid/micrite) and most altered (e.g. sparry cement/recrystallized spar) fractions within a single sample. Grains or micrite laminae were separated from the spar cement or matrix using a 100μm diamond tipped percussion drill. Component analyses and

corrections have been carried out on a limited number of samples representing different lithofacies from each formation. These analyses are plotted on Figures 6.8a, 6.8b and 6.8c. Where cement sub-samples display a consistent pattern of $\delta^{13}C$ depletion and greater negative $\delta^{18}O$ there is scope for correcting $\delta^{13}C$ values for this diagenetic alteration. If we accept that the heavier oxygen isotope values represent samples closer to the composition of the primary carbonate (Fairchild *et al.* 1990), then lighter samples can be corrected by adjusting $\delta^{13}C$ values upward by the median slope of lines connecting the sub-samples cf. Brasier *et al.* (1993). 'Least-altered' oxygen-isotope values for Precambrian dolostones have been reported at around -4‰ while 'least-altered' oxygen values of Precambrian limestones are considered to be around -5.5‰ to -6.6‰ (Fairchild *et al.* 1990). Therefore, if the component correction between an ooid grain and cement in a dolostone was 0.5‰ and its $\delta^{18}O$ value was -6‰ then a correction of 1‰ would be levied on all the samples from that ooid grainstone facies. Facies that show no consistent trends cannot, however, be corrected in this way.

In the Khufai Formation there was no consistent trend obvious within the subsamples of the grainstones, laminites or stromatolite facies (Figure 6.8a) where the cement (open symbol) is often more positive than the grain (filled symbol). The oxygen isotope values for the dolostones of the Khufai Formation are all around -4‰ which might infer a lack of alteration (Fairchild *et al.* 1990). The limestones have $\delta^{18}O$ values of -6 to -7.7‰ in the Huqf area and -9.3‰ in the Oman Mountains which suggest alteration of these samples. No correction was applied to the Khufai Formation data.

It is interesting that the micritic laminae within the stromatolites is relatively depleted in $\delta^{13}C$ possibly reflecting the incorporation of ^{12}C due to organic matter degradation (Figure 6.8a). The grainstones also show a similar trend but recrystallization made sampling of the grains very difficult so these data may not be very reliable. The peritidal facies are the most enriched in $\delta^{13}C$ and $\delta^{18}O$, which would reflect restricted environments with high evaporation rates.

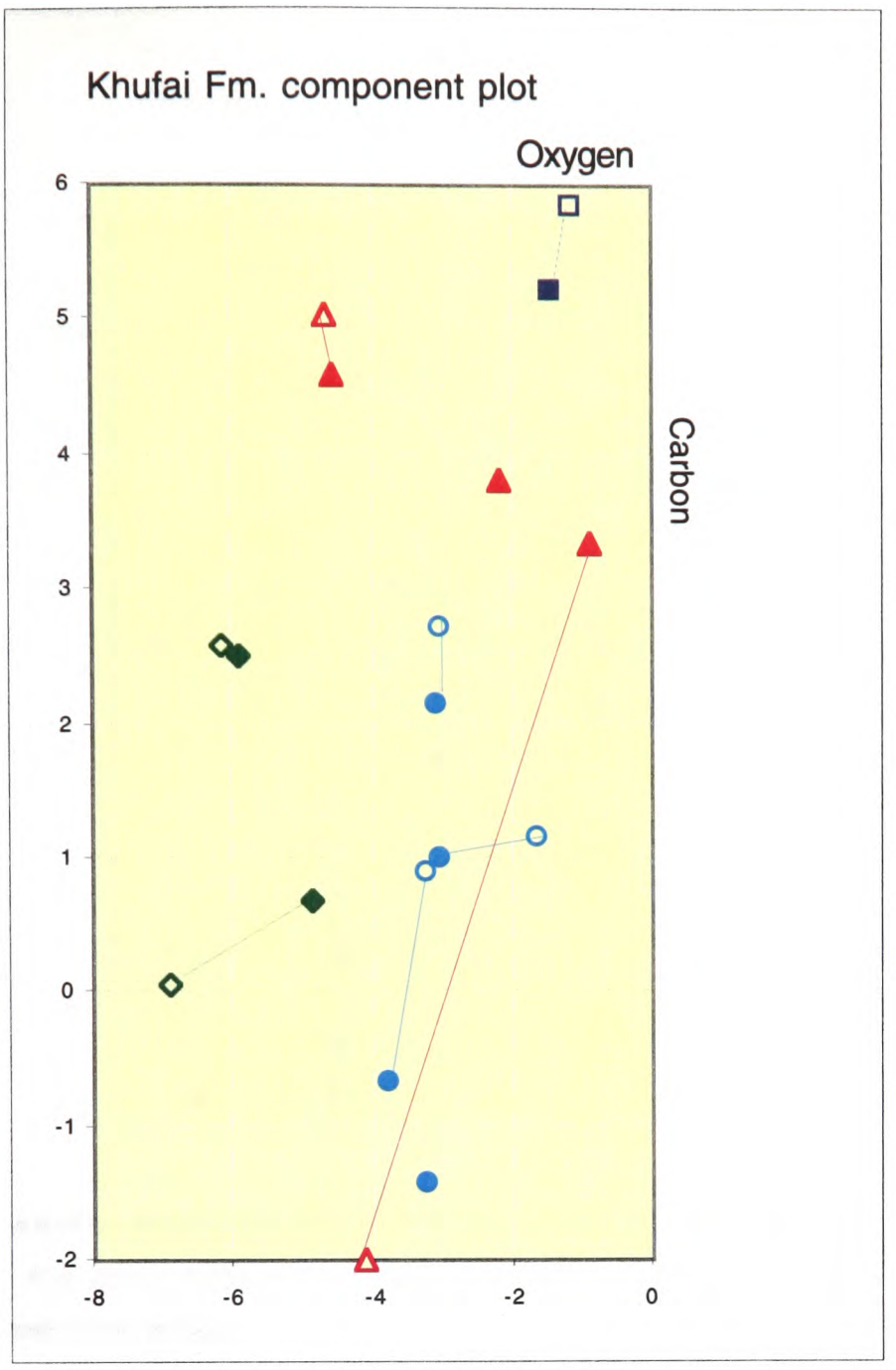


Figure 6.8a Khufai Formation component correction plot; filled blue circles are ooid grains while open blue circles are the cements with lines joining same sample components. Filled triangles are stromatolite micrite laminae with spar laminae represented by open triangles. Filled diamonds are spar and micritic limestones. Squares are peritidal facies. Corrections could not be applied as no consistent diagenetic trend occurs.

The Shuram Formation data show quite variable trends between facies (Figure 6.8b). Oosparites (S4) show a negative change in $\delta^{13}C$ and $\delta^{18}O$ between ooid and cement subsamples. Oosparite had an average 1.3‰ correction applied to all data points from the facies. Flat-pebble conglomerates (S2) record a similar trend, with the matrix recording more negative values. The averaged correction applied was 0.7‰. There is least component variation within the pelsparites (S3) averaging a 0.5‰ difference resulting in a correction of plus 0.5 for each permil oxygen below the -5.5‰ least altered limestone value.

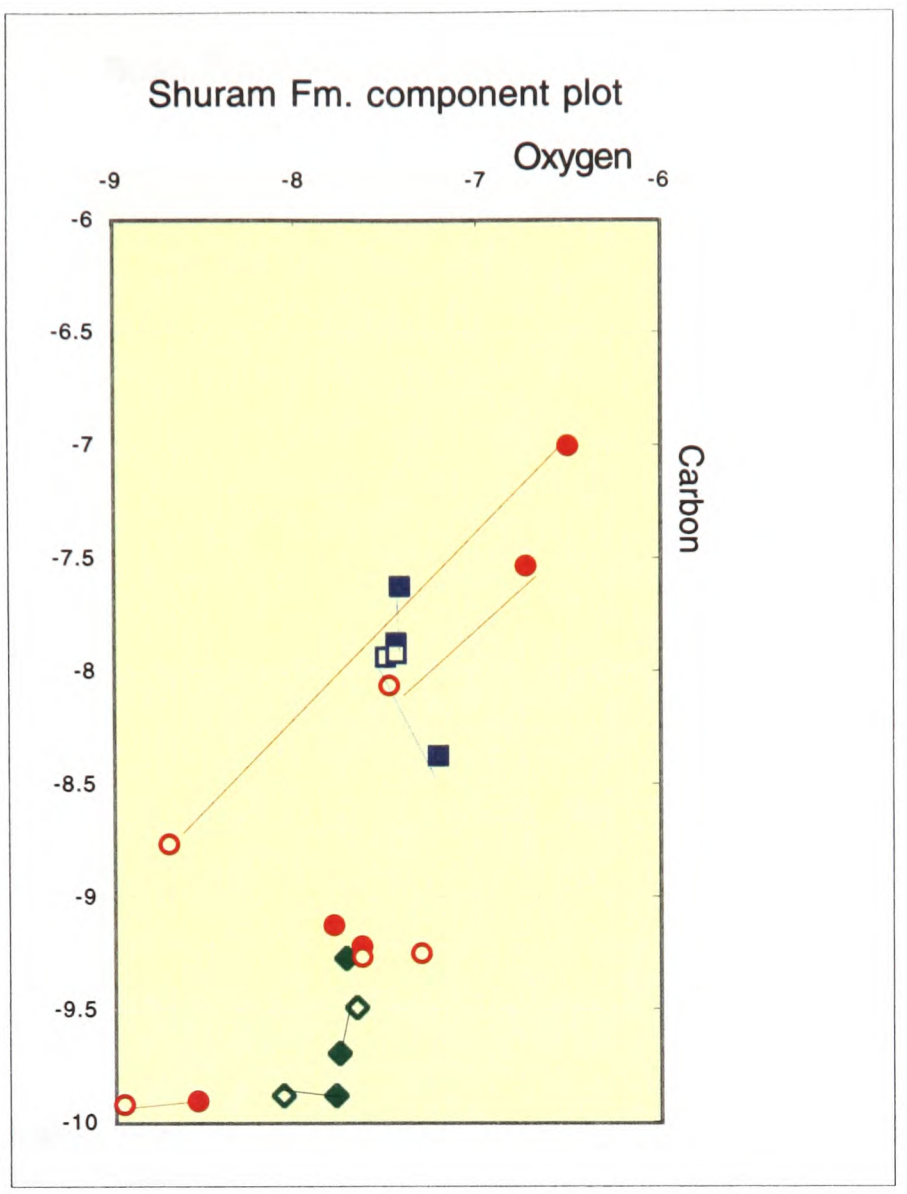


Figure 6.8b Shuram Formation component plot; with filled red circles representing ooid grains while open red circles are the cements with lines joining same-sample components. Filled squares are flat-pebble conglomerate clasts while filled diamonds are peloids.

The more positive ooidal grainstone values are from samples taken from the middle of the bed have ooid grain values relatively close to the original primary value (closest to the heaviest oxygen value) while these cements are greatly altered. The most negative ooids are taken from the top of the beds interpreted as hardground surfaces, here, the ooid grain oxygen- and carbon-isotope values have been reset. The component analysis shows a slight alteration between clast and matrix within the flat-pebble conglomerates (squares) measured at 0.5‰. Pelsparites show extensive alteration, with both peloids and cement values being reset. Pelsparites tend to form the base of the carbonate cycles and commonly contain variable amounts of siliciclastics. These data would suggest that core of the carbonate bed retains more primary values than samples taken from the perimeters of the beds. This suggests that flushing of porewaters through the siliciclastic interbeds has resulted in more open system diagenesis for samples from the Shuram Formation.

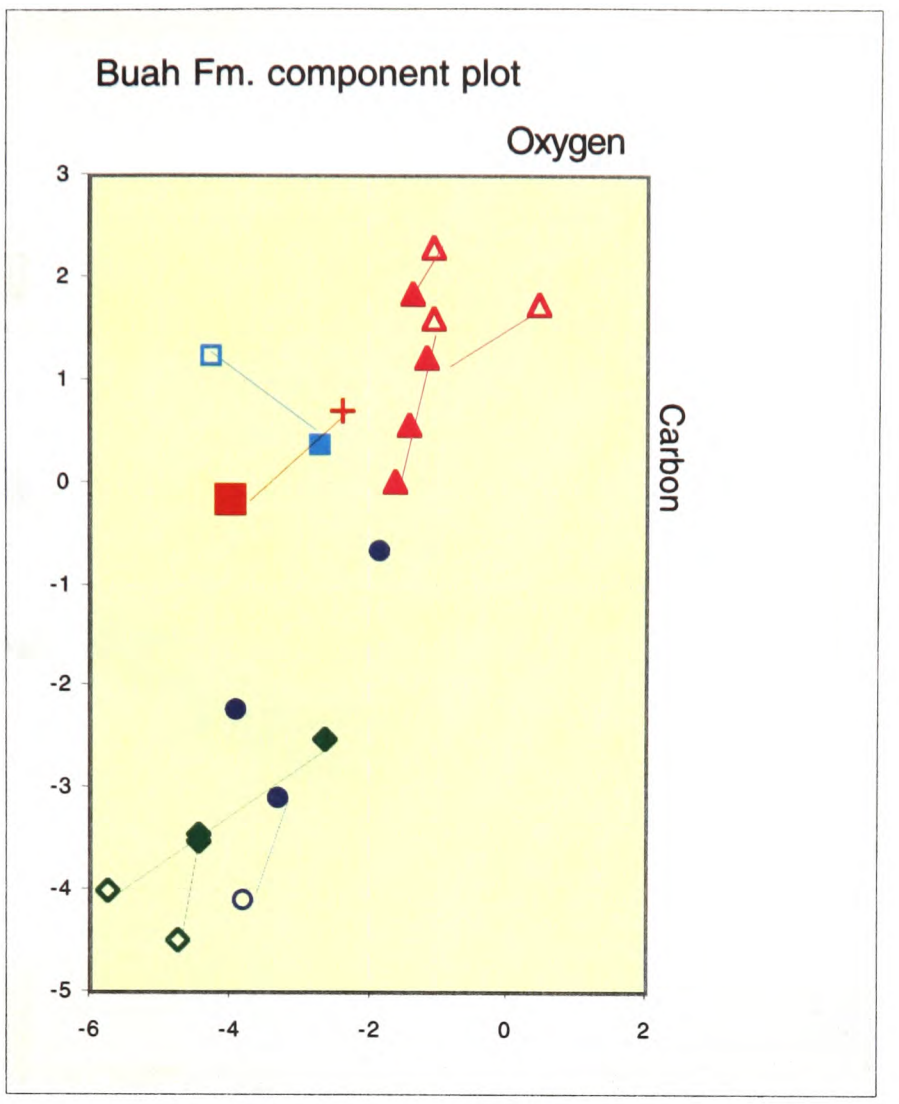
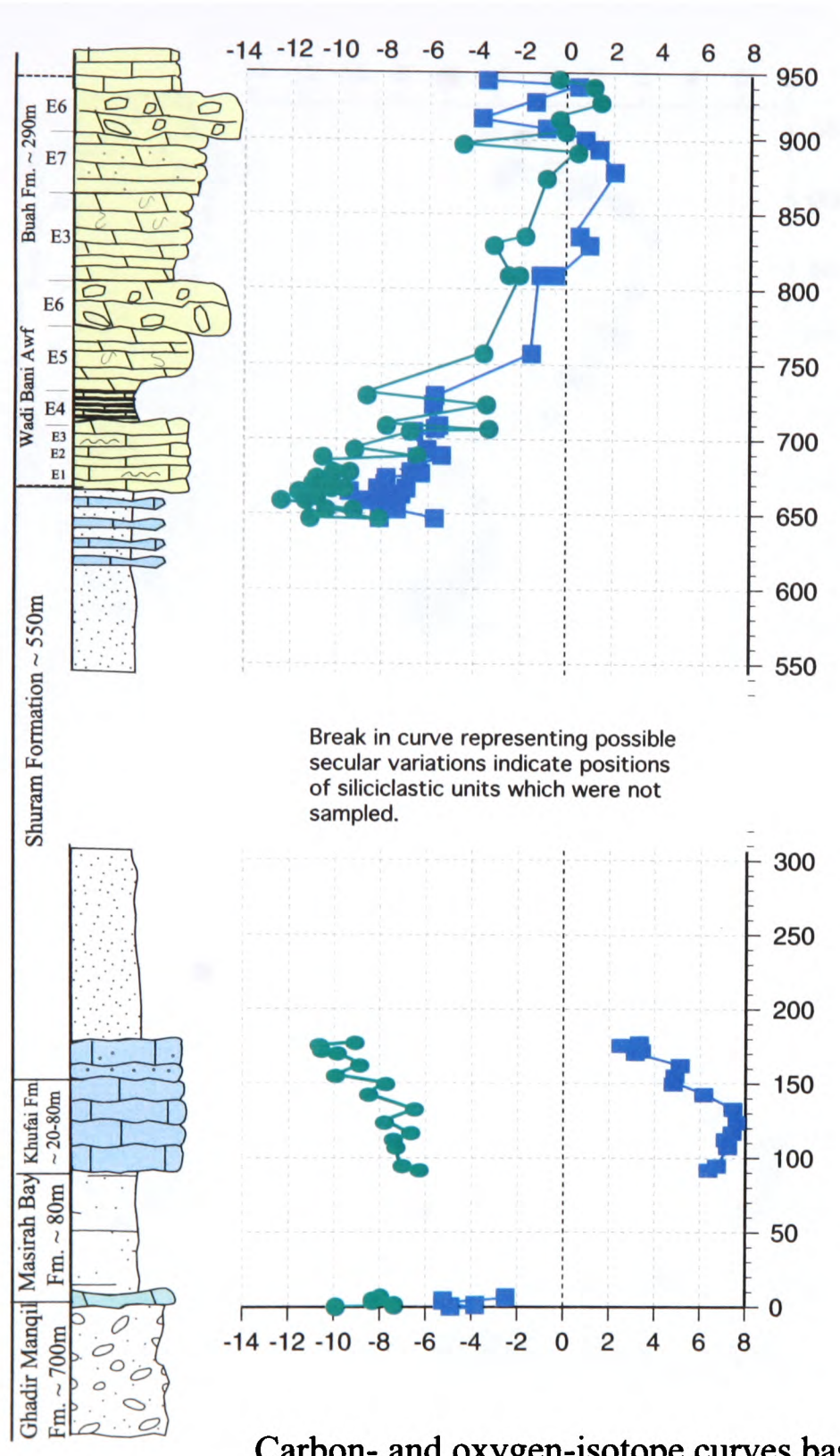


Figure 6.8c Buah Formation component plot with filled triangles representing stromatolite micritic laminae and open triangles spar laminae. Filled circles represent ooid grains whilst open circles represent ooid cement. Squares represent peritidal facies while the diamonds represent crinkly laminites with filled diamond represent microspar and open diamond representing the clay/micritic interlamination.

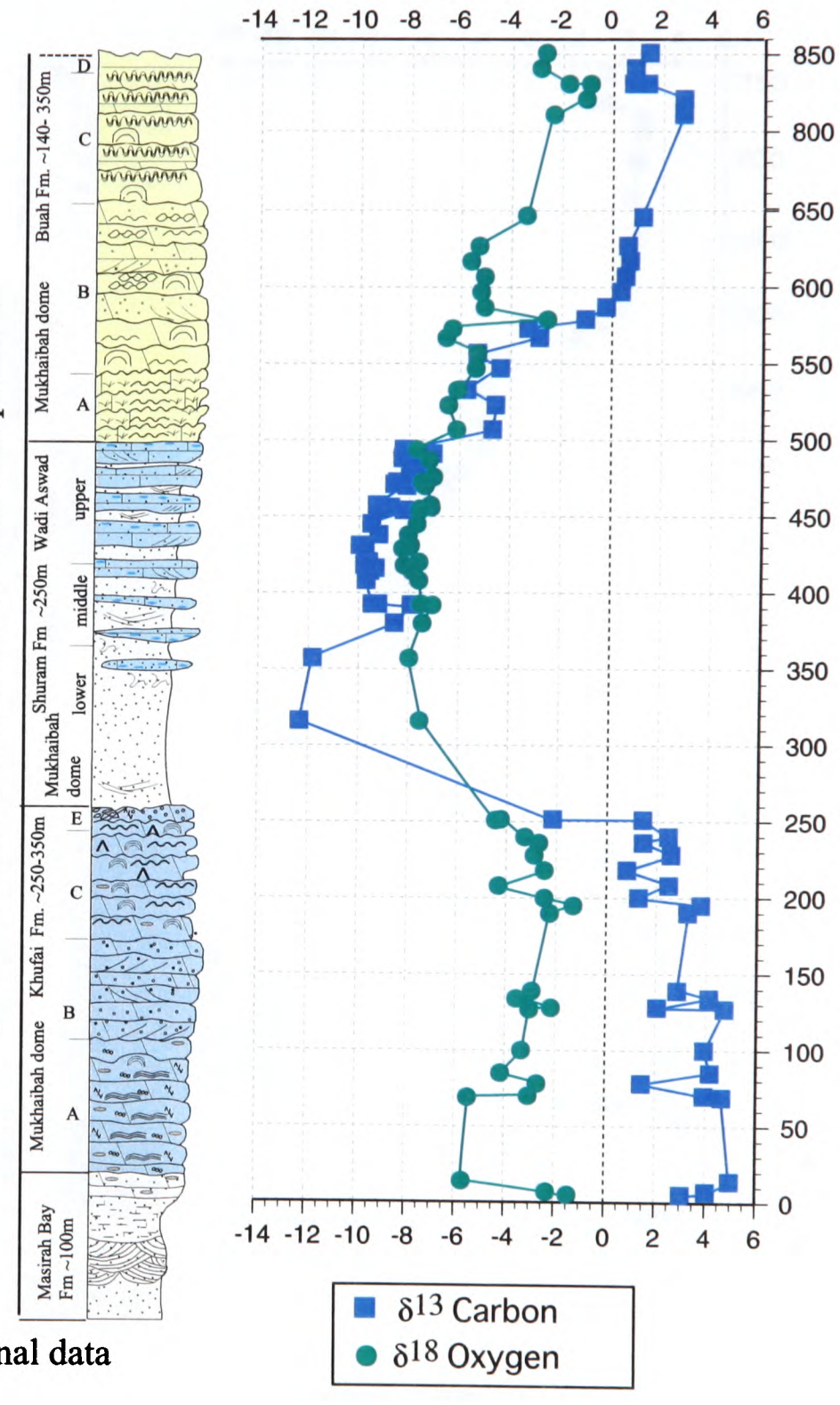
The Buah Formation data occur in clusters. The more negative values are recorded in samples from the base of the formation (Figure 6.8c), within the crinkly limestone facies (A1) where values are similar values to those of the upper Shuram Formation. For the Buah Formation Facies A (crinkly laminites) a 1.5‰ $\delta^{13}C$ correction was applied while Facies B stromatolites had a 1.4‰ correction. Recrystallized grainstones of Facies B require a correction of 1.65‰ $\delta^{13}C$ with peritidal dolomites (Facies C) needing a correction of 0.5‰ (Figure 6.8c).

The facies associations within the Buah Formation appear to show similar trends to those of the Khufai Formation mentioned earlier. As in the Khufai Formation the recrystallization of the grainstones within the Buah Formation made it difficult to identify components which may help explain the scatter in the results.

Huqf Formations in the Oman Mtns with isotope curve

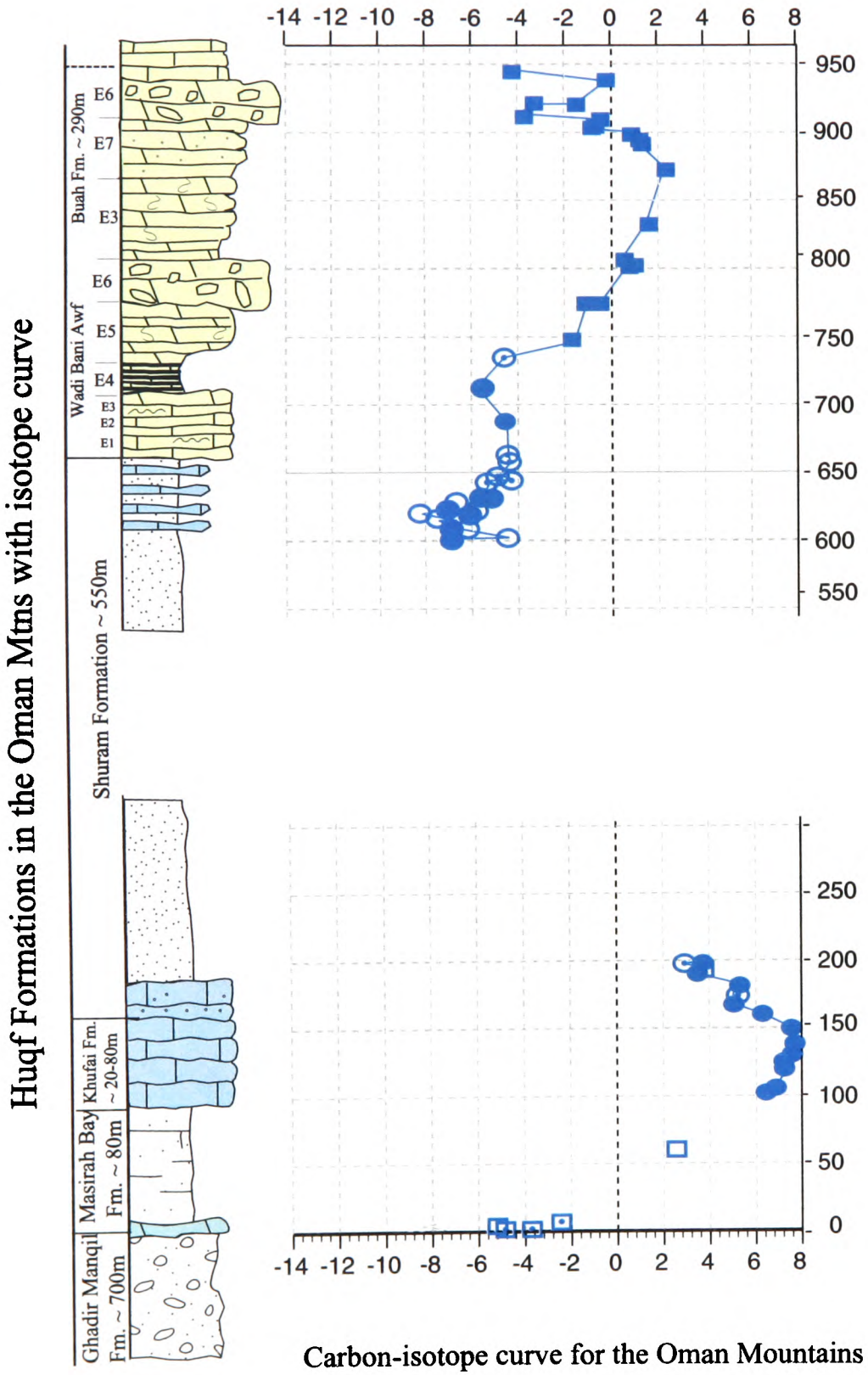


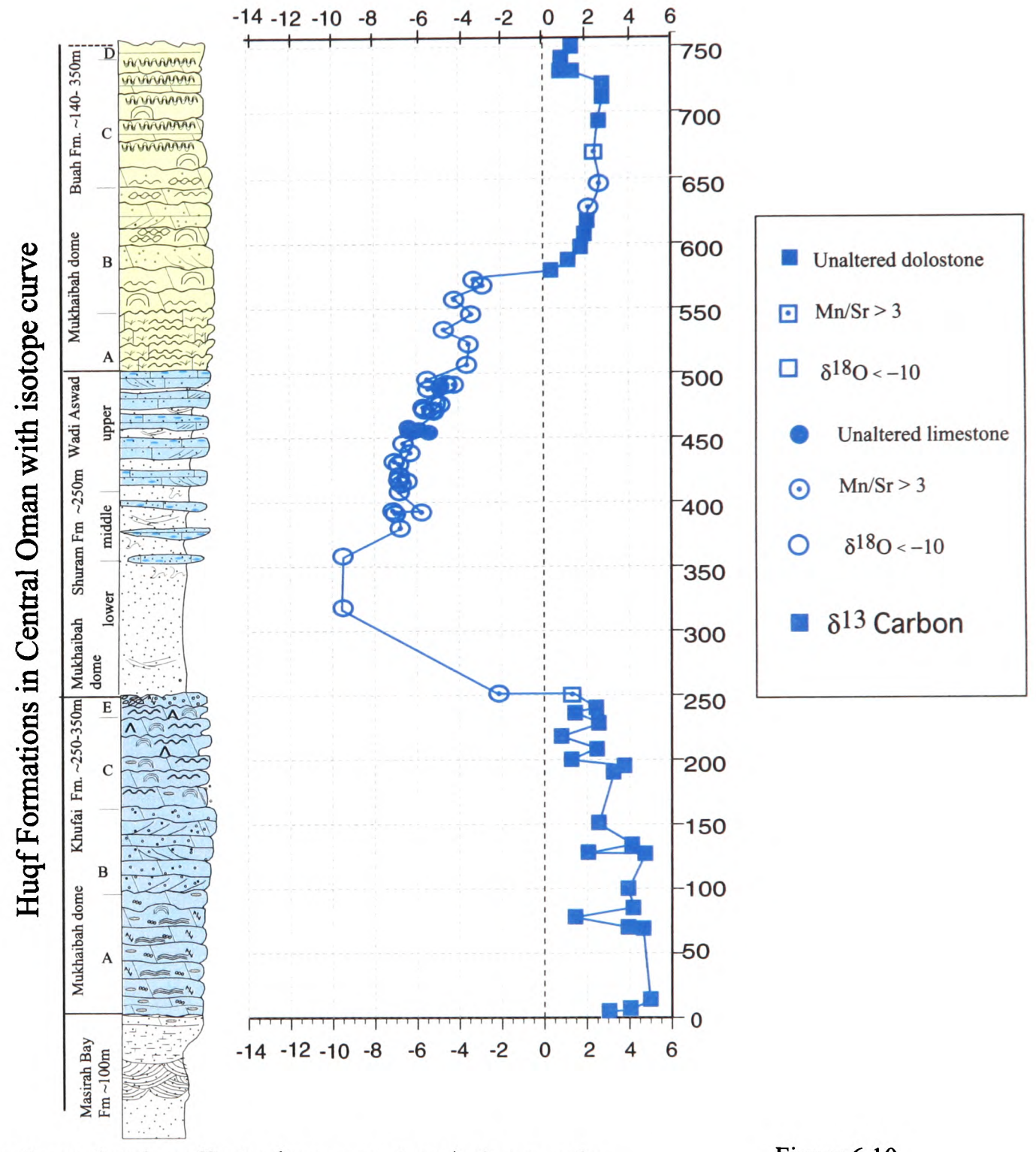
Huqf Formations in Central Oman with isotope curve



Carbon- and oxygen-isotope curves based on original data

Figure 6.9





Carbon-isotope curve for the Oman Mountains and Huqf area showing effects of component-analysis correction

Figure 6.10

Where a consistent diagenetic trend occurs, a subsample average was taken and this correction was then applied to all the data points from that lithofacies. The original data can be viewed in Figure 6.9 whilst the corrected data are displayed in Figure 6.10. These plots show that although the $\delta^{13}C$ values change slightly the general isotopic trend appears robust, suggesting that diagenesis accentuates rather than changes the primary signature.

One significant result of the component-analysis correction exercise (Figure 6.10) is that it removes the unusual situation in which the $\delta^{18}O$ curve is paradoxically heavier than the carbon curve in the Shuram Formation of the Huqf area (Figures 6.9). This would suggest that the very light $\delta^{13}C$ signature is a local diagenetic effect that is specific to the Shuram Formation in the Huqf area.

6.4.2 Carbon/Oxygen-isotope covariation

When plots of $\delta^{13}C$ against $\delta^{18}O$ produce a straight line of positive slope, covariation is said to occur. In such a case, only those samples with the most enriched $\delta^{13}C$ and $\delta^{18}O$ values are considered to be potentially unaltered (Fairchild *et al.* 1990).

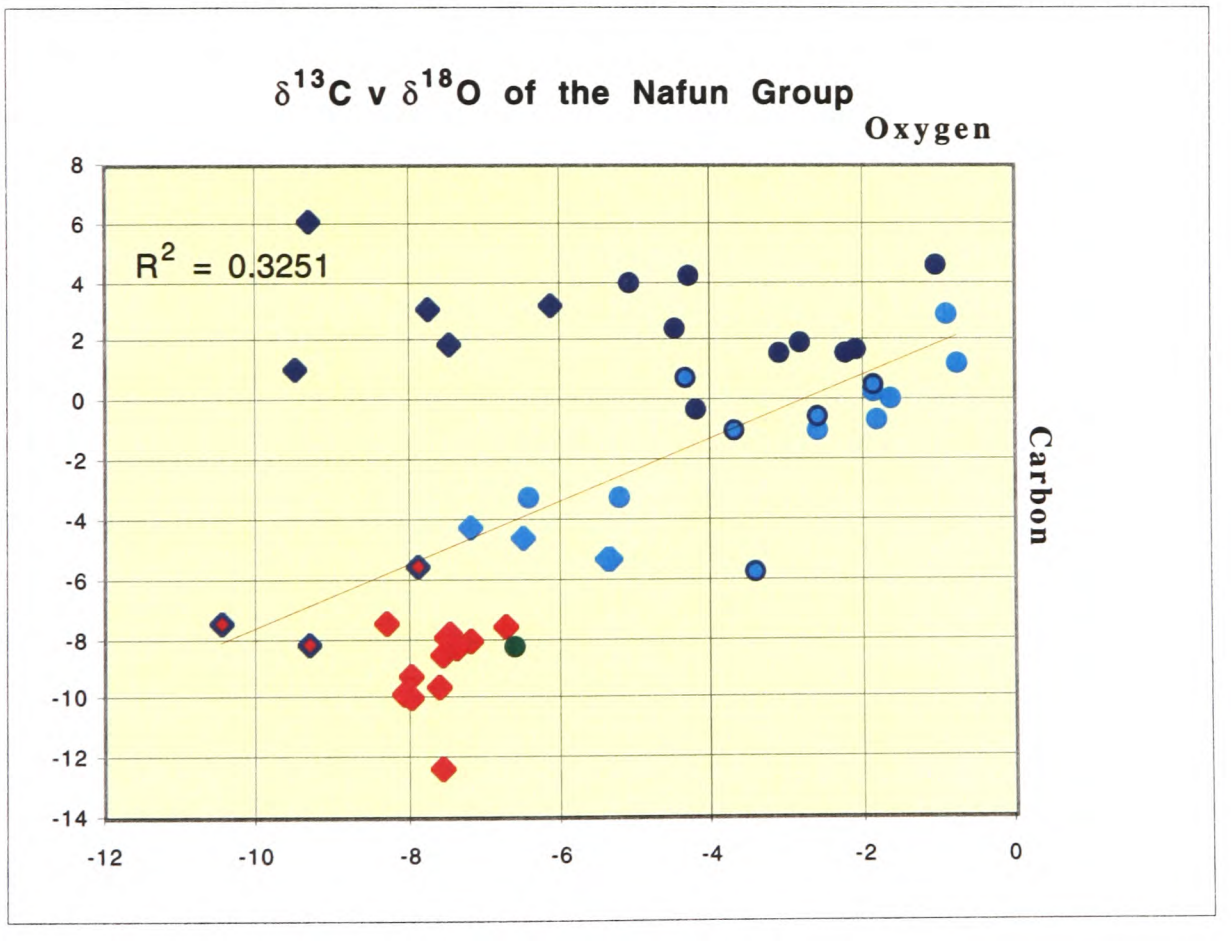


Figure 6.11a Carbon and oxygen covariation for the Khufai, Shuram and Buah formations. A hint of covariation occurs in the Shuram Formation to overlying Buah Formation (see figure 6.11b below). The R^2 value for all three formations (0.3) is not significant. Circles represent dolostones while diamonds represent limestones; darkened rims represent Oman Mountains samples. Dark-blue is Khufai Formation, red is Shuram Formation and light-blue is Buah Formation.

Figure 6.11a and 6.11b shows $\delta^{13}C/\delta^{18}O$ covariation plots for samples representing different lithofacies from all the formations. The data for all the formations plotted on Figure 6.11a do not show a strong covariance while the plot of the Shuram and Buah formations data (Figure 6.11b) illustrate a significant covariance at R^2 value of 0.7691. This shows, along with the tight cluster of oxygen-isotope values within the Shuram Formation, some re-equilibration during burial diagenesis.

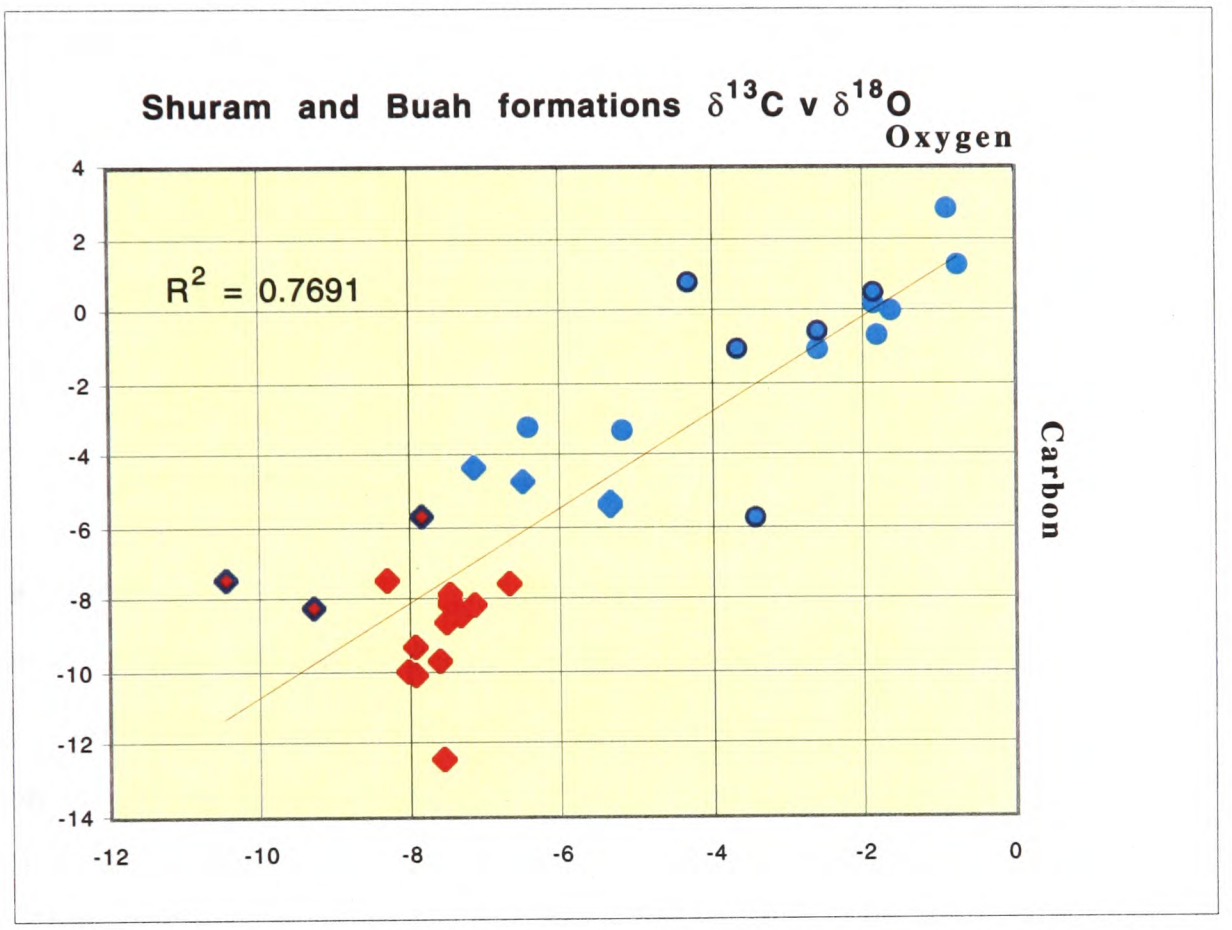


Figure 6.11b The Shuram and Buah formations data show a statistically more significant covariation. Key as for Figure 6.11a.

6.4.3 Oxygen-isotope values

Oxygen-isotopic compositions are sensitive indicators of diagenesis, with a decrease in $\delta^{18}O$ values resulting from isotopic exchange with meteoric, burial or hydrothermal fluids (Kaufman & Knoll 1995). These workers consider that $\delta^{18}O$ values of limestones that are more negative than -5‰ indicate a degree of oxygen-isotopic alteration; samples with values below -10‰ are considered unacceptably altered. Very few of the samples in the present study have $\delta^{18}O$ values of <-10‰.

A literature review (Veizer 1978; Brand & Veizer 1981; Fairchild *et al.* 1990; Veizer *et al.* 1992; Kaufman & Knoll 1995) suggests that oxygen values of -4‰ might be considered as typical of least-altered Precambrian dolomites, and that corrections could in theory be

applied to dolomite samples with lighter values. For limestones, this least-altered value appears to be approximately - 5.5‰ to -6.5‰.

One can observe from the Huqf area data in Table 6.1 that the Khufai Formation dolostones have oxygen-isotope values between -1‰ and -4.5‰ while the limestones have values of between -6‰ and -7.7‰. The Shuram Formation limestones have a relatively tight cluster of values of between -6.3‰ and -8.3‰. The basal limestones of the Buah Formation have values of between -6.3‰ and -7.2‰ while the overlying dolomites have between -0.7‰ and -6.4‰. It is worth noting that in the Oman Mountains, both the Khufai Formation limestones and those of the Shuram/Buah Formation cycles have more negative oxygen isotope values that are around -9‰ and -10‰. It is apparent therefore, that carbonates of the Buah and Khufai Formations can retain oxygen-isotope signatures that are well within the scope of the presumed least-altered Precambrian values, whilst $\delta^{18}O$ isotope values from the limestones of the Shuram and Khufai Formations in the Oman Mountains suggest some degree of alteration.

6.4.4 Summary

This exercise of data correction has shown that, while the $\delta^{13}C$ curve for the Nafun Group (Figure 6.9 and 6.10) is reasonably robust, $\delta^{13}C$ values for the limestones of the Shuram Formation to lower Buah Formation have been reset in a negative direction during diagenesis. This negative shift is indicated by: (a) Mn and Fe ppm enrichment (Table 6.1) which is quite prominent in the upper Shuram Formation and again in the upper part of the lower Buah Formation; (b) a Mn/Sr plot of these samples (Figure 6.4) which suggests a slight correlation, with R^2 values of 0.122; (c) Mn/Sr against $\delta^{13}C$ plots (Figure 6.6a) which show a relatively good correlation of $R^2 = 0.7161$ for the Shuram Formation; (d) Mn against $\delta^{13}C$ plots for the Shuram Formation (Figure 6.7a) which show a slight correlation of 0.3384; and (e) $\delta^{13}C$ against $\delta^{18}O$ plots (Figure 6.11b) show a relatively good correlation of $R^2 = 0.7691$.

Analysis of $\delta^{13}C/\delta^{18}O$ covariance in components (Figures 6.8a,b and c) allows some attempt to backstrip the diagenetic resetting of the Shuram and Buah Formations to values which may be closer to original sea-water values (Figure 6.10) This resetting, which assumes an original $\delta^{18}O$ of limestones of *c.* -6.5‰, does not eliminate, however, the negative $\delta^{13}C$ trend, which appears to be a real part of the original seawater signature.

The evidence for significant differences in seawater depths between the shallow Huqf area and the deeper Oman Mountains successions provides an opportunity to test the impact of locality, water depth and sequence stratigraphy on the $\delta^{13}C$ curve. This is examined in the following section.

6.5 DISCUSSION OF KHUFAI FORMATION DATA

The carbon- and oxygen-isotope curves from the Khufai Formation in the Huqf region are shown in Figure 6.12 and from the Oman Mountains in Figures 6.13. These data show that the $\delta^{13}C$ values from the Khufai Formation are, for the most part, strongly positive across the whole region, with good potential for preservation of a primary signature as shown above. Broadly speaking, the values become heavier from the base of the formation to the top of Association B (at 180m in the Mukhaibah dome), fluctuate through Association C, and then show a sharp decrease in values in the uppermost part of the formation (Figure 6.12).

Association A: Fetid dolostones and limestones

The fine-grained fabrics of the fetid dolostones did not take a stain, indicating iron-free dolomite. Some stained pale-blue indicating iron-poor dolomite. In samples that are partially dedolomitized, the replacement limestone yielded a pale-mauve stain of iron-poor calcite. The interbedded recrystallized peloidal grainstones impart a pale-blue iron-poor stain while the sparry cement is iron-free to iron-poor. The laminated fetid dolostones and limestones of Association A (Figures 6.12 and 6.13) tends to record a rather zigzag pattern with values between 2‰ and 5‰ with a presumably spurious value of -2‰ in interbedded black and white laminated limestones. In the Oman Mountains, the recrystallized limestones are dull-luminescent with pale yellow-luminescent matrix (Plates 6.1a/b). Their iron-free stain is masked by the dark colour of the limestone which, at Wadi Hajir, reveals a very positive $\delta^{13}C$ of between 6 and 8‰ for the most part.

Interpretation

The non-ferroan nature of these sediments along with the lack of a significant diagenetic trend within the trace elements and dull-luminescence, suggest that they preserve a relatively reliable signature (Fairchild 1983). Although care was taken to avoid veins and fractures, the Oman Mountains limestones contain many hairline veins which, if included in the analyses, could affect the results.

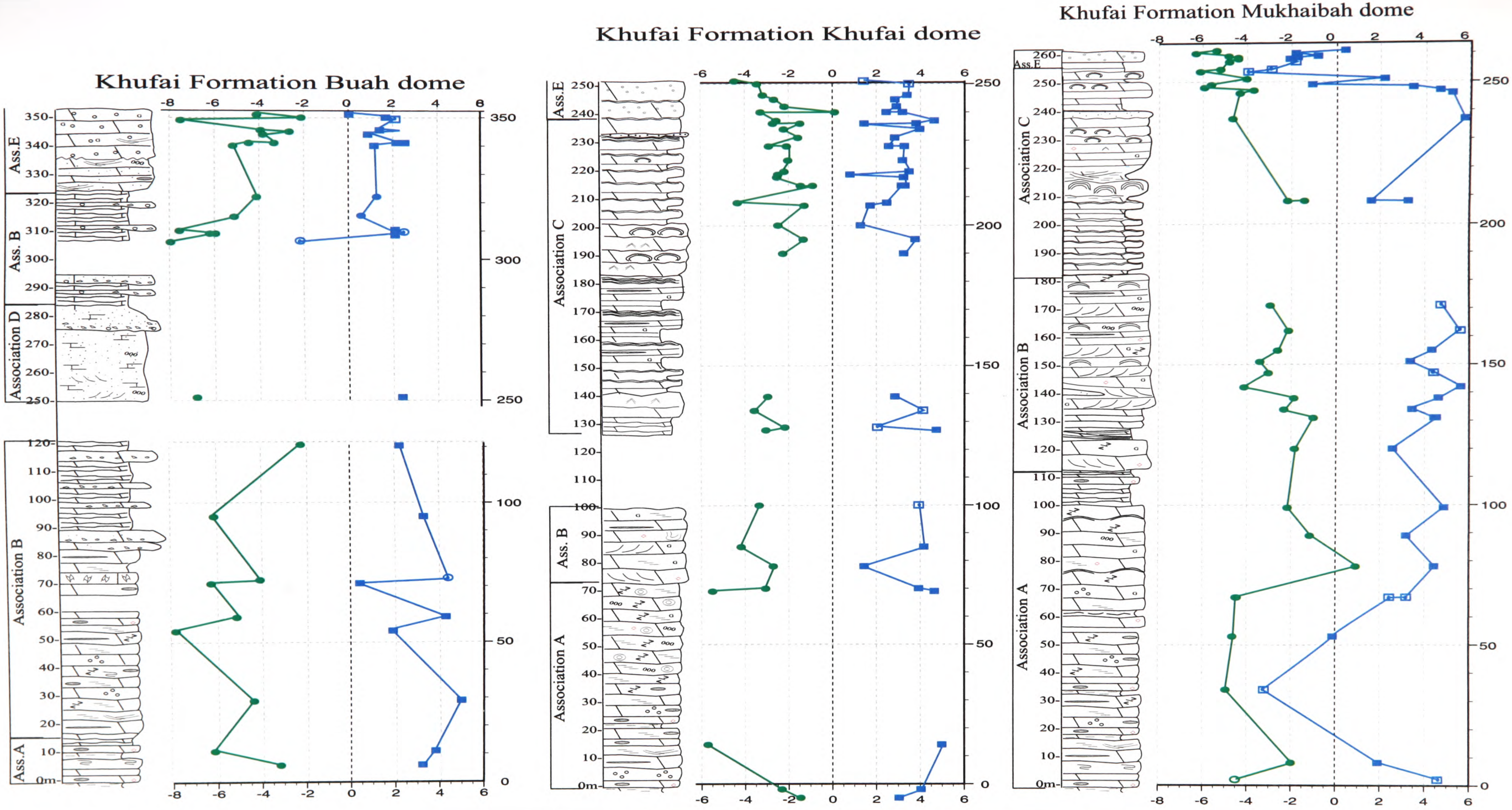

Khufai Formation Buah dome
Khufai Formation Khufai dome
Khufai Formation Mukhaibah dome
Ass.E
Ass. B
Association D
Association C
Association B
Association A
Ass.A
δ 13C Carbon
δ 18O Oxygen
Unaltered dolostone
Mn/Sr >3
∂18O <-10´‰
Unaltered limestone
Mn/Sr >3
∂18O <-10´‰

Figure 6.12

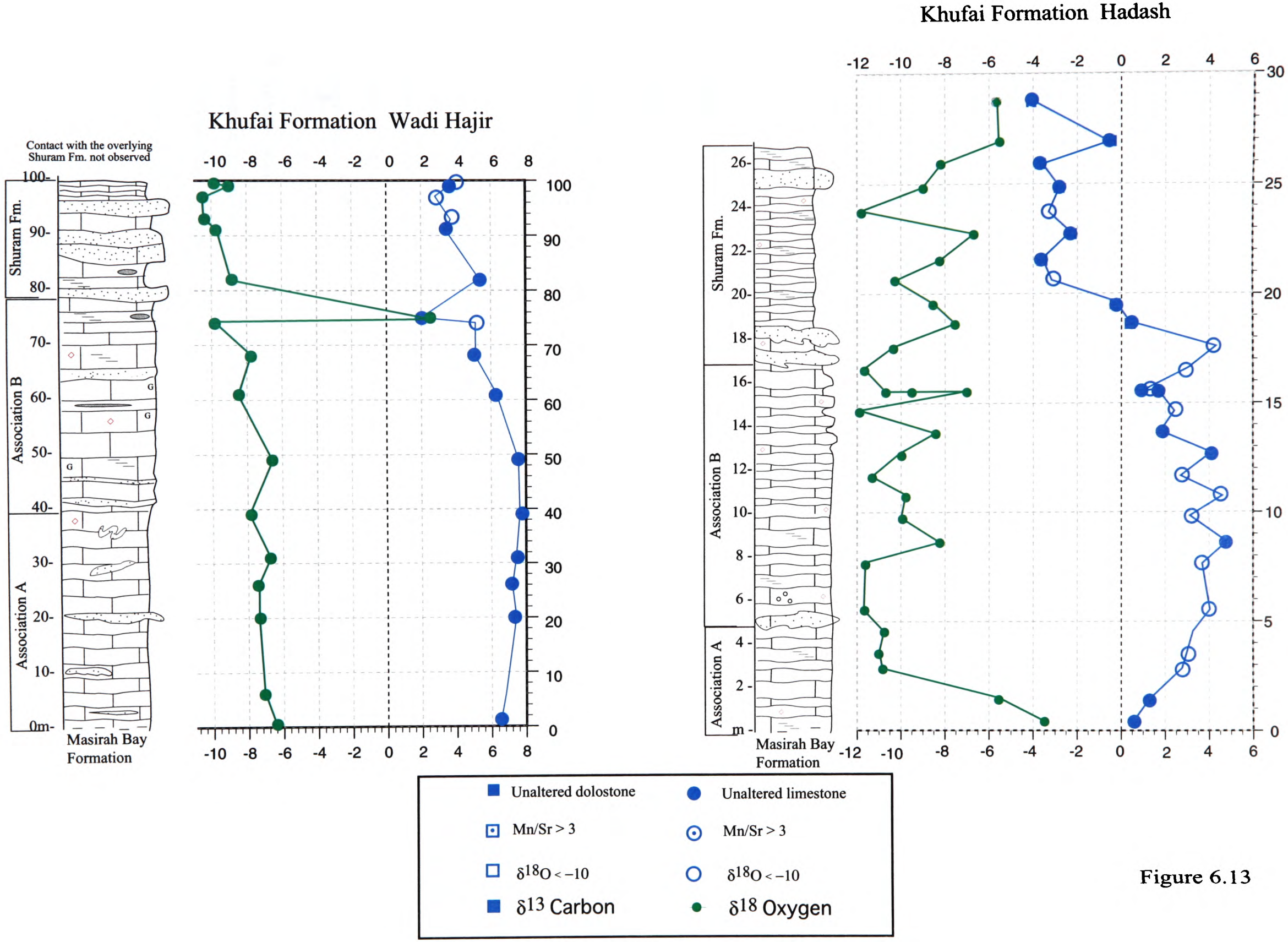

Khufai Formation Wadi Hajir
Contact with the overlying Shuram Fm. not observed
Shuram Fm.
Association B
Association A
Masirah Bay Formation
-10 -8 -6 -4 -2 0 2 4 6 8
100- 90- 80- 70- 60- 50- 40- 30- 20- 10- 0m-
Khufai Formation Hadash
-12 -10 -8 -6 -4 -2 0 2 4 6
26- 24- 22- 20- 18- 16- 14- 12- 10- 8 - 6 - 4 - 2 - m -
30 25 20 15 10 5 0
Unaltered dolostone
Unaltered limestone
Mn/Sr > 3
Mn/Sr > 3
δ18O < –10
δ18O < –10
δ13 Carbon
δ18 Oxygen

Figure 6.13

Association B: Grainstones and stromatolites

Component analysis (Figure 6.7) indicates, surprisingly, that the ooids are slightly more enriched in ^{12}C than the cement. This might reflect a microbial participation in the ooid formation (Dave Wright, pers. comm). Ooids and oncoliths tend to have blotchy-red to pink/blue luminescence while the cements have a sharply zoned yellow-orange luminescence. These grainstones generally remain unstained but where recrystallized or where oomouldic porosity is occluded by calcite they have a pink to mauve stain indicating iron-free to iron-poor calcite. The grainstones facies of Association B (Figures 6.12 and 6.13), with intermittent stromatolites, has samples that are relatively enriched in ^{13}C, with values of between 2‰ and 6‰. In the Oman Mountains, the grainstones of the Khufai Formation are formed of micritic, organic-rich intraclasts of non- or bright-red luminescing carbonate, with some detrital quartz grains, set in a microspar cement which shows yellow luminescence (Plates 6.1c/d). The carbon-isotope signature is approximately 6 to 8‰ at Wadi Hajir but only 3 to 5‰ in Hadash.

Interpretation

Blotchy luminescence can indicate some measure of dissolution (Fairchild *et al.* 1990) and zoned cements suggest different phases of precipitation. The bright-red luminescing cements within the grainstones in the Oman Mountains suggest late dolomite precipitation. The trace element data, however, suggests that these were most likely recrystallized within a 'closed system' so that the primary $\delta^{13}C$ may well be preserved.

Association C: Grainstone-stromatolite cycles

Component analysis indicates that the spar laminae are more enriched in ^{12}C than the micrite laminae, which may be due to incorporation of light carbon released during degradation of the microbial mat. Under cathodoluminescence (Plates 6.1e/f), the micritic laminae luminesce a dull pink/blue while the spar lamina either have none and/or they have orange luminescence with sharply defined zones. Some stromatolites consist of alternating micritic dolomite and sparry limestone laminations; staining indicates that these are formed of iron-free dolomite and iron-poor calcite. The stromatolite cycles tend to have $\delta^{13}C$ values in the range of 0.5‰ to 6‰ (Figure 6.12).

Interpretation

The orange luminescence of the spar lamina suggest a high Mg-calcite which was deposited from pore fluids with varying amounts of Fe and Mn as suggested by the zoned luminescence (Marshall 1988). The well-preserved cathodoluminescence zoning, defining early precipitation, argues along with the micrite for a lack of recrystallization and hence the preservation of a primary to early diagenetic signature.

Association E: Ooidal grainstones

The intraclast grains have dull-red luminescence to non-luminescence with a non-luminescent fringe while the cements are zoned yellow, green and orange (Plates 6.1g/h). The grains do not stain. Component analysis shows that the cement is 0.5‰ more positive in $\delta^{13}C$ and 0.04‰ more negative in $\delta^{18}O$. Trace-element data show a slight enrichment in Fe and Mn. The ooidal/intraclast grainstones of Association E have values that become more negative upward ranging from 3‰ to 0‰ (Figure 6.10). This is further supported by the lower oxygen-isotope values at this level.

Interpretation

The intraclasts are well-preserved while the zoned cement suggests precipitation of low Mg-calcite (yellow), high Mg-calcite (orange) and anhydrite (green) (Miller 1988). The very similar signature of the cement and grains is interpreted as primary to early diagenetic as none of the other characteristics indicate recrystallization.

Oxygen

It is worth recording here the marked difference in oxygen values, between the shallower carbonates of the Huqf area, recording values of between -2 and -8‰, and the Oman Mountains, recording values mostly between -6 and -12‰ (Figures 6.12, 6.13).

6.5.1 Regional variation

There appears to be a slight lateral variation in the $\delta^{13}C$ signature in the Huqf area. Facies Associations A, B and C record heavier values in the Mukhaibah dome (up to 6‰) while the most positive values in the Khufai and Buah domes are generally around 2 to 4‰ (Figure 6.12). At the top of Association C in the Mukhaibah dome there is a negative kick in $\delta^{13}C$ to values of -4‰, followed by more positive values within Association E to about 0.5‰. A negative kick of -2‰ is followed by a positive kick of 1‰ in Association E in the Buah and Khufai domes, where a second negative shift brings values down to 0.5‰ or zero at the top

of the Khufai Formation exposure (Figure 6.12). Lateral variation is also recorded in the Oman Mountains, where Wadi Hajir $\delta^{13}C$ values are between 6 and 8‰ whereas Hadash values are in the range of 1 to 5‰. Oxygen-isotope values are also more negative at Hadash with values of -8 to -12‰ (Figure 6.13).

6.5.2 Interpreting the Khufai Formation signature

These data reveal no consistent trends related to facies-association changes up section during shallowing of the carbonate ramp from fetid carbonates, to grainstones to stromatolite facies. Had there been such a change it would have been possible to argue that the $\delta^{13}C$ signal was overprinted by the effects of water depth and $\delta^{13}C$ gradient through the water column. The anomalously positive values from Wadi Hajir in the Oman Mountains (Figure 6.13) also continue through into the inferred base of the Shuram Formation. Interestingly, if allowance is made for greater diagenesis of oxygen and carbon-isotopes in the Hadash section (Figure 6.13), then $\delta^{13}C$ values may be corrected to comparably positive signatures. One surprising conclusion, therefore, is that the $\delta^{13}C$ of the nearshore Huqf area may have been depleted in ^{13}C relative to the inferred more open-ocean aspect of the Oman Mountains. Such ^{13}C depletion of restricted lagoonal settings is known also from modern Florida Bay, where it has been attributed to biological recycling of organic matter (Patterson & Walter 1994). The greater diagenetic variability of the Oman Mountains section does suggest greater variability in $\delta^{13}C$ inputs.

A sharp fall in $\delta^{13}C$ values is seen at the top of the Khufai Formation in the Mukhaibah dome (Figure 6.12) and in the lower Shuram Formation of Hadash (Figure 6.13). This feature is not recorded in the thicker Wadi Hajir section because the contact with the overlying Shuram Formation was not exposed. Neither is correlated with sharply negative $\delta^{18}O$ values, and trace-element data, suggesting that this fall is not due to meteoric diagenesis at the top of the sequence. This suggests that the falling $\delta^{13}C$ profile may provide a marker that shows Khufai-type facies persisting in the Mukhaibah dome coeval with transgressive Shuram-type facies in the Oman Mountains.

6.6 DISCUSSION OF THE SHURAM FORMATION DATA

The Shuram Formation stable-isotope curve (Figures 6.9 and 6.14) show very low carbon- and oxygen-isotope values. One of the most striking phenomena about the Shuram Formation data from the Huqf area is that the oxygen isotopes are heavier than the carbon values. However, after the application of a component correction (correcting the whole-rock signature for the negative effect of cement recrystallization, see Figure 6.8) this

situation is reversed (Figure 6.10). This correction renders the carbon isotopic data slightly less negative (cf. Figures 6.9 and 6.10). From the lower member of the Shuram Formation upward there is a gradual increase in values into the middle member of the formation, which has very consistent values of around -10‰ (uncorrected) whilst in the upper Shuram Formation uncorrected values are approximately -8‰. The most reliable corrected data from the middle Shuram Formation suggests a value for $\delta^{13}C$ at around -5 to -6‰ (Figure 6.10). The oxygen-isotope values (Figures 6.9 and 6.14) appear to stick at around -8‰ throughout, which would suggest resetting at higher temperatures during burial.

The good preservation of most of the ooids in the oosparites of the Shuram Formation suggest a relatively stable low Mg-calcite precursor (Sandberg 1975; Wilkinson *et al.* 1984) (Plates 6.2a to 6.2f). Many of the pelsparites appear to be formed of grains that have undergone variable amounts of dissolution and reprecipitation (Plates 6.2g/h). In stained thin-sections of facies S4, the ooids are red, suggesting an iron-free calcite mineralogy. These have an isopachous fringe cement of non-luminescent calcite which is sometimes masked by late equant spar which stains a pale-blue, suggesting iron-rich calcite. The cements and grains of the pelsparites and oosparites all luminescence a dull or bright yellow colour without zonation (Plates 6.2a to 6.2h). Vadose cements are commonly non-luminescent (Meyers 1974) while bright luminescence may be a reflection of oxidation state (Frank *et al.* 1982) with brighter luminescence suggesting higher oxygen levels within the diagenetic environment. Thus the diagenetic sequence entails iron-poor ooids cemented by an iron-poor calcite fringe cements with late iron-rich calcite pore-filling cements.

Flat-pebble conglomerates are ubiquitous throughout the Shuram Formation and clearly suggest rapid early cementation on or near the seafloor. This early cementation should help to preserve a primary $\delta^{13}C$ signature for these rocks. This is presumably reflected in a variation of only approximately 0.5‰ between the clast and cement in some samples analysed (Figure 6.8).

The low oxygen-isotope values for the Shuram Formation (c. -7‰) would, using the criteria of Kaufman & Knoll (1995), suggest some degree of oxygen isotopic alteration. The tight cluster would also suggest resetting. However, these values are not very different from the values of -5.5‰ to -6.5‰. suggested as primary oxygen-isotope values for Precambrian limestones by Fairchild *et al.* (1990). Oxygen isotopes are relatively easily exchanged due to the higher concentration of oxygen in porewaters relative to the rock.

Shuram Formation isotope curve

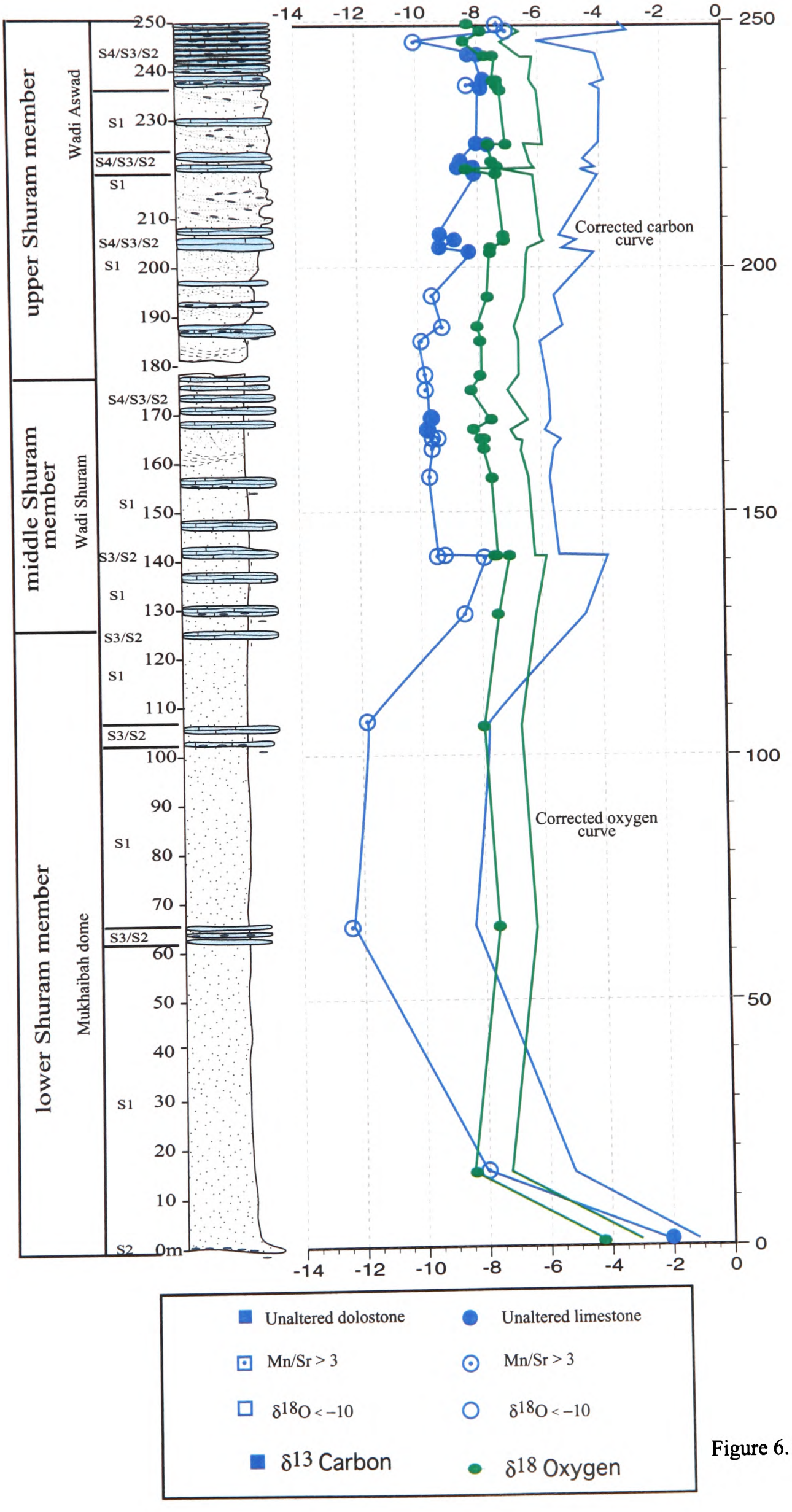


Figure 6.14

As there is evidence for dissolution and reprecipitation within the Shuram facies, oxygen isotopes are considered to have been reset.

Interpretation

The moderate Sr content (average 271ppm) of these Shuram Formation limestones is, like the ooid fabrics and yellow luminescence, suggestive of a primary low Mg-calcite mineralogy. The higher Mn and Fe contents (Table 6.1; Figure 6.7), along with the tight cluster of $\delta^{18}O$ values, indicate that a strong diagenetic overprint took place, involving precipitation in a burial environment where pore waters were enriched in Fe and Mn.

6.6.1 Regional variation

The regional variation of isotopic signatures within the Shuram Formation is not easily defined because of the difficulty of correlating fragmented exposures in the Huqf area. The lack of carbonate facies in the middle member of the Shuram Formation in the Oman Mountains further limits comparison. The sharp carbon-isotope change reported by earlier workers from the base of the Shuram Formation (Burns *et al.* 1993) falls within the uppermost Khufai Formation (as herein defined) at the Mukhaibah dome (Figure 6.12) where a negative shift of up to 6‰ is followed by a positive shift of c. 4‰ before the final decline into Shuram Formation values. Elsewhere, however, this negative shift is confined to the lower Shuram Formation (Figure 6.12).

6.6.2 Interpreting the Shuram Formation signature

Although the negative peak of the Shuram Formation is accentuated by diagenesis, correction for diagenetic effects does not remove the negative signature (Figure 6.9 and 6.10). As has been shown above, the anomalously negative $\delta^{13}C$ values from the upper Shuram Formation in the Huqf area (Figure 6.9) become similar to those from the Oman Mountains section after backtracking for diagenetic resetting (Figure 6.10). Comparably negative $\delta^{13}C$ values are recorded from across Oman at this level (Burns *et al.* 1993). The lower Shuram Formation contains planar bedded siltstones and local organic-rich shales, suggesting quiet deposition, whereas the swaley cross-stratification and dewatering structures of the middle Shuram Formation suggest a predominance of storm deposition. The homogenous and fine-grained character of the siliciclastic sediments as well as their red, iron-rich nature suggests a humid and presumably subtropical to tropical weathering source. Such tropical weathering could have enhanced the availability of Fe and P within surface waters. In Precambrian environments, both Fe and P may have been linked together as ferriphosphates in an oxidised state and therefore not available as nutrients to micro-

organisms (Brasier 1992c; Bühn & Stanistreet 1997). Organic productivity might, therefore, have been limited at this time. A very turbulent water column would remain well oxidised and, as such, would inhibit the preservation or burial of organic matter. A lack of productivity and burial of organic matter, will result in an enrichment of surface waters in ^{12}C. The lack of evidence for organic matter within these sediments certainly makes it hard to invoke bacterial degradation of organic matter as the whole reason for negative $\delta^{13}C$ values, unless degradation went to complete removal of carbon from the sediment under, for example, high levels of oxygen availability.

6.7 DISCUSSION OF THE BUAH FORMATION DATA

The Buah Formation isotope results are shown in Figures 6.15 and 6.16. In all sections except for Wadi Bani Awf, the lowermost association of the Buah Formation, the crinkly laminated limestones, have uncorrected negative $\delta^{13}C$ signatures of between -4‰ and -6‰ like those of the underlying upper member of the Shuram Formation. The sharp contact with overlying stromatolite and grainstone dolostones is accompanied by a minimum 2‰ shift towards more positive values (i.e. between Association A and Association B, Figure 6.15). This shift could be due in part to the change in mineralogy (cf. Fairchild *et al.* 1990) and to the observation that fabric retentive dolostones tend to preserve better the primary $\delta^{13}C$ signal (Kaufman & Knoll 1995). There is a second positive shift of values at the contact between the overlying limestones (peloidal wackestones) and the dolomitized recrystallized grainstones (Figure 6.15) with values close to 0‰ at the top of the Lower Buah Formation. The peritidal cycles of Association C in the upper Buah Formation have negative values in the supratidal sediments at the base (Figure 6.15) but upward have rather consistent values at around 2‰. In the more complete Mukhaibah dome section, there are two negative shifts that appear to correspond to positive oxygen shifts. Similar shifts are recorded in the uppermost Buah Formation in Wadi Bani Awf (Figure 6.16).

Association A: Crinkly laminites

This lithofacies demonstrates dull-cathodoluminescence very similar to that of the Shuram Formation (Plates 6.3g/h). The stain is mauve to purple, indicating an iron-poor calcite with non-staining calcite spar in vugs. Trace elements show moderate Fe and Mn with relatively high Sr contents (Table 6.1). The limestones at the base of the Buah Formation record carbon-isotope values that are slightly more positive than those of the Shuram Formation (Figure 6.9). The oxygen values of between -5‰ and -8‰ must be at least partly altered. The corrected $\delta^{13}C$ value is around -3.7‰ throughout both the crinkly laminated limestones and edgewise flake-breccias of Association A.

Interpretation

The dull-luminescence and moderate Fe and Mn concentrations might be taken to suggest a lack of alteration. However, these rocks have very negative $\delta^{13}C$ signatures and are stylolitized suggesting some measure of pressure dissolution and alteration. This is also suggested by the covariance of $\delta^{13}C$ against ^{18}O plots (Figure 6.11b).

Association B: Stromatolites and grainstones

The wackestones of Association B in the Buah dome have dull-red luminescing intraclasts with a dull to non-luminescing matrix and late pore-filling bright-yellow luminescing cement. The recrystallised grainstones of the platform shoal complex show individual rhomb shaped crystals with a clotty red/orange luminescence in the core within a zoned-luminescent cement in intracrystalline pore space (Plates 6.3e/f). This facies remains unstained in Alizarin red S and potassium ferricyanide solutions. The recrystallised large-scale stromatolites have a corrected $\delta^{13}C$ signature of approximately -1.6‰ in the Khufai dome and the Buah dome (shift 1 on Figure 6.15) whilst the overlying peloidal wackestones have corrected values closer to -2.4‰ (negative part of shift 2 on Figure 6.16).

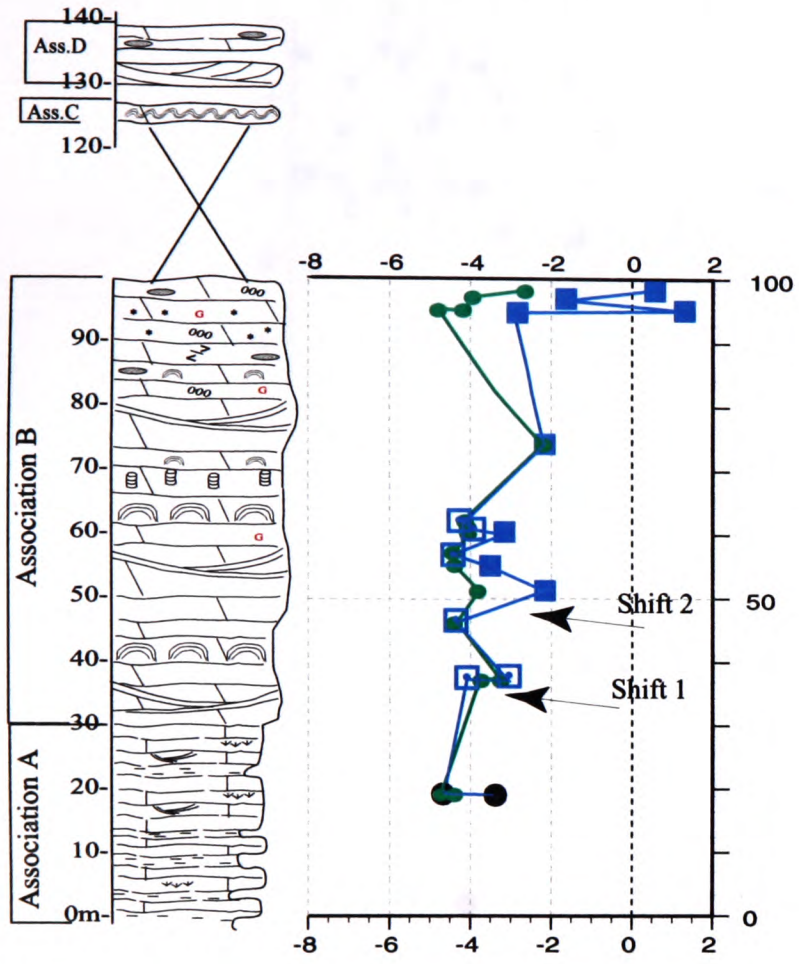
Interpretation

The dull-luminescence of the wackestone intraclasts and matrix would suggest that these are not altered, following the criteria of Kaufman & Knoll 1995). The clotty fabric of the overlying grainstone luminescence is considered an indication of wet recrystallization (Fairchild *et al.* 1990) whilst the zoned nature of the intracrystalline pore filling suggests changing pore-fluid chemistries.

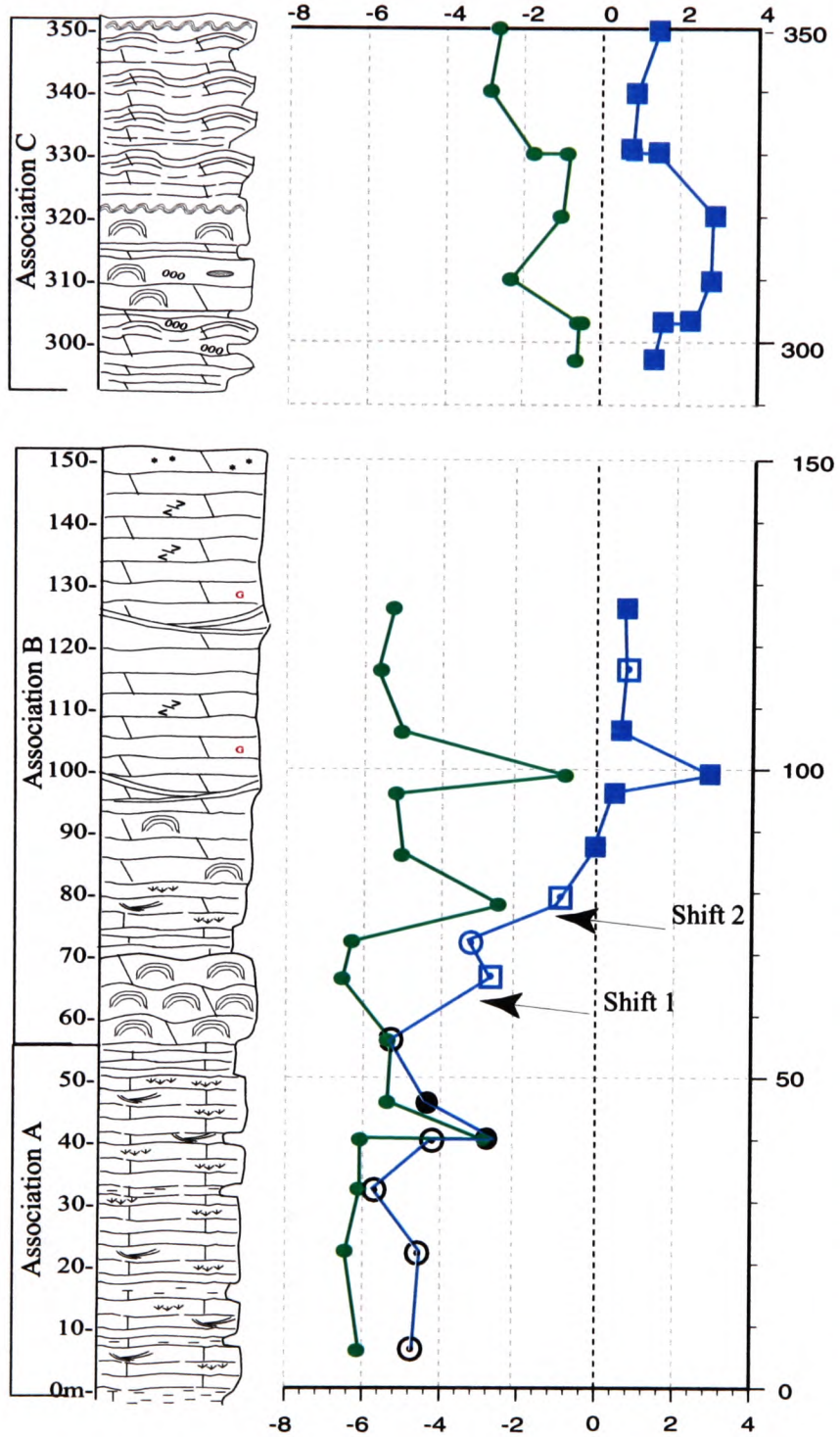
Association C: Peritidal cycles

Cathodoluminescence of interbedded columnar stromatolites show a dull pink/blue luminescence with red-luminescing spar and non-luminescent interbedded chert (Plates 6.3a/b). There is a slight negative shift associated with the appearance of this facies in the Mukhaibah dome (131m in Figure 6.15). It is noticeable that at the level of the anhydrite-rich supratidal facies (185m, Mukhaibah dome) both $\delta^{18}O$ and $\delta^{13}C$ have similar values within the host micrites. The overlying peritidal cycles maintain positive $\delta^{13}C$ values whilst the oxygen values lie close to 0‰ (Figure 6.15). Supratidal beds toward the top of the formation

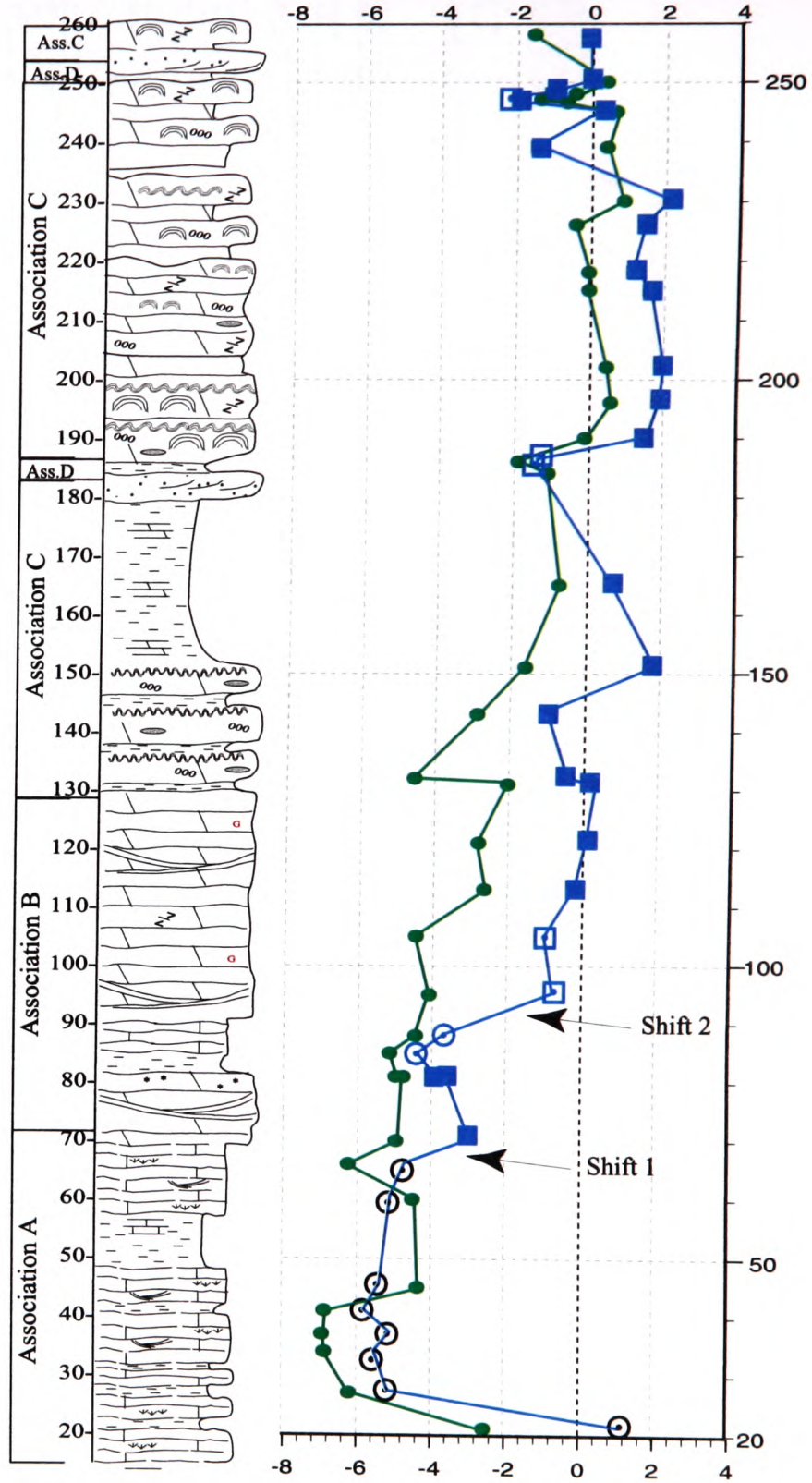
Buah Formation in Buah dome



Buah Formation in Khufai dome



Buah Formation in Mukhaibah dome



Unaltered dolostone
Unaltered limestone
Mn/Sr > 3
Mn/Sr > 3
$\delta^{18}O < -10$
$\delta^{18}O < -10$
Mixed limestone and dolostone
δ^{13} Carbon
δ^{18} Oxygen

Figure 6.15

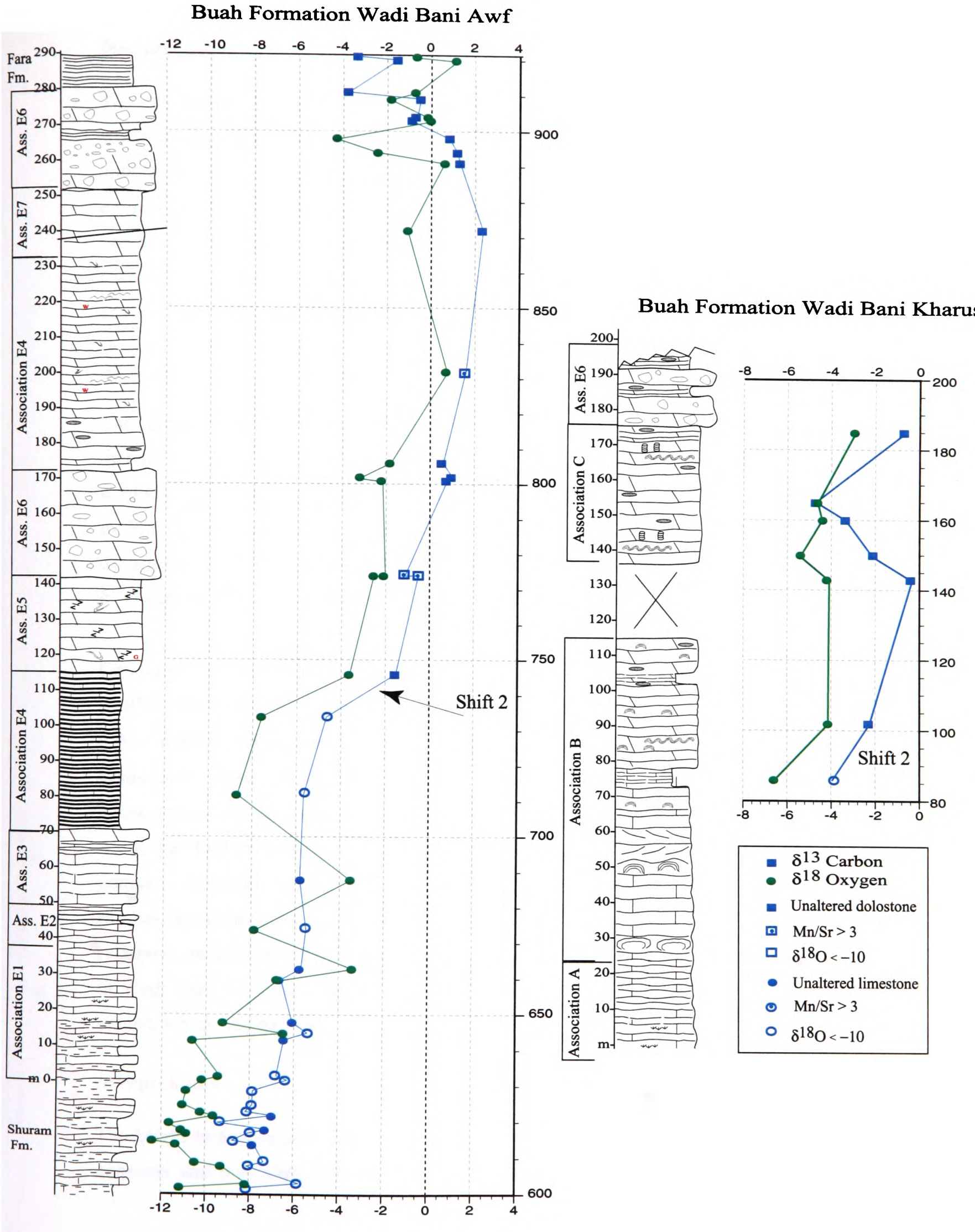

Buah Formation Wadi Bani Awf
Buah Formation Wadi Bani Kharus
Fara Fm.
Ass. E6
Ass. E7
Association E4
Ass. E6
Ass. E5
Association E4
Ass. E3
Ass. E2
Association E1
Shuram Fm.
Association C
Association B
Association A
Shift 2
Shift 2
δ13 Carbon
δ18 Oxygen
Unaltered dolostone
Mn/Sr > 3
δ18O < –10
Unaltered limestone
Mn/Sr > 3
δ18O < –10

Figure 6.16

also record $\delta^{18}O$ values equivalent to or richer than the $\delta^{13}C$ values, while the $\delta^{13}C$ values change from positive to negative and back.

Interpretation

The stromatolitic luminescence suggests lack of alteration within the microspar laminae while the spar laminae have primary dolomite cements followed by iron-rich spar which appears to quench the signal. The relatively high $\delta^{18}O$ values could result from the arid environment where high evaporation rates caused the enrichment of ^{18}O in the seawater, resulting in a positive shift relative to carbon (cf. Pierre 1988). The fluctuations within the carbon-isotope signature possibly result from periodic restriction within the lagoonal environment, with restricted periods recording heavier signatures.

Association E: Deeper facies from Wadi Bani Awf

The basal crinkly laminites have a dull-yellow luminescence whilst upwards there is an increase in red luminescence with most of the thin-sections showing dull- to bright-red luminescence (Plates 6.3e/f). Trace-element analyses do not show any significant enrichment in Mn or Fe within these deeper-water facies and they contain similar Sr values to the dolostones of the Huqf area. While elemental data do not show any covariance the plot of $\delta^{13}C$ against $\delta^{18}O$ shows a covariance of R^2=0.7691 (Figure 6.11b).

Generally, the deeper-water facies through the Buah Formation in Wadi Bani Awf shows similar trends in $\delta^{13}C$ values to those seen elsewhere (Figure 6.15 and 6.16). The very light $\delta^{13}C$ values (c. -8‰ with corrected values of -4‰) in the Shuram/Buah Formation cycles grade-up to about -4‰ (corrected) in the crinkly laminites to shaley carbonates of facies E4. These values are very similar to those recorded from the Huqf area at this level (Figure 6.15). As in the Huqf area, there is a sharp (2‰) positive shift in values at the limestone/dolostone contact, between facies E4 and E5. Upward through the breccia beds (E6) and rhythmites/wackestones (E3), there is a gradual increase to 2‰, a value which remains relatively steady until the uppermost breccia unit at 260m. At the top of the Buah Formation in Wadi Bani Awf, the oxygen-isotope values become more positive than the carbon-isotope values, which fall to -4‰.

Interpretation

The bright luminescence recorded in some of these samples is not complimented by high Mn contents and may therefore be a result of increased beam pressure (Miller 1988). Although

the trace-element data does not show significant evidence of alteration, the $\delta^{13}C/\delta^{18}O$ plot would suggest otherwise (Figure 6.11b). The isotopic trends compare well with those from the shallower Mukhaibah dome section (Figure 6.15). Note that the uppermost part of the Buah Formation was not observed in the Khufai dome and was not sampled in the Buah dome.

6.7.1 Regional variation

There appears to be some facies-associated shifts in isotopic signature through the section during shallowing of the carbonate platform from crinkly limestones, to grainstones and stromatolite facies to peritidal carbonates. These large-scale changes can be seen across the Huqf area (Figure 6.15). Since similar shifts and values occur in the deeper facies of the Wadi Bani Awf section, the changes may not be related to the $\delta^{13}C$ gradient through the water column. The basal Association A of the Buah Formation has carbon-isotope signatures of approximately -5‰ (*c.*3.5‰ corrected) in the Huqf area whilst in the Oman Mountains -6‰ (*c.*-4‰ corrected) is the average. Oxygen-isotope values are around -7‰ in the Huqf area while they fluctuate between -7 and -10‰ in the Wadi Bani Awf section. A notable feature of Association A in the Mukhaibah dome is that the oxygen and carbon-isotope signature cross-over each other continuing the situation in the Shuram Formation. The 'kick' recorded between limestones of Association A and dolostones of Association B in the Huqf area is also seen in the Wadi Bani Awf section between the limestone facies E4 and the dolostone facies E5. The carbon-isotope and oxygen-isotope signatures both tend to become more positive upwards, with the signature recorded in Wadi Bani Awf being very similar to that of the Mukhaibah dome section.

6.7.2 Interpreting the Buah Formation signature

The $\delta^{13}C$ of the Buah Formation sees a gradual return to more normal signatures. Both the carbon- and oxygen-isotope signatures show similar trends in the Huqf area and the Oman Mountains. The lowermost Buah Formation has a signature very similar to that of the upper Shuram Formation and is considered to result from the same processes that affected the latter. It shares, for example, limestones that have undergone rapid cementation as evidenced by the presence of edgewise flake-breccias. The first positive kick of significance in the lower Buah Formation (Shift 1) appears to coincide with the disappearance of flat-pebble conglomerates and edgewise flake-breccias. This more positive signature occurs in large scale stromatolitic dolostones of Association B that are laterally extensive across the whole region (Figure 6.15). Above this, there is a brief return to more negative values within silty peloidal lime-wackestones that are iron-rich.

A further rise (Shift 2) occurs with the disappearance of limestones and a return to shallow marine conditions with dolomitic grainstones and stromatolites. These are dolomitized to a coarse dolospar and retain values of between -2‰ and 1‰. This positive shift might relate to the mineralogical change from limestone to dolostone (Sheppard & Schwarcz 1990) although some authors would dispute such a control (Tucker 1983; Knoll *et al.* 1986). This dolostone facies is persistent throughout the Huqf area and marks the top of the lower Buah Formation (Figure 6.15).

Associations C and D of the upper Buah Formation contain peritidal facies and record $\delta^{13}C$ values of between -2‰ and 2‰. Evaporative conditions are further suggested by the positive values of the oxygen curve in Associations C and D of the upper Buah Formation in the Mukhaibah dome area (Figure 6.15).

6.8 CARBON ISOTOPIC SIGNATURE SYNTHESIS

Two major negative to positive carbon isotopic oscillations are recorded across Oman from the Huqf area to the Oman Mountains, a present day distance of c. 600km. They are thought to preserve a signature that reflects the composition of late Neoproterozoic seawater. The Khufai, Shuram and Buah Formations are noted for their layercake stratigraphy (Bell 1993, Kapellos *et al.* 1992) which must have formed during conditions of relative tectonic stability. Major tectonism is not, therefore, considered to be a cause of the fluctuating carbon isotopic signature.

The relatively deeper-water facies of the Khufai Formation in the Oman Mountains, and of Facies Associations A and B of the Huqf area, are both dominated by fetid carbonates with a very positive signature. This could be taken to indicate globally enhanced rates of organic productivity and burial of organic carbon under anoxic conditions during episodes of marked oceanic stratification (cf. Scholle & Arthur 1980). The shallower water, non-fetid, Facies Association C also tends to have highly positive values. Petrography and cathodoluminescence of the carbonates of the Khufai Formation indicate a primary aragonitic or high Mg-calcite mineralogy, both of which are considered to be preferentially precipitated in warm seas (Fairchild & Spiro 1987; Tucker 1992). This, along with the evidence of evaporitic conditions within Associations C and E, might suggest a rather warm, dry, equitable climate in Khufai Formation times (Kendall & Harwood 1996). Thus the Khufai Formation positive excursion is taken to indicate a period of oceanic stratification that enabled the burial of significant organic matter during warm climatic conditions.

The transgression of the Shuram Formation siliciclastics drowned the Khufai ramp and reworked some of the upper sediments, as seen in Wadi Bani Awf and Wadi Bani Kharus in the Oman Mountains. The only example of organic-rich black shales is recorded from this level in Wadi Bani Awf, suggesting quiet deposition beneath an oxygen-minimum zone. Elsewhere, the lower Shuram Formation sediments tend to comprise planar-bedded red siltstones and shales. By middle Shuram Formation times wave energies had increased dramatically, leading to ubiquitous swaley cross-stratification as well as dewatering and soft-sediment deformation structures, suggesting stormy conditions. In upper Shuram Formation times, cross-stratified prograding ooidal and peloidal grainstones were deposited along with swaley laminated siliciclastics. The fine-grained character and iron-rich nature of the siliciclastic sediments probably result from humid, subtropical to tropical weathering of the hinterland, with deposition rates enhanced by storms. A prolonged period of anoxic conditions in the deep ocean in Khufai Formation times would allow for the build-up of large quantities of ferrous iron, probably sourced from hydrothermal input (Veizer 1983; Derry *et al.* 1989). Upwelling of these waters could result in iron-rich sediments and enhanced nutrient availability in surface waters. However, diminished organic productivity is suggested by the negative carbon-isotopes and the red oxic nature of the sediments, which would also suggest a lack of carbon burial.

Above the flat-pebble conglomerate and edgewise flake-breccias of Association A in the Buah Formation, there is a laterally extensive biostrome of compound stromatolites that are formed of dolostones for the most part. Between these facies there is a marked positive $\delta^{13}C$ shift of about 2‰ across the Huqf area, which is most likely related to the change in mineralogy (cf. Fairchild *et al.* 1990). Superseding the compound stromatolites are thin beds of silty, peloidal lime-grainstones and wackestones. There is a second positive carbon-isotope shift in the overlying beds with dolomitized grainstones and stromatolites that is also recorded laterally across the Huqf area. The stratigraphically similar horizon in Wadi Bani Awf records a similar positive shift and here the underlying sediments are limestone and shales that are considered to represent a flooding surface. There is then a gradual increase to normal isotopic values toward the top of the lower Buah Formation.

The upper Buah Formation sees a continuation of positive values (2‰) with minor negative carbon-isotope shifts correlated with positive oxygen-isotope shifts within evaporitic and sabkha facies. These fluctuations are considered to reflect variations in restriction within a lagoonal environment.

depth	association	petrography	Al ppm	Fe ppm	MgO	CaO	Na ppm	Mn ppm	Sr ppm	13C	18O	MgO/CaO	Mn/Sr	Fe/Mn
Buah Formation														
237	C2a	microspar dolo	0	279.76	12.53	24.76	445.12	130	109	1.249	-0.726	0.506	1.19	2.15
225	C2	spar and microspar	52.93	349.7	15.93	17.7	296.74	244	147	-3.331	-5.196	0.900	1.66	1.43
199	C2a	microspar dolo	52.93	489.58	17.08	17.59	222.56	240	50	2.836	-0.886	0.971	4.80	2.04
160	B3	recryst. dolostone	105.85	20.982	5.45	7.81	296.74	76	25	0.213	-1.856	0.698	3.04	0.28
135	B3	recryst dolomite gs	105.85	1888.4	15.3	21.7	222.56	1643	31	0.032	-1.62	0.705	53.00	1.15
119	B3	recryst dolomite gs	158.78	489.58	15.54	19.15	148.37	356	34	-0.688	-1.806	0.811	10.47	1.38
78	A1	microspar lime	158.78	2587.8	20.66	25.02	222.56	1081	67	-1.084	-2.592	0.826	16.13	2.39
69	B3	microspar dolo	52.93	2657.7	14.02	21.15	816.05	1860	66	-3.245	-6.434	0.663	28.18	1.43
56	B2	peloidal limestone	158.78	1119	1.75	41.27	296.74	2850	284	-5.372	-5.379	0.042	10.04	0.39
52	B2a	ooidal sparite	52.93	699.4	0.57	43.39	148.37	275	231	-5.269	-5.352	0.013	1.19	2.54
43	B1	recryst dolo/lime	52.93	419.64	0.27	43.03	148.37	347	369	-4.258	-7.203	0.006	0.94	1.21
22	A1	microspar lime	211.7	1049.1	0.82	53	445.12	554	1854	-4.627	-6.511	0.015	0.30	1.89
mean			97.03	1004.22			309.11	804.6667	272.25					1.25
stdev			63.16	900.66			189.36	876.45	510.40					1.03
Mtns														
890	B3c	recryst dolospar	1217.3	979.16	20.75	27.92	222.56	132	92	0.799	-4.321	0.743	1.43	7.42
818	E5	peloidal-dolospar	158.78	489.58	15.02	20.14	222.56	182	35	0.495	-1.864	0.746	5.20	2.69
774	E6	recryst dolospar	52.93	349.7	14.54	20.58	148.37	143	40	-0.565	-2.58	0.707	3.58	2.45
746	E3	microspar lime	52.93	209.82	15.54	18.09	148.37	55	30	-1.0583	-3.671	0.859	1.83	3.81
663	E1	microspar lime	423.41	839.28	21.36	28.44	222.56	161	48	-5.759	-3.428	0.751	3.35	5.21
mean			381.07	573.51			192.88	134.60	49.00					4.26
stdev			491.39	325.80			40.64	48.37	24.94					6.74
Shuram Formation														
250	S1a	silty lime microspar	1376.08	4965.7	2.44	41.9	1038.6	3726	552	-8.076	-7.181	0.058	6.75	1.33
244	S1a	silty lime microspar	211.7	1958.3	0.65	42.4	370.93	665	983	-7.412	-8.322	0.015	0.68	2.94
237.5	S4	ooidal sparite lime	317.56	3357.1	1.59	41.99	741.86	1098	403	-7.803	-7.483	0.038	2.72	3.06
237	S2	peloidal spar/microsp	952.67	2517.8	1.07	40.94	667.67	1063	221	-8.316	-7.375	0.026	4.81	2.37
227	S1a	silty microspar lime	211.7	3007.4	1.72	43.03	370.93	755	373	-8.087	-7.5	0.040	2.02	3.98
225	S4	ooidal sparite lime	317.56	1468.7	1.54	42.4	519.3	1842	468	-7.94	-7.508	0.036	3.94	0.80
225	S4	ooidal sparite lime	264.63	1888.4	1.19	41.9	519.3	527	328	-7.526	-6.738	0.028	1.61	3.58
220	S4	ooidal sparite lime	158.78	1748.5	1.18	43.88	519.3	972	271	-8.53	-7.56	0.027	3.59	1.80
204	S4	ooidal sparite lime	264.63	909.22	0.8	44.39	370.93	1378	219	-9.239	-7.988	0.018	6.29	0.66
185	S3	pelsparite lime	264.63	629.46	1.06	43.23	445.12	1560	190	-9.991	-7.988	0.025	8.21	0.40
178	S2	peloidal spar/microsp	423.41	699.4	1.37	42.5	593.93	1509	298	-9.872	-8.079	0.032	5.06	0.46
169	S4	ooidal sparite lime	105.85	279.76	0.41	42.61	222.56	648	251	-9.644	-7.637	0.010	2.58	0.43
65	S1a	silty lime microspar	158.78	349.7	0.59	44.41	296.74	3855	281	-12.36	-7.578	0.013	13.72	0.09
mean			386.77	1829.19			513.63	1507.54	372.15					1.21
stdev			365.01	1364.52			215.16	1087.51	211.30					1.25
Mtns														
626	S9	lime microspar	52.93	2797.6	0.86	43.45	148.37	1067	1010	-7.421	-10.489	0.020	1.06	2.62
74	S9	lime microspar	52.93	559.52	0.61	43.45	148.37	357	2476	-5.596	-7.877	0.014	0.14	1.57
8	S9	lime microspar	158.78	4616	1.4	41.83	222.56	621	3390	-8.141	-9.304	0.033	0.18	7.43
mean			88.21	2657.71			173.10	681.67	2292.67					3.90
stdev			61.11	2031.86			42.83	358.87	855.11					5.66
Khufai Formation														
245	E1? E2a	micrite/dolospar	52.93	629.46	9.22	21.45	148.37	225	39	1.529	-3.092	0.430	5.77	2.80
219	B2b	lime micrite/spar	105.85	419.64	3.36	41.49	445.12	101	594	1.969	-7.456	0.081	0.17	4.15
208	C2	dolomicrite/spar	52.93	209.82	10.57	27.42	593.49	28	120	1.581	-2.206	0.385	0.23	7.49
190	C1	dolospar	105.85	909.22	12.6	24.05	222.56	573	97	-0.27	-4.212	0.524	5.91	1.59
186	C4	lime micrite/spar	52.93	489.58	14.46	20.64	296.74	32	65	1.956	-2.804	0.701	0.49	15.30
131	C2	dolomicrite/spar	52.93	209.82	10.61	26.82	222.56	15	33	4.538	-1.03	0.396	0.45	13.99
109	B2b	lime micrite/spar	52.93	139.88	1.71	40.77	296.74	50	338	3.139	-7.734	0.042	0.15	2.80
95	B2b	lime micrite/spar	52.93	69.94	1.14	42.31	667.67	61	2275	3.296	-6.137	0.027	0.03	1.15
69	A1	dolomicrite	52.93	1538.7	13.68	21.18	148.37	181	36	3.942	-5.08	0.646	5.03	8.50
67	B2b	lime micrite/spar	158.78	559.52	12.84	23.04	370.93	353	51	2.433	-4.459	0.557	6.92	1.59
15	B2	peloidal limesparite	52.93	629.46	15.52	18.74	222.56	234	58	1.727	-2.068	0.828	4.03	2.69
2	A1	dolomicrospar	52.93	909.42	15.67	19.61	148.37	1507	26	4.245	-4.285	0.799	57.96	0.60
mean			70.57	559.54		27.29	315.29	280.00	311.00					2.00
stdev			34.47	415.40			173.62	419.93	641.07					0.99
Mtns														
100	A2	recryst microspar I	105.85	2308	17.88	16.16	222.56	362	221	1.085	-9.498	1.106	1.64	6.38
15	B3	peloidal microspar I	158.78	769.34	1.53	42.51	222.56	103	2351	6.128	-9.304	0.036	0.04	7.47
mean			132.32	1538.67			222.56	232.5	1286					6.62
stdev			37.43	1088.00			0.00	183.14	1506.14					5.94
cap' dolostone														
	Cap	dolospar	264.63	9092.2	13.31	20.3	148.37	1720	188	-8.309	-6.616	0.656	9.15	5.29

Table 6.1

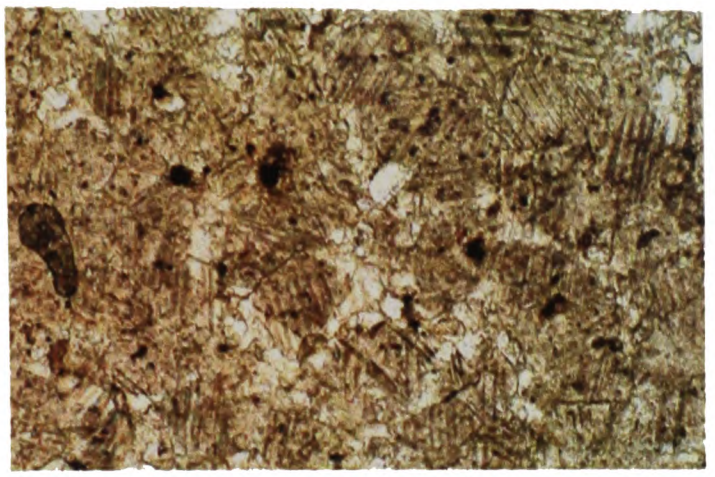


Plate 6.1a Photomicrograph of FaciesA1 recrystallized lime-mudstone. Horizontal fov. 2.45mm. 90m Wadi Sahtan.

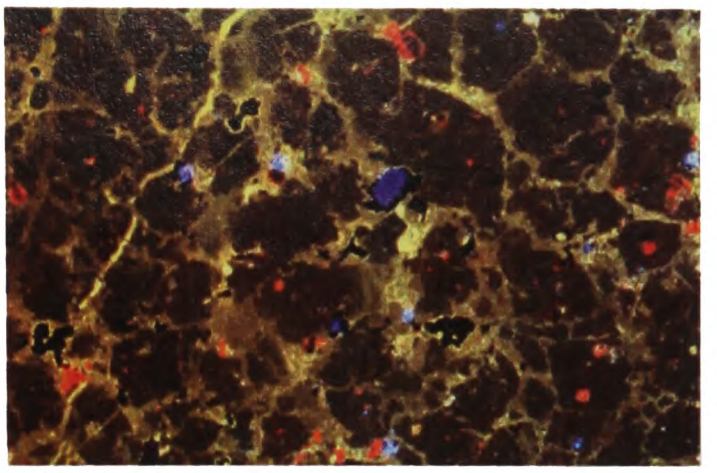


Plate 6.1b Cathodoluminescence photomicrograph of Facies A1 recrystallized lime-mudstone. Horizontal fov. 2.45mm. Wadi Sahtan.

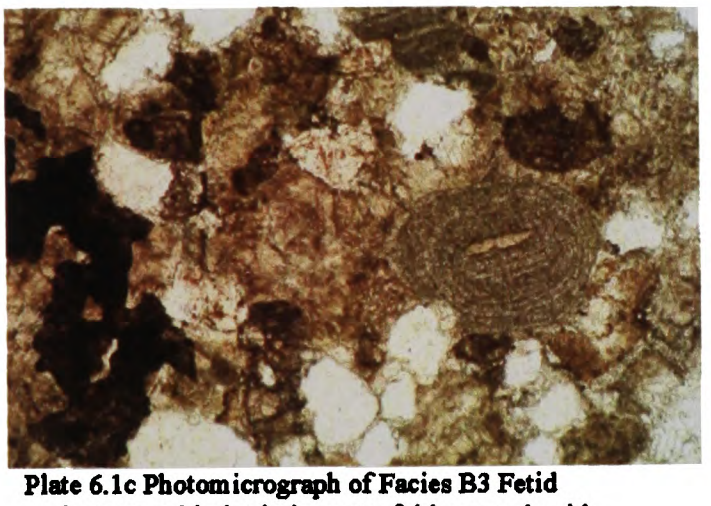


Plate 6.1c Photomicrograph of Facies B3 Fetid grainstone, with detrital quartz, feldspar and ooid grains within a carbonate spar matrix. Horizontal fov. 0.95mm. 87m Wadi Hajir.

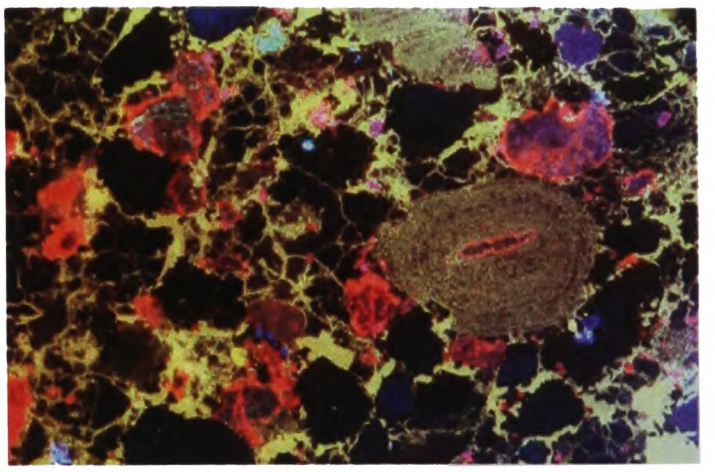


Plate 6.1d Cathodoluminescence photomicrograph of Facies B3 fetid grainstone. Horizontal fov. 0.95mm. 87m Wadi Hajir.



Plate 6.1e Photomicrograph of Facies C2 'Type A' stromatolite with micrite and spar laminations. Horizontal fov. 2.45mm. 235m Md.

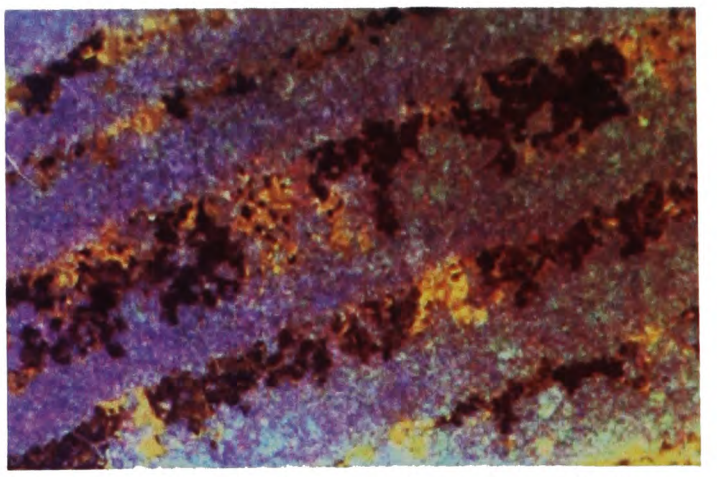


Plate 6.1f Cathodoluminescence photomicrograph of Facies C2 'Type A' stromatolite. Horizontal fov. 2.45mm. 235m Md.

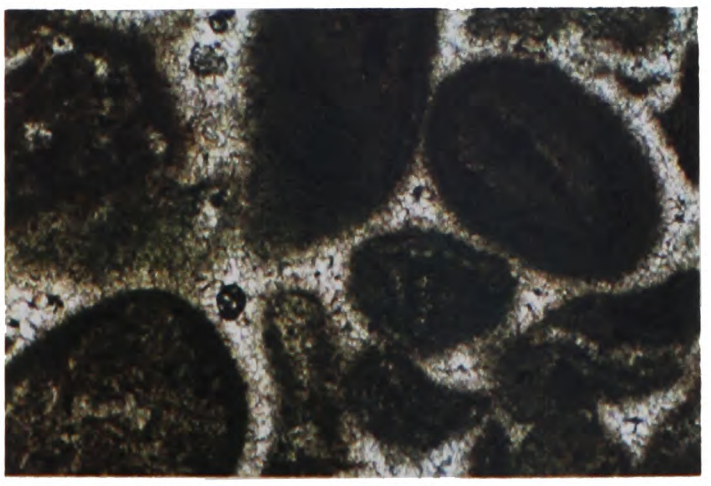


Plate 6.1g Photomicrograph of Facies E1 ooidal-intraclast grainstone. Horizontal fov. 2.45mm. 260m Md.

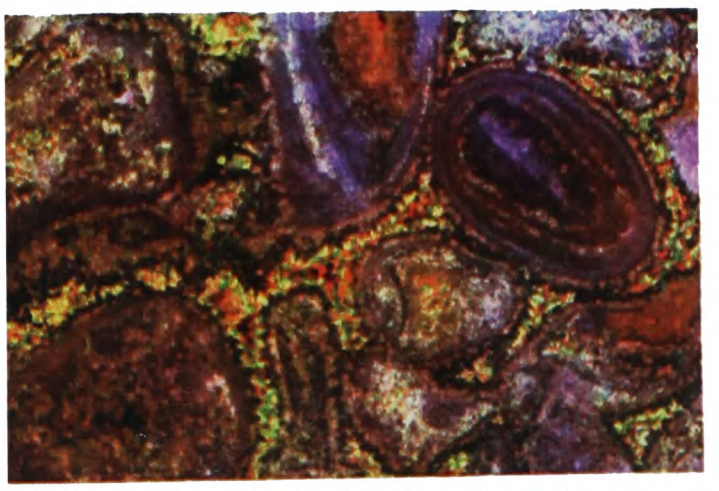


Plate 6.1h Cathodoluminescence photomicrograph of Facies E1 ooidal-intraclast grainstone. Horizontal fov. 2.45mm. 260m Md.

Plate 6.1

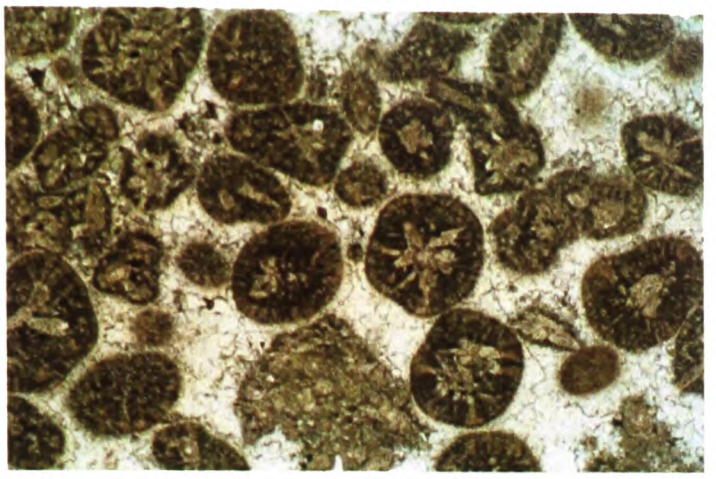


Plate 6.2a Photomicrograph of Facies S4 oosparite with fringe cement and late spar. Horizontal fov. 2.45mm. 220m Wadi Aswad.

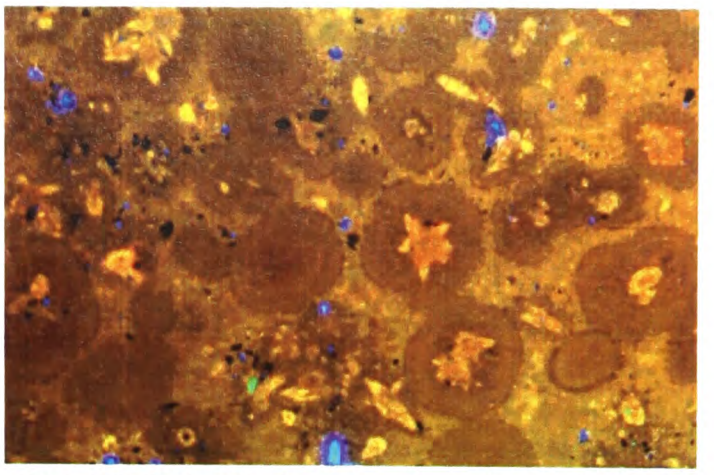


Plate 6.2b Cathodoluminescence photomicrograph of Facies S4 oosparite. Horizontal fov. 2.45mm. 220m Wadi Aswad.

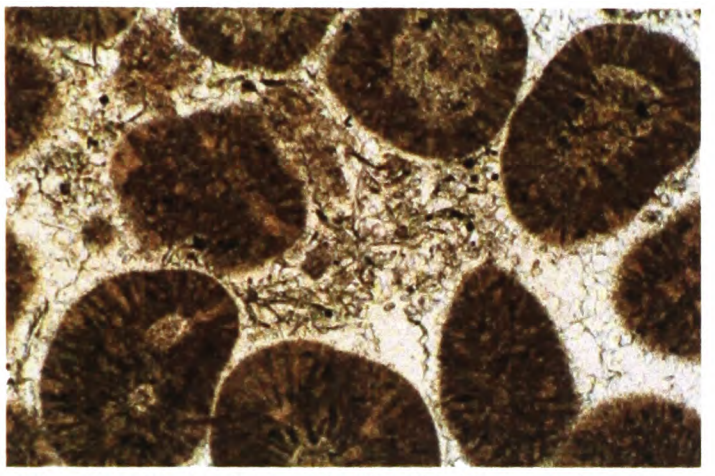


Plate 6.2c Photomicrograph of Facies S4 oosparite with intergranular silt and fitted fabric. Horizontal fov. 2.45mm. Upper Shuram Fm. Sedrah.

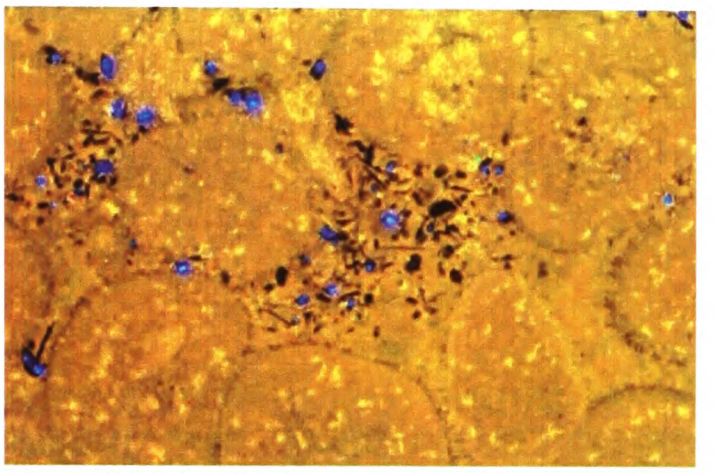


Plate 6.2d Cathodoluminescence photomicrograph of Facies S4 oosparite. Horizontal fov. 2.45mm. Upper Shuram Fm. Sedrah.

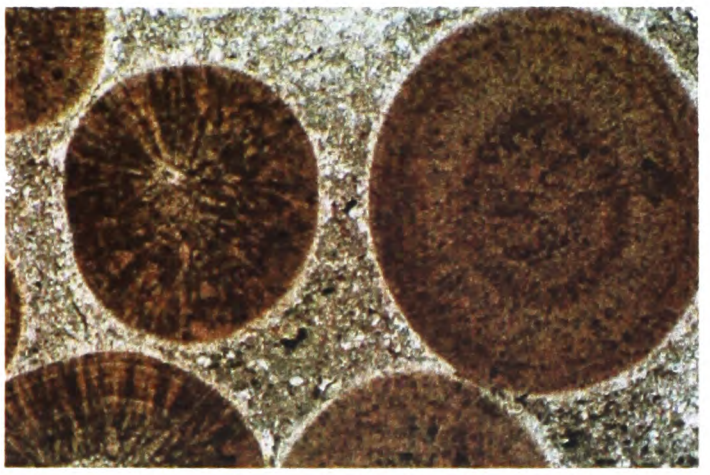


Plate 6.2e Photomicrograph of Facies S4 oosparite with intergranular silt and fringe cement. Horizontal fov. 2.45mm. ppl. 205m Wadi Aswad.

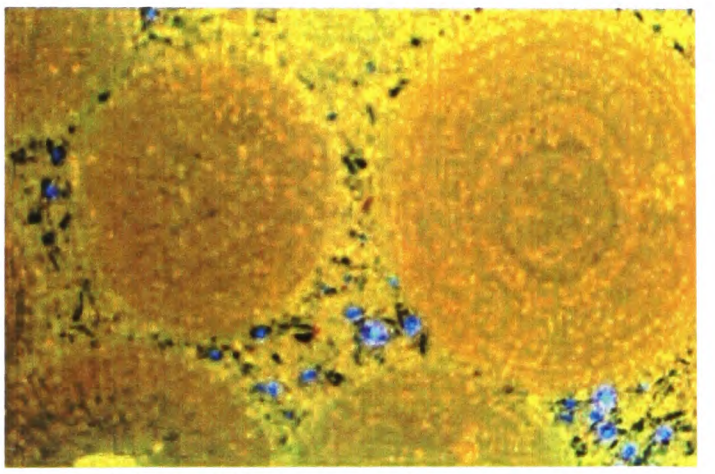


Plate 6.2f Cathodoluminescence photomicrograph of Facies S4 oosparite. Horizontal fov. 2.45mm. ppl. 205m Wadi Aswad.

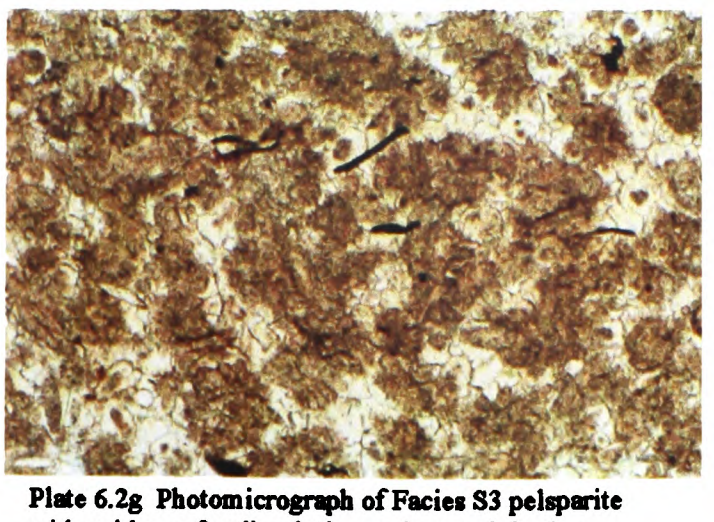


Plate 6.2g Photomicrograph of Facies S3 pelsparite with evidence for dissolution and reprecipitation. Horizontal fov. 2.45mm. ppl. 168m Wadi Shuram.

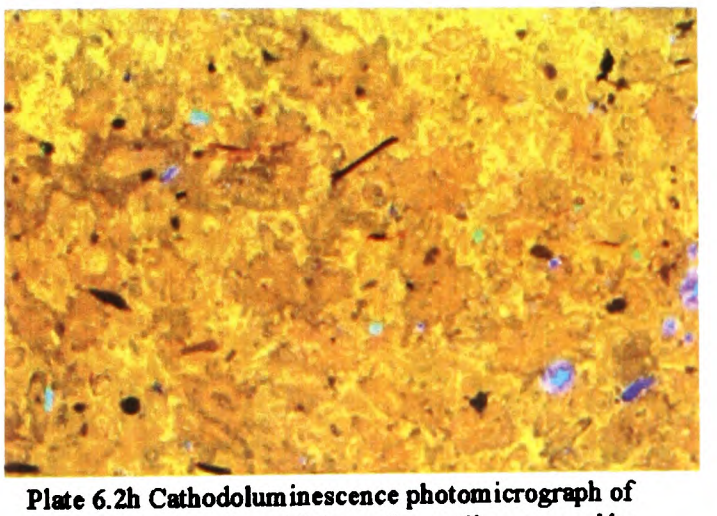


Plate 6.2h Cathodoluminescence photomicrograph of Facies S3 pelsparite with irregular outlines caused by dissolution. Horizontal fov. 2.45mm. 168m Wadi Shuram.

Plate 6.2

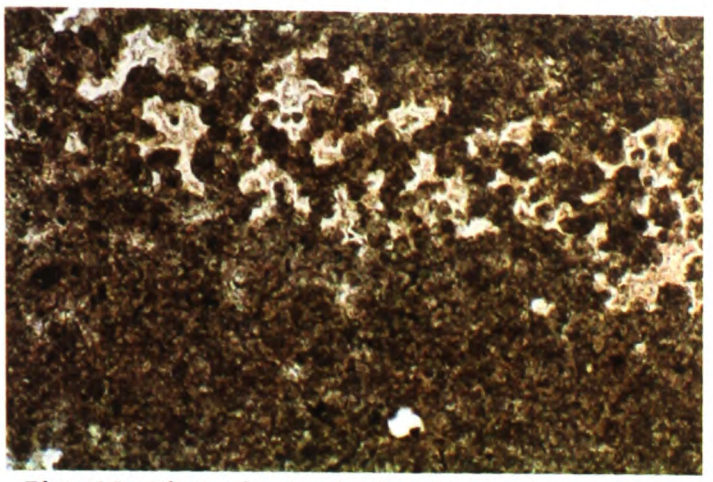


Plate 6.3a Photomicrograph of Facies C2 columnar stromatolites, microspar and spar laminations. Horizontal fov. 0.95mm. ppl. 237.5 Kd.

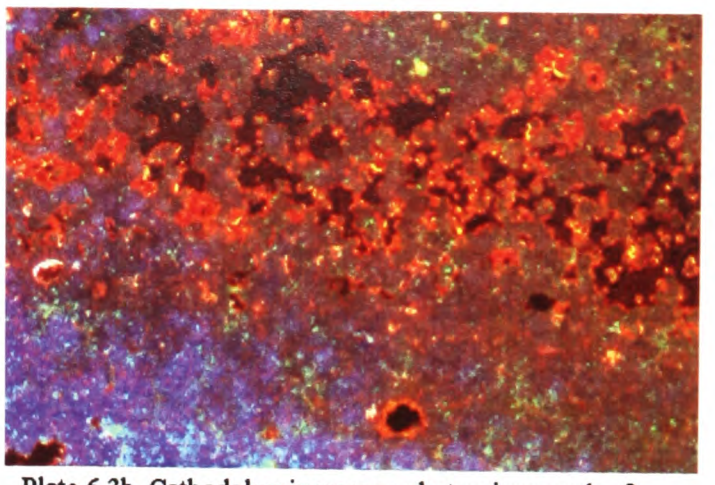


Plate 6.3b Cathodoluminescence photomicrograph of Facies C2 columnar stromatolites, microspar and spar. Horizontal fov. 0.95mm. ppl. 237.5 Kd.



Plate 6.3c Photomicrograph of Facies C3 recrystallized dolospar with relict peloids. Horizontal fov. 0.95mm. ppl. 55m Bd.

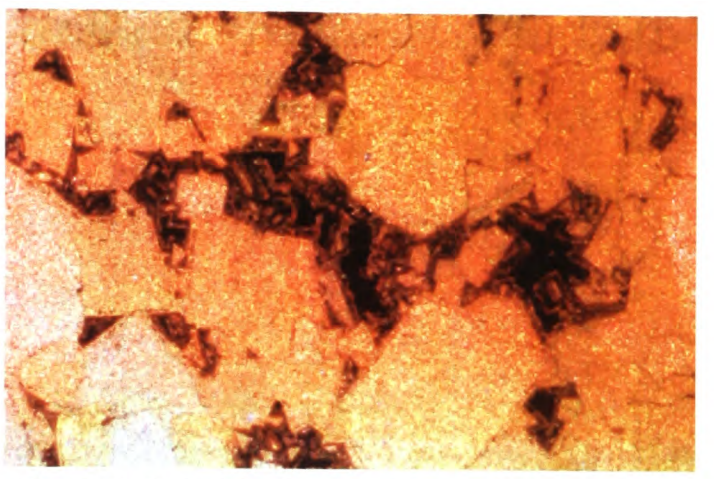


Plate 6.3d Cathodoluminescence photomicrograph of Facies C3 recrystallized dolospar with relict peloids. Horizontal fov. 0.95mm. ppl. 55m Bd.

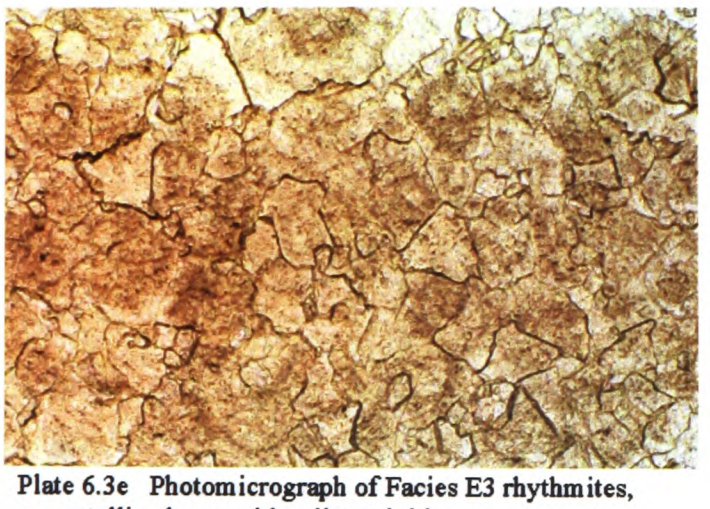


Plate 6.3e Photomicrograph of Facies E3 rhythmites, recrystallized spar with relict peloids. Horizontal fov. 0.95mm. ppl. 112m Wadi Hajir.

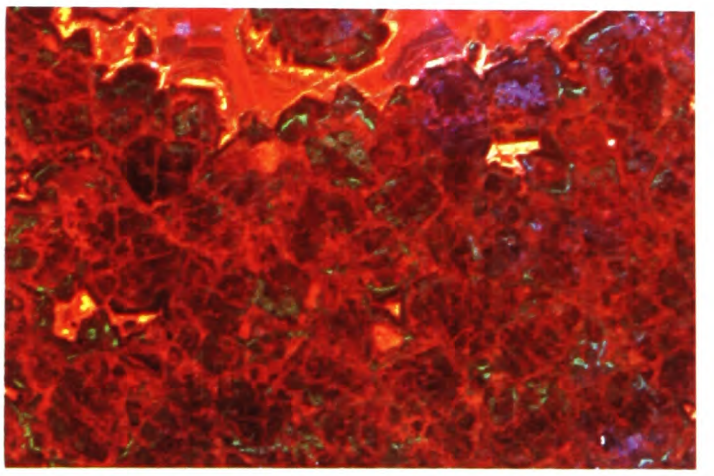


Plate 6.3f Cathodoluminescence photomicrograph of Facies E3 rhythmites, recrystallized spar with relict peloids. Horizontal fov. 0.95mm. 112m Wadi Hajir.



Plate 6.3g Photomicrograph of Facies E1 crinkly laminites formed of calcispar. Horizontal fov. 2.45mm. ppl. 22m Wadi Bani Awf.

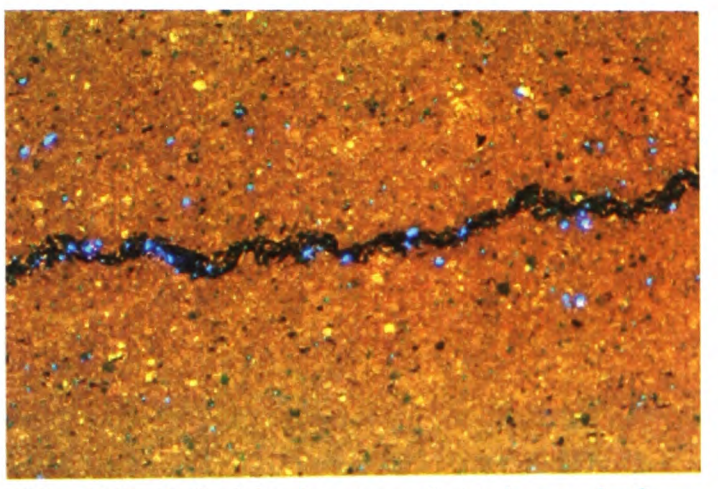


Plate 6.3h Cathodoluminescence photomicrograph of Facies E1 crinkly laminites formed of calcispar. Horizontal fov. 2.45mm. 22m Wadi Bani Awf.

Plate 6.3

Chapter Seven - Discussion

7.1 INTRODUCTION

7.2 CHRONOSTRATIGRAPHIC POSITION

7.3 BASIN SEQUENCE STRATIGRPAHY

7.4 CHEMOSTRATIGRAPHY - BASINAL AND GLOBAL

7.5 BASINAL REVIEW

7.1 INTRODUCTION

An attempt will be made in this chapter to integrate all the data from the previous chapters with a view to identifying major tectono-stratigraphic events within the Nafun Group, leading to a recommended revision of the existing nomenclature for the Huqf Supergroup. These events will be discussed in light of their effect on ocean chemistry, circulation patterns and climate, with consequent changes in organic productivity, carbon burial and the carbon-isotope signature. Finally, an attempt will be made to relate these signatures and events to global events at this time.

7.2 CHRONOSTRATIGRAPHIC POSITION

In order to understand the significance of the carbon isotope signatures and the tectono-stratigraphic relations of the formations we need to consider the chronostratigraphic position of the Nafun Group at this time. Over the past few years the exact position of the Precambrian/Cambrian boundary within the Huqf Supergroup has been the subject of much speculation. Most authors have based their hypothesis on lithological and/or chemostratigraphic correlations (Husseini & Husseini 1990; Rabu 1993: Kimura *et al.* 1997; Brasier *et al.* 1997) and have considered the boundary to be within the Shuram Formation negative carbon isotope excursion. Mattes & Conway Morris (1990) and Conway Morris *et al.* (1990) assigned the boundary to a similar position based on the presence of the 'Cambrian' calcimicrobe *Angulocellularia* in the Ara Group. Kaufman & Knoll (1995), Saylor *et al.* (1998) and Pelechaty (1998) all place the Precambrian-Cambrian boundary within the Ara Group in their global correlations. The new dates defined during the present study help to resolve some of these ambiguities; Figure 7.1 shows a global correlation of the Oman dates and stratigraphy with those recognised globally. This correlation places the whole Nafun Group firmly into the late Neoproterozoic, based on a correlation of the basal Ghadir Manqil Formation diamictites with the Sturtian glaciation in Australia. The Hadash Formation 'cap carbonate' is correlated with that above the Marinoan glaciation, estimated at approximately 590 Ma. The Nafun Group and the base of the Fara Formation fill the stratigraphic interval up to the Neoproterozoic-Cambrian boundary at 543±1 Ma (Bowring *et al.* 1993; Grotzinger *et al.* 1995). This is based on the assumption that there are no major breaks in sedimentation within the Nafun Group or between the Nafun and the Ara groups. This assumption is considered quite reliable as no large unconformities were noted in the field, nor were any recorded from the subsurface.

The suggested placement of the Huqf Supergroup within the global chronostratigraphic framework is shown in Figure 7.1. The carbon-isotope curve from this study and the strontium-isotope curve from Burns *et al.* (1994) have also been plotted on Figure 7.1.

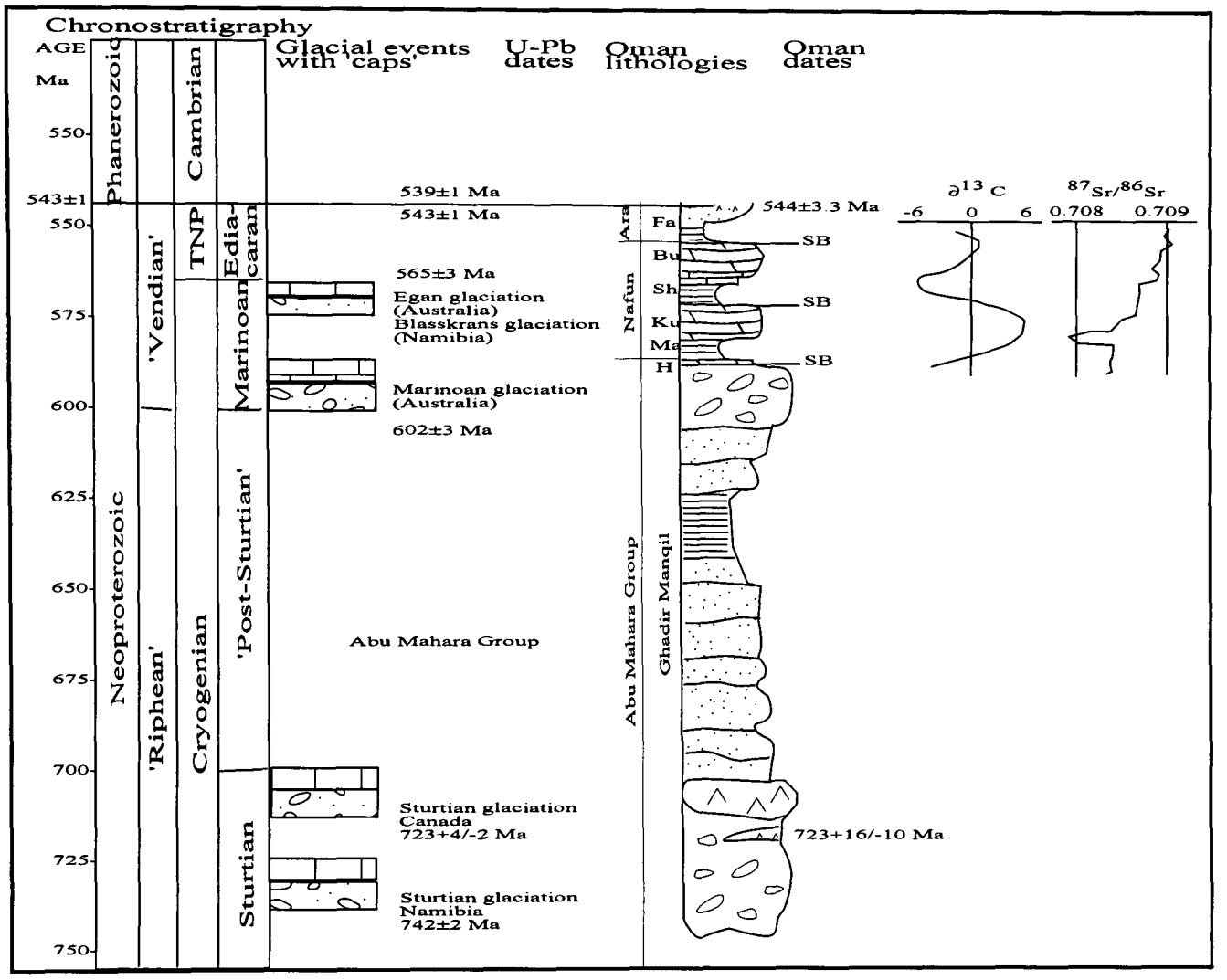


Figure 7.1 The sediments of the Huqf Supergroup fitted within a global chronostratigraphic framework. The new U-Pb dates from this study firmly place the Abu Mahara and Nafun Groups within the Neoproterozoic. Strontium-isotope data is from Burns *et al.* 1994.

7.3 BASIN SEQUENCE STRATIGRAPHY

Depositional sequences are composed of relatively conformable stratigraphic successions, bounded by unconformities or their correlative conformities (Van Wagoner *et al.* 1988; Sarg, 1988). Sequence boundaries are recognised on the basis of regionally extensive surfaces or zones, marked either by: *a)* erosion or valley incision; *b)* an abrupt change in facies; and *c)* a transition from regressive to transgressive facies stacking pattern.

PDO geologists have applied seismo-sequence stratigraphic techniques to the Huqf Supergroup (Borgomano *et al.* 1992, figure 14). In Figure 7.2, the gamma ray log from SMP-1 in Masirah Bay near the Huqf area has been correlated with the Nafun Group and with the carbon- and oxygen-isotope curves described in Chapter 6 from the Huqf area and

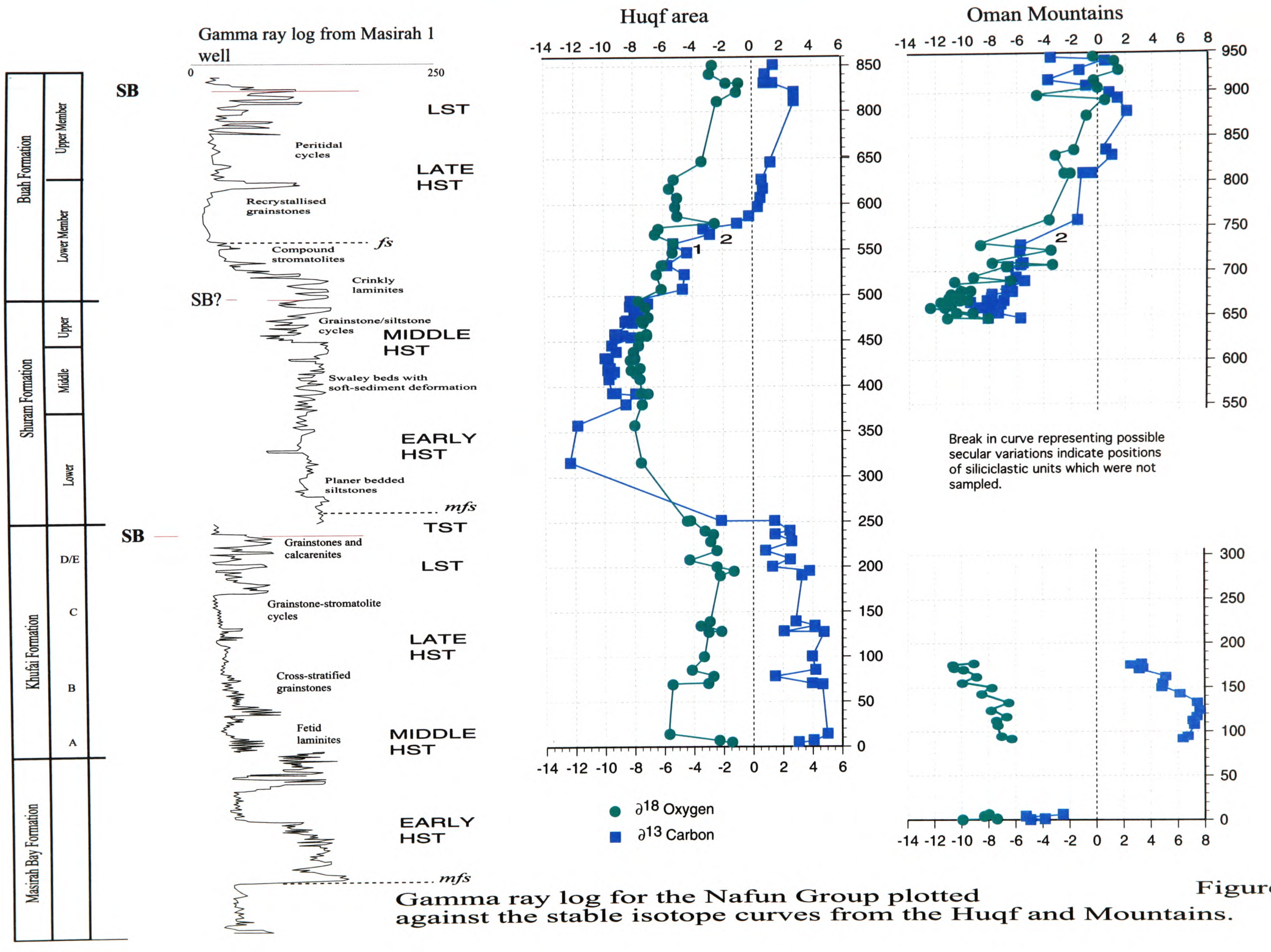


Figure 7.2

Gamma ray log for the Nafun Group plotted against the stable isotope curves from the Huqf and Mountains.

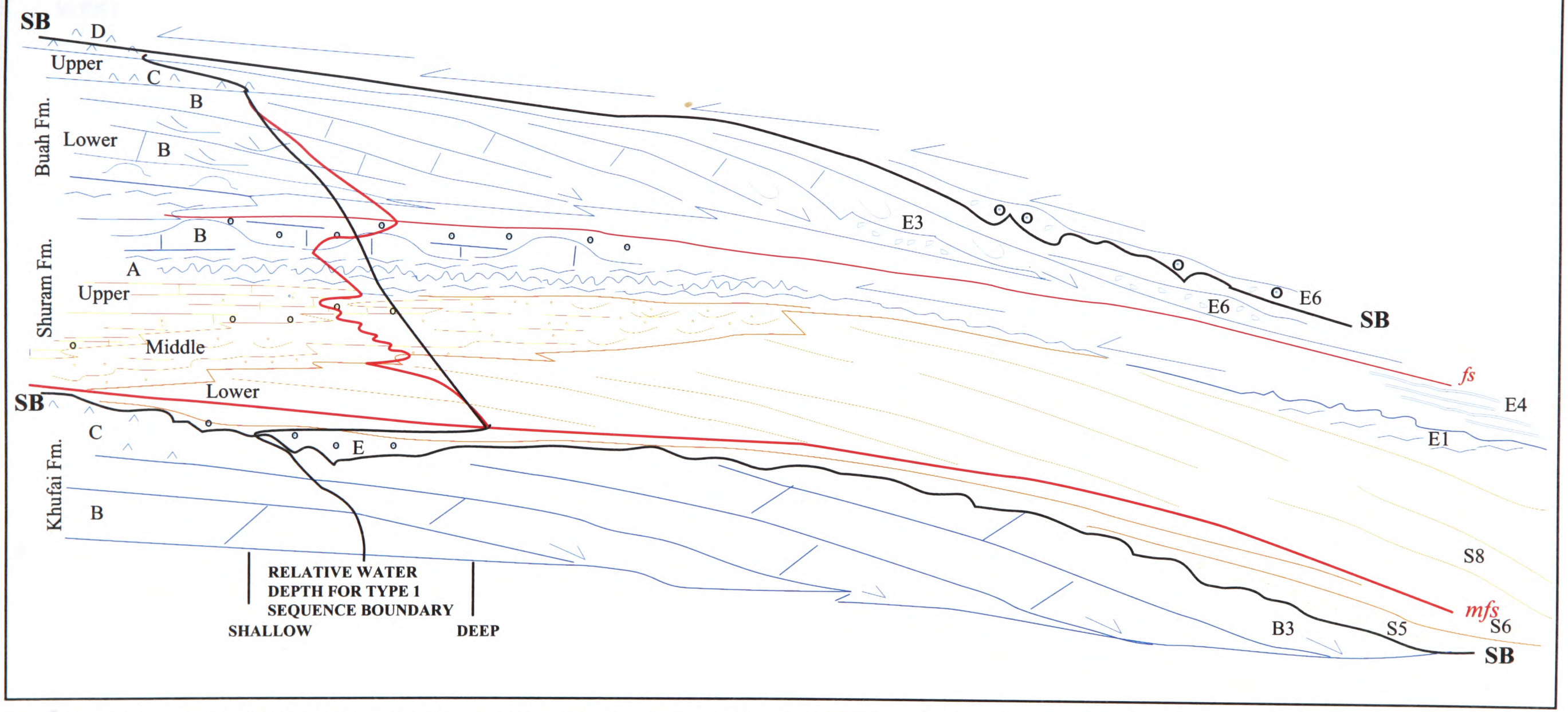


Figure 7.3 Schematic diagram showing sequence stratigraphic interpretation of the Khufai, Shuram and Buah formations in the Huqf area and the Oman Mountains.

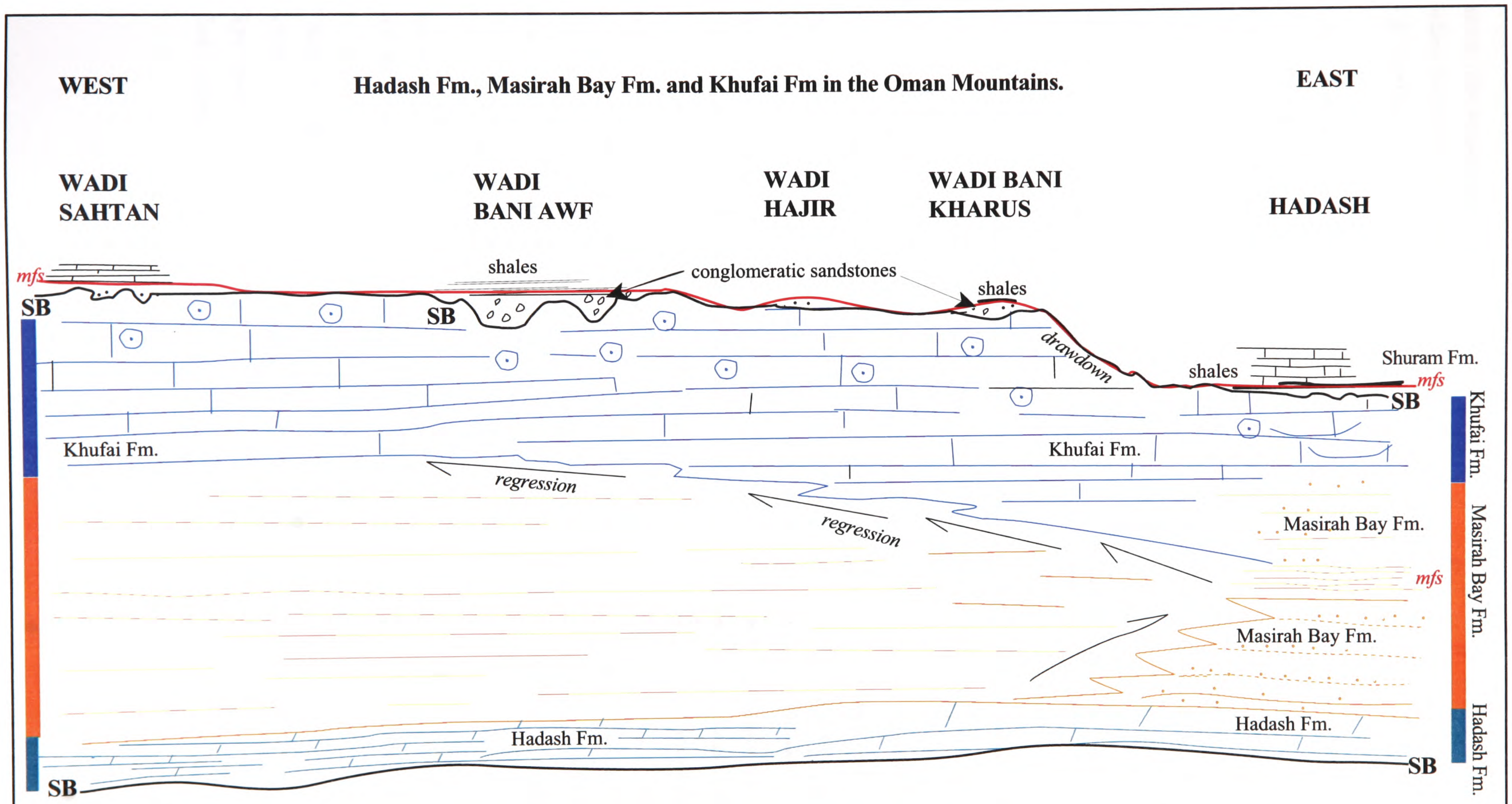


Figure 7.4 Schematic diagram of the sequence stratigraphic interpretation of the Hadash, Masirah Bay and Khufai formations in the Oman Mountains.

Mountains. The sequence-stratigraphic interpretations are based on lithological character of the surface exposures described in Chapters 3, 4 and 5. Due to the formidable terrain and extent of exposure only some of these surfaces have been mapped laterally.

There are two sequence boundaries within the Nafun Group and these are marked on Figure 7.2. The lowermost, is just below the Khufai/Shuram Formation contact while the uppermost marks the contact between the Buah and Fara formations. These interpretations are illustrated diagrammatically in Figure 7.3 showing the more proximal sediments in the Huqf area and the more distal sediment in the Oman Mountains. The lowermost sequence comprises the Masirah Bay and Khufai formations. Dark organic-rich shale beds are observed in the Masirah Bay Formation near Hadash about 30m above the Hadash Formation 'cap carbonate'. The blacks shales are interpreted as *mfs* deposits (Figure 7.4). The upper Masirah Bay Formation and the lower Khufai Formation (Association A) were deposited during the early highstand. The carbonates of the Khufai Formation (lower-blue, Figure 7.3), including Facies Associations B (grainstones and stromatolites) and C (peritidal cycles), comprise part of the middle and late highstand. The peritidal cycles of Association C are locally overlain by thin siliciclastic sandstones of Association D. The uppermost Association E contains cross-stratified ooidal-intraclast grainstones (E1) and locally grainstones with fabrics indicative of evaporite dissolution (E2). The siliciclastics and evaporitic grainstones are taken to indicate an episode of drawdown which is followed by transgression onto the cross-stratified grainstones. In the Oman Mountains, the more distal black, fetid limestones of Association B are overlain by conglomeratic sandstones (S5) which often have scoured contacts with the underlying limestones and contain limestone clasts. These conglomerates sandstones are considered part of the transgressive phase of the following sequence. A large negative peak in the carbon- and oxygen-isotope curves marks the Khufai/Shuram Formation contact. However a gradual shift to more negative values in the carbon-isotope signature occurs just below the contact in the Huqf area and the Oman Mountains suggesting that transgression began in the latest Khufai Formation times.

The second sequence is formed of the Shuram and Buah formations. Although the contact between the two sequences can only be observed at one locality in the Huqf area, this contact is easily observed at numerous localities in the Oman Mountains (Figure 7.4). In Wadi Bani Awf and Wadi Bani Kharus, the basal conglomeratic sandstones of the Shuram Formation are locally overlain by black, shaly carbonates that are considered to represent a *mfs*. The planar-bedded siltstones of the lower Shuram Formation and the swaley cross-stratified, storm-dominated siltstones of the middle Shuram Formation represent early

highstand deposition. The prograding carbonate beds of the upper Shuram Formation and the basal limestones (facies A1, B1 and B2) of the lower Buah Formation probably represent middle highstand deposition. The upper Buah Formation peritidal cycles (Association C) and sabkha (Association D) deposits represent late highstand to lowstand deposition. The sequence boundary is taken to occur in the uppermost sabkha horizon in the Mukhaibah dome section in the Huqf area whilst in the Oman Mountains it is considered to occur with the first influx of volcaniclastics beneath a cherty, breccia horizon (Figure 7.3).

Superimposed on these 400-500m thick sequences are smaller <20m thick parasequences. These include the siliciclastic/carbonate cycles of the middle and upper Shuram Formation. Within Association B of the lower Buah Formation, there is an influx of siliciclastic sediments throughout the Huqf area and also at a stratigraphically equivalent level in Wadi Bani Awf, where shaley organic-rich carbonates are found. Together, these suggest a significant flooding event. The end of this event is marked by a change in mineralogy from limestone to dolostone and is characterised by a positive shift in carbon isotopes.

Although these geochemical perturbations may partly result from the change in mineralogy, they most likely also reflect changes in shoreline or sea level at this time.

7.3.1 Recommended revision of nomenclature

In light of the sequence stratigraphic interpretations above and the data of the previous chapters, it is considered that the present subdivisions of the Huqf Supergroup do not reflect the formational relationships observed (Figure 7.5). It is, therefore, recommended that the sequence boundary at the base of the Hadash Formation should mark the top of the Abu Mahara Group. The members identified in the Ghadir Manqil Formation by Rabu *et al.* (1986) would then become formations. The Nafun Group would consist of two siliciclastic/carbonate cycles. The basal cycle comprising the Hadash Formation overlain by the Masirah Bay Formation with the late highstand Khufai Formation. A sequence boundary separates this cycle from the following cycle comprising the Shuram and Buah formations. The Nafun Group is separated from the overlying Ara Group by a sequence boundary at the top of the Buah Formation.

7.4 CHEMOSTRATIGRAPHY - BASINAL AND GLOBAL

7.4.1 Khufai, Shuram and Buah Formation mineralogy

This study has highlighted the fact that the mineralogy of the ooid grains changes throughout the Nafun Group formations. The dolomitized grainstones of Khufai and Buah formations are considered to have formed of an aragonitic precursor whereas the Shuram Formation ooid grainstones retain a primary calcitic mineralogy.

Under most near-surface temperatures, pressures, and water compositions, aragonite is thermodynamically less stable than its polymorph calcite (Carlson 1980). Aragonite is more soluble that pure calcite because it is a more disordered polymorph (Bathurst 1980). Therefore, aragonite should dissolve and calcite should precipitate. Determination of original, ancient ooid fabric and mineralogy has been based in large part upon the relationship of mineralogy and microstructure preservation in biogenic components (Sandberg 1975). Diagenesis of aragonite bioclasts and ooids has generally been interpreted to result in the destruction of fine fabrics, whereas calcitic ooids should retain detailed microstructures with diagenesis (Sandberg 1975; Tucker 1985). The precursor mineralogy of these two polymorphs is generally recognised by petrographic and geochemical techniques.

Despite the fact that no relict aragonite has been found in the Buah and Khufai Formation ooids they are considered to have an aragonite precursor because:

a) their pervasive recrystallization (Plate 3.5b; 5.8f) (Sandberg 1975; Tucker 1985)

b) evidence for oomoldic porosity indicates wholesale dissolution (Plate 5.8d)

c) there is only one preservation mode within the ooid which would suggest a mono-mineralic origin

d) the calcite replacement of some of the ooids retain a brick-like texture (Plate 5.10a) which is considered to indicate precursor aragonite (Tucker 1984).

On the other hand the Shuram Formation ooids are considered to have had an original low Mg-calcite precursor because:

a) the excellent preservation of fabrics (Plates 4.3d/f)

b) the absence of oomoulds and deformed radial ooids indicates little wholesale dissolution

c) syntaxial calcite cement forms on the ooids. This type of cement has been shown to precipitate on calcitic particles during early meteoric diagenesis (Land 1986).

Geochemistry is often used by workers to augment their petrographical interpretations. As Sr^{2+} is enriched by 9000 ppm in aragonite relative to co-precipitated calcite (Kinsman 1969; Heydari & Moore 1994), Sr contents should be a good indication of precursor mineralogy. The Shuram Formation ooids retain a greater mean Sr content than the Khufai or Buah Formation ooids (Table 6.1). However, this may result from diagenesis which results in a decrease in Sr^{2+}, Mg^{2+} and $\delta^{18}O$ contents and increased Fe^{2+} and Mn^{2+} values of unstable carbonates (aragonite and high Mg-calcite) (Brand & Veizer 1980). Elemental modelling (Chapter 6) suggests that the Shuram Formation and the lowermost Buah Formation have suffered the greatest diagenetic alteration.

Environmental significance

The fact the Khufai and Buah Formation ooids were formed in arid conditions whereas the Shuram Formation ooids were formed in humid conditions might suggest the mineralogical change through the Nafun Group has been strongly controlled by environmental conditions. Cyclic changes in ooid mineralogy during the Phanerozoic are attributed to variations in the Mg^{2+}/Ca^{2+} ratio and pCO_2 compositions of seawater (Sandberg 1983). Palaeoceanographic conditions that modified salinity, Ca^{2+}, dissolved CO_2, CO_3^{2-}, and Mg^{2+}/Ca^{2+} ratio of seawater are considered to have caused precipitation of aragonite ooids during greenhouse conditions in the Smackover Formation (Wilkinson *et al.* 1984). These same authors considered calcitic ooids of the Pennsylvanian Plattsburg Formation to have formed during icehouse episodes. Tucker (1985) has similar conclusions for Precambrian occurrences of aragonitic and calcitic ooids.

A dry climate and evaporative conditions recorded in the Khufai Formation and Buah Formation times could have produced a negative water balance in the basin. This would affect an increased salinity resulting in modification of the physical and chemical characteristics of the seawater in several ways (Garrels & Christ 1965; Morse & Mackenzie 1990). During seawater evaporation, Ca^{2+}, pH, alkalinity and CO_3^{2-} increase up to a salinity of 90‰. Heydari & Moore (1994) suggest this should result in a progressive increase in carbonate saturation state and these conditions would favour the precipitation of aragonite over calcite. This hypersaline restricted intertidal environment would also have facilitated early dolomitization (Folk & Land 1975).

The Shuram Formation ooids however were formed during times of immense oceanic turbulence and possibly very humid conditions. Such invigorated palaeoceanographic

circulation patterns might have affected salinity sufficiently to result in undersaturation in respect to aragonite.

7.4.2 CHEMOSTRATIGRAPHIC SIGNATURE

Within each formation there does not appear to be a significant difference in the carbon-isotope signature across the basin. While the more distal deposits have slightly more positive values in the Khufai Formation (possibly reflecting diagenesis), the proximal to distal signatures of the Shuram and Buah formations remain similar. The excursions recorded are considered to represent genuine changes in net primary productivity and carbon burial rates through time. Although the two sequences of the Nafun Group are lithologically quite similar, their carbon-isotope signatures are very different. The basal siliciclastic Masirah Bay Formation was not sampled because of the lack of carbonates.

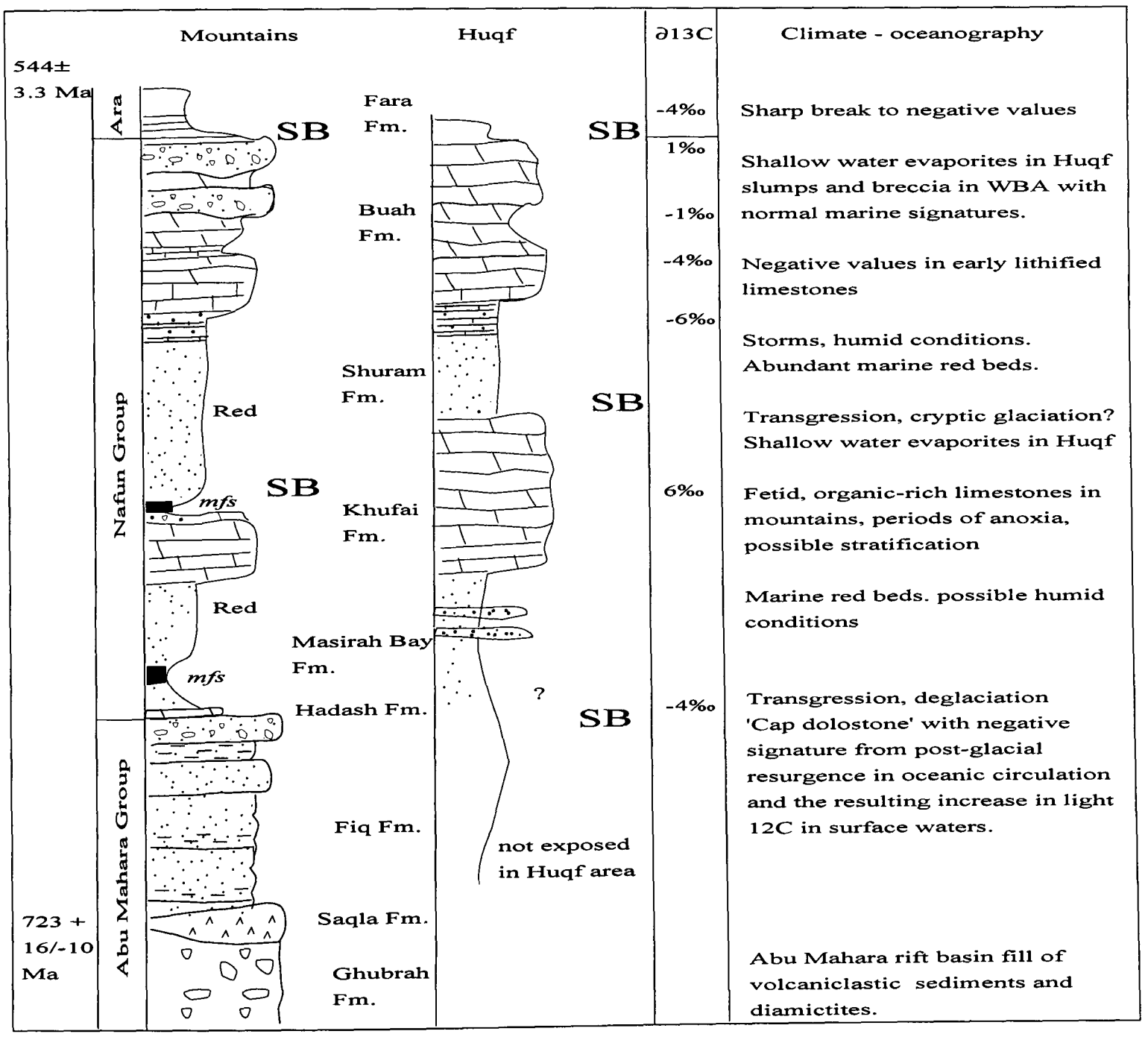


Figure 7.5 Summary log of the Huqf Supergroup with climatic and environmental interpretations as well as the new recommendations for the Huqf Supergroup nomenclature.

Hadash Formation

This 'cap carbonate' (Figure 7.5) represents the initial transgression at the onset of deglaciation, an event considered equivalent to the Marinoan deglaciation in Australia (Figure 7.1). This carbonate records a negative carbon-isotope signature (-4‰). Similar negative values are recorded from other 'cap carbonates' around the world and have been explained by oceanic overturn that occurred during deglaciation (Kaufman *et al.* 1991, 1997; Kaufman & Knoll 1995; Grotzinger & Knoll 1995) or by transgression induced upwelling (Kennedy 1996; Kennedy *et al.* 1998).

Masirah Bay Formation

The Masirah Bay Formation in the Huqf area is composed of shallow-marine high-energy tidal trough cross-bedded sandstones overlain by moderate to low-energy marine fine sandstones. In the Oman Mountains, the Masirah Bay Formation is composed of planar-bedded fine-sandstones indicative of low-energy marine deposits. The black-shale interbeds exposed near Hadash village are considered representative of the *mfs*. The more proximal deposits of the Huqf area are storm-dominated (Leather 1998). The red, iron-rich nature of these sediments may have resulted from invigorated thermohaline circulation after glacial stagnation which would result in upwelling of ferrous ions into surface waters where they could precipitate as ferric oxides and hydroxides along the chemocline (Kaufman *et al.* 1991).

Khufai Formation

Masirah Bay facies grade-upward into basal Khufai Formation dolostones. These are fetid and laminated with some evidence for slumping, suggestive of deeper environments that were periodically oxygen-depleted. The upper Khufai Formation carbonates are intertidal and evaporitic, indicating arid climatic conditions.

The Khufai Formation retains a positive carbon-isotope signature with values up to 5‰ in the Huqf area and up to 8‰ in the Oman Mountains. Such heavy values have elsewhere been explained by prolific production and burial of organic carbon which would result in the enrichment of seawater with heavy ^{13}C. This process would be enhanced by oceanic stratification and anoxia.

Post-glacial warming could account for this increased organic productivity and the precipitation of aragonite precursor carbonates of the Khufai Formation dolostones. Photosynthetic activity can also induce precipitation whereby disequilibrium is caused by the

photosynthetic extraction of CO_2 from surface waters. Much fine-grained carbonate is precipitated in this manner (Tucker 1986b).

Shuram Formation

The influx of Shuram Formation siliciclastics drowned the carbonate ramp, an event correlated chronostratigraphically with the Australian Egan glaciation (Grey & Corkeron 1980) and with post-Blässhrans glacial sediments in Namibia (Saylor *et al.* 1998; figure 6) (Figure 7.1). There is, however, no evidence for glacial deposits within the Shuram Formation sediments. The lower Shuram Formation consists of planar bedded fine sandstones and siltstones whilst the middle Shuram Formation records an increase in storm sedimentation. The stormy character of these sediments suggests greater wind strengths at this time which may indicate greater latitudinal temperature gradients.

The Shuram Formation carbonates are dominantly peloidal and ooidal grainstones with very well-preserved textures suggestive of an original calcitic mineralogy, whereas the Khufai and Buah Formation grainstones textures suggest an original aragonite mineralogy. As mentioned in the previous section, aragonite precipitation is considered to occur within warm saline waters whilst calcite appears to precipitate when the waters are colder and fresher (Hsü & Kelts 1978). Fresher conditions would have prevailed during glacial events.

As in figure 7.1, Saylor *et al.* (1998) and Grey & Corkeron (1980) suggests it is quite probable that the Shuram Formation is the stratigraphic equivalent to post-glacial sediments in Namibia and Australia. It may be tempting to explain the very negative Shuram Formation carbon-isotope signature in a similar manner to that of the Hadash Formation. Negative carbon-isotope excursions related to overturn would be short-lived, limited by the residence time for carbon in the ocean which is estimated at 10^5 years (Kump 1991). The use of this ocean overturn hypothesis for the Shuram Formation, where the negative excursion spans up to 500m of sediments is, therefore, inadequate.

The very negative (-5‰ corrected value) signature of the Shuram Formation would, on first principles, suggest a total shutdown of organic productivity and burial thus allowing surface waters to remain enriched in ^{12}C. Only if productivity ceased for hundreds of thousands of years would $\delta^{13}C$ approach the ocean input value of -5‰ (Kump 1991). The stormy character of the sediments along with their red colour would suggest the depositional environments were kept well oxidised, which would ensure the oxidative recycling of organic matter. Although turbid waters and oxidation has already been suggested as a possible cause of

the light Shuram Formation signature, this hypothesis cannot be extrapolated to explain the continued negative signature in the basal carbonates of lower Buah Formation. Also, this present study has shown that organic-rich shales were deposited at the base of the Shuram Formation in the Oman Mountains and PDO sources maintain that the Shuram Formation is a source of Oman's petroleum. The light carbon-isotope signature might be explained by the incorporation of ^{12}C produced by the bacterial decay of organic matter. Apart from the organic-rich beds at the very base of the formation, there is no great evidence for the presence of organic matter within the middle and upper Shuram Formation.

Thus, the causes of the Shuram Formation negative excursion remain enigmatic but it most likely results from a combination of factors, that might well be specific to this late Neoproterozoic era.

Buah Formation

The Buah Formation Association A limestones, crinkly laminites and edgewise flake-breccias record similar isotopic values to the upper Shuram Formation. There is a small 2‰ positive kick into the overlying stromatolites but a negative shift back into the silty peloidal wackestones then a positive shift to -1‰ for the overlying dolomitic grainstones. These dolostones and the dolostones of the upper Buah Formation in the Huqf area and the Oman Mountains record values close to those of normal marine conditions. Therefore, it is most likely that whatever processes (diminished organic productivity and burial or oceanic overturn) created the Shuram Formation signature, these were still ongoing, up to the flooding surface marked on (Figure 7.3) in the lower Buah Formation. Overlying this surface dolomitization became ubiquitous and the carbon-isotope signatures indicate normal shallow marine conditions prevailed.

7.4.3 Global correlation

The chemostratrigraphic framework of the Neoproterozoic-Cambrian is now emerging from studies of carbon and strontium isotopes preserved in abundant carbonate rocks of platform environments (Derry *et al.* 1989; Kaufman & Knoll 1995; Brasier *et al,* 1996; Saylor *et al.* 1998; Brasier *et al.* 1998). Globally proven temporal fluctuations in $\delta^{13}C$ are thought to reflect global changes in photosynthesis and/or organic carbon burial (Kaufman & Knoll 1995).

Negative $\delta^{13}C$ values span and follow all late Precambrian glacial pulses (Figures 7.1 & 7.6) with values down to -5‰ in 'cap carbonates' (Kaufman & Knoll 1995; Kennedy *et al.* 1998).

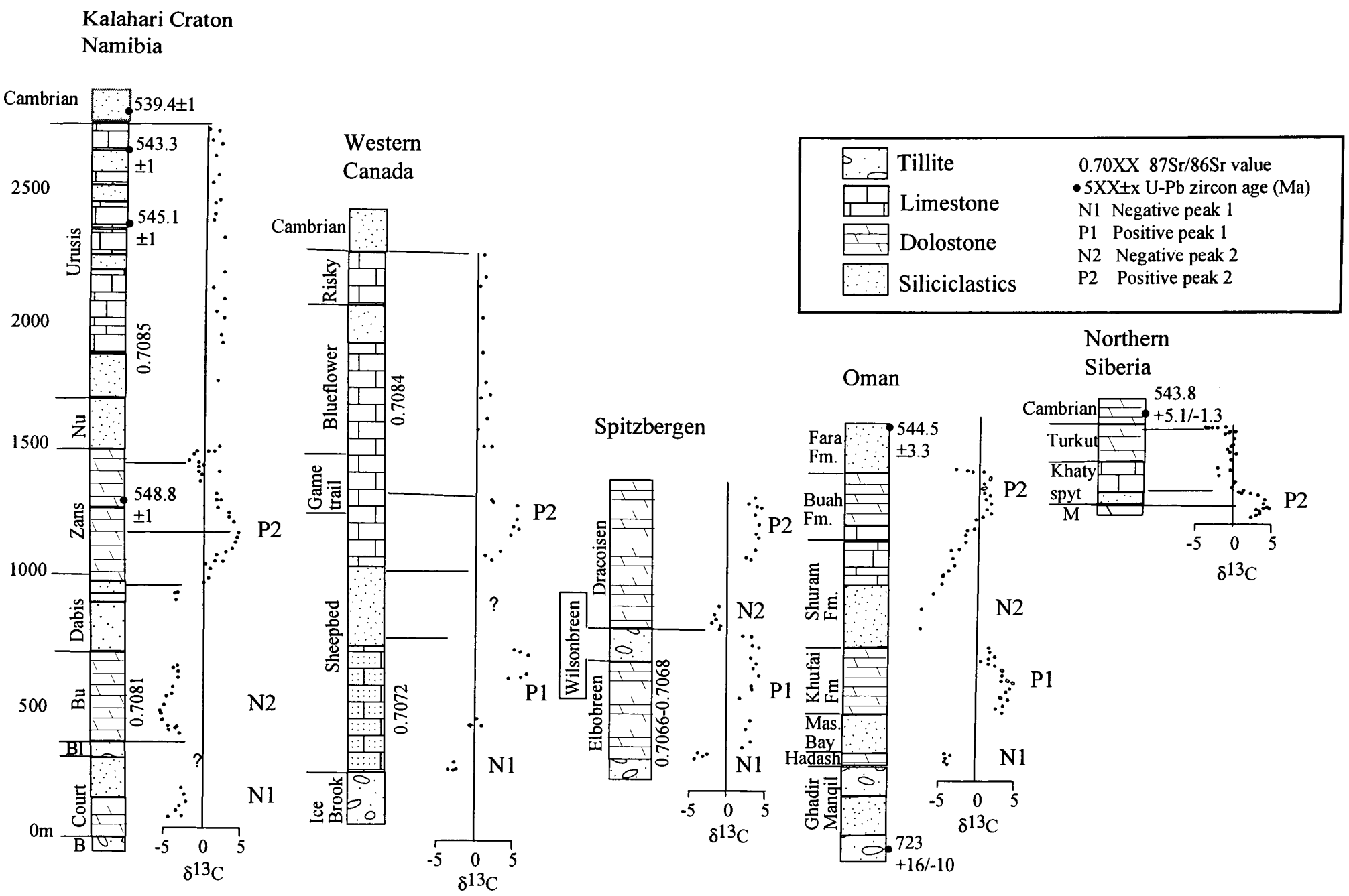


Figure 7.6 Stratigraphic columns (modified from Saylor *et al.* 1998) showing carbon-isotope excursions, the most reliable limestone Sr-isotope values and glacial horizons in the Oman reference section and other correlative sections. All sections are drawn to the same scale as the Namibian section. Sources of data: Namibia-Saylor *et al.* (1998), Western Canada-Narbonne *et al.* (1994); Spitsbergen-Fairchild and Spiro (1987); Oman-present study; and Siberia- Knoll *et al.* (1995).

These cap carbonates are typically found immediately above glaciogenic sequences and are characteristically thin (<15m) (Kennedy 1996; Prave 1999). The intimate association of deglaciation with cap carbonates characterised by low $\delta^{13}C$ values has been explained by the rapid turnover of poorly ventilated deep oceans (where organic matter was mineralised via sulphate reduction to CO_2 and HCO^-_3), possibly driven by glacial invigoration of deep circulation. This would have brought isotopically light dissolved inorganic carbon to the surface with abundant CO_2 degassing into the atmosphere and melting of ice sheets, while excess HCO^-_3 in surface oceans resulted in rapid precipitation of cap carbonates depleted in ^{13}C (Knoll *et al.* 1986; Grotzinger & Knoll 1995). Massive release of methane from continental shelf and slope sediments provides a possible alternative for achieving simultaneous greenhouse warming, increased HCO^-_3 and ^{12}C enrichment of surface ocean waters (Dickins *et al.* 1995). Mechanisms of strong $\delta^{13}C$ depletion whether they involve oceanic overturn or mass mortality of primary producers would likely operate on a short time scale (Kump 1991). Therefore the persistence of low carbon-isotope values through large stratigraphic thicknesses (<600m Saylor *et al.* 1998) must reflect high rates of sediment accumulation.

The Hadash Formation negative $\delta^{13}C$ (N1; Figure 7.6) signature has been correlated with carbonates that transgress glacial deposits in Namibia, Western Canada and the older Varanger glacial horizon in Spitzbergen. These have all yielded negative $\delta^{13}C$ values and low Sr^{87}/Sr^{86} (0.7072) values. This correlation is strengthened by the new zircon age dates from this study, suggesting a Sturtian age for the lowermost glacial unit in the Ghadir Manqil Formation (Chapter 2) and supported by the observation that the Hadash Formation is similar to supposedly Marinoan cap carbonates from Australia described by Kennedy *et al.* (1998) and from California by Prave (1999).

The positive excursion of the Khufai Formation (P1; Figure 7.6) is correlated with the Sheepbed Formation of Canada, the Elbobreen Formation in Spitzbergen and possibly the uppermost Court Formation of Namibia. These strata all record similar positive $\delta^{13}C$ values and have Sr^{87}/Sr^{86} values in the range of 0.7066-0.7072.

The sharp negative $\delta^{13}C$ excursion at the base of the Shuram Formation is correlated with an excursion of similar magnitude in the Namibian Buschmannsklippe Formation which overlies that Blässkrans glacial unit. Similarly, in Spitsbergen the negative signature recorded in the Dracoisen Formation overlies the Wilsonbreen tillite. These latter horizons record Sr^{87}/Sr^{86}

values in the region of 0.7081 whereas the Shuram Formation limestones record values between 0.708557 and 0.708788 (Brasier 1999). A slow progression towards more positive values in the Shuram Formation is mirrored in the other sections.

The Buah Formation becomes more positive upwards with $\delta^{13}C$ values of 2'‰ in the upper Buah Formation. Positive excursions of slightly greater magnitude occur in Namibia, Spitsbergen and Northern Siberia. Values return to around zero in the uppermost Buah Formation with negative values in the lower Fara Formation in the Oman Mountains. Globally the signature remains positive but close to zero until the negative excursion recorded at the Neoproterozoic-Cambrian boundary. This negative interval has been dated at no older than 543.3±1 Ma and no younger than 543.8+5.1/-1.3 Ma (Grotzinger *et al.* 1995). This and the new dates from this study place the Neoproterozoic-Cambrian boundary close to the middle Fara Formation.

The Sr^{87}/Sr^{86} values from Oman are significantly higher that that recorded elsewhere at the same stratigraphic level. This might suggest that the Oman signature is younger that the correlation suggested here. However, correlation based on this approach results in unmatched and more complex carbon-isotope patterns. It is possible the highly sensitive Sr system was reset during dolomitization but, although the values are higher, the trend is consistent with other terminal Neoproterozoic sections.

7.5 Basinal Review

The Ghadir Manqil Formation was deposited in a NE-SW trending rift basin developed in eastern Oman whose existence is poorly recognisable on seismic but is confirmed by subtracting the top-Middle-Huqf depth-map from the top-magnetic-basement depth-map (Bell 1993; Marle van *et al.* 1994; Looseveld *et al.* 1996). A series of N-S to NE-SW trending basement highs may have developed separating different basement segments with associated volcanic activity (Ghubrah Member). This was followed by thermal subsidence allowing the deposition of siltstones and carbonates of the Masirah Bay Formation and the Nafun Group. These latter formations The lack of volcanics and coarse-grained clastics within these formations implies tectonic quiescence through most of their deposition at least until the upper Buah Formation and lower Fara Formation times. Volcanism and large breccia units close to the Buah/Fara contact would suggest a reactivation of the Abu Mahara rift configuration which probably resulted in the formation of the salt-basins.

The Huqf area of east-central Oman remained on a high throughout most of its history and was never subjected to major orogenic movements. No angular unconformities were observed and the fine-grained nature of the Shuram Formation siliciclastics would preclude the existence of high relief in the area. Deposition in the Huqf area represents sedimentation in the basin marginal area which was subjected to minor fluctuations in relative sea-level. As the shallow-marine sediments of the Huqf area are separated from the deeper-water deposits of the Oman Mountains by 350km, it is difficult to reconstruct the palaeogeographic dynamic.

The lack of evidence for any slope redeposition in the Khufai Formation suggests a gentle slope from shoreline to low-energy deeper water (Figure 3.3). Such homoclinal ramps occur when subsidence rates are slow (Markello & Read 1981). The fact that the Shuram Formation is twice as thick in the Oman Mountains as in the Huqf area suggests that greater subsidence occurred towards the basin interior. Carbonate sedimentation kept pace with subsidence during Buah Formation times to produce a shallow carbonate platform that possibly stretched from the Oman Mountains the Huqf area into (Figure 5.1). Large scale slope failure led to the formation of breccia units in the middle Buah Formation in Wadi Bani Awf. Toward the top of the Buah Formation in the Oman Mountains the occurrence of breccias is probably tectonically driven as they grade-upwards into the volcaniclastic Fara Formation.

Adams, A.E., MacKenzie, W.S. & Guilford, C. 1984. *Atlas of sedimentary rocks under the microscope,* Longman Scientific & Technical, England.

Aitken, J.D. 1967. Classification and environmental significance of cyptalgal limestones and dolomites, with illustrations from the Cambrian and Ordovician of southwestern Alberta. *Journal of Sedimentary Petrology,* **37 (4)**, 1163-1178.

Allen, J.R.L. 1968. *Current ripples.* Amsterdam, Netherlands.

Allen, J.R.L. 1970. Physical processes in sedimentation. *In:* Sutton, J & Watson, J.V. (eds.) *Earth Science Series 1*, Allen & Unwin. 248pp.

Allen, J.R.L. 1984. Sedimentary structures: their character and physical basis. *Developments in Sedimentology*, Elsevier Press.

Allen, P.A. & Underhill, J.R. 1989. Swaley cross-stratification produced by unidirectional flows, Bencliff Gritt, (Upper Jurassic), Dorset, UK. *Journal of the Geological Society, London,* **146**, 241-252.

Allen, P.A. & Allen, J.R. 1990. *Basin Analysis: Principles and Applications.* Blackwell Scientific Publications, Oxford. 451pp.

Anderson, T.F. & Arthur, M.A. 1983. Stable isotopes of oxygen and carbon and their application to sedimentologic and palaeoenvironmental problems. In: Arthur, M.A. & Anderson, T.F. (eds.) *Stable isotopes in sedimentary geology,* 1-151.

Arnott, R.W.C. 1992. Ripple cross-stratification in swaley cross-stratified sandstones of the Chungo Member, Mount Yamnuska, Alberta. *Canadian Journal of Earth Sciences.* **29**, 1802-1805.

Asserto, R.L.A. & Kendall, C.G.St.C. 1977. Nature, origin and classification of peritidal tepee structures and related breccias. *Sedimentology*, **24**, 153-210.

Bathurst, R.G.C. 1975. *Carbonate sediments and their diagenesis.* Elsevier, Amsterdam. 658pp.

Bell, A. 1993. The Stratigraphy of the Abu Mahara Group. *PDO Exploration Report* **324,** 12pp.

Benus, A.P. 1988. Sedimentological context of a deep-water Ediacaran fauna (Mistaken Point Formation, Avalon Zone, eastern Newfoundland). *Bulletin of the New York State Museum,* **463**, 8-9.

Berner, R.A. 1981. A new geochemical classification of sedimentary environments. *Journal of Sedimentary Petrology,* **51 (2)**, 359-365.

Berner, R.A. 1984. Sedimentary pyrite formation: An update* *Geochimica et Cosmochimica Acta.* **48**, 605-615.

Bertrand-Sarfati, J. 1976. An attempt to classify Late Precambrian Stromatolite microstructures. *In:* Walter, M.R. (ed.), *Stromatolites,* Developments in Sedimentology **20**, 251-259. Elsevier Scientific Publishing Company, Amsterdam.

Bertrand-Sarfati, J. 1992. Stromatolites from the Huqf Supergroup. *PDO Exploration Note for File* No. **122**.

Bertrand-Sarfati, J. & Moussine-Pouchkine, A. 1983. Platform-to-basin facies evolution: The carbonate of Late Proterozoic (Vendian) Gourma (West Africa). *Journal of Sedimentary Petrology,* **53 (1)**, 275-293.
Bertrand-Sarfati, J., Moussine-Pouchkine, A., Amard, B. & Ait Kaci Ahmaed, A. 1995. First Ediacaran fauna found in western Africa and evidence for an Early Cambrian glaciation. *Geology,* **23**, 133-136.

Beukes, N.J. & Klein, C. 1993. Models for iron-formation deposition. *In:* Schopf , J.W. & Klein, C. (eds.) *The Proterozoic Biosphere*. Cambridge University Press, Cambridge. 147-151.

Beurrier, J. Bechennec, R., Rabu, D. and Hutin, G. 1986. Geological Map of Rustaq: Sheet NF 40-3D, Explanatory Notes. *Bureau de Recherches Géologiques et Minières*, Orléans, Cedex 2, France.

Beydoun, Z.R. 1960. Synopsis of the geology of East Aden Protectorate. *Retport of the 21st International Geological Congress, Copenhagen.* **Part 21**, 131-149.

Beydoun, Z.R. 1964. The stratigraphy and structure of the Eastern Aden Protectorate. *Overseas Geology and Mineral Resources Supplement Series.* **Bulletin Supplement 5**, 1-107.

Beydoun, Z.R. 1986. The petroleum resources of the Middle East: a review. *Journal of Petroleum Geology,* **9**, 5-28.

Beydoun, Z.R. 1988. *The Middle East: Regional Geology and Petroleum Resources*. Scientific Press, UK. 292p.

Beydoun, Z.R. 1991. *Arabian Plate Hydrocarbon Geology and Potential - A Plate Tectonic Approach.* AAPG Studies in Geology **33**, Tulsa, Oklahoma.

Blatt, H. Middleton, G. & Murray, R. 1980. *Origin of Sedimentary Rocks.* Prentice-Hall Inc. New Jersey. pp782.

Bond, G.C., Nickeson, P.A., & Kominz, M.A. 1984. Break-up of a supercontinent between 625 Ma: new evidence and implications for continental histories. *Earth and Planetary Science Letters,* **70**, 325-345.

Bond, G. C. & Kominz, M.A. 1984. Construction of tectonic subsidence curves for the early Palaeozoic miogeocline, southern Canadian Rocky Mountains: Implications for subsidence mechanisms, age of break-up, and crustal thinning. *Geological Society of America Bulletin,* **95**, 155-173.

Bond, G.C., Kominz, M.A., Steckler, M.S. & Grotzinger, J.P. 1989. Role of thermal subsidence, flexure, and eustasy in the evolution of early Paleozoic passive-margin carbonate platforms. *In:* Crevello *et al.* (eds.) *Controls on Carbonate Platform and Basin Development.* Society of Economic Paleontologists and Mineralogists Special Publication, **44**, 39-61.

Bowring, S.A., Grotzinger, J.P., Isachsen, C.E., Knoll, A.H., Pelachty, S.M. & Kolosov, P. 1993. Calibrating rates of early Cambrian evolution. *Science*, **261**, 1293-1298.

Brand, U., & Veizer, J. 1980. Chemical Diagenesis of a Multicomponent Carbonate System-1: Trace Elements. *Journal of Sedimentary Petrology*, **50 (4)**, 1219-1236.

Brand, U. &. Veizer, J. 1981. Chemical Diagenesis of a Multicomponent Carbonate System-2: Stable Isotopes. *Journal of Sedimentary Petrology*, **51 (3)**, 987-997.

Brasier, M.D., Anderson, M.M. & Corfield, R.M. 1992a. Oxygen and carbon isotope stratigraphy of early Cambrian carbonates in southeastern Newfoundland and England. *Geological Magazine,* **129**, 265-279.

Brasier, M.D. 1992b. Global ocean-atmosphere change across the Precambrian-Cambrian transition. *Geological Magazine,* **129 (2)**, 161-168.

Brasier, M.D., Khomentovsky, V.V. & Corfield, R.M. 1993. Stable isotopic calibration of the earliest skeletal fossil assemblages in eastern Siberia (Precambrian-Cambrian boundary) *Terra Nova*, **5**, 225-232.

Brasier, M.D. 1995. Fossil indicators of nutrient levels. 1: Eutrophication and climate change. *In.* Bosence, D.W.J. & Allison, P.A. (eds), *Marine Palaeoenvironmental Analysis form fossils,* Geological Society of London, Special Publication **83**, 113-132.

Brasier, M.D., Shields, G., Kuleshov, V.N. & Zhegallo, E.A. 1996. Integrated chemo- and biostratigraphic calibration of early animal evolution: Neoproterozoic-early Cambrian of southwest Mongolia. *Geological Magazine,* **133 (4)**, 445-485.

Brasier, M. D., Green, O.R. & Shields, G. 1997. Ediacarian sponge spicule clusters from SW Mongolia and the origins of the Cambrian fauna. *Geology,* **25**, 303-306.

Brasier, M.D., McCarron, G., Tucker, R.E. & Allen, P.A. 1998. Preliminary report on U-Pb zircon isochrons from the Huqf Supergroup, Oman Mountains. *PDO Report*, pp15.

Brasier, M.D. 1999. A chronostratigraphy of the Huqf Supergroup of Oman from the existing data base. *Internal PDO Report.* 39pp. 10figs.

Bühn, B. & Stanistreet, I.G. 1997. Insight into the enigma of Neoproterozoic manganese and iron formations from the perspective of supercontinental break-up and glaciation. *From:* K. Nicholas, Hein, J.R., B. Bühn, & S. Dasgupta, (eds.), *Manganese Mineralization: Geochemistry and Mineralogy of Terrestrial and Marine Deposits,* Geological Society Special Publication No. **119**, 81-90.

Burchette, T.P., & Wright, V.P. 1992. Carbonate ramp depositional systems. *Sedimentary Geology*, **79**, 3-57.

Burne, R.V. & Moore, L.S. 1987. Microbialites: organo-sedimentary deposits of benthic microbial communities. *Palaios,* **2**, 241-254.

Burns, S.J., & Matter, Albert 1993. Carbon isotopic record of the latest Proterozoic from Oman. *Eclogae geol. Helv.*, **86 (2)**, 595-607.

Burns, S.J., Haudenschild, U., & Matter, Albert 1994. The strontium isotopic composition of carbonates from the late Precambrian (~560-540 Ma) Huqf Group of Oman. *Chemical Geology (Isotope Geoscience Section),* **111**, 269-282.

Carlson, W.D. 1980. The calcite-aragonite equilibrium: effects of Sr substitution and on orientational disorder. *American Mineralogist,* **65**, 1252-1262.

Carter, H.J. 1852. Memoir on the geology of the south east coast of Arabia, *Journal Royal Asiatic Society, Bombay Br.,* **4**, 21-96.

Cheel, R.J. & Leckie, D.A. 1993. Hummocky cross-stratification. *In:* Wright V.P. (ed.) *Sedimentology Review/1.* 103-138, Blackwell Scientific Publications, Oxford.

Chow. N. & James N.P. 1987. Facies-Specific, Calcitic and Bimineralic Ooids From Middle and Upper Cambrian Platform Carbonates, Western Newfoundland, Canada. *Journal of Sedimentary Petrology,* **57, (5)**, 907-921.

Cloud, P.E. 1960. Gas as a sedimentary and diagenetic agent: *American Journal of Science*, **258**, 35-45.

Conway Morris, S., Mattes, B.W. & Chen Menge 1990. The early skeletal organism *Cloudina*: new occurrences from Oman and possibly China. *American Journal of Science,* **290-A**, 245-260.

Conway Morris, S. 1993. The fossil record and the early evolution of the Metazoa. *Nature*, **361**, 219-225.

Cook, H.E. & Taylor, M.E. 1977. Comparison of continental slope and shelf environments in the Upper Cambrian and Lowest Ordovician of Nevada. SEPM Special Publication No. **25** 51-81.

Cook, P.J., & Shergold, J.H. 1979. Proterozoic~Cambrian Phosphorites

Dalziel, I.W.D. 1997. Neoproterozoic-Palaeozoic geography and tectonics: Review, hypothesis, environmental speculation. *GSA Bulletin,* **109 (1)**, 16-42.

Davies, G. R. 1970. Algal-laminated sediments, Gladstone Embayment, Shark Bay, Western Australia. *In:* Logan *et al.* (eds.) *Carbonate Sedimentation and Environments, Shark Bay, Western Australia.* American Association of Petroleum Geologists Memoir **13**, 169-205.

Demicco, R.B. & Hardie, L.A. 1994. Sedimentary structures and early diagenetic features of shallow marine carbonate deposits *In:* P.A.Scholle, (ed.) *SEPM Atlas Series No.1,*. SEPM (Society of Sedimentary Geology) Oklahoma.

Derry, L.A., Keto, L.S. Jacobsen, S., Knoll, A.H. & Swett, K. 1989. Sr isotopic variations of upper Proterozoic carbonates from East Greenland and Svalbard. *Geochimica et Cosmochimica Acta,* **53**, 2331-2339.

Derry, L.A., Kaufman, A.J. and Jacobsen, S.B. 1992. Sedimentary cycling and environmental change in the Late Proterozoic: Evidence from stable and radiogenic isotopes. *Geochimica et Cosmochimica Acta*, **56**, 1317-1329.

Derry, L.A., Brasier, M.D., Corfield, R.M., Rozanov, A.Yu. & Zhuravlev, A.Yu. 1994. Sr and C isotopes in Lower Cambrian carbonates from the Siberian craton: A palaeoenvironmental record during the "Cambrian explosion". *Earth and Planetary Science Letters,* **128**, 671-681.

Dickins,

Dubreuilh, J, Platel, J.P., Le Métour, J., Roger, J., Wyns, R., Béchennec, F., & Berthiaux, A. 1992. Geological Map of Khaluf: Sheet NF 40-15, Explanatory Notes. *Bureau de Recherches Géologiques et Minières*, Orléans, Cedex 2, France.

Dunham, J.B. & Olson, E.R. 1980. Shallow subsurface dolomitization of subtidally deposited carbonate sediments in the Hanson Creek Formation (Ordovician-Silurian) of central Nevada. *SEPM Special Publication,* **28**, 139-161.

Fairchild, I.J. 1980. Sedimentation and origin of a Late Precambrian 'Dolomite' from Scotland. *Journal of Sedimetary Petrology,* **50 (2)**, 423-446.

Fairchild, I.J. 1983. Chemical controls of cathodoluminescence of natural dolomites and calcites: new data and review. *Sedimentology,* **30**, 579-583.

Fairchild, I.J. & Spiro, B. 1987. Petrological and isotopic implication of some contrasting Late Precambrian carbonates, NE Spitzbergen. *Sedimentology,* **34**, 973-989.

Fairchild, I.J., Hendry, G., Quest, M. & Tucker, M.E. 1988. Chemical analysis of sedimentary rocks. *In:* Tucker M.E. (ed.) *Techniques in Sedimentology,* Blackwell Scientific Press. Oxford.

Fairchild, I.J., Hambrey, M.J., Spiro, B. & Jefferson, T.H. 1989. Late Proterozoic glacial carbonates in northeast Spitsbergen: new insights into the carbonate-tillite association. *Geological Magazine,* **126 (5)**, 469-490.

Fairchild, I.J. & Herrington, P.M. 1989b. A Tempestite-Stromatolite-Evaporite Association (Late Vendian, East Greenland): a Shoreface-Lagoon Model. *Precambrian Research,* **43**, 101-127.

Fairchild, I.J., Marshall, J.D. & Bertrand-Sarfati, J. 1990. Stratigraphic shifts in carbon isotopes from Proterozoic stromatolitic carbonates (Mauritania): Influences of primary mineralogy and diagenesis. *American Journal of Science,* **290-A**, 46-79.

Fedonkin, M.A. 1980. New Precambrian Coelenterata in the north Russian platform. *Palaeontologicheskiy Jhurnal,* **2**, 5-15.

Folk, R.L. 1962. Spectral subdivision of limestone types. *In:* Ham, W.E. (ed.) Classification of Carbonate Rocks, *Memoir American Association of Petroleum Geologists,* **1**, 62-84.

Folk, R.L. 1974. *Petrology of sedimentary rocks.* Hemphill Publishing Co. Austin, Texas 78712. 198pp.

Folk, R.L. & Land, L.S. 1975. Mg/Ca Ratio and Salinity: Two Controls over Crystallization of Dolomite *The Americal Association of Petroleum Geologists Bulletin,* **59 (1)**, 60-68.

Folk, R.L., & Pittman, J.S. 1971. Length-slow chalcedony: A new testament for vanished evaporites. *Journal of Sedimentary Petrology*, **41 (4)**, 1045-1058.

Flügel, E. 1982. *Microfacies Analysis of Limestones,* Springer-Verlag, Berlin. 588pp.

Frank, J.R., Carpenter, A.B. & Oglesby, T. W. 1982. Cathodoluminescence and composition of calcite cement in the Taum Sauk limestone (upper Cambrian), southeast Missouri. *Journal of Sedimentary Petrology,* **52**, 631-638.

Fuzesy, L.M. 1980. Origin of nodular limestones, calcium sulphates and dolomites in the Lower Magnesian Limestone in the neighbourhood of Selby, Yorkshire, England. *In:* Fuchtbauer, H. and Peryt, T. (eds.) *The Zechstein Basin with emphasis on carbonate sequences,* Contributions to Sedimentology, **9**, 35-44.

Garrels, R.M. & Christ, C.L. 1965. *Solutions, Minerals, and Equilibria.* San Francisco, Freeman, Cooper, Co., 450pp.

Garret, P. 1970. Phanerozoic stromatolites: Noncompetitive ecologic restriction by grazing and burrowing animals. *Science*, **169**, 171-173.

Gass, I.G., Ries, A.C., Shackleton R.M. & Smewing, J.D. 1990. Tectonics, geochronology and geochemistry of the Precambrian rocks of Oman. *In:* Robertson, A.H.F., Searle, M.P., & Ries, A.C. (eds.), *The Geology and Tectonics of the Oman Region*. Geological Society Special Publication **49**, 585-599.

Gebelein, C.D. 1969. Distribution, morphology, and accretion rate of Recent subtidal algal stromatolites, Bermuda. *Journal of Sedimentary Petrology,* **39**, 49-69.

Glennie, K.W., Boeuf, M.G.A., Hughes Clarke, M.W., Moody-Stuart, M., Pilaar W.F.H., & Reinhardt, B.M. 1974. Geology of the Oman Mountains. *Verhandelingen van het Koninklijk Nederlands geologisch mijnbouwkundig Genootschap,* KSEPL, Rijswijk, NL.

Gorin, G.E. 1977. Study of the Huqf Group outcrops and comparison with subsurface data in Oman. *Exploration Report No:112,* Petroleum Development (Oman) Ltd.

Gorin, G.E., Racz, L.G. & Walter, M.R. 1982. Late Precambrian-Cambrian Sediments of Huqf Group, Sultanate of Oman. *The American Association of Petroleum Geologists Bulletin,* **66**, 2609-2627.

Grant, S.W.F. 1990. Shell structure and distribution of *Cloudina*, a potential index fossil for the Terminal Proterozoic. *In*: Knoll, A.H. & Ostrom, J.H. (eds.) Proterozoic evolution and environments, *American Journal of Science*, **290-A**, 261-294.

Greenwood, W.R., Anderson, R.E., Fleck, R.J. & Roberts, R.J., 1980. Precambrian geologic history and plate tectonic evolution of the Arabian Shield. *Saudi Arabian Dir.Gen. Miner. Resources Bull.,***24**, 35pp.

Grey, K. & Corkeron, M. 1998. late Neoproterozoic stromatolites in glaciogenic successions of the Kimberley region, Western Australia: evidence for a younger Marinoan glaciation. *Precambrian Research*, **92**, 65-87.

Grotzinger, J.P. 1986a. Cyclicity and palaeoenvironmental dynamics, Rocknest platform, northwest Canada. *Geological Society of America Bulletin*, **97**, 1208-1231.

Grotzinger, J.P. 1986b. Evolution of early Proterozoic passive-margin carbonate platform, Rocknest Formation, Wopmay Orogen, Northwest Territories, Canada. *Journal of Sedimentary Petrology,* **56 (6)**, 831-847.

Grotzinger, J.P. 1989. Facies and Evolution of Precambrian carbonate depositional systems: Emergence of the modern platform archetype. *In:* Crevello, P.D., Wilson, J.L., Sarg, J.F. & Read, J.F. (eds.) *Controls on Carbonate Platform and Basin Development,* SEPM Special Publication, **44**, 79-106.

Grotzinger, J.P. & Knoll, A.H. 1995. Anomalous Carbonate Precipitates: Is the Precambrian the Key to the Permian?. *Palaios,* **10**, 578-596.

Grotzinger, J.P. & Bowring, S.A., Saylor, B.Z. & Kaufman, A.J. 1995. Biostratigraphic and geochronologic constraints on early animal evolution. *Science*, **270**, 598-604.

Grover, G. Jr. & Read, J.F. 1978. Fenestral and associated vadose diagenetic fabrics of tidal flat carbonates, Middle Ordovician New Market Limestone, Southwestern Virginia. *Journal of Sedimentary Petrology,* **48 (2)**, 453-473.

Haeman, L.M. LeChaminant, A.N. & Rainbird, R. H. 1992. Nature and timing of Franklin igneous events, Canada: implications for a Late Proterozoic mantle plume and the break-up of Laurentia. *Earth and Planetary Science Letters*, **109**, 117-131.

Hagan, G.M. & Logan, B.W. 1974. Development of carbonate banks and hypersaline basins, Shark Bay, Western Australia. *Memoir American Association Petroleum Geologists,* **22**, 61-139.

Hallam, A. 1992. *Phanerozoic Sea-level Changes*. Columbia University Press, New York.

Hamblin, A.P. & Walker, R.G. 1979. Storm dominated shallow marine deposits: the Vernie-Kootney (Jurassic) transition, southern Rocky Mountains. *Canadian Journal of Earth Sciences,* **16**, 1673-1690.

Handke, M.J., Tucker, R.D., Ashwal, L.D. 1999. Neoproterozoic continental arc magnatism in west-central Madagascar. *Geology*, **27 (4)**, 351-354.

Hardie, L.A. 1977. Algal structures in cemented crusts and their environmental significance. *In:* Hardie, L.A. (eds.) *Sedimentation on the Modern Carbonate Tidal Flats in Northwest Andros Island, Bahamas.*The Johns Hopkins University Studies in Geology, **22**, 159-177.

Hardie, L.Al & Ginsburg, R.M. 1977. General environmental setting *In:* Hardie L.A. (ed.) *Sedimentation on the Modern Carbonate Tidal Flats of Northwest Andros Island, Bahamas.* John Hopkins Studies in Geology, **22**, 12-49.

Harris, P.M., Kendall, C.G. St.C & Lerche, I. 1985. Carbonate cementation - A brief review. *Society of Economic Paleontologists and Mineralogists Special Publication,* **36**, 79-96.

Harwood, G. 1988. Microscopic techniques: 11. Principles of sedimentary petrography *In:* Tucker M.E. (ed.) *Techniques in Sedimentology,* Blackwell Scientific Press, Oxford.

Hesse, Reinhard 1989. Silica Diagenesis: Origin of Inorganic and Replacement Cherts. *Earth-Science Reviews,* **26**, 253-284.

Heydari, E. & Moore, C.H. 1994. Paleoceanographic and Paleoclimatic controls on ooid mineralogy of the Smackover Formation, Mississippi Salt Basin: Implications for Late Jurassic seawater composition. *Journal of Sedimentary Research*, **A64, (1)**, 101-114.

Hoffman, P. 1974. Shallow and Deepwater Stromatolites in Lower Proterozoic Platform-to-Basin Facies Change, Great Slave Lake, Canada. *The American Association of Petroleum Geologists Bulletin,* **58**, 856-867.

Hoffman, P. 1976. Stromatolite morphogenesis in Shark Bay, Western Australia. *In:* Walter, M.R. (ed), *Stromatolites,* Developments in Sedimentology **20**, 261-271. Elsevier Scientific Publishing Company, Amsterdam.

Hoffman, P., Kaufman, A.J., & Halverson, G.P. 1998. Comings and Goings of Global Glaciations on a Neoproterozoic Tropical Platform in Namibia. *GSA Today,* **8 (5)**, 1-9.

Hoffman, P.E. 1967. Algal stromatolites - use in stratigraphic correlation and paleocurrent determination. *Science,* **157**, 1043-1045.

Hoffman, P.F. 1975. Shoaling-upward shale-to-dolomite cycles in the Rocknest Formation (lower Proterozoic), N.W.Territories, Canada. *In:* Ginsburg, R.N. (ed.) *Tidal Deposits,* Springer-Verlag, Berlin. 257-265.

Hoffman, P.F., Hawkins, D.P., Isachsen, C.E. & Bowring, S.A. 1996. Precise U-Pb zircon ages for early Damarian magmatism in the Summas Mountains and Wrlwitschia inlier, northern Damara belt, *Namibia. Namibia Geological Survey,* Communication **11**, 47-52.

Hofmann, H.J., Narbonne, G.M. & Aitken, J.D. 1990. Ediacaran remains from intertillite beds in northwestern Canada. *Geology*, **18**, 1199-1202.

Hofmann, H.J. 1973. Stromatolite characteristics and utility: *Earth Science Reviews,* **9**, 339-373.

Hsü, K.J. & Kelts, K. 1978. Late Neogene chemical sedimentation in the Black Sea. *In:* Matter, A. & Tucker, M.E. (eds.) *Modern and Ancient Lake Sediments.* Special Publication of International Association of Sedimentologists, **2**, 129-145.

Hudson, J.D. 1977. Stable isotopes and limestone lithification. *Journal of the Geological Society London.* **133**, 637-660.

Hughes-Clarke, M.W. 1988. Stratigraphy and rock nomenclature in the oil-producing area of interior Oman. *Journal of Petroleum Geology,* **11**, 5-60.

Husseini, M.I. 1989. Tectonic and Deposition Model of Late Precambrian-Cambrian Arabian and Adjoining plates. *The American Association of Petroleum Geologists Bulletin* **73(9)** (September 1989), P.1117-1131.

Husseini, M.I. & Husseini, S.I. 1990. Origin of the Infracambrian salt basins of the Middle East. *In:* Brooks, J. (ed), *Classic Petroleum Provinces.* Geological Society of London Special Publication, **50**, 279-292.

Jackson, M.J., Muir, M.D. & Plumb, K.A. 1987. *Geology of the southern McArthur Basin, Northern Territory.* Bureau of Mineral Resources, Geology and Geophysics, Bulletin **220**, Australian Government Publishing Service, Canberra.

James, N.P. 1979. Shallowing upward sequences in carbonates. *In.* Walker, R. G (ed.), *Facies Models. Geological Association, Ontario, Canada. Geoscience Reprint Series,* **1**, 109-119.

Jenkyns, H.C. 1997. Mesozoic anoxic events and palaeoclimate. *Sbl. Geol. Paläont. Teil 1* H. **7-9**, 943-949.

Kapellos,C., Knox, G.J., Borgamano, J.R.F. & Mohammed, A.R. 1992. Stratigraphical Review of the Huqf Supergroup. *PDO Exploration Report* **308**,13pp.

Kapp, H.E. & Llewellyn, P.G. 1965. The Geology of the Central Oman Mountains. *Report S00005-9,* Geological Group, Petroleum Development (Oman) Ltd.

Kassler, P. 1965. The Geology of the Haushi, Central Huqf and Masirah Island areas (Southern Oman). *Report No: 19,* Petroleum Development (Oman) Ltd., Doha Geological Group.

Kaufman, A.J., Hayes, J.M., Knoll, A.H. & Germs, G.J.B. 1991. Isotopic compositions of carbonates and organic carbon from upper Proterozoic successions in Namibia: stratigraphic variation and the effects of diagenesis and metamorphism. *Precambrian Research,* **49**, 301-327.

Kaufman, A.J. & Knoll, A.H. 1992. Biostratigraphic and chemostratigraphic correlation of Neoproterozoic sedimentary successions: Upper Tindir Group, northwestern Canada, as a test case. *Geology*, **20**, 181-185.

Kaufman, A. J., Jacobsen, S.B. & Knoll, A.H. 1993. The Vendian record of Sr and C isotopic variations in seawater: Implications for tectonics and paleoclimate. *Earth and Planetary Science Letters,* **120**, 409-430.

Kaufman, A. J. & Knoll, A.H. 1995. Neoproterozoic variations in the C-isotopic composition of seawater: stratigraphic and biogeochemical implications. *Precambrian Research*, **73**, 27-49.

Kaufman, A. J. & Knoll, A.H. & Narbonne, G.M. 1997. Isotopes, ice ages, and Terminal Proterozoic earth history. *Proceedings of the National Academy of Sciences,* USA, **94**, 6600-6605.

Kaye, C.A. & Zartman, R.F. 1980. *Memoir 2: Proceedings "The Caledonides in the USA"* D.R.Wones (ed.) Virginia Polytechnic Institute and State University, Blacksburg. 257-261.

Kendall, A.C. & Harwood, G.M. 1996. Marine Evaporites: arid shorelines and basins. *In:* Reading H.G. (ed.), Sedimentary environments and facies. 281-323.

Kennedy, M.J. 1996. Stratigraphy, Sedimentology, and Isotope geochemistry of Australian Neoproterozoic postglacial cap dolostones: Deglaciation, $\delta^{13}C$ excursions, and carbonate precipitation. *Journal of Sedimentary Research,* **66 (6)**, 1050-1064.

Kennedy, M.J., Runnegar, B., Prave, A.R., Hoffman, K.H. & Arthur, M.A. 1998. Two or four Neoproterozoic glaciations? *Geology*, **26**, 1059-1063.

Kimura, H., Matsumoto, R., Kakuwa, Y., Hamdi, B. & Zibaseresht, H. 1997. The Vendian-Cambrian $\partial^{13}C$ record, North Iran: evidence for overturning of the ocean before the Cambrian explosion. *Earth and Planetary Science Letters,* **147**, E1-E7.

Kinsman, D.J.J. 1969. Interpretation of Sr^{2+} concentrations in carbonate minerals and rocks. *Journal of Sedimentary Petrology,* **39**, 486-508.

Knoll, A.H. 1985. Exceptional preservation of photosynthetic organisms in silicified carbonates and silicified peats. *Phil. Trans. R. Soc. London,* B **311**, 111-122.

Knoll, A.H., Hayes, J.M., Kaufman, A.J., Sweet, K. and Lambert, I.B. 1986. Secular variations in carbon isotope ratios from upper Proterozoic successions of Svalbard and East Greenland. *Nature*, **321**, 832-838.

Knoll, A.H. 1990. Report on palynological samples from the Huqf Group, Oman. PDO Exploration Report No. **B0173**, 8pp. 2pls.

Knoll, A.H. & Walker, M.R. 1992. Latest Proterozoic stratigraphy and Earth history. *Nature,* **356**, 673-678.

Knoll, A.H. 1994. Neoproterozoic evolution and environmental change. *In:* Bengtson, S. (ed.) *Early life on Earth* , Nobel Symposium No. **84**, Columbia U.P., New York.

Knoll, A.H., Grotzinger, J.P., Kaufman, A.J. & Kolosov, P., 1995. Integrated approaches to terminal Proterozoic stratigraphy: an example from the Olenek Uplift, northeastern Siberia: *Precambrian Research*, **73**, 251-270.

Kramers, J.K. & Frei, R. 1992. Report on age determinations carried out on rocks from Mirbat region, South Oman. *Mineralogisch Petrographisches Institut*, University of Berne, unpublished report.

Krauskopf, K.B. & Bird, D.K. 1995. *Introduction to geochemistry.* McGraw- Hill Inc. NY. 647pp.

Kump, L.R. 1991. Interpreting carbon-isotope excursions: Strangelove oceans. *Geology,* **19**, 299-302.

Kump, L.R., Arthur, M.A., Patzkowsky, M.E., Gibbs, M.T., Pinkus, D.S. & Sheehan, P.M. 1999. A weathering hypothesis for glaciation at high atmospheric *p* CO2 during the Late Ordovician. *Palaeogeography, Palaeoclimatology, Palaeoecology* **152**, 173-187.

Lake, S. 1996. Hydrocarbon plays of Oman. *Exploration in Oman: New ideas from Old basins.* PDO Report, 122pp.

Land, L.S. 1967. Diagenesis of skeletal carbonates. *Journal of Sedimentary Petrology,* **37**, 914-930.

Land, L.S. 1973. Holocene meteoric dolomitization of Pleistocene limestones, North Jamaica: *Sedimentology,* **20**, 411-424.

Land, L.S. 1980. The isotopic and trace element geochemistry of dolomite: the state of the art. *In:* Zenger *et al.* (eds.) *Concepts and Models of Dolomitization.* SEPM Special Publication, **28**, 87-110.

Land, L.S. 1986. Limestone diagenesis-some geochemical considerations. *In:* Mumpton, F.A. (ed.) *Studies in Diagenesis: United States Geological Survey Bulletin,* **1578,** 130-137.

Leather, J. 1998. An Outcrop Study Of The Abu Mahara Formation, Huqf Supergroup, Oman. *PDO Report*, pp47.

Leeder, M.R. 1982. *Sedimentology: Process and Product.* Chapman & Hall, London. 344pp

Lees. G.M., 1928. The Geology and Tectonics of Oman and Parts of South Eastern Arabia, *Quarterly Journal of the Geological Society London,* **84**, 585-670.

Logan, B.W., Rezak, R. & Ginsburg, R.N. 1964. Classification and environmental significance of algal stromatolites, *Journal of Geology,* **72**, 68-83.

Logan G.A., Hayes, J.M., Hleshima, G.B. & Summons, R.E. 1995. Terminal Proterozoic reorganization of biogeochemical cycles. *Nature*, **376**, 53-56.

Loreau, J.P. & Purser, B.H. 1973. Distribution and Ultrastructure of Holocene ooids in the Persian Gulf. *In:* Purser, B.H. (ed.) *Holocene carbonate sedimentation and diagenesis in a shallow epicontinental sea.* 234-278.

Lorens, R.B. 1981. Sr, Cd, Mn and Co distribution coefficients in calcite as a function of calcite precipitation rate. *Geochimica Cosmochimica Acta,* **45**, 553-561.

Looseveld, R.J.H., Bell, A. & van Beusekom, G. 1995. The Najd Tectonic event in Oman, A model. PDO Exploration Report **353**, 15pp

Loosveld, R.J.H., Bell, A. & Terken, J.J.M. 1996. The Tectonic Evolution of Interior Oman. *GeoArabia,* **1 (1)**, 28-50.

Maliva, R.G., Knoll, A.H. & Siever, R. 1989. Secular Change in Chert Distribution: A Reflection of Evolving Biological Participation in the Silica Cycle. *Palaios,* **4**, 519-532.

Mann, A & Hanna, S.S. 1990. The tectonic evolution of pre-Permian rocks, Central and Southeastern Oman Mountains. *From:* Robertson, A.H.F., Searle, M.P. & Ries, A.C. (eds.) *The Geology and Tectonics of the Oman Region.* Geological Society Special Publication No. **49**, 307-325.

Markello, J.R. & Read, J.F. 1981. Carbonate ramp-to-deeper shale shelf transitions of an Upper Cambrian intrashelf basin, Nolichucky Formation, Southwest Virginia Appalachians. *Sedimentology,* **28**, 573-597.

Marle val, L.J., Bell, A., Borgomano, J.R.F. & Love, C.F. 1994. Abu Mahara study summary report. *Internal PDO Report* **340**.

Marshall, D.J. 1988. *Cathodoluminescence of Geological Materials.* Unwin Hyman Publications. 146pp.

Marshall, J. D. 1992. Climatic and oceanographic isotopic signals from the carbonate rock record and their preservation. *Geological Magazine*, **129 (2)**, 143-160.

Mattes, B.W., & Conway Morris, S. 1990. Carbonate/evaporite deposition in the Late Precambrian - Early Cambrian Ara Formation of Southern Oman. *In:* Robertson, A.H.F., Searle, M.P., & Ries, A.C. (eds), *The Geology and Tectonics of the Oman Region.* Geological Society Special Publication **49**, 617-636.

McCarron, M.E. 1996. An outcrop study, with microfacies and lithofacies interpretations, of the Nafun Group, in the Huqf area, East-Central Oman. *PDO Report*, pp63.

McCrory, V.L.C. & Walker, R.G. 1986. A storm and tidally-influenced prograding shoreline - Upper Cretaceous Milk River Formation of Southern Alberta, Canada. *Sedimentology,* **33**, 47-60.

McKerrow, W.S., Scotese, C.R. & Brasier, M.D. 1992. Early Cambrian continental reconstructions. *Journal of the Geological Society, London,* **149**, 599-606.

Meyers W.J. 1974. Carbonate cement stratigraphy of the lake Valley Formation (Mississippian), Sacramento Mountains, New Mexico. *Journal of Sedimentary Petrology,* **44**, 837-861.

Miller, J. 1988. Cathodoluminescence microscopy. *Techniques in Sedimentology.* Blackwell Scientific Press, Oxford. 174-191.

Milliken, K.L. 1979. The silicified evaporite syndrome-Two aspects of silicification history of former evaporite nodules from Southern Kentucky and Northern Tennessee. *Journal of Sedimentary Petrology,* **49 (1)**, 245-256.

Millson, J.A., Mercadier, C.G.L., Livera, S.E. & Peters, J.M. 1996. The Lower Palaeozoic of Oman and its context in the evolution of a Gondwanan continental margin. *Journal of the Geological Society, London,* **153**, 213-230.

Morse, J.W. & Mackenzie, F.T. 1990. *Geochemistry of Sedimentary Carbonates.* New York Elsevier, 707pp.

Morton, D.M. 1959. The geology of Oman. *5th World Petroleum Congress. Proceedings,*
New York, **1**, 277-294.

Nahon, D. & Trompette, R. 1982. Origin of siltstones: glacial grinding versus weathering. *Sedimentology,* **29**, 25-35.

Narbonne, G.M., Kaufman, A.J. & Knoll, A.H. 1994. Integrated chemostratigraphy and biostratigraphy of the Windermere Supergroup, northwestern Canada: Implications for Neoproterozoic correlations and the evolution of animals. *Geological Society of America Bulletin,* **106**, 1281-1292.

Nederlof, P. & al Ruwehy, N. 1996. The quality of the Huqf source rocks. *Exploration in Oman: New ideas from Old basins.* PDO Report, 122pp.

Nicholas, C.J. 1994. *Strontium isotope stratigraphy in the Cambrian System.* PhD. Thesis, University of Cambridge.

Nicholas, C.J. 1996. The Sr isotope evolution of the oceans during the 'Cambrian Explosion'. *Journal of the Geological Society, London,* **153**, 243-254.

Odin, G.S. & Letolle, R. 1980. Glauconitization and phosphatization environments: A tentative comparison. SEPM Special Publication No. **29**, 227-237.

Pallister, J.S., Stacey, J.S., Fischer, L.B. & Premo, W.R. 1988. Precambrian Ophiolites of Arabia: Geologic Settings, U-Pb Geochronology, Pb-isotope Characteristics and Implications for Continental Accretion. *Precambrian Research,* **38 (1)**, 1-54.

Park, R & Epstein, S. 1960. Carbon isotope fractionation during photosynthesis. *Geochim Cosmochim Acta* **21**, 110-126.

Patterson, W.P. & Walter, L.M. 1994. Depletion of ^{13}C in seawater $\sum CO_2$ on modern carbonate platforms: Significance for the carbon isotope record of carbonates. *Geology*, **22**, 885-888.

Pelechaty, S.M., Grotzinger, J.P., Kashirtev, V.A. & Zhernovsky, V.P. 1996. Chemostratigraphic and sequence stratigraphic constraints on Vendian-Cambrian basin dynamics, northeast Siberian craton. *Journal of Geology,* **104**, 543-563.

Pelechaty, S.M., Khaufman, A.J. & Grotzinger, J.P. 1996b. Evaluation of $\partial^{13}C$ chemostratigraphy for intrabasinal correlation: Vendian strata of northeast Siberia. *GSA Bulletin*, **108**, 992-1003.

Pelechaty, S.M. 1998. Integrated chronostratigraphy of the Vendian System of Siberia: implications for a global stratigraphy. *Journal of the Geological Society, London,* **155**, 957-973.

Pflüger, F. & Gresse, P.G. 1996. Microbial sand chips - a non-actualistic sedimentary structure. *Sedimentary Geology,* **102**, 263-274.

Pierre, C. 1988. Applications of Stable Isotope Geochemistry to the Study of Evaporites. *In:* Schrieber B.C. (ed.) *Evaporites and Hydrocarbons*, 300-344.

Pilcher, R. & Buckley, R. 1995. An Outcrop Study of the Huqf Supergroup. *PDO Report.* pp68, 23plates.

Platel, J.P., Bechennec, F., Berthiaux, A., Dubreuilh, J., LeMetour, J., Rojer, J. & Wyns, R. 1992a *Geological Map of Duqm and Madraka*, Sheet NF 40-03/07, 1:250,000. Directorate General of Minerals, Oman Ministry of Petroleum and Minerals.
Dubreuilh,

Platel, J.P., Berthiaux, A., LeMetour,J., Beurrier, M. & Rojer, J. 1992b. *Geological Map of Juzor Al Halaaniyaat*, Sheet NE 40-10, 1:250,000. Directorate General of Minerals, Oman Ministry of Petroleum and Minerals.

Platel, J.P., Bechennec, F., J., Chevrel, S., Rojer, J., LeMetour,J. & Wursten, F. 1992c. *Geological Map of Salalah*, Sheet NE 40-09, 1:250,000. Directorate General of Minerals, Oman Ministry of Petroleum and Minerals.

Pope, M., Grotzinger, J.P, & Schreiber, C. 1999. Evaporitic subtidal stromatolites Produced by *In-Situ* Precipitation. *Journal of Sedimentary Research*.....in press

Pratt, B.R. & James, N.P. 1986. The St. George (Lower Ordovician) of western Newfoundland: tidal flat island model for carbonate sedimentation in shallow epeiric seas. *Sedimentology,* **33**, 313-343.

Prave, A.R. 1999. Two diamictites, two cap carbonates, two $\partial^{13}C$ excursions, two rifts: The Neoproterozoic Kingston Peak Formation, Death Valley, California. *Geology*, **27 (4)**, 339-342.

Prothero, D.R. 1994. The Eocene- Oligocene Transition- paradise lost.*In:* Bottjer, D.J. & Bambach, R.K. (eds.) *Critical moments in Palaeobiology and Earth History Series,* Columbia University Press.

Rabu, D., Bechennec, F., Beurrier, M., Hutin, G. 1986. Geological Map of Nakhl: Sheet NF 40-3E, Explanatory Notes. *Bureau de Recherches Géologiques et Minières*, Orléans, Cedex 2, France.

Rabu, D. 1988. *Geologie de l'autochtone des Montagnes d'Oman; la Fenêtre du Jabal Adhdar*. Thesis BRGM Document No. **130**, 582p.

Rabu, D. 1993. Stratigraphy and structure of the Oman Mountains. *Document du BRGM,* **221**, 21-47.

Read. J.F. 1980. Carbonate Ramp-to-Basin Transitions and Foreland Basin Evolution, Middle Ordovician, Virginia Appalachians. *AAPG Bulletin,* **64 (10)**, 1575-1613.

Read, J.F. 1985. Carbonate Platform Facies Models. *The American Association of Petroleum Geologists Bulletin*, **69**, 1-21.

Reineck, H.E. & Singh, I.B. 1973. *Depositional Sedimentary Environments.* Springer-Verlag. 439pp.

Riding, R. & Voronova, L. 1982. Recent freshwater analogue of the lower Palaeozoic calcareous algae *angulocellularia. Lethaia,* **15**, 105-114.

Riding, R. & Voronova, L. 1984. Assemblages of calcareous algae near the Precambrian/Cambrian boundary in Siberia and Mongolia. *Geological Magazine,* **121**, 205-210.

Ries, A.C. & Shackleton, R.M. 1990. Structures in the Huqf - Haushi Uplift, east Central Oman. *From:* Robertson, A.H.F., Searle, M.P., & Ries, A.C. (eds.), *The Geology and Tectonics of the Oman Region.* Geological Society Special Publication **49**, 653-664.

Roger, J., Bechennec, F., Janjou, D., LeMetour, J., Wyns, R., & Beurrier, M. 1991. *Geological Map of Ja'alan,* Sheet NF 40-08E, 1:100,000 with explanatory notes. Directorate General of Minerals, Oman Ministry of petroleum and Minerals.

Russell, J. & Amthor, J.E. 1996. Pb/Pb radiometric dating and isotope analysis of Huqf carbonates. South Oman. *SIEP 96-5083.*

Sandberg, P.A. 1975. New interpretations of Great Salt Lake ooids and of non-skeletal carbonate mineralogy. *Sedimentology,***22**, 497-537.

Sandberg, P.A. 1983. An oscillating read in Phanerozoic non-skeletal carbonate mineralogy. *Nature*, **305**, 19-22.

Sarg, J.F. 1988. Carbonate sequence stratigraphy. *In:* Wilgus *et al.* (eds.) Sea Level Changes: An Integrated Approach. *SEPM, Special Publication,* **42**, 155-181.

Saylor, B.Z. 1996. *Sequence stratigraphic and chemostratigraphic constraints on the evolution of the terminal Proterozoic to Cambrian Nama basin, Namibia.* (unpublished Ph.D thesis) Massachusetts Institute of Technology, Cambridge Mass. pp164.

Saylor, B.Z., Kaufman, A.J., Grotzinger, J.P, & Urban, F. 1998. A composite reference section for Terminal Proterozoic strata of southern Namibia. *Journal of Sedimentary Research,* **68**, 1223-1235.

Schindlowski, M. & Aharon, P. 1988. Carbon Cycle and Carbon Isotope Record: Geochemical Impact of Life over 3.8 Ga of Earth History *In:*Schindlowski, M., Golubic, S., Kimberley, M.M., McKirdy, D.M. & Trudinger, P.A. (eds.) *Early Organic Evolution,* Springer-Verlag, 555pp.

Scholle, P.A. 1978. Carbonate Rock Constituents, Textures, Cements, and Porosities. *The American Association of Petroleum Geologists,* Memoir **27**, Tulsa, Oklahoma. 241pp.

Scholle, P.A. 1979. Constituents, Textures, Cements, and Porosities of Sandstones and Associated Rocks. *The American Association of Petroleum Geologists,* Memoir **27,** Tulsa, Oklahoma. 201pp.

Scholle, P.A. & Arthur, M.A. 1980. Carbon isotope fluctuations in Cretaceous pelagic limestones: potential stratigraphic and petroleum exploration tool. *American Association of Petroleum Geologists Bulletin,* **64**, 67-87.

Schreiber, B.C. 1986. Arid Shorelines and Evaporites. *In:* Reading, H.G. (ed.) *Sedimentary facies and environments.* Blackwell Scientific Press, Oxford. 178-206.

Sepkoski, J.J. Jr. 1982. Flat-pebble conglomerates, Storm Deposits, and the Cambrian Bottom Fauna. *In:* Einsele & Seilacher (eds.) *Cyclic and Event Stratification.* Springer Verlag. 370-385

Sheldon, R.P. 1980. Episodicity of phosphate deposition and deep ocean circulation - A hypothesis. *SEPM Special Publication No.* **29**, 239-247.

Sheppard, S.M.F. & Schwarcz, H.P. 1990. Fractionation of carbon and oxygen isotopes and magnesium between coexisting metamorphic calcite and dolomite. *Contributions to Mineral Petrology,* **26**, 161-198.

Shields, G., Stilles, P., Brasier, M.D. & Atudorei, N.V. 1997. Stratified oceans and oxygenation of the late Precambrian environment: a geochemical record from the Neoproterozoic of W. Mongolia. *Terra Nova,* **9**, 218-222.

Shields, G. 1999. Working towards an isotopically based stratigraphic calibration scheme for the Terminal Proterozoic and Early Cambrian. *Eclogae Geologicae Helvetiae,* in press.

Shinn, E.A. 1968. Practical significance of birds eye structures in carbonate rocks. *Journal of Sedimentary Petrology,* **38**, 612-616.

Smith, D.B., 1980. The evolution of the English Zechstein basin. *In:* Fuchtbauer, H. and Peryt, T. (eds.) *The Zechstein Basin with emphasis on carbonate sequences,* Contributions to Sedimentology, **9**, 7-34.

Spjeldnaes, Nils 1981. Lower Palaeozoic Palaeoclimatology. *In:* C.J. Holland (ed.) *Lower Palaeozoic of the Middle East, Eastern and Southern Africa, and Antarctica.* John Wiley & Sons Ltd.

Spriggs, A. 1994. An overview of Radiometric dating techniques and their application in PDO. *Exploration Report* No. **336**. 11pp.

Spriggs, A. & Russell, J. 1997. Pb-Pb isotope dating of the Birba Formation, Oman. *In:* Geology. Barren Sequences Workshop. *Shell Exploration and Production News Letter,* Special Issue. 46-50.

Stanley, S.M. & Hardie, L.A. 1998. Secular oscillations in the carbonate mineralogy of reef-building and sediment-producing organisms driven by tectonically forced shifts in seawater chemistry. *Palaeogeography, Palaeoclimatology, Palaeoecology* **144**, 3-19.

Stoeser, D.B. & Camp, V.E. 1985. Pan-African microplate accretion of the Arabian Shield. *Geological Society of America Bulletin*, **96**, 817-836.

Török, Á. 1998. Controls on development o Mid-Triassic ramps: examples from southern Hungary. *In:* Wright, V.P. & Burchette,T.P.(eds) *Carbonate Ramps.* Geological Society, London, Special Publications, **149**, 339-367.

Torsvik, T.H., Lohmann, K.C. & Sturt, B.A. 1995. Vendian glaciations and their relation to the dispersal of Rodinia: Paleomagnetic constraints. *Geology*, **23 (8)**, 727-730.

Tschopp, R.H. 1967. The General Geology of Oman. *Proceedings of the 7th World Petroleum Congress, Mexico.* **2**, 231-242.

Tucker, M.E. 1981. *Sedimentary Petrology: An Introduction to the Origin of Sedimentary Rocks.* Blackwell Scientific Publications, 252pp.

Tucker, M.E. 1982. Precambrian dolomites: Petrographic and isotopic evidence that they differ from Phanerozoic dolomites. *Geology*, **10**, 7-12.

Tucker, M.E. 1983. Diagenesis, geochemistry and origin of a Precambrian dolomite: The Beck Spring Dolomite of eastern California. *Journal of Sedimentary Petrology,* **53**, 1097-1119.

Tucker, M.E. 1984. Calcitic, aragonite and mixed calcitic-aragonite ooids from the mid-Proterozoic Belt Supergroup, Montana. *Sedimentology,* **31**, 627-644.

Tucker, M.E. 1985. Calcitized aragonite ooids and cements from the Late Precambrian Biri Formation of Southern Norway. *Sedimentary Geology,* **43**, 67-84.

Tucker, M.E. 1986a. Formerly aragonitic limestones associated with tillites in the Late Proterozoic of Death Valley, California. *Journal of Sedimentary Petrology,* **56 (6)**, 818-830.

Tucker, M.E. 1986b. Carbon isotope excursions in Precambrian/Cambrian boundary beds, Morocco. *Nature,* **319 (6048)**, 48-50.

Tucker, M.E. 1989. Carbon isotopes and Precambrian-Cambrian boundary geology, South Australia: ocean basin formation, seawater chemistry and organic evolution. *Terra Nova* , **1**, 573-582.

Tucker, M.E. & Wright, V.P. 1990. *Carbonate Sedimentology*. Blackwell Scientific Publications, 467pp.

Tucker, M.E. 1991. Sequence stratigraphy of carbonate-evaporite basins: models and applications to the Upper Permian (Zechstein) of northeast Eangland and ajoining North Sea. *Journal of Geological Society, London,* **148**, 1019-1036.

Tucker, M.E. 1992. The Precambrian-Cambrian boundary: seawater chemistry, ocean circulation and nutrient supply in metazoan evolution, extinction and biomineralization. *Journal of the Geological Society, London,* **149**, 655-668.

Tucker, R.D., Krogh, T.E., Ross, R.J. Jr. and Williams, S.H. 1990. Time-scale calibration by high-precision U-Pb zircon dating of interstratified volcanic ashes in the Ordovician and Lower Silurian stratotypes of Britain. *Earth and Planetary Science Letters,* **100,** 51-58.

Tucker, R.D. & Mc Kerrow, W.S. 1995. Early Palaeozoic chronology: a review in light of new U-Pb zircon ages from Newfoundland and Britain. *Canadian Journal of Earth Sciences,* **32**, 368-379.

Turner, P. 1978. Diagenetic origin of Cambrian marine red beds: Caerfai Bay Shales, Dyfet, Wales. *Sedimentary Geology,* **24**, 269-281.

Van Wagoner, J.C., Posamentier, H.W., Mitchum, R.M. Jr., Vail, P.R., Sarg, J.F., Louth, T.S. & Hardenbol, J. 1988. An overview of the fundamentals of sequence stratigraphy. *In:* Wilgus *et al.* (eds.) Sea-Level Changes: An Integrated Approach. *SEPM Special Publication,* **42**, 39-46.

Vasconcelos, C. & McKenzie, J. 1997. Microbial mediation of modern dolomite precipitation and diagenesis under anoxic conditions (Lagoa Vermelha, Rio de Janeiro, Brazil. *Journal of Sedimentary Research,* **67**, 378-390.

Veevers, J.J. 1994. Pangea: Evolution of a supercontinent and its consequences for Earth's paleoclimate and sedimentary environments. *In:* G.D.Klein (ed.) *Pangea: Paleoclimate, Tectonics, and Sedimentation During Accretion, Zenith, and Break-up of a Supercontinent.* Bounder, Colorado, Geological Society of America Special Paper **288**.

Veizer, J., Lemieux, J., Jones, B., Gibling, M.R. & Savelle, J. 1978. Paleosalinity and dolomitization of a Lower Paleozoic carbonate sequence, Somerset and Prince of Wales Islands, Arctic Canada. *Canadian Journal of Earth Sciences*, **15**, 1448-1461.

Veizer, J. 1978. Secular Variations in the Composition of Sedimentary Carbonate Rocks, II. Fe, Mn, Ca, Mg, Si and Minor Constituents. *Precambrian Research*, **6**, 381-413.

Veizer, J. 1983. Chemical diagenesis of carbonates: Theory and application of trace element technique. *In:* Arthur, M.A. *et.al.*(eds.), *Stable Isotopes in Sedimentary Geology. SEPM Short Course* **No. 10.** 3/1-3/100.

Veizer, J., Plumb, K.A., Clayton, R.N., Hinton, R.W. & Grotzinger, J.P. 1992. Geochemistry of Precambrian carbonates: V, Late Paleoproterozoic seawater. *Geochimica et Cosmochimica Acta*, **56**, 2487-2501.

Walker, J.C.G. 1990. Precambrian evolution of the climate system. *Palaeogeography, Palaeoclimatology, Palaeoecology (Global and Planetary Change Section)*, **82**, 261-289.

Walker, R. G. 1982. Shelf and Shallow Marine Sands. *In*: Walker, R.G. (eds.) *Facies Models*, Geoscience Canada, Reprint Series **1**, 75-90.

West, I.M. 1964. Evaporite Diagenesis in the Lower Purbeck beds of Dorset. *Proc. Yorkshire Geol. Soc.*, **34**, 315-326.

Wilkinson, B.H., Buczynski, C. & Owen, R.M. 1984. Chemical control of carbonate phases: implications from upper Pennsylvanian calcite-aragonite ooids of southeastern Kansas. *Journal of Sedimentary Petrology,* **54**, 932-947.

Wright, V.P., Ries, A.C. & Munn, S.G. 1990. Intraplatformal basin-fill deposits from the Infracambrian Huqf Group, east Central Oman *From:* Robertson, A.H.F., Searle, M.P., & Ries, A.C. (eds.), *The Geology and Tectonics of the Oman Region.* Geological Society Special Publication **49**, 601-616.

Wursten, F., Flish, M., Michalski, I., LeMetour, J., Mercolli, I., Matthaus, U. & Peters, Tj. 1991. Basement of the Jebel Ja'lan (Sur area): *In:* Peters, Tj, Nicolas, A. & Coleman, R.G. (eds.) *Ophiolite Genesis and evolution of the oceanic lithosphere,* Muscat Ophiolite Conference, 613-626.

Zempolich, W.G., Wilkinson, B.H. & Lohmann, K.C. 1988. Diagenesis of Late Proterozoic carbonates: The Beck Spring Dolomite of Eastern California. *Journal of Sedimentary Petrology,* **58**, 656-672.

Appendix 1

Satellite images showing:
Mukhaibah dome,
Khufai Dome and
Buah dome in the Huqf area
Satellite image showing localities in the Oman Mountains

2211984 m 570000 m 578600 m

565144 m

2210000 m

2211220 m

2210000 m

2200000 m

2191848 m

2193400 m



565144 m 570000 m 578600 m

0 1 2 3 4 5 10 km

Projection:		UTM Zone 40
Spheroid:		Clarke 1880
Coordinate Datum:		PSD93
Height Datum:		PHD93
Origin	57°E	500 000 FE
	0°N	0 FN
Scale Factor:		0.9996
Semi Major Axis (a):		6378249.145m
Inverse Flattening (1/f):		293.46500

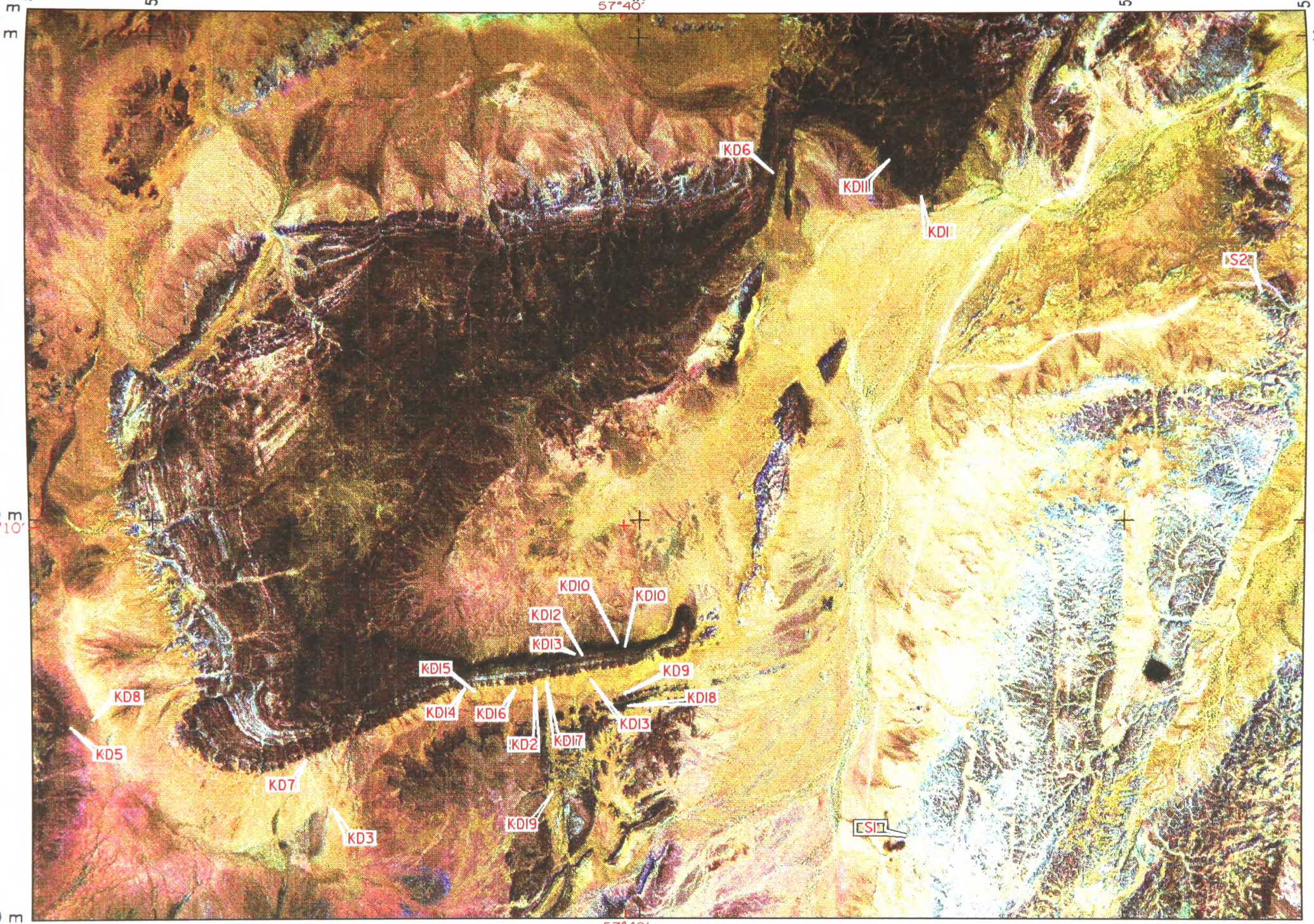
PETROLEUM DEVELOPMENT OMAN

MUSCAT | EXPLORATION DEPARTMENT

MUKHAIBAH DOME

LANDSAT TM IMAGE

Produced By: XTD Dept.	Date: 14-2-1999
Base Design: 00030471 .dgn	Drg. No.: 016192 (Int)



2240600 m
2240000 m
2230000 m
20°10′
2221700 m
55
560
57°40′
570
5800
5836
557500 m
560000 m
570000 m
580000 m
583687 m

0 1 2 3 4 5 10 km

Projection:		UTM Zone 40
Spheroid:		Clarke 1880
Coordinate Datum:		PSD93
Height Datum:		PHD93
Origin	57°E	500 000 FE
	0°N	0 FN
Scale Factor:		0.9996
Semi Major Axis (a):		6378249.145m
Inverse Flattening (1/f):		293.46500

PETROLEUM DEVELOPMENT OMAN

MUSCAT | EXPLORATION DEPARTMENT

KHUFAI DOME

LANDSAT TM & SPOT HRV IMAGE

Produced By: XTD Dept.	Date: 14–2–1999
Base Design: 00030472 dgn	Drg. No.: 016193 (Int)

567500 m

570000 m

575060 m

2256692 m

57~40'

BD6

BD5

BD3

BD4

BD7

BD2

20~20'

BD1

2250000 m

2246000 m

0 1 2 3 4 5 10 km

Projection:		UTM Zone 40
Spheroid:		Clarke 1880
Coordinate Datum:		PSD93
Height Datum:		PHD93
Origin	57°E	500 000 FE
	0°N	0 FN
Scale Factor:		0.9996
Semi Major Axis (a):		6378249.145m
Inverse Flattening (1/f):		293.46500

PETROLEUM DEVELOPMENT OMAN

MUSCAT | EXPLORATION DEPARTMENT

BUAH DOME

LANDSAT TM & SPOT HRV IMAGE

Produced By: XTD Dept.	Date: 14–2–1999
Base Design: 00030473 .dgn	Drg. No.: 016194 (Int)

530000 m 540000 m 550000 m 560000 m 570000 m 580000 m 584354 m

57°20′ 57°30′ 57°40′

2582510 m

23°20′

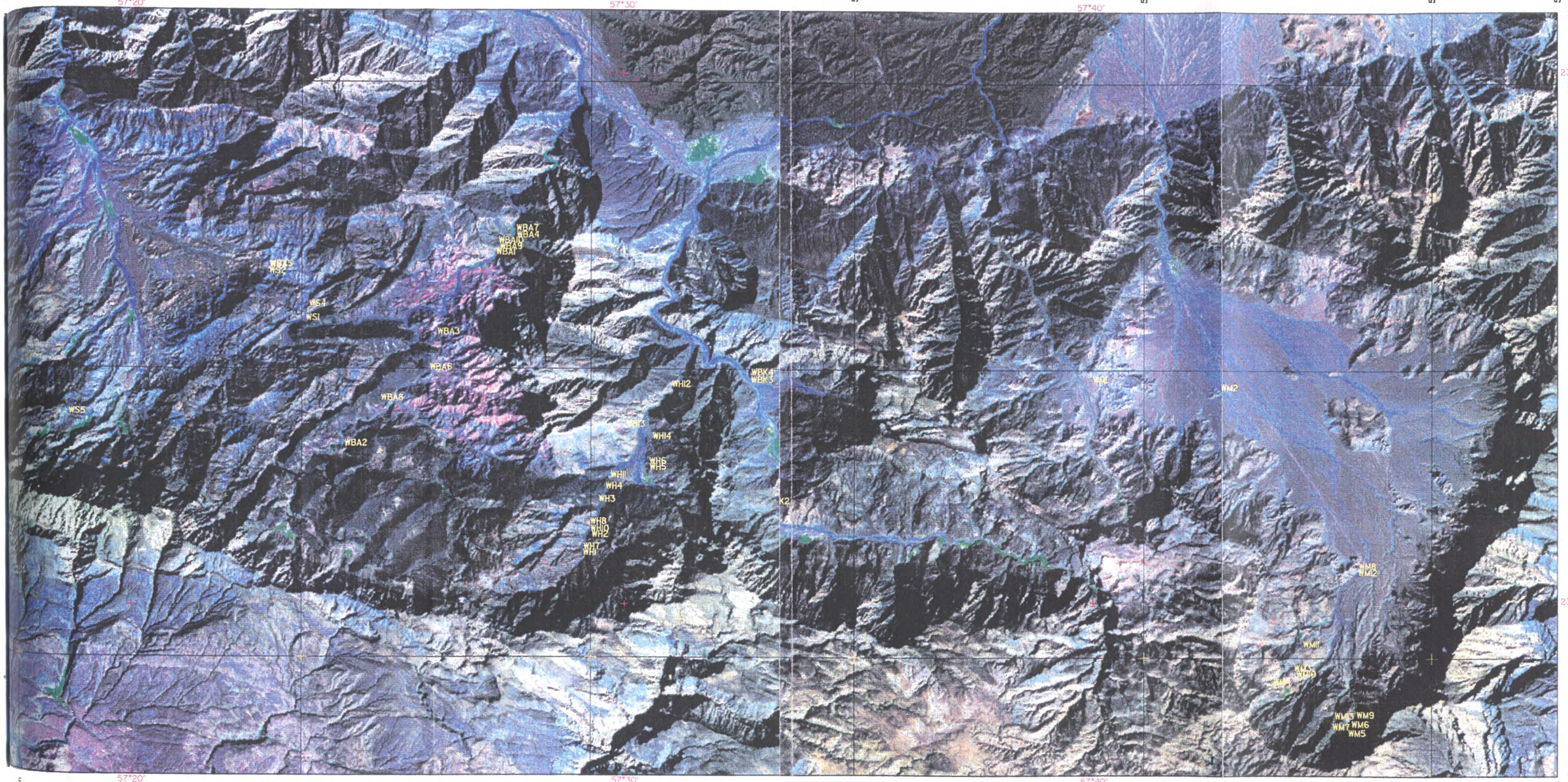
2580000 m

2570000 m

23°10′

2560000 m

2555896 m



0 1 2 3 4 5 10 km.

SCALE
1 : 100,000

Projection:		LTM Zone 40
Spheroid:		Clarke 1880
Coordinate Datum:		PSD93
Height Datum:		PHD93
Origin	57°E	500 000 FE
	0°N	0 FN
Scale Factor:		0.9996
Semi Major Axis (a):		6378249.145m
Inverse Flattening (1/f):		293.46500

PETROLEUM DEVELOPMENT OMAN

MUSCAT | EXPLORATION DEPARTMENT

NORTH OMAN MOUNTAINS LOCATION IMAGE

LANDSAT TM IMAGE

Produced By: XTD Dept.	Date: 21–02–1998
Base Design: 00024472 .dgn	Drg. No.: 011269 (Int)

Appendix 2

2.1 Zircon separation methods

2.2 U-Pb dating technique

2.1 ZIRCON SEPARATION

Powder samples gently in mortar and pestle to 500μm.
Set in beaker with (x3 times) acetic acid and 3 drops of detergent and leave for up to 3 days
Rinse out acetic acid with running distilled water to get rid of extra clay particles.
Agitate sample with distilled water in sonic bath to help separate clay, for up to 2 hours.
Remove liquid and leave grains in oven to dry, preferably over the weekend.
Then sieve to 300μm, use two sieves and save 100μm for dust.
Use fraction between 100-300μm and wash with water and sonic bath. Rinse off fine dust then repeat a few times until the water is clear.
Dry for a day or two.

In a fume cupboard
Flush funnel through with diodomethane (to clean)
Put sample in funnel and cover with diodomethane, stir well and again within 10 minutes, tapping funnel gently on occasion to move grains.
After 4 hours open the tap slowly and let heavies out, pouring half the mixture into very fine filter paper.
Wash with acetone.
Pour lights onto another filter paper and wash with acetone.
Leave to dry.

When dry, the zircon crystals were hand-picked under a binocular microscope to isolate specific morphological zircon types and to ensure high quality (i.e. low colour, no-overgrowths) crystals free of fractures and inclusions where possible. These were then forwarded by mail to Prof. R. Tucker for analysis.

2.2 U-PB DATING TECHNIQUE

Fractions were abraded using the technique described by Krogh (1982). The dissolution with 50% HF in Teflon bombs, and the chemical dissolution, follow essentially the technique of Krogh (1973). Major modifications include: (1) the use of a mixed $^{205}Pb/^{235}U$ spike; (2) the use of micro-columns with a 10 times lower volume than in the original design; and (3) the mass spectrometric analysis of U and Pb loaded together on the same filament. Blank corrections were <10 pg. for Pb and 0.2 pg. for U. Regression lines were calculated using the method developed by Ludwig (1980). Quoted errors represent 95% confidence level. Decay

constants are those of Jaffey *et al.* (1971) recommended by the I.U.F.S. (Steiger and Jäger 1977).

Appendix 3

Khufai Formation Logs:

Mukhaibah dome

Khufai dome

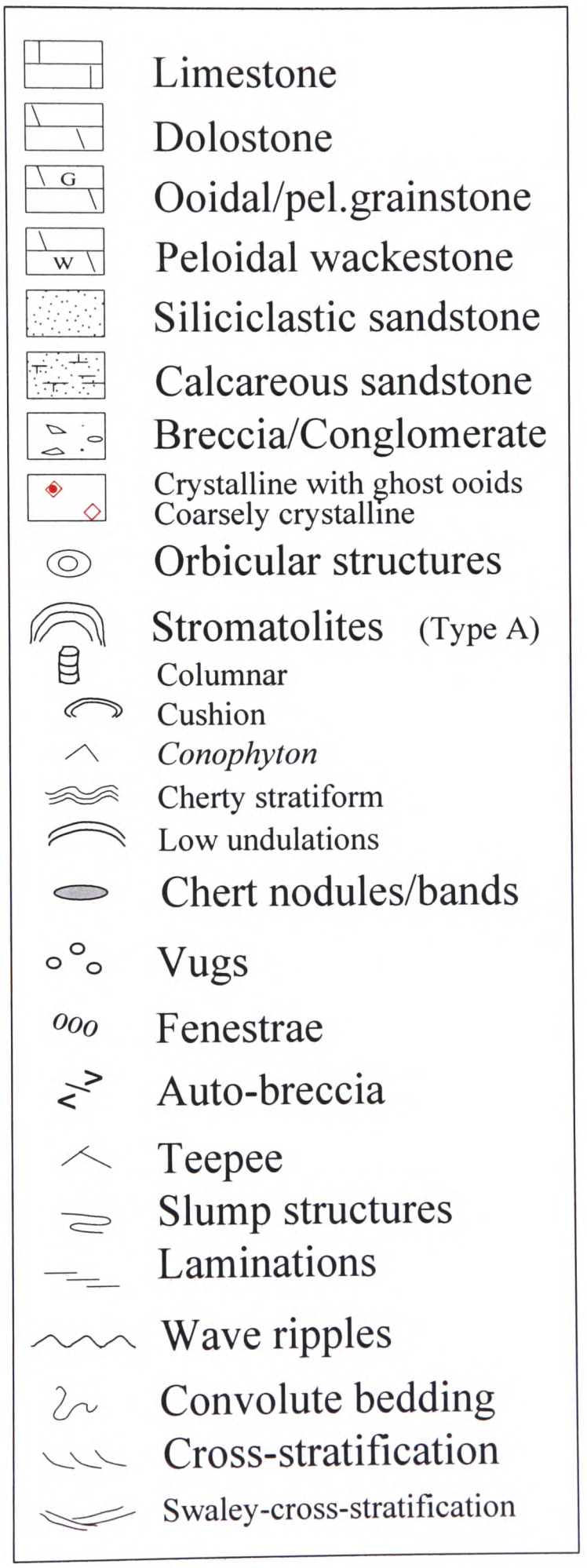
Buah dome

Wadi Hajir

Wadi Mistal (Hadash)

Ternary diagrams

Khufai Formation Key



Khufai Formation in Mukhaibah dome Locality Md 18 40Q 573485 UTM 2204582

Association A Fetid dolostones

Lithofacies	Metres	Lithology (m s f m c)	Geological points of note	Description	Environment Interpretation
A1	50			Chert nodules and dm scale bands with dolomitic cores.	
	48			Massive dolomite with bed partings m scale containing auto-breccia patches, faint laminations with chert nodules and bands up to dm scale. Bed contacts are undulating.	
	46			Chert laminated stromatolitic bedding surface.	
	44				Subtidal
	42		Dark grey	Neomorphosed dolospar with calcite veins	
			K3 26.1.96	Metre scale faintly laminated dolomite beds with undulating contacts.	
	40			Recessive bleached dolomite	
	38			Gy weathering dolomite containing low domal undulations with dispersed chert nodules, auto-breccia beds and faint laminations.	
	36	ooo			
	34	ooo		Rectangular mud clasts 1-2cm in diameter possibly after salt dissolution?	
	32			Massive fetid dolomite with bed partings m scale, containing auto-breccia patches, faint laminations and chert nodules and bands up to dm scale. Bed contacts are undulating.	
	30				
	28	ooo			
	26			Flaggy thin recessive beds cm scale with chert nodules	Subtidal
	24			Massive fetid dolomite with lenticular bk chert nodules and lenses. Faintly laminated with auto-breccia patches and possible fenestrae. Bed contacts are undulating.	
	22				
	20			Recessive auto-breccia beds with chert nodules.	
	18			Heavily veined recessive beds with chert	
	16	ooo	Dark grey	Grainy dolomite with domal bedding surface Fractured massive grey dolomite	
	14			Thin recessive beds a few cm thick heavily veined with calcite spar.	
	12	ooo	K2 26.1.96	Vuggy weathered massive dolomite beds 50cm thick	
	10			Fenestral domes; undulations have a few cm relief	
	8			Massive gy dolomite faintly laminated with cherts slightly undulating beds.	Subtidal
	6			Pellet grainstone with faint mm laminations contain planar chert bands and nodules bk-bn internally laminated Recessive vuggy bleached bed.	
	4			Neomorphosed vuggy dolospar, some vugs have rectilinear outlines possibly after evaporites	
	2		K1 26.1.96	Dk brown/grey weathering m scale beds of fetid dolomite with irregular to sub-spherical vugs and faint mm laminations.	
	0m			Gradational boundary with Masirah Bay Formation.	

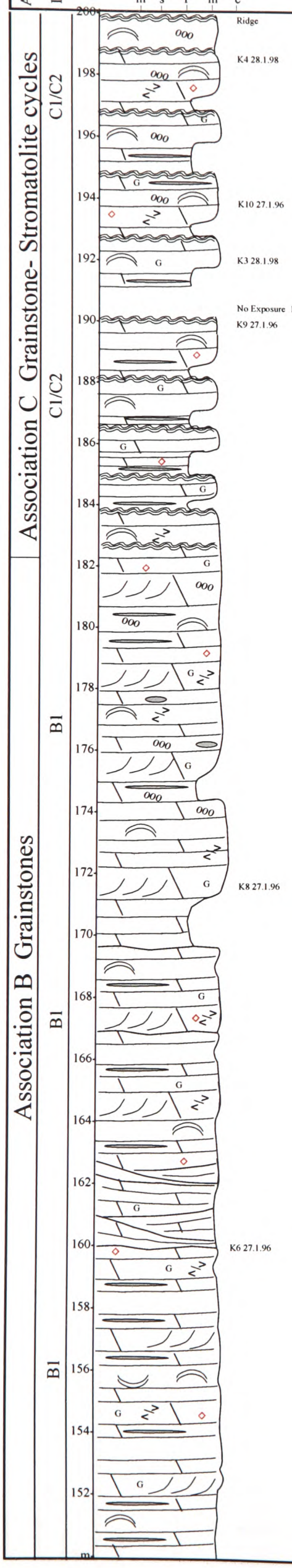
Khufai Formation in Mukhaibah dome Locality Md 18 40Q 573485 UTM 2204582

Association	Lithofacies	Metres	Lithology (m s f m c)	Geological points of note	Description	Environment Interpretation
Association A Fetid dolostones	A1	100			Thin 20cm scale beds of laminated dolomite, planar to undulating.	
		98		K1 27.1.96	Mm scale fine and coarse laminations some brecciated *in-situ* with calcite veins perpendicular to bedding	
		96			Beds of gr-bn dolomite with undulating laminations and low domes?, fenestrae and auto-breccia beds. Fenestrae are sub-spherical and partially occluded by later calcite.	
		94	G	K2 27.1.96	Intraclast grainstone neomorphosed to dolospar and dolomicrospar laminations with oomoldic porosity	
		92			Thin tabular beds recessive.	Subtidal
		90			Massive beds of gy-bn weathering dolomite with auto-brecciation and faint laminations are interbedded with minor undulating laminations.	
		88	G			
		86			Auto-breccia patches change laterally into coherent laminae Minor irregular fenestrae also occur.	
		84			Bleached poorly exposed cavernous dolomite	
		82	G		Bn weathering planar lam crinkle textured dolomite	
		80			No exposure 1m	
		78			Undulating laminations are extensively auto-brecciated with minor chert.	
		76	G	Top of Ridge	Neomorphosed dolomite with quartz veins.	
		74	G	K5 26.1.96		Subtidal
		72			Massive grey/brown 2-3m beds, prominent in outcrop. Laminations are undulating and faint with patches of chertified auto-breccia.	
		70			Undulating laminations with auto-breccia pockets.	
		68		K1 26.1.97	Thin finely laminated carbonate beds planar with tabular lenses - recessive in outcrop. Neomorphosed spar and micrite laminations slightly undulating with minor detrital fine-grained silts within micrite laminations	
		66	G			
		64			On bedding surface domes are preserved, metre diameter with 10-20 synoptic relief - interpreted as possible stromatolites. These occur in grainy dolomite with faint undulating laminations and auto-breccia pockets.	
		62				
		60	G		Thin 4-10cm flaggy beds which are recessive in outcrop	Subtidal
		58			Neomorphosed peloidal grainstone with micritic laminations Thin 1-2cm flaggy beds which are recessive in outcrop	
		56	G			
		54			No exposure for 1.5m Recessive thin flaggy auto-brecciated beds.	
		52	G	K4 26.1.96	Massive gy-bn dolomite with m scale partings and bk-bn chert nodules 1cm to 10 cm in size.	
		50			Recrystallized dolomite with micritic intraclasts	

Khufai Formation in Mukhaibah dome Locality Md 18 40Q 573485 UTM 2204582

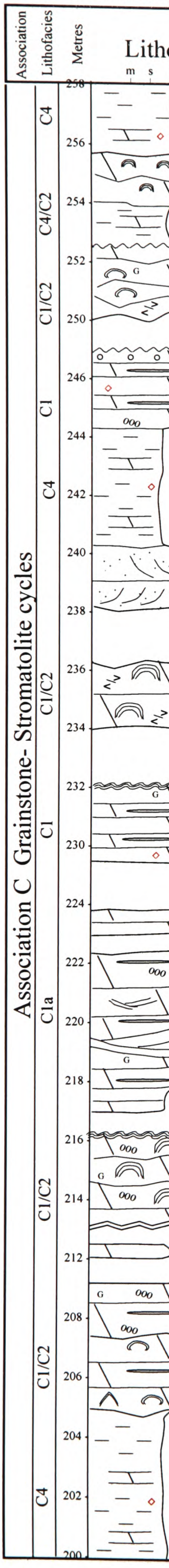
Association	Lithofacies	Metres	Lithology (m s f m c)	Geological points of notes	Description	Environment Interpretation
Association B Grainstones	B1	150			Intraclast/oncolithic grainstone partly neomorphosed with microquartz filled fractures.	
		148	K5 27.1.96 G		Low domal stromatolites with crinkle laminites within pale grey weathering intraclast grainstone beds. Chert stringers occur and are desert varnished brown. Some beds have a brecciated texture.	Shoal/ backshoal
		146	K2 27.1.98 G		Oncolithic/ooidal packstone within a micritic cement	
		144			Stromatolites with chert stringers.	
		142	G		Stromatolites which nucleated on cross-bedded ooidal/ peloidal grainstone have formed dm. scale domes.	
		140		Pale beds	There are dk bn lenses of coarse feldspathic quartz sandstone form channels within the ooidal grainstones. Concave upward dish structures occur in dm scale bands.	Shoal
		138	G			
		136	K1 27.1.98 G		Neomorphosed peloidal grainstone/packstone formed of inclusion-rich dolospar with vuggy intercrystalline porosity.	
		134	G			
		132			Flaggy recessive beds.	
		130	K3 26.1.97 K2 26.1.97		LSH stromatolites with 10-20cm synoptic relief above stratiform stromatolites within a cross-bedded grainstone. Stromatolite laminations formed of micrite and microspar. Intraclast/oncolithic grainstone partly neomorphosed into microspar with oomoldic porosity.	
		128			Poorly exposed tabular beds with vague cross-bedding.	
	B1	126			Pale gy weathering ooidal grainstone with cross-bedding. Cross-sets on a 50cm scale. The base and top of the bed contains concave up dish structures approximately. 10-20cm may be de-watering structures.	Subtidal/ Shoreface
		124	G		Chert laminated dolomites.	
	A1	122			Thin dm scale beds with local low-angle cross-lamination These beds are flaggy and some contain vugs with minor auto-breccia pockets.	
		120				
		118	G G		Massive pale gy/white weathering dolomitic grainstone. These m scale beds are locally cross-laminated and laterally have scour bases.	
	B1	116		Pale beds	Flaggy slightly recessive with low-angle cross-lamination.	
			K4 27.1.96		Neomorphosed peletoidal grainstone, w/numerous intergranular porosity occluded by microquartz.	
		114	G			
		112			Massive dolomite with auto-breccia pockets above thin (cm) beds of finely laminated chert dolomite.	
		110			Bleached vuggy recessive beds with possible evaporite moulds with thin cherty laminites above.	Subtidal
Association A Fetid dolostones		108		Dark beds	Obvious change in colour of dolomites from dk grey to pale grey in outcrop. The darker dolomites are fetid.	
	A1		K3 27.1.96		Dk gy laminated dolomite with 20cm scale beds which have slightly undulating contacts. These contain sporadic auto-breccia pockets throughout.	
		106				
		104			These beds are fetid.	
		102			Fine grained neomorphosed dolomite with mm vugs occluded by pale sparry carbonate. Vugs are formed by intracrystalline porosity. No primary textures preserved.	
		m				

Khufai Formation in Mukhaibah dome Locality Md 18 40Q 573485 UTM 2204582



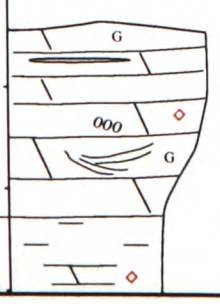
Geological points of note	Description	Environment Interpretation
	Ridge forming resistant beds of desert varnished cherty microbial laminites, locally containing stromatolite domes. These have rare desiccation cracks and fenestrae with minor auto-breccia beds. These beds overlay recessive thin cm-dm scale flaggy beds containing bk and wh lam chert. The latter are fine grained to porcelainous dolomitic grainstones.	Shoal/ backshoal
	Vuggy neomorphosed dolomite primary texture not preserved, vugs partly occluded by calcite containing relict evaporites.	
egg carton stromatolites	Some cycles contain wave ripples with wave ripple cross-lamination. There is also evidence for micro-swales and soft-sediment deformation.	
	Intraclast grains within undulating micritic stromatolite laminae w/evaporite relicts	
	Cycles: C2 Resistant cherty microbial laminites w/local stromatolites C1 Flaggy recessive porcelainous grainstone beds w/chert and vugs.	
	These cycles occur on less than a metre to decimetre scale and are persistent laterally.	
	Resistant ridge of undulating low domal and stratiform stromatolites with desert varnished chert mimicking the microbial lamination. Minor cherty auto-breccia pockets with vugs within oncolithic grainstones.	Shoal/ backshoal
	Intraclast packstone/boundstone with chalcedonic and microquartz in vugs.	
	Cherty laminations with auto-breccia pockets and fenestrae above thin dm beds of pale gy weathering micritic dolomite with flaky concave up dish structures. These undulating beds are slightly recessive and pinch and swell laterally.	
	Massive grey beds of stratiform stromatolitic laminations with chert nodules and bands. Grainstone towards the top, contacts are undulating.	
	Fine laminations with low angle cross-lamination and micro-scour structures Brown weathering chert rich beds (desert varnished) with structures that mimic the laminations.	
	Intraclast oncolithic grainstone/packstone with sparry cement and thin microquartz veins.	Shoal/ backshoal
Pale beds	Cherty stromatolites of dm. scale domes with cherty microbial laminites and minor concave-up dish structures on bedding surfaces.	
	Cross-bedded oncolithic grainstones with vugs.	
	Crinkle laminated stratiform and low domal stromatolites, replaced by chert form resistant pale grey weathering beds.	

Khufai Formation in Mukhaibah dome Locality Md 18 40Q 573485 UTM 2204582



Geological points of note	Description	Environment Interpretation
	Recessive muddy carbonates poorly exposed	
	Mm laminated pale grey beds of stromatolites which form laterally spaced domes with up to 10cm synoptic relief	Subtidal
	Recessive muddy carbonates poorly exposed	
	Ooidal grainstone with wave ripples on bedding surface also contain mm laminated domal cushion and conophyton stromatolites with 50cm synoptic relief. Microbially bound climbing wave ripples also occur. Teepee structures with auto-breccia	
	Wave ripples Micritic dolomite with scouring ooidal sand stringers and cherty lenses overlie vuggy dolomite.	
	Micritic dolomite with evaporite pseudomorphs replaced by sparry calcite with relict evaporites.	
	Recessive dm scale beds of red/blue weathering muddy carbonate with undulating contacts. Thin coarser lenses have scour bases.	Lagoonal
	Cross-bedded, coarse-grained, cream weathering carbonate cemented quartz arenite.	
	Mm laminated metre scale stromatolite domes which contain a brecciated core. These form a bioherm of 100's metres lateral extent.	Subtidal
	Auto-brecciated neomorphosed dolomite with calcite containing relict evaporites occluding vugs. Resistant ridge of desert varnished cherty laminations alternating with blue weathering grainstone beds. Bedded on a 10-30cm scale.	
	Recessive lime mudstone	
	Cavernous pale blue fine grained carbonates with spherical vugs partly occluded by calcite and desert varnished chert. Swaley-cross-beds. Desert varnished cherty limestones with undulating laminations.	Shoreface/ Subtidal
	Recessive red siliciclastic rich carbonate. Muddy carbonate with microquartz replacing dolomite	
Type A stromatolites	Desert varnished chert algal laminations. Mm laminated stromatolites metre scale domes which are vuggy and intercalated with ooidal/intraclast grainstones. These contain wave ripples.	
	Lime mudstone with faint laminations Pink grey weathering muddy carbonate with detrital quartz grains (20μm) and vuggy laminations.	
	Pale blue/grey vuggy beds of stratiform stromatolites and minor intraclast grainstones.	
Conophyton and cushion stromatolites	Mm laminae form egg-carton stromatolites with 15cm synoptic relief also conophyton structures up to 50cm synoptic relief. Cushion stromatolites also occur.	
	Pale weathering neomorphosed dolomite with primary texture not preserved. Micrite and microspar laminations with microquartz in vugs.	Lagoonal
	Recessive beds of lime mudstone pale grey weathering dm. scale beds. Planar with some minor chert bands.	

Khufai Formation in Mukhaibah dome Locality Md 18 40Q 573485 UTM 2204582

Association	Lithofacies	Metres	Lithology (m s f m c)	Geological points of note	Description	Environment Interpretation
E Oncolith	E1	262		Shuram Formation red siltstones and silty flat-pebble conglomerates disconformably overlie the ooidal-intraclast grainstones of the Khufai Formation.	White weathering ooidal-intraclast grainstone overlies the brown cherty laminites of the top Khufai cycle.	Shoal
	C4	260			Swaley cross-lamination within recrystallized grainstones.	
		258			Recessive flaggy pale lime-mud beds dm. scale.	Subtidal

Khufai Formation in Khufai dome

Locality KD10 40Q 569547 UTM 2227429

Association	Lithofacies	Metres	Lithology (m s f m c)	Geological points of note	Description	Environment Interpretation
Association A Fetid dolostones	A1	50			Chert nodules and bands with minor auto-breccia beds within laminated dolomite.	
		48			Orbicular structures replace laminated dolomites. laminated dolomites.	Subtidal
		46		K1 21.1.98	Laminoid vugs and auto-brecciated beds within mm laminated dolomite.	
		44			Orbicular structures up to 30cm diameter form laterally from faint laminations. These concentrically laminated structures generally 1-10cm in diameter occur within a sparry calcite matrix and are associated with zebroic dolomite.	
		42				
		40			Buff coloured dolomite with laminoid fenestrae? which are at an angle to the bedding. Auto-brecciation is extensive with porcelainous laminae broken and moved in situ.	
		38				
		36	G		Massive brown grainstone with faint laminations.	Subtidal
		34			Mm laminations within dolomite with auto-breccia pockets and laminoid fenestrae dm scale - fenestrae are partly occluded with sparry calcite.	
		32		K2 21.1.98		
		30	G		Laminations are locally undulating and laterally down-cut into underlying laminations.	
		28			Faint mm laminations in dolomitic grainstone with minor auto-brecciated beds.	Subtidal
		26				
		24			Faintly laminated dolomite within undulating beds, with laminoid fenestrae and white chert nodules. Fenestral beds tend to be recessive.	
		22				
		20	G		Minor auto-breccia pockets in structureless grainy dolomite.	
		18	G		Undulating mm laminations with minor breccia bands and chert nodules.	
		16			Recessive unit of thinly bedded dolomite, beds are nodular to undulating.	
		14	G		2-3 m massive beds of grainy brown dolomite with faint lamination and zebroic vugs. Laterally these contain slump folds and vague cross-lamination. Thin chert stringers.	Subtidal
		12	G			
		10			Brown weathering dolomitic grainstone with coarse and fine banding cm scale, beds 15cm scale. No vugs. Chert nodules and stratiform bands. Some calcite veins.	
		8				
		6			Sub-spherical vugs up to 5mm in diameter partly occluded by sparry calcite within mildly fetid dolomite. Chert nodules and stratiform chert bands also occur.	
		4		K1 24.1.97		
		2			Basal Khufai is cherty dolomite, 50cm beds, conformably overlying silty carbonates of the underlying Masirah Bay Formation.	
		0m				

Khufai Formation in Khufai dome Locality KD10 40Q 569547 UTM 2227429

Association	Lithofacies	Metres	Lithology (m s f m c)	Geological points of note	Description	Environment Interpretation
Association B Grainstones	B1	100–98	G		Desert varnished grainy dolomite with undulating laminations.	
		98–96	ooo G		Slightly leached dolomite with laminoid fenestrae Grey dolomites with graded beds on a 2cm scale.	
		96–94	G			
		94–92	G			
		92–90	G	Top of ridge	Faintly laminated grey/brown weathering grainstone with porcelainous appearance. Beds on a 20-30cm scale. Minor slump-folds locally developed. Some low-angle swaley cross-lamination.	Shoal
		90–88	G G			
		88–86	G	Slump- fold palaeoflow to NW (292)		
		86–84	G		Grey beds, dm scale grainstones with faint lamination and chert nodules	
		84–82	G		Locally developed low-angle x-lamination with scour structures and isoclinal slump-folds locally developed.	
		82–80	G			
		80–78	G		White weathering cavernous limestone (de-dolomitized dolomite) with pseudo-nodular structures and auto-brecciation.	
		78–76	G	Forms cliff overlooking the core of the Khufai anticline.	Pale grey weathering cross-bedded siliceous grainstone. Thin 20cm bed of red quartz arenite.	
Association A Fetid dolostones	A1	76–74	ooo		Brown weathering finely laminated dolomite with auto-breccia pockets and fenestrae.	Subtidal
		74–72	ooo			
		72–70	ooo			
		70–68	ooo		Brown weathering finely laminated dolomite with auto-breccia pockets and laminoid vugs. Some chert nodules.	
		68–66	ooo	K3 21.1.98		
		66–64	ooo			
		64–62	ooo		Mm laminations undulating with auto-brecciated pockets and laminoid vugs, laterally contain Orbicular structures. White chert nodules throughout.	
		62–60	ooo			
		60–58				
		58–56	ooo		Brown weathering dolomite with vugs which are partly occluded by calcite.	
		56–54	ooo			
		54–52	ooo		Undulating laminations with laminoid fenestrae laterally replaced by orbicular structures within a calcite matrix. Some spherical chert nodules.	
		52–50				

Khufai Formation in Khufai dome Locality KD10 40Q 569547 UTM 2227429

Association C Grainstones -Stromatolites cycles

Lithofacies	Metre	Lithology (m s f m c)	Geological Points of note	Description	Environment Interpretation
C1	176			Desert varnished chert microbial laminites, forming undulating crinkle laminations.	
	174		K12 23.1.96	Vuggy peloidal grainstones which fine up on mm scale with micritic caps. Vugs are sub-spherical and occur along laminae	Intratidal
C1a	172			Recessive thinly bedded dolomite	
	170		K13 23.1.96	Brown weathering cherty bands dm scale are undulating to domal	
	168			Peloidal grainstone with undulating microquartz laminations	Lagoonal
	166			Thinly bedded pale altered dolomite forms recessive unit partly covered by scree.	
C1	164		K14 23.1.96	Intraclast grainstone with micritic laminations which are brecciated . Vugs occluded by sparry calcite.	
	162		K15 23.1.96	Undulating stromatolitic dolomite with auto-breccia pockets above laminated chert microbial dolomite with fenestrae. Chert bands dm scale.	Intratidal
	160			Chalcedonic chert and megaquartz replaces stromatolitic dolomitic laminations which are overlain by neomorphosed ooidal/intraclast grainstone w/geopetal void fill.	
	158			Fenestral faintly laminated dolomite	
C1a	156		K16 23.1.96	Thinly bedded recessive altered dolomite with chert bands and minor teepee structures.	
	154			Fining-up pellet laminations interbedded with micrite sub-cm scale beds. Micro-scours and soft sediment deformation. Chalcedonic quartz nodules.	Lagoonal
C1	152			Desert varnished chert which mimics microbial/ stromatolitic laminations forms resistant cap to altered recessive unit.	
	150			Recessive units of pale altered dolomite, chalky appearance with minor teepee structures.	
C1a	148		K17 23.1.96	Cherty stromatolitic laminations, desert varnished to dark brown forms resistant ridge.	
	146			Recessive pale grey weathering flaggy dolomite contains chert bands 10cm scale.	
	144			Chalky white beds,recessive in outcrop with laterally spaced metre-scale teepee structures and chert bands.	Lagoonal
C1	142				
	140			Brown weathering grainstone with low-angle cross-lamination and chert beds.	
	138				Shoal
	136			Heavily altered de-dolomitized limestone with chert bands very vuggy.	
C1a	134				Lagoonal
	132			Faintly laminated dolomite with white chert bands 20cm thick with original parallel lamination, irregular boundaries.	
	130			Lensoidal chert bands dm scale in dolomite	
			No exposure 27m peneplained top of dome		
	m			Massive grainy dolomite overlain by peneplaination scree, that is all desert varnished.	Shoal

Khufai Formation in Khufai dome

Locality KD10 40Q 569547 UTM 2227429

Association C Grainstone-Stromatolite cycles

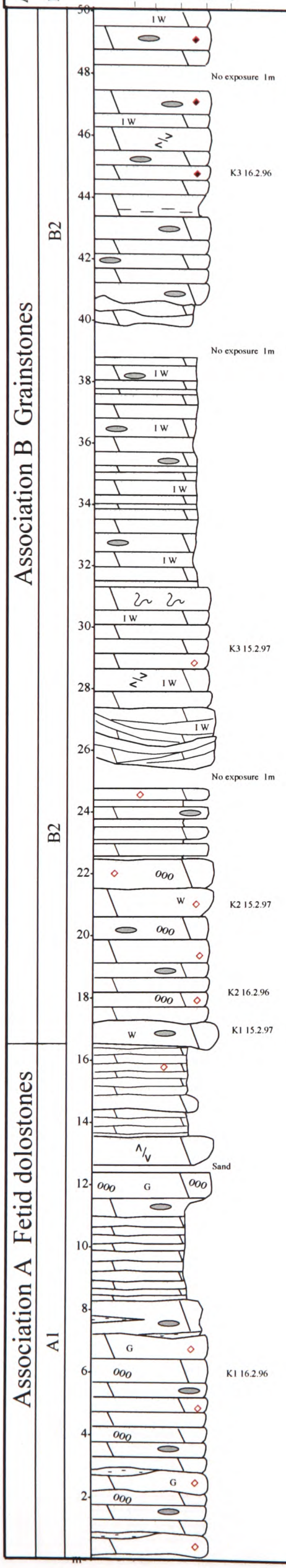
Lithofacies	Metre	Lithology (m s f m c)	Geological points of note	Description	Environment Interpretation
C1a/C2	226			Desert varnished cherty microbial laminites with lateral development of teepee structures and cushion stromatolites. Neomorphosed microspar and micrite laminations	
	224		K6 23.1.96 K6 22.1.98		
	222	1 G	K1 22.1.98 K7 23.1.96	Undulating beds with intraclast. Stromatolites replaced by cherts. Neomorphosed ooidal/intraclast grainstone with sparry calcite occluding oomoldic and intergranular porosity.	Intratidal
C3	220			Pale-grey flaggy porcelainous dolomites above recessive auto-breccia beds. Some contain intraclast conglomerate beds.	
	218	G	K4 22.1.98		
			K5 22.1.98		
C3	216		K3 22.1.98	Cherty microbial laminites with teepee structures and brecciated contorted cap. Metre scale beds of fenestral porcelainous faintly laminated dolomite with minor chert. Thin recessive siliciclastic beds form base of cycle.	
	214	G			
	212	G		Stromatolitic cap partly eroded Cycle C2: Microbial laminites with stromatolites and teepee structures above Cycle C1: Flaggy porcelainous grainstones with chert and vugs Cycle C3: Recessive convoluted/brecciated beds with intraclast lenses.	
C1a/C2	210	1 G ooo			
C3	208		K8 23.1.96 K1 22.1.98	Intraclast grainstone with micrite cement and minor detrital quartz, feldspar and mica.	Intratidal
	206				
	204	ooo		Chert microbial laminated dolomite form resistant ridges with minor teepee structures Flaggy porcelainous dolomite with minor auto-breccia pockets and chert bands.	
	202	ooo G	K9 23.1.96	Micrite and intraclast laminations alternate on mm to cm scale	
	200	G			
		ooo		Recessive thinly bedded auto-brecciated dolomite with chert nodules and bands.	
	198				
		ooo		Flat topped domal stromatolites laterally spaced hemispheroids with 50cm synoptic relief.	
C1a/C2	196				
	194		K10 23.1.96	Stromatolite laminations formed of 3-5mm micrite and microspar laminations, fenestrae occluded by sparry calcite which contains relict evaporites.	Intratidal
	192			Up to dm scale planar chert bands	
	190			Pale weathering laminated chert rich beds with vague hints of cross-lamination.	
	188		Stromatolite elongation 256 K11 23.1.96	Stromatolite domes with 20cm synoptic relief are elongate with current direction. These become undulating to planar chert laminations laterally. Microbial laminations are interbedded with pockets of auto-breccia and chert bands.	
	186				
	184			Recessive unit of thin flaggy dolomite	
				Recrystallized dolomite with intraclast laminations	
	182	ooo		Resistant ridge of chert microbial dolomite with brown weathering (desert varnish) containing auto-breccia pockets.	Subtidal
	180	ooo			
C1b	178	ooo			
	m			Recessive brecciated dolomite	

Khufai Formation in Khufai dome Locality KD10 40Q 569547 UTM 2227429

Association	Lithofacies	Metre	Lithology (m s f m c)	Geological points of note	Description	Environment Interpretation
C Grainstone-Stromatolite cycles	Association E Oncolith	E1				
					Contact with the overlying Shuram Formation not observed	
		250	I/O G	K16 22.1.98 K2 24.1.97	Flaggy beds of porcelainous grainstone, pale grey weathering which are rich in silica. These beds are generally less than 50cm thick and are planar. Low-angle cross lamination in oncolithic grainstones.	Subtidal
		248	I/O G	K1 23.1.96	Ooidal-intraclast grainstone laminations mm scale alternate with microspar laminations mm scale	
				K15 22.1.98	Stromatolites with 20cm synoptic relief.	
		246	I/O G	K14 22.1.98	Contorted brecciated beds.	Intratidal
		244	G	K12 22.1.98	Pale flaggy grainstone with chert rich beds and solitary stromatolites. Some low-angle cross-lamination.	Subtidal
		242		K13 22.1.98	Microquartz rich laminations alternate with recrystallized. microdolospar.	
		240	G	K2 23.1.96	Porcelainous grainstone beds thicken up from 10cm to 40cm.	
		238		K11 22.1.98 Stromatolite elongation toward NW.	Stromatolites with elongation toward NW are erosively overlain by grainstones.	
	C1a/C2	236	ooo I/O G		Cycles of chert microbial/stromatolitic dolomite with teepee structures and fenestrae above flaggy porcelainous grainstone beds with chert bands and lenses overlying recessive auto-breccia beds.	Intratidal
		234		K10 22.1.98		
	D1			K3 23.1.96 K2 22.1.98	Medium grained,well sorted quartz arenite with carbonate cement forms recessive unit.	
		232		K8 22.1.98		
		230	I/O G	K4 23.1.96	Micritic laminations or intraclasts are partially replaced by microquartz and sparry calcite. Vugs possibly after evaporites	Intratidal
	C1a/C2	228		K7 22.1.98	Chert microbial laminations with occasional teepee structures and stromatolite domes overlying flaggy porcelainous grainstones beds, and recessive cross-bedded siliciclastics.	
		m		K5 23.1.96	Intraclast/oncolithic grainstone with sparry calcite occluding oomoldic and intragranular porosity.	

Khufai Formation in Buah dome

Locality Bd1 40Q 571324 UTM 2250303



Geological points of note	Description	Environment Interpretation
	Flaggy beds of porcelainous brown dolomite with sand lenses and chert nodules interbedded with fining up intraclast wackestone beds.	
	Neomorphosed dolospar with relict micritic intraclasts.	Subtidal
	Blocky dolomite beds 50cm to 100cm scale with auto-breccia pockets and undulating laminations may be slump structures.	
	Micritic dolomite with calcite veins and silt patches, faint laminations with auto-breccia and undulating beds.	
	5mm chert nodules and 10cm chert bands.	
	Siliceous intraclast grainstone, cm to dm scale beds with some evidence for fining-up. Grainy chalcedonic quartz forms circular nodules 5mm in size the weather-out on bedding surfaces.	Subtidal
	Brown/grey weathering siliceous intraclast wackestone beds with undulating fine and coarse laminations which are convoluted laterally and alternate with cm. scale muddy dolomite beds.	
	Swaley and low-angle x-lamination within wackestone form downcutting channels, chert nodules.	Subtidal
	.	
	Alternating cm scale beds of muddy (fetid) dolomite and grainstone.	
	Vuggy dolomicrospar with micritic intraclasts. Vugs partly occluded by calcite. Some chalcedonic quartz nodules.	
	Dm scale cherty micritic dolomite with vugs.	
	Recrystallised. microspar with lath shaped vugs possibly after evaporites.	
	Grainy dolomite with minor chert and sand lenses.	
	Thin bedded recrystallized dolomite, contains fining-up conglomerate beds and laminated beds. Pale grey sandier beds occur with down-cutting lower contacts forming channels.	Subtidal
	Grey dolomite with spheroidal vugs above cm. scale light and dark beds.	
	Thin planar laminated carbonate poorly exposed	
	Vuggy beds of muddy dolomite interfinger with silt, irregular lower contacts.	
	Grey dolomite with faint laminations containing spheroidal vugs and chert bands. Ferruginous nodules on bedding surface.	Subtidal
	Neomorphosed dolomicrospar with vugs partly occluded by sparry calcite.	
	Dk grey/blue carbonate interfingers with siltstones which pinch and swell laterally. Dolomite occurs in cm to dm scale beds.	
	Recessive Abu Mahara silts partly obscured by sand	

Khufai Formation in Buah dome

Locality Bd1 UTM 571324 40Q 2250303

Facies Association B Grainstones

Association	Lithofacies	Metres	Lithology (m s f m c)	Geological points of note	Description	Environment Interpretation
	B2a	104	No exposure 1.8m		Micritic cap to conglomeratic intraclast bed.	Subtidal
		102	No exposure 1m			
	B2a/b	100	1 W		Recrystallized dolospar with relict ooids/peloids alternate with micritic lamination. Chalcedonic chert nodules.	
		98	1 W		Siliceous flaggy grainstone beds with dark grey micritic dolomite, planar thinly bedded with intermittent conglomeratic beds dm scale.	
		96	1 W			
		94	No exposure 50cm			
	B2	92	W		Intraclast conglomerate bed with scour base	
		90	1 W	K6 15.2.97	Thin flaggy beds planar of dark micritic dolomite alternating with siliceous grainstone beds. These are recessive and poorly exposed.	Subtidal
		88			Recrystallized dolospar with relict ooids/peloids alternate with micritic lamination. Chalcedonic chert nodules.	
	B2a	86			Siliceous grainstone with thin intraclast conglomerate beds and chert nodules.	
		84	No exposure 1m			
		82			Planar mm laminations of siliceous grainy dolomite (fetid)	
		80	1 W	K8 16.2.96	Mixed med/coarse quartz sand with micritic clasts within a microspar cement.	
					Siliceous grainstone conglomerate	
		78			Irregular laminations of dark grey micritic dolomite and white sparry calcite forming zebra rock.	Subtidal
		76	1 W		Intraclast wackestone breccia with fining-up beds on a dm scale.	
		74	1 W	K7 16.2.96	Micritic and peloidal intraclast wackestone with microspar cement.	
					Thin cm scale beds of intraclast ws and micritic dolomite	
		72		K5 15.2.97	Intraclast wackestone with cherts	
	B2		1 W		Vertical spar and micrite lamina (zebra rock)	
		70	1 W		Recrystallized spar with relict peloids, micritic intraclasts and chalcedonic quartz nodules.	
		68		K6 16.2.96	Flaggy dark grey dolomite of planar dm scale wackestone beds some of which fine up. Chert bands occur and one unit is formed of micritic dolomite and calcite laminations (dark grey and white) that are perpendicular to bedding (zebra rock).	Subtidal
		66	base of ridge			
			No exposure 6m			
		60		K5 16.2.96	Intramicrite - poorly sorted angular to sub-rounded micritic clasts within a microspar matrix.	
			1 W	K4 16.2.96	Micritic siliceous dolomite alternating with intraclast wackestone beds with chert nodules.	
		58			Recrystallized sparry carbonate with micritic intraclasts, relict ooids within chert band.	
		56		K4 15.2.97	Resistant wackestone beds with chert nodules above recessive silty carbonates	
	B2	54			Intraclast beds 10-50cm thick, pale intraclasts up to a few mm in diameter with stratiform chert and circular chert nodules.	Subtidal
		52	1 W		Intraclast wackestone with circular white chert nodules.	
		m				

Khufai Formation in Buah dome Locality Bd1 40Q 571324 UTM 2250303

Association	Lithofacies	Metres	Lithology (m s f m c)	Geological points of note	Description	Environment Interpretation
Association B Grainstones | Facies Association D Calcareous quartz-arenite	B2	311				
			TW		Grey silty calcarenites with climbing wave-ripples lamination 1-5mm above recessive thin brown quartz sand intercalations.	Subtidal
		309	K10 16.2.96			
	B2a		9m poorly exposed silty carbonates			
		299	K8 15.2.97		Detrital quartz sand and micritic clasts within a sparry carbonate cement	
			4.5m poorly exposed silty carbonates		Pale yellow medium grained quartz arenite, with soft-sediment deformation structures	
	B2b	294	TW		Wackestone with dolomite clasts above dm scale conglomeratic beds which alternate with cherty micritic beds (cm scale) very planar. Conglomeratic erosive bases downcut mudstone beds.	
		292				
	B2		No exposure 4m			
			No exposure 4m			
		282			Grey recrystallized fine-grained limestone beds dm scale with planar contacts.	
		280				
					Conglomeratic quartz-arenite with scour contacts and pebble sized carbonate clasts normally graded on a 40cm scale.	Subtidal
		278				
	D1	276			Low-angle x-stratification in sandstone which contain up to boulder size carbonate clasts.	
					Normally graded, matrix supported conglomerate	
		274	K10 16.2.96		50% micritic intraclasts (250μm) and 50% sub-angular quartz and feldspar grains (250-500μm) within a micro-spar matrix	
		272			Cream-grey medium and fine quartz-arenite with caries weathering.	
		270			Undulating beds of coarse and medium quartz-arenite in 10-30cm scale beds	
		268		Palaeoflow toward 320°	Silty crinkle laminated limestone	
					Fining up sandstone beds with very planar contacts	
		266		Palaeoflow toward 320°		
			ooo		Symmetrical wave ripples with ripple x-lamination above massive calcareous quartz-arenite bed.	Subtidal
		264				
			ooo		Thin flaggy grey weathering carbonate cemented quartz-arenite	
		262				
		260	ooo		More weathered, recessive vuggy sands.	
		258			More blocky sandstone with silt partings roughly fine-up on a cm scale with swaley lamination.	
	D1	256			Creamy yellow weathering well-sorted quartz sandstone with carbonate cement. These contain low-angle, tabular, x-stratification with erosional basal contacts.	
		254				
			No exposure 130m			
Association B Grainstones	B2a/b	122	TW		Grainy dolomite beds 10-30cm scale with thin (fining up) conglomeratic intervals with irregular lower contacts above pale silty carbonates. Tabular chert bands occur.	Subtidal
			K9 16.2.96			
		120	TW		Recrystallized dolospar with relict ooids, vuggy intercrystalline porosity	
		118	No exposure 1m			
			TW K7 15.2.97		Cherty dolomicrospar	
	B2	116	TW		Intraclast wackestone with minor conglomeratic beds and chert nodules	
		114				
			No exposure 8m			
		m	TW		Conglomeratic bed fines-up to wackestone	

Khufai Formation in Buah dome Locality Bd1 40Q 571324 UTM 2250303

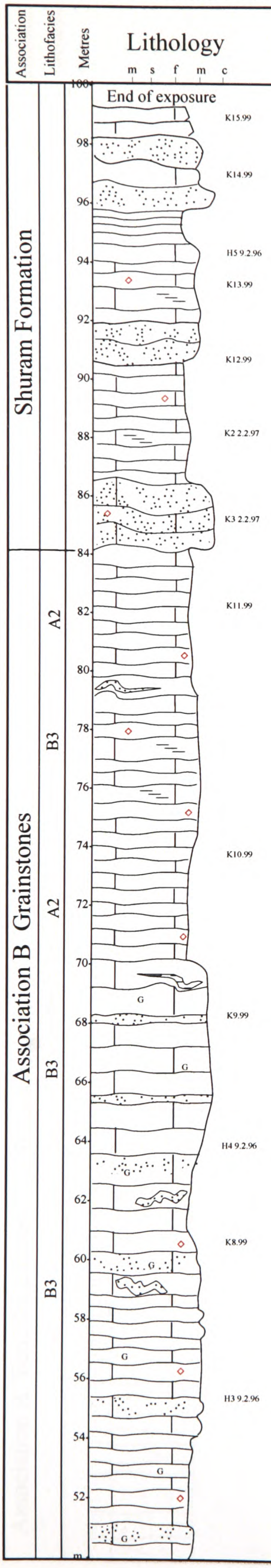
Association	Lithofacies	Metres	Lithology (m s f m c)	Geological points of note	Description	Environment Interpretation
Association E Oncolithic grainstones	E1		End of Khufai exposure contact with Shuram Formation not observed			
		352	K5 16.2.97		Pale grey weathering ooidal-intraclast-grainstone with low-angle cross-lamination.	Subtidal
			K2 10.1.97		Ooidal-intraclast grainstone with fringe cement contains detrital quartz and feldspar that form laminae	
		350			Wave ripples on bedding surface of cross-bedded quartz-arenite with carbonate cement	
		348		Palaeoflow toward 336°	Intraclast grainstone with lath shaped intraclasts forms a micro-conglomerate	
	E1a		K4 16.2.97		Grey weathering dolomite with fenestrae (partially filled with calcite) and with auto-breccia pockets.	Intertidal
		346	K1 16.2.97		Porcelainous planar bedded dolomitized peloidal, ooidal grainstone with chert.	
	E2	344	K3 16.2.97		Pale medium-coarse quartz arenite with carbonate cement containing relict evaporites.	Subtidal
		342	K10 15.2.97		Ooidal grainstone pale creamy white weathering with low-angle x-stratification.	
	D1	340		Palaeoflow toward 290°	Climbing wave-ripples in pale grey swaley-cross- bedded quartz-arenite.	
		338	No exposure 5m		Recessive thin flaggy beds of brown weathering silty dolomite.	
Quartz-arenites/Wackestones	D1	331			Vuggy pale grey weathering hybrid quartz arenite/ dolomitic grainstone in dm scale beds with chert nodules and bands.	
		329	K2 16.2.97	Dol		
		327			Recessive laminated limestones alternate with well-sorted medium-coarse quartz-arenites, dm scale beds.	Subtidal
		325	No exposure 2m			
	D1	323		Lst	Limestone beds (2-10cm) with quartz-arenite lenses that pinch out laterally, detrital quartz sand decreases upward.	
		321			Conglomerate channels within light and dark laminites	
	B2/B2a	319				
	B2a	317		Dol	Light and dark planar laminated (mm-cm scale) limestone. 20-30cm conglomerate beds with angular dolomite clasts up to 1 cm	
	B2b	315			Dark grey intraclast grainstone with minor conglomeratic beds with micritic dolomite clasts.	
	B2b	313	K9 15.2.97	PLATE K3-D	Grey calcareous quartz-arenite with scour base Mm to cm scale laminates of dark grey and white limestone planar bedded with minor quartz-arenite intercalations forming channel-type lenses.	Lagoonal

Khufai Formation in Wadi Hajir Locality WH 11 Q40 550555 UTM 2565838

Association	Lithofacies	Metres	Lithology (m s f m c)	Geological points of note	Description	Environment Interpretation
Association B Grainstones	B3	50		K7. 99	Beds contain stylolaminites and weathered out pyrite grains.	
		48				
		46			Sandy beds dm scale alternate with black fetid crystalline lime mudstone.	
		44		H2 9.2.96		
		42			Undulating beds with weathered out pyrite	Subtidal
		40		K6. 99	Grainstone beds 20cm scale with faintly laminated black crystalline limestone.	
		38			Wadi floor Coarse sandy beds with scour bases.	
		36				
		34				
		32		K5. 99	Quartz sand lenses within dm bedded limestone.	
		30		H1 9.2.96	Dm scale grainy limestone alternate with mm laminated black fetid limestone. Some of the grainstone beds coarsen up.	
Association A Fetid Limestones	A2	28		K2 6.2.97		
		26		K4. 99	Beds are 20-30cm scale - intraclasts at base fine-up to mudstones	
		24				
		22			Convoluted lenses of grainstone within the fetid crystalline limestone indicates soft sediment deformation.	
		20		K3. 99		
		18				
		16			Intraclast grainstone beds with scour bases, fine up while crystalline black limestone beds have undulating contacts, bed thickness increases to 10-40cm.	
	A2	14				
		12			Intraclast grainstone of micritic intraclasts in a partly recrystallized matrix. Rare detrital quartz and mica grains also occur.	
		10		K1 2.2.97		Subtidal
		8			Grainy limestone beds fine up on a decimetre scale and are interbedded with black crystalline limestone.	
		6		K2. 99		
		4			Sand lenses pinch out laterally and have irregular lower contacts.	
		2			Black fetid crystalline limestone. beds 15-20cm with weathered out pyrite grains.	
		0m		K1. 99	Transitional with underlying Masirah Bay Formation	

Khufai Formation in Wadi Hajir

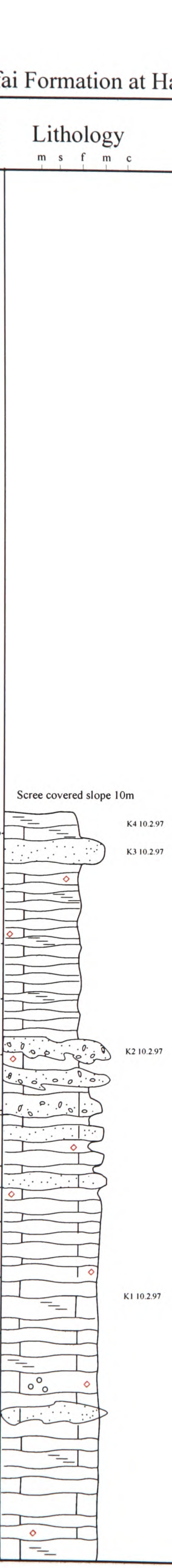
Locality WH 11 Q40 550555 UTM 2565838



Geological points of note	Description	Environment Interpretation
	End of exposure.	
	Sandstone and limestone interbeds on a 20-30cm scale. Sandstones pinch and swell laterally	
	Mud clasts in massive black fetid limestone.	
	Thin 2-5cm scale beds with shale partings which are weathered out.	Subtidal
	Intraclast grainstone with pale dolomitic clasts, quartz sand and mica.	
Wave ripples	Light and dark grey laminated limestone planar with possible wave ripples	
	Dark laminations are recrystallized intraclast grainstone with relict grains preserved while pale bands contain detrital and authigenic quartz.	
	Coarse conglomeratic grainstone with scour bases possible storm beds which alternate with fetid recrystallized limestone containing mud clasts.	
	Coarse intraclast grainstone with quartz and feldspar. Intraclasts of ooids and micrite within a recrystallized matrix. Calcite veins rich in iron oxides.	
	Massive black crystalline limestone with calcite veining.	
	Brown weathering muddy dolomitic clasts within black fetid limestone.	
	Grainstone beds fining up on cm scale alternate with limestone beds dm scale	
	Undulating grainstone beds recrystallized with possible auto-breccia. Calcite veining.	
	Brown muddy dolomite clasts within black limestone also dolomitic patches which are very irregular, almost flaser bedded.	
	Dm scale beds of quartz rich grainstones.	
	Undulating grainstone beds fine up dm. scale alternating with fetid limestone beds.	
	Massive limestone with very irregular quartz sandstone/ intraclast grainstone patches.	Subtidal
	Undulating beds of alternating fetid limestone and grainstone, 20cm scale beds. Weathered out pyrite grains.	
	Black fetid crystalline limestone with quartz sand lenses, outcrop is very weathered and poorly exposed.	

Khufai Formation at Hadash

Locality WM 7 40Q 576607 UTM 2557519

Association	Lithofacies	Metres	Lithology (m s f m c)	Geological points of note	Description	Environment Interpretation
Association A Fetid limestones	A2	0		K1 10.2.97	Scree covered slope 10m	
				K4 10.2.97	Mm crinkle laminated dark organic rich shaley limestone	
				K3 10.2.97	Massive well sorted, well rounded coarse quartz sandstone with muddy limestone clasts in a carbonate cement.	
					Recessive unit of shaley organic-rich limestone with dark mm laminations. Beds up to 30cm thick.	
	B3				Mixed quartz arenite and intraclast grainstone with micritic cement. Oomoldic porosity occluded by microquartz.	
B Grainstones	Shuram Formation			K2 10.2.97	Erosional conglomeratic base to coarse quartz sandstone with limestone clasts which fines up. Coarse limestone breccia with sandy matrix with granule sized micritic clasts. 5cm scale beds fine grained with mud flakes while coarse bands are rich in detrital quartz. Dm scale alternating beds of fine crystalline. limestone and grainstone with breccia pockets and vugs.	Subtidal
					Stylolites Massive dark fetid limestone with breccia pockets (tectonic?) Cm scale grainstone beds with lenticular mud lenses.	
					Neomorphosed microspar with minor detrital micritic intraclasts Coarse beds fine up to mm laminated beds.	
					Laminated beds cm scale Stylolites along bedding. Erosional base to grainstone beds which contain mud flakes and breccia pockets.	Subtidal
					Massive brown/purple weathering fetid limestone with alternating muddy and grainstone beds. Coarse grainstones fine up on a cm scale with irregular bed contacts. Chert nodules occur Basal contact with Masirah Bay Formation obscured by scree.	

Sample k8 16.1.97 260m Bd

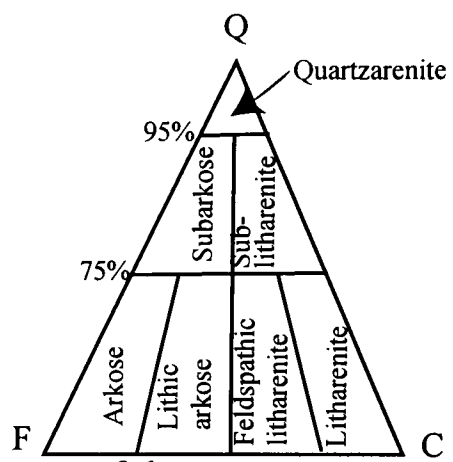
Quartz	Feldspar	Carbonate clasts	Cement	Voids	Fe Oxide	Other
123	53	63	104	0	4	3
52%	22%	26%	Feldspathic-litharenite			

Sample k9 24.2.96 267m Bd

Quartz	Feldspar	Carbonate clasts	Cement	Voids	Fe Oxide	Other
115	25	132	75	0	0	3
42%	9%	49%	Calci-litharenite			

Sample k8 15.2.97 299m Bd

Quartz	Feldspar	Carbonate clasts	Cement	Voids	Fe Oxide	Other
114	28	67	131	5	5	0
55%	13%	32%	Feldspathic-litharenite			



Ternary diagram of Folk (1974).

Sample k3 23.1.96 232m Kd

Quartz	Feldspar	Carbonate clasts	Cement	Voids	Fe Oxide	Other
135	57	23	130	1	1	3
63%	26%	11%	Lithic-arkose			

Sample k9 18.2.96 231m Kd

Quartz	Feldspar	Carbonate clasts	Cement	Voids	Fe Oxide	Other
155	53	0	114	17	1	2
75%	25%		Sub-arkose			

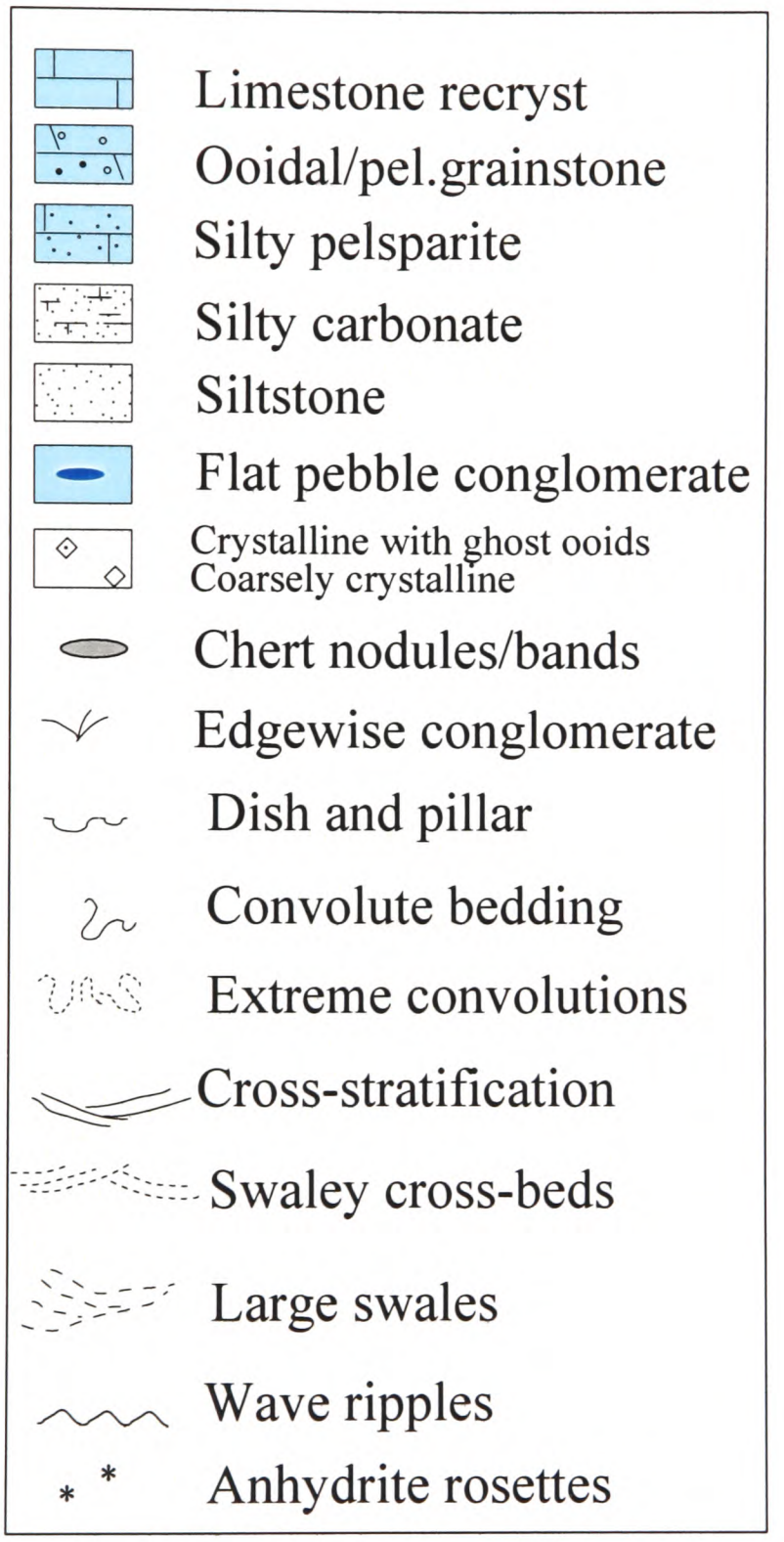
Appendix 4

Shuram Formation Logs:

Composite log from Mukhaibah dome, Wadi Shuram and Wadi Aswad

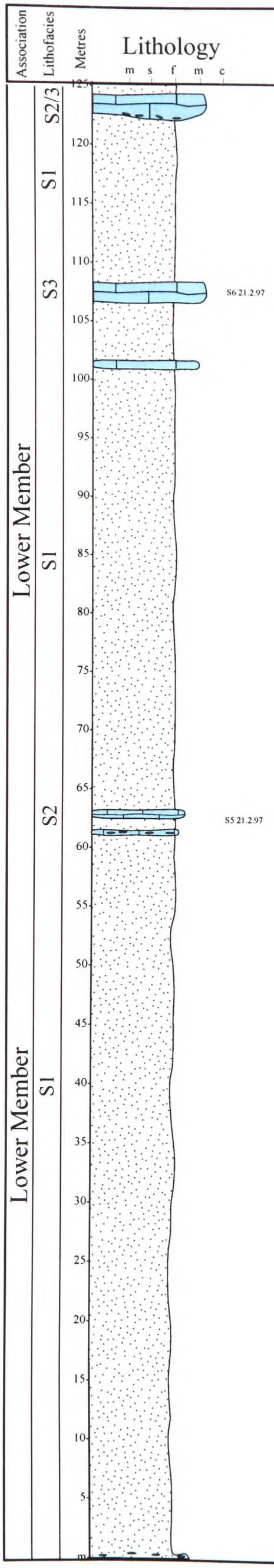
Base of Shuram Formation in Wadi Bani Awf

Shuram Fm. Key



Shuram Formation in Nafun

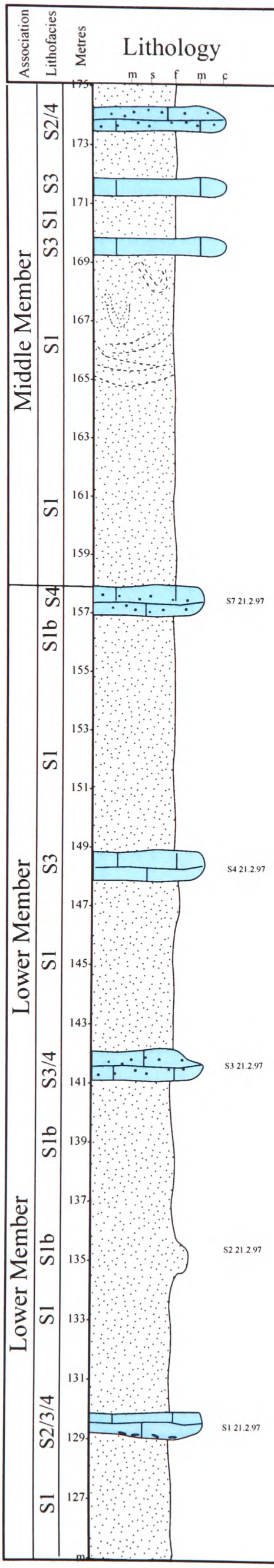
Locality MD9 40Q 572958 UTM 2196098



Description	Environment Interpretation
Flat pebble downcutting shallow channel Sandstone becomes more coarse grained and forms resistant ridge in outcrop. Thin silty carbonates.	
Ooidal grainstone, radial ooids partially obscured by neomorphism. Sparry inclusion free cement. Decimetre scale silty carbonate bed pinches out laterally 2cm carbonate lense	Shallow marine
Red weathering siltstone with very minor intercalations of flat pebble conglomerates forming lenses within this homogenous unit.	
Decimetre band of grey weathering peloidal carbonate with silt laminations Pelsparite with micritic peloids 100 microns in diameter within a sparry carbonate cement. Minor detrital quartz, feldspar and mica laminations	Shallow marine
Micaceous red sandstones, very fissile consisting of fine to medium grained quartz, feldspar and abundant micas within an iron rich matrix. No evidence of structure within this basal unit.	
Flat pebble conglomerate marks the contact with the underlying Khufai carbonates.	

Shuram Formation in Nafun

Locality MD9 40Q 572958 UTM 2196098



Geological points of note	Description	Environment Interpretation
	Ooidal grainstone with cross -stratification and lenses of flat pebble conglomerate which form down-cutting channels	Prograding carbonates
	Recessive red/green siltstones	
PCL 058/238		
	Grey weathering flat pebble conglomerate beds - flat pebbles formed of silty peloidal grainstone.	
	Convoluted beds of green and red siltstone overlie low-angle swaley cross-laminations. Laterally, metre scale dish and pillar structures form.	Shallow marine
Wavecrest orientation 150-330		
PCL 068/248		
	Radial ooids, micro-inclusion rich, well-sorted with suture contacts within a sparry cement. Some ooids squashed may have been soft while compacted. Neomorphic sparry cement contains relict ooids.	
	Grey weathering sandstone with a sparry carbonate cement forms a 50cm thick bed. Beds are finely laminated.	Prograding carbonates
		Shallow marine
	Structureless micritic peloids within a sparry matrix, detrital laminations containing quartz, mica, organic fragments and pyrite.	Prograding carbonates
	More resistant sandstone unit within recessive silts.	
	Packstone laminations alternate with grainstone laminations. Radial ooids 300microns to 1mm in diameter in some lamina are compacted pre-cementation while in others have a sparry cement. Detrital lamina rich in quartz and mica with algal filaments?. Authigenic glauconite within cement.	Shallow marine
	Carbonate cemented sandstone, with detrital quartz, feldspar and mica with organic laths and pyrite grains.	Prograding carbonates
	Detrital quartz, feldspar and mica grains 50-100 microns within a carbonate matrix. Iron rich with pyrite.	Shallow marine
	50cm to 1m thick sandy carbonate beds forms resistant bed within the more recessive red weathering siltstones.	
	Ooidal grainstone with flat-pebble intraclasts of silty peloidal grainstone. Coccoid cyanobacteria within core of ooids.	Prograding carbonates
	Medium to coarse sandstone with a carbonate cement, forms a resistant ridge in outcrop.	Shallow marine
	Red weathering micaceous siltstone-fine sandstone, no evidence of sedimentary features.	

Shuram Formation in Wadi Aswad Locality WA 40Q 606237 UTM 2312125

Association	Lithofacies	Metres	Lithology (m s f m c)	Geological points of note	Description	Environment Interpretation
Upper Member	S2/4	222	S6.3 17.2.97 S6.2 17.2.97 S6.1 17.2.97	4 Wave ripples	Flat pebble conglomerate on top of pink/grey weathering ooidal grainstone which overlies recessive silty laminated carbonate.	Shallow marine hardgrounds
		220			Ooidal grainstones with fringe cements alternate with sutured, silty peloidal/ooidal packstone.	
	S1/S1b	218		PCL 125/305 fpc imbrication >120	Laminated beds of very micaceous fine sands	
		216			Swaley cross beds in green silty carbonate	
					Dm scale bowl shaped convoluted structures	
		214			Flat pebbles along swaley lamination	
	S2				Low angle cross-lamination with flat pebble conglomerate	Shallow marine
		212		Wave ripples	Green sandstone has an average grainsize of 300 microns while red sandstone average grainsize is ~200 microns	
	S1	210				
		208			Dm scale alternations of blocky ooidal/peloidal limestones and recessive cross laminated fine micaceous sandstone	
	S3/4	206	S5.4 17.2.97 S5.3 17.2.97 S5.2 17.2.97 S5.1 17.2.97	3	Ooidal grainstones with fringe cements and hardground surfaces, intraclasts of silty peloidal/ooidal wackestone. Some compaction pre-cementation with clay rich sutures.	Prograding carbonates
	S1	204			Convoluted beds above alternating carbonate rich and carbonate poor beds	
		202			Low-angle cross lamination with green and red colouration cutting across lamination.	
	S1b	200			More carbonate rich green silts with low angle swales	Shallow marine
		198			Recessive red siltstones	
		196			Cross laminated green silts above more recessive red silts	
		194	S4.1 17.2.97	2	Oosparite with packstone and grainstone laminations, ooids have irregular outlines due to dissolution. Ooids are of iron free calcite while sparry cement is of iron rich calcite.	
	S2/4	192	S5		Ooidal grainstone cap to silty carbonate beds containing flat pebble conglomerates.	
	S2/3	190			Flat pebble conglomerates overlie cross-stratified silty carbonates above recessive red/green siltstones	Prograding carbonates
		188		fpc imbrication >300°	No exposure 1m	
	S2/4	186	S4	1	Dm scale alternations of cross-stratified ooidal grainstones containing flat pebbles and recessive siltstones. Recessive green and red siltstones	
	S2	184			Cross-stratified silty ooidal carbonate with flat pebble bed	Shallow marine
	S1b	182			Recessive red and green siltstones with low-angle swales of up to 3m wavelength; amplitude ~50cm Some more carbonate rich lenses containing flat pebbles	
		180			base of exposure in Wadi Aswad, outcrops above sabhka	
Middle Member					End of Nafun exposure	
	S3	179			50cm thick carbonate beds alternating with red siltstone beds with planar contacts.	
	S1	177	S2	fpc imbrication >357°	Silty peloidal/ooidal grainstones with planar low angle cross-stratification overlying recessive red/green siltstones with large scale swaley cross-lamination.	
	S3	m	S1			

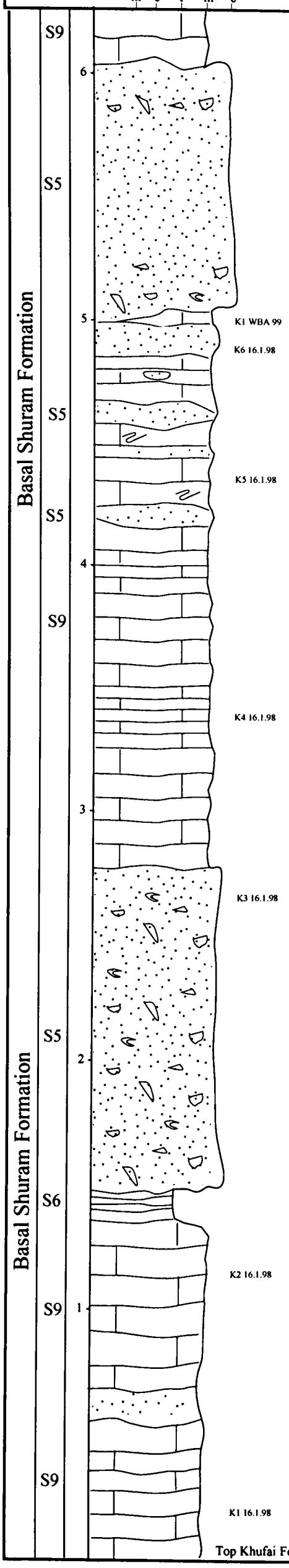
Shuram Formation in Wadi Aswad Locality WA 40Q 606237 UTM 2312125

Association	Lithofacies	Metres	Lithology (m s f m c)	Geological points of note	Description	Environment Interpretation
Upper Member	S2/3/4	248	S5 18.2.97	7	Ooidal grainstone with dog-tooth fringe cement and late evaporitic? pore-filling cement alternate with silty, peloidal flat-pebble conglomerates.	
	S2/3/4	246	S418.2.97		Sub-metre cycles consisting of planar laminated calcareous siltstones overlain by ooidal grainstones often containing flat pebbles.	Carbonate platform
	S2/3/4	244	S3 18.2.97		Sub-metre scale alternations of cross-bedded ooidal flat-pebble conglomerates with recessive silty carbonates which contain rare intraclasts (edgewise conglomerates).	
	S2/3/4	242	S2 18.2.97		Blocky ooidal/peloidal grainstones with minor cross laminated silty carbonates. Ooidal beds contain flat-pebble conglomerates with irregular contacts.	
	S2/3/4	240	S1 18.2.97		Ooids have suture contacts and vague fringe cements in a sparry matrix. Siltstones contain quartz, mica, detrital pyrite and authigenic glauconite and are carbonate cemented.	
	S1b	238	S7.1 17.2.97 S7.2 17.2.97 S7.3 17.2.97		Cross laminated silty carbonate above red weathering fine sandstone containing minor green bands. More recessive units partially covered by scree - dish shaped convoluted beds ~10-20cm.	
	S1	236				
	S1b	234			More carbonate rich beds	Shallow marine
	S1b	232			Slightly more resistant beds with low angle cross-lamination	
	S1	230				
		228			Recessive red and green fine sandstones, difficult to see structure as they are covered in scree, some convoluted beds and swaley cross-lamination was observed.	
		226				
		224				
		m				

Basal Buah Formation

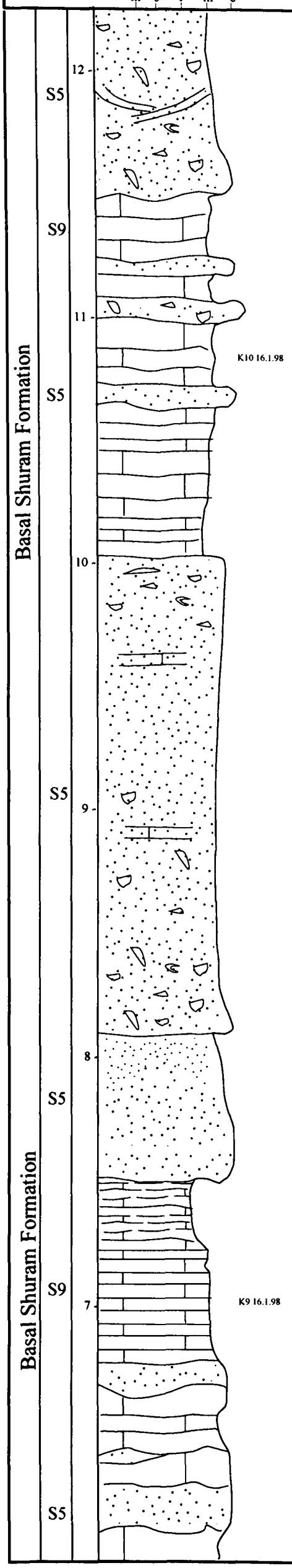
End of exposure

Shuram Formation in Wadi Bani Awf Gorge Locality WBA 6 40Q 544464 UTM 2569963



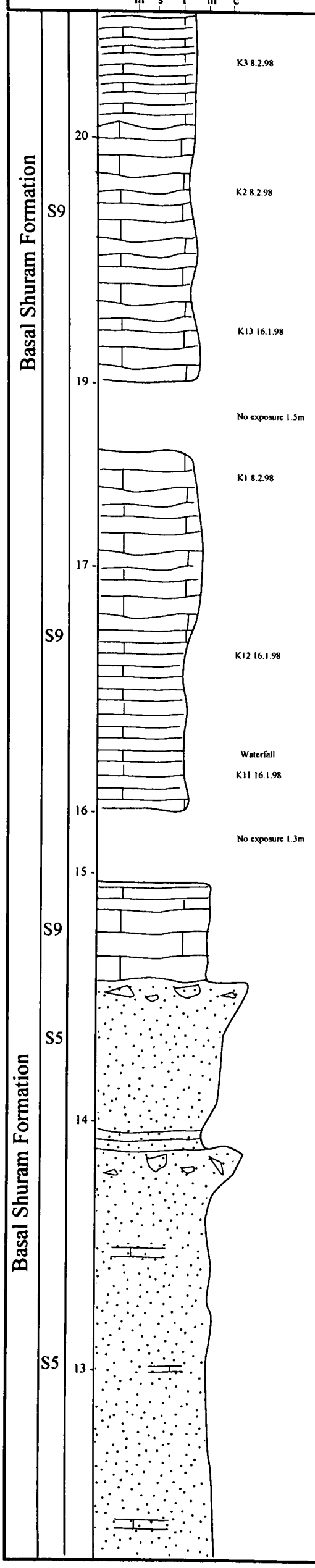
Geological points of note	Description	Environment Interpretation
	Limestone lenses infill undulating upper surface of sandstone.	Outer-ramp
	Conglomeratic lenses in the top of the sandstone unit.	
	Basal sandstone contains rip up dolomitic clasts in rippled contorted beds.	
	Sandstone downcuts into underlying limestones.	
	Laminated grainstone beds pinch-out laterally. Black limestone contains mud interbeds and sandstone lenses up to 50cm scale.	
	Limestone beds 10cm scale, grainstone interbeds contain minor detrital quartz. Some low-angle cross-lamination and isoclinal fold, slump structures.	
	Very fine grained dark organic-rich laminations containing detrital quartz and feldspars (fine-grained) alternate with relict peloids within a recrystallized spar matrix.	Outer-ramp
	Black limestone bedded 2-3cm scale with red muddy interbeds which have planar lamination and sharp planar contacts.	
	Cm scale peloidal laminations alternate with detrital fine-grained siltstone with organic rich matrix. Normal grading	
	Dm scale bedded black fetid limestones interbedded with red/brown muddy horizons with swaley lamination pinch-out laterally.	
	Sub-rounded to sub-angular quartz grains with boehm lamellae and composite grains indicative of metamorphic precursor. Carbonate intraclasts formed of stromatolites, ooidal grainstones and micritic clasts.	
	Brown weathering coarse sandy limestone, sub-angular quartz grains with angular dolomitic mud clasts up to 3cm in diameter. Mud clasts increase towards top of unit.	
	Pink muddy bands interbedded with thin limestones cm scale.	Outer-ramp
	Black recrystallized limestone with pale brown muddy dolomitic bands 1cm thick, undulating contacts	
	Grainstones weather a flecky brown colour, grade up on a 1-2cm scale. Upper parts of beds contain numerous stylolites.	
	Vuggy weathering on bedding surface, sub-circular vugs with diameters of 2-4mm.	

Shuram Formation in Wadi Bani Awf Gorge Locality WBA 6 40Q 544464 UTM 2569963



Geological points of note	Description	Environment Interpretation
	Brown blocky quartz rich limestone with rafted limestone clasts up to 25cm in diameter. Low-angle cross bedding.	Outer-ramp
	Black limestone bands 20cm thick alternate with detrital quartz rich beds 10-20cm thick with irregular scour contacts.	
	Conglomeratic bed Dark organic-rich micritic laminations with boundstone texture containing detrital quartz and feldspars	
	Heterolithic beds of sandy limestones and muddy limestones with dm scale beds and undulating contacts forms more recessive unit.	
	Top sandstone has rafted mud clasts up to 10cm in diameter.	Outer-ramp
	Blocky quartz rich limestone with dolomitic mud clasts and rafted black limestone lenses. Detrital quartz grains are rounded and up to 500μm while detrital spherical black limestones are 1-2mm in diameter.	
	Conglomeratic base lst clasts up to 1m, grades up. Some clasts folded and contorted.	
	Scour base to quartz sandstone with mud intraclasts.	
	Very fine grained red/brown laminated mudstone. Limestone and mud interbeds 2cm scale. Limestone beds are formed of microspar with micritic clotty intraclasts possibly peloids alternate with more organic-rich laminations containing detrital silts.	Outer-ramp
	Heterolithic beds. Sandy limestones, black limestones and red laminated muddy beds are dm scale. Cross bedded siliciclastic limestones grade up to background carbonate grainstone on a 2-3cm scale then finally grades into laminated muds.	

Shuram Formation in Wadi Bani Awf Gorge Locality WBA 6 40Q 544464 UTM 2569963



Geological points of note	Description	Environment Interpretation
K3 8.2.98	Blocky black limestones containing 2-3cm muddy beds with swaley laminations. Undulating contacts.	Outer-ramp
K2 8.2.98	Dm scale beds of recrystallized black limestone.	
	Black limestone, dm scale beds with numerous calcite veins.	
K13 16.1.98	Wispy micritic laminations alternate with more sparry peloidal? laminations. Detrital quartz and feldspars with numerous pyrites.	
No exposure 1.5m		
K1 8.2.98	Blocky black limestone very fractured with calcite veins.	
K12 16.1.98	Organic-rich lime mudstone with detrital fine-grained quartz and feldspars and numerous euhedral pyrites.	Outer-ramp
	Recessive unit under water formed of limestone with thin mud interbeds mm scale.	
Waterfall K11 16.1.98	Clotty, brecciated texture to micrite with calcite spar matrix. Calcite spar and authigenic quartz in veins	
No exposure 1.3m		
	More recessive limestone with minor detrital quartz and limestone clasts.	
	Conglomeratic carbonate clasts	
	Blocky brown sandstone locally developed with well-sorted, well-rounded quartz grains.	
	Planar laminated sandstone.	Outer-ramp
	Conglomeratic bed with rafted mud clasts up to 10cm diameter.	
	Thin black limestone stringers 10cm thick and a few metres long.	

Shuram Formation in Wadi Bani Awf Gorge Locality WBA 6 40Q 544464 UTM 2569963

Lithology (m s f m c)	Geological points of note	Description	Environment Interpretation
Shuram Formation red and green siltstones (S1)			
30 - K7b 8.2.98		Thin cm beds of planar limestone black and shaley	Outer-ramp
K7 8.2.98			
S6		Recessive red weathering shaley beds with thin cm scale sandy lenses.	
29 - K16 16.1.98		Cm bedded highly fractured black limestones with numerous calcite views.	
S9 K6 8.2.98			
Basal Shuram Formation		Black shaley organic rich limestones.	
28 - K15 16.1.98			Outer-ramp
S6			
K5 8.2.98			
27 - No exposure 5m			
22 -		Black shaley organic rich limestones.	
K14 16.1.98			Outer-ramp
K4 8.2.98		Dark organic rich fine grained carbonate with detrital feldspars, mica and quartz. Quartz grains up to 500μm have mermekitic texture	
S6			
21 -			

Appendix 5

Buah Formation Logs:

Mukhaibah dome

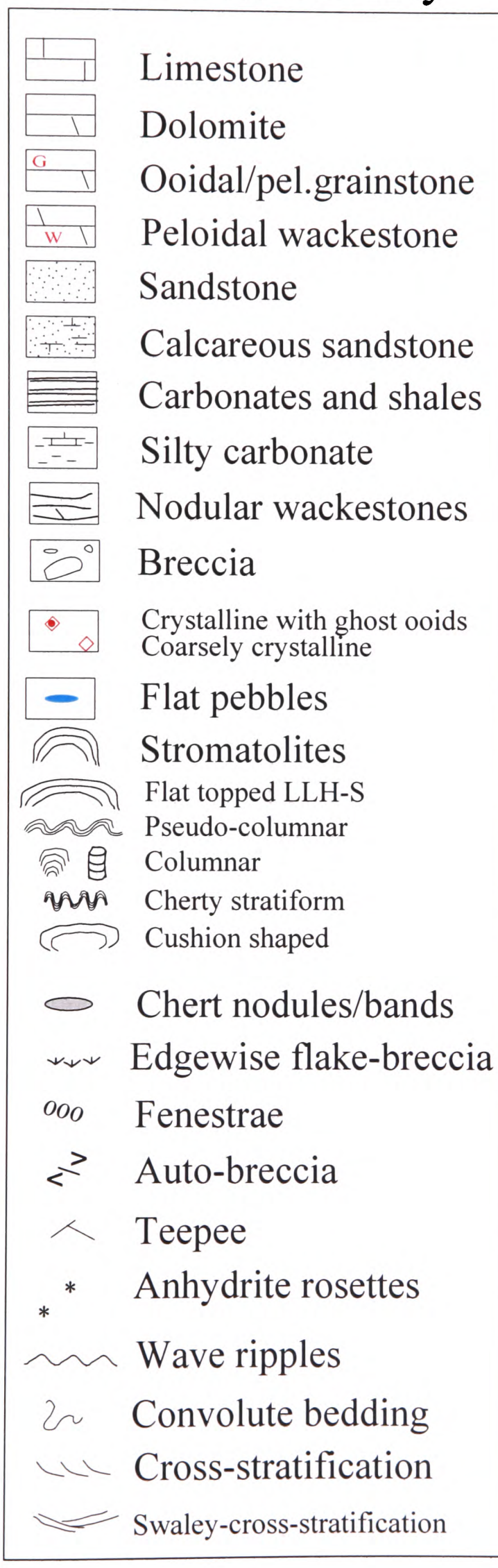
Khufai dome

Buah dome

Wadi Bani Kharus

Wadi Bani Awf

Buah Formation Key



Buah Formation in Mukhaibah dome Locality Md 40Q 573319 UTM 2203216

Association	Lithofacies	Metres	Lithology (m s f m c)	Geological points of note	Description	Environment Interpretation
Association A Crinkly laminites	A2	50			Poorly exposed very fine grained pale grey carbonates are heavily weathered and recessive.	
		48				
		46		Ridge		
				B8 26.1.98	Flat pebble conglomerate	
		44			Crinkly laminated beds with edgewise flake-breccia lenses form cm thick beds which alternate with silty carbonate containing low-angle swales with wave ripples?.	
	A1	42		B7 26.1.98		
		40			Minor channels cut laminated beds.	
		38			Recessive silty carbonates, paper shale facies.	
				B6 26.1.98		
		36			More carbonate-rich beds with crinkly laminites and edgewise flake-breccia lenses, laminated with nodular appearance.	
		34		B5 26.1.98		
		32			Finely laminated silty pink/grey peloidal carbonate forms cm scale flaggy beds. These locally contain low-angle cross-stratification and ripples.	Subtidal
		30				
		28		Ridge		
				B4 26.1.98		
		26		Ridge	Flaggy laminations of nodular texture containing silt laminations and fenestrae. Decimetre scale bands with minor cross-lamination.	
	A2	24				
		22		B3 26.1.98	Edgewise flake-breccia lenses within crinkle laminated carbonates which are of recrystallized limestone.	
	A1	20				
		18				
		16			Laminations thicken upward to 2-5 mm which weather-out as thin plates.	
	A2	14			Silty red weathering carbonate with thin mm swales and low-angle cross laminations.	
		12		Ridge	More carbonate-rich beds, edgewise flake-breccia and crinkly laminations are more resistant.	Subtidal
				B2 26.1.98		
		10			Micrite and microspar neomorphosed limestone with undulating laminations.	
	A1	8		B1 27.1.97	Crinkly carbonates dominantly formed of edgewise flake-breccia minor lenses of silty carbonates in hollows.	
		6			Edgewise flake-breccia lenses within silty pink/grey carbonates 10cm high and 50cm long.	
		4		Base Buah Fm.	Recessive silty mm. laminated carbonates pink/grey weathering with low-angle swales.	
		2		B1 26.1.98		
		0m			Transitional contact with Shuram Fm.	

Buah Formation in Mukhaibah dome Locality MD 20 40Q 573019 UTM 2202962

Association	Lithofacies	Metres	Lithology (m s f m c)	Geological points of note	Description	Environment Interpretation
Association B Grainstones and stromatolites	B3b	101			Flat pebble conglomerate bed 20cm thick.	Shoal
		99	G		Vague hints of swales and low-angle cross lamination in silty bands within the grainstone. Vugs are concentrated along laminations.	
		97			Flat topped stromatolites with 60cm synoptic relief onlap onto grainstones are elongate in 030.	Backshoal
		95	G B16 26.1.98			
	B3	93			Pink/grey weathering recrystallized peloidal grainstones with dark mm laminations form massive beds with cavernous weathering.	
		91	G B2 27.1.97 ooo		Recrystallized sparry dolomite with vague relict ooids and minor chalcedonic chert.	Shoal
		89				
		87	B15 26.1.98		Neomorphosed calcisiltite with detrital quartz, feldspar and mica, pyrite, minor peloids and phosphate.	
	B2	85	B14 26.1.98		Brown weathering heterolithic beds of shales and wackestones form nodular flaggy beds 3-4cm scale with mm laminations, low-angle swales and scour structures.	
		83				Subtidal
	B3	81	B13 26.1.98		Neomorphosed sparry dolostone with relict ooids, oncoliths and intraclasts of silty peloidal wackestone. Intraclasts are fragmented, also contains minor fine grained quartz and feldspars	
		79			Brown weathering silty wackestones with wave-ripples, mm laminations within cm scale flaggy beds.	
		77	B12 26.1.98		Grey weathering neomorphosed peloidal/ooidal grainstone with evaporite moulds	Shoal
		75				
		73	No exposure 1.9m.		Poor exposure results from recessive shale beds	
		70	B11 26.1.98		Neomorphosed ooidal/peloidal grainstone	Shoal
Association A Crinkly laminites	B3	68	ooo	Brown Dolomite	Yellow weathering silty peloidal grainstone with small scale low-angle swales alternating with crinkly laminations containing edgewise flake-breccia.	
		66	B10 26.1.98			
	A1	64			Peloidal wackestone has a recrystallized nodular texture with swales locally developed.	
		62			Low-angle swales in a peloidal wackestone with minor intraclast flakes.	
		60	B9 26.1.98		Sharp planar contact with underlying fine grained carbonate	
	A2	58		Limestone		Subtidal
		56			Poorly exposed fine grained pale grey carbonates weathers as paper shale	
		54				
		52				
		m				

Buah Formation in Mukhaibah dome Locality MD 20 40Q 572980 UTM 2202554

Association	Lithofacies	Metres	Lithology (m s f m c)	Geological points of note	Description	Environment Interpretation
Association C Peritidal stromatolites and evaporites	C2	151	IG	Recessive poorly exposed beds form inter-ridge area.	Very vuggy grainstone containing micritic intraclasts with evaporite pseudomorphs.	
		149			Fine-grained carbonate with chert and evaporite moulds	Peritidal
		147			Flaggy beds of fine grained dolomite with chert.	
	C1	145			Recessive pink weathering flaggy porcelainous limestones.	
	C2	143	B22 26.1.98		Yellow weathering vuggy ooidal intraclast grainstone with domal stromatolites 80cm diameter, 30cm relief laterally	Peritidal
		141			Vuggy stromatolitic laminations very altered.	
	C1	139			Dimple stromatolites 1cm diameter	
		137			Pale green-grey fine-grained carbonate with undulating contacts.	
	C2	135			Columnar stromatolites within ooidal grainstone beds overlie desert varnished cherty stromatolitic laminations.	
		133	B21 26.1.98		Thin flaggy beds with tabular chert.	
	C1	131	Top of major ridge B20 26.1.98		Heterolithic silt and sand beds with scour structures	Peritidal
					Recessive very fine-grained green-grey silty carbonate	
Association B Grainstones and stromatolites	B3b	129			Stromatolite domes form resistant ridge in outcrop and overlie cross-bedded grainstones	Backshoal
					Low flat topped stromatolites form biostrome 100's m along strike synoptic relief approximately 20cm.	
	B3a	127				
		125			Brown weathering cross-laminated grainstone with vugs along lamination.	Shoal
		123			Low flat topped stromatolites form biostrome 100's m along strike synoptic relief approximately 20cm.	
	B3b	121	B19 26.1.98			Backshoal
		119	B3 27.1.97		Neomorphosed coarsely crystalline dolospar with wispy clay rich laminae and minor detrital millet-seed quartz, feldspar and mica grains.	
		117			More massive pink/grey weathering nodular dolomite form prominent ridge in outcrop formed of neomorphosed dolomitic peloidal grainstone and low domal stromatolites	
	B3a	115				Shoal
		113	B18 26.1.98			
		111			More coarse grained dolomite with a nodular to massive texture. Blocky beds metre scale. Minor breccia pockets.	
	B3b	109			Low flat topped stromatolites form biostrome 100's m along strike synoptic relief approximately 20cm.	Backshoal
		107				
		105	B17 26.1.98		Massive beds of pink/grey grainstones which laterally interfinger with stromatolites form massive ridge.	
		103			Nodular laminites with local developments of swales and low-angle cross-stratification.	
		m			Some brecciated patches occur within interdome areas	

Buah Formation in Mukhaibah dome Locality MD 20 40Q 572980 UTM 2202554

Association	Lithofacies	Metres	Lithology (m s f m c)	Geological points of note	Description	Environment Interpretation
Association C Peritidal stromatolites and evaporites	C2	226			Cherty laminations with vugs and auto-breccia pockets stromatolitic laterally.	Peritidal
		224				
		222				
		220			Recrystallized cherty laminations with evaporite moulds and columnar stromatolites laterally.	
		218		B32 26.1.98		
		216		B31 26.1.98	Brown weathering faintly laminated grainstone.	
		214		No exposure 3m		
		210			Grey brown weathering LLH with cm scale synoptic relief. Sub-mm laminations thicken and thin laterally, tending to thicken in domes and interdome hollows and thin on edges. Irregular fenestrae are partially occluded by yellow stained sparry calcite.	Peritidal
		208		No exposure 6m		
	C1	202		B4 27.1.97 B30 26.1.98	Red weathering breccia beds cut down into laterally linked hemispheroid stromatolites with 1m synoptic relief and 2 m diameters.	
		200			Recessive flaggy muddy carbonate.	
	C2	198		B29 26.1.98	Cherty pseudo-columnar stromatolite, mm laminated with up to 10 cm synoptic relief and 2 cm diameters.	
		196				
		194			Massive beds of domal stromatolites, laterally linked hemispheroids with metre scale synoptic relief. Very weathered with vugs and auto-breccia.	Peritidal
		192			Dark grey vuggy grainstone with stromatolites laterally, very altered.	
		190		B28 26.1.98	Green-grey muddy dolomites with minor pyrite and vugs with rectilinear outlines.	
		188			Altered grey weathering stromatolitic beds, vuggy and brecciated.	
	D3	186		B26 26.1.98	Recessive red carbonate with chert-rich lamina and muddy lamina, undulating and slightly brecciated Med. crystalline with iron-rich clay laminations and spherulitic quartz rich in anhydrite	Supratidal Sabhka
	C1	184		B25 26.1.98	Pale pink-grey faintly laminated micritic carbonate.	
		182		B24 26.1.98	Recessive fine-grained carbonate Soft, yellow-brown weathering saccharoidal, porous limestone. Coarsely crystalline anhedral calcite crystals with minor dolomite and quartz.	
		180				
		155		B27 26.1.98	Recessive pale green-grey weathering muddy carbonate poorly exposed under boulders and scree.	Peritidal
		153			Very fine-grained limestone with minor irregular vugs sometimes occluded by spar	
		m		B23 26.1.98	Pale-grey micro-breccia with micritic intraclasts and evaporite pseudomorphs.	

Buah Formation in Mukhaibah dome Locality MD 20 40Q 573384 UTM 2202208

Association	Lithofacies	Metres	Lithology (m s f m c)	Geological points of note	Description	
			The top Buah Fm. in the Mukhaibah dome is taken to be the sabhka horizon (D3) which is considered equivalent to a similar horizon in the Buah dome area which contains a silcrete surface and is unconformably overlain by the Cambrian Thumailah Formation.			
Association D Sabhka	D3 C2	258-	B41b 26.1.98	Brown	Brown weathering carbonate forms ridge containing laterally linked hemispheroid stromatolites overlain by mm laminated, columnar stromatolites.	Lagoonal
				Red brown	Red-brown weathering fine-grained recessive unit with gypsum? crystals	Sabhka
	D2	256-				
		254-	B41 26.1.98	Yellow brown	Cross-bedded coarse sandstone pale yellow weathering. Well sorted quartz grains within a porous cement. Subrounded quartz arenite, quartz cemented with glauconite	
	D1	252-			Poorly exposed fine-grained muddy carbonate.	Peritidal
Association C Peritidal stromatolites and evaporites	C1	250-	B40 26.1.98 Contorted beds		Very contorted beds with large domes, pseudo-columnar stromatolites, auto-breccia and muddy laminations.	
	D1	248-	B39 26.1.98 B38 26.1.98	Yellow	Fine-grained grey dolomite with weathered out grains. Peloidal grainstone with chert.	
			B37 26.1.98	Pink	Recessive fine grained chalky pink dolomite with low-angle cross-lamination.	
	C2	246-	B5 27.1.97			Peritidal
		244-	B36 26.1.98	Pale grey	Increase in chert upwards, chert-rich undulating bedding surface, brecciated in places with mm laminated pseudo-columnar stromatolites.	
		242-			Fine grained pink/grey carbonate with mm laminations and blocky weathering.	
			No exposure 1m			
		240-	B35 26.1.98		Pink brown weathering thinly bedded flaggy dolomite, recrystallized with fine laminations.	
		238-	No exposure 7m			
	D1 C2	230-	B34 26.1.98		Pink and grey mm laminated pseudo-columnar stromatolites with vuggy fenestrae and auto-breccia. Stacked hemispheroid stromatolites 1-8cm scale. Fine grained dolomite with evaporite pseudomorphs.	Peritidal
		228-			Poorly exposed recessive chalky carbonate beds	
		m	B33 26.1.98		Pink and grey cherty columnar stromatolites with auto-breccia patches.	

Buah Formation in Khufai dome Locality Kd9 40Q 569656 UTM 2226372

Association	Lithofacies	Metres	Lithology (m s f m c)	Geological points of note	Description	Environment Interpretation
Association A Crinkly laminites	B2	50			Poorly exposed finely laminated fissile silty limestones with vague ripples?	
	A2	48		Top of cycle		
		46		B18 23.2.97		
		44			Green/grey weathering crinkly laminated limestones with minor edgewise flake-breccia.	
		42			Structureless microspar with vague hints of nodular texture with minor bitumen	Subtidal
	A1	40				
		38		B3 23.1.97	Neomorphosed intraclast flake-breccia with silt-rich undulating laminations above.	
		36				
	A2	34				
		32		Top of cycle B19 23.2.97	Fissile recessive silty brown laminites. Edgewise flake-breccia consists of micritic clasts up to 1cm long and 2mm wide within a microcrystalline matrix. Shadow/stalagtitic sparry cement associated with clasts.	
	A1	30			Dm scale alternations of planar crinkly laminites and laminites containing edgewise flake-breccia bundles or lenses.	
		28				
	A2	26				
		24		Top of cycle		
		22		B20 23.2.97	Dm scale bands of pale and dark grey laminites with nodular texture alternating with edgewise flake-breccia beds.	
	A1	20			50cm unit of edgewise flake-breccia with minor crinkly laminites form more resistant ridge.	
		18			Nodular laminites form dm scale beds that alternate with planar crinkly laminations containing edgewise flake-breccia	
	A2	16			Silty carbonates with scours and wave-ripples	
		14				Subtidal
		12		Top of cycle	Flat pebbles on bedding surface Laminites containing spaced edgewise flake-breccia bundles (4cm thick) alternating with crinkly laminations on a dm scale. Intraclast band with pale micritic intraclasts 5mm long and 1mm wide.	
	A1	10		B1 23.1.97	Crinkly laminites are formed of microcrystalline carbonate with nodular texture surrounded by darker aphanocrystalline limestone containing detrital silts.	
	A2	8				
		6		Top of cycle B21 23.2.97	Prominent flake breccia? bed 30cm thick above dm variation in edgewise flake-breccia beds and crinkly laminated beds.	
	A1	4			Green/grey laminites planar, mm thick, with rare lenses of edgewise flake-breccia	
		2				
		m			Contact with underlying Shuram Fm. not exposed	

Buah Formation in Khufai dome

Locality Kd9 40Q 569656 UTM 2226372

Association	Lithofacies	Metres	Geological points of note	Description	Environment Interpretation
Association B Grainstones and stromatolites	B3	98	Top of major ridge	Metre scale domal stromatolites, poorly preserved, possibly LLH. Laminations contain laminoid fenestrae.	
		96	B12 23.2.97	Laminated dolomites with low stromatolite domes and anhydrite rosettes and vuggy fenestrae. Minor occurrence of auto-breccia. PLATE	
		94	Stromatolite orientation 188°	Nodular crinkly laminations form low-domal stromatolites on a 1-5 m scale which are interbedded with peloidal grainstones. Lath shaped vugs (after evaporites) are partly occluded by calcite.	Backshoal
		92	B5 23.1..97	Neomorphosed carbonate with microspar and spar undulating laminations. 5% intergranular porosity.	
		90			
		88	B4 23.1..97	Channel with low-angle cross-lamination down-cuts 23 cm into fenestral beds.	
		86	B13 23.2.97	Undulating laminations of sparry carbonate with relict peloids and micritic laminations containing detrital silts.	
		84		Laminite beds up to 30 cm thick contain nodular carbonate with silty partings and fenestrae. Evaporite moulds are partly occluded by calcite.	
		82		Beds thicken up to 20 cm.	Backshoal
		80	Top of Ridge	75 cm unit of edgewise flake-breccia overlies dm scale alternations of planar laminations and edgewise flake-breccia laminites.	
	A2	78	B14 23.2.97	Microspar and sparry laminations with nodular texture, minor silt in microspar laminations	
		76		Dm scale bedded laminites with nodular texture and rare edgewise flake-breccia.	
		74	B15 23.2.97	Microcrystalline limestone with nodular texture with clay coatings and sparry calcite in vugs.	
	B2	72	B4 23.1.98 Top of cycle B3 27.1.97	Brown sandy peloidal wackestone with cross-lamination forms recessive unit which infills underlying stromatolite topography and contains carbonate clasts and flat pebbles.	Shoal
	B1	70		Stromatolites overlie grey weathering vuggy bleached dolomite which overlies fine mm laminated dolomite containing low-angle-cross stratification.	
		68	B16 23.2.97	Flaggy recrystallized beds with no evidence for stromatolites	
		66		Large LLH stromatolites domal, yellow weathering with up to 5 m in diameter and 2 m synoptic relief. These are generally composite formed of domes with metre scale diameters. Laminations are a few mm thick are porcelainous, undulating and pinch and swell laterally.	
		64	B2 23.1.97		Shoal
		62			
		60		Massive beds of nodular limestone Very coarse crinkly laminites, 5-10 mm thick, which pinch and swell laterally. Thin partings of yellow silty carbonate are recessive and surround limestone nodules.	
		58		Massive intraclast breccia beds have sharp contact with underlying silty carbonates.	
		56	B2 23.1.98	Iron rich ooidal wackestone with detrital quartz, feldspar and mica. Microcrystalline carbonate cement.	
		54	B17 23.2.97		Subtidal
	B2	52	B8 17.2.96 B1 23.1.98	Poorly exposed recessive unit of fissile silty yellow peloidal wackestone with swaley cross-lamination and wave ripples. Wavelength 10 cm wave height 2.5 cm wave-crest orientation 154°	
		m	Wave crest orientation 154°		

Buah Formation in Khufai dome

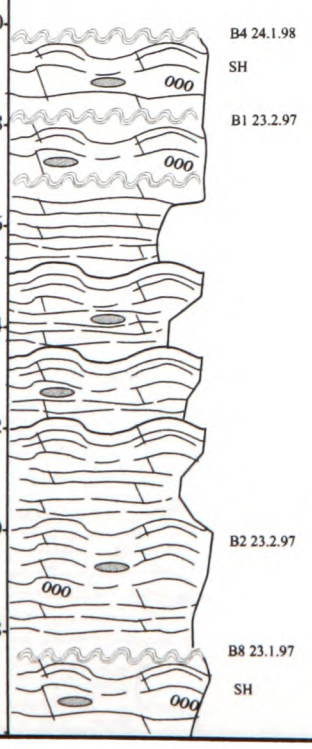
Locality Kd9 40Q 569656 UTM 2226372

Unit	Lithofacies	Metres	Lithology (m s f m c)	Geological points of note	Description	Environment Interpretation
		150				
		148			Brown weathering recrystallized nodular laminites with laminoid fenestrae and evaporite moulds. Most porous but some are occluded by calcite	Shoal
		146		B7 23.2.97	Euhedral dolomites packed with skeletal organic matter with detrital quartz, feldspar and mica. Irregular porosity partly occluded by calcite	
		144	G		Domes preserved within the laminites have m scale synoptic relief and 3-6 m diameter.	
		142		LSH		
		140			Coarsely recrystallized fenestral dolomite vuggy.	
		138			Fine and coarse crystals of euhedral dolomite. Finer grained bands rich in iron oxide with minor detrital silts. Some authigenic quartz. Intercrystalline porosity occluded by calcite with relict evaporites.	
		136		B8 23.2.97		
		134	G		Grey/brown weathering fenestral laminations. Laminations are on a mm scale and are slightly undulating. The fenestrae are sub-mm irregular to spheroidal. Some laths up to 2 mm occur. Fresh surface shows fenestrae are partially occluded by calcite while many of the laths are empty.	
		132				
		130				
		128				Shoal
		126		B9 23.2.97	Contorted laminations of dolomicrospar and dolomicrite with rare detrital silt. Vugs occluded by iron rich sparry dolomite.	
		124				
		122	G		Grey/brown dolomite containing dark mm laminations with a stromatolitic texture. 1-3 mm scale vugs some with a rosette outline. Many are empty while some are occluded by sparry calcite.	
		120				
		118	G		Neomophosed undulating fine and coarse lamination with nodular texture. Vertical stylolites.	
		116		B10 23.2.97		
				LSH		
		114		Elongation 188°	Domes preserved within the laminites have m scale synoptic relief and 3-6 m diameter.	
		112			Pale-grey nodular carbonate, recrystallized coarse and fine laminations with evaporite moulds.	
		110	G			
		108	G		Neomorphosed sparry carbonate packed with skeletal micro-inclusions with vague hints of relict peloids. Fine and coarse undulating laminations.	Shoal
		106		B11 23.2.97		
		104	G		Brown/grey recrystallized dolomite with relict ooids fresh surface reveals pink and grey laminites.	
		102				
		m				

Buah Formation in Khufai dome Locality Kd9 40Q 569656 UTM 2226372

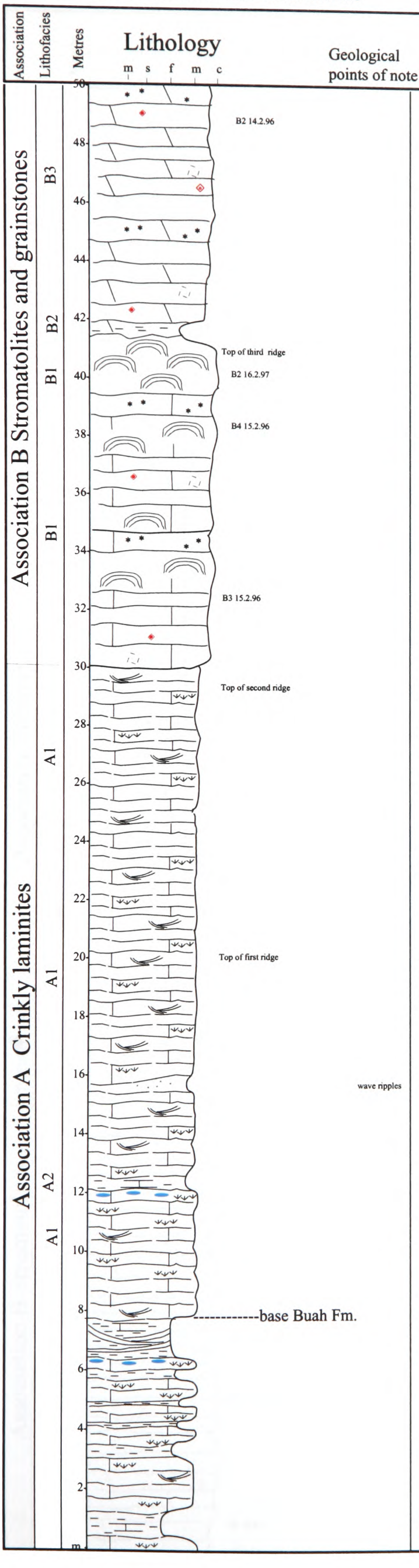
Association	Lithofacies	Metres	Lithology (m s f m c)	Geological points of note	Description	Environment Interpretation
Association C Peritidal stromatolites and evaporites	C1	336			Cherty low domal stromatolites, mm laminated with undulations sub-dm. scale.	
	C2	334	G			
		332			Recessive fine grained dolomite forms flaggy cm. thick beds.	Peritidal
		330	B3 23.2.97			
		328	G B5 23.1.98		Grainstone interbeds with stromatolites. Dolomicrite laminations with evaporite pseudomorphs occluded by sparry calcite and microquartz.	
	C2	326				
		324	G B7 23.1.97		Grey/brown weathering dolomites containing stromatolites with 10 cm synoptic relief, with chert laminites and fenestrae.	
		322			Subhedral dolomicrospar rich in micro inclusions with relict peloids. Evaporite pseudomorphs and microquartz.	
		320	B4 23.2.97		Cm scale cherty pseudo-columnar stromatolites - stacked hemispheroids above massive stromatolites. These are mm laminated composite stromatolites with up to 2 m synoptic relief and 3-4 m in diameter. They are pale yellow/brown weathering, crinkle laminated whose edges dip at approximately 45° .	Peritidal
	C1	318				
		316	G B7 24.1.98		Columnar stromatolites are formed of alternating micritic and microspar laminations with relict peloids.	
	C2	314			Columnar stromatolites mm laminated with 1-2 cm synoptic relief.	
		312	B6 24.1.98	Pale cream	Laterally spaced-hemispheroid stromatolites, mm laminated metre scale domes with chert	
		310	B5 23.2.97		Cream/yellow weathering dolomite with low cm. scale domes. Rich in fenestrae with brown chert bands dm. thick.	
	C2	308	G			
			1m No exposure			
	C2	306	B1 24.1.98		Dark cherty cap of stromatolites which consist of low domes (cm scale) within a pale creamy grey matrix of mm laminated dolomites. The latter contain fenestrae 2 mm in diameter which are partly occluded by sparry calcite.	
		304		Pale cream		Peritidal
	C1	302			Dolomicrite laminations alternate with more calcic microspar laminations.	
	C2	300	B6 23.2.97		Trochoidal wave ripples in fine grained dolomite beneath stromatolites	
		298				
	C1	296			Recessive beds of pale grey weathering muddy dolomite	
			138m No exposure and scree covered exposure			
Association B	B3	158			Metre scale domal stromatolites up to 5 m in diameter form major ridge. These interfinger with grainstones	
		156	G			
		154		Brown beds	Large domes have cavernous weathering in outcrop	Backshoal
		152	G		Brown/grey recrystallized dolomite with relict ooids fresh surface reveals pink and grey laminites.	
		m	B6 23.1.98			

Buah Formation in Khufai dome Locality Kd9 40Q 569656 UTM 2226372

Association	Lithofacies	Metres	Lithology (m s f m c)	Geological points of note	Description	Environment Interpretation
Association C Peritidal stromatolites and mudstones	C2 C1 C2	350 348 346 344 342 340 338 m		Top of Ridge and end of Buah exposure in Khufai dome	Cherty columnar stromatolites with dark brown desert varnish. These form synoptic relief of 3-6 cm and are approximately 2-4 cm in diameter. The weathered surface shows undulation chert algal lams with the bedding surface containing cylindrical laminations of juxtaposed columnar stromatolites. Low domal cherty stromatolitic dolomite overlying thin flaggy micritic beds which are recessive in outcrop. Micritic laminations alternate with microquartz laminations. Some are auto-brecciated with calcite infill. Partly silicified pseudo-columnar stacked-hemispheroid stromatolites within pale weathering laminated dolomites.	Peritidal Peritidal

Buah Formation in Buah dome

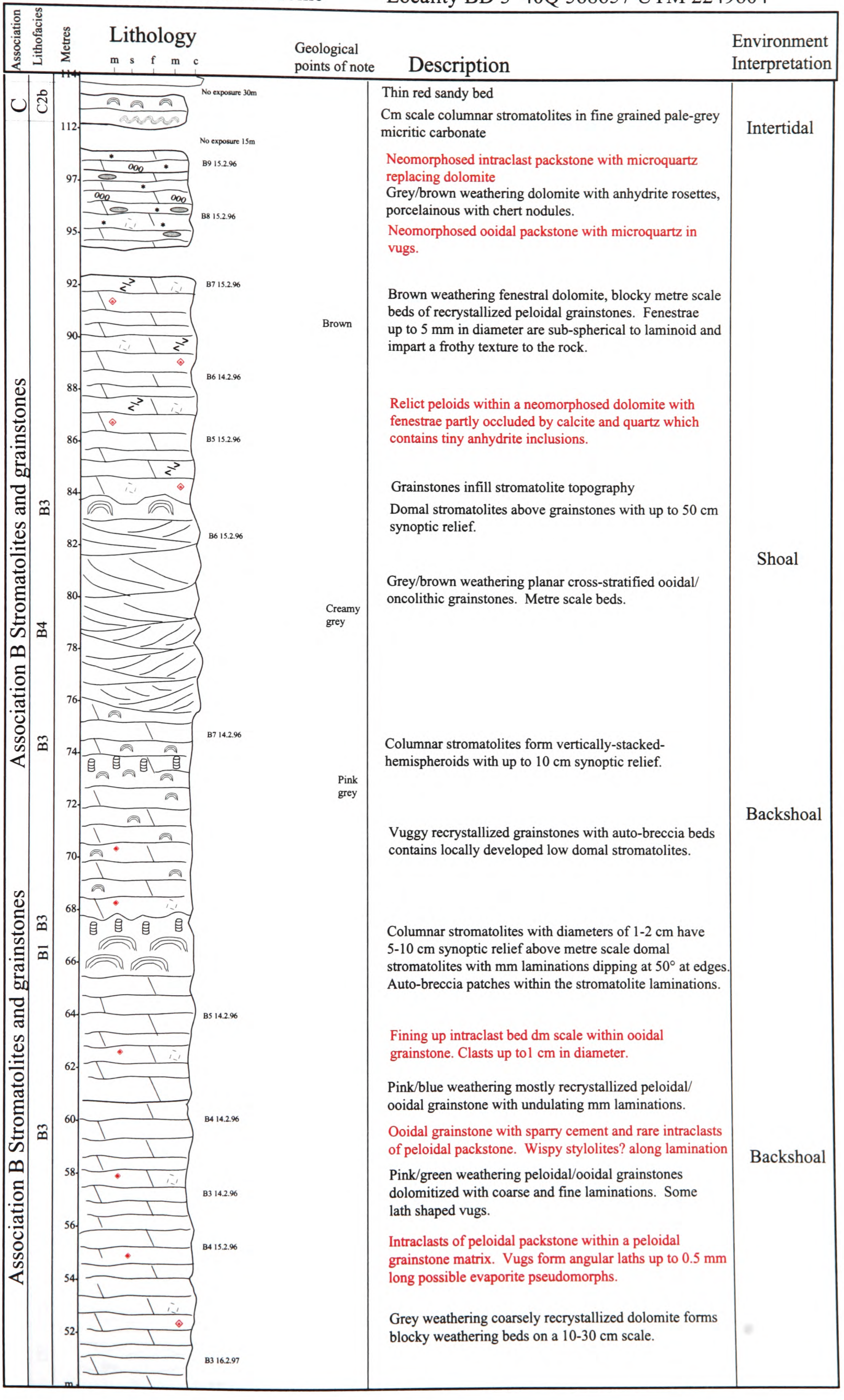
Locality BD 3 40Q 568657 UTM 2249604



Geological points of note	Description	Environment Interpretation
	Neomorphosed dolospar replaces concentric ooids. Bitumen along stylolites	Backshoal
	More flaggy planar beds grey weathering 10-20 cm thick mostly recrystallized peloidal grainstones.	
	Recessive unit above stromatolites laterally consists of silty red carbonates containing polygonal rills.	
	Large composite stromatolites, domes up to 10 m in diameter with approximately 2 m synoptic relief. These are composed of smaller stromatolites of 1-2 m diameter. This bioherm extends for 100's metres along section.	Backshoal
	Stromatolites consist of neomorphosed crinkly laminations	
	Subhedral dolomite rhombs containing relict inclusions of iron rich ooids.	
	Subhedral hypidiotopic mosaic of dolomite crystals with micro-inclusions and undulating (stylolitic?) laminations which are clay rich.	
	Pink/grey weathering coarse crinkly laminations up to 5 mm thick. Lath shaped vugs are possible evaporite pseudomorphs.	
	Edgewise flake-breccias decrease in abundance upwards and beds become more cohesive.	
	Massive crinkly laminite beds with minor beds 2-3 cm thick containing edgewise flake-breccia lenses.	Intertidal
	Unusual polygonal rills on bedding surface	
	More massive unit of crinkly laminites with edgewise flake-breccia on a dm scale.	
	Dm scale beds of grey weathering planar crinkly laminites that alternate with crinkly laminites containing edgewise flake-breccia lenses.	
wave ripples	Minor incursions of silt which is wave rippled.	
	Silty carbonate channel 30 cm deep detrital quartz rich and is low-angle cross-laminated.	
	Green/grey carbonate beds crinkly laminated with low-angle swales and edgewise flake-breccia.	
	Buah Fm. marked by first metre of carbonates without siltstone	
	Poorly exposed red silty carbonates with low-angle swales above flat-pebble conglomerate bed.	Subtidal
	Thin recessive red/grey weathering crinkly laminated beds with dm scale lenses of edgewise flake-breccia	
	Gradational boundary with Shuram Fm.	

Buah Formation in Buah dome

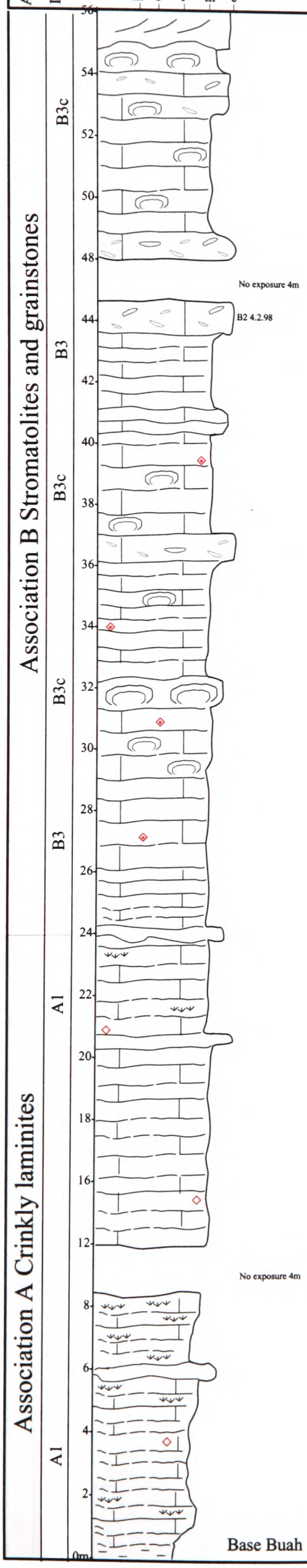
Locality BD 3 40Q 568657 UTM 2249604



Buah Formation in Buah dome Locality BD 3 40Q 568657 UTM 2249604

Association	Lithofacies	Metres	Lithology (m s f m c)	Geological points of note	Description	Environment Interpretation
D Sabhka	D3	122	The Upper Buah Formation forms an angular unconformity beneath the clastics of the Cambrian Haima Group.		Breccia which laterally becomes cherty laminated crust brecciated and ferruginous locally.	Sabhka
		120			Recessive red silty beds are poorly exposed, laterally contain micro-teepee structures, *in-situ* brecciation and minor detrital quartz laminae	
	C2		No exposure 1m.			
		118	B4 18.2.97		Very fine grained pale grey carbonate with faint mm laminations	
			No exposure 50cm.			
			B3 16.2.97		Blue/grey laminated micritic carbonate with cottage-loaf stromatolites with a few cm relief and up to 10 cm diameter	Peritidal
	D2	116	No exposure 50cm.			
		m	No exposure 90cm.		Red weathering cross-laminated silty carbonate Undulating laminations cherty above a breccia base - karst?	Sabhka

Buah Formation in Wadi Bani Kharus Locality WBK 3 40Q 555810 UTM 2569620



Geological points of note	Description	Environment Interpretation
	Pale-grey cross-laminated grainstone	
	Low-domal stromatolites under tree where rocks jut into wadi	
	Pale-grey intraclast grainstone with stromatolite domes laterally	Backshoal
	Dark grey limestone with pale muddy clasts - rock art	
	Brown weathering flat pebble conglomerate with muddy intraclasts up to 10 cm long	
	Ooidal intraclast grainstone with muddy laminations	
	Light and dark laminations 2-5 mm scale give recrystallized limestone a stripy appearance.	Shoal
	Light and dark laminations undulating stratiform stromatolite	
	Recrystallized grey limestones with light and dark (coarse and fine) bands with intraclast conglomerate beds.	Backshoal
	Brown weathering grainstone with muddy clasts 5 cm long and 5 mm thick	
	Undulating laminations with low-domal stromatolites	
	Cushion-shaped stromatolite laminations with 50 cm relief laminations 2 mm thick but can thin laterally.	Backshoal
	Cushion-stromatolites with 40 cm domal relief and 2 m diameter	
	Light and dark grey bands 10-20 cm thick of recrystallized limestone.	
	Light and dark laminations 2 mm thick form beds up to 20 cm thick.	Shoal
	Brown grainy band thickens and thins laterally, swaley at base.	
	Crinkly limestone in nodular beds with intraclast bands on a decimetre scale.	
	Brown weathering intraclast bed.	
	Limestone has crinkly/nodular texture in decimetre scale beds.	Subtidal
	Pale and dark grey banded limestone recrystallized, fine-grained with stylolites.	
	Edgewise conglomerates increase in thickness upwards forming stacked beds.	
	Intraclast breccia bed thickens and thins laterally.	
	Dark grey carbonate bedded on a 2-10 cm scale with pale weathering thin partings. Possible wave ripples.	
	Carbonate and silt interbeds, carbonates contain edgewise conglomerates and low-angle cross beds.	Subtidal
	Log started above faulted beds with possibly 20 m of laminites below	

Buah Formation in Wadi Bani Kharus Locality WBK 3 40Q 555810 UTM 2569620

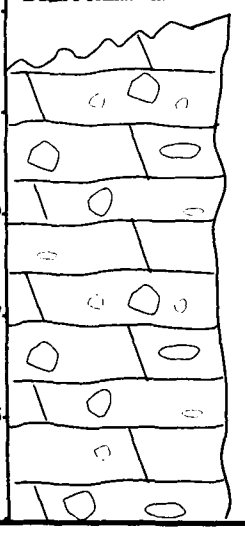
Association	Lithofacies	Metres	Lithology (m s f m c)	Geological points of note	Description	Environment Interpretation
Association B Stromatolites and grainstones	B3	10.5		B5 5.2.98	Ooidal grainstone with edgewise intraclast beds on a 30 cm scale. Mm chert nodules weather out brown.	
		08.5	G		Peloidal grainstone replaced by dolospar interbedded with ooidal-intraclast grainstone partially recrystallized. Inclusion-free spar cement	
		06.5	G		Grey, fetid, recrystallized ooidal and peloidal grainstone with lath intraclasts and mm chert nodules. Bedded on a 30 cm scale.	Backshoal
		04.5	G		Fine grained, laminated thin beds with mm chert grains weathering out.	
		02.5			Breccia related to fault.	
		00.5	G		Massive beds of brown/grey weathering ooidal grainstone which becomes more peloidal towards the top. Neomorphosed ooidal/oncolithic grainstone formed of subhedral dolomite rhombs	
		98.5		B4 5.2.98	Laterally linked hemispheroid stromatolites with ooidal/ oncolithic packstone within interdome area.	
	B3c	96.5	G		Pale grey weathering laminated beds form domes with 50 cm synoptic relief. Laterally spaced hemispheroids. Small domes with 1-2 cm relief overlie the larger domes.	Backshoal
		94.5		B3b 5.2.98	Fetid intraclast grainstone, beds on a 20-30 cm scale. Intraclasts weather in.	
		92.5		B3a 5.2.98	Intraclast grainstone with lath shaped pale weathering mud clasts 2 mm wide and 2-3 cm long.	
		90.5		B2 5.2.98	Grainstone with hints of low-angle cross-lamination. Intraclast breccia, clasts of angular microspar within a matrix which is inclusion-rich. Coarse calcispar in vugs.	
		88.5			Thin beds of recrystallized limestone.	
		86.5		B1 5.2.98	Flat-lying intraclasts interbedded with stromatolites Rock with nodular texture	
		84.5			Pale-grey limestone with grainstone texture and low domal stromatolites laterally	Backshoal
				No exposure 1.5m	Breccia with intraclasts up to 10 cm diameter.	
		82			Grainstone with zebroic texture in dm scale beds, numerous calcite veins.	
		80		5m fault gauge	Recrystallized grainy cap to stromatolite bed. Stromatolites are laterally-linked hemispheroids and have 20-30 cm synoptic relief.	
		74		B1 4.2.98	Brown weathering intraclast grainstone with weathered out grains. Large clasts up to 20 cm diameter.	
		72			Fine-grained recrystallized limestone Intraclast conglomerate	
		70			Ooidal grainstone with cross-lamination.	Shoal
		68				
		66				
		64				
		62				
		60				
	B4	58				

Buah Formation in Wadi Bani Kharus Locality WBK 3 40Q 555810 UTM 2569620

Association	Lithofacies	Metres	Lithology (m s f m c)	Geological points of note	Description	Environment Interpretation
Association E	E1	183			Beds heavily fractured with chert nodules.	
				B13 5.2.98	Neomorphosed dolospar with chalcedonic chert and micro-quartz, vugs occluded by sparry calcite	
		181			Fine-grained, dm scale, planar beds of dolomite	
	E6	179			Coarse breccia of recrystallized dolomitic matrix and clasts poorly sorted, massive blocky beds. Clasts up to 20 cm in diameter.	Slope
		177				
		175			Circular chert nodules up to 10 cm diameter on bedding surface	
	E1				Recrystallized pale grey porcelainous dolomite with fracture weathering.	
		173			Stromatolite laminations formed of irregular undulating microspar and spar up to 0.5 mm thick. Interdome area contains detrital ooids and peloids.	
		171		B12 5.2.98	Brown weathering columnar stromatolites with 10 cm synoptic relief.	
	B4	169	G		Recrystallized grainstone with muddy intraclasts and mm quartz in bands has sharp contact with underlying stromatolites.	
		167	G			
	B3d	165			Columnar stromatolites with 10 cm relief at base of bed have 2-3 cm relief at top of bed.	
		163	G	B11 5.2.98	Brown weathering chert band.	
					Microquartz and megaquartz replaces ooid grainstones, intergranular porosity occluded by chalcedonic quartz	Shoal
	B4	161	G		Ooidal/grapestone grainstone with muddy flake intraclasts. Brown weathering chert bands a up to 10 cm thick.	
				B10 5.2.98		
		159	G			
	B3d	157			Columnar stromatolites with 20 cm synoptic relief.	
					Recessive light and dark laminations.	
		155			Columnar stromatolites with 1-2 cm synoptic relief.	Backshoal
					Blocky beds of recrystallized fine-grained dolomite	
		153				
	B3d				Columnar stromatolites brown weathering, mm laminated with 10 cm synoptic relief.	
		151	G	B9 5.2.98	Ooids, peloids and grapestone intraclasts form partly neomorphosed grainstone	
		149		B8 5.2.98	Low domal stromatolites colonize ooidal grainstone	
	B4	147	G		Grainstone with mud clasts up to 20 cm and chert nodules has sharp contact with underlying stromatolites.	
		145	G		Stromatolites formed of microspar and spar laminations which nucleated upon peloids and intraclasts	
	B3c/d	143		B7 5.2.98	Columnar stromatolites with 13 cm relief, 2 cm base and 20 cm top. Some pseudo columnar stromatolites occur.	Backshoal
		141	G		Peloidal grainstone with detrital/authigenic quartz grains and muddy intraclasts.	
		139				
				Fault gauge 25m		
	B3			B6 5.2.98	Intraclasts of grapestones up to 1 cm in diameter, are subrounded within a neomorphosed grainstone matrix	
		114			Flat-pebble conglomerate bed.	
		112				
		m	G		Ooidal grainstone with intraclasts	

Association B Stromatolites and grainstones

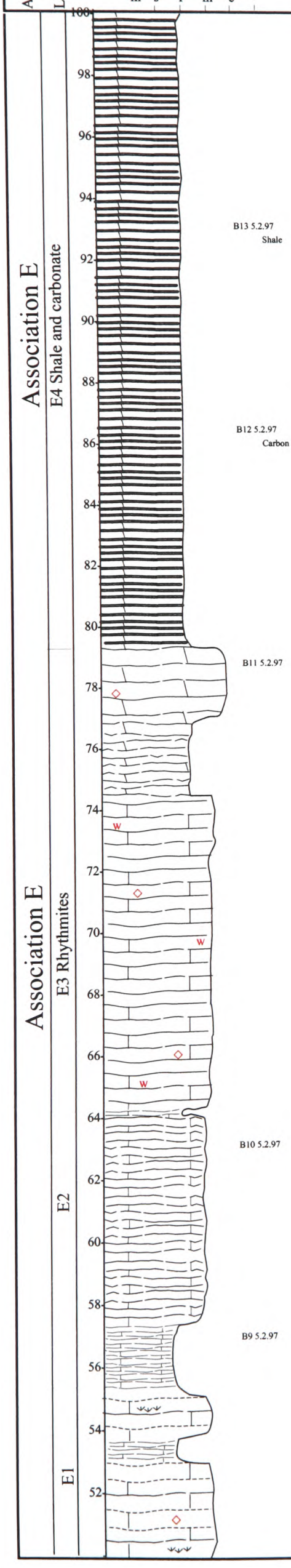
Buah Formation in Wadi Bani Kharus Locality WBK 3 40Q 555810 UTM 2569620

Association	Lithofacies	Metres	Lithology (m s f m c)	Geological points of note	Description	Environment Interpretation
Association E	E6	193 191 189 187 185		Permian unconformity downcuts Buah Formation.	Upper beds of the Buah Formation are eroded under the Permian unconformity Coarse breccia, massive, poorly sorted clasts of pale dolomite within a recrystallized dolomitic matrix. Clasts are up to metres in diameter and are matrix supported. Chert clasts also occur. Rock is fetid.	Slope

Buah Formation in Wadi Bani Awf Locality WBA 1 40Q546741 UTM 2573968

Association	Lithofacies	Metres	Lithology (m s f m c)	Geological points of note	Description	Environment Interpretation
Association E	E1 Black crinkly laminites	50				
		48	B8 5.2.97		Dark grey weathering carbonate, crinkly laminated in places, but may be thrombolitic. Beds 10-50 cm with very minor intraclast breccias	
		46			Microspar laminites retain faint nodular texture. Pyrite occurs with late hairline calcite veins.	
		44		Black beds	Mm laminated limestone and nodular texture alternate on a dm scale	Subtidal
		42				
		40			Blocky weathering grey carbonate with crinkly laminations with undulating contacts.	
		38				
		36				
		34				
		32	B7 5.2.97		Nodular limestone with intraclasts neomorphosed to calcimicrospar. Lath shaped vugs occluded by calcispar with relict anhydrites.	
		30			Sharp contact between massively bedded crystalline grey carbonate and underlying beds.	
	E1	28				
		26	B6 5.2.97		Massively bedded crystalline grey carbonate with calcite veins and sharp contact with underlying sandstone	Subtidal
	E1 Black crinkly laminites	24		Green/ brown beds	Thin carbonate beds 2-3 cm poorly exposed	
		22	B5 5.2.97		Green/brown silts with minor carbonates	
					Homogenous microspar, no texture preserved, organic rich with pyrites up to 100 µm.	
		20			Grey carbonate beds 4-10 cm thick of crystalline carbonate with intraclast breccias, laminated beds and possible thrombolites	
		18				
		16	B4 5.2.97		Pure crystalline carbonate with minor silt	
					Green/brown weathering fine sandstone with minor carbonate lenses	
		14	B3 5.2.97		Flat intraclast breccia, 2 cm long and a few mm thick within with pellet texture microspar matrix, stains iron rich.	
	E1	12			Alternating intraclast and laminated beds with weathered out pyrite grains	
		10			Lenticular carbonate lenses 1 cm thick and 10 cm long with cubic pyrites a few mm in diameter	
		8	B2 5.2.97		Decimetre scale carbonate beds with intraclasts (edgewise conglomerates) within grainstones	Subtidal
		6			Interlaminated micrite and microspar mm-cm scale undulating contacts, organic-rich with pyrites and relict peloids	
		4			Silts with minor carbonate lenses and beds on a decimetre scale	
		2	B1 5.2.97		Edgewise conglomerates within intraclast grainstone	
		0m			Low-angle cross-lamination with lenticular beds of carbonate within silts.	

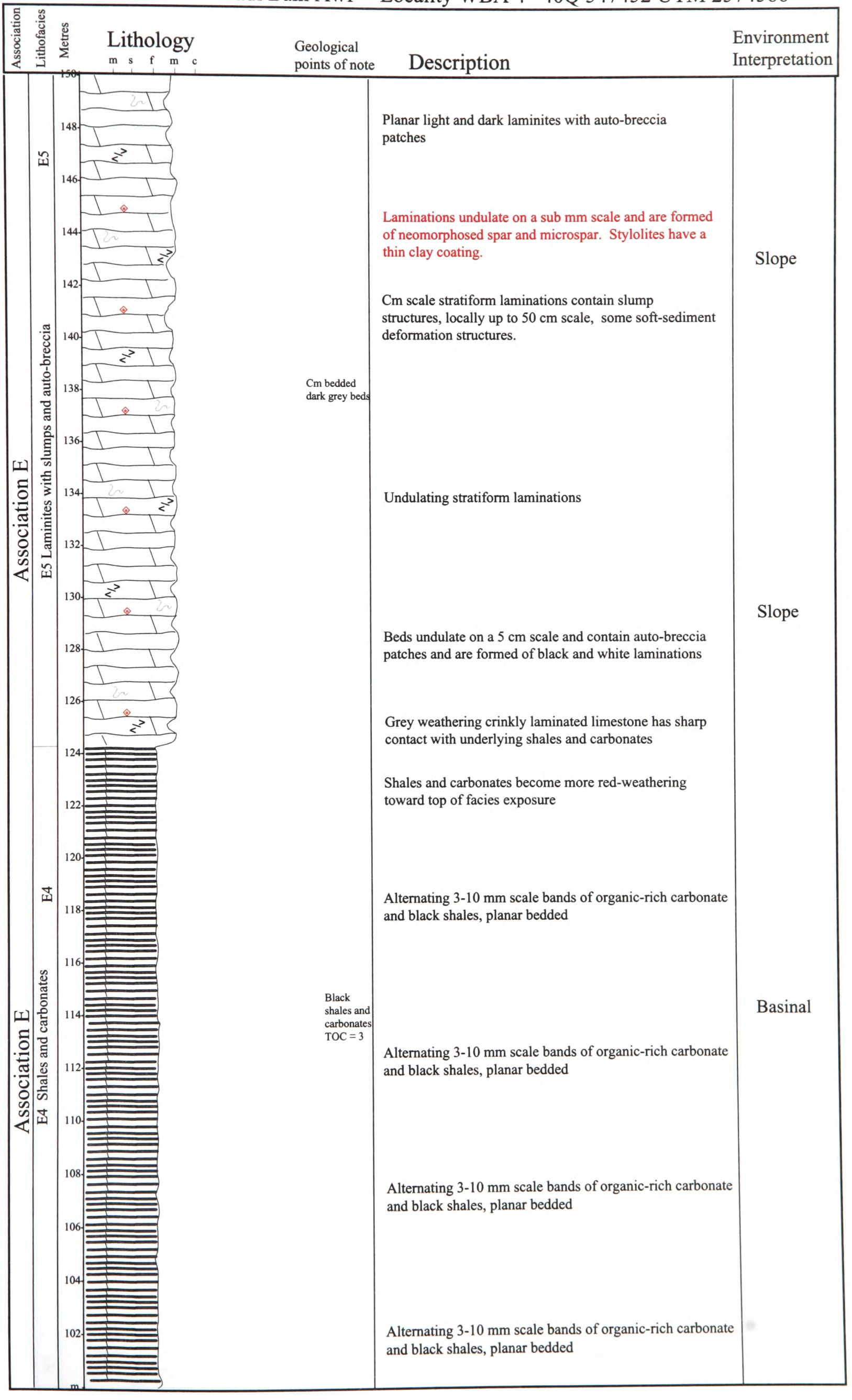
Buah Formation in Wadi Bani Awf Locality WBA 4 40Q 547452 UTM 2574566



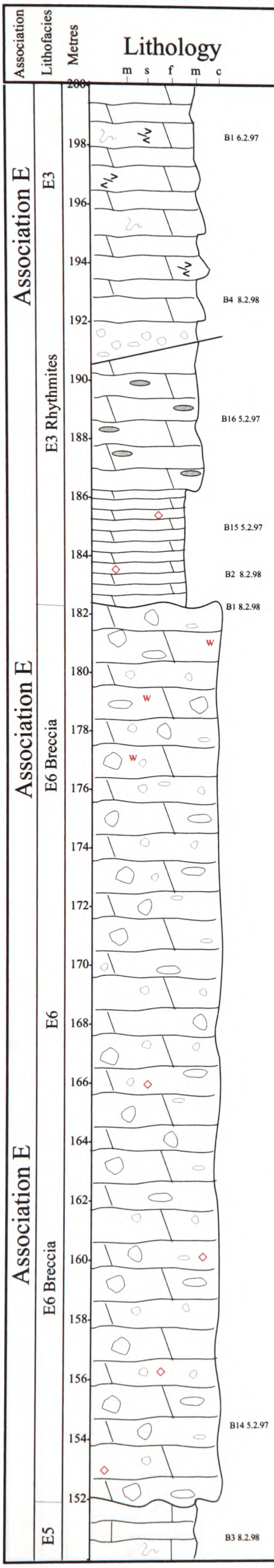
Geological points of note	Description	Environment Interpretation
	Organic rich silt and carbonate alternations on a sub-cm scale very planar and laterally extensive	
	Silt increases with silt bands 2-3 cm thick and carbonate bands 1 cm thick. Silt contains minor white laminations 1 mm thick	
		Basinal
	Black and brown weathering shale and organic rich carbonate bands mm-cm scale very planar. Carbonate has black mm laminations while shale is black fissile and platy	
Lst		
----	Massive recrystallized dolomite with intraclasts of fine grained angular dolomite and mud clasts	
	Recrystallized intraclast breccia with stylolites	
Dol	Recessive thin flaggy beds 1-10 cm thick with crinkly laminations and increasing silt partings upwards	

Lst	Cm scale beds with minor scour structures	
	Light and dark laminations with more wackestone interbeds	
Grey beds		Subtidal
	Light and dark coarse and fine mm laminations	
	Brown weathering recessive thin flaggy beds	
	Undulating to nodular grey limestone beds with minor shale partings, possible thrombolitic texture	
	Nodular calcite spar with surrounding micrite and anhydrite pseudomorphs	
	Undulating, laminated grey carbonate beds with thin mm-cm silt intercalations weathering orange, pyrite cubes and authigenic quartz	
	Laminations of spar and micrite with authigenic quartz pseudomorphs of anhydrite	
	Cm bedded carbonate with mm laminations and silt partings	
	Decimetre beds of grey carbonate with intraclast breccia	
	Recessive orange weathering thin flaggy carbonate beds with silt partings	Subtidal
Black beds	Dark-grey nodular limestone beds 10-50 cm thick with rare intraclast breccia	

Buah Formation in Wadi Bani Awf Locality WBA 4 40Q 547452 UTM 2574566



Buah Formation in Wadi Bani Awf Locality WBA 9 40Q 546816 UTM 2574299



Geological points of note	Description	Environment Interpretation
	Microspar with minor micritic intraclasts and thin mm laminations of detrital quartz, Muscovite and pyrites often with scour bases. Stylolites and late quartz veins.	
	Minor slumps and auto-breccia	
Normal grading	Porcelainous limestones light and dark grey cm scale banding with minor detrital sand intercalations with normal grading.	Slope
	Fault breccia Grey micritic limestones with grainstone bands of sub-cm scale chert nodules which are circular to ellipsoid and less than 1cm in diameter	
	Micritic bands alternated with intraclast bands cm scale. Intraclasts are micritic within a microspar matrix with authigenic quartz and mica. Numerous disseminated iron oxides	
Normal grading	Light and dark laminated porcelainous dolomite, very planar mm-cm fine and coarse laminations - some evidence for normal grading.	
	Alternating micritic, microspar and sparry laminations with minor micritic intraclasts and stylolites	
	Oncolithic wackestone is the background sedimentation to the intraclast breccia. Angular breccia clasts are composed of micrite, stromatolites and ooidal wackestone.	
	Massively bedded breccia unit containing brecciated angular intraformational clasts, of micritic dolomite and intraclast grainstones. Clasts are poorly sorted, with a random fabric	
	Massively bedded breccia unit containing brecciated angular intraformational clasts, of micritic dolomite and intraclast grainstones. Clasts are poorly sorted, with a random fabric and are matrix supported	Slope
	Neomorphosed microspar with intraclasts barely discernible. Clasts are micritic, or ooidal/oncolithic grainstone tend to be angular and are sometimes broken and fragmented. They are matrix supported.	
	Massively bedded breccia unit, blue-grey weathering with pale dolomitic clasts up to 2 m in diameter and minor small mm sized clasts, randomly orientated and matrix supported.	Slope
Dol		
------	Breccia down-cuts into underlying beds	
Lst	Planar beds with minor slump structures.	

Buah Formation in Wadi Bani Awf Locality WBA 10 40Q546826 UTM 2574375

Association	Lithofacies	Metres	Lithology (m s f m c)	Geological points of note	Description	Environment Interpretation
Association E	E7	250	G		Ooidal-intraclast grainstone	
		248				
	E3 Rhythmites	246	W	B9 8.2.98	Finely recrystallized grey weathering dolomite with quartz feldspar and mica rich bands with scour contacts	
		244				
		242	W	B3 6.2.97	Dark laminations with micro-relief alternate with intraclast wackestone of broken and fragmented micritic intraclasts. Vugs occluded by spar containing relict anhydrite. Pyrite and stylolites.	Slope
		240	W		Dark organic-rich laminites alternating with paler coarser laminations	
		238	W			
		236	W	Grey/ pale grey	Stripy planar pale grey fine grained beds and grey (detrital) intraclast wackestone beds cm scale	
		234				
		232	W	B8 8.2.98	Microspar laminations alternate with peloidal wackestones containing variable amounts of siliciclastics	
		230				
		228	W		Flaggy laminated beds planar pale grey weathering with slump structures and minor *in-situ* brecciation	
		226				Slope
		224	W		Muddy dolomite with thin grainstone bands and minor detrital silts	
		222		B7 8.2.98		
		220	W			
		218		B2 6.2.97	Intraclast laminations alternating with slightly undulating micritic laminations	
		216	W		Thin mm laminae slightly undulating	
		214		B6 8.2.98	Detrital beds of intraclasts possibly peloids fine up on a 5mm scale. Stylolites and sparry calcite within brecciated laminations	
		212	W			
		210		Normal grading	Pale grey muddy dolomite interbedded on a cm scale with grainy beds which fine up	
		208	W			
		206			Undulating contact with flaggy beds	Slope
		204			Grey/brown weathering laminites with calcite stringers fine and coarse bands	
				B5 8.2.98		
		202			Laminated beds broken in situ	
					Undulating beds with cm scale fining up detrital bands and auto-breccia pockets with sparry calcite	

Buah Formation in Wadi Bani Awf Locality WBA 10 40Q546826 UTM 2574375

Association	Lithofacies	Metres	Lithology (m s f m c)	Geological points of note	Description	Environment Interpretation
Association E	E6	296	Pale grey weathering ashy silts of the overlying Fara Formation		No exposure 8 m Thin dark grey weathering flaggy carbonate beds planar to slightly undulating laminites	
		294		B17 8.2.98	Pale grey weathering ashy siltstone (Fara Formation?) Thin cm scale bedded limestone beds flaggy with silt partings?	
		292		B16 8.2.98	Dark organic rich limestone beds dm scale	
		290			Breccia unit has irregular upper contact with overlying flaggy limestone which appears to infill breccia topography	
		288			Breccia unit is massively bedded, no preferred orientation of clasts and without clast sorting.	Slope
		286				
		284			Poorly sorted matrix supported breccia unit with large micritic dolomite clasts up to 2 m in diameter with fine mm sized clasts. Clasts of underlying laminated beds are angular and randomly orientated. Breccia matrix is ooidal grainstone.	
		282				
		280			Basal breccia down-cuts into underlying laminated beds.	
	E7 Cherty grainstone	278	G	B21 8.2.98	Planar bedded laminations alternating with intraclast grainstone beds, 2-3 cm scale.	Platform
		276	G	B15a 8.2.98		
				B15b 8.2.98		
		274			Concentric ooids and grapestones up to 2 mm in diameter are replaced by brick carbonate (calcite after aragonite) or megaquartz and minor calcite spar. Matrix is inclusion rich calcite spar	
		272	G		Metre scale bedded massive grainstone beds of grey weathering dolomite	
		270	G			
		268	W	B14 8.2.98	Massive beds of fine grained dolomite, bedded on up to a metre scale	
		266	W		Angular micritic intraclasts within ooidal wackestone, ooids are replaced by spar with geopetal micrite.	Platform
	E6	264			Planar laminated dolomitic beds with breccia bands at base of beds	
		262				
		260			Massively bedded breccia unit, of poorly sorted angular dolomicritic clasts in a grey carbonate has faulted contact with underlying sandy dolomites	
		258	P	B11 8.2.98	Broken and fragmented ooids and grapestones have been replaced by calcispar	
	E7 Cherty grainstone	256	P		Sandy grey laminated dolomites	
		254	P	B10 8.2.98		Platform
		252	P		Ooids and grapestones replaced by medium-coarse spar within an inclusion-rich microspar matrix with a clotty texture. Minor chert.	
				B20 9.2.98		

Appendix 6

6.1 Methods of sample evaluation

6.2 Isotopic analysis methodology

6.3 Trace element analysis methodology

6.4 Carbon and oxygen isotope data for all the samples analysed

6.1 METHODS OF SAMPLE EVALUATION

The isotopic composition of C in marine carbonates are susceptible to alteration. This process may include early diagenesis, late diagenetic fluid-rock reactions, metamorphism and weathering among others. The steps undertaken to decipher the effects of post-depositional alteration on the C isotopic composition of the carbonates of the present study are listed below. These enable the determination of samples most likely to record the isotopic composition of coeval seawater, so the C curve can be constructed with confidence.

Petrography

The thin sections and polished thin sections prepared for this thesis were cut to a thickness of 30μm and mounted in araldite epoxy resin. The thin sections were covered with a glass slip, whereas the polished sections were left uncovered. All thin section photomicrography were taken on a binocular microscope using Kodak EKTA 320T (tungsten) 35mm film. Petrographic evaluation of micritic, oolitic and stromatolitic carbonates for degree of recrystallization, authigenic and detrital components, stylolites and veins or vugs. Samples with significant recrystallization, secondary veins and vugs were removed from the sample population. Fine grained samples with good textural preservation are least altered and therefore likely to retain primary isotopic values. To determine carbonate mineralogy, half the section was stained with potassium ferricyanide and Alizarin red S (Dickson, 1966).

Cathodoluminescence

Cathodoluminescence (cold-cathode) examination of highly polished, 300μm thick, thin-sections cut from rock surfaces that are mirror images of those used for petrographic study. A Nuclide Luminoscope set between 14-16kV and 80-100μA under a vacuum of approximately 50 mtorr was used in the cathodoluminescence examination. Luminescence in sedimentary carbonates is commonly activated by Mn^{2+} concentrations of approximately 100pm and quenched by Fe^{2+} concentrations greater than 10,000ppm (Marshall, 1988; Hemming *et al.* 1989). As seawater contains relatively little Mn compared with freshwater, manganese enrichment is often the result of meteoric diagenesis while iron enrichment may result from the dissolution and reprecipitation of carbonate during surficial weathering. Samples without secondary veining and with non- to moderate-luminescence were chosen. Thick sections were photographed during examination.

Component analysis

Component analysis where micro-samples are taken from fine-grained micrite, ooids and early diagenetic cements to ascertain within-sample variations in isotopic signature. Micro-samples of 5-10mg are isolated using a 100μm diamond percussion drill.

6.2 ISOTOPIC ANALYSIS METHODOLOGY

Isotopic abundance measurements for this study were determined on a VG Isogas PRISM stable-isotope mass spectrometer, attached to an on-line VG Isocarb preparation system in the Oxford University stable-isotope laboratory. This instrument separates and detects ions based on the motions of charged particles with different masses in magnetic or electrical fields. Reviews of mass spectrometer theory can be found in Hoefs (1980), Anderson & Arthur (1983) and Corfield (1995). The mass spectrometer consists of four fundamental parts: 1. the preparation system and inlet; 2. the ion source; 3. the mass analyser; and 4. the ion detectors.

Preparation system and inlet

The carbonate to be analysed is converted to CO_2 by acidification in hydrated 100% orthophosphoric acid at 90°C in a reaction vessel as in the following reaction:

$$CaCO_3 + H_3PO_4 \leftrightarrow CaHPO_4 + CO_2 + H_2O$$

Samples are placed in the carousel on top of the vessel and dropped at regular intervals into the phosphoric acid, producing CO_2 and H_2O. These gases are purified cryogenically by trapping water in an alcohol slush at -90°C and trapping CO_2 in a liquid nitrogen cold finger at -196°C. The pure CO_2 is then admitted into the symmetrical inlet system which permits rapid alternation and comparison between the sample gas and a reference gas.

Ion source

The ionisation chamber contains a heated filament focused by a weak magnetic field that emits electrons which bombards the gaseous molecular CO_2 to produce positive ions. These are accelerated in a high voltage electric field until the ions of each isotopic mass have essentially the same kinetic energy.

Mass analyser

This ion beam passes through a magnetic field which deflects the ions into circular paths whose radii are proportional to the charge and mass of the particular ionic species. This motion is defined by $M/Z = B^2R^2/2V$ where an ion of mass M and charge Z is accelerated in a

potential V and injected into a uniform magnetic field B. The ion experiences a force and moves in a circular orbit of radius R. For single-charged ions, the radius is determined by a combination of magnetic and electric fields and effectively forms a mass filter. This is the underlying principle of all magnetic sector mass spectrometers and the equation is called the "mass spectrometer equation". Thus, the ions are separated into beams emerging from the analyser region with particular values of mass/charge.

Ion detectors

After the beams are filtered in the magnetic field, the ions of a chosen mass are transmitted through a resolving slit and detected by a Faraday cup. Here, the ion current from the cup is proportional to the number of incident ions and hence the partial pressure of the corresponding isotopic molecular species in the sample gas. Multiple slits and Faraday cups allow the simultaneous detection of different masses and are used to measure a major beam, representing the most abundant isotopic species, and minor beams from the less abundant isotopic species. The ratio between the heavy and light isotope is measured as the ratio between two masses. To measure $\delta^{13}C$ in carbon dioxide, the ratio between mass 45 ($^{13}C\ ^{18}O\ ^{18}O$) and 44 ($^{12}C\ ^{16}O\ ^{16}O$) is used. The isotopic data generated are displayed and stored on an attached computer.

6.2.1 Isotope delta notation and reference standards

The isotopic composition of oxygen and carbon from a carbonate sample is expressed in per mil (‰) differences relative to a standard, as follows:

$$\delta^{18}O = \frac{^{18}O/^{16}O_{Sample} - (^{18}O/^{16}O)_{Standard}}{(^{18}O/^{16}O)_{Standard}} \times 1000$$

$$\delta^{13}C = \frac{^{13}C/^{12}C_{Sample} - (^{13}C/^{12}C)_{Standard}}{(^{13}C/^{12}C)_{Standard}} \times 1000$$

A value of $\delta = +1.0‰$ indicates that the ratio of the sample is 1.0‰ higher than the standard. Seawater samples are normally standardised against Standard Mean Ocean Water (SMOW). Carbonate material is standardised with reference to the rostrum of a belemnite from the Cretaceous Pee Dee Formation of South Carolina (PDB). SMOW has $\delta^{18}O = -0.2‰$ PDB but the $\delta^{13}C$ of both is 0.0‰. Results are reported with reproduceabilities of 0.1‰.

6.2.2 Analytical errors

Analytical uncertainty during mass spectrometry comprises both precision error and bias error. In this study, precision error was estimated by inserting 8 standards of Carrera Marble with every run of 36 samples. Four standards were placed at the beginning and four at the end of each run. Their average (χ) and standard deviation (σ) was calculated and the precision error was estimated a 2σ. A precision of $\leq 0.1‰$ was considered acceptable. Data where precision errors were greater than 0.1‰ were disregarded.

The bias of the analytical technique can be estimated by comparing the Carrera marble standard with the value of the accredited Pee Dee Belemnite (PDB) standard. The mean value (χ) of the reference material analysed can be used to calculate the absolute bias of the analytical measurement:

$$Bias_{absolute} = \chi - C_a$$

The relative bias can be calculated as a percentage:

$$Bias_{relative} = \chi - C_a/C_a$$

In order to determine whether this bias is significant, a t-test can be used and the calculated t is equal to the following:

$$t_{calc} = Bias \div \sigma/\sqrt{n}$$

where n is the number of samples taken.

If $t_{calc} > t_{tables} \Rightarrow$ bias is significant.

Data were disregarded if the difference between the Carrera marble standard and PDB was significant.

6.3 ELEMENTAL ANALYSIS

6.3.1 Preparation of sample powders

All the samples used in the geochemical analyses were first dried in air, then rough crushed in a mortar and pestle and finally powdered in a Teemer swing mill, using agate milling equipment. The samples were ground to a fine, homogenous powder. This process took, on average, 40 seconds per sample. The agate mill was thoroughly cleaned between samples using acetone. Care was taken to ensure that the samples did not cake in the mill. The powdered samples were then stored in air-tight glass jars.

6.3.2 Sample preparation for ICP AES elemental analysis

Analysis for major and minor elements were undertaken on a Phillpis PV8060 Internally Coupled Plasma-Atomic Emission Spectograph (ICP) linked to the ES40 program at Royal

Holloway & Bedford College, under the guidance of Nikki Paige and Sarah James. The ICP is a NERC facility. Whole-rock samples are prepared by Procedure A while the carbonate dissolution method for carbonate fraction analysis is outlined in Procedure B. The major elements are reported (by convention) as wt% oxides and the trace elements in ppm.

Procedure A: The total dissolution method and bulk rock geochemical analyses

1. Exactly 0.2g of powdered sample was weighed into a clean, dry crucible. The weights of the crucible were recorded before and after the addition of the sample.
2. 6mls of a 1:2 mixture of $HClO_4$ and HF acids was added to each crucible with the automatic dispenser. The crucibles were placed on a hotplate set on 5 or 4, in the fume cupboard and evaporated down to dryness (3-4 hours).
3. These were removed from the hotplate and allowed to cool. Using the automatic dispensing pipette 2mls of HCI was added to each crucible. This was topped up with distilled water and returned to the hotplate to warm for 15 minutes. The crucibles were removed from the hotplate and allowed to cool.
4. When cooled distilled water was added to make up to 20ml volume (20.4g by weight).
5. Before running on the ICP, the solutions were shaken thoroughly.

Procedure B: Solution of carbonate fraction

1. The empty vial was weighed. Then 0.5g of powdered sample was added.
2. Approximately 6ml of 5% formic acid was added to each vial.
3. This was left for 24 hours on a hot plate. When effervescence stopped more acid was added and the sample was shaken. This process continued until the addition of fresh acid no longer resulted in effervescence.
4. The samples were then centrifuged at 1,500 revolutions per minute for 1 minute.
5. The liquid was then very carefully pipetted off so as not to include any silicate fraction from the bottom of the vial. Better to strain through paper (grade 6 or less) and wash with deionized water.
7. The solution was evaporated down to dryness overnight on hotplate.
8. The dry residue was then weighed. (use xrd to check contents i.e. if any carbonate remains or if silicates have also been attached by acid).
9. The evaporated carbonate fraction was weighed.
10. The carbonate fraction was dissolved in 5ml of HCI, the solution was left to heat and cooled down.
11. The resultant solution was made up to 20ml volume with distilled water.

12. Before running on the ICP, the solutions were thoroughly shaken.

Notes for this preparation technique

When doing these preparations do (1) one pure carbonate and (2) the same sample 3 times using the same prep method. This will provide a check to establish if (a) if all the carbonate actually dissolved (or if acid contamination occurred) (b) the results are reproducible

NB. Remember Weigh All Vials Before Use

Powders Should Be Measured To ±0.010 Precision

Notes on the ICP

a. A blank was run every ten readings. If the detection limit of the blank falls below 15.5% Al_2O_3, then the reading is invalid, as are the previous ten. This did not occur during use of the machine in the present study.

b. Blanks or minus readings indicate that the sample contains none of the particular element, or the concentration is below the detection limit.

Defects in the technique

According to Loveland (1988), the potential problems of the ICP are threefold: firstly, the detection limits are unfavourable compared to other techniques (e.g. Atomic Absorption Spectroscopy). Secondly, various inter-element interferences occur, which are internally corrected for. Finally, the Fe signal is suppressed by Ca.

Khufai Fm (Md)

Khufai Formation in the Mukhaibah dome				
Depth	Carbon	Oxygen	Sample	Description
261	0.408	-5.394	k10	top khufai oncolithic gs
260	-1.824	-6.328	k9	grainstone
259	-0.826	-4.849	k8	muddy carb lst
258.5	-1.742	-4.423	k7b	recryst white lst
258	-2.092	-4.425	k7	chalky lst
257	-1.831	-4.83	k5	crud
254.4	-2.906	-5.225	k4	hybrid sst
253.6	-3.967	-6.133	k3	hybrid sst
251	2.168	-4.052	k2	crinklw lams
249	-1.088	-5.64	k1	micrite
248	3.446	-5.957	k0 Md 98	lt+dk lams lst
247	4.661	-3.731	K4 25/1	fenestral stromatolite
246	5.203	-4.349	K6 25/1	grainstone
237	5.777	-4.678	K3 25/1	fenestral dol
208	1.581	-2.206	k2 25.1.97	strom dk lam
208	3.26	-1.453	k2 25.1.97	strom lt lam
171	4.746	-2.981	K12 27/1	micritic dol
162	5.623	-2.155	K11 27/1	lt&dk lams
155	4.331	-2.644	K10 27/1	micritic dol
151	3.357	-3.443	K9 27/1	auto-breccia
147	4.41	-3.059	K8 27/1	grainstone
142	5.636	-4.145	K7 27/1	micritic dol
138	4.631	-1.901	K6 27/1	grainstone
134	3.442	-2.35	K5 27/1	auto-breccia
131	4.538	-1.03	k3 26.1.97	strom dk lam
131	4.437	-1.023	k3 26.1.97	strom lt lam
120	2.567	-1.87	K4 27/1	grainstone
99	4.878	-2.18	K3 27/1	micritic dol
89	3.177	-1.175	K2 27/1	lam dol
78	4.437	0.897	K5 26/1	auto-breccia
67	2.433	-4.459	k1 26.1.97	rec lam dk & lt
67	3.194	-4.512	k1 26.1.97	rec lam dk & lt
53	-0.121	-4.654	K4 26/1	peloidal dol
34	-3.211	-4.957	K3 26/1	fetid dol
8	1.908	-2.011	K2 26/1	dol
2	4.593	-4.521	k126/1md	fenestral dol

Khufai Fm (Kd)

Khufai Fm in the Khufai dome				
Depth	Carbon	Oxygen	Khufai dome	description
251	1.392	-4.486	k9 18/2/96	hybrid sandstone
250	3.446	-3.465	k16 22/1/98	hybrid sst lst
246	3.37	-3.195	k15 22/1/98	vuggy microbial lams lst
244.5	2.818	-2.693	k14 22/1/98	intraclast gs lst
242	2.889	-2.219	k12 22/1/98	cherty lams
240	3.161	0.068	k13 22/2/98	flaggy cherty dol
240	2.42	-3.304	k1 23/1/96	cherty dolomicrite
237	4.6	-2.591	k11 22/1/98	grainstone
236	3.782	-1.511	k9 22/1/98	strom lams dol
236	1.418	-2.742	k1 22/1/98	porcellaneous lams
234	3.945	-2.25	k10 22/1/98	lam khufai cycle
231	2.81	-1.607	k8 22/1/98	muddy dol
228	2.536	-2.928	k2 23/1/96	chert lam
228	3.247	-2.115	k7 22/1/98	porcel recryst lst
223	3.156	-2.055	k6 22/1/98	porcel recryst lst
219	3.457	-2.226	k4 22/1/98	cherty dol
218	0.776	-2.509	k4 23/1/96	chert algal dol
217	3.213	-2.558	k5 22/1/98	lam cherty dol
214	3.114	-0.939	k3 22/1/98	auto-breccia - micrite
214	3.274	-1.483	k3 22/1/98	auto-breccia - cement
208	2.449	-4.343	k7 23/1/96	peloidal grainstone
207	1.693	-1.317	k1 Kd	lam porcell dol
200	1.246	-2.51	k3 22/2/96	chert dol
195	3.733	-1.353	k9 23/1/96	algal lam
190	3.218	-2.286	k4 22/2/96	fen dol
139	2.82	-2.978	K12 23/1/96	fenestral dol
134	4.093	-3.596	k6 18/2/96	chert algal dol
128	2.023	-2.201	K13 23/1/96	chert algal dol
127	4.71	-3.065	k5 18/2/96	strom? dol
100	3.909	-3.375	k6 22/2/96	muddy dol
85	4.146	-4.204	K14 23/1/96	grainstone
78	1.418	-2.742	K16 23/1/96	cherty dol lt+dk lams
70	3.911	-3.093	k8 22/2/96	ooidal grainstone
69	4.624	-5.512	k3 18/2/96	fetid lams
14	4.961	-5.734	K1 18/2/96	chert dol breccia
-2	4.015	-2.35	MB1 12/1	silty dolomite
-5	3.015	-1.491	MB2 20/2	silty dolomite

Shuram Fm. data

Shuram Fm. data				
depth	CARBON	OXYGEN	SAMPLE	Description
249.5	-7.412	-8.322	B2 18.2.97	pel gs
248	-7.105	-7.896	B1 18.2.97	silty pel gs
246	-10.02	-8.455	S4 18.2.97	silty pel evap
243	-8.087	-7.5	S3 1.2.96	flat pebble
243	-8.278	-7.767	S3 1.2.96	matrix
238	-7.441	-7.378	S7.1 17.2.96	flat pebble
238	-7.803	-7.483	S7.1 17.2.96	matrix
237	-8.316	-7.375	S7.3 17.2.97	pel gs
236	-7.917	-7.264	S4 21.1.96	silty carb
225	-7.741	-7.082	S1 1.2.96	cement
225	-8.012	-7.668	S1 1.2196	ooid
221.5	-8.53	-7.56	S6.3 17.2.97	ooid gs
220.5	-8.203	-7.386	s6.2 17.2.97	recryst
220	-8.629	-8.408	S6.1 17.2.97	pel gs
219	-8.137	-7.429	S3 1.2.96	fpc
206.5	-9.32	-7.195	S5.4 17.2.97	ooid gs
205.5	-8.786	-7.177	S5.2 17.2.97	ooid gs
204	-9.239	-7.626	S5.1 17.2.97	ooid gs
203	-8.246	-7.639	S1 21.1.96	pel gs
194	-9.533	-7.731	S4.1 17.2.97	pel gs
188	-9.238	-8.078	S1 1.2.96	oolite
185	-9.991	-7.988	S4 24.1.96	oosparite
178	-9.824	-7.994	S2 24.1.96	pel gs
175	-9.784	-8.297	S1 24.1.96	pel gs
169	-9.644	-7.637	S8 21.2.97	ooid gs
167	-9.805	-8.232	S5 25.1.96	intraclast gs
165	-9.557	-8.003	S5 25.1.96	matrix
165	-9.372	-7.885	S5 25.1.96	intraclast
163	-9.584	-7.901	S6 25.1.96	pel gs
157	-9.734	-7.642	S7 21.2.97	pel gs
141	-9.26	-7.525	S3 21.2.97	matrix
141	-9.496	-7.589	S3 21.2.97	ooidal gs
141	-7.938	-7.098	S3 21.2.97	ooidal gs
129	-8.597	-7.499	S1 21.2.97	fp lams
106	-11.852	-8.012	S6 21.2.97	recryst ooid
65	-12.36	-7.578	S5 21.2.97	pel gs
15	-8.052	-8.454	S1 20.1.96	flake brecia
1	-2.198	-4.281	K5 25.1	silty top k Lr sh

Khufai Fm (Bd)

Khufai Fm in the Buah dome				
Depth	Carbon	Oxygen	Samples	Description
351	0.083	-4.055	k5 16.2.97	ooidal gs
350	1.727	-2.068	k2 16.2.97	micritic dol
349	2.105	-7.455	k14 24.2.96	fenestral dol
345.5	1.458	-3.879	k1 16.2.97	ooidal gs
345	2.417	-2.598	k2 10.1.97	intraclast gs
344	0.932	-3.773	k11 23.2.96	micritic dol
341	2.213	-4.41	k9 23.2.96	grainstone breccia
341	2.595	-3.283	k10 15.2.97	ooidal grainstone
340	1.21	-5.118	k3 10.1.97	peloidal grainstone
322	1.34	-4.072	k5 23.2.96	laminated grainstone
315	0.642	-5.06	k2 23.2.96	fetid grainstone
310	1.928	-7.505	k11 16.2.96	fetid dol
309	2.516	-5.894	k9 15.2.97	lt & dk lams
309	2.595	-6.143	k9 15.2.97	lt & dk lams
306	-2.315	-7.901	k1 23.2.96	lt & dk lams
251	2.433	-6.783	k11 24.2.96	intraclast breccia
126	-0.593	-5.12	k7 24.2.96	lam grainstone
95	3.296	-6.137	k6 15.2.97	dk lams
72	4.511	-4.057	k4 15.2.97	hybrid sst
71	0.401	-6.275	k5 16.2.96	fetid dol
59	4.288	-5.138	k4 24.2.96	fetid grainstone
54	1.89	-7.882	k3 16.2.96	micritic dol
29	4.984	-4.397	k3 15.2.97	sandy dol
11	3.808	-6.165	k2 24.2.96	micritic dol
6	3.214	-3.208	k1 16.2.96	auto-breccia

Buah Fm in the Mukhaibah dome				
Buah Md	depth	Carbon	oxygen	Description
B3	21	0.851	-2.613	crinkle lams
B4	27	-5.221	-6.261	thick crinkle
B5	34	-5.539	-6.931	recryst crinkle
B6	37	-5.146	-6.996	grey lst
B7	41	-5.911	-6.937	edgewise cong
B8	45	-5.445	-4.412	intraclast gs
B9	60	-5.171	-4.556	crinkles
B10	66	-4.762	-6.309	swaley gs
B11	70	-3.046	-5.02	crinkles
B12	81	-3.676	-4.834	black ooids
B13	81	-3.935	-5.039	black ooids cement
B14	85	-4.311	-5.208	muddy carb pink
B15	88	-3.756	-4.514	recyst dol sandy?
B16	95	-0.824	-4.153	recryst vuggy dol
B17	105	-1.109	-4.522	recryst vuggy gs
B18	113	-0.259	-2.697	intraclast gs
B19	121	0.066	-2.868	intraclst gs
B20	131	2.615	0.397	columnar strom
B21	132	-0.561	-4.614	pink muddy carb
B22	143	-1.093	-2.948	cherty lams
B23	151	1.753	-1.674	vuggy intraclast gs
B27	165	0.634	-0.804	green br muddy carb
B25	184	-1.429	-1.153	muddy pkgy carb
B26	186	-1.429	-1.95	red sandy carb
B28	190	1.463	-0.167	grey carb w/vugs
B29	196	1.863	0.513	cherty carb
B30	202	1.967	0.386	columnar strom
B31	215	1.554	-0.106	lam beds
B32	218	1.108	-0.114	vuggy anhydrite
B33	226	1.427	-0.467	cherty lams
B34	230	2.084	0.82	columnar strom
B35	239	-1.491	0.351	brown dol
B36	245	0.229	0.589	muddy grey dol
B37	247	-1.984	-0.735	pink chalky carb
B38	247	-2.243	-1.429	yellow silty carb
B39	248	-1.131	-0.502	grey carb with vugs
B40	250	-0.02	0.337	columnar strom
B41	258	-0.135	-1.611	columnar strom sandy
B42	350	-0.111	-4.035	intraclast gs
B43	358	-2.202	0.146	recryst lst
B44	360	-0.822	0.881	carb muddy clasts
B45	364	-0.197	-1.317	top buah carb with clasts

Buah Fm in the Khufai dome				
Sample	Depth	CARBON	OXYGEN	Description
b1 23.2.97	350	1.385	-2.714	col strom
b2	340	0.827	-2.923	cherty strom
b3	330	0.762	-0.949	altered dol
b4	330	1.335	-1.809	strom
b5	320	2.766	-1.111	col strom
b6	310	2.761	-2.395	micritic lam
b8 23.1.97	297	1.249	-0.726	col strom
b5 27.1.97	303	2.272	-0.672	strom pale
b5 27.1.97	303	1.521	-0.563	strom dark
b9	126	0.582	-5.329	fen lam
b10	116	0.67	-5.647	algal mat
b11	106	0.497	-5.104	lam dol
b5 23.1.97	99	2.836	-0.886	col strom
b12	96	0.313	-5.242	fine grained dol
b13	86	-0.268	-5.098	recryst gs
b14	78	-1.084	-2.592	recryst gs
b15	72	-3.349	-6.37	nodular lst
b16	66	-2.902	-6.613	flaggy lst
b17	56	-5.372	-5.379	wackestone
b18	46	-4.45	-5.432	edgewise cong
b3 23.1.97	40	-4.348	-6.133	nod lst nodule
b3 23.1.97	40	-2.648	-2.909	nod lst lam
b19	32	-5.784	-6.164	intraclast lam
b20	22	-4.627	-6.511	nodular lst recryst
b21	6	-4.752	-6.183	nodular lst recryst
Buah Fm in the Buah dome				
b9 15.2.96	98	0.356	-2.689	rosette dol bd
bd b9	97	-1.638	-3.985	gr w evaps
b6 14.2.96	95	1.234	-4.225	rosette dol yellow
bd b11	95	-2.953	-4.835	recryst dol evaps
b8 14.2.96	80	-8.073	-8.113	recyrst dol
B7 14.2BD	74	-2.204	-2.244	recryst dol
B5 14.2BD	62	-4.132	-4.172	ooidal gs
b4 14.2.96	61	-4.062	-4.102	edg cong
bd b4	60	-3.241	-4.096	recryst ghost ooids
B3 14.2BD	57	-4.44	-4.48	peloidal gs
b3 14.2.97	55	-3.51	-4.43	crinkle lams laths
b3 16.2.97	51	-2.223	-3.864	recryst dol
B2 14.2BD	46	-4.4	-4.44	recryst ghost ooids
b3 15.2.96	37	-4.088	-3.781	pk & gr lam pink lam
b3 15.2.96	37	-3.084	-3.3	pk & gr lam green lam
b1 11.1.97	19	-4.48	-4.748	nodular lst clay
b1 11.1.97	19	-3.436	-4.442	nodular grey lst

Shuram and Buah formations
data from Wadi Bani Awf

DEPTH	CARBON	OXYGEN	SAMPLE	description
940	-13.624	-0.254	F7 6.1.98	mm wispy lams
930	-6.924	-0.709	F1 9.2.98	black carb
930	-9.535	-2.2	F1 8.2.98	mm siliceous lams
924	-4.352	-0.687	B24 9.2.98	undulating wispy lams
922	-0.293	0.352	B23 9.2.98	blocky lams phosphate?
921	-3.388	-0.696	U7 9.2.98	breccia
920	-1.578	1.088	B16	wispy lams
911	-3.821	-0.76	U2 9.2.98	breccia
909	-0.527	-1.867	B21	ooidal gs
904	-0.745	-0.192	B15A	wispy lams recyst
903	-0.911	-0.056	B15B 9.2.98	grainstone
898	0.799	-4.321	B20	grainstone
894	1.148	-2.469	B14 9.2.98	recryst gs calcite vugs
891	1.266	0.586	B18	lam carb
872	2.287	-1.098	B10 8.2.98	recryst gs
832	1.544	0.661	B6 8.2.98	recryst lams
806	0.495	-1.864	B16 5.2.97	chert lst
802	0.931	-3.233	B15 5.2.97	lam sts
801	0.704	-2.246	B2 8.2.98	
774	-1.196	-2.122	B14 5.2.97	breccia matrix
774	-0.565	-2.58	B14 5.2.97	breccia clast
746	-1.583	-3.671	B4 3.2.97	recryst lst
734	-4.681	-7.626	B13 9.2.98	shaley carb
712	-5.772	-8.731	B12 5.2.97	shaly org carb
688	-5.838	-3.536	B11 5.2.97	massive dol
674	-5.596	-7.877	B10 5.2.97	massive lst
663	-5.759	-3.428	B3 3.2.97	edgewise cong
660	-6.692	-6.834	B9 5.2.97	mm dk lams
648	-6.112	-9.257	B8 5.2.97	lst
645	-5.476	-6.518	B1 3.2.97	recryst lst
643	-6.538	-10.64	M11 4.3.96	recryst lst
633	-6.802	-9.462	M9 4.3.96	recryst lst
632	-6.383	-10.187	B7 5.2.97	lam lst
629	-7.88	-10.907	M8 4.3.96	
625	-7.933	-11.067	M7 4.3.96	
623	-8.248	-10.251	M5 4.3.96	
622	-7.01	-9.664	B5 5.2.97	dk lst
620	-9.478	-11.668	M3 4.3.96	
618	-7.232	-11.126	B4 5.2.97	pure lst
617	-8.1	-10.89	M4 4.3.96	
615	-8.761	-12.433	M2.5 3.3.96	
614	-7.848	-11.369	B3 5.2.97	fine lst
609	-7.421	-10.489	M2 4.3.96	
608	-8.141	-9.304	B2 5.2.97	mm lams
603	-5.777	-8.189	B1 4.3.96	lst
602	-8.17	-11.181	B1 5.2.97	intraclast lams

Khufai Fm and 'cap dolo[illegible]or'
Oman Mountains

Khufai Fm. Wadi Hajir			
Depth	Carbon	Oxygen	description
99.5	3.985	-9.906	grainy lams K15b
99	3.623	-9.081	muddy lst K15
97	2.859	-10.552	recryst muddy lst K14
93	3.711	-10.453	recryst grainy K13
91	3.456	-9.807	grainy lst K12
82	5.312	-8.894	coarse recryst lst K11
75	2.009	2.463	muddy br lst K10b
74	5.098	-9.882	muddy blk lst K10
68	5.028	-7.828	grainy bed K9
61	6.293	-8.527	recryst lst K8
49	7.499	-6.649	vuggy lst K7
39	7.679	-7.877	vug grainy k6
31	7.47	-6.796	grainy lst K5
26	7.189	-7.508	reycrst vug k4
20	7.291	-7.403	lam lst K3
6	6.834	-7.144	recryst lst K2
0.5	6.487	-6.444	muddy carb K1
Khufai Fm. Hadash			
108.7	-4.097	-5.689	K27 12.2.98
106.9	-0.5	-5.548	K26 12.2.98
105.9	-3.704	-8.221	K25 12.2.98
104.8	-2.857	-9.02	K24
103.7	-3.313	-11.833	K23
102.7	-2.303	-6.721	K22
101.5	-3.632	-8.27	K21
100.6	-3.199	-10.307	K20 12.2.98
99.5	-0.318	-8.573	K19
98.6	0.365	-7.574	K18
97.5	4.228	-10.383	K17
96.5	2.998	-11.699	K16
95.5	0.925	-10.732	K15C
95.5	1.574	-9.54	K15A
95.5	1.049	-7.04	K15B
94.6	2.326	-11.925	K14 12.2.98
93.6	1.852	-8.457	K13
92.6	4.004	-10.014	K12
91.6	2.68	-11.351	K11
90.7	4.538	-9.814	K10 12.2.98
89.7	3.133	-9.965	K9
88.6	4.765	-8.267	K8
87.6	3.652	-11.651	K7
85.5	3.995	-11.697	K6
84.5	3.241	-10.789	K5 12.2.98
83.5	2.972	-11.041	K4
82.8	2.758	-10.86	K3
81.4	1.237	-5.579	K2
80.4	0.588	-3.505	K1 12.2.98
Cap dolostone			
6	-2.538	-8.015	C4 6.12.97 hadash cap dol
4	-5.276	-8.361	C3 6.12.97 sandy dol
1	-3.867	-7.413	C2 6.12.96 pale s gorge
0	-4.947	-9.963	C1 6.12.96 dk.gy sahtan
Khufai/Shuram contact in Wadi Bani Awf			
21.6	0.343	-4.305	K14 organic rich
19.2	-1.807	-4.824	K13 org rich w/veins
16.8	1.056	-8.943	K12 pale grey muddy
16.2	2.37	-10.066	K11 micrite
10.8	1.77	-11.096	K10 muddy limey
7	1.658	-11.653	K9 recryst muddy
6.3	2.058	-10.55	K8 recryst lams
5.9	-0.729	-6.67	K7 crinkly lams
4.3	0.117	-8.293	K5 pink grey interbeds
3.5	0.893	-6.058	K4b red limey cap
3.4	2.244	-9.88	K4 organic lst
2.6	2.463	-8.169	K3 hybrid sst
1	2.633	-8.848	K2 vuggi lst